Volume 1, June 2015 ISSN 2356-8569

مركز الأكاديمية للنشر
ACADEMY Publishing Center

Journal of Renewable Energy and Sustainable Development

RESD

Academy Publishing Center
Journal of Renewable Energy and Sustainable Development (RESD)
First edition 2015

Volume 1, Issue 1, June 2015

ISSN: 2356-8518 Print Version

ISSN: 2356-8569 Online Version

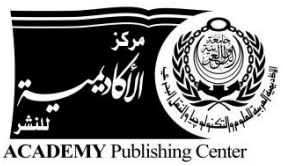

Journal of Renewable Energy and Sustainable Development

RESD

Renewable Energy and Sustainable Development (RESD) is a biannual international peer-reviewed journal which presents a global forum for dissemination of research articles, case studies and reviews focusing on all aspects of renewable energy and its role in sustainable development. The topics of focal interest to RESD include, but are not limited to, all aspects of wind energy, wave/tidal energy, solar energy, as well as energy from biomass and biofuel. The integration of renewable energy technologies in electrical power networks and smart grids is another topic of interest to RESD. Experimental, computational and theoretical studies are all welcomed to RESD.

Sustainable development is a multidisciplinary advancing to the center of energy research with the declaration of UN millennium development goals for the first time in 2000, and continued to constitute a challenge in energy technologies in the past decade. RESD is mainly interested in case studies of sustainable development and its relation to transition economies in the Middle East, Africa, Asia and Oceania.

RESD has an outstanding editorial board of eminent scientists, researchers and engineers who contribute and enrich the journal with their vast experience in different fields of interest to the journal. The journal is open-access with a liberal Creative Commons Attribution-NonCommercial-NoDerivatives 4.0 International License. Which preserves the copyrights of published materials to the authors and protects it from unauthorized commercial use or derivation. The journal is financially supported by Arab Academy for Science, Technology and Maritime Transporting in order to maintain quality open-access source of research papers on renewable energy and sustainable development.

Editorial Commitee

Editor-in-Chief

Yasser Gaber Dessouky, Ph.D
Professor of Electrical Engineering and Renewable Energy Technologies
Arab Academy for Science and Technology and Maritime Transport (AASTMT)
Abu Kir Campus, POBox: 1029 Miami,
Alexandria, EGYPT
E-mail: ygd@aast.edu

Associate Editors

Rania El Sayed Abdel Galil, Ph.D.
Associate Professor, Architectural Engineering and Environmental Design
Arab Academy for Science and Technology and Maritime Transport (AASTMT)
Abu Kir Campus, POBox: 1029 Miami,
Alexandria, EGYPT
Email: rania@aast.edu

Ahmed Kadry A. Abdel-Salam , Ph.D.
Assistant Professor, Electrical and Control Engineering
Arab Academy for Science and Technology and Maritime Transport (AASTMT)
Abu Kir Campus, POBox: 1029 Miami,
Alexandria, EGYPT
Email: ahmed.abdel-salam@ieee.org

Aly Ismail Shehata , Ph.D.
Assistant Professor, Mechanical Engineering
Arab Academy for Science and Technology and Maritime Transport (AASTMT)
Abu Kir Campus, POBox: 1029 Miami,
Alexandria, EGYPT
Email: aliismail@aast.edu

Editorial Board

Advisory Board

Table of Contents

Editorial Articles

Journal Articles

Editorial Articles

Journal of Renewable Energy and Sustainable Development

Prof. Yasser Gaber A. Dessouky

Energy is one of the basic needs of humanity and, for ages, the sun seemed to be the main source of all energy in the universe and that is why the ancient Egyptians used to venerate it. Many wastes and corpses – under pressure and heat – have been converted throughout the years inside the earth into the oil on which recent development is totally based to support humans' life, particularly in transportation and power generation. As time passes, it has been proven that oil will vanish. For the first moment, it seemed like mankind will certainly suffer due to such a hard situation and some people thought that we will get back to stone ages when oil no longer exists.

Thanks for the Renewable Energy scientist who has looked at the issue from a different prospective, that is, even if oil vanishes, the main reason of its existence is still there, that is the sun .

The sun has the capability to still make people enjoy their life not only by enjoying the sunny weather in many places of the world and having good times on the beach for those who live by the sea but also the sun can still provide man with required energy and cause the wind to blow, the waves to raise, the plants to be converted to biomass, and the earth to store its geothermal energy.

As long as life goes on, the sun will always rise and will always grant its energy to mankind. It is the clean, renewable and sustainable energy, which guarantees sustainable development.

Because of the high correlation between renewable energy and sustainable development, the editorial team of this journal thought of offering a hub to researchers interested in these two important fields to present their work and share it with others who have the same interest in such a wide area of research .

Thanks to the Academy Publishing Center, 'APC' owned by the Arab Academy for Science, Technology and Maritime Transport 'AASTMT' for hosting this international journal.

We call upon researchers in this area to share their thoughts and their work through this journal, free of charge through the online submission system, and have it on hard copy through a Print On Demand 'POD' base.

Last but not least, we would like to thank the authors of the four editorial articles which were useful to researchers in the field of Renewable Energy and Sustainable Development.

About Prof. Yasser Gaber A. Dessouky

Professor Yasser Gaber Dessouky graduated from Alexandria University in 1991. He got his PhD from Heriot Watt University, UK in 1998. He is a professor at the Department of Electrical and Control Engineering, Arab Academy for Science, Technology and Maritime Transport (AASTMT) since 2006. Currently, he is the Dean of Scientific Research and Innovation in the AASTMT. He is the Chair of Industry Relations Subcommittee, IEEE Alexandria. He is a Renewable Energy Expert in the ESCWA of the UN and he is a member of the World Renewable Energy Network (WREN) UK and the DeserTech University Network (DUN) Hamburg Germany. He is also a member of the Research, Development and Innovation Network (RDIN) and the Egyptian Science, Technology and Innovation Observatory (ESTIO). Professor Dessouky is an editorial board member of many journals and a consultant for many industrial companies. He is a peer reviewer in many transactions, periodicals and conferences. He has a patent from the Patent Office in UK. He is leading Technology, Innovation and Commercialization Office (TICO) in the AASTMT. He is also leading many research projects funded by the EU such as ErAfrica project entitled, 'Development of a High-Efficient Power-Generation from Hybrid-Fuel Supplies', 2014-2017 and a TEMPUS project, 'Highway and Traffic Engineering', 2013-2016.

Renewable Energy and Sustainable Development and Their Relation with Remote Sensing

Prof. Farouk El-Baz

It is with pleasure that I welcome this initiative of the Arab Academy of Science and Technology (AASTMT). I applaud the AASTMT for emphasis on the applications of renewable energy to sustainable development. This new journal will assist in popularizing the significance of this important effort.

Because the topic is rather new to many developing countries, emphasis is to be placed on communicating the significance of the endeavor. Thus, scientists and technologists should attempt to convey the expected benefits to the society at large. Articles and case studies in this new journal will be case studies in an easy to follow explanation of the proper procedures and their expected benefits.

There is no limitation to subjects that would have an impact on the topic. For example, my own field of studying the earth with data collected from space would have an impact. For example, the potential use of satellite image data to the selection of sites for the generation of solar energy. This would be based on the topography, measurements of the aridity index, and preferred locations near large cities, as well explained by Dr. Hany El-Nokrashi in this volume.

It is clear that in Egypt and throughout the Arab world there is a need to emphasize the use of solar energy. Our region includes some of the driest places on Earth. The impinging solar radiation during most of the year would be invaluable to the production of all energy needs. In addition, many regions are endowed with utilizable wind for the production of additional energy. The use of such research would go a long way in sustaining a clean environment for a vast number of citizens.

For these reasons, I congratulate all those who embarked on bringing this valuable effort to fruition. It is particularly significant that many participants in this effort represent younger generations of Egyptians. I applaud you all and wish you continued success.

About Prof. Farouk El-Baz

Egyptian American space scientist, Born on January 2, 1938 in the Nile Delta village of Touqh el aklaam, El Senbellawein city, Dakahlia Governorate. In 1958, at the age of 20, he received a Bachelor of Science in chemistry and geology from Ain Shams University. In 1961, he received a Master of Science in geology from the Missouri School of Mines and Metallurgy (now Missouri University of Science and Technology). In 1964, at the age of 26, he received a Doctor of Philosophy in geology from the Missouri University of Science and Technology after conducting research from 1962 to 1963 at the Massachusetts Institute of Technology.

In 1978, El-Baz was appointed Science Adviser to President Anwar Sadat of Egypt. He was charged with the selection of regions for land reclamation in the desert without detrimental effects on the environment. For his distinguished service, President Sadat awarded him Egypt's Order of Merit - First Class.

In recognition of his professional standing, he received the following honorary degrees: Doctor of Science from the New England College, Henniker, NH (1989); Professional Degree from the Missouri University of Science and Technology (2002); Doctor of Philosophy from Mansoura University, Mansoura, Egypt (2003); Doctor of Laws from the American University in Cairo (AUC), Egypt (2004); Doctor of Engineering from the Missouri University of Science and Technology, United States (2004).

Currently, El-Baz is Research Professor and Director of the Center for Remote Sensing at Boston University in Boston, Massachusetts. He is a Professor of Geology at the Faculty of Science, Ain Shams University, Cairo, Egypt.

He is also a member of the Board of Trustees of the Geological Society of America Foundation, Boulder, Colorado, a member of the Board of Directors of CRDF Global, and a member of the U.S. National Academy of Engineering, Washington, DC.

Future of Energy in Egypt and the World

Dr.-Eng. Hani Mahmoud El-Nokraschy

If the whole world, which Egypt is a part of, continues business as usual in the field of electricity generation, namely, using the same regimes adopts today, burning fossil fuels and Uranium fission, both fuels will run out within sixty years at most and the world will definitely return to the Stone Age. Shall this be the end of the Egyptian people … the history makers?

Generating energy is the next necessity to human life after water and food, since it is the major stimulus of development. However, what is the aim of development if it is only momentary; then followed by an endless abyss?

Shall we wait till fossil and nuclear fuels run out? Jostling over the remaining fuel will certainly be fierce and we will pay a high price for it, a matter that will subsequently lead to demolishing the ingredients of development.

Considering that oil is now dominating our way of life, it shall be wise to start immediately planning for the post-oil age, provided that it is a sustainable plan set up to continue its validity as long as humans live on this planet; this cannot be achieved except if we shift to renewable energies.

Looking at Egypt and its available renewable energy sources, it becomes evident that the solar energy, particularly in Upper Egypt, can give more than the present and future needs of the Egyptian society and even cover the demand of the whole world for electricity.

However, success of any plan in this regard depends mainly on the appropriate techniques adopted to realize it. There are two techniques to utilize solar energy in order to generate electricity:

Firstly, solar cells that transform sun light directly to electricity. However, this technique does not allow storing - on a large scale – of the daily produced electricity to be used at night and therefore, there will be no electricity after sunset.

Secondly, mirror focusing of sunrays to obtain high temperature that makes it possible to heat water and generate high temperature and high-pressure steam, exactly like fossil-fueled boilers do in the majority of conventional power stations in the world. This technique is capable of storing a significant portion of the heat collected during the sunny hours to be used during night to produce electricity. This means that the Concentrating Solar Power (CSP) technique can replace fossil fuels completely, because thermal storage costs a hundredth of that of electricity storage. Egypt's qualitative advantage is the availability of direct sunrays, in contrast to northern countries having mainly diffuse sunrays; only direct sunrays can be bundled and thus concentrated on a focus, obviously the condition for utilizing this technique.

Therefore, solar thermal power stations equipped with storage will spare Egypt importing fuels to generate electricity as well as establishing nuclear plants since they are less in costs than nuclear plants of same capacity and reveal equal performance; moreover, decrease in costs when multiple units are put in operation. Another significant advantage is that they can be much more rapidly manufactured, commissioned and operated than conventional or nuclear power stations, giving them the ability to cope with the highly increasing demand on electricity. Besides, they do not produce dangerous wastes or emissions. Finally, most of their components can be manufactured locally thus providing job opportunities and encourage establishing of complementary industries.

For such power stations, standardizing a small capacity unit, offers better chances for financing and paves the way to mass production. Small units with air cooled condensers can be placed anywhere in the desert, thus giving flexibility in regards to selecting their location as no special site conditions are

required as to be in vicinity of a water stream. Thus the power station can be placed near new residential complexes or along the south-north electricity line to inject power to it instead of reinforcing the line. This strategy decreases load over lines as well as electricity transfer losses; since selecting the location for the power station does not necessitate having a water stream. In case that the power station is located near the seashore, its waste heat can be used for desalting seawater resulting in very low cost drinking water because energy used for desalination is available as waste heat.

Following such a policy will definitely boost Egypt's rank in the countries exporting expertise and special equipment to establish such stations. Furthermore, Egypt possesses all the ingredients of development and atop of which are its intelligent persistent people and imperishable energy sources.

It is also worth mentioning that desalination of seawater is the only way out for Egypt to provide enough water and consequently food. Limitation of the River Nile water forces the farmers to reduce irrigation water thus reducing wash out of salts from the earth and consequently increasing land salinity that damages the land for years to come. Experience provides evidence for such dangerous exercises.

Let us have a glans at the civilization history of the Egyptian people. A civilization that extends for more than 7000 years, whereas during the last 5000 years the oldest state on earth was established, that still exists and glares with its donation. Looking that way raises a significant question: is our generation entitled to spoil the fertile land that we have inherited from our ancestors and on which we have lived in dignity and pride the last millenniums.

For all these reasons, we have proposed adopting a sustainability framework in the Egyptian Constitution:

> **Preserving the country's resources by applying sustainability principles in agriculture, energy production and other community requirements to guarantee the wellbeing of future generations**

We are truly grateful to Almighty God that the Founding Committee of the Egyptian Constitution has responded to this proposal and required to adopt sustainability principles in at least six articles including article 32 stipulating that the government should abide by using renewable energies:

> **"The State is committed to the optimum utilization of sources of renewable energy"**

Hereunder are some examples of solar thermal power stations using different schemes that have been successfully implemented and are commercially operating:

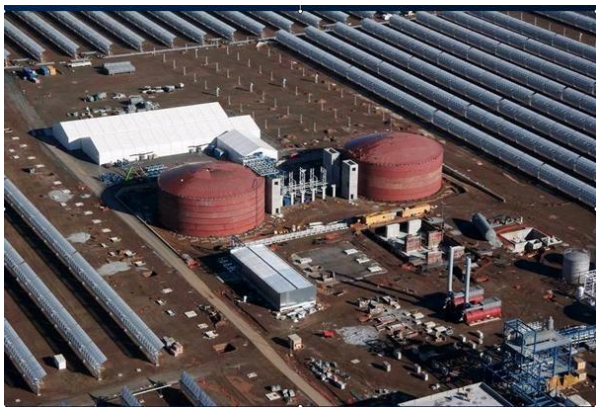

Rows of solar reflectors consisting of longitudinal parabolic mirrors (Parabolic troughs) in the 50 MW solar power station in Spain "ANDASOL". It has thermal storage that allows it to operate for seven and a half hours after the sunset

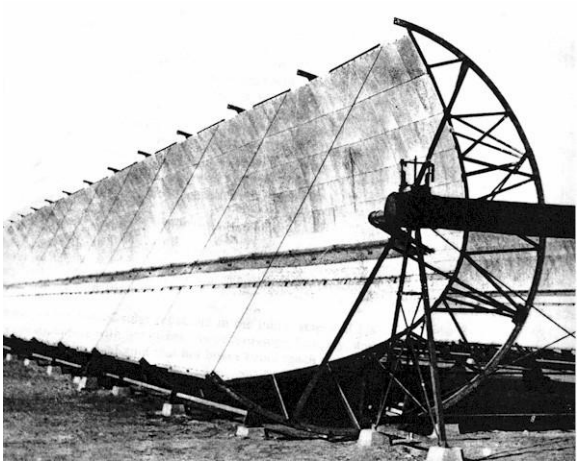

Longitudinal parabolic mirror (crescent shaped) This was the first commercial application of concentrating thermal solar power. Installed in Maady, near Cairo 1913 to produce steam for pumping the Nile water to the cotton fields

Solar Power Tower Technology, Gemasolar in Spain, 19.9 MW with 15 hours storage

Fresnel Flat Mirror Technology, Puerto Errado in Spain, 30 MW with 0.5 hours Storage

About Dr.-Eng. Hani Mahmoud El-Nokraschy

After graduating with a BSc. in Mechanical Engineering from the Faculty of Engineering, Cairo University in 1958, he pursued his graduate studies in Germany at the Technical University of Darmstadt where he received his Dipl.-Ing. (MSc.) in 1963 and his Dr.-Ing. (PhD) in 1968 .

Dr. El Nokraschy worked at the Transport and Engineering Company in Cairo from 1957 to 1958 .

After receiving his PhD in 1968 he joined SCHENCK in Darmstadt, Germany. He was appointed as Head of the Research Department for Vibrating Machines in 1983. He continued working at SCHENCK until he moved to MOGENSEN in Wedel, Germany in 1991, where he occupied the position of Head of Design and R&D .

In 1998, he founded his own consultancy services, NOKRASCHY ENGINEERING GmbH in Germany, where he discovered the attractiveness of renewable energies, especially for his birth country Egypt which is blessed by excellent sun and wind conditions.

He participated as a team member at the German AeroSpace Center (DLR), from 2004 to 2007 to the research on renewable energies around the Mediterranean and deploying renewable energies for seawater desalination. In 2007, he also participated as a member of the renewable energy team at the German-Egyptian Year of Science and Technology .

In 2009, he was appointed by the Centre of Future Studies at the Information and Decision Support Centre (IDSC) of the Egyptian Cabinet to conduct a study on the future of electricity in Egypt. He suggested therein a gradual but definitive shift to renewable energies within this century.

Dr. El Nokraschy is a member of Advisory Board, and MSc. lecturer and examiner at REMENA joint program of Cairo University in collaboration with Kassel University, Germany .

He was one of the founders of the DESERTEC foundation in Jan. 2009 and vice Chairman of the Supervisory Board. His last position at the Foundation was Chairman of Board of Trustees till September 2014 when he was nominated as a member of the Scientific Advisory Council to the President of Egypt.

Further activities and positions :

- Founding member - 1996 - of the Egyptian Businessmen Association in Germany and Secretary General since 2013 .
- Member of the General Union of Egyptians Abroad (Cairo).
- Head of the Supervisory Board to the Supreme Council of Egyptian Associations in Germany .
- Member of the German Association of Scientists (VDW) since 2013.

مستقبل الطاقة في مصر و العالم

د .مهندس هانئ محمود النقراشي

إذا استمر العالم - و مصر جزء منه - في إنتاج الكهرباء بالنمط الحالي، أي حرق الوقود الحفري و شطر اليورانيوم، فسينفد كلاهما في غضون ستين سنة و يعود العالم للعصر الحجري .فهل تكون هذه هي نهاية شعب مصر الذي صنع التاريخ ؟
إن إنتاج الطاقة يأتي في المرحلة التالية من الضروريات بعد توفير الماء و الغذاء للإنسان لأنها المحرك الأساسي للتنمية،و لكن ما فائدة التنمية إذا كانت مؤقتة و يتبعها الهبوط إلى الهاوية؟

إذا انتظرنا إلى قرب نفاد كلا الوقود الحفري و الإنشطاري، سيكون التزاحم على شراء ما تبقى منه على أشده و لن نحصل عليه إلا بغالي الثمن الذي يقوض مقومات التنمية.

إذا من الحكمة أن نبدأ فورا في التخطيط لما بعد عصر النفط الذي طغى على حياتنا .... شريطة أن يتصف المخطط بالاستدامة، أي يسمح بالاستمرار على نهجه طالما وُجدت البشرية على وجه الأرض، و هذا لا يتأتى إلا إذا اتجهنا إلى الطاقات المتجددة.

بنظرة إلى المتاح في مصر من الطاقات المتجددة المعروفة، نجد أن الطاقة الشمسية - و خاصة في صعيد مصر- أكثر من احتياجات المجتمع المصري الآن و في المستقبل، بل تكفي لتلبية متطلبات العالم كله.

و لكن نجاح أي مخطط في هذا الصدد يعتمد في الدرجة الأولى على التقنية المناسبة لتحقيقه .و لاستخدام الطاقة الشمسية لإنتاج الكهرباء نجد تقنيتين:
الخلايا الشمسية التي تحوّل ضوء الشمس إلى كهرباء مباشرة، و هذه لا تتيح تخزين الكهرباء المُنتجة نهارا لاستخدامها ليلا، فلا كهرباء بعد غروب الشمس.
ثم تقنية تركيز أشعة الشمس بالمرايا للحصول على درجة حرارة عالية تسمح بإنتاج بخار الماء بحيث تلبي نفس الغرض الذي أنشئت من أجله المراجل التي تعمل بالوقود الحفري في أغلب محطات الكهرباء في العالم .و هنا تظهر فائدة هذه التقنية، فبجانب أنها تحل محل الوقود الحفري فهي تفتح المجال للتخرين الحراري و هذا التخرين متاح بتكلفة أقل مائة مرة من تكلفة تخزين الكهرباء .كذلك تظهر الميزة النوعية لمصر حيث أن الأشعة المباشرة لشمسها - بخلاف تلك في دول الشمال- يمكن تركيزها في بؤرة و هذا هو شرط تفعيل هذه التقنية.

و على ذلك فإن المحطات الشمسية الحرارية ذات التخزين الحراري تغني مصر كليا عن إستيراد الوقود لإنتاج الكهرباء و تغني كذلك عن المحطات النووية، حيث أنها تتميز بنفس الأداء و لكنها أسرع في بنائها و إدخالها الخدمة و لا ينتج عنها نفايات خطيرة فضلا عن أنها أقل منها في السعر الذي ينخفض مع تزايد إنتاج وحداتها .و مقارنتها بالمحطات النووية يُظهر لنا مميزات أخرى بجانب سرعة بنائها، مما يقدرها على تواكب التزايد على الطلب فإن مكوناتها تُضنّع محليا فتفتح مجالا كبيرا للعمل و إنشاء صناعات مكملة.

إختيار قدرة نمطية صغيرة للمحطة فيه يُسر للتمويل و يتيح إنتاجها بأعداد كبيرة .و اختيار موقعها قرب التجمعات السكنية و نشرها على طول خطوط الكهرباء ينقص الحمل على الخطوط و يُنقص فواقد نقل الكهرباء .خاصة أن إختيار الموقع لا يُراعى فيه وجود مجرى مائي لأن تبريد المحطة النمطية يجب أن يكون بالهواء .و إذا كان موقعها قرب البحر يُستغل فائضها الحراري لتحلية مياه البحر، فيكون الحصول على مياه الشرب بأقل التكاليف لعدم استخدامه طاقة إضافية.

عند إتباع هذه السياسة سترقى مصر إلى مصاف الدول المُصدّرة للكهرباء الشمسية، بل أيضا إلى مصاف الدول
المصدرة للخبرة و المعدات الخاصة ببناء هذه المحطات حيث يتوافر لديها كل مقومات التنمية :شعب ذكي دؤوب على العمل و مورد طاقة لا يفنى.

و لا ننسى أن تحلية مياه البحر هي المخرج الوحيد أمامنا لتوفير الماء و بعده الغذاء .فإن قلة المتاح من ماء النيل يدفعنا إلى إنقاص مياه الري مما يتسبب في تناقص الصرف الزراعي و هذا بدوره سبب تزايد ملوحة الأرض و إفسادها لأجيال كما حدث لمن سبقونا في هذه التجربة الخطيرة.

لختام هذا الحديث، إذا نظرنا إلى تاريخ شعب مصر الذي تمتد حضارته لأكثر من سبعة آلاف عام أرسى في الآلاف الخمس الأخيرة منها أقدم دولة على وجه الأرض مازالت على مر كل هذه السنين و للآن تتألق بعطائها، فيجب أن نتساءل بأي حق نسمح لأنفسنا أن نفسد هذه الأرض الطيبة بعد أن ورثناها من أجدادنا في حالة صحية خصبة سمحت لنا بالعيش فيها بكرامة و عزة.

لكل هذه الأسباب اقترحنا تثبيت إطار الإستدامة في دستور مصر:

الحفاظ على مقومات الدولة بتطبيق مبادئ الإستدامة في الزراعة و إنتاج الطاقة
و غيرهما من ضروريات المجتمع، و ذلك لضمان سلامة البيئة للأجيال القادمة.

و نحمد الله عز و جل أن استجابت لجنة وضع الدستور لهذا الاقتراح و ضمنت مبادئ الاستدامة في ستة مواد على الأقل منها المادة 32و التي تلزم الحكومة باستخدام الطاقات المتجددة:

"كما تلتزم الدولة بالعمل على الاستغلال الأمثل لمصادر الطاقة المتجددة"

أمثلة عملية لمحطات شمسية بتقنيات مختلفة نُفذت بنجاح:

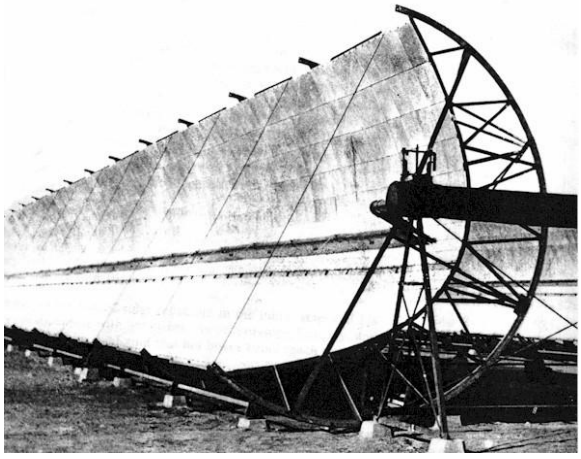

مرآة طولية ذات قطع مكافئ (هلالي) لتركيز الإشعاع أول تفعيل عملي للطاقة الشمسية الحرارية عالميا كان سنة 1913 في المعادي لإنتاج بخار لضخ ماء النيل

تقنية المرايا ذات القطع المكافئ
أنداسول، محطة شمسية في إسبانيا بها تخزين حراري يسمح لها بالعمل سبع ساعات بعد غروب الشمس

تقنية فرينل بالمرايا المستوية
بويرتوإرادو في إسبانيا تخزين 0.5 ساعة

تقنية البرج الشمسي
جيماسولار في إسبانيا تخزين 15 ساعة

Energy Mix between Renewable Energy and Nuclear Energy

Prof. Yousri AbuSahdy

Energy is the backbone of any development in any State. Renewable Energy (wind, solar and biomass) appears currently as a major strategic energy source for a sustainable development particularly for developing or under developing societies. Use of renewable Energy will challenge major technological changes, by achieving energy production and saving. In particular by replacing fossil fuel, a significant cut of environmental impact and green house gas emission (GHG) could be achieved. In addition Renewable Energy could offer a sustainable development for different societies particularly those in rural area (e.g. desert or isolated islands). The significant technical renewable energy tool developments in developed States could be much easier to be transferred to or copied in developing States .

Due to the lack of continuity of energy production throughout the entire days for solar and wind resources, it would either need an important increase in their cost to save energy from the hours it works to use it during the dead production period, or to use a base-load other energy source. One of the best clean and relatively sustainable is the nuclear energy. The use of energy mix between renewable energy and nuclear energy could offer the best energy strategy for a developing State like Egypt.

The issue of a Journal for renewable energy and sustainable development from the Arab Academy for Science and Technology and Maritime Transport in Alexandria is an important step to address many scientific and technical researches and technical applications in the field and could offer an important reference to national and international affiliations and academic researches. I wish all success to the new Journal in its important field.

About Prof. Yousri AbuSahdy

Prof. Yousri AbuSahdy was awarded his BSc, MSC and PhD in Nuclear Engineering from Alexandria University and France. He was former head of the Nuclear Engineering Department (NED), Alexandria University till 1982.

Prof. AbuShady is an international expert in the field of energy, nuclear energy and designing reactors, in particular. He is also a senior inspector at the International Atomic Energy Agency (IAEA) and former head of its Safeguards Operation Section.

Prof. AbuSahdy assumed duty at IAEA since 1984 till 2009 (for 25 years) during which he was assigned several tasks, held various positions and took part in inspection of hundreds of nuclear facilities in more than 40 countries.

Prof. AbuSahdy was awarded several honorary rewards and certificates of merit, atop of which is the Nobel Peace Prize in 2005 jointly awarded with the IAEA, as well as the International IAEA Distinguished Award for Excellence in Work in 2003 in addition to Alexandria University Encouragement Award in 1981. He also chaired and took part in various international and local scientific conferences and seminars, has a multiplicity of scientific research papers, publications, references and a number of books and articles. Furthermore, he was able to design and manufacture the first prototype of an Egyptian nuclear reactor in collaboration with ten BSc students as their graduation project at the Nuclear Energy Department, Alexandria University in 2012-2013 supported by an Egyptian national factory.

Now, he is a member of the Egyptian Council for Foreign Affairs (ACFA), member of PUGWASH International Association that is countering nuclear weapons. Recently, he is a visiting professor at a number of Egyptian universities.

Power Electronics and Renewable Energy Systems – a perfect match for a sustainable society

Prof. Frede Blaabjerg

The energy consumption is steadily increasing very rapid due to more people on the earth, better living conditions as well as we are trying to live in areas where the energy demand is high. The economy growth in the last century has not been possible without low prize of energy which has been achieved by fossil fuels. Looking into the future – the fossil fuel resources have a time limit – which can appear faster than expected – both because of the limited resources but also because the market can suddenly increase the prize. Therefore there is a demand to come up with sustainable energy solutions for energy production like wind turbines, hydro power as well as photovoltaics. At the same time it is evident that by the use of new technology it is possible to make energy saving. In both situations power electronics are making this possible – we are using power electronics to interface renewable sources to maximize the energy yield from wind turbines and photovoltaics as well as smoothly integrate it to the grid. Also in many applications we use power electronics to interface a load with the grid and control the behavior of the electrical equipment according to the demand. In many cases power electronics is able to ensure a large amount of energy saving like in pumps, compressors as well as in ventilation systems. Also the transportation gain a lot of using electricity instead of fossil fuel – clearly made possible due to the power electronics.

Denmark is one of the societies which have been the frontier of implementing the renewable technology and has today covered more than 50 % of the electrical energy consumption by means of renewable and has as ambition to be fully independent on fossil fuels in 2050. Already in 2035 100 % of the electricity will be covered by renewables. At the same time the energy consumption has not really increased for 20 years despite the GDP has grown by more than 60 % - much is enabled by energy efficient technologies based on power electronics. So renewables and power electronics are a perfect tool for a sustainable society.

About Prof. Frede Blaabjerg

Frede Blaabjerg (S'86–M'88–SM'97–F'03) was with ABB-Scandia, Randers, Denmark, from 1987 to 1988. From 1988 to 1992, he was a Ph.D. Student with Aalborg University, Aalborg, Denmark. He became an Assistant Professor in 1992, an Associate Professor in 1996, and a Full Professor of power electronics and drives in 1998. His current research interests include power electronics and its applications such as in wind turbines, PV systems, reliability, harmonics and adjustable speed drives.

He has received 15 IEEE Prize Paper Awards, the IEEE PELS Distinguished Service Award in 2009, the EPE-PEMC Council Award in 2010, the IEEE William E. Newell Power Electronics Award 2014 and the Villum Kann Rasmussen Research Award 2014.

He was an Editor-in-Chief of the IEEE TRANSACTIONS ON POWER ELECTRONICS from 2006 to 2012. He has been Distinguished Lecturer for the IEEE Power Electronics Society from 2005 to 2007 and for the IEEE Industry Applications Society from 2010 to 2011. He is nominated in 2014 by Thomson Reuters to be between the most 250 cited researchers in Engineering in the world. He has more than 1000 publications and more than 37000 citation in Google Scholar.

Adaptive Artificial intelligence based fuzzy logic MPPTcontrol for stand-alone photovoltaic system under different atmospheric conditions

L. Zaghba[1,2], N.Terki [2], A .Borni [1], A.Bouchakour [1]

[1] Unité de Recherche Appliquée en Energies Renouvelables, URAER, Centre de Développement Des Energies Renouvelables, CDER, 47133, Ghardaïa, Algeria
[2] Electrical Engineering Department, University of Biskra, Algeria
Layachi40@yahoo.fr

Abstract— There is an increased need for analysing the effect of atmospheric variables on photovoltaic (PV) production and performance. The outputs from the different PV cells in different atmospheric conditions, such as irradiation and temperature, differ from each other, evidencing knowledge deficiency in PV systems. Maximum power point tracking (MPPT) methods are used to maximize the PV array output power by tracking continuously the maximum power point (MPP). Among all MPPT methods existing in the literature, perturb and observe (P&O) is the most commonly used for its simplicity and ease of implementation; however, it presents drawbacks, such as slow response speed, oscillation around the MPP in steady state, and even tracking in wrong way under rapidly changing atmospheric conditions. In order to allow a functioning around the optimal point Mopt, we have inserted a DC-DC converter (Buck– Boost) for a better matching between the PV and the load. In this paper, we study the Maximum power point tracking using adaptive Intelligent fuzzy logic and conventional (P&O) control for stand-alone photovoltaic Array system. In particular, the performances of the controllers are analyzed under varying weather conditions with constant temperature and variable irradiation. The proposed system is simulated by using MATLAB-SIMULINK. According to the results, fuzzy logic controller has shown better performance during the optimization.

Keywords- Solar photovoltaic; MPPT; P&O; fuzzy logic Controller; PV array; DC/DC Buck-Boost converter

I. INTRODUCTION

In order to obtain an adequate output voltage, PV cells are connected in series to form a PV module. If higher voltages or currents are not available from a single module, modules must be connected into arrays. Series connections result in higher voltages, while parallel connections result in higher currents (Fig 1).The maximum power point tracking, MPPT technique, not only enables an increase in the power delivered from the PV module, but also enhances the operating lifetime of the PV system [2].

Various MPPT methods have been developed and implemented [3][4]. These methods can be differentiated based on various features including the types of sensors required, convergence speed, cost, range of effectiveness, implementation hardware requirements, and popularity [4].

MPPT techniques, such as the Perturb & Observe and the Fuzzy logic methods, will be compared using Matlab tool Simulink, considering different types of irradiation and temperature variations. The partially shaded condition will not be considered in the simulation: the irradiation is assumed to be uniformly spread over the PV array [4].

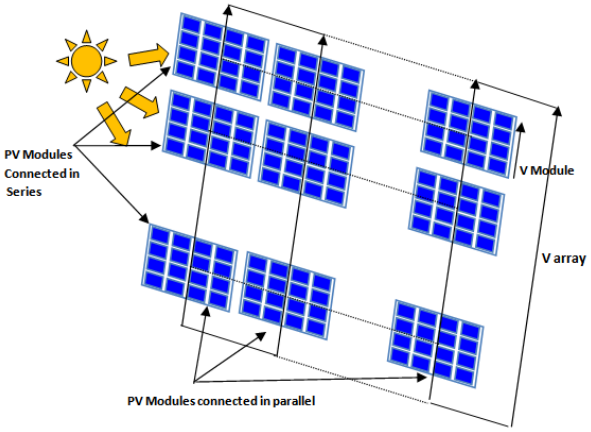

Fig 1. Example of PV arrays

II. MODELLING AND CHARACTERISTIC OF PV ARRAY

1. *Modeling of PV array*

A solar PV array is developed in Simulink. This array is used as a source for the maximum power point tracker system. The PV array makes use of the equations of a typical solar cell. The typical model of a solar cell is shown in Fig. 2. The current and voltage of the solar cell is given as follows [01]:

$$Icell = Iph - ID - \frac{Vcell + RsIcell}{Rp} \quad (1)$$

$$ID = Isat\left\{\exp\frac{q}{kT}[(\mathrm{Vcell} + \mathrm{RsIcell})] - 1\right\} \quad (2)$$

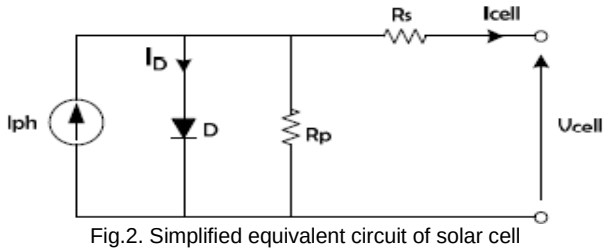

Fig.2. Simplified equivalent circuit of solar cell

where $Icell$ and $Vcell$ are the cell output current and voltage. The definitions of the parameters are

given in table 1.The equivalent circuit for the solar cells arranged in Np parallel and Ns series is shown in fig.3. Array current and array voltage become:

$$Ipv = NpIph - NpIsat\left\{exp\left[\frac{q}{KT}\left(\frac{Vpv}{Ns}+\frac{RsIpv}{Np}\right)\right]-1\right\} - \frac{Np}{Rp}\left(\frac{Vpv}{Ns}+\frac{RsIpv}{Np}\right) \quad (3)$$

Np : represents the number of parallel modules. It should be noteded that each module is composed of Ns cells connected in series. $NpIph$ Corresponds to the short circuit current of the solar array.

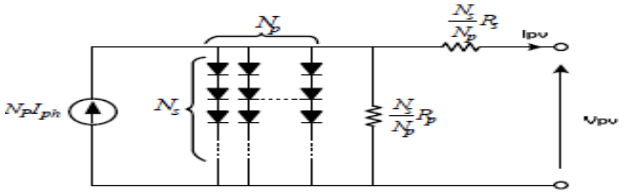

Fig.3. Electrically equivalent of solar array circuit (N_p parallel- N_s series)

The output of Simulink model is shows first; the V-P characteristics of PV module, for various irradiation levels (Fig.7), and then V-I characteristics, reference to the key specifications of the MSX60 array are illustrated in table 2 [01]. The results of Simulink PV module show the excellent correspondence to the model.

Table 1. Electrical specifications of the -60 W mono-crystalline photovoltaic module MSX60

Parameter		Value
Maximum Power	P_{PV}	200W
Tension at Pmax	V_{MPP}	26.3 V
Current at Pmax	I_{MPP}	7.61A
Open Circuit Voltage	Voc	32.9V
Short Circuit Current	Isc	8.21A
Ideality factor	A	1.3

Table 2. Electrical specifications of the - 6KW mono-crystalline photovoltaic array of 100 module of MSX60

Parameter		Value
Maximum Power	P_{PV}	60X100 = 6000W
Tension at Pmax	V_{MPP}	17.1X20 = 342 V
Current at Pmax	I_{MPP}	3.5X5 = 17.5A
Open Circuit Voltage	Voc	21.1 X20 = 422V
Short Circuit Current	Isc	3.8X5 = 19 A

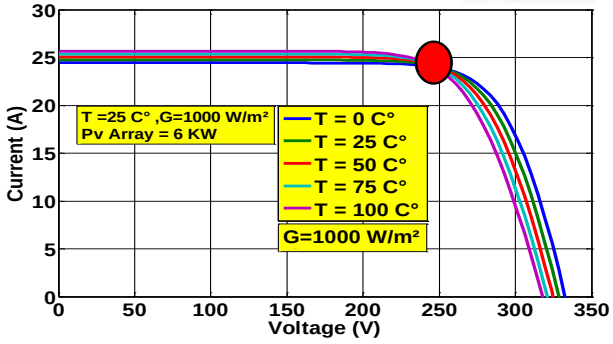

Fig .4. V-I, Characteristics of PV Array (6KW) at constant insulations and varying temperature

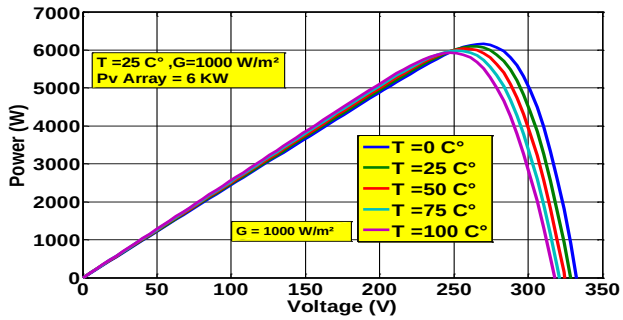

Fig.5.P-V Characteristics of PV Array (6KW) at constant insulations and varying temperature.

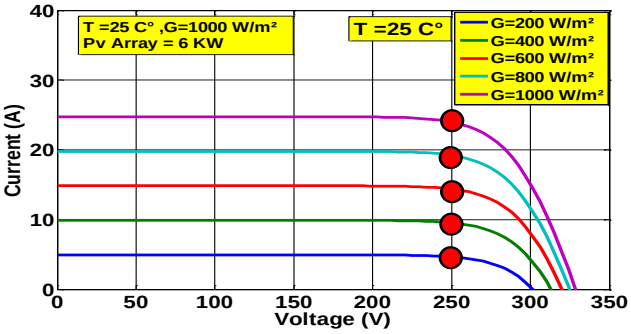

Fig .6. V-I Characteristics of PV Array (6KW) at constant temperature and varying insulations

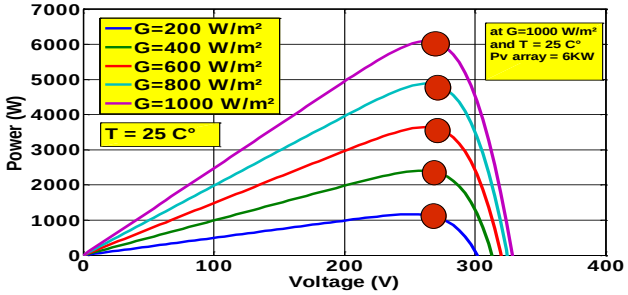

Fig .7. V-P Characteristics of PV Array (6KW) at constant temperature and varying insulations

2. DC-DC Buck-Boost Converter

The DC-DC converter is an electronics circuit, which is used to provide a loss less transfer of energy between different circuits at different DC voltage levels. There are many DC-DC converters. One of the popular types of DC-DC converters is buck-boost converter. The Buck-boost converter is used to step down and step up the DC voltage by changing the duty ratio of the MOSFET. If the duty ratio is less than 0.5, the output voltage is less than the input voltage; however, if the duty ratio is greater than 0.5, the output voltage will be greater than the input voltage. Duty ratio is the time at which the MOSFET is on to the total switching time. The buck-boost converter is shown in Figure 8.The relation between the input and the output voltages of the buck-boost converter is given as follows: [7].

$$Vout = \frac{-D}{1-D}Vin \quad (4)$$

Table 3. Buck-boost converter parameters

Buck-boost converter parameters	
L	1mH
C1	1000 µF
C2	330 µF
fs	40KHZ
Resistive Load R	5Ω

When applying Kirchhoff's laws, we find:

$$\begin{cases} \frac{dV_{PV}}{dt} = \frac{i_{PV}}{C_{PV}} - \frac{i}{C_{PV}} D \\ L\frac{di}{dt} = (1-D).V + D.V_{PV} \\ C\frac{dV}{dt} = -(1-D)i - \frac{V}{R} \end{cases} \quad (5)$$

I is the current through the inductance; V is the voltage across the capacitor; D is the duty ratio and Vpv is the voltage measured from the photovoltaic panel Fig 8.

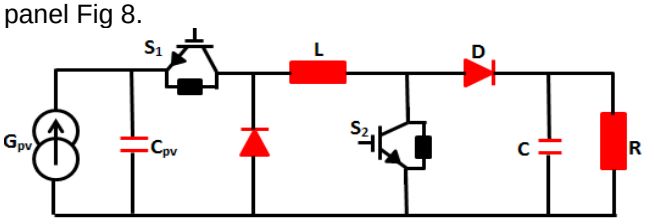

Fig. 8. The buck-Boost converter circuit

3. Maximum Power Point Tracking

Maximum Power Point tracking controller is basically used to operate the Photovoltaic modules in manner that allows the load connected with the PV module to extract the maximum power, which the PV module is capable to produce at given atmospheric conditions. PV cells have a single operating point, where the value of the current and voltage of the cell results in a maximum power output. With the varying atmospheric condition and because of the rotation of the earth [4], the irradiation and temperature keeps on changing throughout the day. So it is a big challenge to operate a PV module consistently on the maximum power point and for which many MPPT algorithms have been developed [1]. The most popular among the available MPPT techniques is Perturb and Observe (P&O) method. This method is having its own merits and demerits. The aim of the present work is to develop the Simulink model of P&O MPPT controller and then the fuzzy intelligent control has introduced on it to improve its overall performance

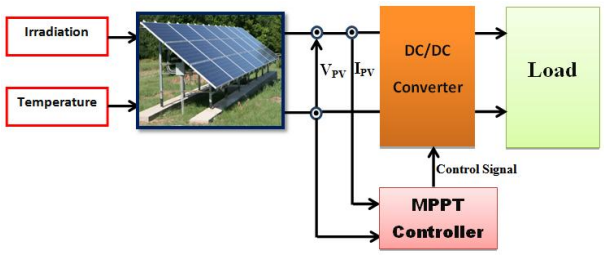

Fig. 9. Block diagram of PV Module with MPPT Controller

A. MPPT using Perturbation & Observe

This technique introduces a slight perturbation by decreasing or increasing the PWM duty cycle of the Buck converter. This perturbation changes the power of the solar module. If the power increases due to the perturbation, the perturbation is continues in that direction [06]. After the peak power is reached, the power at the next instant decreases and hence that the perturbation reverses. When the steady state is reached, the algorithm oscillates around the peak point. To keep the power variation small, the perturbation size is kept very small. The flow chart of algorithm has 4 cases as shown in Fig.10 [06].

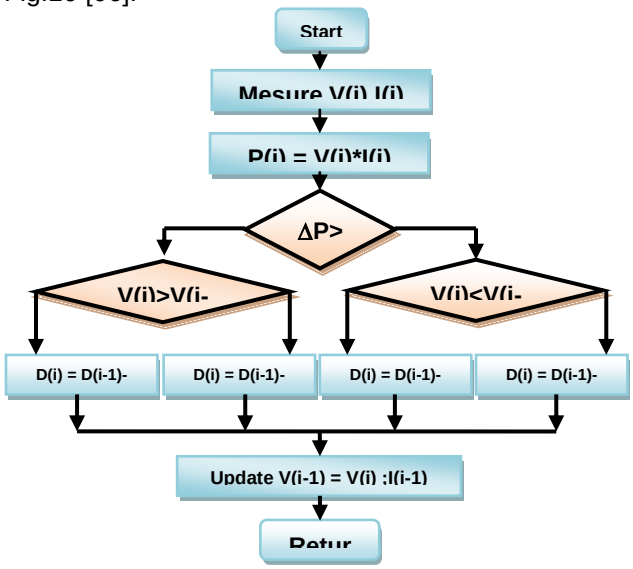

Fig .10. Configuration of Fuzzy Logic Controller in matlab/simulink

B. MPPT using Fuzzy Logic Control

Fuzzy logic controllers have been introduced recently in the tracking of the MPP in PV systems. They have the advantage to be robust and relatively simple to design as they do not require complete knowledge of the exact model and can handle nonlinearity. The proposed fuzzy logic MPPT Controller, shown in Figure 11, has two inputs and one output. The two input variables are the error E and change of error CE at sampled times k defined by eq. 6 and 7, where P and V are the PV panel power and voltage respectively at instant k: [8][9] [10][11]

$$E(k) = \frac{P(K)pv - P(K-1)pv}{V(K)pv - V(K-1)pv} \quad (6)$$

$$CE(K) = E(K) - E(K-1) \quad (7)$$

Where:
$P(K)pv$ and $V(K)pv$ are the power and the voltage of the PV generator respectively at instant k.
The power of the PV system:

$$P(K) = i(K).V(K) \quad (8)$$

The input E(k) shows the following: the operation point at the instant k is located on the right or on the left of the MPP on the PV characteristic curve as shown in figure 12, while the input CE(k) shows moving the direction of this point.
Where the control action D is duty cycle of PWM signal that control the Buck Boost converter [5] [6][7][8].

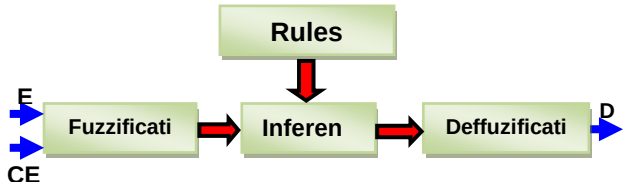

Fig.11. Block diagram of the fuzzy controller

The fuzzy controller design contains the three following steps:

• *Fuzzification*
The fuzzification is the process of converting the system actual inputs values E and CE into linguistic fuzzy sets using fuzzy membership function. These variables are expressed in terms of five linguistic variables (such as ZE(zero), PB (positive big), PS (positive small), NB (negative big), NS (negative small)), using basic fuzzy sub sets as shown in Fig.13

• *Rule base & inference engine*
Fuzzy rule base is a collection of if-then rules that contain all the information for the controlled parameters. It is set according to professional experience and the operation of the system control. The fuzzy rule algorithm includes 25 fuzzy control rules listed in table 3 [5] [6][7][8].

Fuzzy inference engine is an operating method that formulates a logical decision, based on the fuzzy rule setting and transforms the fuzzy rule base into fuzzy linguistic output. In this paper, Mamdani's fuzzy inference method, with Max-Min operation fuzzy combination, has been used [9][10][11].

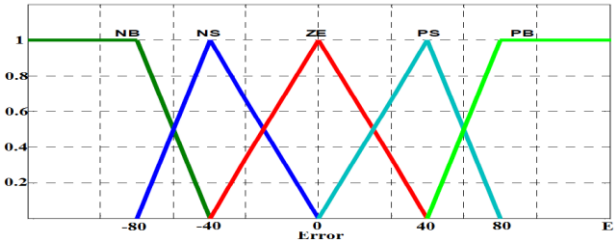

(a)

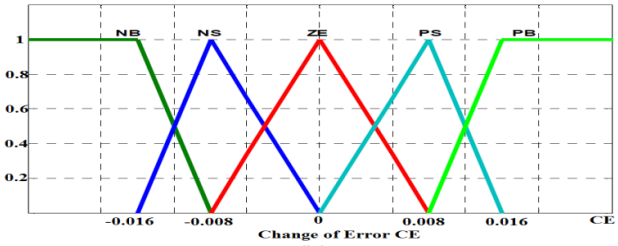

(b)

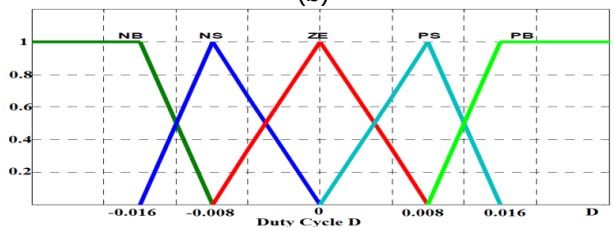

(c)

Fig.12. Membership function of E, CE and D

• *Defuzzification*
Defuzzification of the inference engine evaluates the rules, based on a set of control actions, for a given fuzzy inputs set. This operation converts the inferred fuzzy control action into a numerical value at the output by forming the union of the outputs resulting from each rule. The center of area (COA) algorithm is used for defuzzification of output duty control parameter, i.e. If E is NB and CE is ZO, then crisp D is PB. This means that if the operating point is far away from the MPP by the right side, and the variation of the slope of the curve is almost Zero, this will increase the duty cycle.
The Output of duty cycle D is expressed by [10][11][12][13]:

$$D = \frac{\sum_{j=1}^{n} \mu(D_j).D_j}{\sum_{j=1}^{n} \mu(D_j)} \quad (9)$$

Table 4. Fuzzy Rules Table

E/CE	NG	NP	ZE	PP	PG
NG	ZE	ZE	PG	PG	PG
NP	ZE	ZE	PP	ZE	PP
ZE	PP	ZE	ZE	ZE	NP
PP	NP	NP	NP	ZE	ZE
PG	NG	NG	NG	ZE	ZE

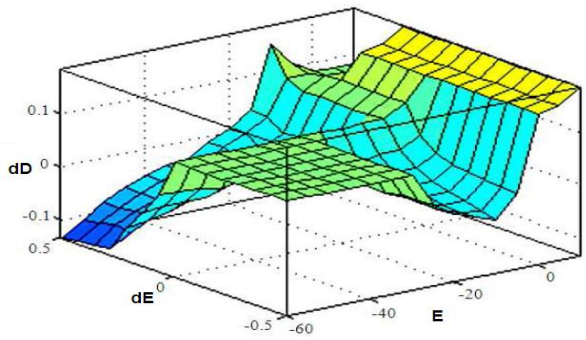

Fig. 13.The input-output surface waveform of the FLC

III. SIMULINK MODEL OF PV SYSTEM WITH P&O AND FUZZY LOGIC CONTROLLER

The performance of the tow systems, namely perturb &observe (P&O) and fuzzy logic controller, are analyzed. The performances of the controllers are analyzed in the following conditions:
Constant temperature and variable irradiation

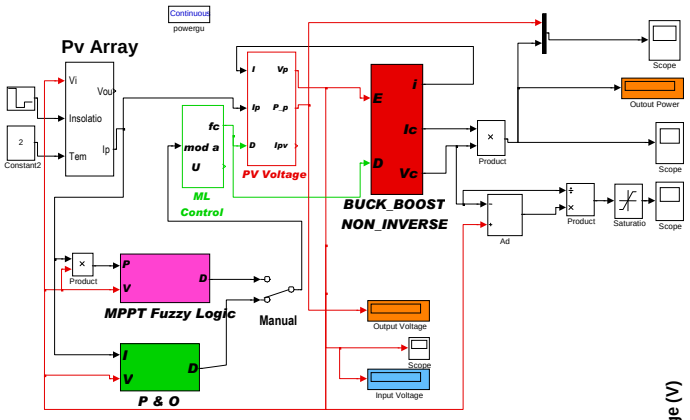

Fig 14.Simulation Block Diagram of MPPT PV systems for Maximum using P&O and Fuzzy Logic Controller

A. *Operation under Constant Conditions*

In this case, the temperature and irradiation are considered constant. the values are taken under standard conditions: temperature25°Cand irradiation in 1000W/m2.

B. Operation with Variable Conditions

In this case the temperature and irradiation are changing with time under different weather condition. Fig. 9 shows how the irradiance is changing for the PV solar panel. The voltage and the current vary depending on irradiance. The curve of variable irradiance is plotted using a signal builder, where the irradiance is not very realistic, because these are instantaneous changing irradiances. The simulation results are shown in the next figures. :

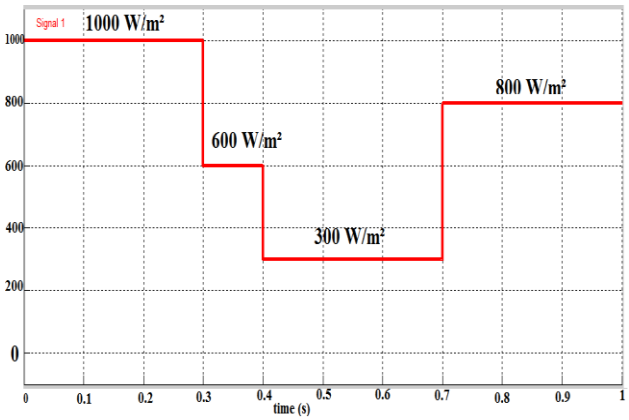

Fig.15. Variation of irradiance used in simulation.

C. *P&O Mppt Controller*

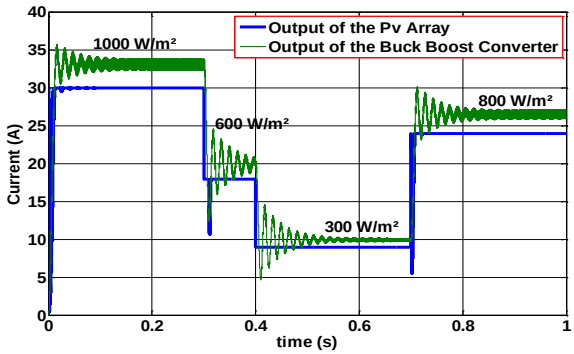

Fig.16. Input and Output Current of the Buck Boost converter with P&O Mppt Controller at constant temperature (T=25 C°) and varying insulation

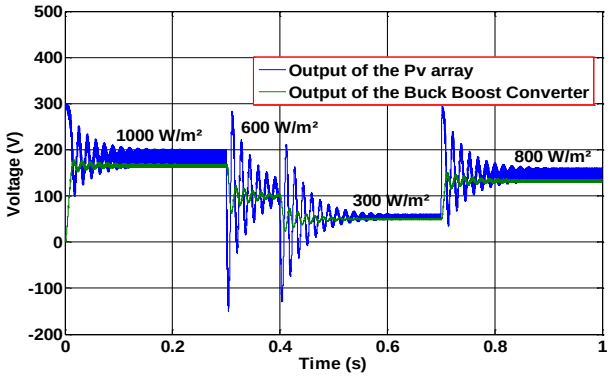

Fig.17. Input and Output Voltage of the Buck Boost converter with P&O Mppt Controller at constant temperature (T=25 C°) and varying insulation

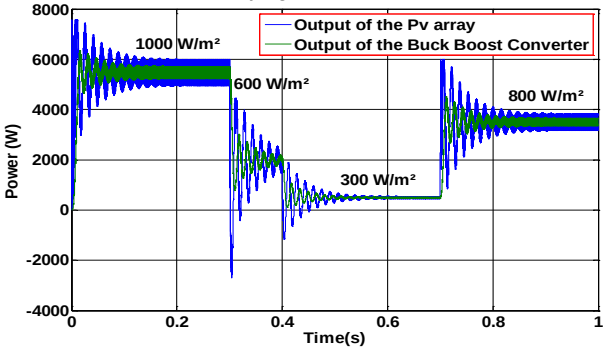

Fig.18. Input and Output Power of the Buck Boost with P&O Mppt Controller at constant temperature (T=25 C°) and varying insulation

D. *Fuzzy Logic Mppt Controller*

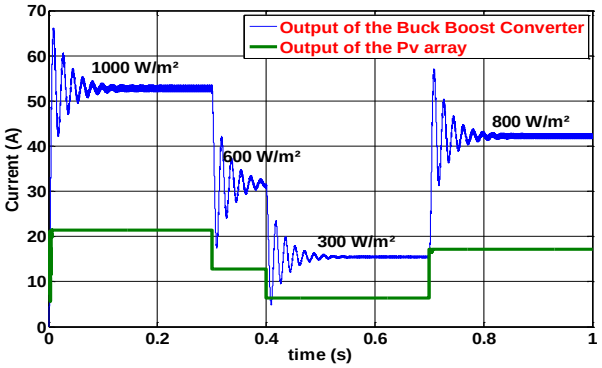

Fig.19. Input and Output Current of the Buck Boost converter with fuzzy logic Mppt Controller at constant temperature (T=25 C°) and varying insulation

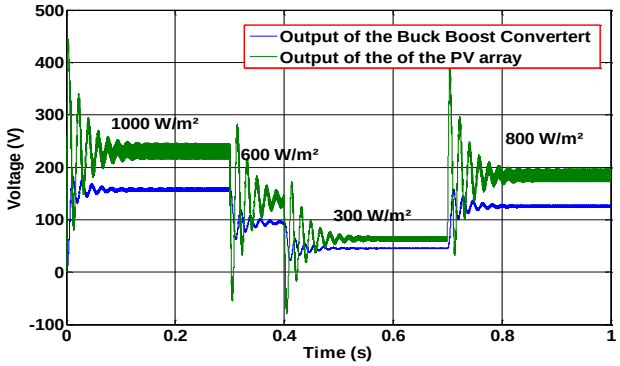

Fig.20. Input and Output Voltage of the Buck Boost with fuzzy logic Mppt Controller at constant temperature (T=25 C°) and varying insulation

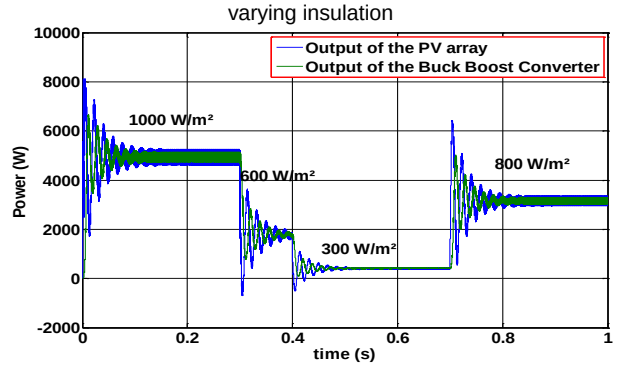

Fig.21. Input and Output Power of the Buck Boost converter with fuzzy logic Mppt Controller at constant temperature (T=25 C°) and varying insulation

As shown, fuzzy controller gives smother power signal line, less oscillation and better stable operating point than P&O. From the simulation results, it can be deduced that the fuzzy controller gives better performance than P&O, and it has more accuracy for operating at Maximum Power Point.

IV. CONCLUSION

This paper presents the performance of tow MPPT algorithms for tracking the maximum power available in PV array system, with Fuzzy Logic controller and P&O. The algorithms works as a direct method of MPPT through a buck-boost converter placed in parallel with the PV array. Based on the simulation results with MATLAB/SIMULINK, it can be observed that all of the tow MPPT controllers can be used to track the MPP under variable changes of solar irradiance and cell temperature. The tow controllers regulate the PV array voltage to operate at MPP operating voltage in order to produce the maximum power. However, it can be concluded that fuzzy logic has a better steady state, less oscillation around the MPP and dynamical performance than traditional P&O.

REFERENCES

[1] Aurobinda Panda,.Pathak, M.K., and Srivastava, S.P.« Fuzzy Intelligent Controller for the Maximum Power Point Tracking of a Photovoltaic Module at Varying Atmospheric Conditions ». *Journal of Energy Technologies and Policy*. Vol.1, no.2. pp.18-27, 2011.

[2] Mahammad, Abd Kadir, Saon, Sharifah and Chee, Wong Swee. «Development of Optimum Controller based on MPPT for Photovoltaïque System during Shading Condition, *Procedia Engineering* 53 (2013) 337 – 346 .

[3] Salas, V., Olias, E., Làzaro, A. , and. Barrado, A "Review of the maximum power point tracking algorithms for stand-alone photovoltaic systems," *Solar Energy Material Solar Cells*, 2006, 90:1555–78.

[4] Esram, T., and Chapman, P. "Comparison of photovoltaic array maximum power point tracking techniques," *IEEE Transactions on Energy Conversion*, 2007, 22:2.

[5] H.E.A. Ibrahim, Comparison Between Fuzzy and P&O Control for MPPT for Photovoltaic System Using Boost Converter, Journal of Energy Technologies and Policy. Vol. 2, No.6. 2012.

[6] Fares, Ahmed M., Belal, A. Abo Zalam, El Nashar, Salwa G.,and Aka1, Haitham. **«** Comparison Between Different Algorithms for Maximum PPT in Photovoltaic Systems and its Implementation on Microcontroller ». *Journal of Energy Technologies and Policy*, Vol.3, No.5, 2013.

[7] Abdullah M., Noman,Khaled E. Addoweesh, and Hussein M. Mashaly, « DSPACE Real-Time Implementation of MPPT-Based FLC Method". Hindawi Publishing Corporation *International Journal of Photoenergy.* Vol. 2013, Article ID 549273, 11. Pages:

[8] Rahmani, R., Fard, M., Shojaei, A. A., Othman, M. F., and Yusof, R. "A Complete Model of Stand-alone Photovoltaïque Array in MATLAB-Simulink Environment." *IEEE Student Conference on Research and Development 2011*.

[9] Singh,S., Mathew,L. , Shimi, S. L, " Design and Simulation of Intelligent Control MPPT Technique for PV Module Using MATLAB/ SIMSCAPE". *International Journal of Advanced Research in Electrical Electronics and Instrumentation Engineering* . Vol. 2, Issue 9, September 2013.

[10] Rahmani, R., Seyedmahmoudian, M., Mekhilef, S. and Yusof, R. " implementation of fuzzy logic Maximum power point tracking Controller for photovoltaic system". *American Journal of Applied Sciences*. 10 (3): 209-218, 2013.

[11] Messai, A., Mellit A., Guessoum, A. and Kalogirou, S.A. 2011. "Maximum power point tracking using a GA optimized fuzzy logic controller and its FPGA implementation". *Solar Energy*. 85: 265-277. DOI:10.1016/j.solener.2010.12.004

[12] Hari Prasad, K.V., Uma Maheswar Rao, CH. "Design And Simulation Of A Fuzzy Logic Controller For Buck & Boost Converters". *International Journal of Advanced Technology & Engineering Research* (IJATER). Vol. 2. Issue 3. May 2012.

[13] Aït Cheikh, C. Larbes, G.F., Kebir, T and Zerguerras, A. "Maximum power point tracking using a fuzzy logic control scheme". *Revue des Energies Renouvelables* Vol. 10 N°3 (2007).

[14] Jardine, C. N., Conibeer, G. J. and Lane, K. "PVCOMPARE: Direct Comparison of Eleven PV Technologies at Two Locations in Northern and Southern Europe". In *17th European Conference on Photovoltaic Solar Energy Conversion*. Munich. Vol. 17th . Europ, 2001.

Power Quality Improvements in Wind Diesel Power Generation System

Omar Feddaoui[1], Riad Toufouti[1], Salima Meziane[1]
Department of Electrical Engineering University of Mohammed ChérifMessaadia Souk Ahras, Algeria
omarispower@hotmail.com, toufoutidz@yahoo.frmeziane_elc@yahoo.fr

Abstract— Generation of electricity using diesel is costly for small remote isolated communities. At remote location electricity generation from renewable energy such as wind can help reduce the overall operating costs by reducing the fuel costs. However, the penetration of wind power into small diesel-based grids is limited because of its effect on power quality and reliability. This paper focuses on the combination of Wind Turbine and Diesel Generator systems for sustained power generation to improve the power quality of wind generation system. The performance of the optimal control structure are assessed and discussed by means of a set of simulations.

Keywords- Triple – renewable energy, wind diesel system, a synchronous generator, asynchronous generator, diesel generators, micro grid;

I. INTRODUCTION

Global warming is one of the most serious environmental problems facing the world community today. Scientistsare highly interested in solving it. It is characterized by the increase in the average temperature of the earth and extreme weather conditions[1]. On top of that, the rapid depletion of fossil fuels worldwide has necessitated an urgent search for another alternative energy sources to meet the current human requirements. Wind power is one of the renewable energy sources that scientists have recently drawn attention to[2]. Being an abundantly availableand non-pollutingenergy, it can make a wonderful alternative source of power. Moreover, this clean alternative source of energycan fit attractively for many usesand applications. On the hand, only 6.4% of total renewable energy sources available in the world are in use today. To get more consistent flow of energy to the user request, there has been a growing trend to combine renewable energy sources with diesel generators, giving a hybrid power generation system[4].They are activated to serve as an electrical energy source in telecommunication systems or clinics in border crossings,remote areas, desertsand isolated habitats. These locationsneed systems which are generally independent from large interconnected networks[5]. In literature thousands of researches have been doneto find a way that hybrid systems could becontinually utilized in an isolated area or be connected to a power grid. In[6] a study a hybrid autonomous system was introduced and presented as[7] a power system in an island in Bangladesh. Several parameters are entered in the study as well as in the system design, but in books it is difficult to find how to measure the various components of an autonomous system.Most of the books focus on the basic technologicaltheory of the device, not the measurements of equipment. Variable parameters of most of renewable energy sources often take a complex control system[8]. However,the design of the right voltage and frequency used tocontrol a wind-diesel system is shown in[9]. In[10]*P. S. Panickar* et *al* study a strategy of adaptive control by a variable wind speed for an application for a wind-diesel hybrid system. Modeling is also a major factor in studies developed to simulate a functioning system. Much software allows us to do that. There is an example of modeling and simulating various hybrid systems presented with MATLAB-Simulink software in [11],[12]. In [13] a model of a hybrid power generation is made by the HOMER software.To improve the quality of the energy produced by a system of wind energy production, a wind-diesel hybrid system is proposed in this study. Simulation results in Matlab \ Simulink are presented to confirm the proper functioning of the wind diesel hybrid system to reduce greenhouse gas emissions.

II. DIFFERENT STRUCTURES OF HYBRID SYSTEM

The configuration of the hybrid system obviously depends on the availability and use constraints of energy resources. This requires a measurement and a preliminary analysis of site conditions.

There are several structures of an autonomous wind-diesel hybrid system: wind-diesel system with short-term storage, wind-diesel system with long-term storage (Batteries, compressed air, hydrogen, etc.)[14] and wind-diesel system without energy storage. The choice of a suitable structure of a hybrid system is connected to two parameters. The first is the satisfaction of the technical performance in meeting the requirements of power quality;whereas the second is theeconomicincrease of saving fuel. Thus, the costs of electricity production in the autonomous systemswill beminimized[15].

III. WIND-DIESEL WITHOUT STORAGE

In our study we chose to work on the third structure of wind-diesel system without energy storage (Figure 1).

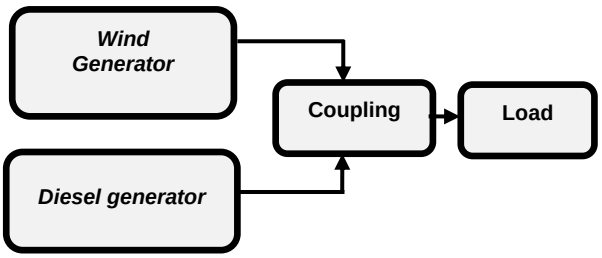

Fig.1. Simplified diagram of a wind diesel hybrid system

It is able to meet the need for electricity for consumers in isolated zones.It consists of the following subsystems: a wind generator and some diesel both connected to a load.

During the functionality of the system studied, if the electricity generated by the wind generator is sufficient for the load demand, the diesel generator is inactive to producereactive energy compensation. Except in the case where wind energy is insufficient to load demand, the diesel generator goes on to provide additional energy.

A. Wind generator

A wind turbine consists of four main components: a turbine which is the main tool for the conversion of wind energy into mechanical energy,an electromechanical system as a tool for transformation of mechanical energy into electrical energy.It includes the asynchronous generator and associated electrical components. An interconnect system and a control system [13].

The low cost and the standardization of the asynchronous machine that does not require a complex installation has led to a wide domination of this type of generators installed in a wind system. It is less demanding in terms of maintenance and has a failure rate which is very low. In the wind turbine consequent size, rotation speed is low. It is therefore necessary to inserta mechanical speed multiplier between the turbine and the induction motor. In this work we will focus to study on an asynchronous machine squirrel cage self-excited. (Figure 2)
PSM requires reactive energy to start (generation of rotating magnetic field). In a general case a capacitor connected in parallel with the stator circuit provide this energy [16].

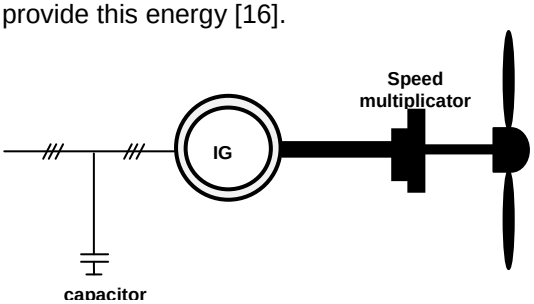

Fig.2. Wind System

B. Diesel generator

The diesel generator (Figure 3) is generally composed of a synchronous generator coupled to a diesel engine. The frequency of the alternating output current is maintained by a speed regulator. The regulator operates by adjusting the flow of fuel to keep the engine speed and the speed of the generator constant.In the case of high speed wind, the clutch decouples the synchronous generator from the diesel engine, and the machine functions as a synchronous generator and provides reactive energy [16, 23].
Diesel engines are more efficient than internal combustion engines. The speed of rotation of such generator depends on the amount of injected fuel and the load applied to the engine crankshaft. The diesel engine is a nonlinear system. It presents delays, which makes it difficult to control. Diesel engines are equipped with cruise control: mechanical, electromechanical or electronic. It carries out the automatic control of the speed of the diesel engine by adjusting the fuel injection depending on the load. It acts on the acceleration mechanism [16, 23].

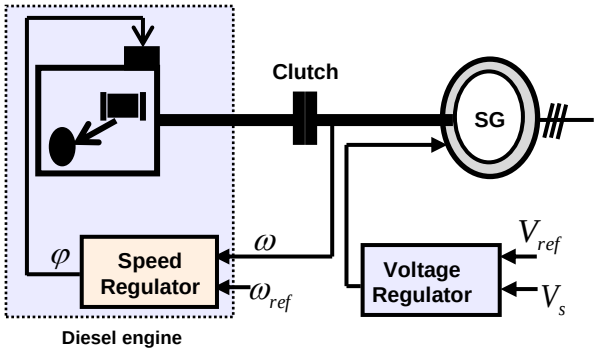

Fig.3. The diesel generator

IV. MODELING OF WIND DIESEL GENERATOR

To optimize a hybrid power generation system, it is necessary to know the various elements of it. For this, we will begin modeling the wind turbine with the asynchronous generator and as in a second step we model the diesel generator.

A. Modeling the wind system generator

In the literature, several studies have been devoted to the modeling of different components of a wind power system for a quality generated. A single autonomous wind-poweredturbine model was presented in [17]. The authors in [18] did an analysis of different modeling methods; the first deals with themodel theoretically;whereasthe second relied on the experimental data.
We can say that wind system transforms wing energy of the air mass to a mechanical power, characterized by the speed of rotation and mechanical torque. (Figure 4).

Fig.4. Model of the wing

In our case the turbine is formed with a horizontal axis, the principle of wind conversion was established by Betz.It assumes that the blades are placed in lively air to infinity upstream speed V_1 and downstream of an infinite speed V_2 with an air mass moving through the density ρ with surface S of the blades [19].

$$m = \frac{\rho.S.(V_1 + V_2)}{2} \quad (1)$$

The power p_m; extracted is expressed as half the product of the mass and the change in wind speed.

$$P_m = \frac{m.(V_1^2 - V_2^2)}{2} \quad (2)$$

By replacing the expression of m in the equation Number (2)

$$P_m = \frac{\rho.m.(V_1 + V_2)(V_1^2 - V_2^2)}{2} \quad (3)$$

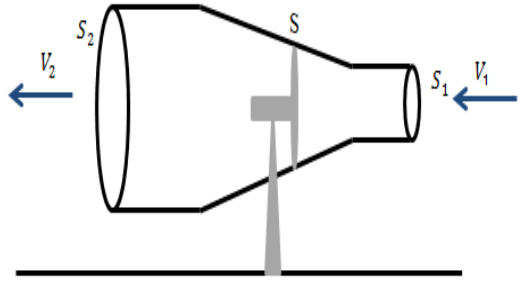

Fig.5. Tube of the current around the wind system

Undisturbed wind theoretically pass through the same area S with no variation in speed V_1 , the total power p_{mt} would be written:

$$P_{mt} = \frac{\rho.S.V_1^3}{2} \quad (4)$$

The ratio of the power extracted from the wind and the total power available is:

$$C_p = \frac{P_m}{P_{mt}} = \frac{\left(1 + \left(\frac{V_1}{V_2}\right)\right).\left(1 - \left(\frac{V_1}{V_2}\right)^2\right)}{2} \quad (5)$$

Where C_p : The power coefficient

If we represent the corresponding feature in the equation above, we see that the power coefficient C_p has a maximum of 0.59, see Figure 6. This theoretical limit called Betz limit which determines the maximum extractable power for a given wind speed. The evolution of the power coefficient is a specific data for each wind [20].

Fig.6. Coefficient of power

With the combination of the equations (1), (4) and (5),the mechanical power P_m available on the shaft of a wind turbine is expressed by [19]:

$$P_m = \frac{P_m}{P_{mt}}.P_{mt} = C_p.P_{mt} = \frac{1}{2}C_p(\lambda).p.\pi.R^2.V_2^3 \quad (6)$$

The specific rate λ is written as follows:

$$\lambda = \frac{\Omega_1.R}{V_1} \quad (7)$$

Given the ratio of speed multiplier K, the mechanical power p_{mg} available on the shaft of the electric generator is expressed by:

$$P_{mg} = \frac{1}{2}.C_p\left(\frac{\Omega_2 R}{KV_1}\right).\rho.\pi.R^2.V_1^3 \quad (8)$$

With:

R : Radius of the wind turbine

Ω_1 : Rotational speed before the multiplier

Ω_2 : Rotational speed after the multiplier

B. Modeling the wind system generator

Modeling of the diesel engine must consider the moving parts of the engine, the power output p_i and the total power dissipated P_{diss} p_{diss} P_{diss}. The motor runs at constant speed for a given order to maintain the voltage and frequency of the current supplied by the alternator constant load. The principle of energy conversion can be written as follows [21]:

$$P_i - P_{diss} = 0 \quad (9)$$

The power delivered can be represented by the following expression:

$$P_i = P_{ci}.n_i.m_f \quad (10)$$

With

P_{ci} : The calorific value of the fuel

n_i : The indicated engine performance

m_f : The flow of fuel injected into the combustion chamber

The total dissipated power includes the effect of friction of the moving parts as (rods, pistons, crankshaft), and that of the load applied on the engine, can be expressed by the following formula:

$$P_{diss} = P_{mf}.\frac{C_y}{4\pi}.\omega + C_r.\omega \quad (11)$$

P_{mf} : The average pressure of the friction losses

C_y : The total displacement of the engine

C_r : The resistive torque to the applied load

The modeling of friction at different parts of the engine was the subject of numerous studies that lead to a variety of forms. Given the complexity to treat each element separately, it was preferred to use the comprehensive assessment of the losses formulas [22].

The most accurate formula which represents the variation of the power of friction depending on the speed and pressure of the intake air of the engine as follows:

$$P_{mf} = (1+\omega.S_{eng}.\left(K_{f1} + K_{f2}.\frac{P_{in}}{P_a}\right) + K_{f3}\omega^2).P_a.\frac{C_y}{4\pi}.\omega \quad (12)$$

V. SIMULATION OF WIND DIESEL SYSTEM

The general structure of the wind diesel system is illustrated by Figure 7.

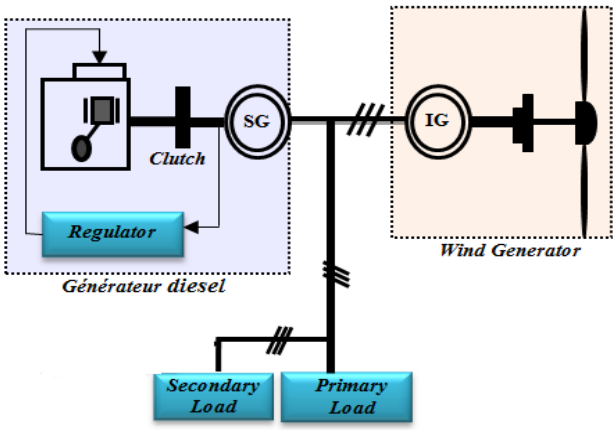

Fig.7. Tube of the current around the wind system

In our system the configuration of the electrical energy provided by means of a system consisting of a wind turbine connected to an asynchronous generator with an apparent power 250kVA diesel and another system which comprises a diesel engine coupled to a permanent magnet synchronous generator with power of 300kVA, which provides the necessary reagent to initiate the asynchronous generator. This hybrid power generation system feeds a load of 250kW and a secondary variable load associated with a frequency regulator. The system operates on a voltage of 380V and a frequency of 50Hz. The simulation time is 20s with a sampling period of 1ms. The primary load is 120kW up to t=5s, at this time we add another charge to reach a total 250kW (Figure 8). The simulation results are shown in the figures below.

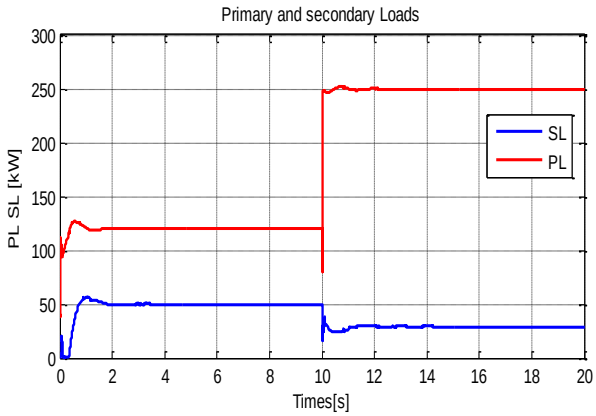

Fig.8. Primary and secondary load

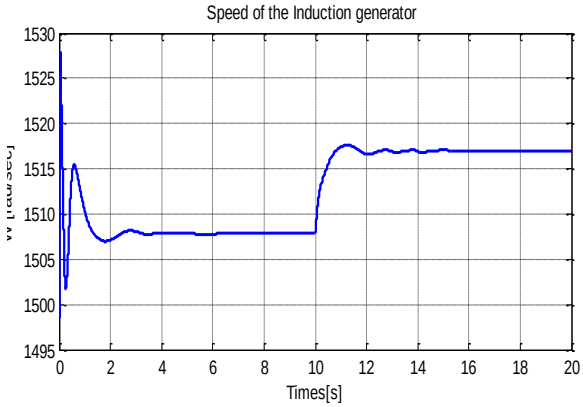

Fig.9. Speed of the asynchronous generator

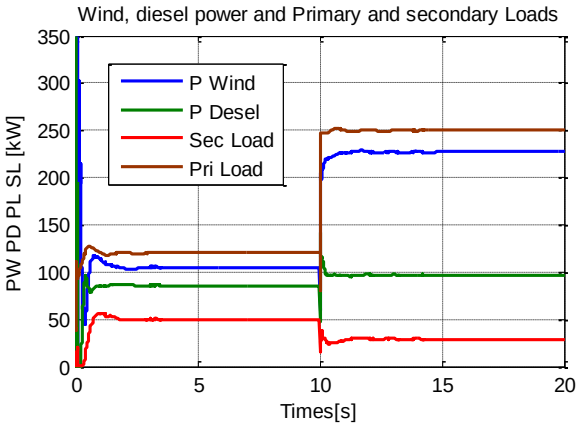

Fig.10. Power in the hybrid system

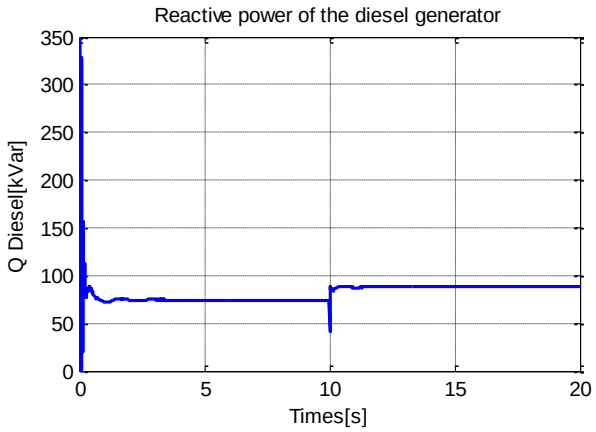

Fig.11. Reactive power of the diesel generator

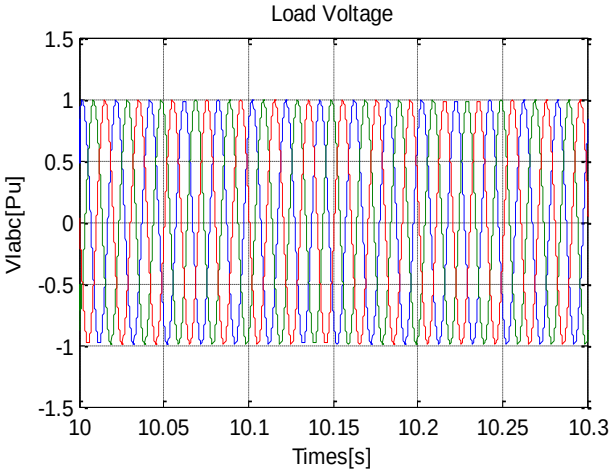

Fig.12. Zoom of load voltage

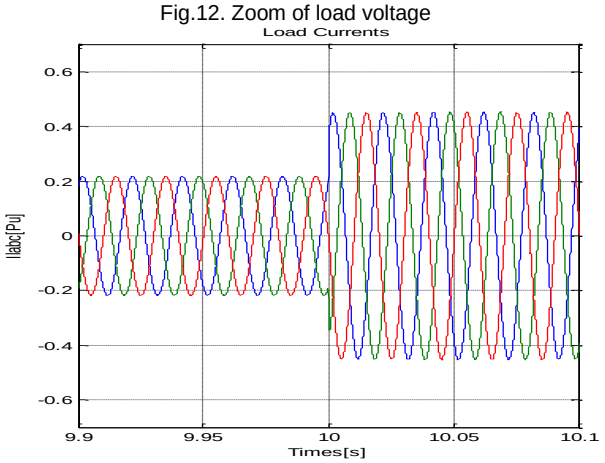

Fig.13 .Zoom of the Load Currents

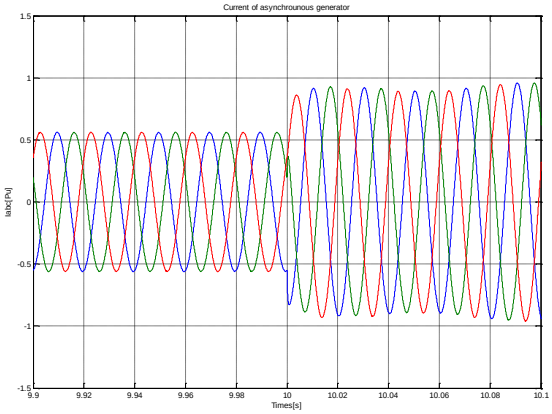

Fig.14. Zoom of the wind currents

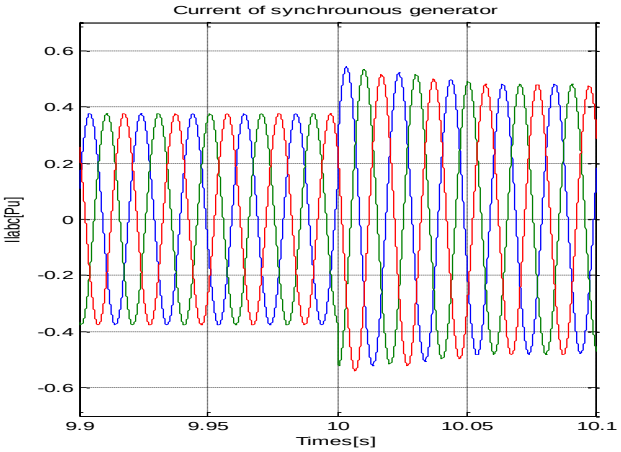

Fig.15. Zoom of the diesel currents

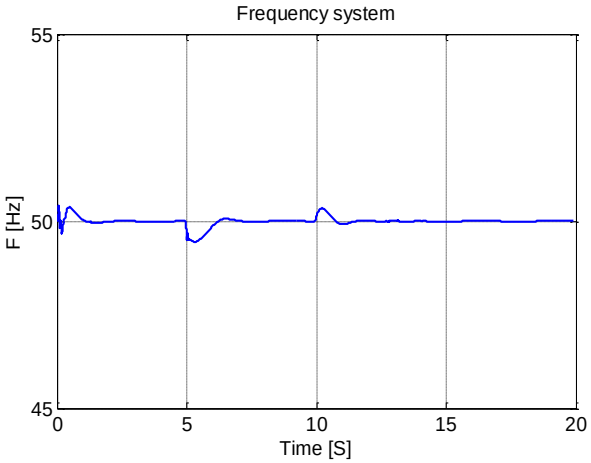

Fig.16 .Frequency system

From the simulation results it is noted that the turbine connected to the induction generator operates at a speed which is slightly greater than the synchronous speed (figure 9).

We note that at t=5s the total load power is 250kW and according to the characteristic of the turbine for a wind speed 8m/s, the power generated by the wind turbine is 120kW, the latter is less the total power of the load, and for that at this moment the power generated by the diesel generator increases (figure 10) to meet the demand.

In the same figure at time t=10s, we note that if the wind speed increases (8 to 10m/ s), the power supplied by the wind system increases, the power supplied by diesel generator decreases, which leads to a decrease the fuel consumption which is accompanied by a proportional reduction in toxic emissions and greenhouse gas emissions. Conversely, if the wind speed decreases again, the power of GAS decreases power diesel generator (that of the GS) increases to ensure the power demanded by the load. Figure 11 shows the required reactive power generated by the diesel system to initiate the asynchronous generator. The load voltage and load, wind diesel currents are in sinusoidal shapes, see Figuress (12-15). The phase current has fewer ripples and a nearly sinusoidal

wave form. Figure 14 shows that the frequency regulator maintains the frequency of the load at 50Hz, after some changes are made in the load.

VI. CONCLUSION

In This paper we have discussed a modeling of a micro-grid with Wind-Diesel generator hybrid system and its operations. The simulations in Matlab-Simulink are presented. According to these simulation results we show the importance and flexibility of operation of a diesel generator and a wind generator to reduce fuel consumption which is associated with a proportional reduction in toxic emissions and greenhouse gas emissions. We also showed how to improve the power quality of wind generation system by means of a wind-diesel hybrid system.

REFERENCES

[1] Supriyadi A.N and Hashiguchi T., Control Scheme of Hybrid Wind-Diesel Power Generation System, Japon Indonisia.

[2] Sebastiin, R. ,Castro, M. ,Sancristobal, E., Yeves, F. and Peire J., Approaching Hybrid Wind-Diesel Systems and Controller Area Network. Ciudad University. Spain.

[3] Borowy, B.S. Ziyad Salameh M., (September 1994) Optimum Photovoltaic Array Size for a Hybrid Wind/PV System, IEEE Transactions on Energy Conversion, Vol. 9, No. 3,.

[4] Trifkovic,M. ,Sheikhzadeh,M., Nigim K. and Daoutidis,P. Hybrid Energy System Modeling and Control, University of Minnesota, Canada.

[5] Devine, M.M. (February 2005) Analysis of Electric Loads and Wind- Diesel Energy Options for Remote Power Stations in Alaska, University of Massachusetts: Amherst. Master.

[6] Rekioua, D., Z. Roumila et Rekioua T. (2008), Etude d'une Centrale Hybride Photovoltaïque - Éolien - Diesel, University A. Mira, Bejaia. Bejaia, Algeria

[7] Al-Masood,N. Mirza, R. and Jubaer, A.(2011) Design of a Cost Effective Off-Grid Wind-Diesel Hybrid Power System in an Island of Bangladesh, World Academy of Science, Engineering and Technology 60.

[8] Stott, P.A. and Mueller, M.A. Modelling Fully Variable Speed Hybrid Wind Diesel Systems, Edinburgh University, UK.

[9] Murthy,S.S. Mishra,S. Mallesham, G. and Sekhar,P. C. (December 2010) Voltage and Frequency Control of Wind Diesel Hybrid System with Variable Speed Wind Turbine, IEEE magazine 20-23.

[10] Panickar,P. S. S. ,Rahman,S. Islam, M. and Pryor,T. L. Adaptive Control Strategies in Wind-Diesel Hybrid Systems, Curtin University, Western Australia.

[11] Taylor ,J.H. and Kebede,D. (1995) Modeling and Simulation of Hybrid Systems, University of New Brunswick. Conference on Decision & Control. Canada.

[12] Kasera,J., Chaplot, A. and Jai, K. (2012) Maherchandani, Modeling and Simulation of Wind-PV Hybrid Power System using MATLAB/Simulink, IEEE Students' Conference on Electrical, Electronics and Computer Science.

[13] Kansara, B.U and . Parekh, B.R (2011) Modelling and Simulation of Distributed Generation System Using HOMER Software, International Conference on Recent Advancements in Electrical.

[14] Ibrahima,H. Ilincaa ,A. and Younesc, R. (2007) Study of a Hybrid Wind-Diesel System with Compressed Air Energy Storage, IEEE Electrical Power Conference. Canada.

[15] Ibrahim,H., Lefebvre, J., Methot, J. F. and Deschenes, J. S. (2011) No-Storage Wind-Diesel System: Mechanical Modeling Based on Power Flow Models, IEEE electrical power conference.

[16] Vechiu, I. (2005) Modelling and Analysis of the Renewable Energy Integration in an Autonomous Grid, PhD thesis. University de Havre..

[17] Idjdarene1, K.(December 2008)Contrôle d'une Génératrice Asynchrone à Cage dédiée à la Conversion de L'énergie Éolienne, JCGE'08 Lyon..

[18] J. Chen and D. Jiang, Study on Modeling and Simulation of Non-grid Connected Wind Turbine,Tsinghua University. China.

[19] Poitiers, F. (2003)Study and Control of Induction Generators for Wind Energy Conversion Systems, PhD thesis. University of Nantes..

[20] Heier,S. (1998) Grid Integration of Wind Energy Conversion Systems. Publications John Wiley & Sons..

[21] Ibrahim,H. R. ,Younès, A., Ilinca, M. Dimitrova and Perron, J. May (2010) Study and Design of a Hybrid Wind-Diesel System with Compressed Air Energy Storage System for Remote Areas, Applied Energy, Vol. 87, Issue 5, pp 1749-1762,.

[22] Younes,R. (1993) Elaboration d'un modèle de connaissance du moteur diesel avec turbocompresseur à géométrie variable en vue de l'optimisation de ses émissions, PhD Thesis. École Centrale de Lyon. France.

[23] Gagnon, R. Saulnier,B. Sybille, G. and Giroux, P. (April 2002) Modeling of a Generic High-Penetration No-Storage Wind-Diesel System Using Matlab/Power System Blockse.Global Windpower Conference, Paris, France.

Maximum Power Tracking by VSAS approach for Wind Turbine, Renewable Energy Sources (RES)

Billel Maghni [1], Nacer Kouider M'Sirdi [2] , Ahmed Saadoun [3]
[1] Electrical engineering Department, University of Badji Mokhtar ,Annaba Algeria and Laboratoire de recherche des systèmes électromécaniques
maghni_1990@yahoo.fr
[2] Aix Marseille Université, CNRS, ENSAM, Université de Toulon, LSIS UMR 7296 LSIS UMR CNRS UMR, Domaine Universitaire St Jérôme, Avenue Escadrille Normandie-Niemen, 13397 Marseille Cedex 20, France
nacer.msirdi@lsis.org
[3] Electrical engineering Department,
University of Badji
Mokhtar ,Annaba Algeria and Laboratoire de recherche
des systèmes électromécaniques
Abdallahsaadoun555@gmial.com

***Abstract*—** This paper gives a review of the most efficient algorithms designed to track the maximum power point (MPP) for catching the maximum wind power by a variable speed wind turbine (VSWT). We then design a new maximum power point tracking (MPPT) algorithm, using the Variable Structure Automatic Systems approach (VSAS). The proposed approach leads efficient algorithms as shown in this paper by the analysis and simulations.

***Keywords*—** Wind Turbine; MPP; VSWT; VSAS; MPPT

I. INTRODUCTION

Wind energy is one of the most promising renewable energy resources for generating electricity due to its cost competitiveness compared to other conventional types of energy resources. Variable speed operation and direct drive Wind Turbines (WT) have been the modern aspect of the Wind Energy Conversion System (WECS) technology Variable-speed has many advantages over fixed-speed [1, 2].

The MPPT algorithms are necessary to maximize, at each time instantly, the produced power is shown in Fig.1. Many MPPT techniques have been proposed as in Figs. [3, 4, 5, 6 and 7]. A lot of them are well established in the literature. They have different aspects and can be classified by: simplicity, convergence speed, digital or analogical implementation, hardware implementation, need for parameterization, sensors required, cost, range of effectiveness, and other aspects. There are several methods: Tip Speed Ratio method (TSR), Sliding Mode Control methods (SMC), Perturbation and Observation method (P&O), Hill Climbing method, Fuzzy Logic Control method (FLC) and Modified Enhanced (MEPO) among others.

The main objective of this paper is to find the best control for catching the maximum wind power. We then recall the most used techniques and then design a new MPPT algorithm, using the (VSAS) approach to design a robust and efficient algorithm. This approach has been used successfully for PV Systems and can be applied for WTs as shown in this paper [8].

The paper is organized as follows. The problem formulation is given in Section 1. Section 2, presents the mathematical models of the different parts of the considered Wind Energy Conversion System used for simulation. The models of the WT, the Permanent Magnet Synchronous Generator (PMSG) and the converters with connection to the grid are presented. Section 3, presents the most often used MPPT control strategies, for wind turbine driving and then we introduce our new algorithm deduced from the approach considered in [7 ,8]. After its definition, we compare its results with the widely used MPPT algorithms. The fourth section gives some simulation results. Finally, a conclusion summarizes the work and proposes perspectives.

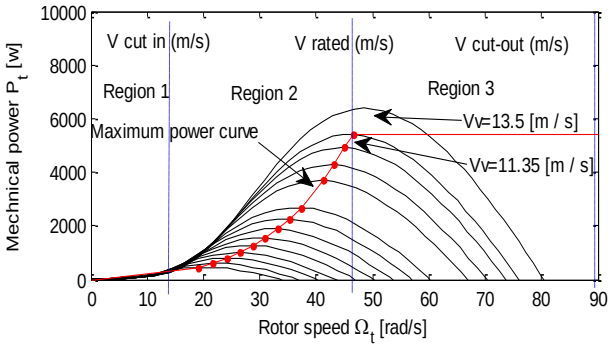

Fig.1.The power characteristic of the considered WT

II. MODEL OF WIND ENERGY CATCHING SYSTEM

In order to ensure extraction of the maximal wind energy, it is necessary to use a power electronic device between the WT generator and the grid,

where the frequency is constant as shown in Fig.2. A WT, a PMSG, AC-DC and DC-AC converters and transformers are to be connected to the grid composing the system. All these parts have to be modeled and simulated.

A. The Wind Turbine model

The input of the WT is the wind and the output is the mechanical power turning the PMSG rotor [9]. For a VSWT, the output mechanical power can be expressed as:

$$P_t = \frac{1}{2}\rho\pi R_t^2 v^3 C_p(\lambda,\beta) \quad (1)$$

The tip speed ratio is given by:

$$\lambda = \frac{R_t \Omega_t}{v} \quad (2)$$

$$P_t = K1\ v^3 C_p(\lambda,\beta)\ ,Were\ K1=\frac{1}{2}\rho\pi R_t^2 \quad (3)$$

Where $P_t\ in\ (w)$ is the output mechanical power available from a wind turbine, $\rho\ (\text{in kg/m}^3)$ is the air density, $R_t\ (\text{in meters})$ is turbine radius, $v\ (\text{in m/s})$ is the wind speed, C_p is the power coefficient, λ is the tip speed ratio, $\beta\ (\text{in degree})$is the blade pitch angle and $\Omega_t\ (\text{in rad/s})$ is the rotational speed of the wind turbine shaft.

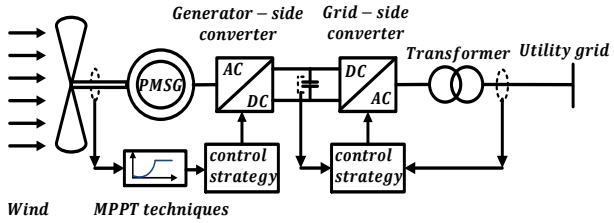

Fig.2. Schematic diagram of the overall system

According to the manufacturer's data of the wind turbine and the curve-fitting technique, the power coefficient C_p can be expressed, with β the adjustable pitch angle of the blade, as [10].

$$C_p = 0.073\left(\frac{151}{\lambda_i} - 0.058\beta - 0.002\beta^{2.14} - 13.2\right)e^{\frac{-18.4}{\lambda_i}} \quad (4)$$

Where $\lambda_i = \frac{1}{\frac{1}{\lambda - 0.02\beta} - \frac{0.003}{\beta^2+1}}$

By using "Equation (4)," the typical C_p versus λ curve is shown in Fig.3. In a wind turbine, there is an optimum value of λ_{opti} that leads to C_{pmax}. When λ in "Equation (2)," is adjusted to its optimal value λ_{opt}, the maximum C_p is reached when $\beta = 0$. The maximum power extraction is achieved. From "Equation (1, 2)," we get:

$$P_{t\,max} = \frac{1}{2}\rho\,\pi\,R_t^5\left(\frac{C_{p.max}}{\lambda_{opt}^3}\right)\Omega_{t\,opt}^3 \quad (5)$$

$$\Omega_{t\,opt} = \frac{\lambda_{opt} v}{R_t} \quad (6)$$

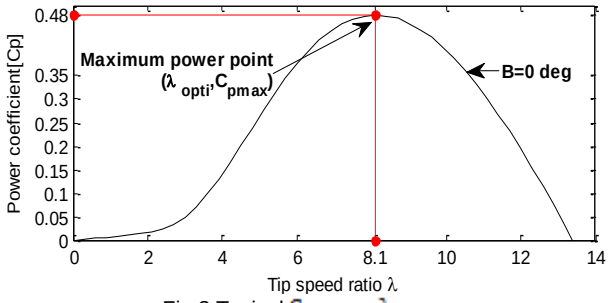

Fig.3.Typical $C_p$versus λ curve

B. The PMSG model

The PMSG are usually modeled assuming uniform distribution of stator 3-phase windings. So, a simple model of the generator can be obtained by conversion from the three phases reference frame a, b, c to the d, q frame [11, 12].

The model of a three phases PMSG in the d, q reference frame is given by:

$$V_{sd} = R_s I_{sd} + L_d\frac{dI_{sd}}{dt} - \omega_e L_q I_{sq} \quad (7)$$

$$V_{sq} = R_s I_{sq} + L_q\frac{dI_{sq}}{dt} + \omega_e\left(L_d I_{sd} + \psi_m\right) \quad (8)$$

Where $V_{sd}, V_{sq}\ (\text{in V})$ are the direct and quadrature components of the PMSG voltages, R_s, L_d and L_q represent respectively the stator winding resistance, the direct and the quadrature inductance of the PMSG stator winding,$\psi_m\ (\text{in wb})$ represents the magnet flux, $\omega_e\ (\text{in rad/s})$ is the electrical rotational speed of PMSG and I_{sd}, $I_{sq}\ (\text{in A})$ are respectively the direct and quadrature components of the PMSG currents.

Let $T_e\ (\text{in N.m})$ be the electromagnetic torque and n_p be the number of pole pairs. The electromagnetic torque developed by a n_p machine is given by [11, 12]:

$$T_e = \frac{3}{2} n_p\left(\psi_m I_{sq} + (L_d - L_q) I_{sd} I_{sq}\right) \quad (9)$$

C. The Grid model

The dynamic model of the grid connection, is referred to the rotating frame synchronized with the grid voltage, this allow us to express the model as: [13].

$$V_{dg} = V_{di} - R_g I_{dg} - L_{dg}\frac{dI_{dg}}{dt} + L_{qg} w_g I_{qg} \quad (10)$$

$$V_{qg} = V_{qi} - R_g I_{qg} - L_{qg}\frac{dI_{qg}}{dt} - L_{dg} w_g I_{dg} \quad (11)$$

Where $V_{dg}, V_{qg}(\text{in V})$ represent the direct and quadrature components of voltages on grid side, while $V_{di}, V_{qi}(\text{in V})$ are the direct and quadrature components of voltages on inverter side, $(R_g, L_{dg}\text{ and }L_{qg})$ are resistance, the direct and quadrature grid inductance respectively. The direct and quadrature components of the grid currents are $I_{dg}, I_{qg}(\text{in A})$ respectively.

By aligning the d-axis of the reference frame along with the grid voltage position, $V_{qg} = 0$, the active and reactive power can be obtained from the following equations:

$$P_g = \frac{3}{2} V_{dg} I_{dg} \quad (12)$$

$$Q_g = \frac{3}{2} V_{dg} I_{qg} \quad (13)$$

Where P_g, Q_g are active and reactive grid powers.

For simulations of complete WECS chain, the converters, the grid and their connections, Maltlab Simulink programs have been developed and used.

III. CONTROL TECHNIQUES

The control technique (MPPT) aims to optimize the generator speed in order to maximize the wind turbine output power. Many strategies were investigated to achieve the MPPT. Three control methods are presented (TSR, SMC, P&O) and compared to the proposed MEPO algorithm [8].

A. The tip speed ratio control (TSR)

The TSR MPPT method controls the rotational speed of the generator in order to preserve λ to an optimum value at which the power extracted is maximal. This method needs the measure of both the wind and the turbine speed. A speed sensor must be used; this increases its overall system cost. Furthermore, the knowledge of λ_{opti} of the turbine is required. Fig.4, shows the block diagram of a WECS with TSR control [2].

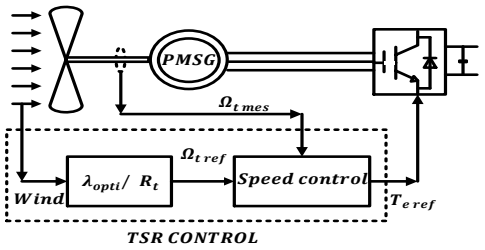

Fig.4.The block diagram of tip speed ratio (TSR) MPPT method

B. The Sliding Mode Control (SMC)

This part uses a SMC for tracking the optimal power of a variable speed PMSG based WECS as used in [14]. The sliding surface is systematically extracted from imposing a required reduced-order dynamics to enable the WT to work, more or less, close to the optimal regime characteristics. This depends on imposed trade-off between the torque control input ripple and the optimum tracking. In this manner, by torque controlling the PMSG, a multipurpose energy-reliability optimization is actually executed and illustrated in Fig. 5. The two components of the sliding-mode control law are: the equivalent control input U_{eq} and the commutation component U_n that must now be calculated [14].

$$U_{eq} = T_g - \frac{T_t}{(1 + a_2 J_t)} (a_1 J_t \Omega_t + a_2 J_t T_g)(a_1\ A(\lambda, v)) \quad (14)$$

Where $A(\lambda, v) = \left(\frac{K v R_t^2}{i^2}\right)\left(\frac{C_p'(\lambda)\lambda - C_p(\lambda)}{\lambda^2}\right)$, $k = \frac{1}{2}\rho\pi R_t^2$

$$a_1 = \frac{-1}{T_{sm}} \quad (15)$$

$$a_2 = \frac{-a_1 \Omega_{t\,otp}}{T_{e\,opt}} \quad (16)$$

Where: T_{sm} is a time constant, i is gearbox (drive train) ratio, $\Omega_{t\,otp}$ is optimal rotational speed of the turbine shaft, $C_p'(\lambda)$ is the derivative of power coefficient and $T_{e\,opt}$ is optimal electromagnetic torque.

$$U_n = -\alpha\ sgn_h(\sigma) \quad (17)$$

$sgn_h(\sigma)$ is a hysteretic sign function of width h and α is the control gain. Finally, the total sliding mode control law is the sum of the equivalent component and on-off component:

$$U = U_{eq} + U_n \quad (18)$$

$$U = T_g - \frac{T_t}{(1+a_2 J_t)} (a_1 J_t \Omega_t + a_2 J_t T_g)(a_1 - A(\lambda, v)) - -\alpha\ sgn_h(\sigma) \quad (19)$$

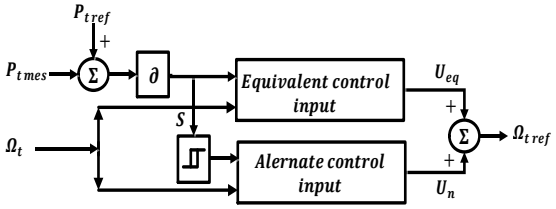

Fig.5.The block diagram of the sliding mode control (SMC) MPPT method

C. The Perturbation and Observation control (P&O)

The P&O method is one of the simplest MPPT techniques as it involves measurement of the power only. It is based on perturbing the speed Ω_t in small step $d\Omega_t$ and perceiving the resulting changes in turbine mechanical power P_t, as illustrated by Fig.6, [15, 5]. This algorithm is based on the following procedure: if the operating speed of the WT generator is perturbed in a given direction and if the power supplied by the generator increases, it means that the operating point has moved toward the MPP, and therefore the speed of the machine must still be settled in the same direction (see Fig.7). Otherwise, if power operated generator decreases, the operating point is far from the MPP and therefore the direction of the disturbance in the speed of operation must be reversed see eg [12, 13].

Additionally, selecting an appropriate step size is not a simple task: though larger step-size means a faster response and more oscillations around the peak point, and hence, less efficiency, a smaller step-size improves efficiency but decreases the convergence speed [5, 16] as represented in Fig.7 and compared to the MEPO and the TSR methods.

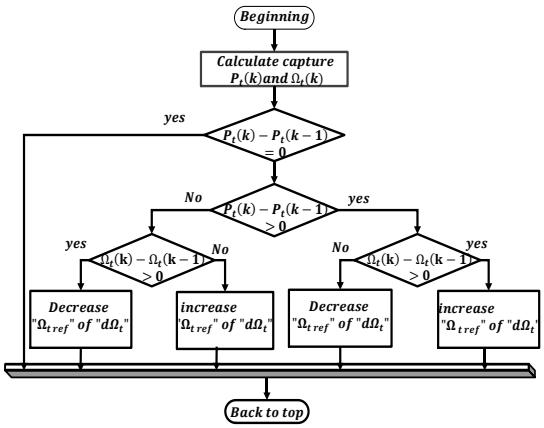

Fig.6. Flowchart of the perturbation and observation (P&O) MPPT method

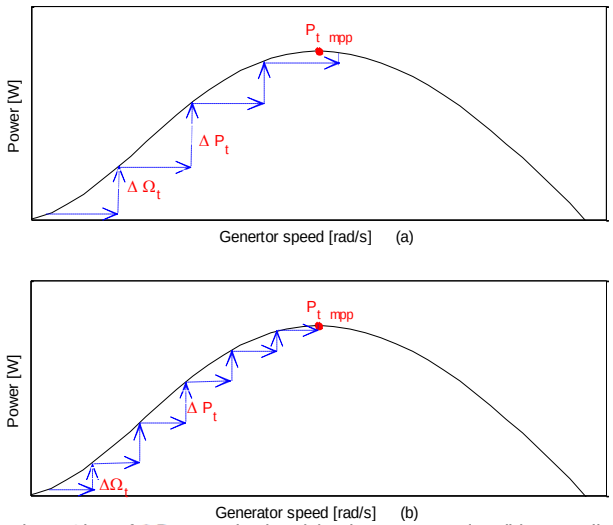

Fig.7. Size of $\Delta\Omega_t$ perturbation,(a) a larger step-size,(b) a smaller step-size

C. The Modified Enhanced P&O Algorithm (MEP&O)

For fast and good converging algorithms, the Operation Point moves essentially on a wind dependant characteristic. The change of wind velocity forces it to change from one characteristic curve to another, generally more or less near the new optimum. The maximum Power depends on the WT rotation speed Ω_t and time: $P_t(t) = P_t(\Omega_t(t))$.

Then the required Maximum Power Point to Track is really defined by the following objective function:

$$\frac{dP_t(t)}{dt} = 0 \; or \; \frac{dP_t(t)}{dt} = \frac{dP_t}{d\Omega_t}.\frac{d\Omega_t}{dt} = 0 \qquad (20)$$

We can define as Lyapunov function the positive function W(t) where we use a positive constant $P_0 > P_t$ greater than the maximum power which can be got by the WT. W is always positive.

$$W(t) = (P_0 - P_t(t))^2 > 0 \qquad (21)$$

Its time derivative $\frac{dW(t)}{dt}$ must be negative to make $W(t)$ always decreasing and then convergence of the algorithm.

$$\frac{dW(t)}{dt} = -\frac{dP_t(t)}{dt}(P_0 - P_t(t)) < 0 \qquad (22)$$

Then, to verify this condition, $\frac{dP_t(t)}{dt} > 0$ must be positive. Let us now consider the control in case of discrete time, like do all the above-presented algorithms. We can estimate the Power derivative $\frac{dP_t(t)}{dt} = \frac{dP_t}{d\Omega_t}.\frac{d\Omega_t}{dt}$ by:

$$(P(\Omega_t + \Delta\Omega_t) - P(\Omega_t)).\Delta\Omega_t = \Delta P.\Delta\Omega_t > 0 \qquad (23)$$

Then we choose for the rotational speed perturbation $\Delta\Omega_t = K.sign(\Delta P.\Delta\Omega_t)$

The fetched MPPT may be defined, in the MEPO algorithm by the following: $\Delta\Omega_t = Ksign(\Delta P.\Delta\Omega_t)$

In case of no change in the output power after perturbation: $\Delta P_t(k) = 0$, then as

In case of $\Delta P_t(k) \geq 0$, the power increase after positive perturbation delta w then let us continue in the same direction .

In case of $\Delta P_t(k) \leq 0$, the power decreases after positive perturbation delta w then let us continue in the reverse direction .Finally for the rotation speed control we get the following control law:

$$\Omega_{tref} = \Omega_t + Ksign(\Delta P.\Delta\Omega_t) with \; k = 1 \qquad (24)$$

IV. SIMULATION RESULTS AND DISCUSSION

The simulation has been carried out using Matlab Simulink package, under a wind speed profile whose mean value is (11.5 m/s). The evaluation tests have been done with the wind speed input defined by Fig.8, got from a Matlab Simulation. The system parameters are given in the appendix A.

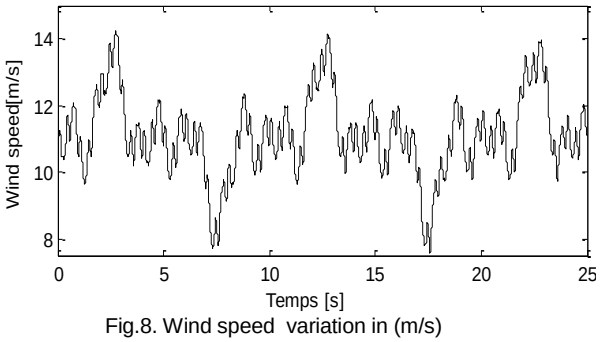

Fig.8. Wind speed variation in (m/s)

The C_p and the output power is shown in the following for each one of the presented algorithms. The studied and proposed algorithm MEPO based on VSAS approach is tested in simulation and compared with the different MPPT methods (TSR, SMC, P&O) are shown in Figs (9, 10, 11 ,12 and 13); The simulation results are summarized in Table I [2].

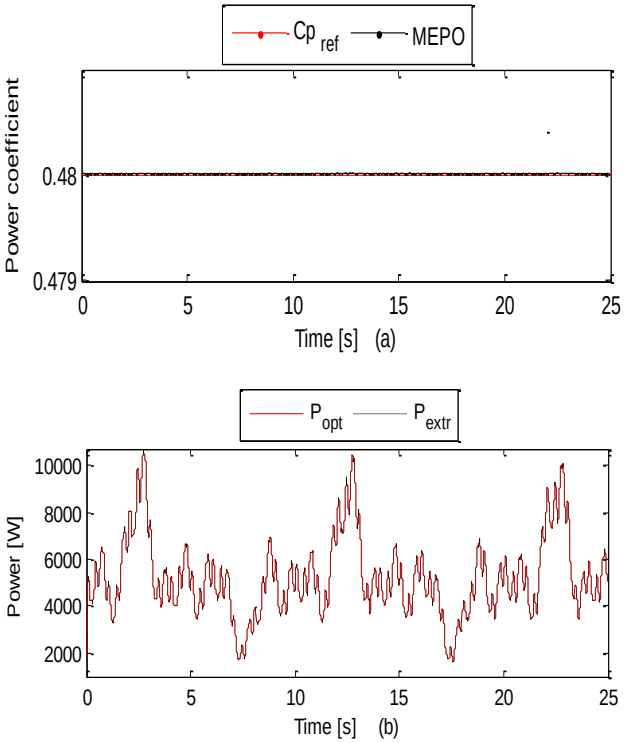

Fig.9. (a) C_p and (b)optimal and extracted power For [MEPO MPPT]

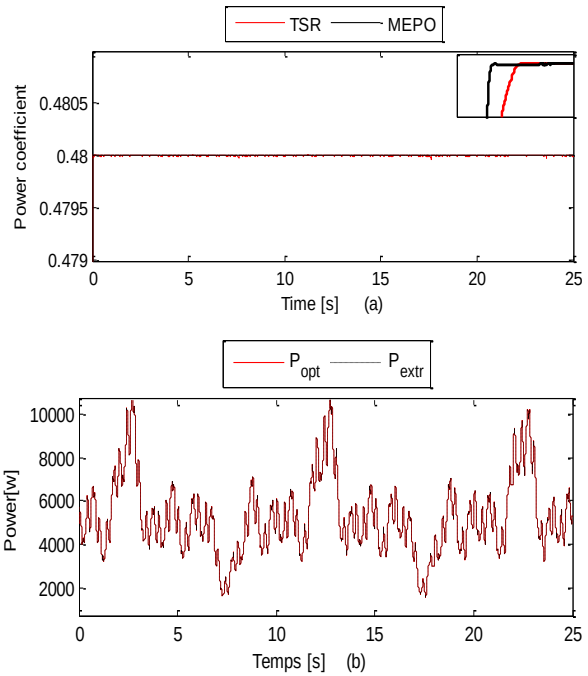

Fig.10. (a) C_p and (b)optimal and extracted power For [TSR MPPT]

The MPPT controller ensures the tracking of the optimum power points at variable wind speeds, by maintaining the power coefficient to its maximum value $C_{p\,max} = 0.48$ as shown in Fig.9 (a). Based on the results demonstrated in Figs (9(a), 10(a), 11(a), 12 (a), 13(a))the MEP&O method were found to be the fastest to reach the steady-state, This shows the effectiveness of the proposed algorithms. While the other algorithms exhibiting a slight difference. In contrast with MEPO, the classical P & O for (**x=5**) and SMC methods of are very slow.

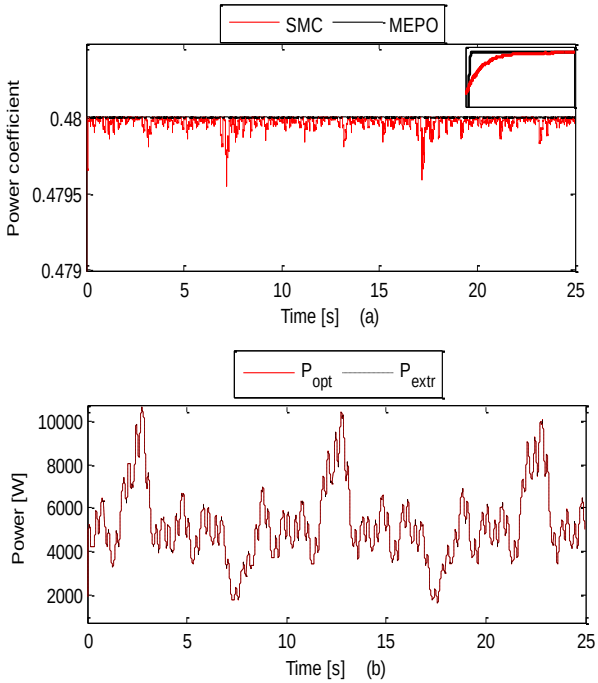

Fig.11. (a) C_p and (b)optimal and extracted power For [SMC MPPT]

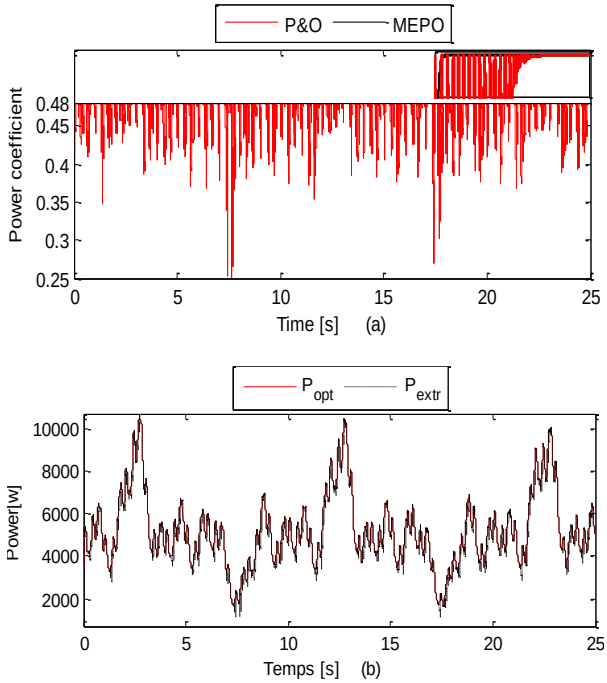

Fig.12. (a) C_p and (b)optimal and extracted power For [P&O MPPT ,**x=5**]

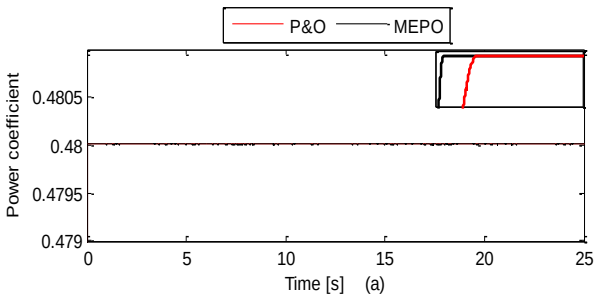

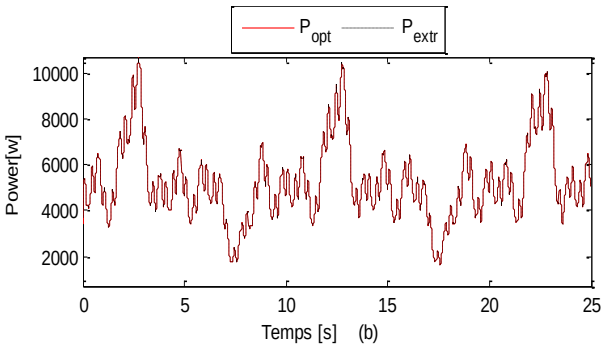

Fig.13. (a) C_p and (b)optimal and extracted power For [P&O MPPT ,**x=0.1**]

The control algorithm based on MEPO and TSR achieve the highest average value of $C_{p\,max}$ to an approximate value of 0.480. By comparison, the SMC gives an average value of $C_{p\,max} = 0.4794$, which is approximately equal to the $C_{p\,max}$ value obtained from the P&O for (**x=0.1)** control. Since the average value of $C_{p\,max}$ of the classical P&O for (**x=5**) method is 0.4780, this method is the least effective.

Table 1 .Summary of performance of four algorithms

MPPT technique	Average power Pt kw	Losing power Pt (w)	Power coefficient	Tip speed ratio	Response time (s)	Efficiency (Pt/Popt) %
TSR	2.2628	0.0211	0.4800	8.0994	0.0295	≅ 100
SMC	2.2489	2.5941	0.4794	8.1044	0.4982	99.87
P&O X=0.1	2.2598	0.1982	0.4794	8.0983	0.215	99.97
P&O X=5	2.2463	7.4252	0.4780	8.1233	0.0405	99.57
MEP&O	**2.2613**	**0.0877**	**0.4800**	**8.0992**	**0.01**	≅ 100

The verification of maximum power tracking control is illustrated in Figs (9(b), 10(b), 11(c), 12 (b) and 13(b)).The wind speed profiles of maximum power tracking control P_{opt} is also shown in Figs (9(b), 10(b), 11(b), 12 (b) and 13(b)).From the figures, it has been found that, in the four methods (TSR, SMC, FLC, P&O), the extracted power by the turbine follow the desired trajectory P_{opt} with different efficiency; the calculated efficiencies are listed in Table I.

V. CONCLUSION

In this paper we present the models of the different parts of a Wind Energy Conversion System: the WT, the PMSG, and the converters with connection to the grid are presented. The most often used MPPT control strategies are reviewed, for wind turbine driving and then we propose a new MEPO algorithm deduced from the VSAS approach. We compare our algorithm with the widely used MPPT algorithms.

The verification of maximum power tracking control is illustrated in the presented figures show that the best MPPT algorithm is the MEPO. The wind speed profiles of maximum power tracking control P_{opt} and the dynamic difference between the turbine powers P_t is also shown. From the figures, it has been found that, in the four methods (MEPO, TSR, SMC, P&O), the extracted power by the turbine follow the desired trajectory P_{opt} with different efficiency; the calculated efficiencies are listed in Table III. As perspective, we will focus on the control and stabilization for the grid connection of multiple sources and Hybrid Renewable Energy Systems by using again VSAS like used in MEPO.

APPENDIX A

Table 1 . Wind turbine Parameters

Radius of the turbine	$R_t = 2$ m
Volume density of the air	$\rho = 1.225$ kg. m^3
The pitch angle	$\beta = 0^*$
specific optimal speed	$\lambda_{opti} = 8.1$
Coefficient of maximum power	$C_{p\,max} = 0.48$

Table 2 . PMSG Parameters

Rated power	$P = 10$ kw
Stator resistance	$R_s = 0.00829\Omega$
Direct stator inductance	$L_d = 0.174$ mH
Stator inductance quadrature	$L_q = 0.174$ mH
Field flux	$\psi_{fl} = 0.071$ wb
Number of pole pairs	$n_p = 6$ paire pole

REFERENCES

[1] Oghafy, V., & Nikkhajoei, H. (2008, July). *Maximum Power Extraction For a Wind-Turbine Generator with No Wind Speed Sensor*. In Power and Energy Society General Meeting-Conversion and Delivery of Electrical Energy in the 21st Century, 2008 IEEE (pp. 1-6). IEEE.

[2] Abdullah M A, Yatim A H M, Tan C W, et al.(2012) *A Review of Maximum Power Point Tracking Algorithms for Wind Energy Systems. Renewable and Sustainable Energy Reviews*.; vol. 16, no 5, p. 3220-3227.

[3] Raza Kazmi S M, Goto Hiroki, Guo Hai-Jiao, et al(2010) *Review and Critical Analysis of the Research Papers Published Till Date on Maximum Power Point Tracking in Wind Energy Conversion System*. In: Energy Conversion Congress and Exposition (ECCE). IEEE; p. 4075-4082.

Joanne, H., and Alireza. B (2008) *A New Adaptive Control Algorith for Maximum Power Point Tracking for Wind Energy Conversion Systems*. In: Power Electronics Specialists Conference (PESC). IEEE; p. 4003-4007.

[4] Raza Kazmi S M, Goto Hiroki, Guo Hai-Jiao, et al. (2011) *A Novel Algorithm for Fast and Efficient Speed-Sensorless Maximum Power Point Tracking in Wind Energy Conversion Systems*. Industrial Electronics. IEEE Transactions on.; vol. 58, no 1, p. 29-36.

[5] Shravana, M., and Ginn H L. (2011) *Comprehensive Review of Wind Energy Maximum Power Extraction Algorithms*. In: Power and Energy Society General Meeting. IEEE,; pp. 1-8.

[6] M'Sirdi, N. K.., Nehme, B., Abarkan, M .and Rabhi, A. (Nov. 2014) *The Best MPPT Algorithms by VSAS Approach for Renewable Energy Sources (RES)* . Int. Conference EFEA 2014, Paris.

[7] M'Sirdi, N. K., Rabhi, A., & Abarkan, M. (2013). *A New VSAS approach for Maximum Power Tracking for Renewable Energy Sources (RES). Energy Procedia*, *42*, 708-717.

[8] Kelvin, T., and Syed, I. (2004) *Optimum Control Strategies in Energy Conversion of PMSG Wind Turbine System Without Mechanical Sensors. Energy Conversion*. IEEE Transactions on.; vol. 19, no 2, p. 392-399.

[9] LIN, Whei-Min et HONG, Chih-Ming. (2010) *Intelligent Approach to Maximum Power Point Tracking Control Strategy for Variable-Speed Wind Turbine Generation System: Energy*, vol. 35, no 6, p. 2440-2447.

[10] Iulian, M., Iuliana , B. A., and Nicolaos-Antonio, C., ET AL. (2008) *Optimal Control of Wind Energy Systems: Towards a Global Approach*. Springer..

[11] Ming ,Y., Gengyin, L. and Ming, Z., Et Al. (2007) *Modeling of the Wind Turbine with a Permanent Magnet Synchronous Generator for Integration.* In: Power Engineering Society General Meeting. IEEE.pp. 1-6.

[12] Monica, C. , Santiago, A. Et Juan Carlos, B. (2006) *Control Of Permanent-Magnet Generators Applied to Variable-Speed Wind Energy Systems Connected to the Grid. Energy Conversion*. IEEE Transactions on.; vol. 21, no 1, p. 130-135.

[13] Munteanu I, Guiraud J, Roye D, ET AL. (2006) *Sliding Mode Energy-Reliability Optimization of a Variable Speed Wind Power System*. In: Variable Structure Systems.. VSS'06. International Workshop on. IEEE. pp. 92-97

[14] Eftichios K. , and Kostas K. (2006) *Design of a Maximum Power Tracking System for Wind-Energy-Conversion Applications.* Industrial Electronics. IEEE Transactions on.; vol. 53, no 2, p. 486-494.

[15] Ching-Tsai P.and Yu-Ling, J.(2010) *A Novel Sensorless MPPT Controller for a High-Efficiency Microscale Wind Power Generation System.* Energy Conversion. IEEE Transactions on; vol. 25, no 1, pp. 207-216.

A review of Indirect Matrix Converter Topologies

Lazhar Rmili [1], Salem Rahmani [1], Kamal Al-Haddad [2]
[1] Laboratory of Biophysics and Medical Technology (BMT),
ISTMT of the University of Tunis El-Manar, Tunisia
Av. Dr. Zouhaier Essafi, 1006, Tunisia
rmili_lazhar@yahoo.fr, rsalem02@yahoo.fr
[2] Canada Research Chair in Energy Conversion and Power Electronics CRC-ECPE,
École de Technologie Supérieure, 1100 Notre-Dame, Montréal, Québec H3C 1K3, Canada
kamal@ele.etsmtl.ca

***Abstract*—** Matrix Converter (MC) is a modern direct AC/AC electrical power converter without dc-link capacitor. It is operated in four quadrants, assuring control of the output voltage, amplitude and frequency. The matrix converter has recently attracted significant attention among researchers and it has become increasingly attractive for applications of wind energy conversion, military power supplies, induction motor drives, etc. Recently, different MC topologies, which have their own advantages and disadvantages, have been proposed and developed. Matrix converter can be classified as direct and indirect structure. In this paper, the indirect MCs are reviewed. Different characteristics of the indirect MC topologies are mentioned to show the strengths and weaknesses of such converter topologies.

***Keywords*—** Matrix converter; AC/AC conversion; topologies; bidirectional switches;

I. INTRODUCTION

Matrix converter is a new generation of the direct power converter controlling the output voltage, amplitude and frequency. It has an adjustable power factor to control the input, regardless of the load. The absence of heavy and susceptible-to-failure capacitors, matrix converters can perform operations at high temperature, gain reliability, control input and output current and adjust voltage sine waves with an adjustable phase shift. These are considered some advantages of this type of converters. The controlling of output voltage, amplitude and frequency represents one more advantage over the previously mentioned advantages and over other types of converters as well. Those advantages promote the integration of this new topology in several areas of industrial applications. For example, aerospace industries have a great interest in that converter [1], [2], marine propulsion industries, electrical drive machines with variable speed [3]-[10], embedded systems and other fields of renewable energy which are based on wind and fuel cells [11]-[14].

Various research works on the topologies of matrix converters, led to the discovery of appropriate structures that minimize the number of semi-conductors. Two types of topologies for the matrix converter have been established by researchers including direct and indirect matrix converter topologies [15]-[26]. It has been shown that the indirect topology is handled easier. Other studies have been published on the design of multilevel and Z-Source Matrix Converters.

In previous work [24], authors showed the primary concerns of the MCs on bidirectional switches as well as the direct MC topologies and associated modelling. In this paper, the indirect topologies for MCs are investigated. Various features of those topologies are studied and a brief summary of the research will be shown at the end.

II. INDIRECT MATRIX CONVERTER TOPOLOGY

A new topology, developed in the early 2000s, can be proposed as an alternative to the matrix converter. This configuration consists of a combination of two conventional converters through a fictitious intermediate floor without capacitive storage element. It is called "double stage converter". The first floor is a controlled rectifier directly connected to the second floor, which consists of a voltage inverter, traditionally used in variable speed AC machines as presented in figure 1.

This indirect converter topology has two stages:

- Rectifier stage and inverter stage

The rectifier stage is formed of two switching cells, denoted (R) and (R'), modeled by the (1). One switch is closed at each switching time for both cells; this condition is expressed by the relation (2).

$$[S_{rect}] = \begin{bmatrix} S_A & S_B & S_C \\ S'_A & S'_B & S'_C \end{bmatrix} \quad (1)$$

Where …. $[S_{red}]$ is the connection matrix of the rectifier.

$$\begin{cases} S_A + S_B + S_C = 1 \\ S'_A + S'_B + S'_C = 1 \end{cases} \quad (2)$$

The operation of the rectifier is described by (3) and (4).

$$\begin{bmatrix} v_p \\ v_o \end{bmatrix} = [S_{rect}] \begin{bmatrix} v_A \\ v_B \\ v_C \end{bmatrix} \quad (3)$$

$$\begin{bmatrix} i_A \\ i_B \\ i_C \end{bmatrix} = [S_{rect}]^T \begin{bmatrix} i_{dc} \\ -i_{dc} \end{bmatrix} \quad (4)$$

The inverter stage of the indirect matrix converter consists of three switching cells called a, b, c as shown in figure 1. This floor is modeled by equation (5) and satisfies the constraints described by (6).

$$[S_{inv}] = \begin{bmatrix} S_a & S'_a \\ S_b & S'_b \\ S_c & S'_c \end{bmatrix} \quad (5)$$

Where … $[S_{inv}]$ is the connection matrix of the inverter stage.

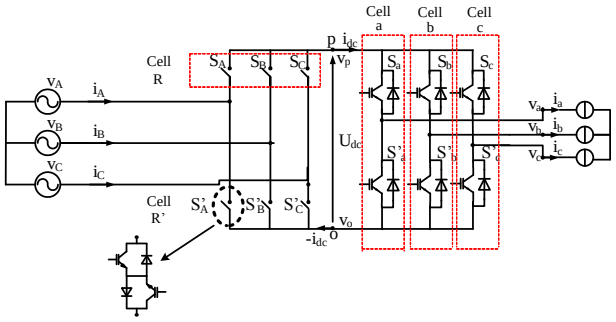

Fig. 1. Dual-stage indirect matrix converter

Every rectifier switch may be one of the following switches Fig. 2

$$\begin{cases} S_a + S'_a = 1 \\ S_b + S'_b = 1 \\ S_c + S'_c = 1 \end{cases} \quad (6)$$

The inverter operation is set by the relations (7) and (8).

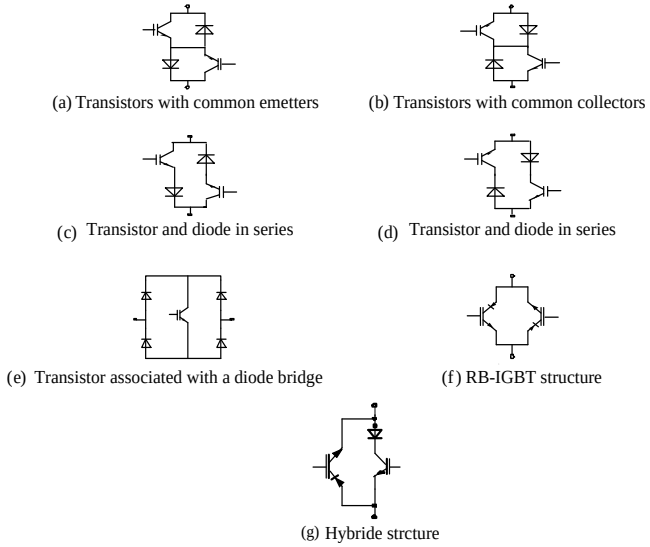

Fig.2. Different topologies of the bidirectional switches

$$\begin{bmatrix} v_a \\ v_b \\ v_c \end{bmatrix} = [S_{inv}] \begin{bmatrix} v_p \\ v_o \end{bmatrix} \quad (7)$$

$$\begin{bmatrix} i_{dc} \\ -i_{dc} \end{bmatrix} = [S_{inv}]^T \begin{bmatrix} i_a \\ i_b \\ i_c \end{bmatrix} \quad (8)$$

The connection matrix of two-stage matrix converter named $[S_{DE}]$ is obtained by the product of the connecting matrices of the inverter and rectifier, as shown in equation (9).

$$[S_{DE}] = [S_{inv}].[S_{rect}] = \begin{bmatrix} S_a & S'_a \\ S_b & S'_b \\ S_c & S'_c \end{bmatrix} . \begin{bmatrix} S_A & S_B & S_C \\ S'_A & S'_B & S'_C \end{bmatrix} \quad (9)$$

A tie between two matrices connections can be established as shown in (10).

$$[S] = [S_{DE}] \Rightarrow \begin{bmatrix} S_{Aa} & S_{Ba} & S_{Ca} \\ S_{Ab} & S_{Bb} & S_{Cb} \\ S_{Ac} & S_{Bc} & S_{Cc} \end{bmatrix} = \begin{bmatrix} S_a & S'_a \\ S_b & S'_b \\ S_c & S'_c \end{bmatrix} . \begin{bmatrix} S_A & S_B & S_C \\ S'_A & S'_B & S'_C \end{bmatrix} \quad (10)$$

In the same manner as the direct matrix converter,

a formulation based on modulation of the switches may also be set for the dual stage matrix converter. The equations described above in "connection function" are transposed in "modulation function" and the conversion matrices defined by the modulation functions of each stage of "dual-stage" matrix converter are described by (11), (12) for the rectifier stage and (15), (16) for the inverter stage.

$m_i = \frac{t_i}{T}$ where t_i represents the conduction time of switch (S_i) during the commutation period T .

$$[M_{rect}] = \begin{bmatrix} m_A & m_B & m_C \\ m'_A & m'_B & m'_C \end{bmatrix} \quad (11)$$

$$\begin{cases} m_A + m_B + m_C = 1 \\ m'_A + m'_B + m'_C = 1 \end{cases} \quad (12)$$

The laws of conversion of electrical values, whatsoever voltage/voltage or current/current are set by relations (13), (14) for the recovery block and (17), (18) for the inverter stage.

$$\begin{bmatrix} v_p \\ v_o \end{bmatrix} = [M_{rect}] \begin{bmatrix} v_A \\ v_B \\ v_C \end{bmatrix} \quad (13)$$

$$\begin{bmatrix} i_A \\ i_B \\ i_C \end{bmatrix} = [M_{rect}]^T \begin{bmatrix} i_{red} \\ -i_{red} \end{bmatrix} \quad (14)$$

$$[M_{inv}] = \begin{bmatrix} m_a & m'_a \\ m_b & m'_b \\ m_c & m'_c \end{bmatrix} \quad (15)$$

$$\begin{cases} m_a + m'_a = 1 \\ m_b + m'_b = 1 \\ m_c + m'_c = 1 \end{cases} \quad (16)$$

$$\begin{bmatrix} v_a \\ v_b \\ v_c \end{bmatrix} = [M_{inv}] \begin{bmatrix} v_p \\ v_o \end{bmatrix} \quad (17)$$

$$\begin{bmatrix} i_{dc} \\ -i_{dc} \end{bmatrix} = [M_{inv}]^T \begin{bmatrix} i_a \\ i_b \\ i_c \end{bmatrix} \quad (18)$$

Product conversion matrices of inverter and rectifier stages are the conversion matrix of "double stage" matrix converter, denoted $[M_{inv}]$. It is expressed by (19).

$$[M_{DE}] = [M_{inv}].[M_{rect}] = \begin{bmatrix} m_a & m'_a \\ m_b & m'_b \\ m_c & m'_c \end{bmatrix}.\begin{bmatrix} m_A & m_B & m_C \\ m'_A & m'_B & m'_C \end{bmatrix} \quad (19)$$

As explained before; there is a relationship between "modulation functions" of the direct matrix converter and the indirect matrix converter, which is the equality of two conversion matrices according to (20).

$m_{ij} = \frac{t_{ij}}{T}$ where t_{ij} represents the conduction time of switch (S_{ij}) during the commutation period T .

$$[M] = [M_{DE}] \Rightarrow \begin{bmatrix} m_{Aa} & m_{Ba} & m_{Ca} \\ m_{Ab} & m_{Bb} & m_{Cb} \\ m_{Ac} & m_{Bc} & m_{Cc} \end{bmatrix} = \begin{bmatrix} m_a & m'_a \\ m_b & m'_b \\ m_c & m'_c \end{bmatrix}.\begin{bmatrix} m_A & m_B & m_C \\ m'_A & m'_B & m'_C \end{bmatrix} \quad (20)$$

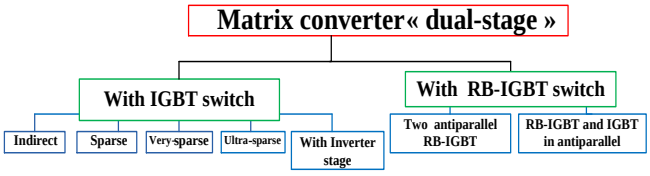

Fig. 3. Different indirect MC topologies

This two-stage indirect matrix converter structure developed by “J.W. Kollar” has a major advantage which is the ability to minimize the number of power transistors. The different topologies derived from indirect dual-stage MC have been shown in figure 3. Based on the two-stage indirect MC configuration, the following topologies have been derived:

A. Indirect matrix converter:

The configuration shown in figure 4 includes a rectifier stage comprising six bidirectional switches connected to a common emitter or common collector. This configuration generates less switching and conduction losses compared to other

configurations. It has a complex control for the number of switches to handle. All this leads to the development of other configurations with the aim of reducing the number of required transistors which facilitates the monitoring and control of the matrix converter.

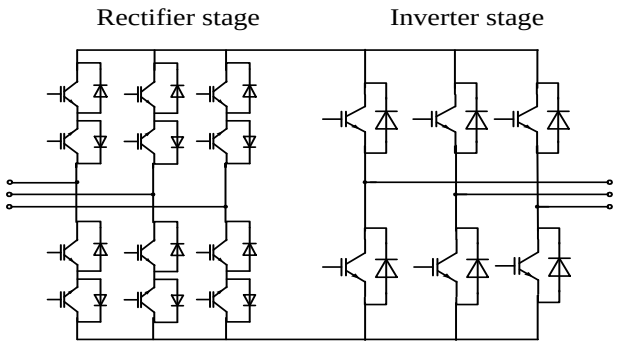

Fig. 4. Indirect matrix converter

B. Sparse matrix converter:

The configuration shown in figure 5, leads to remove an IGBT from each arm of the rectifier, so three components will be eliminated totally compared to the previous configuration, which facilitates the development of control algorithm of the converter. Conduction losses will be greater than those generated by the first configuration since three transistors and diodes are working during the feeding phase of the load as well as two transistors and two diodes in the feedback phase to the network.

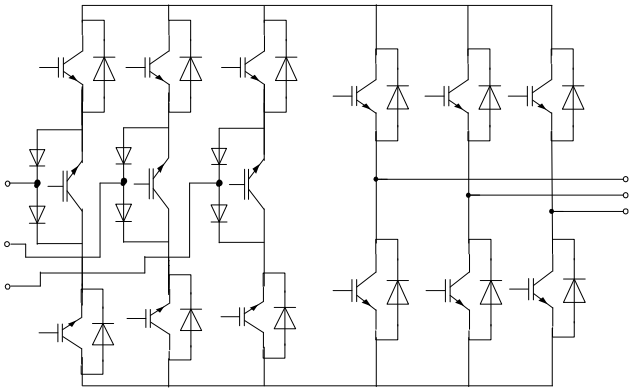

Fig. 5. Sparse Matrix converter

C. Very-Sparse matrix converter:

The structure of this topology illustrated in figure 6 is based on the implementation of bidirectional IGBT switches connected to a diode bridge, where the number of the controlled components in the rectifier is reduced compared to the two configurations mentioned above. Each active element of the rectifier requires the activation of a transistor with two diodes in each commutation phase, the rectifier requests two transistors and four diodes, bearing in mind that conduction losses are then a matter of importance.

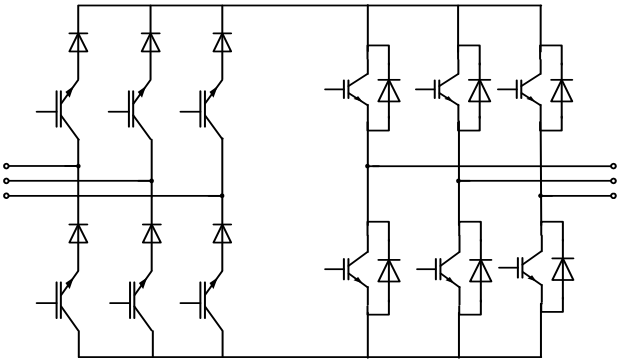

Fig. 6. Very-Sparse Matrix Converter

D. Ultra-Sparse Matrix Converter:

In this configuration, the least number of switches is employed. There is a single switch via input phase as shown in figure 7. In each arm, one transistor and two diodes are controlled. This structure generates similar conduction losses to those produced by the "Very- Sparse" structure. Yet, this configuration does not allow bi-directional power flow which limits its practical application.

(19)

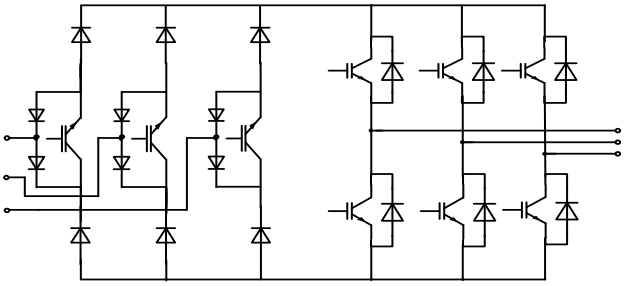

Fig. 7. Ultra-Sparse matrix converter

E. Matrix Converter "to inverter stage"

The first stage of this configuration includes a rectifier in cascade with an inverter circuit as shown in figure 8. This structure has many controlled components than the "Sparse" topology. It creates additional switching losses and has a high complexity level in control. Consequently, this configuration will not be an objective study.

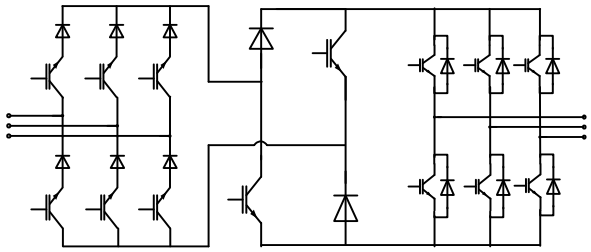

Fig. 8. Matrix converter with rectifier stage

F. Matrix Converter based on RB-IGBT:

The structure shown in figure 9 incorporates RB-IGBTs into the rectifier stage with advantages like reduction of conduction losses. The poor diode recovery behavior of the RB-IGBT is of less concern here than in a matrix converter because it is possible

to switch the rectifier stage at zero current as soft switching pattern. At low switching frequencies, a matrix converter built with RB-IGBTs will be more efficient than the one built with IGBTs.

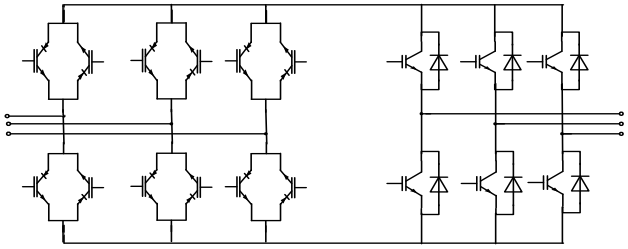

Fig. 9. Matrix converter or rectifier unit switches are based on RB-IGBT

G. Matrix Converter based hybrid switches:

The topology of matrix converter using hybrid bi-directional switches in the rectifier stage (as shown in figure 10), provides low conduction losses in motoring operation as well as soft turn-on commutation of the RB-IGBTs, whereas in the rectifier stage the standard IGBTs and diodes provide low switching losses in regenerative operation.

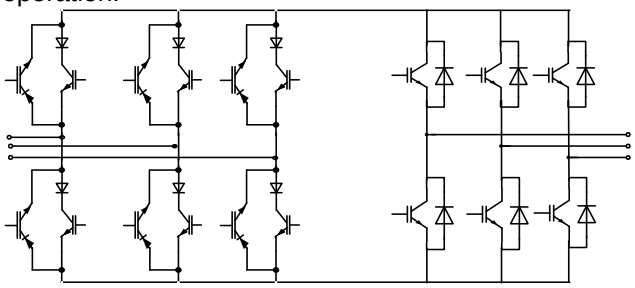

Fig. 10. Matrix converter or rectifier unit switches are based on a RB-IGBT on anti-parallel to an IGBT with a series diode

Table 1 shows the summary of the above-mentioned MC topologies considering various points including some elements such as a number of components, power losses, control strategy complexity and reversibility.

III. SIMULATION RESULTS

The SimPowerSystem toolbox of MATLAB has been used as the simulation tool. The simulation results before and after compensation of the three-level sparse matrix converter feeding an RL load as illustrated in Fig.11, also shown in Figs.12 to 17. Table II gives the system parameters used in the simulations.

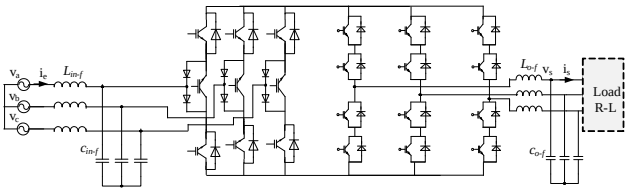

Fig. 11. Three-level Sparse Matrix Converter

Table 1. Summary of the indirect topologies features

Topology	Number of transistors	Number of diodes	Energetic losses	Reversibility power	Control
Indirect Matrix	18	18	low	yes	fairly complicated
Sparse	15	18	important	yes	fairly complicated
Very-Sparse	12	12	low	yes	easy
Ultra-sparse	9	18	low	No	easy
With Stage inverter	14	14	important	yes	complicated
Based on RB-IGBT	18	18	low	yes	fairly complicated
Based-on Hybrid switches	18	18	average	yes	easy

Figs.12 (a)-(b) show the phase a input current (ie) and its harmonic spectrum, respectively. The input current has a THD of 75.33%. The output voltage (vs) of phase (a), and its harmonic spectrum (output voltage THD of 92.21%) are shown in figs.13 (a)-(b), respectively. Figs.14 (a)-(b) show the phase (a) output current (is) and its harmonic spectrum. The output current THD is 2.43%. An input and output LC filters are necessary to compensate the high-frequency ripple from the input currents and output voltages. Thus, an LC filter is connected at the input side to avoid overvoltage and to filter the high-frequency ripple from the input currents. Similarly, on the other side, an output LC filter is connected between the converter and the load which allows controlling the output voltage and mitigates its harmonics. Figs. 15 (a) and (b) show the phase (a) input current and its harmonic spectrum after filtering. The measured THD of the input current in phase (a) is reduced from 75.33% before compensation to 1.78% after compensation. It is important to notice that the input current is kept free of harmonics.

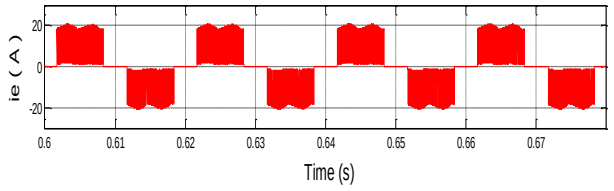

(a)

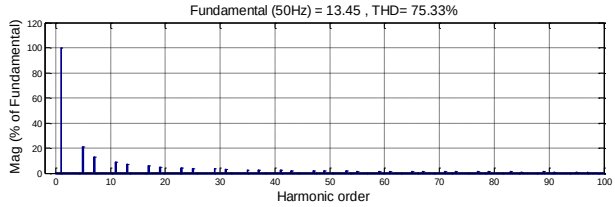

(b)

Fig. 12. (a) Waveform of phase a input current (ie) of three-phase three-level sparse matrix converter before filtering, (b) Harmonic spectrum of input current.

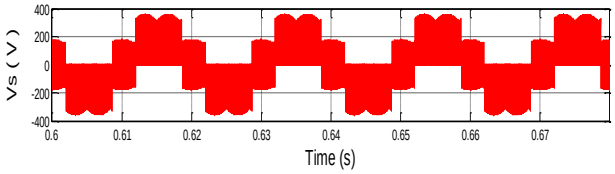

(a)

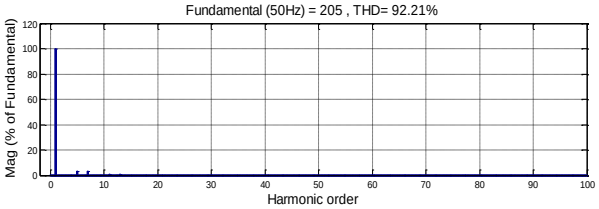

(b)

Fig. 13. (a) Waveform of phase a output voltage (vs) of three-phase three-level sparse matrix converter before filtering, (b) Harmonic spectrum of output voltage

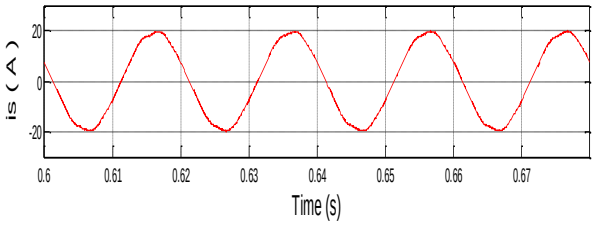

(a)

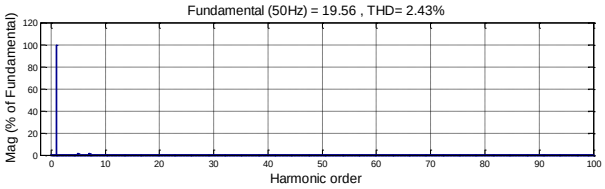

(b)

Fig. 14. (a) Waveform of phase a output current (is) of three-phase three-level sparse matrix converter before filtering, (b) Harmonic spectrum of output current.

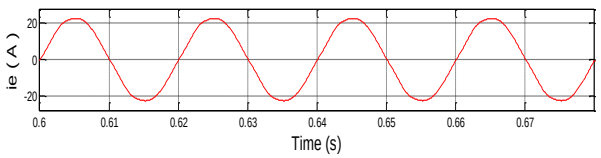

(a)

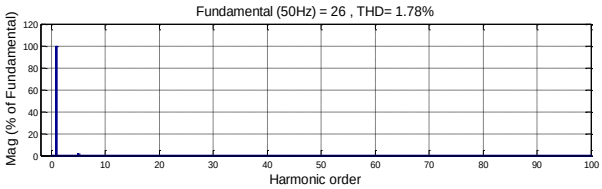

(b)

Fig. 15. (a) Waveform of phase a input current of three-phase three-level sparse matrix converter after filtering, (b) Harmonic spectrum of input current.

The waveforms and harmonic spectra of output voltage and current waveforms after filtering are shown in (figs.16 and 17) respectively. The output filter reduces the THD in the output voltage from 92.21% to 0.26%. The THD of the output current in phase (a) is therefore reduced from 2.43% without output filter to 0.15% after filtering. These results show the output LC filter capability to compensate harmonics of output voltages and output currents.

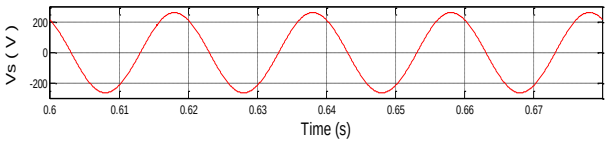

(a)

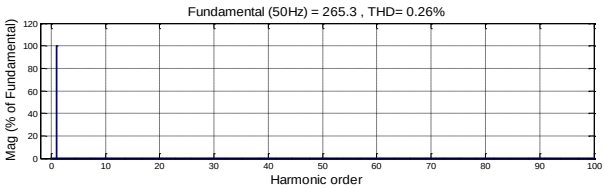

(b)

Fig.16. (a) Waveform of phase a output voltage of three-phase three-level sparse matrix converter after filtering, (b) Harmonic spectrum of output voltage

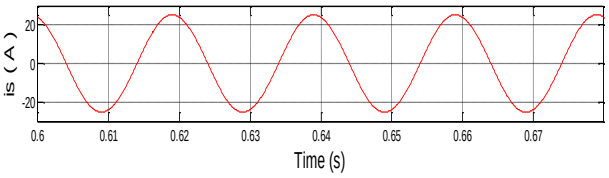

(a)

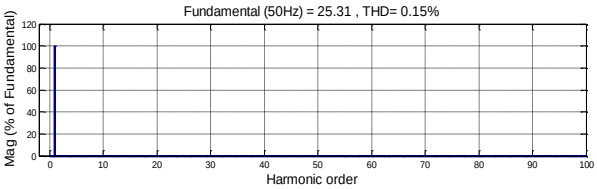

(b)

Fig.17. (a) Waveform of phase a output current of three-phase three-level sparse matrix converter after filtering, (b) Harmonic spectrum of output current

Table 2. Specification Parameters

Circuit Specifications	Value
Input side	$V_{in-max} = 311\ V, f_{in} = 50Hz$
Load	$R = 10\Omega$, $L = 10mH$
Input filter	$R_{in-f} = 0.1\Omega$, $L_{in-f} = 40mH$, $C_{in-f} = 100\mu F$
Output filter	$R_{o-f} = 0.1\Omega$, $L_{o-f} = 27mH$, $C_{o-f} = 200\mu F$
Output side	$V_{o-max} = 256.8\ V, f_o = 50Hz$
Ratio	0.825
Switching frequency	$f_{sw} = 10KHz$

IV. CONCLUSION

This paper proves that the dual stage MC topology has been studied and analyzed. Different topologies based on dual stage configuration of MC have been illustrated. The brief summary at the end shows some facts and characteristics of the afore-mentioned topologies which would be useful for future applications on MC topologies and control aspects. As mentioned before, MC has two main topologies including direct and indirect ones. The comparison between these two topologies made it clear that the two-stage matrix converters have advantages over the direct or conventional ones. For example, the possibility of reducing the number of switches forming the converter enables consumers to reduce the switching power losses and manufacturing cost as well. Less switching difficulties occurs because switches of the input stage (rectifier) can be turned on by the application of the zero vector current. The second stage is controlled as a standard inverter and the Clamp circuit can be simplified only by a capacitor in series with a diode which is not compatible with the direct matrix converter topology. Simulation results for an RL load supplied via a sparse matrix converter with the PWM modulation show that output voltage is controllable with corresponding improvements in power quality and the unity displacement power factor is achieved at the input stage. Eventually, these studies offer a very wide field of research, especially in the study of reliability, maintainability, availability; faults tolerances and stability of these types of converters.

REFERENCES

[1] Alesina, A. and Venturini, M. (April 1988) Intrinsic Amplitude Limits and Optimum Design of 9-switches direct PWM AC-AC converters, Proceedings of Power Electronic Specialist Conference, vol. 2, pp. 1284 – 1291.

[2] Alesina, A. and Venturini, M. (January 1989) Analysis and Design of Optimum Amplitude Nine-Switch Direct AC- AC Converters, IEEE Transactions on Power Electronics, vol. 4, no.1, pp. 101-112.

[3] Alesina, A. and Venturini, M. (1980) Generalised Transformer: A New Bidirectional, Sinusoidal Waveform Frequency Converter with Continuously Adjustable Input Power Factor, IEEE Power Electronics Specialists Conference, pp. 242-252.

[4] Rmili, L., Rahmani, S., Fnaiech, F. and Al-Haddad, K. (2013) Space Vector Modulation Strategy for a Direct Matrix Converter, In Proc.14th international conference on Sciences and Techniques of Automatic control & computer engineering - STA'2013, pp.1-6.

[5] Bradaschia, F., Cavalcanti, M., Neves, F. A. and Helber, E. P. (April 2009) A Modulation Technique to Reduce Switching Losses in Matrix Converters", IEEE Transactions on Industrial Electronics, vol. 56, no. 4, pp. 1186-1195.

[6] Choi, J. and Sul, S. (1995) A New Compensation Strategy Reducing Voltage/Current Distortion In PWM VSI Systems Operating With Low Voltages", IEEE IAS Annual Meeting, vol.31, pp. 1001-1008.

[7] Kang, J., Yamamoto, E., Ikeda, M. and Watanabe, E. (November 2011) Medium-Voltage Matrix Converter Design Using Cascaded Single-Phase Power Cell Modules, IEEE Transactions on Industrial Electronics, vol. 58, no. 11, pp. 5007-5013.

[8] Garcés, A. and Molinas, M. (January 2012) A Study of Efficiency in a Reduced Matrix Converter for Offshore Wind Farms, IEEE Transactions on Industrial Electronics, Vol. 59, no. 1, pp. 184-193.

[9] Klumpner, A. and Blaabjerg, F. (October 2003) Using Reverse Blocking Igbts in Power Converters for Adjustable Speed Drive, Proceedings of IEEE Industry Applications Conference, vol. 3, pp. 1516 – 1523.

[10] Klumpner, A., Nielsen, P., Boldea, I. and Blaabjerg, F. (April 2002) A New Matrix Converter Motor (Mcm) for Industry Applications, IEEE Transactions on Industrial Electronics, vol. 49, pp. 325 – 335.

[11] Changliang, X., Yan, Y., Song, P. and Tingna, S. (January 2012) Voltage Disturbance Rejection for Matrix Converter-Based PMSM Drive System Using Internal Model Control, IEEE Transactions on Industrial Electronics, vol. 59, no. 1, pp. 361-372.

[12] Ortega, C., Arias, A., Caruana, C., Balcells, J. and Asher, G. M. (June 2010) Improved Waveform Quality in the Direct Torque Control of Matrix- Converter-Fed PMSM Drives, IEEE Transactions on Industrial Electronics, vol. 57, no. 6, pp. 2101-2110.

[13] Daning, Z., Sun, K., Huang, L., and Sasagawa, K. (2005) A Novel Commutation Method of Matrix Converter Fed Induction Motor Drive Using RBIGBT, Fourtieth. IEEE IAS Industry Applications Society Annual Meeting, pp. 2347-2354.

[14] Casadei, D., Serra, G., Tani, A., Trentin, A. and Zarri, L. (October 2005) Theoretical and Experimental Investigation on the Stability of Matrix Converters, IEEE Transactions on Industrial Electronics, vol. 52, no. 5, pp. 1409-1419.

[15] Yue, F., Wheeler P., and Clare, J. (March 2006) Relationship of Modulation Schemes for Matrix Converters, 3rd IET International Conference on Power Electronics, Machines and Drives, pp. 266-270.

[16] Rodriguez, J., Rivera, M., Kolar, J. and Wheeler, P. (January 2012) A Review of Control and Modulation Methods for Matrix Converters, IEEE Transactions on Industrial Electronics, vol. 59, no. 1, pp. 58-70,.

[17] Domes, D., Hofman, W.and Lutz, J. (September 11-14, 2005) A First Loss Evolution Using a Vertical Sic-JFET and a Conventional Sic-IGBT in the Bidirectional

Matrix Converter Switch Topology, European Conference on power Electronics and Application.

[18] Hojabri, H., Mokhtari, H. and Chang, L. (March 2011) A Generalized Technique of Modeling, Analysis, and Control of a Matrix Converter Using SVD, IEEE Transactions on Industrial Electronics, vol. 58, no. 3, pp. 949-959.

[19] Mahlein, J. , Weigold , J. , and Simon,O. (November 29-december 2, 2001) New Concepts for Matrix Converter Design, The 27th Annual conference of the IEEE Industrial Electronics Society IECON, vol.2, pp 1044-1048.

[20] Ibarra, I., Kortabarria, J. , Andreu, I., Martin, M. L. and Ibañez, P. (January 2012) Improvement of the Design Process of Matrix Converter Platforms Using the Switching State Matrix Averaging Simulation Method, IEEE Transactions on Industrial Electronics, vol. 59, no. 1, pp. 220-234.

Mahlein,J., Bruckmann , M., and Braun, M. (April 2002) Passive Protection Strategy for Drive System with Matrix Converter and Induction Machine, IEEE Transactions and Industrial Electronics, vol. 49, no. 2, pp. 297-303,.

[21] Ishiguro, A., Furuhashi, T., and Okuma, S. (1991) A Novel Control Method for Forced Commutated Cyclo-converters Using Instantaneous Values of Input Line-To-Line Voltage, IEEE Transactions on Industrial Electronics, pp.166-172,.

[22] Schafmeister F. and Kolar, J. (January 2012) Novel Hybrid Modulation Schemes Significantly Extending the Reactive Power Control Range of All Matrix Converter Topologies with Low Computational Effort, IEEE Transactions on Industrial Electronics, vol. 59, no. 1, pp. 194-210.

[23] Rmili, L., Rahmani, S., Vahedi, H. and Al-Haddad, K. (June 2014) A Comprehensive Analysis of Matrix Converters: Bidirectional Switch, Direct Topology, Modeling and Control, In Proc. 23rd IEEE International Symposium on Industrial Electronics, IEEE-ISIE,

[24] Huang,X., Goodman, A., Gerada, C., Fang, Y. and Lu, Q. (September 2012) A Single Sided Matrix Converter Drive for a Brushless DC Motor in Aerospace Applications, IEEE Transactions on Industrial Electronics, vol. 59, no. 9, pp.3542-3552.

[25] Wheeler, P., Clare, J.C., Empringham, L., Apap, M., Bradley, K., Whitley C. and Towers, G. (June 2004) A Matrix Converter Based Permanent Magnet Motor Drive for an Aircraft Actuator System, Proceedings of IEEE International Electric Machines and Drives Conference, vol. 2, pp. 1295 – 1300.

Comparison of Sliding Mode Control and Fuzzy Logic control applied to Variable Speed Wind Energy Conversion Systems

Zine Souhila [1], Mazari Benyounes [1], Bouzid Mohamed Amine [2]
[1] Laboratory of development of electrical drives (LDEE)
University of Sciences and Technology
Oran, Algeria
souracha2005@yahoo.fr
[2] Laboratory of Intelligent Control and Electrical
Power Systems
University Djilali LIABES
Sidi Bel Abbes, Algeria

***Abstract*—** Wind energy features prominently as a supplementary energy booster does not pollute and is inexhaustible. However, its high cost is a major constraint, especially on the less windy sites. The purpose of wind energy systems is to maximize energy efficiency and to extract maximum power from the wind speed. In this case,the MPPT control becomes important. To realize this control, strategy conventional Proportional and Integral (PI) controller is usually used. However, this strategy cannot achieve better performance. This paper proposes other control methods of a turbine, which optimize its production, such as fuzzy logic, sliding mode control. These methods improve the quality and energy efficiency. The proposed Sliding Mode Control (SMC) strategy and the fuzzy controllers have presented attractive features, such as robustness to parametric uncertainties of the turbine, simplicity of its design and good performances. The simulation result under Matlab\Simulink has validated the performance of the proposed MPPT strategies.

***Keywords*—** Heat transfer enhancement factor, Ceramic Plate-Fin (PFHE) Heat Exchanger, Nusselt number, Schmidt number, pressure drop Wind turbine, maximum power point tracking; Sliding Mode Control; fuzzy logic control.

I. INTRODUCTION

In recent years, the strong industrialization and the increase in household appliances led to huge power needs. To face this growing demand and to avoid pollution fossil fuels (oil, gas), several countries were interested in renewables energies. In this context, wind energy occupies an important place as a supplementary energy booster. It does not pollute and it is inexhaustible. For this, improved control strategies to obtain maximum performance and longevity of its life become increasingly necessary. [1]

Several researches on wind control were conducted. The latest generation of wind turbines operates at variable speed, which offers a higher yield of energy compared to fixed-speed turbines [2%]. The rotational speed of turbine varies with changing wind speed to maintain the operating point of maximum efficiency in order to get the coefficient of maximum power and the maximum power point tracking. In this case, the MPPT control becomes important [3]. The purpose of wind energy systems is to maximize energy efficiency and extract maximum power from the wind speed; this can be achieved through different methods. Optimum power/torque tracking is the most popular control strategy. To realize this control strategy, conventional Proportional and Integral controller is usually used [4]. However, this strategy cannot achieve better performance. To solve this problem, there are other control methods such as fuzzy logic and sliding mode control.

The sliding mode control is a variable structure control , that it's a non-linear control [5]. Proposed in the early 1950s, its success has been proven in control problems, since it is able to tackle system uncertainties and external disturbances with good robustness. This control is characterized by some advantages such as: high precision, rapid dynamic response, stability, simplicity of its design and its implementation. Its major drawback is the presence of chattering. [6]

The fuzzy controllers have presented encouraging performance in the treatment of non-linear systems because they do not require a well-known system. The fuzzy controller is has interesting features, such as simplicity, good performance, and automation [7]. However, its major drawback lies in the hardware and software implementation due to the high computational load. [8]

The main objective of this paper is to propose a robust control to achieve better performance. This paper is organized as follows: Section II describes Wind Energy Conversion System (WECS); Section III develops control strategies. Sliding mode control and fuzzy logic control are designed. In section IV, simulation results show the performance of the proposed approach. Conclusion is presented in section V. The proposed strategy is compared with conventional PI controllers and confirmed superiorly in MATLAB / Simulink environment.

II. WECS SYSTEM MODELING

The Wind Energy Conversion System (WECS) is shown in Fig1. It consists of a turbine, a rectifier, a PMSG and an inverter connected to the grid.

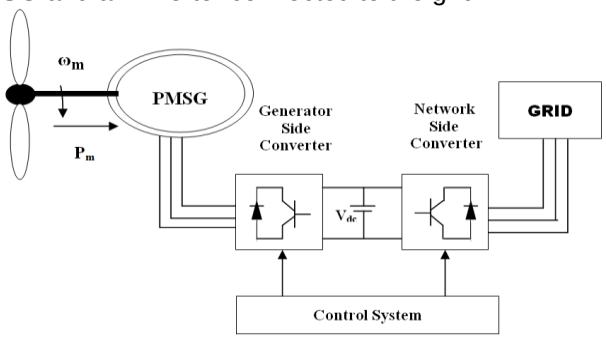

Fig. 1. The structure of wind system based on permanent magnet synchronous machine

Wind turbines are designed to produce electrical energy as cheaply as possible and give maximum power at any speed of the wind. All wind turbines are therefore designed with some sort of power control. This standard control law keeps the turbine operating at the peak of its Cp curve [9]. However, this control has an important problem since wind speed fluctuations force the turbine to operate off the peak of its Cp curve most of the time, resulting in less energy capture [9]. Therefore, our work will be based on the mechanical part of the chain (turbine), in order to propose a robust control to achieve better performance.

A. Modeling of wind turbine

The mathematical relation for the mechanical turbine power can be expressed as follows [10]:

$$P_m = C_p(\lambda,\beta)P_w = C_p(\lambda,\beta)\frac{\rho A V^3}{2} \quad (1)$$

Where Pw is the extracted power from the wind; ρ is the air density [kg/m3]; V_w is the wind speed; A is the area swept by the rotor blades of the wind turbine and $C_{p\ is}$ the power coefficient which is a function of both blade pitch angle β and tip speed ratio λ.

Tip speed ratio as given in the following equation [11]:

$$\lambda = \frac{R\omega_m}{V_w} \quad (2)$$

Where ω_m is the angular speed of the turbine rotor and R is the radius of the turbine blades.

The power coefficient Cp can be expressed as [12]:

$$C_p(\lambda,\beta) = C_1\left(C_2\frac{1}{\lambda} - C_3\beta - C_4\right)exp^{\left(-C_5\frac{1}{\lambda}\right)} + C_6\lambda \quad (3)$$

Where

$$\frac{1}{\lambda_i} = \frac{1}{\lambda + 0.08\beta} - \left(\frac{0.035}{\beta^3 + 1}\right)$$

C1=0.5176, C2=116, C3=0.4, C4=5, C5=21 and C6=0.0068.Ω

Fig 2 indicates the relation between C_p and λ for different pitch angles.

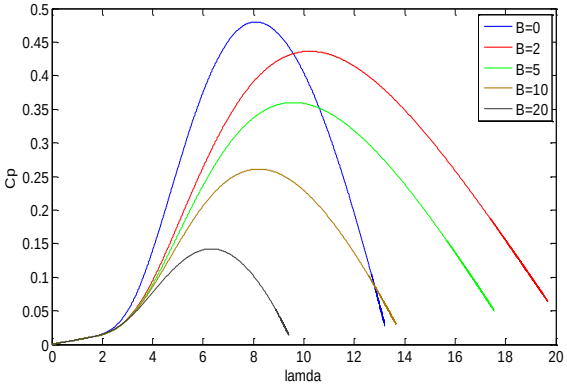

Fig. 2. Characteristics of the power coefficient as function of λ and β

It can be noticed that when pitch-angle are fixed at a value of 0, we get the nominal value of C_p about 0.48 for λ of 8.1. So the maximum power can be obtained from the wind.

The torque of the wind turbine can be expressed as:

$$T = C_p(\lambda,\beta)\frac{\rho A V^3}{2\lambda} \quad (4)$$

The mechanical equation is given by:

$$J\frac{d\,\omega_m}{dt} = T - T_e - Bw_m \quad (5)$$

III. MAXIMUM POWER POINT TRACKING CONTROL

The MPPT control is divided into three parts:

- The first part concerns the realization of the classical MPPT; this strategy can be realized using conventional Proportional and Integral (PI) controller, such as in Fig 3.
- In the second part, we will replace conventional Proportional and Integral (PI) controller by sliding mode control, such as in Fig 4.
- In the third part, conventional Proportional and Integral (PI) controller is replaced by fuzzy logic controller.

A. Maximum Power Point Tracking (MPPT) Principle

To extract the maximum power, we proceed to control the speed of the wind turbine. The wind speed measured using an anemometer is used as the reference for the speed control loop. The Maximum Power Point Tacking (MPPT) algorithm gives the reference torque applied to the turbine, so that extracted power is maximum at any wind velocity below the maximum value [13], as shown in Fig 3.

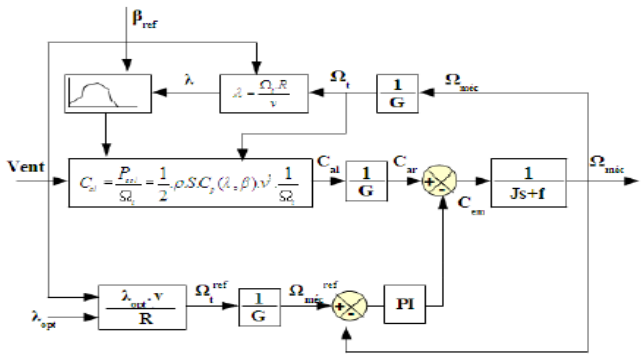

Fig. 3. Bloc diagram of torque control scheme

To ensure maximum efficiency of the turbine, it necessary that power coefficient remains optimum. The use of the linearization approach is common in addressing the control problem of wind turbines. However, due to the inevitable uncertainties inherent in the system, this strategy cannot achieve better performance. To solve this problem, we will use sliding mode control, which takes into account these control problems. [9]

B. Sliding control

The sliding mode is a special mode of operation of the variable structure system. It was a great success in recent years; this is due to the simplicity of its implementation and robustness, compared with the uncertainties of system and external disturbances, vitiating the process. [5]

Control by sliding mode is divided into three parts. The first step is to select a sliding surface, which models the desired closed-loop performance in the state variable space. Then, we impose the condition of convergence, and then the command must be designed so that the system state trajectories are directed towards the sliding surface and stay on it. [14]

1) Choice of the sliding surface

A non-linear system is presented by the following form:

$$\dot{X}=f(X,t)+g(X,t)\,u(X,t) \quad (6)$$

Where $f(X,t)$, $g(X,t)$ are both non-linear functions

Taking JJ Slotine equation, to determine the sliding surface, which is given by [14]:

$$S(X)=\left(\frac{d}{dt}+\lambda\right)^{n-1} e \quad (7)$$

$$e=X^{d}-X \quad (8)$$

e: error on the controlled variable;
-λ: positive coefficient;
-n: order of the system;
-X^{d}: desired size;
-X: state of the controlled variable size.

So that the surface is attractive and invariant, regulator sliding mode should be chosen to satisfy the Lyapunov stability criterion.

2) Convergence condition

The convergence condition is defined by the following equation:

$$S(X)\,\dot{S}(X) \le 0 \quad (9)$$

3) Control

The control structure is defined by the following equation:

$$U=U_{eq}+U_{n} \quad (10)$$

With U_{eq}-the component of the equivalent control,
U_n -component of discontinuous control

$$U_n=U_{max}\,sgn(S(X)) \quad (11)$$

Where:
-sgn(S (X)): sign function,
- U_{max}: positive gain.

4) Speed control

To control the speed, the degree of the sliding surface is taken equal to 1; the sliding surface S (w) is:

$$S(w)=w_{m\,ref}-w_{m} \quad (12)$$

By deriving equation (12), we obtain:

$$\dot{S}(w)=\dot{w}_{ref}-\dot{w} \quad (13)$$

By replacing the expression of speed, we get:

$$\dot{S}(w)=\dot{w}_{ref}-\frac{T-Te}{J}+\frac{F}{J}\dot{w} \quad (14)$$

During the sliding mode surface S (w) = Ṡ (w) =0.

$$\dot{w}_{ref}-\frac{T-Te}{J}+\frac{F}{J}\dot{w}=0 \quad (15)$$

Then we obtain

$$\begin{cases} U_{eq}=T-J\dot{w}_{ref}-F\dot{w} \\ U_{n}=U_{max}\,sgn(S(w)) \end{cases} \quad (16)$$

The proposed control scheme is shown in Fig 4

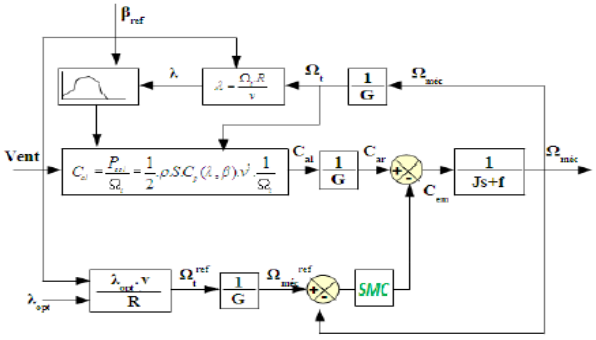

Fig. 4. The proposed strategy scheme

C. Fuzzy Logic Control

Fuzzy logic controllers are similar to how human beings make decisions. The fuzzy control is used where the nonlinearities are significant, as in the case of wind. The fuzzy control did not need to know dynamics of the system [15].

A fuzzy controller generally consists of four subsystems, in which two parts have duty of transformation [16]:

Fuzzifier (first transformation),

Fuzzy rule base,

Inference engine,

And defuzzifier (second transformation).

In a control system, the fuzzy system operates in real time to find the values optimal or near of optimum. The use of fuzzy rules base ensures that the operating the device remains within the desired range of operation [17].

1) Fuzzy logic controller

Fig. 5 shows the general structure of the control system fuzzy logic used in our work. Control output u is deduced from the error (e) and change of error (Δe). Control rules are designed to assign to a fuzzy set of the control output u for each combination of fuzzy sets of e and (Δe).

Fig. 5. Structure of a fuzzy control system

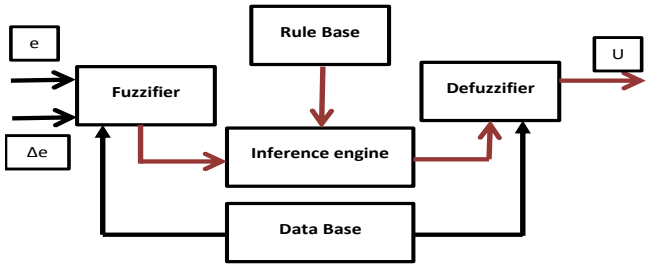

The rules of Kp and Ki are presented in the Table 1 and Table 2. Error is represented by the lines and error change Δe, by columns. Each interaction of e and Δe determines the level of output corresponding to u. [18]

Table 1 . Rule base of Kp

u		Δe				
		NB	NS	ZR	PS	PB
e	NB	VB	VB	VB	VB	VB
	NS	B	B	B	BM	VB
	ZR	ZR	ZR	NM	S	S
	PS	B	B	B	BM	VB
	PB	VB	VB	VB	VB	VB

Table 2. Rule base of Ki

u		Δe				
		NB	NS	ZR	PS	PB
e	NB	M	M	M	M	M
	NS	S	S	S	S	S
	ZR	NM	NM	ZR	NM	NM
	PS	S	S	S	S	S
	PB	M	M	M	M	M

The abbreviations of Table 1 are defined as follows: VB is very big; NB is Negative Big; NM is Negative Medium; NS is Negative Small; ZR is Zero; PS is Positive Small; BM is Positive Medium; PB is Positive Big; M is medium; B is Big and S is small. These abbreviations are labels of fuzzy sets and their corresponding membership functions are depicted in Figures 6-8.

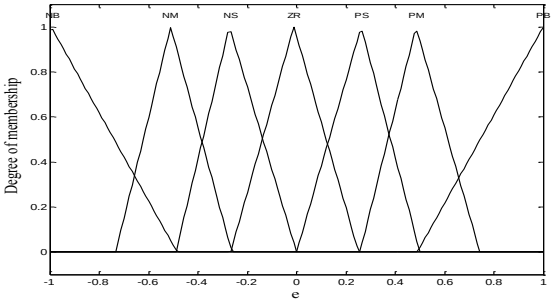

Fig. 6. Membership function for input e

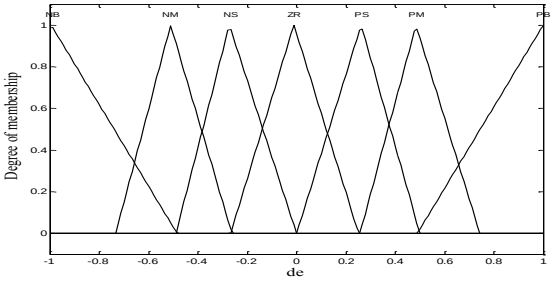

Fig. 7. Membership functions for input Δe

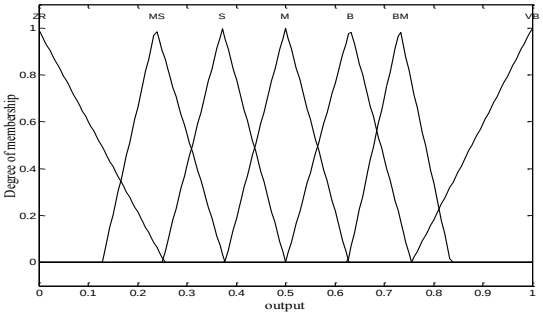

Fig. 8. Membership function of output

In this paper, the triangular membership function, the max–min reasoning method, and the center of gravity defuzzification method are used. The parameters of the PI speed controller are adjusted by using two fuzzy logic controllers to define Kp and Ki.

IV. SIMULATION RESULT

A global simulation of the system under Matlab/Simulink is realized. Table 1 illustrates system's parameters. Fig 9 shows the wind speed.

Table 3. Simulation parameters

Wind Turbine Parameters		
R=3 m	ρ=1.22	J=0.042 Kg.m2
Cp_{opt}=0.48	λopt=8.1	$\boldsymbol{B}$=0.017 N.m.s-1

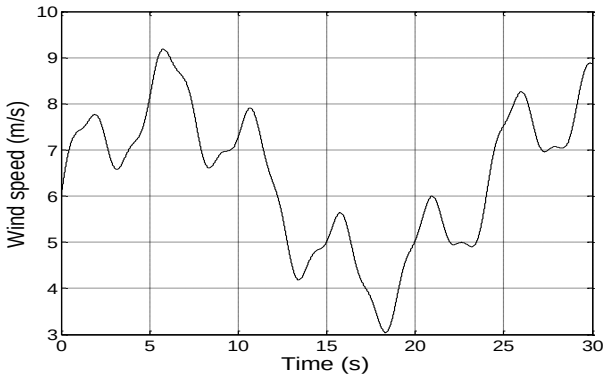

Fig. 9. Variation of wind speed (m/s)

The power coefficient variations are shown in Fig 10. It can be clearly seen that the Sliding Mode Controller provides better than the PI and Fuzzy Logic controllers. The uses of the sliding mode greatly reduces the fluctuation, which ensures optimization of the extracted power.

Figure 11 shows the efficiency of the Sliding Mode Control to maintain the speed ratio at its optimum value under varying wind conditions. The PI and Fuzzy Logic controllers stay oscillating around optimal value.

The average output power as a function of wind speed is shown in Fig 12; this power is the maximum extracted power from available wind power, keeping the value of the power coefficient at its optimum value. One notices the sliding mode controller and fuzzy controller show better performances than PI controller in optimizing the power conversion performance.

The speed curves of Fig 13 illustrate the high performance of the three developed controllers, and allow having high dynamic responses in tracking the desired speed reference, especially with the use of the sliding mode control.

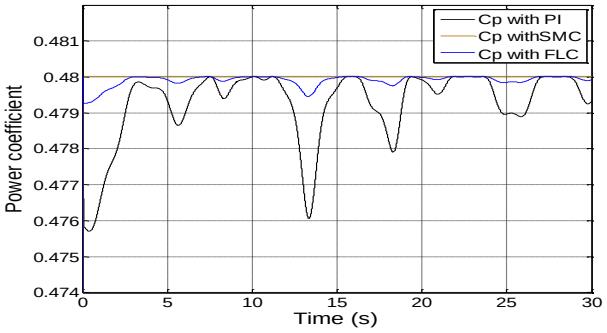

Fig.10. Power coefficient

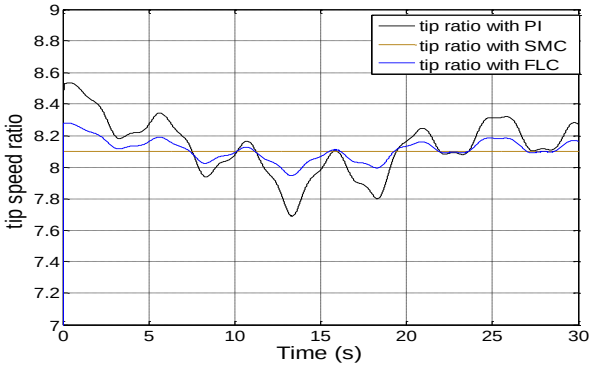

Fig. 11. Variation of tip speed ratio

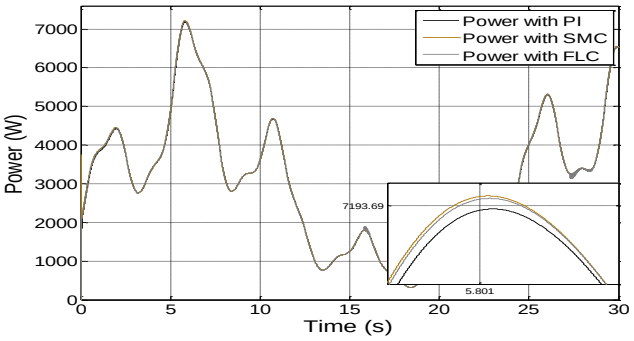

Fig. 12. Turbine Power

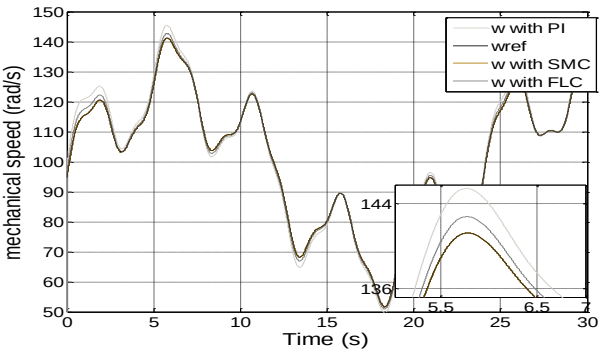

Fig.13. Speed of turbine

This paper adresses the problem of controlling power generation in variable speed wind turbines. A torque controller has been developed to follow a speed trajectory that allows the wind turbine to operate with maximum power extraction in below rated wind speed.

For this purpose, three control strategies have been proposed. The first uses a conventional proportional and integral (PI) controller, the second uses the sliding mode control, whereas the third uses Fuzzy logic controller.

Interesting features, such as high precision, rapid dynamic response, stability, simplicity of its design and its implementation, characterize sliding mode control and fuzzy controllers.

The simulation result shows that Sliding Mode Controller has better performances than a conventional Proportional and Integral controller, since the coefficient is maintained at its optimum value, thereby ensuring the optimization of the extracted power.

REFERENCES

[1] Ghennam, T.« Supervison d'une ferme éolienne pour son intergation dans la gestion d'un réseau électrique, Apports des convertisseurs multi niveaux au réglages des éoliennes à base de machine asynchrone à double alimentation », *Ecole militaire polyctechnique d'Alger*. 2011.

[2] Beltran, B. « Maximisation de la puissance produite par une génératrice asynchrone Double alimentation d'une éolienne par mode glissant d'ordre supérieur ». *JCGe*. 16-17 December 2008.

[3] Hussein, M. H., Orabi, M., Ahmed, M. E., Abd El-Wahab, M. A. and Hamada, M. M. « Simple Direct Sensorless Control of Permanent Magnet Synchronous Generator Wind Turbine ». Proceedings of the 14th international Middle East Power Systems Conference (MEPCON'10). Cairo University, Egypt. 19-December-2010.

[4] Haque, M. E. , Muttaqi, K. M. and Negnevitsky, M.« Control of a standalone variable speed wind turbine with a permanent magnet synchronous generator », in 2008 IEEE Power and Energy Society General Meeting - Conversion and Delivery of Electrical Energy in the 21st Century. 2008. P. 109.

[5] Aissaoui, A. G., ABID, H., ABID, M. and TAHOUR, A. « Commande par la logique floue et mode Glissant d'une machine synchrone autopilotée », *Rev Roum SciTechn–Électrotechn Énerg*, vol. 52, no 1, p. 89–104.

[6] Zhang, L., Chunliang, E., Li, H. and Xu, H. « A new pitch control strategy for wind turbines base on quasi-sliding mode control ». In *Sustainable Power Generation and Supply 2009 SUPERGEN'09 International Conference.* Pp. 1–4.

[7] Gargoom, A., Haruni, A. M. O, Haque, M. E. and Negnevitsky, M. « Voltage and frequency stabilizer based on fuzzy logic control for three-level NPC converters in stand-alone wind energy systems ».In *Power and Energy Society General Meeting*, 2010 IEEE, 2010, p. 1–7.

[8] Y. Mihoub, D. Toumi, B. Mazari, et S. Hassaine, « Design and Implementation of an Adaptive PI Fuzzy Controller to Improve the Speed Control of Induction Motor. », Int. Rev. Electr. Eng., vol. 5, no 2, 2010.

[9] B. Beltran, T. Ahmed-Ali, et M. E. H. Benbouzid, « Sliding mode power control of variable-speed wind energy conversion systems », Energy Convers. IEEE Trans. On, vol. 23, no 2, p. 551–558, 2008.

[10] Chih-Hong Lin, "Recurrent modified Elman neural network control of PM synchronous generator system using wind turbine emulator of PM synchronous servo motor drive", International Journal of Electrical Power & Energy Systems, Volume 52, November 2013, Pages 143-160

[11] S.M. Muyeen, Ahmed Al-Durra, J. Tamura, Variable speed wind turbine generator system with current controlled voltage source inverter, Energy Conversion and Management, Volume52, Issue 7, July 2011, Pages 2688-2694

[12] Robert Gasch, JochenTwele. Wind Power Plants: Fundamentals, Design, Construction and Operation, Springer 2012

[13] M. E. Emna, K. Adel, et M. F. Mimouni, « The Wind Energy Conversion System Using PMSG Controlled by Vector Control and SMC Strategies », Int. J. Renew. EnergyRes. IJRER, vol. 3, no 1, p. 41–50, 2013.

[14] Jiabing Hu; Heng Nian; Bin Hu; Yikang He; Zhu, Z.Q., "Direct Active and Reactive Power Regulation of DFIG Using Sliding-Mode Control Approach," *Energy Conversion, IEEE Transactions on* , vol.25, no.4, pp.1028,1039, Dec. 2010

[15] J. Zhang, M. Cheng, Z. Chen, et X. Fu, « Pitch angle control for variable speed wind turbines », in Electric Utility Deregulation and Restructuring and Power Technologies, 2008. DRPT 2008. Third International Conference on, 2008, p. 2691–2696.

[16] A. Rahideh, M. Karimi, A. Shakeri, et M. Azadi, « High performance direct torque control of a PMSM using fuzzy logic and genetic algorithm », in Electric Machines & Drives Conference, 2007. IEMDC'07. IEEE International, 2007, vol. 2, p. 932–937.

[17] A. G. Aissaoui, A. Tahour, N. Essounbouli, F. Nollet, M. Abid, et M. I. Chergui, « A Fuzzy-PI control to extract an optimal power from wind turbine », Energy Convers. Manag., vol. 65, p. 688–696, 2013.

[18] A. V. A. Macedo et W. S. Mota, « Wind turbine pitch angle control using Fuzzy Logic », in Transmission and Distribution: Latin America Conference and Exposition (T D-LA), 2012 Sixth IEEE/PES, 2012, p. 16.

Position Control of Motor Drive Systems: A Data Driven Approach

Hossein Parastvand [1], Mohammad Javad Khosrowjerdi [1], Nacer Kouider M'Sirdi [2]
[1] Advanced Control Research Laboratory (ACRL), Department of Electrical Engineering Sahand University of Technology (SUT) Tabriz, Iran
[2] Aix Marseille Université, CNRS, ENSAM, Université de Toulon, LSIS UMR 7296 LSIS UMR CNRS UMR, Domaine Universitaire St Jérôme, Avenue Escadrille Normandie-Niemen, 13397 Marseille Cedex 20, France
h_parastvand@sut.ac.ir, khosrowjerdi@sut.ac.ir, Nacer.msirdi@lsis.org

Abstract— A new model-free approach for designing robust PID controllers for the position control of electrical machines (such as induction, synchronous or DC motors) with un-modeled dynamics is proposed.
In this paper, it is illustrated that frequency response data is sufficient to calculate a family of robust PID controllers that satisfy an $\boldsymbol{H}_{\infty}$- norm on the complementary sensitivity function. The approach is illustrated on an induction motor drive system through simulation.

Keywords- motor drive, position control, PID controller, robust control, frequency domain, model free approach;

I. INTRODUCTION

Motion control applications can be found in almost every part of industry by induction motor, synchronous motor and DC motor. They are used to regulate mechanical motions in terms of position, velocity and acceleration. A high performance motor drive must have good position command, tracking and load to regulate response in the presence of external load uncertainty, un-modeled and nonlinear dynamics of plant. Similar to other industrial control problems, PID is the first choice in most of motion control applications.
In [1] the PID controller has been designed based on stability analysis considering passivity in null space motion of redundant manipulator**.** A self-tuning PID control strategy has been proposed in [2] for implementing a motion control system that stabilizes the two-wheeled vehicle and follows the desired motion commands. The controller parameters are tuned automatically, on-line, to overcome the disturbances and parameter variations. In [3] the dynamics of the synchronous motor has been investigated and the motor's response to rapid load changes has been analyzed using decentralized PID controller. Another model-based application with PID has been proposed in [4] on load motion control of two-mass servomechanisms. Although most of the proposed methods in this area rely on plant mathematical model, yet some model-free approaches can be found in the literature such as [5,6,7,8,18,19]. Almost every proposed model-free approach uses time domain data and online adaptive algorithms. A PID position domain control (PDC) is proposed in [6] for reducing contour tracking errors. Fuzzy control is another model-free approach to motion control of motor drives [9,10]. An intelligent PID controller has been proposed in [18,19] based on a newly developed numerical differentiation. The approach use time domain and numerical differentiation to adjust the control.
In this paper, another model-free technique is proposed in frequency domain for robust PID controller design of motor drive systems faced to un-modeled dynamics that can be classified as structured uncertainties. The algorithm used to calculate the family of stabilizing PID controllers for nominal plant proposed in [11] is extended to plants with an uncertain parameter. It is shown that the only required data is the set of frequency responses of motor drive system including frequency responses corresponding to maximum and minimum values of uncertain parameter. Also, the family of robust PID controllers that achieve H_{∞}-norm on complementary sensitivity function is calculated. Some special applications of the proposed approach are reviewed. It is shown that the problem can be solved with more relax conditions if the uncertain parameter appears in the feedforward path.
The paper is organized as follows. The position control problem is introduced in Section II. The algorithm used to calculate the family of stabilizing PID controllers for nominal plants and its extension to uncertain plants are presented in Section III. A review on special cases of application of the proposed approach is presented in Section IV. The proposed approach is simulated on induction motor drive in Section V. Finally, some concluding remarks are given in Section VI.

II. PROBLEM FORMULATION

The basic model for many industrial motor drives can be described by an electrical part and a mechanical part [10]. This structure is shown in Fig. 1. The electrical part is placed between input voltage u and output torque T_e and the mechanical part is between torque T_e and the rotor position θ. The electrical part that is much faster than the other one can be approximated by a first order transfer function plus a small time delay; and the mechanical part of electrical motors can be described by a two-order transfer function [10]. In Fig. 1 the transfer

function "$W(s)\Delta$" where Δ is an unknown constant and $|\Delta| < 1$ represents for the un-modeled dynamics.

The paper investigates the position control of electrical motor drives that can be configured as structure of Fig. 1. This problem is formulated as follows. Consider the basic structure of a motor drive system and assume that

1. The frequency response from voltage *u* to rotor position *θ* is available.
2. Δ is an unknown constant and $|\Delta| < 1$.

Under these assumptions the control objective is to calculate the family of PID controllers that stabilize the uncertain plants $P(s)(1 + W(s)\Delta)$ where $|\Delta| < 1$ and satisfies H_∞-norm consideration on complementary sensitivity function in the presence of un-modeled dynamics.

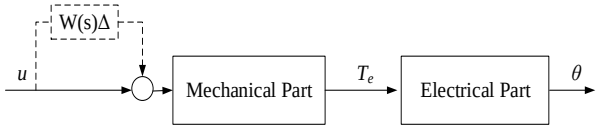

Fig. 1. Motor drive **system with un-modeled dynamics**

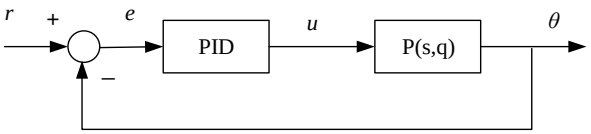

Fig. 2. Feedback structure with uncertain plant and PID

Fig. 2 shows the feedback system with PID controller in which $P(s,q)$ is an uncertain plant and q can be substituted by Δ. In the next section, a survey on the algorithm proposed for nominal stability in [11] and its generalization to uncertain plants is presented and it is illustrated that the control objectives of this paper on motor drive system can be satisfied in a same way.

III. PID CONTROLLER DESIGN: MODEL FREE APPROCH

In this section, the problem of achieving the family of stabilizing PID controllers for nominal stable plant $P(s)$ proposed in [11] is reviewed. Then by verifying a theorem, this approach is generalized to plants with an uncertain parameter. Similar approach is proposed for unstable plants which are omitted here because of room limitation.

The feedback system with PID controller is shown in Fig. 2. First, some mathematical preliminaries are introduced. Consider a real rational function

$$P(s) = \frac{A(s)}{B(s)}$$

where $A(s)$and $B(s)$ are polynomials with real coefficients and of degrees *m* and *n*, respectively. Assume that $A(s)$ and $B(s)$ have no zero on $j\omega$ axis. Let $z^+, p^+(z^-, p^-)$ determine the number of open right halp plane (RHP) (open left half plane (LHP)) zeros and poles of$P(s)$. Also let $\Delta|_0^\infty(P(j\omega))$ denotes the net change in phase of $P(s)$ as ω runs from *0* to $+\infty$. Then

$$\Delta|_0^\infty(P) = \frac{\pi}{2}[z^- - z^+ - (p^- - p^+)] \quad (1)$$

Define the (Hurwitz) signature of $P(s)$ as

$$\sigma(P) = \frac{2}{\pi}\Delta|_0^\infty(P(j\omega)) \quad (2)$$

and since $P(s)$ has no pole and zero on $j\omega$ axis, it can be written

$$\sigma(P) = -(n - m) - 2(z^+ - p^+) \quad (3)$$

The value of $n - m$ can be calculated from the frequency data of $P(s)$ and z^+ can be calculated from (3). Let

$$P(j\omega) = P_r(j\omega) + jP_i(j\omega)$$

where $P_r(j\omega)$ and $P_i(j\omega)$ denote the real and imaginary parts of $P(j\omega)$, respectively. Assume that the real, distinct, finite zeros of $P_i(j\omega) = 0$ denote as $\omega_0, \omega_1, \dots, \omega_{l-1}$ such that

$$0 = \omega_0 < \omega_1 < \cdots < \omega_{l-1}$$

and consider the modified PID controller as

$$C(s) = \frac{k_i + k_p s + k_d s^2}{s(1 + sT)}$$

where k_p, k_i and$k_d$are the proportional, integral and derivative coefficients of PID controller and *T* is a positive constant.

Lemma 1: *Let*

$$F(s) := s(1 + sT) + \left(k_i + k_p s + k_d s^2\right)P(s)$$

and

$\overline{F}(s) = F(s)P(-s)$.

Then the closed loop stability is equal to

$$\sigma\left(\overline{F}(s)\right) = n - m + 2z^+ + 2.$$

Let

$$\overline{F}(j\omega) = \overline{F}_r(\omega, k_i, k_d) + j\omega\overline{F}_i(\omega, k_p)$$

where

$$\overline{F}_r(\omega, k_i, k_d) = (k_i - k_d\omega^2)|P(j\omega)|^2 - \omega^2 T P_r(\omega) + \omega P_i(\omega)$$

and

$$\overline{F}_i(\omega, k_p) = k_p|P(j\omega)|^2 + P_r(\omega) + \omega T P_i(\omega)$$

Consider $\overline{F}_i(\omega, k_p) = 0$ and define

$$k_p = -\frac{\cos\phi(\omega) + \omega T \sin\phi(\omega)}{|P(j\omega)|} := g(\omega) \quad (4)$$

and $J = sgn[\overline{F}_i(\infty^-, k_p)]$ where $k_p^{min} < k_p^* < k_p^{max}$.

Theorem 1: *Let* $\omega_1 < \omega_2 < \cdots < \omega_{l-1}$*denote the distinct frequencies of odd multiplicities which are solutions of*

$$\overline{F}_i(\omega, k_p^*) = 0.$$

Determine strings of integers $I = [i_0, i_1, i_2, \dots, i_l]$ *where* $i_l \epsilon \{-1, 1\}$ *such that:*

for n-m even:

$$[i_0 - i_1 + i_2 + \cdots + (-1)^{l-1}2i_{l-1} + (-1)^l i_l](-1)^{l-1}J = n - m + 2z^+ + 2 \quad (5)$$

and for n-m odd:

$$[i_0 - i_1 + i_2 + \cdots + (-1)^{l-1}2i_{l-1}](-1)^{l-1}J = n - m + 2z^+ + 2 \quad (6)$$

Also let

$$i_l = sgn(\overline{F}_r(\infty^-, k_i, k_d).$$

Then for $k_p = k_p^*$, *the values of*(k_i, k_d) *corresponding to the closed loop stability are given by*

$$\overline{F}_r(\omega_t, k_i, k_d)i_t > 0 \quad (7)$$

where i_t*'s are taken from strings satisfy (5) or (6) and* ω_t*'s are taken from the solutions of (4).*

Next theorem shows how to calculate the admissible range of k_p.

Theorem 2: *The necessary condition of existence the stabilizing PID for LTI plants is that there exists* k_p *such that* $k_p = g(\omega)$ *has at least R distinct roots of odd multiplicities such that*

$$\begin{cases} R \geq \frac{n-m+2z^++2}{2} - 1 & n-m\ even \\ R \geq \frac{n-m+2z^++3}{2} - 1 & n-m\ odd \end{cases}. \quad (8)$$

The procedure for calculation the family of stabilizing PID controllers is summarized in the following algorithm [11].

Algorithm 1.

1. Determine the relative degree r_P of plant $P(s)$ from high frequency slope of bode magnitude of $P(j\omega)$.
2. Determine $\sigma(P)$ from (2).
3. Determine z^+ from (3).
4. Determine $g(\omega)$ for $\omega \geq 0$ from (4).
5. Apply Theorem 2 to determine the range of k_p.
6. For $k_p = k_p^*$, solve (4) and obtain $\omega_1 < \omega_2 < \cdots < \omega_{l-1}$.
7. Let $\omega_0 = 0$ and $\omega_l = \infty$. Determine $i_0, i_1, \ldots, i_{l-1}$from (5) or (6).
8. For $k_p = k_p^*$, determine the (k_i, k_d) values from (7).
9. Change k_p and go to step 6 to obtain the whole family of stabilizing PID controllers.

Now the main result of this paper will be presented. Consider an uncertain real rational plant $P(s,q)$ where $q \in [q_{min}, q_{max}]$ is an uncertain parameter. The control goal is to calculate the family of robust stabilizing PID controllers for the uncertain plant$P(s,q)$. The feedback structure is shown in Fig. 2. The only required data is the set of frequency responses $P(j\omega, q)$ including $P(j\omega, q_{min})$ and $P(j\omega, q_{max})$ for $\omega \geq 0$.

In the proposed approach of Algorithm 1, roots R of function $g(\omega)$ in (8), can be obtained from (4) and the range of k_p is calculated based on the value of$R$. Also the range of admissible(k_i, k_d) values obtain from (7) which have the slope equal to ω_t^2. If by monotonic variation of the uncertain parameter *q*, $g(\omega)$ varies monotonically, some substantial results could be concluded. First of all, the range of admissible $k_p$for stabilizing the uncertain plant $P(s,q)$ is the common range of admissible k_p for two plants $P(s, q_{min})$ and$P(s, q_{max})$. Second, since the slope of linear inequalities in (7) varies monotonically with monotonic varying the uncertain parameter, the inequalities corresponding to $P(s, q_{min})$ and $P(s, q_{max})$have the maximum and minimum slopes, not necessarily respectively. Finally, since variation of the uncertain parameter q, does not lead to monotonic variation in the $y-$intercept, the common space of inequality (7) for $P(s, q_{min})$and $P(s, q_{max})$is larger than the admissible (k_i, k_d) values. An approach to find the exact range of admissible parameters is presented in the following remark.

Remark 1: A simple approach to exclude these regions is to choose some test points in those regions and analyzing their stability. So monotonic variation of the function$g(\omega)$, makes it easy to calculate the family of stabilizing PID controllers for plants with an uncertain parameter.

Theorem 3: *Let* $P(s,q)$ *be a real rational transfer function and* $q \in [q_{min}, q_{max}]$*is an uncertain parameter. If the Number of zeros and poles and the number of RHP zeros of* $P(s,q)$ *are fixed for* $q \in [q_{min}, q_{max}]$ *then the family of stabilizing PID controllers for uncertain plant is a subspace of common space between two set of stabilizing PID controllers for* $P(s, q_{min})$ *and* $P(s, q_{max})$ *if one of the below constraints satisfy*

$$\begin{cases} p_i^2 + P_r^2 + P_i\omega + P_r < 0 \\ -(P_r + P_i\omega) > 0 \end{cases} \quad (9)$$

$$\begin{cases} p_i^2 + P_r^2 + P_i\omega + P_r > 0 \\ -(P_r + P_i\omega) < 0 \end{cases} \quad (10)$$

for only one value of uncertain parameter q and for $\omega \geq 0$.

Proof: If monotonic varying the uncertain parameter leads to monotonic varying the function $g(\omega)$ then the family of stabilizing PID controllers for uncertain plant is a subspace of common space between two set of stabilizing PID controllers for $P(s, q_{min})$ and $P(s, q_{max})$. Then

$$\frac{dg}{dk} = -\frac{(\frac{dP_r}{dk} + \omega\frac{dP_i}{dk})(p_i^2 + P_r^2) - 2\left(P_r\frac{dP_r}{dk} + P_i\frac{dP_i}{dk}\right)(P_r + P_i\omega)}{p_i^2 + P_r^2}$$

Without loss of generality, consider the case of monotonic increasing in $g(\omega)$. Increasing the uncertain parameter leads to increasing in $g(\omega)$ if the following inequality holds:

$$(P_r^2 - P_i^2 + 2\omega P_r P_i)dP_r + (P_i^2\omega - P_r^2\omega + 2P_r P_i)dP_i > 0 \qquad (11)$$

Assumption 1: Let

$$P_i^2\omega - P_r^2\omega + 2P_r P_i > 0. \qquad (12)$$

and note that the symbol '>' could be inversed; but for simplicity it is assumed as '>'. Finally, consider the real rational symbol of (12). So (11) can be transformed to

$$\frac{dP_i}{dP_r} > \frac{(P_i^2 - P_r^2 - 2\omega P_r P_i)}{(P_i^2\omega - P_r^2\omega + 2P_r P_i)} \qquad (13)$$

and by change of variable as:

$$z = \frac{P_i}{P_r}$$

the inequality (13) can be changed to:

$$P_r dz > \frac{-z^3\omega - z^2 - z\omega - 1}{z^2\omega - \omega + 2z}dP_r. \qquad (14)$$

Assumption 2: Let

$$P_r > 0 \qquad (15)$$

and

$$\frac{-z^3\omega - z^2 - z\omega - 1}{z^2\omega - \omega + 2z} > 0 \qquad (16)$$

similar to Assumption 1, the real rational symbol of (15) and (16) will be considered finally. From (15) and (16), the inequality (14) leads to:

$$\ln\left(\frac{-z\omega - 1}{(z^2+1)P_r}\right) > 0 \quad \Rightarrow \quad \frac{-z\omega - 1}{(z^2+1)P_r} > 1$$

and since $z = \frac{P_i}{P_r}$, then

$$p_i^2 + P_r^2 + P_i\omega + P_r < 0$$

that is one of the necessary conditions imply that increasing the uncertain parameter q leads to increasing in $g(\omega)$. Assumptions 1 and 2 imply another necessary condition as

$$-(P_r + P_i\omega) > 0.$$

Remark 2: Bode diagrams corresponding to $P(j\omega, q_{min})$ and $P(j\omega, q_{max})$ could be recognized from the frequency responses set of uncertain plant $P(j\omega, q)$. In fact if (9) or (10) holds, then from monotonic variation of the function $g(\omega)$, it could be deduced that the uppermost and lowermost plots of $g(\omega)$ are corresponding to $P(j\omega, q_{min})$ and $P(j\omega, q_{max})$, not necessarily respectively.

The following Corollary shows that the problem can be solved easier when the uncertain parameter is in the feedforward path of control loop.

Corollary 1. *Let* $P(s,q)$ *be a real rational function for an uncertain LTI plant and* $q \in \{q_{\min}, q_{\max}\}$ *is an uncertain parameter that appears in the feedforward path. Then the family of stabilizing PID controllers for uncertain plant is a subset of common set between two set of stabilizing PID parameters for* $P(s, q_{\min})$ *and* $P(s, q_{\max})$ *if one of the below sets satisfy*

$$\begin{cases} (-P_r + \omega P)_i > 0 \ : \ if \quad g(\omega) \ \ is \ \ ascendant \\ (-P_r + \omega P)_i < 0 \ : \ if \quad g(\omega) \ \ is \ \ decendant \end{cases} \qquad (17)$$

for $\omega \geq 0$ *and for only one value of uncertain parameter* q.

proof: It can be written

$$P(j\omega, q) = qP_r(j\omega) + qP_i(j\omega)$$

and

$$g(\omega) = -\frac{qP_r(j\omega) + \omega qP_i(j\omega)}{q^2(P_r(j\omega) + P_i(j\omega))}.$$

Then

$$\frac{dg}{dq} = \frac{1}{q^2}\cdot\frac{P_r + \omega P_i}{P_r^2 + P_i^2}$$

So $g(\omega)$ is monotonic if (17) satisfies.

The procedure for calculating the family of stabilizing PID controllers is summarized in the below algorithm.

Algorithm 2.

1. Determine $P(j\omega, q_{min})$ and $P(j\omega, q_{max})$ for $\omega \geq 0$ from $g(\omega)$ plots using Remark 2.
2. Using Algorithm 1, calculate the family of stabilizing PID controllers for two plants $P(s, q_{min})$ and $P(s, q_{max})$. Determine the common space of PID parameters between two calculated family. The family of stabilizing PID controllers for uncertain plant $P(s,q)$ is a subspace of this common space.
3. Calculate the exact family of stabilizing PID controllers using the approach proposed in Remark 1.

Now it can be shown that the problem of satisfying some performance specifications for uncertain plant $P(s,q)$ could be transformed to problem of robust stabilizing the uncertain plant $P(s,q)$ with additional virtual uncertain parameter.

Many performance attainment problems for uncertain plant $P(s,q)$ can be cast as the simultaneously stabilization of the uncertain plant and the family of real and complex plants [11]. For example an H_∞-norm achievment on the complementary sensitivity function, that is $\|W(s)T(s)\| < \gamma$, is equivalent to simultaneously stabilizing the uncertain plant $P^C(s,q,\theta)$ as

$$P^C(s,q,\theta)=\{\left(1+\tfrac{1}{\gamma}e^{j\theta}W(s)\right)P(s,q):\theta\epsilon[\theta_{min},\theta_{max}]\} \quad (18)$$

where θ is a virtual uncertain parameter and $W(s)$ is a weight selected by designer.

Let the family of stabilizing PID parameters for uncertain plant $P(s,q)$ can be calculated from Algorithm 1 and Let $P^C(s,q,\theta)$in (18) be a real rational function. If $g(\omega)$ corresponding to (18), varies monotonically by monotonic varying the virtual uncertain parameter θ, for any q and any θ, then the family of stabilizing PID controllers for uncertain plant $P(s,q)$ that satisfy the H_∞-norm specification on the complementary sensitivity function, is a subspace of PID controllers obtained from simultaneously stabilization of two plants

$$P^C(s,q_{min})=\left[1+\tfrac{1}{\gamma}W(s)\right]P \quad (19)$$

$$P^C(s,q_{max})=\left[1+\tfrac{1}{\gamma}W(s)\right]P(s,q_{max}) \quad (20)$$

and the exact family can be obtained using the approach proposed in Remark 1.

IV. A REVIEW ON THE APPLICATIONS OF THE PROPOSED APPROACH

In this section, some applications of the proposed method are presented. In fact, it is illustrated that some control objectives can be cast as robust stabilizing of a plant with an uncertain parameter. For example:

Example 1: Performance achievement

Many performance achievement problems for uncertain plant $P(s,q)$ can be cast as the simultaneously stabilization of the uncertain plant and the family of real and complex plants. Some of these performance achievement problems for nominal plant are listed in [11]; for example, the problem of H_∞-norm achievement on the complementary sensitivity function is equivalent to simultaneously stabilizing the plant P(s) and the family of real plants

$$P^C(s,q,\theta):q\in\{q_{\min},q_{\max}\},\theta\in\{0,2\pi\}$$

and the exact family can be obtained using some test points. The other specifications such as H_∞-norm achievement on the sensitivity function and phase margin can be satisfied by the same approach.

Example 2: Robustness against loss of effectiveness in actuator

Fig. 3 Shows the feedback structure of a plant with PID faced to loss of effectiveness in actuator where L is the parameter corresponding to loss of effectiveness and belongs to $(0,1]$. Obviously this structure can be cast as a plant with an uncertain parameter, i.e., $P(j\omega,L)$ with PID where $L=q$ is the uncertain parameter. There is similar case when loss of effectiveness happens in sensors. Thus the family of robust PID controllers for plants faced to loss of effectiveness can be calculated by the approach proposed in the previous section. For this special case, the problem of controller synthesis could be handled easily using Corollary 1.

Example 3: Robustness in plants with a dominant uncertain parameter

Some plants that are faced to parameter variations can be approximated by plants with a dominant uncertain parameter. Obviously the proposed approach can be applied in this case to calculate the family of robust stabilizing PID controller.

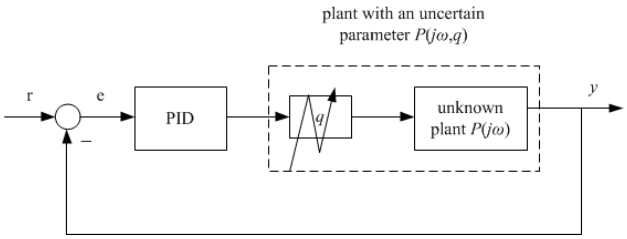

Fig. 3. The feedback structure of plant faced to loss of actuator effectiveness with PID

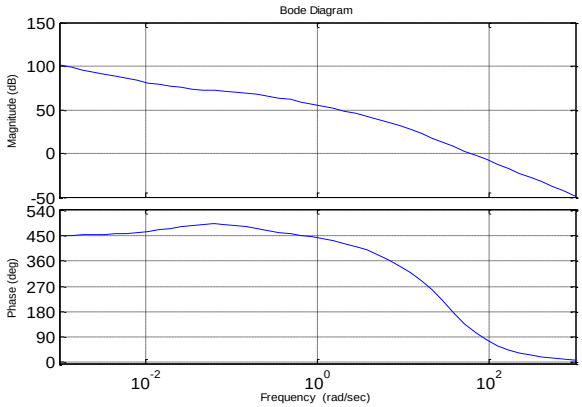

Fig. 4. The frequency response of motor drive system

V. SIMULATION ON INDUCTION MOTOR

The model studied in this section is an induction motor drive system introduced in [9, 12] that has the similar structure to Fig. 1 in [14] and its nominal frequency response is shown in Fig. 4. The frequency response of such systems can be obtained by virtual sine sweeping [13]. The corresponding plot of $g(\omega)$ is shown in Fig. 5. Since $R\geq 3$ (from (8)), the admissible range of k_p is $[-25,395]$. Calculating the(k_i,k_d)values for $k_p=50$ and *T=1* is resulted to the following inequalities

$$\begin{cases} k_i>0 \\ k_i<16.24k_d+270 \\ ki>370.17k_d-21611 \\ k_i<6561k_d+15379 \end{cases}.$$

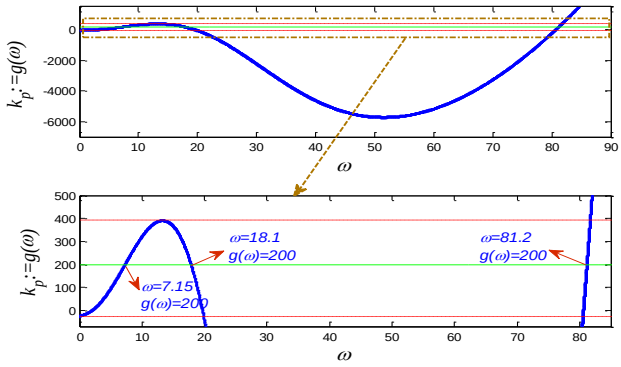

Fig. 5. The plot of function g(ω) with the line *kp*=200

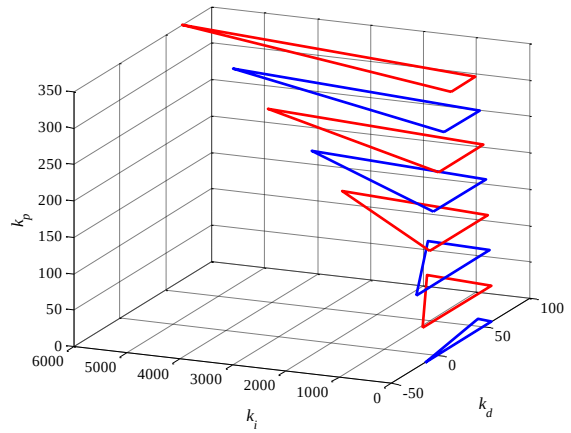

Fig. 6. The whole family of stabilizing PID controllers for nominal model of induction motor drive system

Therefore the family of robust PID controllers for the induction motor drive with uncertainties can be calculated by stabilizing the following two plants

$$\begin{cases} (1+W(s)\Delta_{min})P(s) \\ (1+W(s)\Delta_{max})P(s) \end{cases}.$$

The range of robust stabilizing PID parameters for induction motor faced to un-modeled dynamics is illustrated in Fig. 7-a. The admissible range of (k_i, k_d) for all admissible k_p is shown in Fig. 7-b.

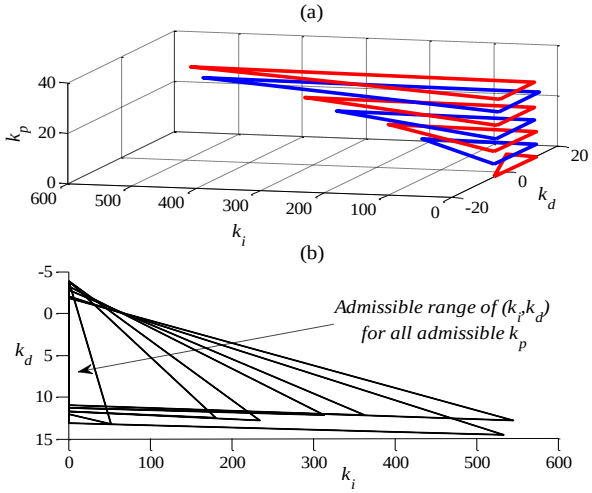

Fig. 7. (a) Robust stabilizing PID parameters for induction motor drive faced to un-modeled dynamics; (b) the admissible range of (k_i,k_d)

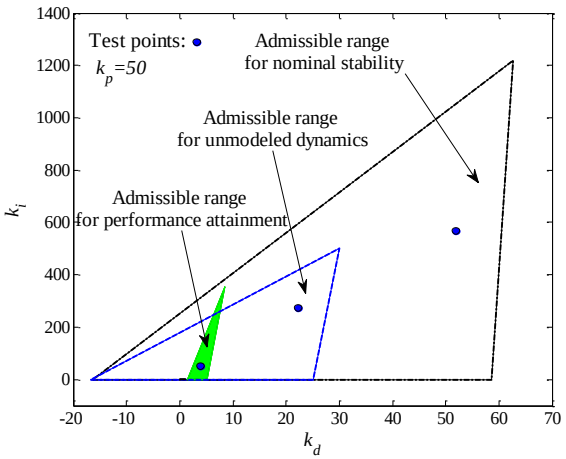

Fig. 8. The range of admissible (k_i,k_d)values that satisfy different control objectives for k_p=50

Now consider the problem of satisfying H_∞-norm on the complementary sensitivity function. The admissible range of(k_i, k_d)values that satisfy this performance criterion for $k_p = 50$ is shown in Fig. 8 together with regions corresponding to nominal stability and stability in the presence of un-modeled dynamics. The whole range of (k_i, k_d) values can be obtained similarly.

The step responses of closed loop system with controllers corresponding to test points marked in Fig. 8 are shown in Fig. 9. Applying the PID controller that satisfies performance consideration is resulted to decreasing the overshoot. Also, the control signals corresponding to selected controllers are plotted in Fig. 10. It can be seen that the control signals drift to zero after the reasonable times.

For better tracking of the proposed approach in this paper, the readers can refer to the many academic examples implemented in [15].

VI. CONCLUSION

In this paper, a robust control approach presented based on a general model for different types of electrical motor drives. The problem of robustness against un-modeled dynamics in motor drives is transformed to the problem of stabilizing a plant with an uncertain parameter. It is shown that knowing the frequency responses of motor drive system corresponding to maximum and minimum values of uncertainty is sufficient to calculate the family of robust stabilizing PID controllers. In fact, there is no need to plant mathematical model. Also it is illustrated that the problem of H_∞-norm achievement on the complementary sensitivity function can be solved by the same approach. Through the paper, it is assumed that the frequency response of plant is available. Such an assumption is often valid in many practical applications. Also, this is an assumption that has already been used several times in other papers dealing with controller synthesis using frequency domain data [5,7,11,13,15-17].

There are open doors to extend this approach to MIMO and nonlinear systems and to improve the performance specifications. Also, it is obvious that many of un-modeled dynamics are more complicated than the constant parameter Δ considered in this paper. So it is of essential interest to extend the approach to more complicated types of uncertainties.

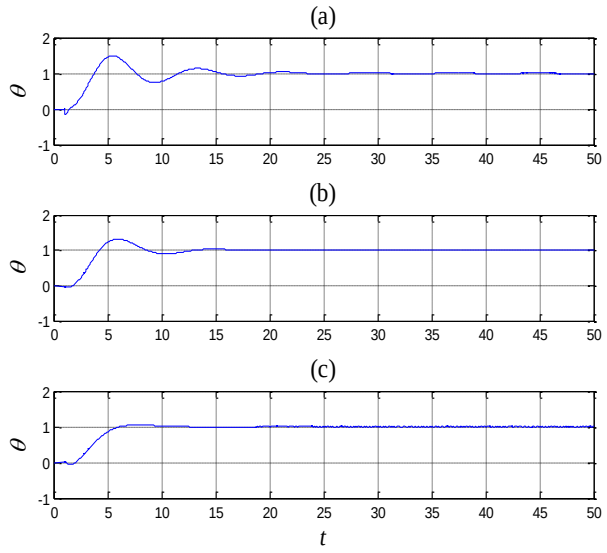

Fig. 9. Step responses corresponding to controllers that satisfy (a) stability for nominal motor drive system, (b) stability for motor drive with un-modeled dynamics, (d) stability and performance attainment for motor drive with un-modeled dynamics (The unit of

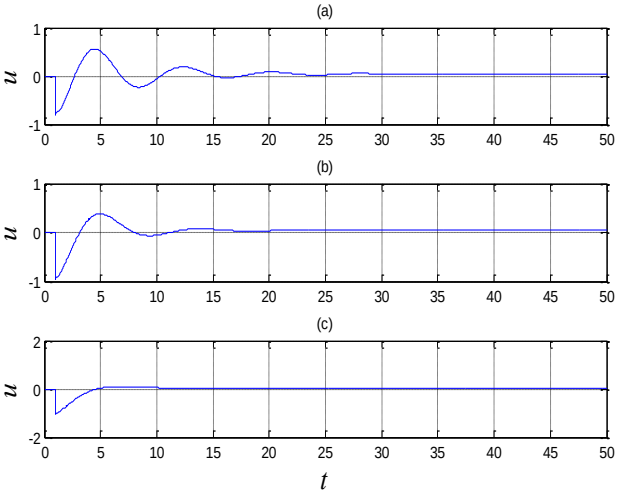

time *t* is second)

Fig. 10. The control inputs corresponding to controllers that satisfy (a) stability for nominal motor drive system, (b) stability for motor drive with un-modeled dynamics, (d) stability and performance attainment for motor drive with un-modeled dynamics (The unit of time t is second)

REFERENCES

[1] Shibata, T. and Murakami, T. (2008) *Null Space Motion Control by PID Control Considering Passivity in Redundant Manipulator*, IEEE trans. Industrial Informatics, vol. 4, no. 4.

[2] Ren, T. J. , Chen T. C. And Chen,C. J. (2008)*Motion Control of a Two-Wheeled Vehicle Using a Self Tunning PID Controller,* Contol Engineering Practice, vol. 16, pp. 365-375.

[3] Mikalsen, R., Roskilly, A. P. (2010) *The Control of a Free-Position Generator. Part 2: Engine Dynamics and Piston Motion Control,* Journal of Applied Energy, pp. 1281-1287.

[4] Ferretti,G., Magnani, G. and Rocco, P. (2001) *Alternative in Precise Load Motion Control of Two Mass Servomechanisms*, IEEE/ASME International Advanced Parastvand Intelligent Mechatronics Proceedings, Como, Italy.

[5] Parastvand, H. and Khosrowjerdi, M. J. (2015) *Controller Synthesis Free of Analytical Model: Fixed Order Controllers,* International Journal of Systems Science, vol. 46, no. 7, pp. 1208-1221.

[6] Ouyang, P. R., Pano, V. and Dam, T. (2015) *PID Position Domain Control for Contour Tracking,* International Journal of Systems Science, vol. 46, no. 1, pp. 111-124.

[7] Parastvand, H. and Khosrowjerdi, M. J. (2014) *A New Data-Driven Approach to Robust PID Controller Synthesis*, Journal of Control Engineering and Applied Informatics, vol. 16, no. 3, pp. 84-93,.

[8] Parastvand, H. and Khosrowjerdi, M. J.(2015) *Parameterized Controller Synthesis for SISO-LTI Uncertain Plants Using Frequency Domain Information,* International Journal of Systems Science, in press,.

[9] Lin,F. J., Chen, S. Y., Teng L. T. and Chu, H. (2009) *Reurrent Functional Link Based Fuzzy Neural Network with Improved Practical Swarm Optimization for A Linear Synchronous Motor Drive,* IEEE trans.Magnetics, vol. 45, no. 8,.

[10] Masiala, M., Vafakhah, B., Salmon J. and Knight A (2008) *Fuzzy Self Tunning Speed Control of An Indirect Field Oriented Control Induction Motor Drive,* IEEE trans. Industry Applications, vol. 44, no. 6.

[11] Keel, L. H. and Bhattacharyya, S. P. (July 2008) *Controller Synthesis Free of Analytical Model: Three term controllers,* IEEE trans. Automatic Control, vol. 53, no. 6.

[12] Liu Z. and Wang, Q. (2008) *Robust Control of Electrical Machines with Load Uncertainty,* Journal of Electrical Engineering, vol. 2, no. 2, pp. 110-112.

[13] Taghirad, H. D. (1997) *Robust Torque Control of Harmonic Drive System,* Ph.D. dissertation, Dept. Electrical Eng., Univ. McGill, Montreal.

[14] Wildi, T. (2002) *Elecctrical Machines, Drives, and Power Systems,* Prentice Hall.

[15] Parastvand, H. (2010) *Model Free Controller Synthesis: Frequency Domain Approaches,* MSc thesis, Sahand University of Technology, Department of Electrical Engineering, Iran.

[16] S. Formentin, A. Karimi, S.M. and Savaresi, (2012) *On Input Design for Direct Data-Driven Controller Tuning,* IFAC Symposium on System Identication, Bruxelles, Belgium.

[17] Silva, G. J., Datta, A. and Bhattacharyya,S. P. (2002) *New Results on the Synthesis of PID Controllers,* IEEE TRANSACTIONS ON AUTOMATIC CONTROL, VOL. 47, NO. 2, pp. 241-25.

[18] Fliess, M. and Join,C., Riachy, S. (2011) *Revisiting Some Practical Issues in The Implementation of Model-Free Control,* 18th IFAC World Congress, IFAC WC'2011, Milan, Italy.

[19] Fliess, M. and Join, C. (2009) Model-free Control and Intelligent PID Controllers: Towards a Possible Trivialization of Nonlinear Control, 15th IFAC Symposium on System Identi_cation (SYSID 2009), Saint-Malo, France.

Location and Parameters of Power System Stabilizer for Small Perturbation of Tunisian Network

BEN SALAH Rim [1], DJEBALI Meriam [1], KAHOULI Omar [1], BOUCHOUCHA Chokri [2], HADJ ABDALLAH Hsan [1]
[1] Control & Energies Management (CEM-Lab)
National Engineering School of Sfax, ENIS
[2] Tunisian Company for Electricity and Gas (STEG)

Abstract - This paper proposes the static stability of Tunisian electrical network while facing small perturbation to maintain the security of the entire power system. In this context, after linearizing the power system, the concept of determining the placement of Power System Stabilizer is based on participation factor to find where it is going to be the most effective on a particular mode. Then, the Power System Stabilizer tuning is calculated by using the method of residue. Our objective is to improve the dynamic behavior of the electricity grid while facing various small disturbances.

Keywords - the static stability of Tunisian electrical network; Power System Stabilizer; Automatic Voltage Regulator; method residue.

I. INTRODUCTION

The purpose of a grid is to generate electrical power, and transport it to the load. A balance between the energy generated and the energy consumed must be maintained at all times. Besides, for a safe and reliable operation, the grid must be able to maintain stability while encountering several types of disturbances.

The electromechanical phenomena of small disturbances often occur with little damped oscillations of the system whose frequency range is between 0 to 2 Hz [1]. These oscillations can lead to destabilize an alternator, a part of the network or the whole network causing a loss of the synchronism and consequently the entire system would collapse.

The objective is to ensure a maximum damping of the inter-area modes as well as of the local modes, using Power System Stabilizers (PSS) which are habitually used for the damping of electromechanical local modes. The additional signal is injected into the input of the AVR

[2].

Conventionally, to adjust PSS tuning, the equations of nonlinear system model are linearized around the operating point. Furthermore, the problem of the PSSs adjustment is that the location must be optimal.

The problem of ensuring better locations for PSSs can be determined by the participation factors and their parameters can be calculated by the method of residues [1]. Then, the final decision for PSS placement was made by looking at the changes of the eigenvalues after installation of a PSS at the machine closely related to this mode.

This work presents the application of our approach in a multi-machine power system as the Tunisian grid [2]. The simulation is done by PSAT / MATLAB.

II. POWER SYSTEM DYNAMIC MODEL

A. Machine Models

The synchronous machine is the main source of electrical energy in power system. The multi-machine modeling adopted in this paper uses as dynamical variables for each generator the angular velocity (ω), the rotor angle (δ), the internal voltage of quadrature axis q E_q^' and the internal voltage of quadrature axis d E_d^'[1, 3, 4].

Nonlinear dynamic equations of the each machine can be summarized as follows [5]:

$$\dot{\delta} = \Omega_b(\omega - 1) \tag{1}$$

$$\dot{\omega} = \frac{T_m - T_E - D(\omega - 1)}{M} \tag{2}$$

$$\dot{e}'_q = \frac{-f_s(e'_q) - (x_d - x'_d)i_d + V_f^*}{T'_{d0}} \tag{3}$$

$$\dot{e}'_d = \frac{-(e'_d) + (x_q - x'_q)i_q}{T'_{q0}} \tag{4}$$

Where ω is electric speed [rd/s], Te is Electrical Torque [p.u], Tm is Mechanical Torque [p.u], M is Mechanical starting time [p.u/s], D is Damping coefficient [p.u/p.u], SE is equation of the magnetic circuit saturation, id is d-axis current [p.u], iq is q-axis

current [p.u], xd is d-axis synchronous reactance [p.u], xd' is d-axis transient reactance [p.u], Td0' is d–axis open circuit transient time constant [p.u], Tq0' is q–axis open circuit transient time constant [p.u], xq is q- axis synchronous reactance [p.u], xq' is q- axis transient reactance [p.u] and Vf is field voltage [p.u].

III. POWER SYSTEM CONTROLLER

There are many types of power system regulators in order to enhance the stability, the margin of safety or the power transmitted by lines.

1. *Turbine governor and frequency controller*

The frequency controller acts on the servomotor to open and to close the control valves, also to change the speed of the generator. Thus, the role of the turbine is to drive the rotor of the synchronous generator speed. The tg is the variable of the speed control.

In our case the speed controller TG is type II, it is described by the following equation [5]:

$$\dot{t}_g = \frac{\frac{1}{R} * \left(1 - \frac{T_1}{T_2}\right)(\omega_{ref} - \omega) - t_g}{T_2} \quad (5)$$

Where ωref is reference speed [p.u], T1 is Transient time constant of turbine governor [s], T2 is Time constant of turbine governor [s].

2. *Voltage regulator*

Automatic voltage regulator (AVR) is used to regulate the output voltage through controlling the excitation field. This regulator is used to vary the external voltage of the filter Vm, the voltage of regulator Vr1, Vr2 and the field voltage Efd. The AVR is Type II.

It can be described as [5]:

$$\dot{V}_m = \frac{V_g - V_m}{T_R} \quad (6)$$

$$\dot{V}_{r1} = \frac{K_A\left(V_{ref} - V_m - V_{r2} - \frac{K_F}{T_F} * E_{fd}\right) - V_{r1}}{T_A} \quad (7)$$

$$\dot{V}_{r2} = -\frac{V_{r2} + \frac{K_F}{T_F} * E_{fd}}{T_F} \quad (8)$$

$$\dot{E}_{fd} = \frac{-(E_{fd}(K_E + S_e(E_{fd}) - V_{r1})}{T_E} \quad (9)$$

Where Vref is reference voltage [p.u], Vg is terminal voltage of the generator [p.u], KA, TA are Amplifier gain and amplifier time constant respectively [p.u/p.u] and [s], KF, TF are stabilizer gain and stabilizer time constant [p.u/p.u] and [s], KE, TE are Parameter stabilizer respectively [p.u/p.u] and[s].

3. *Voltage regulator*

Power System Stabilizers (PSSs) are typically used for damping power system oscillations. The PSS output signal is the state variable vs, which modifies the reference voltage vref of the AVR.

They usually consist of four blocks: an amplifier block, "filter washout" block, a phase compensation block and a limiter block.

In our study, we used type II. PSSs are defined by this equation, as follows:

$$\dot{V}_1 = -\frac{(K_\omega * V_{SI} + V_1)}{T_\omega} \quad (10)$$

$$\dot{V}_2 = \frac{\left(1 - \frac{T_1}{T_2}\right) * (K_\omega * V_{SI} + V_1) - V_2}{T_2} \quad (11)$$

$$\dot{V}_3 = \frac{\left(1 - \frac{T_3}{T_4}\right) * \left(V_2 + \left(\frac{T_1}{T_2} * (K_\omega * V_{SI} + V_1)\right) - V_3\right)}{T_4} \quad (12)$$

$$\dot{V}_{pss} = \frac{V_3 + \frac{T_3}{T_4} * \left(V_2 + \frac{T_1}{T_2} * (K_\omega * V_{SI} + V_1)\right) - V_{pss}}{T_\epsilon} \quad (13)$$

Where Vpss is voltage (PSS) [p.u], Tw is time constant filter [s], Kw is stabilizer gain [p.u], T1 is First stabilizer time constant [s], T2 is Second stabilizer time constant [s], T3 is Third stabilizer time constant

[s], T4 is Fourth stabilizer time constant [s].
"Fig. 1" presents the AVR and the PSS

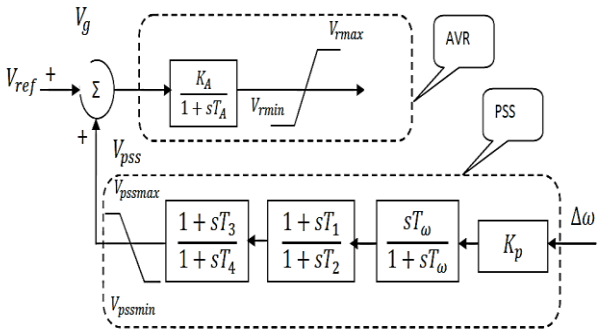

Fig .1. combinaison of AVR and PSS

IV. POWER SYSTEM CONTROLLER

The general dynamic equations of the relevant system can be expressed by a set of nonlinear differential equations in the following form:

$$\begin{cases} \dot{x} = \mathrm{f}(\mathrm{x}, \mathrm{u}) \\ y = \mathrm{g}(\mathrm{x}, \mathrm{u}) \end{cases} \quad (14)$$

Let x0 be the initial state vector, and u0 the input vector corresponding to the equilibrium point.

The linearized system of the equation(14), which includes a synchronous generator connected over transmission lines to an AC network, is represented as the following state-space model [6, 7]:

$$\begin{cases} \Delta\dot{x} = A\Delta x + B\Delta u \\ \Delta y = C\Delta x + D\Delta u \end{cases} \quad (15)$$

Where A is the power system state matrix of size (n * n), B is the input matrix of size (n * r), C is the output matrix of size (m * n), D is the feed forward matrix of size (m * r).

The variables described above and the linearized equations define the linear system are:

$$\begin{cases} \Delta X = [\Delta\delta_1\ \Delta\omega_1 \Delta E'_{q1} \Delta E'_{d1} \dots \Delta\delta_n \Delta\omega_n\ \Delta E'_{qn}\ \Delta E'_{dn} \Delta V_{m1} \\ \quad \Delta V_{r11} \Delta V_{r21} \dots \Delta V_{mn} \Delta V_{r1n}\ \Delta V_{r2n} \Delta tg_1 \dots \Delta tg_n]^T \\ \quad \Delta \mathrm{U} = [\Delta \mathrm{V}_{\mathrm{ref1}} \dots \dots \dots \Delta \mathrm{V}_{\mathrm{refn}}]^{\mathrm{T}} \\ \quad \Delta \mathrm{U} = [\Delta \mathrm{V}_{\mathrm{ref1}} \dots \dots \dots \Delta \mathrm{V}_{\mathrm{refn}}]^{\mathrm{T}} \end{cases} \quad (16)$$

Where ΔX is the state vector of dimension n, ΔY is the output vector of dimension m and ΔU is the input vector of dimension r.

A. Eigenvalues

The analysis of eigenvalues is a very effective tool to study the properties of the dynamic systems. The eigenvalues (λ) of the state matrix are given by the solutions of the characteristic equation of the state matrix A. It is defined by [1, 9, 10, 11]:

$$det(\lambda \mathrm{I} - \mathrm{A}) = 0 \quad (17)$$

Each eigenvalues has a real part of complex eigenvalues which provides the damping coefficient, and an imaginary part which gives the oscillation frequency. These are defined by the following expression.

$$\lambda = \sigma \pm j\omega \quad (18)$$

The system will be stable if all the eigenvalues have a negative real part in the complex plane.

The following relations give the frequency of oscillation:

$$\mathrm{f} = \frac{\omega}{2\pi} \quad (19)$$

The damping factor sets the decreasing of the oscillation amplitude. It is given by :

$$\xi = \frac{-\sigma}{\sqrt{\sigma^2 + \omega^2}} \quad (20)$$

B. Eigenvectors

The linear model of the power system can be represented and described by equation (14).

The eigenvectors is calculated. The right and left eigenvector related to the state matrix of the system by the following equations [12, 13]:

$$A\,\varphi_i = \lambda_i \varphi_i \quad (21)$$

$$\psi_i A = \lambda_i \psi_i \quad (22)$$

λ_i : the ith eigenvalues ; φ_i: the right eigenvector

For a state matrix of dimension n × n, the specific vector is a right column vector of dimension n x 1, while the left eigenvector is a row vector of dimension n × 1.

The two vectors are defined as follows:

$$\varphi_i = \begin{bmatrix} \varphi_{1i} \\ \varphi_{2i} \\ . \\ . \\ . \\ \varphi_{ni} \end{bmatrix} \quad , \quad \psi_i = [\psi_{1i} \quad \dots \quad \psi_{ni}]$$

The set of right eigenvectors of the system to form the right modal matrix is given as follows:

$$\Phi = [\phi_1 \quad \dots \quad \phi_n] \tag{23}$$

The left modal matrix is formed by the left vectors:

$$\Psi = [\psi_1^T \quad \dots \quad \psi_n^T]^T \tag{24}$$

The right vector φi shows the relative influence of each variable in an excited state. The eigenvector left ψi mode, it determines the set of state variables involved regarding the composition of ith mode.

C. Participation Factor

The participation factor, which combines both the right and left eigenvectors, is defined by a matrix of participation in the following form [14]:

$$P = [p_1 \quad p_2 \quad \dots \quad p_i \quad \dots \quad p_n] \tag{25}$$

Which

$$P_i = \begin{bmatrix} p_{1i} \\ p_{2i} \\ \vdots \\ p_{ni} \end{bmatrix} = \begin{bmatrix} \phi_{1i}\psi_{1i} \\ \phi_{2i}\psi_{2i} \\ \vdots \\ \phi_{ni}\psi_{ni} \end{bmatrix} \tag{26}$$

During the study of the stability at small disturbances, the participation factors allow the influence of a source of damping applied to a generator.

In the participation matrix P, as shown in equation (25), the jth column shows how the user participates with respect to the evolution of the state variables of the system while the line ith shows how the different modes involved relatively the evolution of the ith state variable [15].

$$P = \begin{matrix} \begin{bmatrix} p_{11} & \cdots & p_{1n} \\ \vdots & \ddots & \vdots \\ p_{n1} & \cdots & p_{nn} \end{bmatrix} & \begin{matrix} x_1 \\ \vdots \\ x_n \end{matrix} \\ \lambda_1 \dots \lambda_2 & \end{matrix} \tag{27}$$

The participation factors allow to us the identification of variables participants at specific oscillatory mode.

D. Residue

The residues give an idea about the influence of the input stabilization or its optimal location in a multi-machine power system. The transfer function affects only the behavior of inputs-outputs [1, 3].

Considering the following system :

$$\begin{cases} \Delta\dot{x} = A\Delta x + B\Delta u \\ \Delta y = C\Delta x \end{cases} \tag{28}$$

The transfer function is as follows:

$$G(s) = \frac{\Delta y(s)}{\Delta u(s)} = C(sI - A)^{-1}B \tag{29}$$

s: Laplace operator.
The function G (s) can be composed by simple elements as follows:

$$G(s) = \frac{R_1}{s - p_1} + \frac{R_2}{s - p} + \dots + \frac{R_n}{s - p_n} = \sum_{i=1}^{n} \frac{R_i}{s - p_i} = \sum_{i=1}^{n} \frac{R_i}{s - \lambda_i} \tag{30}$$

Where Ri is the residues of G(s) given by:

$$R_i = C\phi_i\psi_i B \tag{31}$$

V. CONTROL POWER SYSTEM

A. Optimal Placement of Power System Controller

When installing such as a controller in multi-machine networks, the first conventional step is to find its optimum location within the network.

To damp the local modes, the choice of location is still easy because the number of generators implicated mostly in local oscillations is very small.

On the other hand, for global modes, a great number of generators are generally associated with oscillations. That complicates the choice of the location of the PSS. In addition, a bad location of PSS can result in amplification of the oscillations, or contribute to the loss of stability of the system.

When a PSS is added in the system, it will affect all the electromechanical oscillation modes. Thus, the interactions between PSS must be considered when several PSSs are used [1].

All PSS should be adjusted to provide sufficient damping of all electromechanical modes because the damping of each mode has a cumulative effect on the contribution of each PSS.

Moreover, adjustment of PSS must be robust: PSS must be efficient not only during the change of the operating conditions but also when changing the network topology.

B. Design of PSS

To improve the stability of the system, the power system stabilizers that are simple and easy to install, practical, effective and cheap are often the most common stabilizers that are used to damp these oscillations as much as possible and also to increase the damping of oscillatory modes.

These parameters of PSS are adjusted sequentially and separately by method of residues [16].

The latter method of sequential setting usually gives satisfactory results for the damping of the oscillations. In this method, PSS are resolved in a phased manner [16]:

- First, the residual of transfer function at open loop system is calculated. Then a PSS is added and used the information of these residues.
- Next, a second PSS is introduced and set based on information of the residues with the first PSS.
- This process continues until the system reaches satisfactory stability characteristics.

The most method used for the selection of machines, which must be equipped with PSS, is the method of Participation Factors [1, 10, 14, 17, 18, 19]. The transfer function of the PSS for a system with an input / output is:

$$H(s) = K_p \frac{sT_w}{1+sT_w}.\left[\frac{1+T_1}{1+T_2}\right]^p = K_p H_f(s) \quad (32)$$

Where T_w: The constant of the high pass filter, T_1,T_2 : The time constants of the controller, p: number of blocks lead / lag phase, K_p:gain
"Fig. 2" presents the moving of eigenvalue to another value.

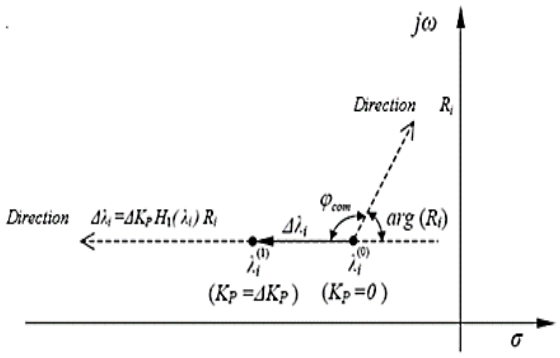

Fig. 2. Moving of eigenvalue

Moving these eigenvalues may be calculated by the following equation [20]:

$$\Delta\lambda_i = |\lambda_{i1} - \lambda_{i0}| = R_i H(\lambda_i) \quad (33)$$

Where are calculated in equation (31)
The methodology of sizing residue is divided into three stages

- Sizing the filter "washout" We usually take Tw = 5s [1].
- Sizing Block lead / lag phase: the total phase shift required φ_com is calculated from the residue of the critical mode. The phase angle required to direct the direction of the residue R_i so that the eigenvalue λ_(i)moves parallel to the real axis can be calculated by the following equation:

$$\varphi_{com} = 180° - \arg(R_i) \quad (34)$$

The time constants T1 and T2 can be determined by:

$$T_2 = \frac{1}{\omega_i \sqrt{\alpha}} \quad (35)$$

$$T_1 = \alpha . T_2 \quad (36)$$

With :ω_i : est la fréquence du mode λ_i en rad/sec

$$\alpha = \frac{1 - \sin\frac{\varphi_{com}}{p}}{1 + \sin\frac{\varphi_{com}}{p}} \quad (37)$$

- With a good lead-lag compensation, controller efficiency is related to the gain 〖 K〗_p [16]. Consequently, when we have a change of K_p, all modes of oscillation will be influenced.

To calculate the gain 〖 K〗_p, here is the transfer function following PSS:

$$H(s) = K_p H_f(s) \quad (38)$$

Based on the equations (33) and (38), the gain value K_p is given by the following expression:

$$K_p = \left|\frac{\lambda_{i1} - \lambda_{i0}}{R_i H_f(\lambda_i)}\right| \quad (39)$$

The output signal y(s) may be selected based on the maximum value of the residue data selected by the outputs [19].

In fact, not all the generators associated with electrical networks need to be equipped with PSS since they do not participate in all of the most dominant electromechanical modes.

Therefore, the first step is to find the optimal locations of PSS needed and determine their number using important information provided by the factor of interests whose goal is to achieve better damping compared to given criteria.

VI. RESULTS AND SIMULATIONS

The local modes are the most recurrent modes encountered in power systems. They are associated with oscillations between a generator (and a group of generators) of a power plant and the rest of the system.

The local modes and inter modes, with frequencies of these oscillations are typically in the range of 0.2 to 2 Hz, are studied. This application was processed on the Tunisian network system generation and transmission of electric power STEG.

It consists of a network for transferring electrical energy production centers to consumption centers which are geographically often far away from each other.

Tunisian network (2012 version) consists of 3 wind farms, 172 lines, 83 transformers, 33 generators, 75 knots consumers.

A. Application on the Tunisian network

Initially, before the use of PSS, yet we had to ensure adequate damping of the oscillations, the method of residues will allow us to provide better localization of PSS and better coordination of their parameters [2].

1. Location of PSS

The electromechanical generator participation factor is the first method used in this study; it allows us to determine the participation of a machine in each mode. Thus, for a desired mode to be damped, the machine that participates the most is the machine where the PSS should be installed.

In our case, 14 generators mainly participate in 11 modes.Next the frequency of each mode and the associated generator, the type of each mode is determined. Then 11 modes are selected:

- 3 modes of interregional –type.
- 8 modes of local type.

The results are given in "Tab.1":

Table 1. Participants Generators

N° Mode	Eigenvalue	Fre-quency	Generators participants	The mode type
1	-0,99146± 10,3388i	1.653	G1	Local
2	-0,66359± 11,8818 i	1.894	G3, G4	Local
3	-0.92013± 7.1822 i	1.1524	G10, G18	Local
4	-0.43648± 8.1696 i	1.3021	G11	Local
5	-0.77795± 11.3363 i	1.8085	G13	Local
6	-0.51007± 5.6611 i	0.90463	G15, G23	Interrégional
7	-0.49009± 5.8498 i	0.93429	G16	Interrégional
8	-0.44439± 11.2483 i	1.7916	G19	Local
9	-0.89544± 7.2212 i	1.1581	G22	Local
10	-0.73736± 11.9208 i	1.9009	G27	Local
11	-0.33778± 5.2691 i	0.84032	G33	Interrégional

Factor analysis of participation shows the influence of each generator in that mode. If the participation of a generator is relatively small, the placement of a PSS on this generator provides little improvement.

"Fig.3" and "Fig.4" show the participation factors (PF) associated to the angle and the speed variations of each generator for the 11 electromechanical modes.

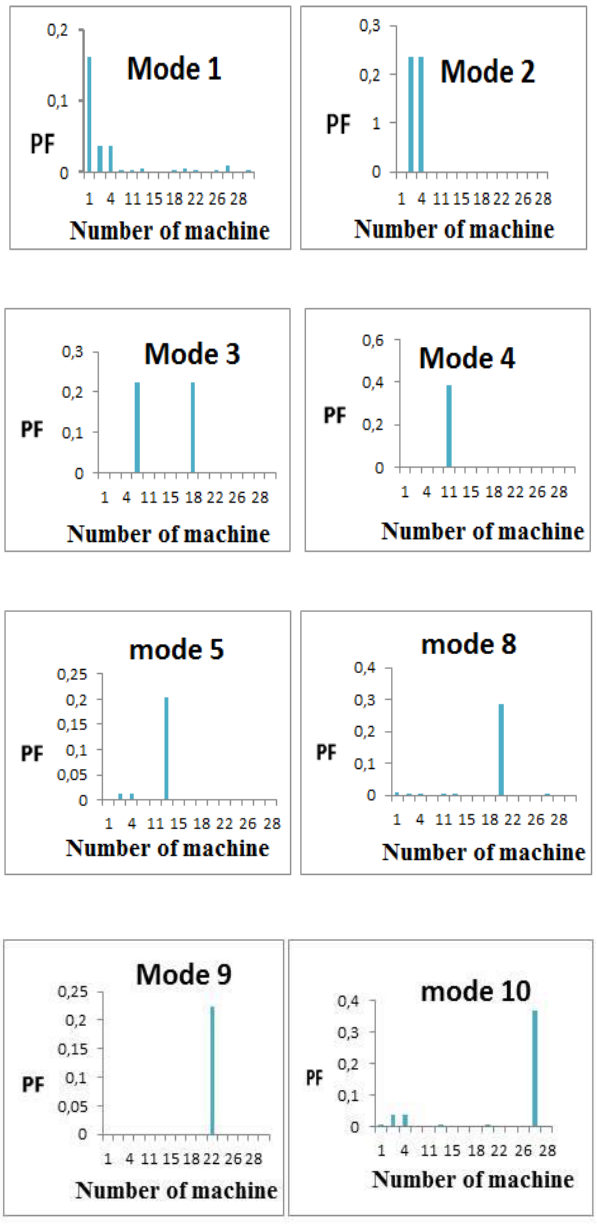

Fig. 3.The participation factors (PF) of local modes

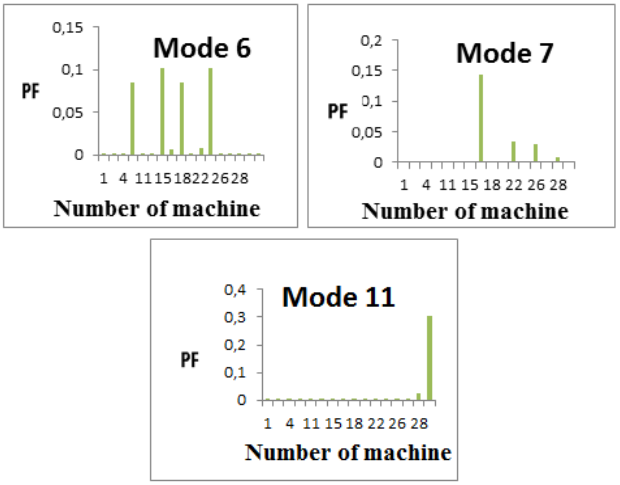

Fig. 4. The participation factors (PF) interregional modes

2. Setting the parameters of the PSS

To restore system stability and improve its overall damping, the PSS is added to the desired generators. In the remainder of this section, the residue method is used to determine the parameters of the PSSs. These are summarized in "Tab.2":

Table 2. Parameters of PSS by the residue method

PSS	N° G	KPSS	T_1=T_3	T_2=T_4
1	1	0.0099	0.7970	0.0117
2	3	0.0538	0.3196	0.0222
3	4	0.6756	0.1053	0.0673
4	10	0.0147	2.9297	0.0066
5	11	1.4230	0.1922	0.0780
6	13	0.0022	0.9039	0.0086
7	15	3.3088	0.1889	0.1652
8	16	0.5092	0.4494	0.0650
9	18	0.0147	2.9324	0.0066
10	19	0.0396	0.5533	0.0143
11	22	8.2752	0.1618	0.1185
12	23	3.3062	0.1888	0.1653
13	27	0.4044	0.1744	0.0403
14	33	0.3312	0.9549	0.0377

1. Analysis of the eigenvalues

To demonstrate the effectiveness of the proposed approach, two cases are considered:

- Without PSS
- With PSS

The eigenvalues electromechanical modes for the both cases, their improvement and the improvements of the damping are given in “Tab.3”:

Table 3. Improving eigenvalue and damping

N° G	Eigenvalue without PSS	Eigenvalue with PSS	improvement of Eigenvalue	Imrovement Of damping
1	-0,99146±10,3388i	-1,0142±10,3394	2%	17%
3	-0,66359±11,8818i	-0,74261±11,9396i	8%	2%
4	-0,66359±11,8818i	-0.71031±11.8841i	5%	2%
10	-0.92013±7.1822i	-0.92906±7.2014i	1%	1%
11	-0.43648±8.1696i	-0.44521±8.0851i	1%	1%
13	-0.77795±11.3363i	-0.8044±11.4987i	3%	2%
15	-0.51007±5.6611i	-0.5361±5.6987i	3%	3%
16	-0.49009± 5.8498i	-0.49903±5.85i	1%	1%
18	-0.92013±7.1822i	-0.92906±7.2014i	1%	1%
19	-0.44439±11.2483i	-0.55527±11.2923i	11%	2%
22	-0.89544±7.2212i	-0.90357±7.228i	1%	1%
23	-0.51007±5.6611i	-0.53523±5.8241i	3%	3%
27	-0.73736±11.9208i	-0.74291±11.9542i	1%	1%
33	-0.33778±5.2691i	-0.48524±5.1309i	15%	1%

Based on the analysis of the eigenvalues of the system, the electromechanical modes (local and inter) are improved.

To see this improvement, here is the breakdown of some eigenvalues in the complex plane which are given respectively in” Fig.5”.

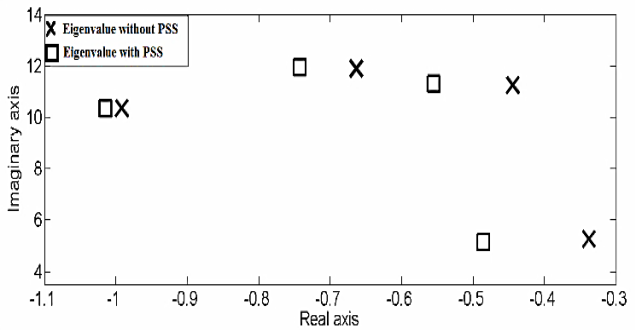

Fig. 5. Distribution of some eigenvalues in the complex space

As a second step, the performance and robustness of the setting of these regulators are evaluated. To do this, time domain simulations of the system in the presence of severe disturbance is done: load variation for both cases “Fig.6” and “Fig.7”:

- Before location of PSS.
- After location of PSS.

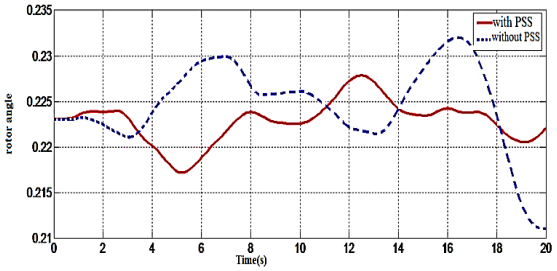

Fig. 6. Variation of the rotor angle for the machine 11

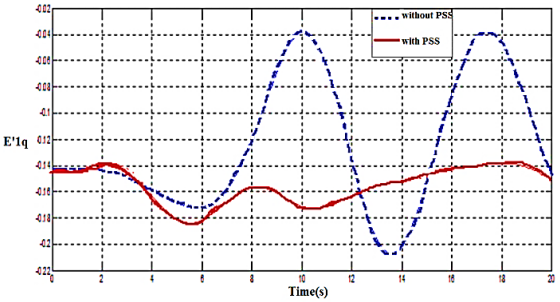

Fig. 7. Variation of the transient voltage 〖E'1〗_q for the machine 11

The amplitude of oscillations is reduced in the presence of PSS and the system becomes more

stable in less time if compared to the network without PSS.Finally and after a simulation of the selected Tunisian improved network software. “Fig.8” showing the location of the eigenvalues of the system in the complex plane.

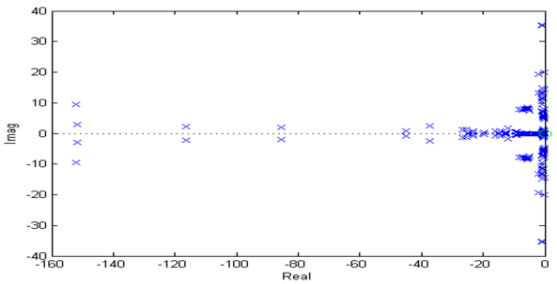

Fig. 8. Position of the eigenvalues of the Tunisian system

The most of the eigenvalues has a negative real part. The system is then stable.

V. CONCLUSION

Power systems continue to grow. The extension of networks interconnected makes them highly sensitive to interregional oscillations. These oscillations can severely restrict the transport of electrical energy.

Under these new conditions, operators of electrical networks are often required to operate the systems to the limits of stability. Therefore, improving the stability to small perturbations represents an objective.In this work, the problem of the dynamics of a network of multi Machine stability distribution was handled. The nonlinear model of a network of electric power multi machine was developed. The nonlinear model was linearized to derive the model Philips-Heffron.Using the method of residues based on the eigenvalues of the system; providing, passing by the conventional method of participation factors, not just a calculation of parameters stabilizers PSSs, but also a better location and an interesting reduction in their number.
In this study, the PSSs satisfy both the damping of inter modes also the damping of local modes As perspective, the utility of using the method of residues on another network that combines two different regions of the world such as interconnection Tunisia-Libya will be validated.

REFERENCES

[1] ALKHATIB, H. (2008) Etude de la stabilité aux petites perturbations dans les grands réseaux électriques : optimisation de la régulation par une méthode méta heuristique. Thèse de doctorat, Université Paul Cézanne d'Aix-Marseille,

[2] Rim, B. S. Mariam, D. (2014) Etude De La Stabilité Statique Du Réseau Tunisien Et De L'interconnexion Tunisie-Lybie. projet de fin d'étude, ENIS,

[3] Kalifullah A. Palanis., H. (2014) Optimal Tuning of PI Power System Stabilizer For Multi Machine Power System Using Harmony Search Algorithm. JATIT,

[4] Asrar Ur Rahman, M. Sabah ul Islam M, and Abdul Hafeez Ansari M. (2014) Enhancing Power System Oscillation Damping Using Coordinated PSS and SVC Controller. IJESI,

[5] Milano, F. (2006) Power System Analysis Toolbox Documentation for PSAT» version 2.0.0

[6] Wang,Sh. K, Ji-Pyng Chiou,Ch. W. L. (2008) Parameters Tuning Of Power System Stabilizers Using Improved Ant Direction Hybrid Differential Evolution . ELSEVIER,

[7] Ali, E. S., Abd-Elazim, S. M. (2013) Optimal Power System Stabilizers Design For Multimachine Power System Using Hybrid BFOA-PSO Approach . dep of wseas transactions on power systems,

[8] Usman, J. Mustafa,M. W.and Aliyu,G. (2012) Design Of AVR And PSS For Power System Stability Based On Iteration Particle Swarm Optimization.

[9] Zitouni M. F. (2010) Amélioration de la Stabilité Transitoire des Réseaux Electriques par l'utilisation des Systèmes FACTS.

[10] Febres C.A.T., Araujo P.B. Damping of Low-Frequency Oscillations by Supplementary Control of Power System Stabilizers .

[11] Sumina .D, Bulic, Miskovic, N.M. (2011) Parameter Tuning Of Power System Stabilizer Using Eigenvalue Sensitivity », ELSEVIER,

[12] Kartubi, L. (2006) Optimisation de la Synthèse des FACTS par les Algorithmes Génétiques et les Essaims Particulaires pour le contrôle des Réseaux Electriques., p43

[13] Bragason R. F. (2008) Damping In The Icelandic Power System Small Signal Stability Analysis And Solutions. Dept. of Industrial Electrical Engineering and Automation Lund University,

[14] Duc, H.N.(2011) Amélioration De L'amortissement Des Oscillations De Puissance Du Réseau Electrique Les Dispositifs Facts Et Les Mesures A Distance .

[15] Custem T.V., (2002) Systèmes Electriques de Puissance II. Cours ELEC 047, Département d'Electricité, Electronique et Informatique : Institut Montefiore, Université de Liège,.

[16] Yee S.K. and Milanovic J.V (June. 2004) Comparison Of The Optimization And Linear Sequential Method For Tuning Of Multiple PSSs. IEEE Power Engineering Society, General Meeting Denver, CO,.

[17] Mekki K. (2002) Mesures Synchronisées par GPS pour une Meilleure Stabilité des Réseaux.

[18] Zea A. A. (2013) Power System Stabilizers for the Synchronous: Generator Tuning and Performance Evaluation.

[19] Sebaa M. K. (2008) Commande intelligente pour l'amélioration de la stabilité dynamique des réseaux d'énergie électrique .

[20] Ammari S. (2000) Interaction des dispositifs Facts avec les charges dynamiques dans les réseaux de transport et d'interconnexion

THE VSAS APPROACH GIVES THE BEST MPPT FOR SOLAR ENERGY SOURCES (RES)

Nacer K.[1], M'Sirdi N. K.[2], Rabhi A.[3], Nehme B.[4]
[1]Laboratory of Systems and Information Sciences of Aix Marseille University (LSIS - AMU),
[2]CNRS UMR 7296, Domaine Universitaire Saint-Jerome, Avenue Escadrille Normandie-Niemen, 13397 Marseille Cedex 20, France.
[3]MIS, Laboratory of Modeling, Information and Systems, University of Picardie Jules Verne Amiens, France
Authors are members of the HYRES Lab and the RMEI Network.
[4] Département de Génie Électrique et Électronique, Faculté d'Ingénierie, Université Saint-Esprit de Kaslik, B.P. 446 Jounieh, Mont Liban – Liban.

Abstract - More and more MPPT (Maximum Power Point Tracking) algorithms are in competition to maximize energy extracted from PV systems. This paper shows how to get the best algorithm (the most simple, fast and robust). VSAS (Variable Structure Automatic Systems) control methodology is applied to develop the control algorithm, to clarify the rationale behind and get the best optimization algorithm.

Keywords - Maximum Power Point Tracking, Renewable Energy Sources, Perturb and Observe, IncCond, Hill Climbing.

I. INTRODUCTION

The PV system operation principle needs a polarization depending on the weather to fix the operation point leading to extraction of the maximum power. The Renewable Energy Systems (RES) include commutations and discontinuities; this is one kind of Variable Structure System (VSS). However, the behaviour of the conversion systems of this kind of renewable energy is VSAS (Variable Structure Automatic Systems)[MsirdiEFEA14] and highly dependent on variations in climate parameters, such as temperature and irradiation.

The MPPT algorithms are necessary to maximize, at each time instant, the produced power. Several techniques have been designed to search this optimal Maximum Power Point (MPP). In the literature, more and more MPPT (Maximum Power Point Tracking) algorithms are in competition to maximize energy extracted from PV systems.

The maximum performance of a photovoltaic system depend, of course, on good weather conditions, but needs also appropriate MPPT algorithm [Mutoh, NianChun]. The great majority of MPPT control strategies are based on the (steady state) characteristics of PV panels, such as I-V or P-V plots, the duty cycle ratio control and sometimes using look-up tables [Amei]. A lot of MPPT techniques are well established in the literature. There are several methods: voltage feedback method, perturbation and observation method, linear approximation method, incremental conductance method, hill climbing method, actual measurement method, fuzzy control method and so on [Ting-Chung, Tavares, Hua Lin, Fangrui, ChihChuanHua, Weidong]. In general, there exist four types of MPPT techniques:

- the PV operation point perturbation and observation (PO) based algorithms in order to get the direction of tracking the MPP.
- the hill-climbing algorithm which makes a perturbation in duty cycle to reach the apex of the characteristics.
- the incremental conductance (InCond) algorithm which periodically checking heslope (conductance) of the P-V curve [Liu].
- the constant voltage algorithm based on keeping constant the ratio between the PV voltage at the maximum power and the open circuit voltage (Voc) value; In this method the effect of solar irradiance variations is neglected [Hohm].

In[IbrahimHoussiny, Amei], Ibrahim and Houssing use a look-up table to track, when other author prefer the use of a dynamic MPP tracker to PV appliances [MidyaKerin]. A single-stage MPP controller using the slope the power versus voltage, like has been done in [KuoLiangChen]. In [Hua Lin] a

DSP chips is used to implement the PO MPPT in order to get maximum power. They, also try to improve the efficiency of the PO and HC methods.

In [Fangrui], the time response of PO [ChihChuanHua]and HC methods [Fangrui, Weidong, Hohm]are compared for a grid connected system. The PO method can fail under rapidly changing atmospheric conditions. Several research activities have been carried out to improve the traditional Hill-climbing and P&O methods. Reference [Xiao] proposes to use three measurement points to compute MPP.

The method compares the obtained power measurement to the two preceding points before choosing the perturbation sign. In [KuoLiangChen] the authors propose a two stage algorithm that offers faster tracking in the first stage and more accurate tracking in the second stage. To prevent divergence from MPP, they use a modified adaptive algorithm.

Table 1. Parameters Definition

Symbol	Units	Definition
q	q=1.6.1 0 −19 C	The electron charge
n	diode non-ideality factor	
K B	1.38065·1 0 −23 N.m/K	the Boltzmann's constant
STC	at (1kW/m2, 25°C)	Standard Test condition
I SC	A	Short Circuit Current
I SC,STC	A	Short circuit current at STC
V OC	V	Open Circuit Voltage
K 0	% calculated for ISC	Temperature coefficient
G	W/m2	Solar radiation
T	in Kelvin °K	the cell temperature
T 1,ref	at 1kW/m2, 298K (25°C)	Reference temperature
T 2,ref	K	Temperature at 2nd STC
V ref	Vref =5V	Reference voltage

In [Tina]Tina et. al. proposed a mathematical model for the electrical-thermal coupling of a PV module with ambient temperature, wind speed, wind direction, relative humidity and electrical operating point (voltage and current values). An MPP tracking based on Dual boost converter is developed using fuzzy logic in [Veerachary]. Artificial neural network (ANN), trained offline with a gradient descent algorithm using a back-propagation have been used by Kaiser et. al.

[Kaiser] to generate (online) the reference voltage for MPPT control, in a solar electric vehicles. Another approach based on variable structure control is applied to a buck converter in [MiaoJie]. In [Ting-Chung],

the authors study and compare three maximum power point tracking (MPPT) algorithms, under different climate conditions, in a photovoltaic simulation: the algorithms of perturbation and observation (PO), incremental conductance (INC) and hill climbing (HC), respectively (see also [Hohm]). They show that the photovoltaic simulation can track the maximum power accurately using the three MPPT algorithms. PO algorithm has fast dynamic response and well regulated PV output voltage than HC algorithm. Since the INC algorithm is more complex, the time response of INC is a little longer.

All of the MPPTs are based on the convex nature of the power characteristic curve and ignore that the characteristic can change in time when the temperature or irradiation changes[Shaefer, Kim]. As the weather conditions change during time, the Maximum Power Point varies also with time. The maximum power point (MPP) changes from one curve to another, with solar irradiation or load variations.

The paper is organized as follows. Section 1 gives the problem formulation and recalls most used algorithms used for MPPT. The second section presents PV system equations and features. Section three introduces our new algorithm design approach. We compare their results with the widely used MPPT algorithms; performance is evaluated considering different actual solar irradiation measured variations. The fourth section gives a conclusion and proposes perspectives.

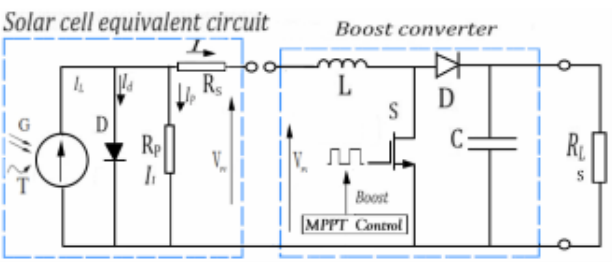

Fig .1. Equivalent circuit model of PV panel

II. PV SYSTEMS CONTROL

A. Solar Energy Sources

In this section we present the models of the PV systems. The simulation of the energy behavior of RES (Renewable Energy Source) is developed and several control methods and parameters can be analyzed. The goal is to obtain a good model of the process and to achieve a realistic simulation to enable us to check and validate our approach of Optimal MPPT and control.

1. *The Solar irradiation Model*

The electric power operating by a PV panel depends on the irradiation intensity of the sun shining, and the temperature of the PV cells. The simplest solar radiation, perturbation free, model that can be used is the following, from (roughly) 7h-19h, the period of sunshine. At the top of the sinusoid, the maximum power is assumed to be 1kw/m², at the time 13 hours. The sunless period is 19h-31h [schijndel1, Sallem]. Note that the wave is assumed piecewise sinusoidal. The solar radiation is represented by the following expression:

$$G_S = \{G_{S-pic} \sin\left(\frac{2\pi t}{3600}\right) \text{ if } t \in [\,7h, 19h\,] \quad (1)$$

The electric diagram is equivalent to an average PV cell as shown in figure 1

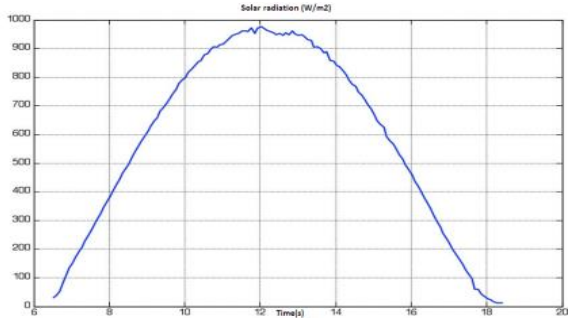

(a)

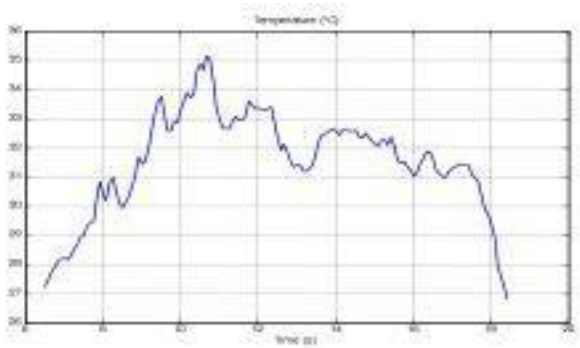

(b)

Fig .2. a) Measurement of Solar irradiance taken for a day; b) Temperature taken for a day

2. *Photovoltaic Systems Model and characteristics*

A PhotoVoltaic Generator consists of a group of PV modules electrically connected in series or parallel or series-parallel combinations with each other in a RES to generate required currents and voltages [MsirdiEFEA14, Liu].

The model is a photo-current source IL one diode with as reverse saturation current I0 , and a serial resistance RS , representing the PV cell resistance. The circuit is connected to the load (R L) trough a converter in order to adjust (adapt) the operating voltage and current of the PV panel at optimal values to maximize the harnessed power and transmit it. The control has to tracks the Maximum Power Point.

The equations describing the I(V) relationship between the current and voltage of a solar cell are given by (2), with the parameters defined in Table1 [Shaefer, Hsiao, Walker].

$$I = I_L - I_0\left[\exp\left(\frac{q(V-R_sI)}{nK_BT_s}\right) - 1\right] - \frac{V+R_sI}{R_P} \quad (2)$$

$$I_0 = I_0(T_1)\left[\exp\left(\frac{V_{OC}(T_{1,ref})}{nK_BT_{1,ref}/q}\right) - 1\right] \quad (3)$$

The internal serial resistance RS relative to one cell in open circuit voltage VOC is:

$$R_S = -\frac{dV}{dI}\Big|_{V_{OC}} - \left(\frac{nK_oT_{1,ref}}{q}\right) / I_0(T_{1,ref}) \exp\left(\frac{V_{OC}(T_{1,ref})}{nK_BT_{1,ref}/q}\right) \quad (4)$$

The PV output voltage of the serial cells can be expressed as V:

$$V = N_S \frac{nK_BT}{q} ln\left(\frac{I_{SC}-I}{qI_0}\right) \quad (5)$$

IL varies as a function of the ambient temperature T and of the solar radiation G as:

$$I_L = I_L(T_{1,ref}) + K_o(T - T_{1,ref}) \quad (6)$$

With $K_o = \frac{I_{SC}(T_{2,ref}) - I_{SC}(T_{1,ref})}{T_{2,ref} - T_{1,ref}}$ (7)

$$I_L = I_{STC}(T_{1,ref,STC}) \frac{G_S}{G_{STC}} \quad (8)$$

The PV system exhibits a nonlinear I(V) characteristic which depend on the temperature and the solar radiation which vary during a day, for exemple, as shown by the figure TempRadiation; where a) and b) show the profile of real irradiation measured and temperature for one day.

The photovoltaic Panel considered, in this paper, contains 36 photovoltaic cells connected in series. To track the Maximum Power Point (MPPT) and achieve the optimum matching, a good control of the DC-DC is necessary. As the temperature, insulation and load vary, an algorithm is used to ensures that the PV module always operates at its maximum power point. The boost converter operation principle is the one of Variable Structure System (VSS). The Switching frequency of the Boost IGBT (changing s) is in general around fsw = 1/Ts =20kHz . We will try to use, in the comparative analysis different frequency values.

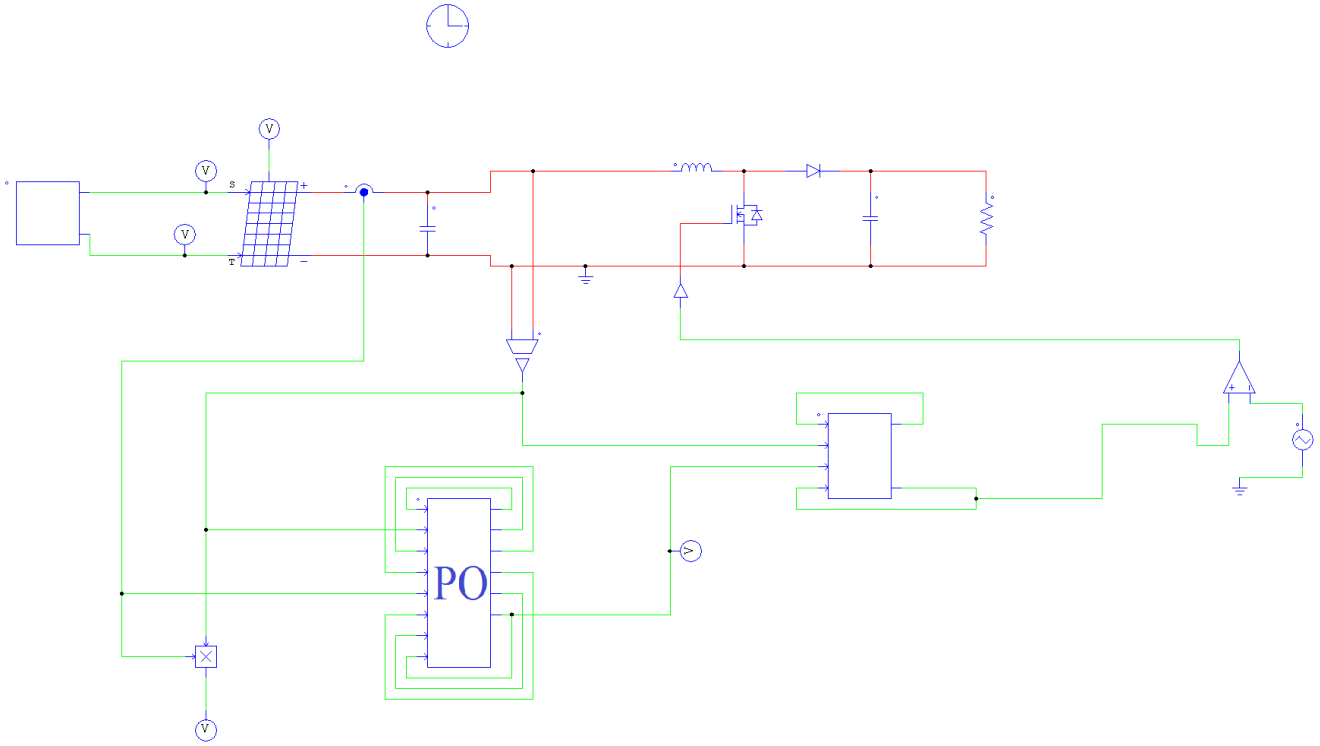

Fig .3 Shows the electric circuit diagram of a PV panel connected to a DC/DC converter with the MPPT control circuit based on PO.

B. The MPPT Controls for PV Systems

This part reviews 3 of the most frequently used control algorithms to get the maximum power. As presented previously, an MPPT controller is used to increase the PV system efficiency. The principle is to calculate the optimal reference output voltage and/or current which ensures that the PV system operate at its MPP. These techniques are different from each other in many aspects, including simplicity, convergence speed, hardware implementation, sensors required, cost, range of effectiveness and need for parametrization (see eg [Shaefer] for a survey).

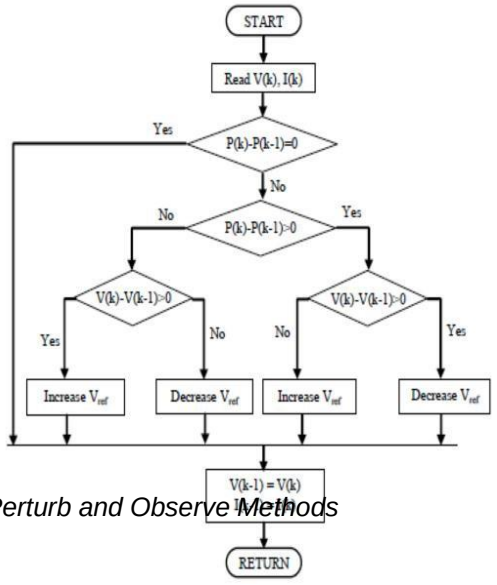

1. Perturb and Observe Methods

The most commonly used MPPT algorithm is the Perturbation and Observation (PO) due to its easy implementation. It uses the P-V characteristics Ppv=f(V) of the PV module. Note that, for constant weather conditions, the operating power point P(n)=V(n)I(n) is obtained when the condition dP/dV=0 is accomplished. We can calculate the slope (dP/dV) using consecutive outputs measurements (voltages and output):

$$\frac{dP}{dV}(n) = \frac{P(n)-P(n-1)}{V(n)-V(n-1)} \quad (8)$$

- If the operating voltage of the PV array is perturbed in a given direction and DP/DV>0, then the perturbation moves the array's operating point toward the MPP. The PO algorithm would then continue to change the PV array voltage in the same direction.

- If DP/DV⟨0 then the change in operating point moves the PV array away from the MPP, and the PO algorithm reverses the direction of the perturbation [Femia].

Some limitations are encountered such as: oscillations around the MPP in steady state operation, slow response speed, and even tracking in wrong way when atmospheric condition instability [Kim, Liu, Femia].
The duty cycle of the Boost is changed and the process is repeated until the maximum power point has been reached. In actual experiments, the system oscillates around the MPP. To minimize the oscillations amplitude, we can reduce the perturbation step size. However, small step size slows down the convergence of the MPPT.

To solve this problem, we can use smaller perturbation size towards the MPP.

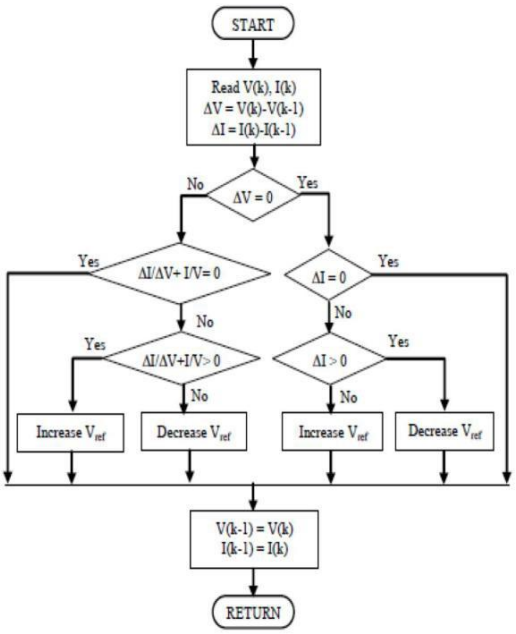

2. Perturb and Observe Methods

The incremental conductance (IncCond) [Femia], method is based on the fact that the slope (or the PV conductance G= dI/dV) of the PV array, in the power curve is zero at the MPP and it is positive (constant) on the left of the MPP. The slope becomes negative on the right of th MPP. These relations can be rewritten in terms of the array current and voltage as:

$$\frac{dP}{dV} = \frac{dVI}{dV} = I\frac{dV}{dV} + V\frac{dI}{dV} = I + \frac{dI}{dV}$$

to keep DP/DV = 0 we need: G=dI/dV=-I/V; DP/DV = 0 at the MPP

- If $G = \frac{dI}{dV} > -\frac{I}{V}$ (this means that $dP/dV > 0$), the operating point is on the left side of the MPP, V has to be raised.
- If $G = \frac{dI}{dV} < -\frac{I}{V}$ (dP/dV<0), the operating voltage is on the right side of the MPP then V has to be reduced.

voltage is on the right side of the MPP then V has to be reduced.

3. Hill Climbing Method

In general the almost applications, use DC-DC converters and DC-AC inverters, as the power interface devices between PV modules and loads. The basic idea of the HC (Hill Climbing) method is the

same as P&O method. It tests if P(n) is greater than P(n-1) or not, to reach MPP. The PO method uses instead a test on dP/dV to determine whether the maximum power point has been found or not. However, the HC method uses a test condition on P(n)-P(n-1) and uses the duty cycle (D) of these switching mode power interface devices as the decision action parameter for the maximum power point tracking. The figure7 shows a flow diagram of the hill climbing algorithm.

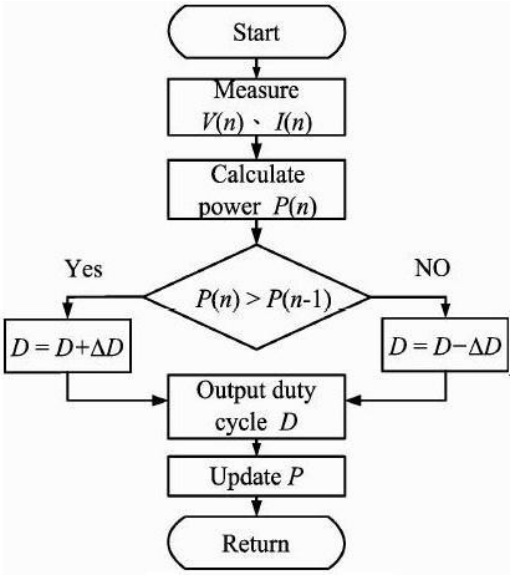

4. The Proposed VSAS-MPPT Algorithms

The desired objective to get is that the MPP reached when the maximum power is obtained (P(t)=Pmax and dP/dt=0). The power is function of the voltage V, the current I and the time t, then the required Maximum Power Point to Track is really defined by the following objective function:

$$\frac{dP}{dt} = \frac{dVI}{dt} = I\frac{dV}{dt} + V\frac{dI}{dt} = 0 \quad (8)$$

Let us consider the control in case of discrete time, then the fetched MPPT may be defined by ΔP(k)=0,

$$\begin{cases} \Delta I = I_{PV}(k) - I_{Pv}(k-1) \\ \Delta V = V_{PV}(k) - V_{PV}(k-1) \\ \Delta P = P_{PV}(k) - P_{PV}(k-1) \\ P_{PV}(k) = V_{PV}(k).I_{PV} \end{cases}$$

$$\Delta P(k) = I(k).\Delta V(k) + V(k).\Delta I(k)$$

$$\Delta P(k) = I(k).u_1(k) + V(k).u_2(k)$$

The two control variables are then u1(k)= ∆V(k) (the voltage variation) and u2(k)=∆I(k) (the current variation).

5. RUCA: Robust Unified Control Algorithm

For the proposed RUCA algorithm, both control inputs can be used if we look for adjusting both variables (V and I), either at each control step or alternatively. It can be noticed that the previous algorithms can be considered as particular cases of this one, when simplifying the proposed control method. P max is a constant chosen greater than the maximum power in any weather condition Pmax≥P(t) . Let us then consider the Lyapunov like function

$$W(t) = (P^2{}_{max} - P(t)^2) > 0$$

which is strictly positive everywhere (∀t, ∀I, ∀V). The derivative of the proposed Lyapunov function W(t)=(P^2〗 _max-〖P(t)〗^2)>0 , is

$$\dot{W}(t) = -P(t)\frac{dP(t)}{dt} = -P(t)(I\frac{dV}{dt} + V\frac{dI}{dt})$$

$$\dot{W}(t) = -I^2V\frac{dV}{dt} - V^2I\frac{dI}{dt})$$

t can be made negative by choosing the appropriate control laws u1(k)= ∆V(k)and u2(k)=∆I(k) to get a decreasing Lyapunov function. The RUCA uses two control inputs which can be done either simultaneously or alternatively or one of them can be frozen depending on the needed voltage or current. Choosing

u1(k)= Kα∆P(k)sign(∆V(k))

u2(k)=K_2 α_2 ∆P(k)sign(∆I(k))

ensures that W ̇(t)<0 and then the convergence of the RUCA algorithm. This proves, theoretically also the convergence of the MEPO algorithm which follows. We can use both inputs or only one of them either, in a first case u1(k)= Kα∆P(k)sign(∆V(k)), or in the second case u2(k)=K_2 α_2 ∆P(k)sign(∆I(k)). In control context, the previously presented MPPT controllers use only one control variable u1 or u2 and impose the second to be zero. The implementation of the proposed enhanced MPPT controller RUCA can be summarised as follows:

- The reference voltage is set be equal to the double of the PV open circuit voltage.
- Measurement of the of input signals (PV voltage,

PV current and Load voltage).

- Estimate the PV power at the sample time k : PPV (k)= Ipv(k).Vpv(k)

- Calculate the PV current and PV power increments (see equation eq:optim).

6. MEPO: Modified Enhanced PO Algorithm

If we take as input u1(k) and put a constant current u2(k)=0 , which means that the voltage is perturbed and the current is fixed u2(k)= ∆I(k)=0 , we are in the same configuration as the PO algorithm. We propose, as a Modified Enanced PO Algorithm which will be more robust, the reference voltage is given by Vref=Vk+ Kα∆P(k)sign(∆V(k)) Knowing that we impose ∆I(k)=0 , we get for the proposed MEPO control algorithm we take u1(k)= Kα∆P(k)sign(∆V(k)) and u2(k)= ∆I(k)=0 . The reference voltage Vref(k) is calculated as below, where α is a gain weighting the perturbation variation step. Note that ΔVref= αsign(∆P(k)∆V(k)) produces exactly the same result as the classical PO algorithm with a much simpler implementation. This method gives an enhanced variable step size algorithm. The step size is adjusted in proportionally to the power variation produced in the previous step. The adaptive step adjustment gain K is used with ∆P(k), for weighting the variation (Voltage perturbation) step. It is useful for oscillation avoidance, fast convergence and noise sensitivity reduction. We can also use only the control variable u2 (k)= ∆I(k) (and put u1(k)=0), the current is perturbed and the voltage is fixed ∆V(k)=0.

C. Comparative Simulations and Tests

The simulation was performed under Psim software as shown in figure 3. The physical model of a PV panel is used. The panel is considered to have 36 cells. A boost converter is built using a MOSFET as a switch. The load is a 100 Ω resistor. The algorithms are implemented in a C block and the duty cycle is calculated from Vref using another C block. The actual, measured irradiation and panel temperature are read from a txt file as inpt to the simulation.

1. MPPT Alghorithms Comparison

In this study we compare four MPPT algorithms under the same experimental conditions. The first algorithm called P&O stands for perturb and observe. The second algorithm called IncCond stands for incremental conductance. The third algorithm called MEPO stands for Modified Enhanced Perturb and Observe (from VSAS- MPPT). And the fourth algorithm called RSMCA (from VSAS-MPPT approach) stands for Robust Sliding Mode Control Algorithm. Note that RUCA algorithm is simply combining use of the two VSAS MPPTs alternatively.

The comparison is made under changing values of irradiation and temperature. Two cases are considered: first we update the irradiance and temperature each time without interpolation to create sudden variation in power output, second we interpolate the values of irradiance and temperature to create quasi-continuous irradiation and temperature. At the end we use real measured data for simulation. In this study we focus on the PWM commutation frequency of the MPPT algorithm.

2. Zero Order Hold Interpolation Analysis

We perform many simulations with varying irradiance and temperature. The values are not interpolated causing sudden variation in power output. For high MPPT algorithm frequencies (25Hz, 50Hz, 100Hz) no difference in power output is noted between the four algorithms. After a change in environmental conditions that makes an increase in power output, MEPO algorithm may present an oscillation because it is based on the value of DP and not on the sign of DP. At high irradiances, the RSMCA algorithm present oscillation caused by the gain in calculation of Vref.For low frequencies (5Hz, 10Hz, 12.5Hz), the MEPO and the RSMCA algorithms excel the PO and IncCond algorithms. We can see in figure 2 that the PO power and the IncCond power are too far from the maximum power that can be generated from the panel. This is due to the fixed or small step size of the Vref. We must recall that the MEPO and the RSMCA algorithms also converge rapidly to the maximum power after the start of the simulation.

3. First Order Interpolation Analysis

When interpolating data for irradiance and temperature (approaching real conditions), we can see that that the difference between PO and IncCond algorithms and MEPO and RSMCA algorithms are emphasized when we have high variation of environmental conditions and low algorithm frequency.

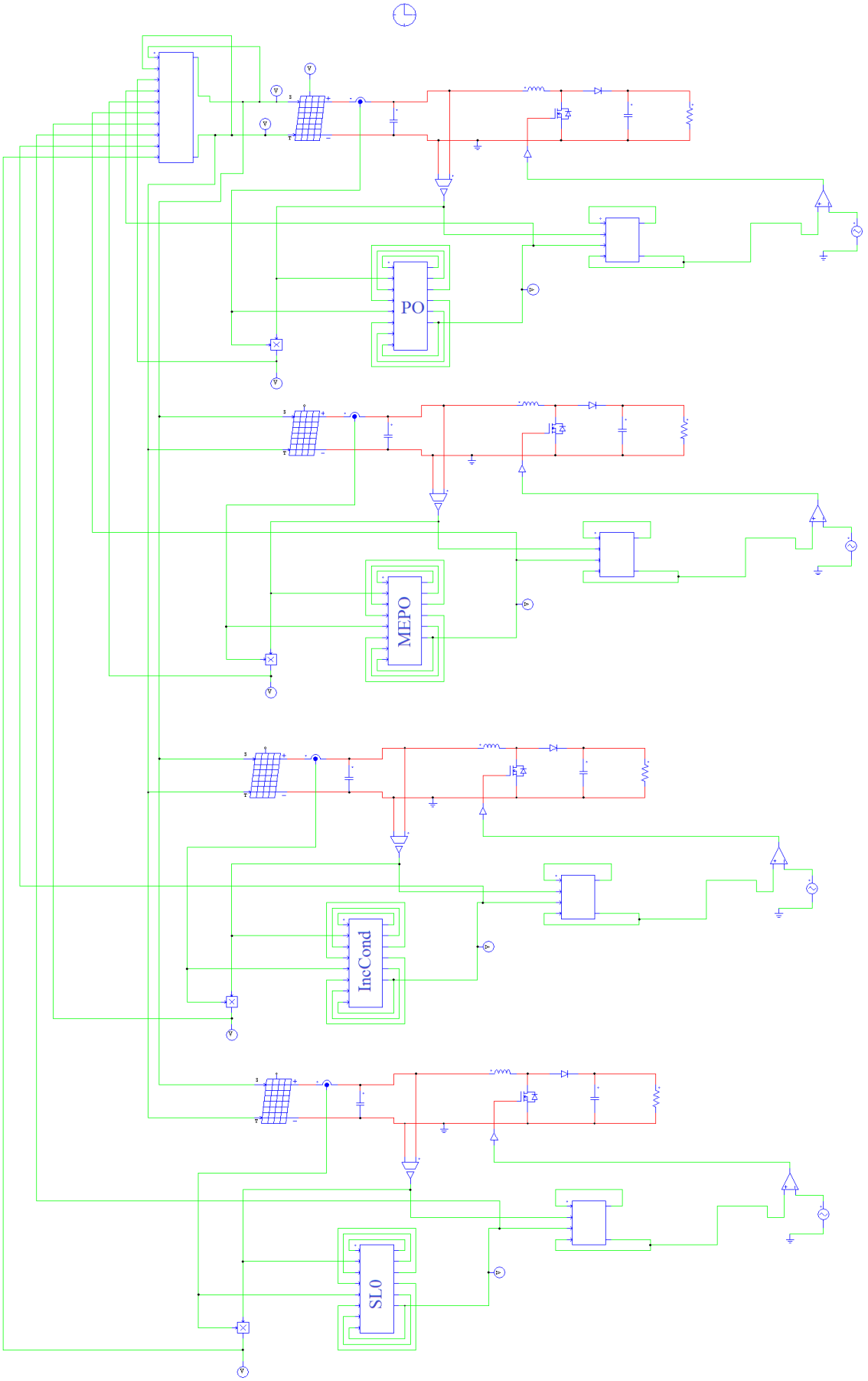

Fig .4. Shows the electric circuit diagram of the 4 MPPT algorithms

4. Real Data Analysis

In this simulation we take real data measured for one day. We choose 20 minutes that present high fluctuations of irradiance (878W/m2 - 126W/m2) and temperature (26°C – 14°C). The data is available each 5 min which mitigates the high variation in environmental conditions. This is why the algorithms results are almost identical even for low frequency.

III. CONCLUSION

In this paper, a new Robust MPPT algorithm is proposed to optimize the production of a photovoltaic (PV) chain. We developed a new technique to design the maximum power point tracking (VSAS-MPPT) based on Variable Structure Automatic Systems approach. This approach generalizes the sliding mode control to systems with commutations in a simplified technique, easy to implement. New and very efficient algorithms are proposed from VSAS-MPPT approach:

- the MEPO (Modified Enhanced Perturb and Observe)
- the RUCA algorithm (Robust Unified Control Algorithm).
-

The MPP is computed online using a very simple algorithm which uses two control inputs (one in current and one in voltage). The other algorithms like Perturb and Observe (PO), Hill Climbing, Incremental Encoder (InCond) and SMC look as particular cases of the proposed Algorithm called RUCA (Robust Unified Control Algorithm).The proposed MPPT has several advantages: simplicity, high convergence speed, and is independent on PV array characteristics. We study and compare execution efficiency for the proposed VSAS-MPPT algorithms to the other methods, including Perturbation and Observation (P&O).

Realistic simulations are presented to show ease of implementation of our new algorithms, and compare its efficiency and accuracy to other MPPTs. The obtained results prove that the MPPT is tracked even under sudden change of irradiation level or temperature. In our comparative tests, a particular case (use only voltage input), called the Modified and Enhanced Perturb and Observe Algorithm (MEPO), is shown to be the most fast and efficient, despite using low frequency commutation and sudden fast temperature and irradiation changes. The proposed MPPT has several advantages: simplicity, high convergence speed, oscillation free and is independent on PV array characteristics. In summary the best algorithms are those designed using the SASV-MPPT approach and considering that the system can move from one characteristic to another. The proposed algorithms are the most efficient despite using low frequency commutation. They are the faster converging. The simulations was performed under PSIM software to use realistic physical models.

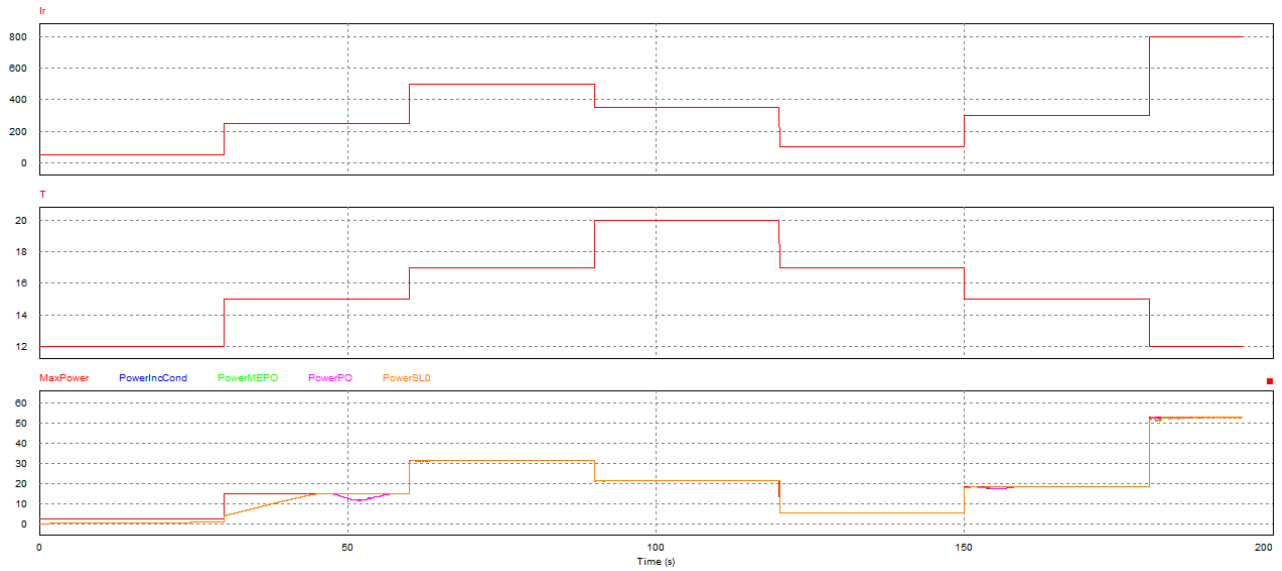

Fig .5. Sudden variation of irradiation and T with frequency (100Hz)

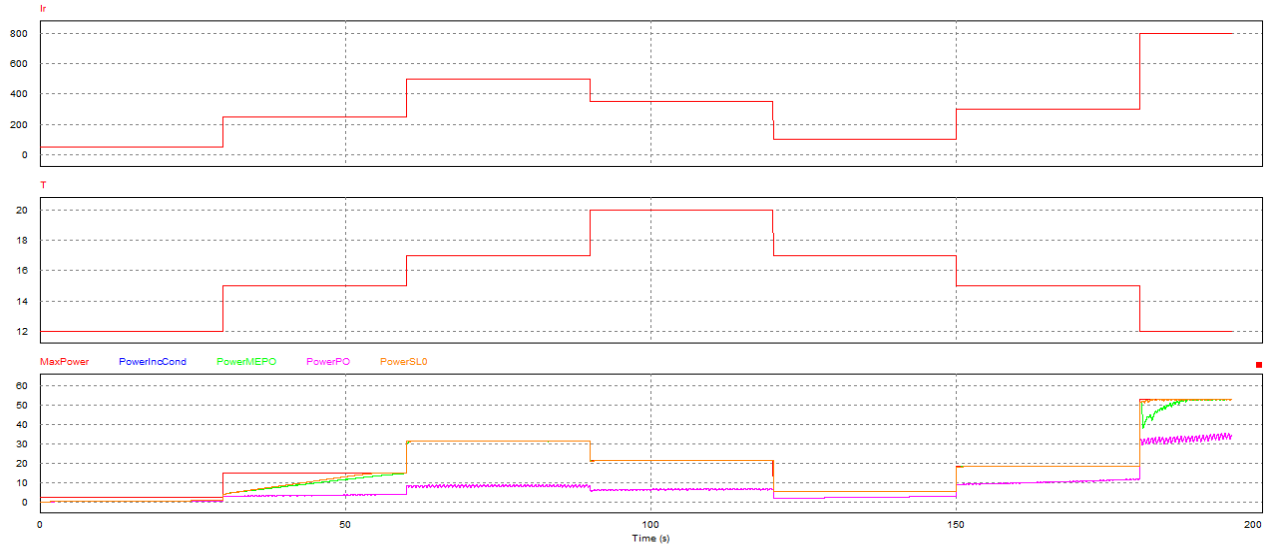

Fig .6. Variation of irradiation and temperature with low frequency (5Hz)

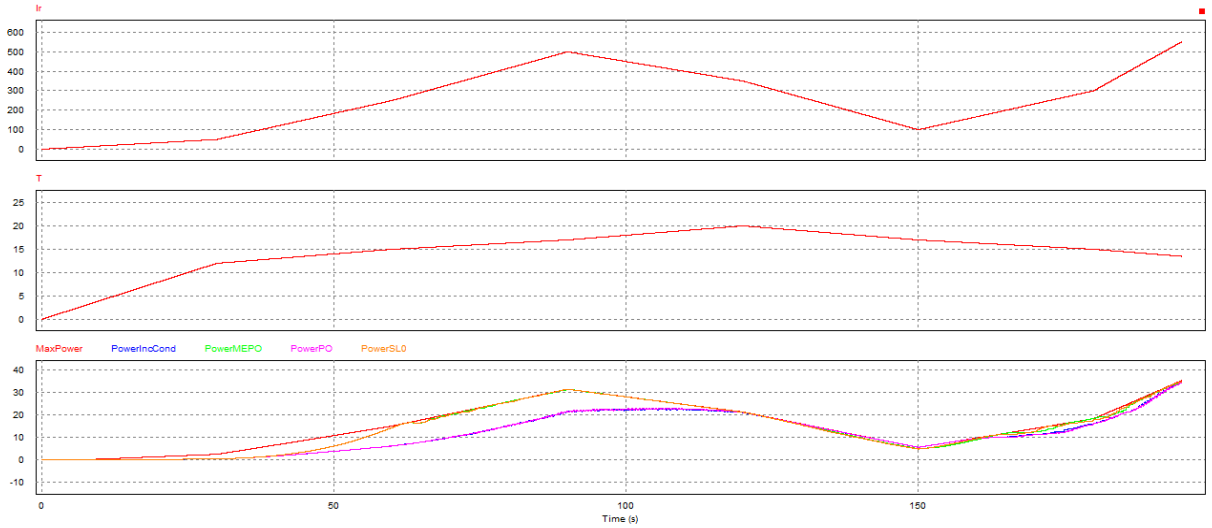

Fig .7. Interpolated variation of irradiation and T with low frequency (10Hz)

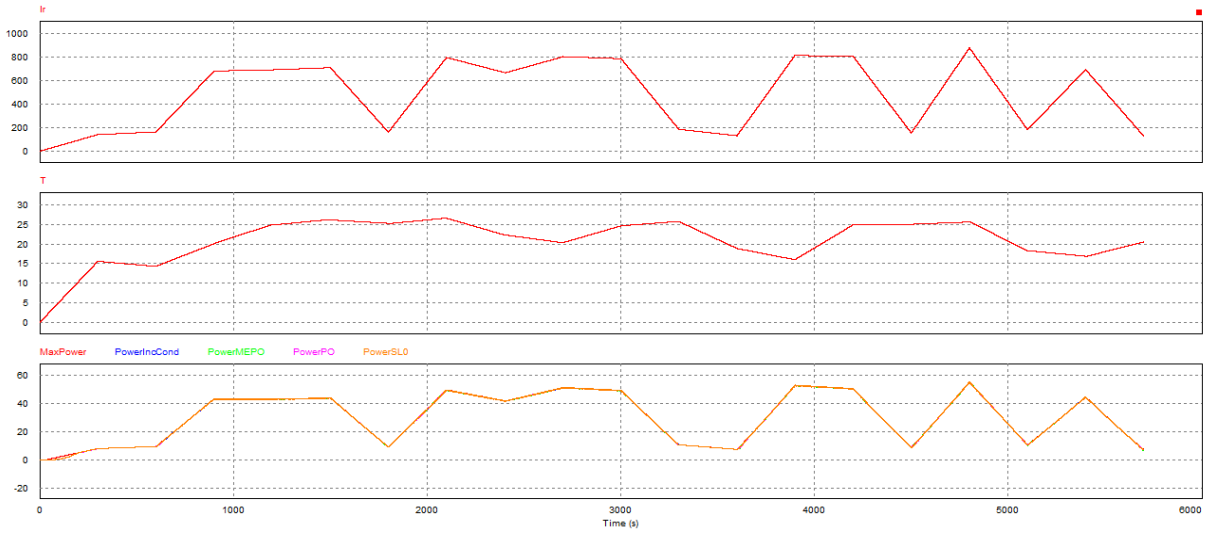

Fig .8. Real data interpolated with low algorithm frequency (10Hz)

REFERENCES

[1] M'Sirdi, N. K., Nehme, B. and Rabhi, A. (November 2014) The Best MPPT Algorithms by VSAS approach for Renewable Energy Sources (RES). EFEA 2014, international IEEE conference PARIS.

[2] Mutoh, N. Ohno, M. and Inoue, T. (June 2006) A method for MPPT control while searching for parameters corresponding to weather conditions for PV generation systems. IEEE Transactions on Industrial Electronics, vol.53, no.4, pp.1055-1065.

[3] Wang, N. C., Sun, Z., Yukita, K., Goto, Y. and Ichiyanagi, K. (March 2010) Research of PV model and MPPT methods in Matlab. Asia-Pacific Power and Energy Engineering Conference (APPEEC 2010), pp.1-4, 28-31.

[4] Amei, K., Takayasu, Y., Ohji, T. and Sakui, M. (2002) A Maximum Power Control of Wind Generator System Using a Permanent Magnet Synchronous Generator and a Boost Chopper Circuit. IEEE Power Conversion Conference, vol. 3, , pp. 1447- 1452.

[5] Yu, T. C., and Shen,Y.T. (Nov. 2009) Analysis and Simulation of Maximum power point tracking for photovoltaic systems. Proceedings of the 30th ROC Symposium on Electrical Power Engineering, Taoyuan, Taiwan, pp. 92-96.

[6] Tavares, C. A. P., Leite, K. T. F., Suemitsu, W. I. and Bellar, M. D. (Nov. 2009) Performance Evaluation of Photovoltaic Solar System with Different MPPT Methods, Industrial Electronics, 2009. IECON '09. 35th Annual Conference of IEEE, pp.719-724.

[7] Hua, C., Lin, J., Shen, C. (1998) Implementation of DSP-Controlled Photovoltaic System with Peak Power Tracking. IEEE Trans. On Industrial Electronics, Vol. 45, No. 1, pp. 99-107.

[8] Liu, F., Kang,Y., Zhang, Y., and Duan, S., (June 2008) Comparison of P&O and hill climbing MPPT methods for grid-connected PV converter. 3rd IEEE Conference on Industrial Electronics and Applications, (ICIEA 2008), pp.804-807, 3-5.

[9] Hua, C. C., Lin, J. R. (June 2001) Fully Digital Control of Distributed Photovoltaic Power Systems. Proceedings of IEEE International Symposium on Industrial Electronics (ISIE 2001), vol. 1, pp. 1-6.

[10] Xiao,W. (July 2003) A Modified Adaptive Hill Climbing Maximum Power Point Tracking Control Method for Photovoltaic Power System. Master Thesis, The University of British Columbia,

[11] Liu X., Lopes L.A.C. (June 2004) An Improved Perturbation and Observation Maximum Power Point Tracking Algorithm for PV Arrays. Power Electronics Specialists Conference, 2004. PESC 04. 2004 IEEE 35th Annual Volume 3, pp. 2005 – 2010.

[12] Hohm, D. P., Ropp, M. E. (January 2003) Comparative Study of Maximum Power Point Tracking Algorithms. Progress in Photovoltaics: Research and Applications, vol. 11, no. 1, pp. 47–62,

[13] Ibrahim, H. E. and Houssiny, F. F., (August 1999) Microcomputer Controlled Buck Regulator for Maximum Power Point Tracker for DC Pumping System Operates from Photovoltaic System. Proceedings of the IEEE International Fuzzy Systems Conference, Vol. 1, pp. 406-411.

[14] Midya, P., Kerin, P. T., Turnbull, R. J., Reppa, R. and Kimball, J. (1996) Dynamic Maximum Power Point Tracker for Photovoltaic Applications. Proceedings of the IEEE Power Electronics Specialists Conference, PESC, Vol. 2, pp. 1710-1716.

[15] Kuo, Y. C., Liang, T. J. and Chen, F. C. (2001) Novel Maximum-Power-Point-Tracking Controller for Photovoltaic Energy Conversion System. IEEE Transactions on Industrial Electronics, Vol. 48, pp. 594- 601.

[16] Kaiser, M., Aditya, S. and Mazumder, R.(July 2006) Performance Evaluation of a Maximum Power Point Tracker (MPPT) for Solar Electric Vehicle Using Artificial Neural Network. Daffodil International University Journal Of Science And Technology, vol. 1, issue 1.

[17] Xiao, W. and Dunford, W. G. (2004) A modified adaptive hill climbing MPPT method for photovoltaic power systems," 35th. Annual IEEE

Power Electron. Specialists Conf., pp. 1957-1963.

[18] Tina, G.M. and Scrofani, S.(May 2008) Electrical and Thermal Model for PV Module Temperature Evaluation. IEEE Electrotechnical Conference. pp. 585-590.

[19] Schaefer, J. (June 1990) Review of Photovoltaic Power Plant Performance and Economics, IEEE Trans. Energy Convers., vol. EC-5, pp 232-238.

[20] Tse, K. K., Ho, M. T., Henry, S., Chung, H. and Hui, S. Y. (November 2002) A Novel Maximum Power Point Tracker for PV Panels Using Switching Frequency Modulation. IEEE Transactions on Power Electronics, Vol. 17, No.6.

[21] Calavia, M., Perie, J.M., Sanz, J.F. and Sallan, J. (March 2010) Comparison of MPPT Strategies for Solar Modules. International Conference on Reneweble Energies and Power Quality, Granada (Spain),

[22] Femia, N., Petrone, G., Spagnuolo, G. and Vitelli, M. (June 2004) Optimizing duty-cycle perturbation of P&O MPPT technique. Power Electronics Specialists Conference, 2004. PESC 04. 2004 IEEE 35th Annual Volume 3, pp.1939 –1944.

[23] Femia, N., Petrone, G., Spagnuolo, G. and Vitelli, M. (July 2005) Optimization of Perturb and Observe Maximum Power Point Tracking Method. IEEE Transactions on Power Electronics, Vol. 20, No. 4.

[24] Fangrui, L., Shanxu, D., Fei, L., Bangyin, L. and Yong, K. (July 2008) A Variable Step Size INC MPPT Method for PV Systems. IEEE Transactions on Industrial Electronics, Vol. 55, No. 7.

[25] Chao, K.H. and Lee, Y.H. (Volume 2012) A Maximum Power Point Tracker with Automatic Step Size Tuning Scheme for Photovoltaic Systems. International Journal of Photoenergy.

[26] Zoua,Y., Yua,Y., Zhangb, Y. and Luc, J. (2012) MPPT Control for PV Generation System Based on an Improved Inccond Algorithm. Procedia Engineering Vol. 29, pp.105-109.

[27] Chen, C. H. (2002) Maximum Power Tracking for Photovoltaic Power System. In Conf. Record of the 37th IAS Annual MeetingInd. Applicat. Conf., pp. 1035-1040.

[28] Walker, G. (2001) Evaluating MPPT Converter Topologies Using a MATLAB PV Model. Journal of Electrical & Electronics Engineering, Australia, IEAust, vol.21, No. 1, pp.49-56.

[29] Veerachary, M., Senjyu, T. and Uezato, K. (July 2002) Feedforward Maximum Power Point Tracking of PV Systems Using Fuzzy Controller. IEEE Transactions on Aerospace and Electronic Systems,Vol. 38, 3, 969-981.

[30] Miao, Z., Jie, W. et al.,(2004) The Application of Slide Technology in PV Maximum Power Point Tracking System. Fifth WorldCongress on Intelligent Control and Automation, WCICA.

[31] Kim,T. Y., . Ahn, H. G., Park, S. K. and Lee, Y. K. (2001) A Novel Maximum Power Point Tracking Control for Photovoltaic Power System Under Rapidly Changing Solar Radiation. In IEEE International Symp. On Ind. Electron, pp. 1011-1014.

[32] MATLAB Simulink. Creating Graphical User Interfaces. Version 7.9 [Online]. Available : http://www.mathworks.com/access/ helpdesk/ help/ techdoc / creating_guis/ bqz79mu.html.

Modelling Of Diesel Generator Sets That Assist Off- Grid Renewable Energy Microgrids

J. Salazar, F. Tadeo, Prada, C.
Dept. of System Engineering and Automatic Control, Dr. Mergelina S/N,
University of Valladolid, 47005 Valladolid, Spain.

Abstract **-** This paper focuses on modelling diesel generators for off-grid installations based on renewable energies. Variations in Environmental Variables (for example, Solar Radiation and Wind Speed) make it necessary to include these auxiliary systems in off-grid renewable energy installations, in order to ensure minimal services when the produced renewable energy is not sufficient to fulfill the demand.

This paper concentrates on modelling the dynamical behaviour of the diesel generator, in order to use the models and simulations for developing and testing advanced controllers for the overall off-grid system. A diesel generator is assumed to consist of a diesel motor connected to a synchronous generator through an electromagnetic clutch, with a flywheel to damp variations. Each of the components is modelled using physical models, with the corresponding control systems also modelled: these control systems include the speed and the voltage regulation (in cascade regulation).

Keywords **-** Microgrids, Off-grid, Speed and voltage control, Diesel generators, Variable dead time, Governors.

I. INTRODUCTION

Remote areas are not frequently connected to a reliable grid supply, so their usual method of electricity generation is the use of diesel generator sets in off-grid configurations. Unfortunately, logistics, safety and environmental concerns impulse the use of electrical energy locally generated using renewable sources, mainly based on the conversion of solar and wind energy, as they are clean, silent and reliable, with low operation costs and small environmental impact. Sunlight and the kinetic energy of the wind are free, inexhaustible, and involve only a small amount of residues or greenhouse gases emissions. Despite these advantages, however, electric power production systems that use as primary sources exclusively solar and wind energy pose technical problems due to uncontrollable wind speed and radiation fluctuations [1,2,3]. As a consequence, the power supply continuity of an off-grid system should be backed-up by other reliable and non-fluctuant sources of primary energy, generally diesel

generator sets. Such systems, designed for the decentralized production of electric power using combined sources of primary energy, are called hybrid systems [4, 5].

A typical configuration is shown in Figure 1, based on an off-grid system designed as part of the Open-Gain project and installed in Borj Cedria (Tunisia): see [6] for more details. The three-phase power supply system comprises photovoltaic panels, maybe a wind turbine, a battery bank for voltage regulation, and a small Diesel Generator.

A central role in the operation of the system is provided by the control power electronics. The Solar Inverter changes the direct current electricity (DC) from a photovoltaic array into alternating current (AC), which is injected into the main AC bus of the system. The Wind Inverter converts the variable frequency voltage from wind generators into grid-conforming AC voltage. The Bidirectional Battery Inverter functions as inverter or rectifier charger mode. In the inverter mode, it converts direct current (DC) from the battery bank into alternating current (AC) which is injected into the main AC bus of the system. In rectifier charger mode, if the total power generated by the PV generator and the wind turbine exceeds the load needs, it will be used to charge the battery bank.

In this system, there are two main operation modes [7]. The first is the island mode, in which the battery inverter defines the operating grid frequency and voltage (The diesel generator might be switched off). In the second operation mode, the diesel generator is the one that defines the frequency and voltage, so the battery inverter acts as a “grid parallel” unit, by synchronizing its output voltage to

the grid voltage. In both cases, wind and solar inverters operate as “grid parallel” units, without any participation in the voltage or frequency regulation.

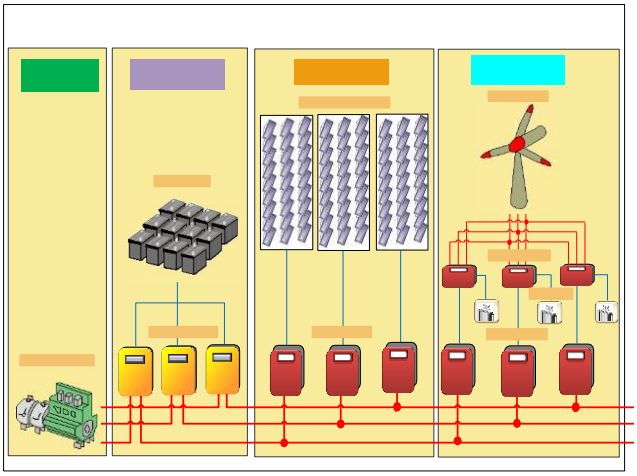

Fig .1. Off-grid Hybrid Energy Generation

frequently carried out in these Micro Grids by small modifications of the grid frequency (for example, by the droop algorithm in [8, 9]). Solar and wind inverters limit their output power based on this grid frequency. In island mode, this is automatically carried out by the battery inverter [10].

In genset mode, only specific diesel generators use the frequency for communications; standard diesel generators supply the voltage and frequency specified in the rating plate, without using a droop factor to operate in parallel with another energy source. Thus, when standard generator sets are connected, the frequency is 50Hz, so solar and wind inverter produce always the maximum available power. When the batteries are fully charged, the battery inverter temporarily increases significantly the grid frequency, to disconnect solar and wind sources from the local grid [11].

This paper focuses on modelling and simulation of the response of the diesel generator for start-up and load disturbances. Models of other components of microgrids have been presented elsewhere (see [12] and references therein). The modelling concentrates on reproducing the dynamic response (especially at start-up). Thus, the models are selected to be precise enough in the time scale of tens of seconds (given by the time dynamics of the loads), but quick enough so that the operation during many months can be evaluated in reasonable time using standard computers.

The diesel generator is then assumed to consist of three main components: the diesel engine, the synchronous generator and the excitation system (see Figure 2). Thus, Models of the diesel engine, the diesel engine governor, the synchronous generator, its excitation system, and the automatic voltage regulation (AVR) module are now presented.

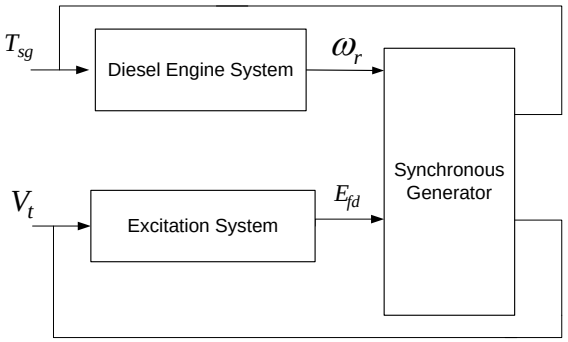

Fig .2. The overall block diagram of diesel generator

II. A MODEL OF DIESEL ENGINE SYSTEM

Although detailed models are available to simulate the complete dynamics of a diesel engine, that include thermodynamic aspects, as the focus here is in electricity production as auxiliary system, it is sufficient to use a much lower order model, so thermodynamic variables may be considered to be constant, but unknown. This approach has been adopted in other internal-combustion engine simulation studies, such as in [13].

The general structure of the diesel engine model is then shown in Figure 3. It can be seen that it is assumed to consist of four main sub-models: the controller, the actuator, the engine and the flywheel. The model of each component is now briefly described.

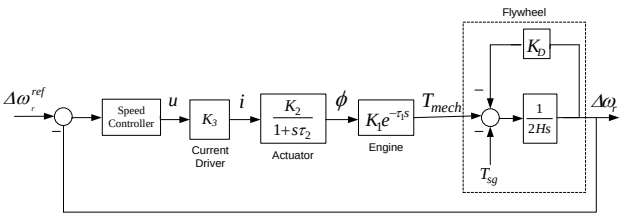

Fig .3. Block diagram of a typical diesel engine system

A. A Controller Model

A "controller" consists of a standard PID speed controller (presented in detail in Section 5), followed by a "current driver" module, represented by a scalar value K3, which depends on the operating point of the system, transforming the control signal into a current sent to the actuator.

B. AN Actuator Model

The "actuator" block represents the governor (actuator) system of the diesel engine. A governor can be defined as a mechanical or electromechanical device for controlling the speed of an engine automatically by relating the intake of fuel. The input driving current (ι) controls the fuel rack position, which in turn determines the amount of fuel (ϕ) to be injected into the combustion chamber. The actuator is usually represented by a first order phase lag function, which is characterized by a gain K2 and a variable time constant (τ2). Here, K2 is the actuator constant, that is considered to be fixed, τ2 is the actuator time constant, which is a complicated function of the temperature of the fuel. For simplicity, the variation of the parameters is ignored and τ2 is assumed to be constant.

C. A Diesel Engine Model

The "Engine" block comprises the combustion system of the diesel engine. The injected fuel is ignited by the compressed hot air in the combustion chamber, causing the movement of the piston during the power strokes. This action drives the crankshaft, so the mechanical torque T_{mech} is produced.

For modelling, this engine combustion system is represented as an engine torque constant with a dead time element □1, which is the result of having several cylinders. For each individual cylinder, this has essentially two components. The "ignition delay" represents the time taken by the fuel-air mixture to reach combustion point at the particular operating temperature and pressure; it can be shown to have a hyperbolic variation with speed deviation.

The "power stroke delay" represents the time that elapses from a load disturbance to the time at which a particular engine cylinder responds to the disturbance. This delay is random and depends on the crank angle value at which a load disturbance is imposed. Its effect can be reduced by increasing the number of cylinders. Since for a particular load disturbance, the time after which the cylinders responds goes down inversely with speed, it may be approximated by an inverse function of speed. The engine dead time (τ1) is a function of the speed deviation Δωρ (pu) through a nonlinear function. An adequate non-linear function to represent the dead time variation is (see Figure 4):

$$\tau_1 = \frac{A\Delta\omega_r^{\,2} + B\Delta\omega_r + C}{\Delta\omega_r^{\,2}}, \quad (1)$$

where A, B and C are parameters that are determined by curve fitting techniques to reproduce empirically determined curves, such as those in [14].

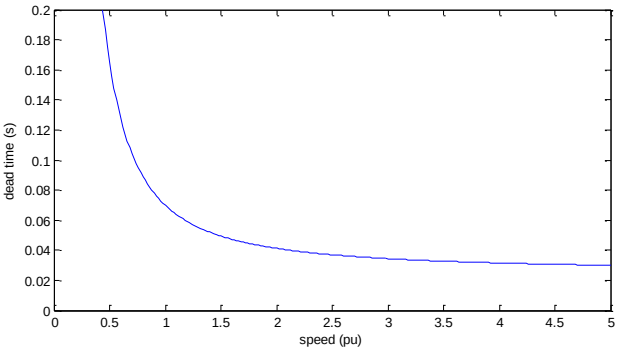

Fig .4. Typical variation of dead time with engine speed

D. A Flywheel Model

The "Flywheel" block comprises the rotating system, so it comprises the dynamics of the engine inertia, the flywheel, the damping factor (KD) and the loaded alternator. The mechanical motion of equation is then:

$$2H\frac{d\Delta\omega_r}{dt} = T_{mech} - T_{sg} - K_D\Delta\omega_r \quad (2)$$

$$\frac{d\delta}{dt} = \omega_0\Delta\omega_r \quad (3)$$

$$\Delta\omega_r = \omega_r - 1 \quad (4)$$

Where time t is in seconds, rotor angle δ is in radians, rated generator speed ω_0 is in rad/s, $\Delta\omega r$ is the speed deviation (pu), ω_r is the angular velocity of the rotor (pu), T_{sg} is the generator torque (pu), H is the per unit inertia constant (s).

III. A SYNCHRONOUS GENERATOR MODEL

The equations of synchronous generator are obtained from Park Transformation, after a per unit representation and some simplifications. The most important simplification is that stator transients are neglected because it is much faster compared to the rotor ones. Considering a salient pole synchronous generator, rotor consists of three windings. A field and a damping winding are considered on the direct axis in order to take into account the transient and subtransient behavior respectively in this axis. Meanwhile, a damping winding is considering on the quadrature axis.

The terminal voltage phasor is determined by, Vt=Vd + jVq, that can be evaluated from:

$$V_d = E''_d - R_s I_d + X''_q I_q \quad (5)$$

$$V_q = E''_q - R_s I_q - X''_d I_d \quad (6)$$

where R_s is the armature resistance, I_q and I_d are the currents flowing in the stator winding, the $X''_{d,q}$ are the so-called subtransient d and q-axis reactances and $E''_{d,q}$ are given by [15].

$$E''_d = \frac{\left(X_q - X''_q\right)}{1+\tau''_{qo}s} I_q \quad (7)$$

$$E''_q = \frac{1}{1+\tau''_{do}s} E'_q - \frac{\left(X'_d - X''_d\right)}{1+\tau''_{do}s} I_d \quad (8)$$

where $X_{d,q}$ and $X'_{d,q}$ are the synchronous and transient reactances, the $\tau''_{d,qo}$ are the open circuit subtransient time constants and E'_q is given by

$$E'_q = \frac{1}{\left(\frac{X_d - X''_d}{X'_d - X''_d}\right)+\tau'_{do}s} E_{fd} + \frac{\left(\frac{X_d - X'_d}{X'_d - X''_d}\right)}{\left(\frac{X_d - X''_d}{X'_d - X''_d}\right)+\tau'_{do}s} E''_q \quad (9)$$

where E_{fd} is the exciter field voltage and τ'_{do} is the open circuit transient time constant.

As it can be seen in Figure 2, there is an additional feedback term from the generator to the diesel engine given by the electromagnetic torque that in flywheel mode can be evaluated from:

$$T_{sg} = E''_d I_d + E''_q I_q - \left(X''_d - X''_q\right) I_d I_q \quad (7)$$

IV. AN EXCITATION SYSTEM MODEL

The main function of an excitation system is to supply and automatically adjust the field current of the synchronous generator considering control and protective functions essential to the satisfactory performance of the system. The control functions include the control of voltage and the enhancement of system stability. The protective functions ensure that the capability limits of the synchronous machine, excitation system, and other equipment are not exceeded. The functional block diagram of a typical excitation control system is shown in Figure 5.

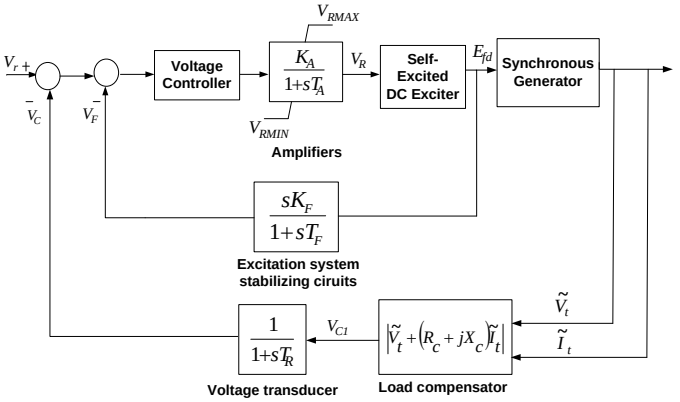

Fig .5. Functional Block diagram of a synchronous generator excitation control system [16]

- Excitation System Stabilizing Circuits: Excitation systems comprised of elements with significant time delays have poor dynamic performance. Hence, excitation system stabilizing circuits is used to improve the dynamic performance of the control excitation control system. A derivative feedback is the most commonly used form of compensation. The aim of the compensation is to minimize the phase shift introduced by the time delays over a selected frequency range.

- Load Compensation: The compensator has adjustable resistance (Rc) and inductive reactance (Xc) that simulate the impedance

between the generator terminals and the point at which the voltage is being effectively controlled. Using this impedance and the measured armature current, a voltage drop is computed and added to or subtracted from the terminal voltage. The magnitude of the resulting compensated voltage (Vc1), which is fed to the AVR, is given by:

$$V_{c1} = \left| \tilde{V}_t + \left(R_c + jX_c \right) \tilde{I}_t \right| \quad (11)$$

This is used to ensure proper sharing of reactive power between generators placed together at their terminals, sharing a common step-up transformer. The compensator functions as a reactive current compensator by creating an artificial coupling between the generators. Without this provision, one of the generators would try to control the terminal voltage slightly higher than the other; hence, one generator would tend to supply all of the required reactive power while the other would absorb reactive power to the extent allowed. When load compensator is not used, Rc and Xc are set to zero.

- Voltage transducer: The time constant TR represents rectification and filtering of the synchronous machine terminal voltage. The voltage transducer output (Vc) forms the principal control signal to the excitation system. If a load compensator is not used and Vc is negligible, Vc =Vt.

- *Amplifiers:* Amplifiers may be magnetic, rotating, or electronic type. Magnetic and electronic amplifiers are characterized by a gain and may also include a time constant.

A. A Self-Excited Dc Exciter

The excitation systems of this category utilize dc generators as source of excitation power and provide current to the rotor of the synchronous machine through slip rings.

The self-excited DC exciter is represented in block diagram form as shown in Figure 6. All variables are in per unit.

$$V_R = K_E E_{fd} + S_E\left(E_{fd}\right) E_{fd} + T_E \frac{dE_{fd}}{dt} \quad (12)$$

There are several mathematical expressions that may be used to approximate the effect of exciter saturation. A commonly used expression is the exponential function

$$S_E\left(E_{fd}\right) E_{fd} = A_{EX} e^{B_{EX} E_{fd}} \quad (13)$$

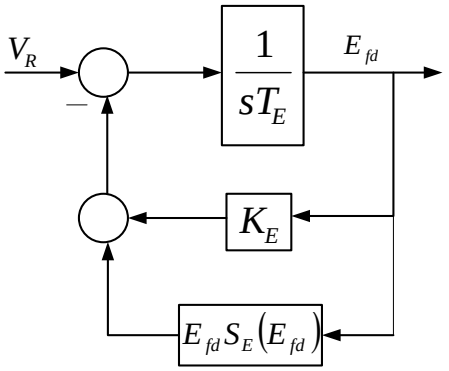

Fig .6. Block Diagram of a self- excited DC exciter

V. A SPEED CONTROLLER

The speed controller is designed to keep constant the internal combustion engine speed by changing the quantity of fuel consumed by the motor. The direct result of this speed controller is a stable frequency for the voltage at the generator terminals. A constant frequency requires good precision and a short response time from the speed controller.

Detailed models of diesel engines are characterized by nonlinear, time-varying parameters including a nonlinear input dead-time variation that introduces an unknown delay ($\tau 1$) between the injection of fuel and the production of engine torque. The presence of this dead time together with some other system parameters gives rise to a serious control problem and significantly degrades the performance especially under varying loads. The dead time is an unknown time delay and is commonly considered as a complicated function of operating conditions and the engine speed [17,18].

Conventional PID controllers are widely employed in diesel engine speed control, which gives acceptable performance. However, PID schemes might not be able to handle large variations in the engine dead time. Here, several advanced control techniques for the speed control of the diesel engine systems have

been reported in the literature, based on the methods of H∞ [19], adaptive control [20] and neural network [21].

VI. AN AUTOMATIC VOLTAGE REGULATOR (AVG)

The Automatic voltage regulator (AVG) controls the exciter field to provide a constant terminal voltage. In the past, the generator response using an analog excitation system was a matter of adjusting potentiometers or adding or deleting capacitors and resistors in the control loops of the voltage regulator stability circuit. Adjustment could be very time consuming because changes would often involve turning the excitation system on and off many times in order to make modifications.

Today, the digital excitation system provides the means to easily access the challenging parameters of the analog system. The most important point of digital controllers is the embedded microprocessors that perform various control functions for the excitation system. These control functions include the automatic voltage regulator, field current regulator, Var/Power factor control, and a host of excitation limiters to regulate and maintain the generator within safe operating limit of the machine [22]. Conventional PID controllers are employed in digital AVG.

VII. A SIMULATION EXAMPLE

To show the typical responses of diesel generators, data from the Open-Gain prototype (see Figure 7) have been used. This prototype included a Diesel Generator of 17/20KVA continuous/emergency power (Pramac GBW 22Y), shown in Figure 8. For this installation the parameters are given in Tables 1 to 3.

The main issue for off-grid renewable energy installations is the connection/disconnection transient, so some simulation results are presented for this situation in Figures 8 to 10: the engine is assumed to be running at 80% of the nominal speed before connection to the grid, at t=0s. The responses presented in Fig. 8 to 10 correspond to a worst case condition (cold oil), that gave an actuator time constant of 0.198 s and a droop of 5% (for comparison the hot oil time constant is 0.072 s.

It can be seen that the simulations reproduce accurately the expected results. Voltage is regulated to the desired output voltage in around 4 seconds, without significant oscillations in torques and speeds.

The model was then integrated into the Micro-grid library (see Figure 11), developed in the EcosimPro© language (selected as it simplifies developing multi-domain simulations thanks to the object oriented and non-causal approach). Results using simulations of the complete installation are presented in [12].

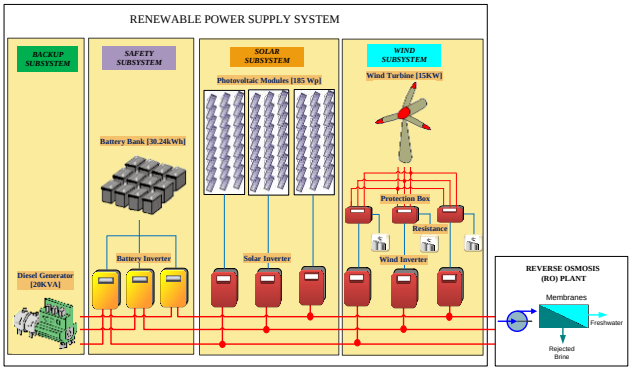

Fig .7. Renewable Energy System proposed in the European Project Open Gain

Fig .8. Diesel generator Pramac GBW 22

A complete set of parameter values and ranges is given in Table 1 and Table 2.

Table 1. System parameters of a typical diesel engine [19]

Parameter	Value	Unit	Definition
K_1	1.15	pu	Engine torque constant
K_2	1	pu	Actuator torque
K_3	1	pu	Current Driver Torque
τ_2	0.125	s	Actuator time constant
A,C	-0.085	-----	Parameters for delay variation
B	0.08	-----	Parameter for delay variation
H	1	s	Inertia constant
K_D	0.1	pu	Damping Factor

Table 2. System parameters of a synchronous generator model E1S13M F/4 provided by Linz Electric.

Parameter	Value	Unit	Definition
X_d	1.57	pu	Synchronous d-axis reactances
X'_d	0.21	pu	Transient d-axis reactances
X''_d	0.076	pu	Subtransient d-axis reactances
X_q	1.35	pu	Synchronous q-axis reactances
T'_{d0}	0.4	s	Transient d-axis open circuit time constant
T'_d	0.053	s	Transient d-axis short circuit time constant
T''_{d0}	0.0064	s	Subtransient d-axis open circuit time constant
J_{gen}	0.083	Kgm^2	Moment of inertia of Generator

Table 3. Data for Self-Excited dc exciter

Parameter	Value	Definition
K_A	187	Gain amplifiers
T_A	0.89	Time constant amplifiers
T_E	1.15	Time constant exciter
A_{EX}	0.014	Parameter for exciter saturation function
B_{EX}	1.55	Parameter for exciter saturation function
K_F	0.058	Gain for stabilizing circuits
T_F	0.62	Time constant for stabilizing circuits
T_B	0.06	Voltage Regulator
T_C	0.173	Voltage Regulator
T_R	0.05	Time constant for Voltage transducer
V_{RMAX}	1.7	Amplifier limitation
V_{RMIN}	-1.7	Amplifier limitation

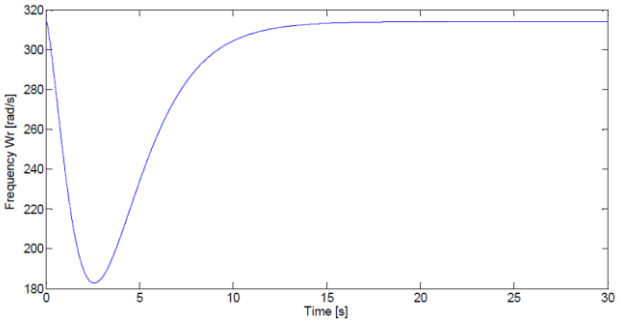

Fig .9. Terminal Voltage Response [V]

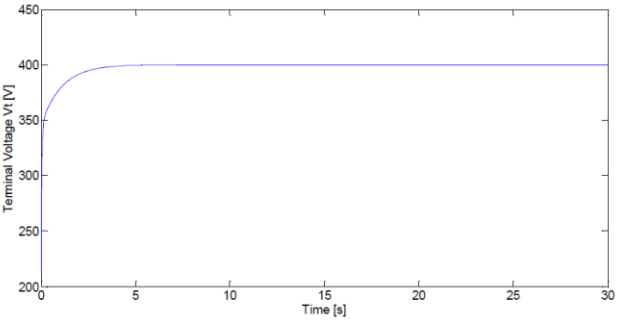

Fig .10. Engine Speed Response [rad/s]

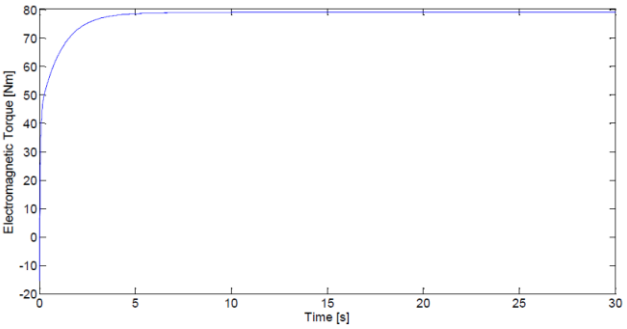

Fig .11. Electromagnetic Torque Response [Nm]

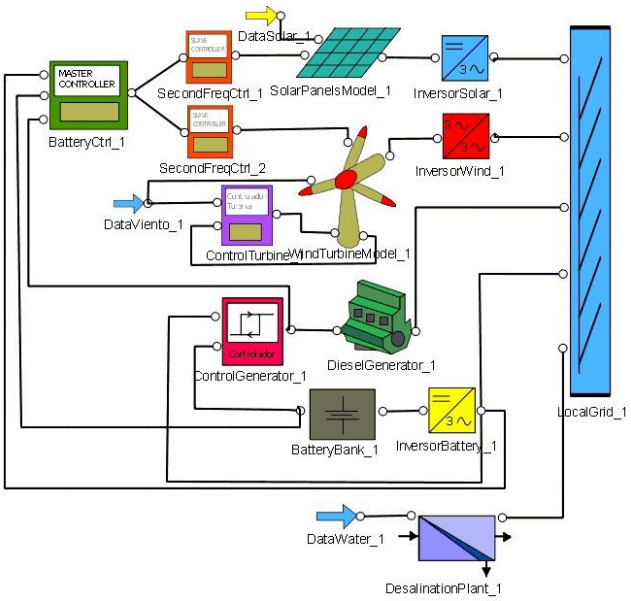

Fig .12. Integration of the models into the EcosimPro Microgrids Library [12]

VIII. CONCLUSION

The paper discusses the modeling of diesel generators in order to integrate them in the simulation of off-grid renewable energy systems. As the objective is to develop models to test Energy Management Systems and High-level control systems (such as those discussed in [23] and references therein), a model is developed as simple as possible, but with the precision required by this application. For this transfer-function based models have been developed with static nonlinear terms that take into account the possible variations in gains due to changes in the operating conditions.

The final model consists of sub-models of the controllers, the diesel engine, the synchronous generator and the excitation system. It is expected to be capable of simulating a number of different events. Some simple simulation results are presented to show the applicability of the model to the problem at hand.

REFERENCES

[1] Chaabene, M. and Annabi, M. (1997) Dynamic Model for Predicting Solar Plant Performance and Optimum Control, Energy Vol. 22, No. 6, pp. 567- 578.

[2] Chaabene, M. (2008) Measurements Based Dynamic Climate Observer, Science Direct, Solar Energy Vol.82 pp.763–771.

[3] Mohandes, M. A., Rehman, S. and Halawani T. O. (1998) A Neural Networks Approach for Wind Speed Prediction, Renewable Energy, Vol. 13, No. 3, pp. 345-354.

[4] Deshmukh, M. K. and Deshmukh, S. S. (2008) Modelling of Hybrid Renewable Energy Systems, Renewable and Sustainable Energy Reviews Vol. 12 pp. 235–249.

[5] Nfah, E.M. and Ngundam, J.M. (2008) Modelling of Wind/Diesel/Battery Hybrid Power Systems for Far North Cameroon, Energy Conversion and Management Vol. 49 pp.1295–1301.

[6] Salazar,J., Tadeo F. and Prada, C. (23th to 25th March, 2010) Renewable Energy for Desalinization Using Reverse Osmosis, International Conference on Renewable Energies and Power Quality (ICREPQ'10), Granada (Spain).

[7] Palizban, O., and Kauhaniemi, K. (2015). "Hierarchical Control Structure in Microgrids with Distributed Generation" Island and grid-connected mode. Renewable and Sustainable Energy Reviews, Vol. 44, pp.797-813.

[8] Loix,T. De Brabandere, K., Driesen, J. and Belmans, R. (Nov. 5-8, 2007) A Three-Phase Voltage and Frequency Droop Control Scheme for Parallel Inverter . The 33rd Annual Conference of the IEEE Industrial Electronics Society (IECON), Taipei, Taiwan

[9] De Brabandere, K., Bolsens, B. J., Den Keybus,V., Woyte, A., Driesen J. and Belmans,R.F. (July 2007) A Voltage and Frequency Droop Control Method for Parallel Inverters, IEEE Transactions on power electronics, Vol. 22, Nº 4.

[10] Engler, A. (2005) Applicability of Droops in Low Voltage Grids, International Journal of Distributed Energy Resources. Vol. 1(1), pp. 3-15.

[11] Sunny Island installation and instruction manual, Operation Together with Sunny Boys, Version 2.1, SI5048-12:EE3107, chapter 14, Section 14.1.8, page 116.

[12] Salazar, J., Tadeo, F., & de Prada, C. (2014, August). A Micro-grid Library in a General Simulation Language. In IFAC World Congress, Cape Town, South Africa (Vol. 19, No. 1, pp. 3599-3604).

[13] Morris, R. L., Hopkins, H. G. and Borcherts, R. H. An Identification Approach to Throttle Torque Modelling, Soc. of Automotive Engrs., paper # 810448.

[14] Mina, T. I. A Detailed Study of the Start and Machinery, McGraw Hill.

[15] Krause, P. C. (1987) Analysis of Electric Machinery, McGraw Hill.

[16] Kundur, P. Power System Stability and Control, McGraw-Hill, Inc.

[17] Haddad, S. and Watson, N. (1984) Principles and Performance in Diesel Engineering, Chichester [West Sussex] : Ellis Horwood,.

[18] Choe ,Y. W. and Jung, B. G. (1994) An H∞ Controller Design for the Speed Control of Large Size and Low Speed Diesel Engine. Proceedings of the SICE Annual Conference, pp. 747-752.

[19] Kuang, B., Wang, Y,and Tan, Y. L. (2000) An

H∞ Controller Design for Diesel Engine System.

[20] Roy,S., Malik, O. P. and Hope, G. S. (1991) A Low Order Computer Model for Adaptive Speed Control of Diesel Driven Power-Plants, IEEE Transactions on Energy Conversion, pp. 1636-1642.

[21] Yacoub,Y. (1999) Mean Value Modeling and Control of a Diesel Engine Using Neural Networks, Ph.D. Dissertation, West Virginia University.

[22] Richard, S. and Kim, K. (March-April 2001) Excitation Control of the Synchronous Generator, IEEE Industry Applications Magazine, Vol 7, no2, pp. 37-43.

[23] Salazar, J., Tadeo, F., and Valverde, L. (2013, November). Predictive Control of a Renewable Energy Microgrid with Operational Cost Optimization. In 39th Annual Conference of the IEEE Industrial Electronics Society, IECON 2013 (pp. 7950-7955).

Pitch Angle Control for Variable Speed Wind Turbines

Mouna BEN SMIDA, Anis.SAKLY
Research Unit: Industrial systems study and renewable energy (ESIER),
Key the National Engineering School of Monastir (ENIM),
University of Monastir, Av. Ibn El Jazzar Skanes (5019), TUNISIA.

Abstract - Pitch control is a practical technique for power regulation above the rated wind speed it is considered as the most efficient and popular power control method. As conventional pitch control usually use PI controller, the mathematical model of the system should be known well.This paper deals with the operation and the control of the direct driven permanent magnet synchronous generator (PMSG).

Different conventional strategies of pitch angle control are described and validated through simulation results under Matlab\Simulink.

Keywords - variable-speed wind turbine; MPPT; pitch control; PMSG.

Nomenclature –

PMSG	Permanent magnet synchronous generator
HAWT	Horizontal-axis wind turbines
VAWT	Vertical axis wind turbines
TSR	Tip speed ratio
MPPT	Maximum Power Point Tracking
PWM	Pulse width modulation
PI	Proportional integral

I. INTRODUCTION

Traditional energy resources, especially from fossil origins, will break off in the following few decades, which predict an energy shortage in the world. In addition, the energy consumption, in its various forms, increased in an exponential way. To satisfy these needs, it was necessary to solve this problem. Actually, there was a simple way to do so, since there were inexhaustible renewable energy resources, which can be easily and properly exploited [1-3]. Nevertheless, being neglected for a long time, power extraction techniques of these resources requires more researches and developments aiming to make the manufacturing costs reliable and lower and to increase the energy efficiency [4-5].

In this general context, this study was interested in the wind energy which seems to be one of the most promising energies with a very high rate growth in the world. Today, the wind power has become a reality with the increase of the installed power all over the world a significant proportion of this type of energy is available in windy areas.

Recently, pitch-adjusting variable-speed wind turbines have become the dominating type of installed wind turbines.Pitch angle control method is a basic approach to improve the performance of the power generation system including different types of wind turbines. Although a wind turbine can be built in either a vertical-axis or horizontal-axis configuration, we focus on horizontal-axis wind turbines (HAWTs) because they dominate the utility-scale wind turbine market. At the utility scale, HAWTs have aerodynamic and practical advantages [6]. Smaller vertical axis wind turbines (VAWTs) are more likely to use passive rather than active control strategies. In fact, generally for vertical axis wind turbine, which consists of several blades rotating about axis in parallel direction, the cycloid blade system and the individual active blade control system are adopted.

Both methods are variable pitch system. For cycloid wind turbine, aerodynamic analysis is carried out by changing pitch angle and phase angle based on the cycloid motion according to the change of wind speed and wind direction. And for more efficient wind turbine, individual pitch angle control of each blade is obtained by maximizing the tangential force in each rotating blade at the specific rotating position, optimal.

Therefore, generally for the variable-speed wind turbines two controllers are used. Below rated value, in low wind speed, the speed controller can continuously adjust the rotor speed to maintain the tip speed ratio constant at the level which gives the maximum power coefficient, so the efficiency of the turbine will be significantly increased. Pitch angle regulation is necessary in conditions above the rated wind speed when the rotational speed is kept constant which can have a dramatic effect on the power output. The purpose of the pitch angle control might be expressed as follows [7-8]:

- Optimizing the wind turbine power output. Below rated wind speed, the pitch setting should be at its optimum value to give maximum power.

- Preventing the mechanical power input to beat the design limits. Above rated wind speed, pitch angle control provides an effective method of regulating the aerodynamic power and loads produced by the rotor.

- Minimizing fatigue loads of the turbine mechanical component. It is clear that the action of the control system can have a major impact on the loads experienced by the turbine. The design of the controller must take into account the effect on loads, and the controller should ensure that excessive loads will not result from the control action. It is possible to go further than this, and explicitly design the controller with the reduction of certain fatigue loads as an additional objective.

In this paper, conventional pitch angle control strategy in which various controlling variables may be used is discussed.

II. WIND TURBINE MODELING

In order to simulate the behavior of the wind turbine, it is necessary to determine the torque exerted on its shaft.The mechanical power extracted from the wind turbine is expressed by [9-10]:

$$P_w = \frac{1}{2} \rho \pi R^2 V_w^3 C_p(\lambda, \beta) \quad (1)$$

The power coefficient Cp depends on the pitch angle of rotor blades β and the tip speed ratio (TSR) λ, with [11]:

$$C_p(\lambda,\beta) = 0.53\left[\frac{151}{\lambda_i} - 0.58\beta - 0.002\beta^{2.14} - 13.2\right] \times \exp\left(\frac{-18.4}{\lambda_i}\right) \quad (2)$$

Where:

$$\frac{1}{\lambda_i} = \frac{1}{\lambda + 0.02\beta} - \frac{0.003}{\beta^3 + 1} \quad (3)$$

$$\lambda = \frac{R\Omega}{V_w} \quad (4)$$

The turbine torque is then defined as the ratio of the mechanical power to the rotational speed:

$$T_m = \frac{P_w}{\Omega} \quad (5)$$

The mechanical speed of the turbine is determined from the fundamental equation of the dynamics as:

$$J\frac{d\Omega}{dt} = T_m - T_{em} - f\Omega \quad (6)$$

The wind turbine speed is controlled in order to extract the maximum power from the wind. According to the Betz theory, the maximum power extractable from a wind turbine is 59.3% of the available wind power, which corresponds to the Betz limit with a power coefficient of 0.593 [12].

For the wind turbine modeled in this study, the curve of Cp versus λ with β =0, represented in Fig. 1, shows an optimum value of the TSR ($\lambda_{opt} = 8$) corresponding to a maximum value of the power coefficient (Cpmax =0.473).

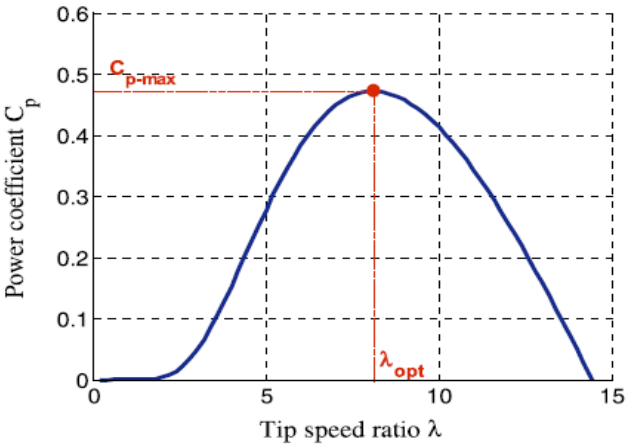

Fig .1. Cp versus λ curve

A. Control of the Wind Generator

The control of the generator power is obtained by the control of the PMSG electromagnetic torque Tem. The role of the pitch control system is to limit the rotational speed of the shaft, the reference electromagnetic torque Tem-ref, can be developed in this method [13]: The strategy of an operating at maximum power, goals to develop the turbine aerodynamic output, aiming to extract the maximum of wind power derived when the turbine operates at maximum power coefficient.

Equation 7 gives the expression of the maximum power obtained using the Maximum Power Point Tracking (MPPT) strategy which adjust automatically the ratio speed at its optimum value , l_{opt}, in order to attain the maximum power coefficient Cpmax, the equation below indicates the relationship between turbine power and turbine speed at maximum power. When regulating the system under the specification of maximum power, it must be considered that turbine power must never be upper than generator rated power. The output power must be limited when generator rated power is attained at rated wind speed.

$$P_{MPPT} = K_{opt}\Omega^3 \quad (7)$$

$$K_{opt} = \frac{1}{2}\frac{rpR^5C_{p\max}}{l_{opt}^3} \quad (8)$$

In the case of high wind, it is necessary to limit the rotational speed to avoid the damage of the turbine and the electric machine. This limitation is obtained by the control of the pitch angle β .

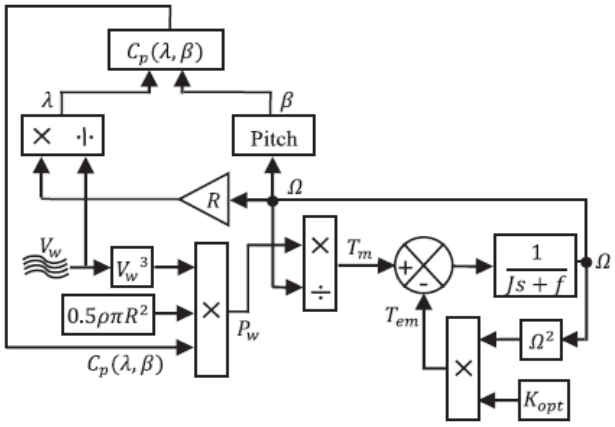

Fig .2. Turbine model

B. Wind Turbine Operating Regions

The Typical power control regions of wind turbine are shown in Figure 3. Three wind speeds are considered as limits of this division, the cut-in wind speed vcut-in, the rated wind speed vrated and the cut-out wind speed vcut-out. For the wind turbine model considered in this study the values of vcut-in, vrated and vcut-out respectively are 6m/s, 10m/sand 13m/s. In region I, the wind turbine is at stop state and the pitch angle usually is set to90°. In the partial load region, region II, the wind speed is limited between vcut-in and vrated. The main objective of the control in this region is maximizing power generated by the wind turbine. The principle control objective in the full load region, region III, is maintaining the generator power P_g around the rated generator power $P_{g,rated}$.

In fact, in the case of high wind, it is necessary to limit the rotational speed to avoid the damage of the turbine and the electric machine. This limitation is obtained by the control of the pitch angle b .In region IV where the wind speed is upper than vcut-out, the wind turbine must be shut down in order to protect wind turbine against the stresses and fatigue damages. In this case, the pitch angle usually is set to 90° and power generation is stopped. The focus of this paper is on full load region (region III) to design an optimal pitch controller.

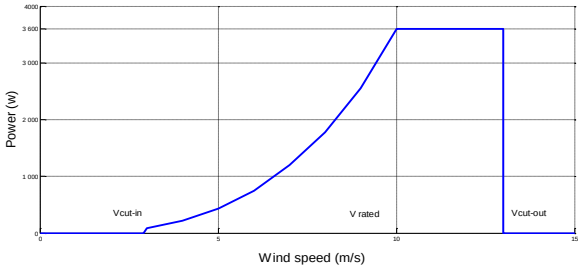

Fig .3. Wind Turbine operating regions

III. PITCH ANGLE CONTROL

The pitch control method is a basic approach for controlling the rotational speed of wind turbine. The conventional blade pitch angle control strategies are developed in this part. The pitch angle reference b_{ref} , is controlled by the input values, which may be as follows:

- Wind speed, as shown in Fig. 5(a). Perfectly, the pitch angle reference can be illustrated from the curve of the pitch angle versus wind speed, as shown in Fig.3. The direct measure of the wind speed makes this control strategy simple; however this is not a pertinent procedure, because it is difficult to measure the wind speed precisely.In fact, when the rotor speed exceeds the maximum rotor speed of turbine Ωtn, the pitch angle is increased to reduce the turbine torque Ct.

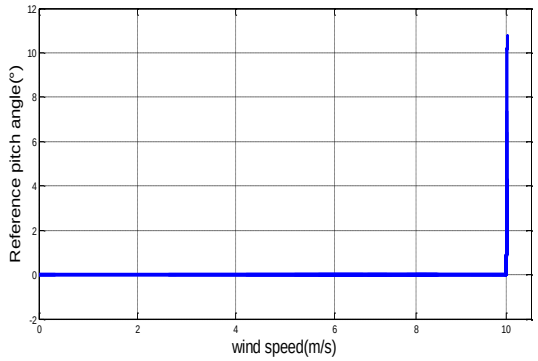

Fig .4. Reference Pitch angle

- Generator rotor speed, as shown in Fig. 5(b). The controlling rotor speed is compared with its reference. The error signal is then sent to the PI controller and produces the reference value of the pitch angle.

- Generator power, as shown in Fig. 5(c). The error signal of the generator power is sent to a PI controller. The PI controller produces the reference pitch angle b_{ref} .

For variable-speed wind turbines, a mechanical actuator is generally used to adjust the pitch angle of the blades in order to decrease the power coefficient Cp and maintain the power at its rated value. By linearization of the model to order 1 [14-16], the torque has been considered proportional to rotational speed of the turbine. The control strategy implemented is as follows:

$$\begin{cases} \beta_{ref} = \beta_0 = 0 & for\ 0 < \Omega_t < \Omega_{tn} \\ \beta_{ref} = \dfrac{\Delta\beta}{\Delta\Omega}\left(\Omega_t - \Omega_{tn}\right) + \beta_0 & for\ \Omega_t > \Omega_{tn} \end{cases} \quad (9)$$

With is the initial pitch angle (optimal value) and (rad/s) is the nominal mechanical turbine speed. Taking into account the blades orientation system which can be hydraulic or electric type, a transfer function of the first order is introduced in order to control the position of the blades according to a reference.

$$b = \frac{1}{1 + t_b s} b_{ref} \quad (10)$$

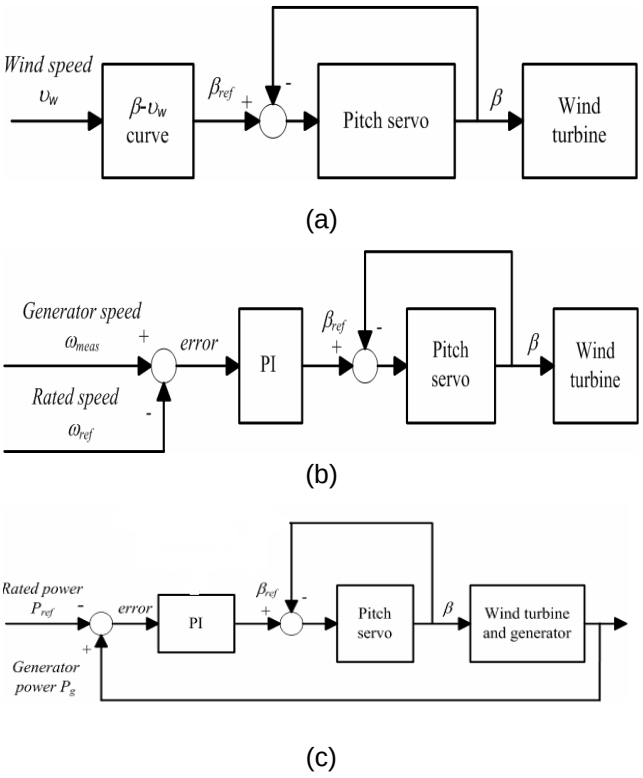

Fig .5. Pitch control strategy.(a) Wind speed; (b) generator rotor speed; (c) generator power

IV. PERMANENT- MAGNETIC SYNCHRONOUS GENERATOR AND RECTIFIER

A. Modeling of the PMSG

In this study a PMSG Park model is used, only the fundamental harmonic of the flux distribution in the air-gap of the machine is considered and the homopolar component is neglected, so the theory of the space vector gives the dynamic equations of the stator currents as follows:

$$\begin{cases} \dfrac{di_{sd}}{dt} = \dfrac{1}{L_s}\left(v_{sd} - R_s i_{sd} + L_s p\Omega_t i_{sq}\right) \\ \dfrac{di_{sq}}{dt} = \dfrac{1}{L_s}\left(v_{sq} - R_s i_{sq} - L_s p\Omega_t i_{sd} - p\Omega_t \varphi\right) \end{cases} \quad (11)$$

Where the phase resistance of the stator winding (Ω), the stator cyclic inductance (H), φ is the flux of the permanent magnetic (Wb), v_{sd} and v_{sq} are the d-q components of the stator voltages respectively (V), i_{sd} and i_{sq} are the d-q components of the stator currents respectively (A), and finally p is the number

of pairs of poles The electromagnetic torque is given by:

$$C_{em} = p\varphi i_{sq} \quad (12)$$

B. Modeling of the Rectifier

For the dynamic model of the system, we will divide the study of the converter to three parts: the alternative part, the discontinuous part which is composed by switches and the DC side. In this context, the function of switches is to establish a connection between the AC side and the DC bus; these switches are complementary, their state is defined by the following function:

$$S = \begin{cases} +1 \\ -1 \end{cases} \quad \text{for S=a,b,c} \quad (13)$$

Then, the input phase voltages and the output current may be written in function of Sj, Udc and input currents ia, ib, ic.

$$i_a + i_b + i_c = 0 \quad (14)$$

The phase between the input PWM rectifier voltages can be described by:

$$\begin{aligned} U_{Sab} &= (S_a - S_b).U_{DC} \\ U_{Sbc} &= (S_b - S_c).U_{DC} \\ U_{Sca} &= (S_c - S_a).U_{DC} \end{aligned} \quad (15)$$

The voltage equations of the system can be written as follows:

$$\begin{bmatrix} e_a \\ e_b \\ e_b \end{bmatrix} = R.\begin{bmatrix} i_a \\ i_b \\ i_c \end{bmatrix} + L.\frac{d}{dt}\begin{bmatrix} i_a \\ i_b \\ i_c \end{bmatrix} + \begin{bmatrix} U_{Sa} \\ U_{Sb} \\ U_{Sc} \end{bmatrix} \quad (16)$$

Avec:

$$\begin{aligned} U_{Sa} &= \frac{2S_a - S_b - S_c}{3}.U_{DC} \\ U_{Sb} &= \frac{2S_b - S_a - S_c}{3}.U_{DC} \\ U_{Sc} &= \frac{2S_c - S_a - S_b}{3}.U_{DC} \end{aligned} \quad (17)$$

Finally, we deduce the equation coupling between AC and DC sides by:

$$C\frac{dU_{Dc}}{dt} = S_a i_a + S_b i_b + S_c i_c \quad (18)$$

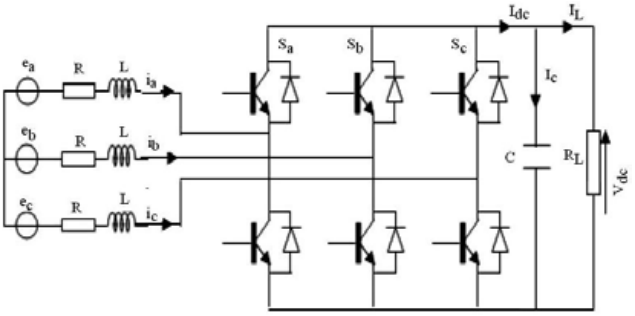

Fig .6. Diagram of MSAP- PWM Rectifier

C. Control

For variable-speed wind turbine, the maximum power is a cubic function of rotational speed. the development of the generator torque is based on the stator q-axis current component, but a freedom degree remains to set direct current. In order to minimize current for a given torque, and therefore, minimize resistive losses the direct-axis current component can be set at zero [17]. Thus, the control of the generator torque depends directly of the quadrature current component. The schematic diagram of the control loops of the permanent-magnet generator-side converter is illustrated on Fig. 7.The required d–q components of the rectifier voltage vector are determinate from two proportional plus integral (PI) current controllers: the first one is controlling the d-axis component of the current and the other one is controlling the q-axis component. In order to improve the dynamic response, compensation terms are added.The control requires the measurement of the stator currents, dc voltage, and rotor position.

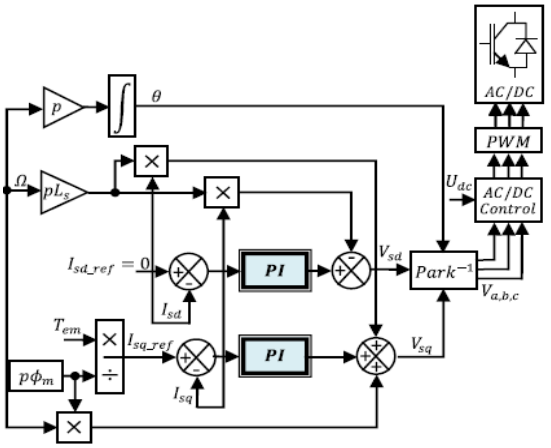

Fig .7. PMSG and converter control

D. Simulation Results and Discussion

Pitch angle control systems of the wind turbine were simulated using MATLAB/SIMULINK tool to test the control strategy and evaluate the performance of the system. The wind model is necessary to obtain realistic simulations of the power control of the wind turbines [18]. During 300 s, we have applied to the wind turbine model a variable wind profile between 6 and 12 m/s with an average value of 10 m/s. This sequence is obtained by adding a turbulent component to a slowly varying signal represented in Fig.8.

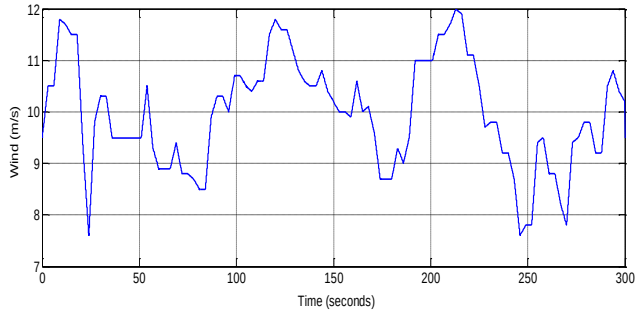

Fig .8. Wind speed

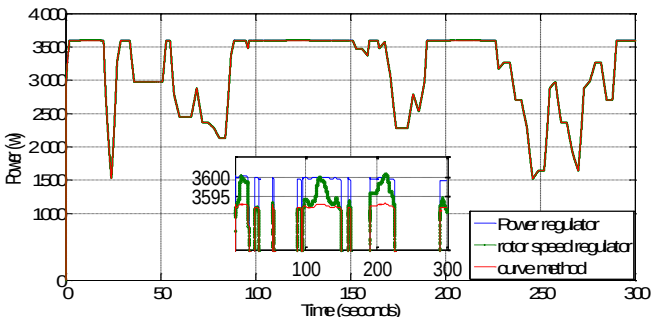

Fig .9. Output power

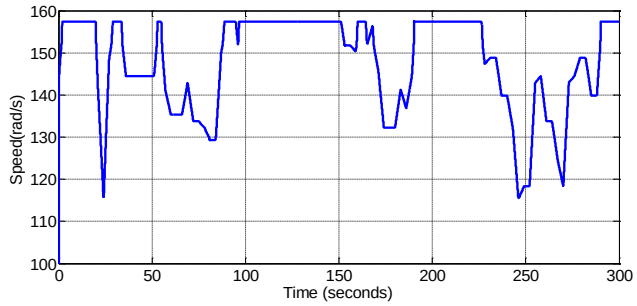

Fig .10. Mechanical speed

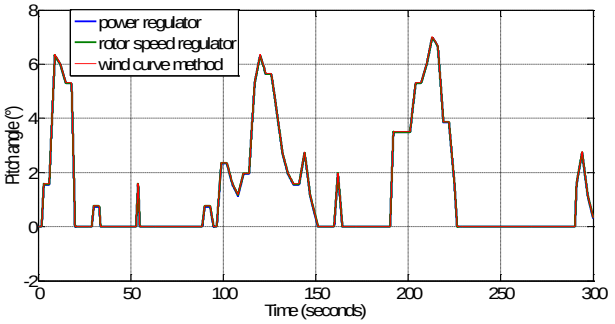

Fig .11. Pitch angle curve

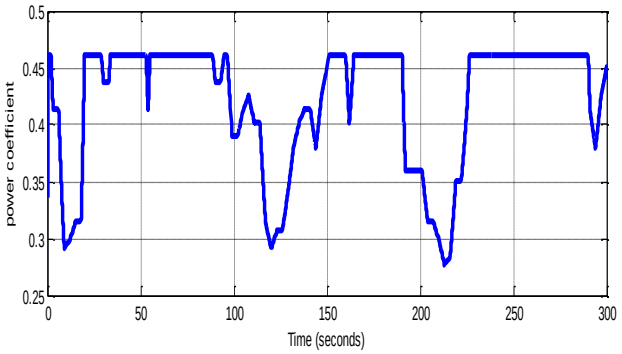

Fig .12. Power Coefficient

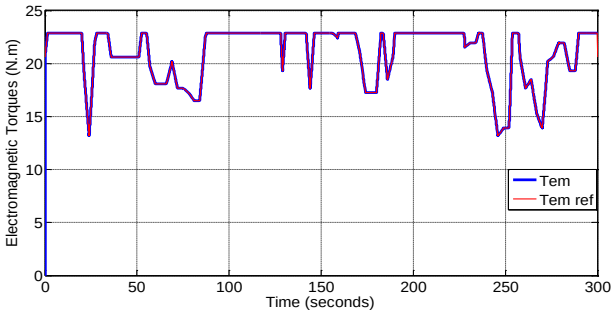

Fig .13. Electromagnetic Torque

The wind turbine is dimensioned to provide a nominal power at a nominal speed of 10 ms-1. Beyond this wind, it is necessary to protect the wind turbine against mechanical failures; therefore, we must limit its speed. This limitation will be obtained by a pitch control. The mechanical speed of the turbine represented in Fig. 10 is obtained next to the variation of the pitch angle illustrated in Fig. 11. The more the pitch angle increases, the more the power coefficient decreases (Fig. 12). The comparisons of different strategies illustrated in the simulation results show that pitch angle control strategy where the generator power is used as the controlling variable has a rapid pitch angle respond to the wind speed variation and minimum power ripples.

The response of the second strategy where rotor speed is used as the controlling variable has a squared error evaluated of 0.79 and the error of the

Response obtained next to the wind curve pitch control method is evaluated of 0.95, these results highlight the robustness of the strategy of the generator power controller.

V. CONCLUSION

In order to handle the pitch control in wind turbines, in this paper conventional methods are proposed. In fact, pitch angle control has an effect on the aerodynamic loads which may be controlled by the controller to achieve lower torque peak as well as lower fatigue loads.The simulation results show that the power controller has lower torque peak and lower power peak.

REFERENCES

[1] Lior, N. (2008) Energy Resources and Use: The Present Situation and Possible Paths to the Future, Energy, 33(6): pp. 842-57.

[2] Lund, P.D, (2009) Effects of Energy Policies on Industry Expansion in Renewable Energy, Renew Energy, 34(1): pp. 53-64.

[3] Østergaard P.A, (2009) Reviewing Optimization Criteria for Energy Systems Analyses of Renewable Energy Integration, Energy, 34(9):1236-45G.

[4] Wen, J., Zheng, Y., Donghan, F. (2009) A Review On Reliability Assessment for Wind Power, Renew Sustain Energy Review, 13(9): pp. 2485-94.

[5] Chowdhury M.A, Hosseinzadeh N, Shen W.X. (2012) Smoothing Wind Power Fluctuations by Fuzzy Logic Pitch Angle Controller. Renewable Energy; 38: pp. 224-233.

[6] Pao, L. Y., and Johnson, K. E. (2011) Control of Wind Turbines: Approaches, Challenges and Recent Development, IEEE Control Systems Magazine April.

[7] Duong, M.Q., Grimaccia, F., Leva, S., Mussetta, M., and Ogliari, E. (2014) Pitch Angle Control Using Hybrid Controller for All Operating Regions Of SCIG Wind Turbine System. Renewable Energy, 70:pp. 197- 203.

[8] Suryanarayanan, S. (2005) A. Dixit, Control of Large Wind Turbines: Review and Suggested Approach to Multivariable Design, Proc. of the American Control Conference, Portland, USA, pp. 686-690.

[9] Firdaus, A. A. (2014) Design and Simulation of Neural Network Predictive Controller Pitch-Angle in Permanent Magnetic Synchronous Generator Wind Turbine Variable Pitch System. In Information Technology, Computer and Electrical Engineering (ICITACEE), 1st International Conference on (pp. 346-350). IEEE.

[10] Yuan, X., & Li, Y. (2013) Control of Variable Pitch and Variable Speed Direct- Drive Wind Turbines in Weak Grid Systems with Active Power Balance. IET Renewable Power Generation, 8(2), pp. 119-131.

[11] Wang, Z., Cai, C., & Jia, K. (2013, July). Neural Network Adaptive Control for Constant Output Power of Variable Pitch Wind Turbine. In Vehicular Electronics and Safety (ICVES), 2013 IEEE International Conference on (pp. 165-170). IEEE.

[12] Muhando, E.B., Senjyua, T., Urasakia, N., Yonaa, A. K,,and Funabashi, T. (2007) Gain Scheduling Control of Variable Speed WTG Under Widely Varying Turbulence Loading, Renew Energy;32(14): p.2407

[13] Courtecuisse,V. Supervision D'une Centrale Multisources a Base D'éoliennes et de Stockage D'énergie Connectée au Réseau Electrique.

[14] Leclercq, L. (2004) Apport du Stockage Inertiel Associé a des Eoliennes dans un Réseau Electrique en Vue D'assurer des Services Systèmes Thèse de Doctorat : Génie Electrique : Université des Sciences et Technologies de Lille, Villeneuve d'Asq, , 171 p, n°3563.

[15] Melício R, Mendes, V.M.F., Catalão J.S. (2011) Transient Analysis of Variable- Speed Wind Turbines at Wind Speed Disturbances and a Pitch Control Malfunction, Applied Energy; vol.88; pp.1322-1330

[16] Rodriguez-Amenedo, J. L., Arnalte, S. et Burgos, J. C. Automatic Generation Control of Wind Farm with Variable Speed Wind.

[17] Kesraoui M, Korichi N, Belkadi A. (2011) Maximum Power Point Tracker of Wind Energy Conversion System. Renewable Energy; 36: pp. 2655-2662.

[18] Xing G. (2011) Research on Application of Fuzzy PID in Collective Pitch Control System. Control, Automation and Systems Engineering (CASE): pp. 1–4.

APPENDIX

- Wind turbine
  Dry friction torque : Cs = 953 Nm
  Number of blades : 3
  Viscous friction coefficient : f = 10-3N.m.s.rad-1
  Total inertia of the mechanical transmission: J =99 10-4 kg.m2

- PMSG
  Nominal power: Pn = 3.6kW
  Number of pole pairs: p=4
  Self-inductance: Ls = 15.1 mH
  Permanent magnetic flux: Φa = 0.5 Nm/A
  Stator resistance: Rs = 0.82Ω

Numerical Analysis of Fluid Flow and Heat Transfer for Different Fin Designs and Arrangements of Ceramic Plate-Fin High Temperature Heat Exchanger – Part I

Vijaisri Nagarajan[a], Yitung Chena*, Qiuwang Wangb[b], Ting Mab[b]

[a] Department of Mechanical Engineering, University of Nevada, Las Vegas, NV 89154-4027, USA

[b] Key Laboratory of Thermo-Fluid Science and Engineering, MOE, Xi'an Jiaotong University, Xi'an, Shaanxi, 710049, China

Abstract - In this study numerical analysis is carried out for four different types of fins namely rectangular, triangular, inverted bolt fins and ripsaw fins for staggered fin arrangement. The obtained results are compared with each other, and the design with best heat transfer and minimum pressure drop is selected. The working fluids used in the model are sulfur trioxide, sulfur dioxide, oxygen and water vapor. The operating pressure is 1.5 MPa and the operating temperature ranges from 973 K to 1223 K.

From the results it was found that the ripsaw fin design with thickness of 0.00005 m gives a good heat transfer rate with minimum pressure drop. The inverted bolt fins has the highest pressure drop due to the flow disturbances caused by the arrangement of the fins. The pressure drop and the heat transfer obtained for the rectangular and triangular fins are similar to each other. Friction factor, Colburn j- factor and dimensionless numbers like Nusselt number, Schmidt number are calculated for all the models. The average Nusselt number obtained for the ripsaw fin design with thickness of 0.00005 m for the top and bottom arrangement is 3.197. The friction factor for the ripsaw fins for the top and bottom arrangement is 0.522.

Keywords - Heat transfer enhancement factor, Ceramic Plate-Fin (PFHE) Heat Exchanger, Nusselt number, Schmidt number, pressure drop.

I. INTRODUCTION

Compact heat exchangers (CHE) plays an important role in the field of aerospace, transportation, nuclear and other industries. The need for lightweight, space saving and economical heat exchangers have driven to the development of compact heat exchangers. Surface area density of greater than $700 m^2/m^3$ is achieved by incorporating fins, ribs tec. The book by Hesselgreaves [1] describes different types of compact heat exchangers like plate-fin heat exchangers, spiral heat exchangers, printed circuit heat exchangers, tube fin heat exchangers etc. A plate-fin heat exchanger is a form of compact heat exchanger made of block of alternating layers of corrugated fins separated by parting sheets. Surface interruption prevents the continuous growth of the thermal boundary layer by periodically interrupting it. Thus the thicker thermal boundary layer which offers high thermal resistance to heat transfer are maintained thin and their resistance to heat transfer is reduced. In a plate-fin heat exchanger, fins are easily rearranged resulting in cross-flow, counter-flow, cross-counter-flow or parallel flow arrangements. From the research done by Kayansayan [2] the effect of the performance of plate-fin and tube cross-flow heat exchangers due to the outer surface geometry was considered.

In this study 10 geometrical configurations were tested and the Reynolds number was varied from 2,000 to 30,000. The results showed that the heat transfer coefficient strongly depends on the finning factor ε and the value of ε increases with decrease in j-factor. Ranganayakaulu & Seetharamu [3] carried out an analysis of a cross-flow compact plate-fin heat exchanger for the combined effects of two-dimensional longitudinal heat conduction through the exchanger wall, flow non-uniformity and temperature distribution was carried out using the finite element method. The exchanger effectiveness and thermal deterioration due to these effects were studied for various design and operating conditions. Wen & Li [4] proposed a study in order to enhance the uniformity of flow distribution. In their study an improved header configuration of plate-fin heat exchanger was proposed. The results showed that the fluid flow misdistribution was very severe in the direction of header length for the conventional header used in the industry due to poor header configuration.

Manglik & Bergles [5] studied the heat transfer and pressure drop correlations for the rectangular offset strip-fin compact heat exchanger. The f and j parameters were also found for laminar, transition and turbulent flow regimes. Steady state three-dimensional numerical model was used to study the heat transfer and pressure drop characteristics of an offset strip-fin heat exchanger by Bhowmik & Lee [6] Three different performance criteria for heat exchangers were tested for different fluids and the appropriate performance criteria for Pr = 7 and Pr = 50 were found to be JF (thermal-hydraulic performance factor) and j/f1/3.

Research has been carried out by Ma et al. [7] to find heat transfer and pressure drop performances of ribbed channels in the high temperature heat exchanger. From the results it was found that the Nusselt number and the friction factor were unsuitable to compare heat transfer and pressure drop performances at different temperature conditions. Schulte-Fischedick et al. [8] proposed a ceramic high temperature plate-fin heat exchanger for externally fired combustion process. Thermal performance and pressure drop in ceramic heat exchanger was evaluated using CFD simulations by Monteiro et al. [9]. Correlations for the Colburn and the friction factors for the Reynolds number ranging from 500 to 1500 were evaluated. Simulations with conjugate heat transfer were conducted and the results show the influence of mass flow rate on pressure drop and effectiveness of the heat exchanger. Ponyavin et al. [10] carried out a numerical analysis on the three-dimensional computational model of the ceramic high-temperature heat exchanger to investigate fluid flow, heat transfer, and chemical reaction and stress analysis within the decomposer. A decomposition rate of 0.515% was achieved for SO_3 using this design.

In this study numerical analysis of ceramic plate fin high temperature heat exchanger was carried out to investigate the fluid flow and heat transfer for different fin designs and fin arrangements. This study is an extension of the work done by Nagarajan et al. [11]. In order to save computational space and time a single channel model of the heat exchanger is modeled and studied. The main operating parameters for the heat exchanger design models for the current study are taken from the research done by Ponyavin et al. [10].

II. GEOMETRY OF THE MODEL AND MATERIAL PROPERTIES

In this study three-dimensional study of the fluid flow and heat transfer on four type of fins namely rectangular, triangular, inverted bolt fins and ripsaw fins for top and bottom arrangement is carried out. The computer aided geometry (CAD) geometry for all the models are modeled in Solid works [12] and simulations are carried out in ANSYS FLUENT 14.5.

The geometry and dimensions for the current study is taken from the work done by Ponyavin et al. [10] and from his study it was found that mass flow rate in all channels can be made almost uniform with a proper design of manifold channels. Hence by applying that concept a single channel model is developed to reduce computational time and memory. Single-banking configuration is used where in the hot and the cold plates are stacked alternatively.

The current study has hot fluid channel, cold fluid channel and two silicon carbide (SiC) solid regions. Helium fluid flows through the hot channel placed above the solid region and mixture of sulfur trioxide, sulfur dioxide, oxygen and water vapor flows through the cold fluid channel which is placed between the two solid regions. The flow is counter flow where the hot and the cold fluids enter the model from –x and +x directions and exit in the +x and –x directions, respectively. Figure 1 shows the geometry and dimensions of the single channel of plate fin heat exchanger.

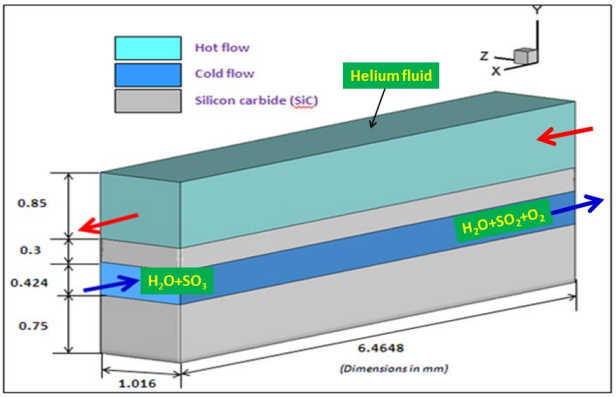

Fig .1. Geometry and dimensions of the channel

To enhance the thermal performance of the PFHE many fin designs are explored and studied. Table 1 shows the dimensions of all the fins

Table 1. Dimensions of various fins

Geometry	Definition
Rectangular fins	Height = 0.4 mm, length = 0.4 mm, width = 0.2 mm
Triangular fins	Height = 0.3 mm, breadth = 0.2 mm, length = 0.4 mm
Inverted bolt type fins	Diameter of top cylinder = 0.2 mm, diameter of bottom cylinder = 0.4 mm
Ripsaw fins	Larger height of the rectangle = 0.3 mm, smaller height of the rectangle = 0.15 mm, thickness = 0.05 m

In order to avoid backflow and provide entrance zone for each channel no fins are placed near the inlet and the outlet region on the cold channel. A study was carried out by increasing the length of the inlet and outlet to 5, 10 and 15 times the hydraulic diameter. At 10 times the hydraulic diameter the flow becomes fully developed and hence the length of the inlet and outlet are taken to be 10 times the hydraulic diameter. The material properties, boundary and operating conditions are taken from the work done by Nagarajan et al.

III. NUMERICAL METHOD AND ALGORITHM

The finite volume method is one of the most versatile discretization techniques used in CFD. The governing equations are solved in the Cartesian coordinate system using a control volume finite difference method that is similar to the approach introduced by Patankar [14]. ANSYS FLUENT [13] a commercial CFD program based on the finite volume method is among the most powerful packages of existing software used for solving fluid flow and heat transfer problems. The pressure-based segregated solution algorithm is used for the given problem. It can be simply described as the process of solving the governing equations in a sequential order as opposed to simultaneously as with a coupled solver.

The geometry of the model is meshed in ANSYS WORKBENCH [13] mesh generator. Hexahedral elements are used for meshing. The mesh is refined near the walls particularly for the cold flow channel with fins. The mesh refinement near the wall helps in calculating the fluid flow and heat transfer properties accurately. In order to check the mesh dependence on fluid flow and heat transfer properties, the grid independent study was done for both staggered and top and bottom arrangement. From the study, optimum nodes with difference in pressure drop and heat transfer of less than 5% is selected for further study. Around 481,558 cells, 1,496,152 faces and 532,599 nodes are selected for further study for all the cases. The friction factor, the Colburn factor and the Prandtl number are calculated using the formula shown below:

$$f = \frac{\left(\frac{\Delta P}{L}\right) * D_h}{(0.5 \cdot \rho \cdot U^2)} \quad (1)$$

$$j = \frac{\overline{Nu}}{Re \cdot Pr^{\frac{1}{3}}} \quad (2)$$

$$Pr = \frac{\mu \cdot C_p}{K} \quad (3)$$

The Schmidt number which is the ratio of the viscous diffusion rate to the mass diffusion rate is calculated based on the average temperature of the reacting channel. The validation of the fluid flow and heat transfer for the rectangular and ripsaw fins was carried out in the previous study done by Nagarajan et al. [11]. The friction factor was compared with the published result by Manson [15] and the Colburn factor was compared with the correlation published by Wieting [16]. The obtained CFD result was in good agreement with the published result and the slight offset is due to the difference in the dimensions of the geometry. Since the numerical results agree closely with the published results and follow the same trend, further research is carried out for the selected design.

IV. RESULTS AND DISCUSSIONS

In this paper studies are done to enhance the heat transfer rate by arranging the fins in the staggered manner. The single channel model with rectangular fins, triangular fins, inverted bolt fins and ripsaw fin with thickness of 0.00005 m are studied in this research. The fluid flow and heat transfer results were discussed in detail in the following.

A. Staggered Arrangement

1. Case 1 (Single Channel Model with Rectangular Fins)

The heat transfer surface area for the staggered rectangular fins is 2.25602·10-5 m^2 and triangular fins is 2.2058·10-5 m^2. The obtained heat transfer rate is high for the staggered arrangement. The obtained

pressure drop for the staggered rectangular and triangular fins is 28.41 Pa and 23.07 Pa, respectively. Due to the staggered arrangement of the fins there is more recirculation and hence higher pressure drop and friction factor are obtained. There is a significant increase in the friction factor for both the fins. The friction factor for rectangular fin is 0.894 and the friction factor for the triangular fin is 0.725. The average Nusselt number and the Colburn j-factor for the rectangular and triangular fins are 3.205, 0.016, and 3.235, 0.016, respectively. The Schmidt number for staggered rectangular and triangular fins is 0.316 and 0.316, respectively.

Flow over staggered rectangular plates produces recirculation in the wake region. In the wake which is formed downstream of the fin the heat transfer is decreased due to the flow disturbances caused by the fins. Relatively low heat transfer distributions are found immediately behind the fin because of flow recirculation with low local velocity. The strong recirculation zone is found behind the fins where the shear layer separates and rolls into vortices. There is no secondary vortex and only one recirculation zone is formed in the wake region. The length of the recirculation region increases with the increase in the Reynolds number. The recirculation region is located at 0.00154 m and the reattachment region of the shear layers is located at 0.00210 m. The velocity streamline for the staggered rectangular fins is shown in Figure 2.

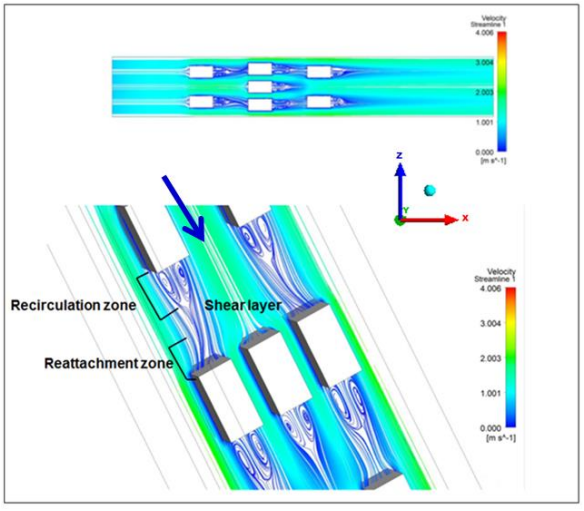

Fig .2. Velocity streamline for single channel model with staggered rectangular fins along y-plane at y=0.003 m and bottom solid regions

The velocity streamline along the z-plane from Figure 3 shows the recirculation zone behind the fins. It can be seen that recirculation zone for the first and the third plane are formed at the rear end of the second row of fins or the before the start of the third row of fins. This is due to the staggered arrangement of the fins. The z-plane is created at a distance of three-fourth of the first and the third fin and near the edge of the second fin. The recirculation vortex is formed in the wake region immediately behind the first and the third fin. Since the fin thickness is very small behind the second fin no vortices are formed behind the second fins. The shear layers continue from the second fin and they separate and form recirculation zone before the start of the third fin for the first and the third z-plane. Another vortex is formed in the wake region of the third fin and thereafter the shear layers reattach and the flow becomes stable without much fluctuation.

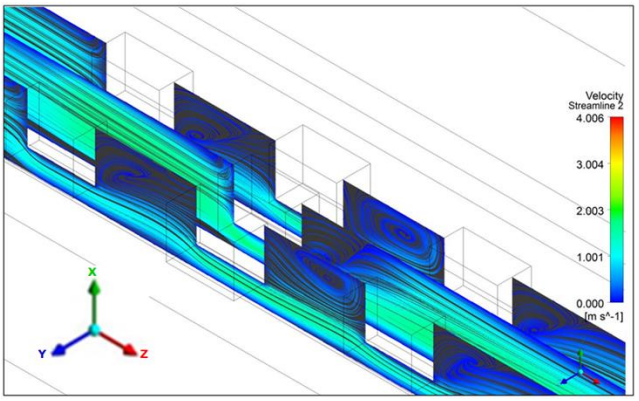

Fig .3. Velocity streamline for single channel model with staggered rectangular fins along z-plane at z=0.0015 m

Figure 4 shows the velocity and local heat transfer coefficient for the single channel model with staggered rectangular fins. The velocity of the fluid decreases from 0.800 m/s and it reaches minimum at the stagnation point P1. The velocity at the stagnation point is 0.101 m/s. The velocity reaches maximum at P2 where the fluid flows without any disturbance and is about 0.975 m/s. The velocity decreases as the fluid travels to the wake region of the fins. The velocity starts decreasing from P3 and becomes minimum at P4. Again the velocity increases and it becomes maximum at P7. The process repeats till the end of the third fin and then the velocity becomes stable till the fluid reaches the outlet. The heat transfer characteristics influenced by the generation of vortex and wake are observed similar to the uniform arrangement of the fins. The heat transfer coefficient is high at point near to the hot solid wall. The heat transfer rate is greatly enhanced due to the fin arrangement and the flow disturbance caused by

the fins. The heat flux is high near the wall and decrease near the bottom region of the fins. The heat transfer coefficient is low at fluid points near the fin bottom. The reason is due to the points are placed away from the hot solid wall and the heat is dissipated by the moving fluid.

The temperature difference is high at points away from the wall and the heat flux is less at these points. After the end of the third fin the heat transfer coefficient increases without much fluctuation till it reaches the outlet. There is increase in heat transfer as the fluid reaches the outlet due to the counterflow arrangement of the heat exchangers.

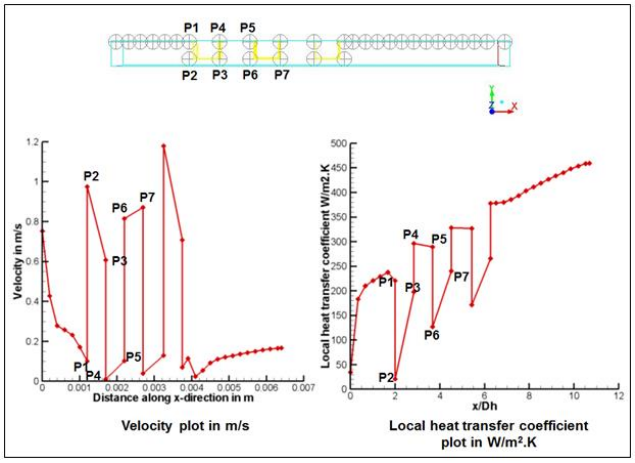

Fig .4. Velocity and local heat transfer coefficient for single channel model with staggered rectangular fins

2. Case 2 (Single Channel Model with Inverted Bolt Fins)

The inverted bolt fins gives a good heat transfer rate compared to all the other cases studied here. The obtained pressure drop for inverted bolt fin case is 31.64 Pa and the friction factor obtained is 0.996. Due to the recirculation and the vortex formed in the fins the obtained pressure drop and the friction factor for the fins are relatively high. The obtained maximum velocity in the fins is 2.027 m/s and the average inlet velocity is 0.8 m/s. The obtained average Nusselt number for the staggered inverted bolt fins is 3.418 and the Colburn j-factor is 0.017. The obtained Schmidt number for the staggered inverted bolt fins is 0.315. The pressure that drives the fluid is the static pressure and the resistance offered to the fluid by the tube causes the pressure drop as the fluid moves towards the exit.

The streamline velocity for the staggered inverted bolt fin is shown in Figure 5. Horseshoe vortices are formed around the cylinder and the pressure increases at the stagnation point. As the fluid flows around the cylinder shear layer separates and forms vortices behind the fins. Recirculation zone occurs at the wake region behind the cylinder. The vortices formed on the first and the third rows are symmetrical and there are two vortices one rotating in clockwise and the other in counter clockwise direction. Since there are three large cylinders in the second row, the vortices formed are not symmetrical. From Figure 5 the vortices can be found in the wake region on the first and third row of the fins but no recirculation is found in the second row of the fins.

Along the middle z-plane strong recirculation zone is found in the wake region. Since there are more recirculation zones found in the staggered arrangement the obtained pressure drop and friction is high compared to the uniform arrangement. The recirculation region of the staggered inverted bolt fins is located at 0.000957 m and the reattachment region of the shear layer is located at 0.00197 m.

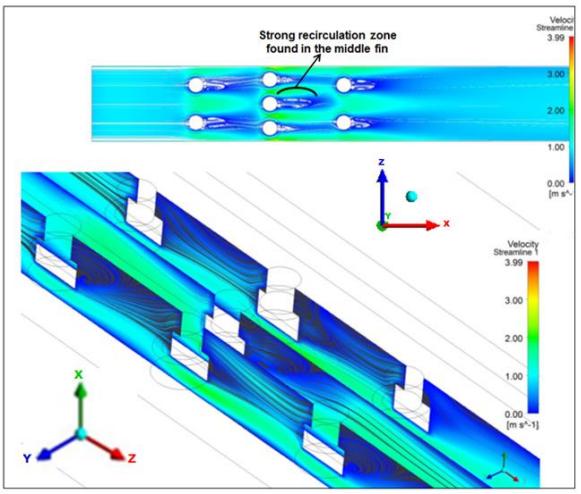

Fig .5. Velocity streamlines for the single channel model with staggered rectangular fins at y=0.003 m and z=0.0048 m

Figure 6 shows the velocity and heat transfer coefficient plot for the staggered inverted bolt fins. The velocity of the fluid decreases and it reaches minimum at P1. P1 is the stagnation point where the pressure is high and the velocity is low. The velocity increases from P2 and it becomes high at P3. The pressure is low at P2 and it starts increasing as the fluid travels to the rear of the cylinder. The velocity is minimum at P4 and the pressure is high at the point due to the adverse pressure gradient. Also the increase in pressure is due to the formation of the

recirculation zone in the wake of the fins. Again as the fluid moves towards the second fin the velocity increases and the pressure decreases until it reaches the wake region of the fins. The velocity is maximum at the end of the second fin due to the staggered arrangement of the fins and there is more space for the fluid to flow without any disturbance. The local heat transfer coefficient is high at points (P1, P4, etc.) near the top solid wall.

The heat flux is high at the top solid wall and it decreases at places away from the top solid wall or near the bottom region of the fins. After P4 the local heat transfer coefficient decreases due to the recirculation formed in the wake region of the fins. The local fluid velocity is low at these points which decrease the heat transfer rate. The temperature and local heat transfer coefficient are low at points (P2, P3 etc.) away from the hot solid wall. After the third fin the local heat transfer coefficient increases without much fluctuation till it reaches the outlet.

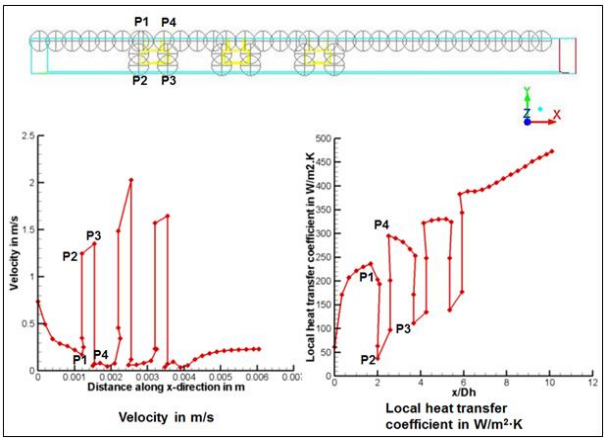

Fig .6. Velocity and local heat transfer coefficient for single channel model with staggered inverted bolt fins

3. Case 3 (Single Channel Model with Staggered Ripsaw Fin of Thickness 0.00005 m)

The single channel model with staggered ripsaw fins of thickness 0.00005 m gives a good heat transfer rate with reasonable pressure drop. The obtained pressure drop and friction factor are 16.59 Pa and 0.522, respectively. The pressure drop increases by about 1.4 Pa between the uniform and the staggered arrangement of the fins. The obtained heat transfer rate for the staggered ripsaw fin is 0.483 W and the average Nusselt number is 3.404. The obtained Colburn j-factor is 0.017. The average heat transfer coefficient increases from 211.18 W/m^2·K to 223.61 W/m^2·K. The Schmidt number obtained is 0.315. The obtained velocity streamlines show that there is no recirculation formed in the wake region. Since the fins are extremely thin and placed close to each other there are no vortices formed in this type of fin arrangement. The heat transfer rate is increased by the increase in the heat transfer surface area. Figure 7 shows the velocity streamline along the y and z-planes.

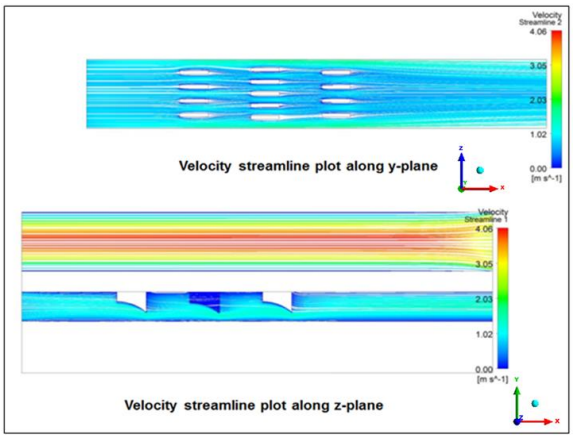

Fig .7. Velocity streamline for single channel model with staggered ripsaw fin with thickness of 0.00005 m at y=0.0037 m and z=0.0047 m

Figure 8 shows the pressure and local heat transfer coefficient for the staggered ripsaw fins with thickness of 0.00005 m. The pressure changes decreases from the inlet until it reaches the fins at P1. At this point the velocity is low due to the stagnation region and after this point the fluid flow around the fins and the flow separation starts. The pressure is low at P2 since there is no obstacle and the velocity is high at this point. As the fluid reaches the rear of the fins there will be a wake region where the pressure increases.

Eventhough there is no recirculation zone in this fin arrangement the pressure increases behind the fins and the velocity decreases due to the obstacles and the narrow space between the fins. This process continues until the fluid reaches the third fin and the flow increases till it reaches the outlet. Due to the resistance offered to the flow the pressure decreases as the fluid moves from the inlet to the outlet. The local heat transfer coefficient is high at points near the hot solid wall and is low at P2 away from the wall. In between P3 and P4 the local heat transfer coefficient decreases due to the decrease in local fluid velocity. The local heat transfer coefficient does not change a lot after the third fin and till the fluid reaches outlet.

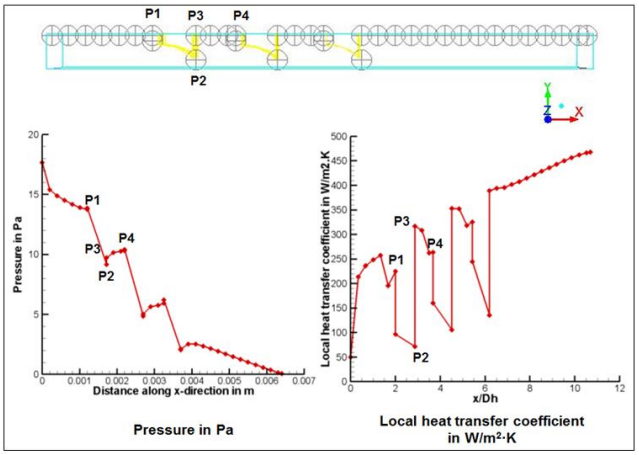

Fig .8. Pressure and local heat transfer coefficient for staggered ripsaw fin with thickness 0.0005 m

Table 2 shows the fluid flow and heat transfer values for the staggered arrangement of different fins. It has been found that the heat transfer and pressure drop increases for the staggered arrangement of the fins. It can be seen that the heat transfer rate is higher for ripsaw fin with thickness of 0.00005 m compared to the other cases. The obtained average Nusselt number is the highest for the inverted bolt fins and least for the ripsaw fins. The rectangular and triangular fins have similar values for the average Nusselt number and pressure drop. The Schimdt number is calculated based on the average temperature and it is found to be similar for all the cases studied. Due to the increase in pressure drop the friction factor is found to be the highest for inverted bolt fins followed by the rectangular fins. The ripsaw fin with thickness of 0.00005 m has the least friction factor.

Table 2. Fluid flow and heat transfer values for the staggered flow arrangement

Staggered arrangement				
Types	Rectangle fins	Triangle fins	Inverted bolt fins	Ripsaw fin with thickness 0.00005 m
Heat transfer rate (W)	0.481	0.478	0.482	0.494
Heat transfer surface area (m^2)	$2.256 \cdot 10^{-5}$	$2.205 \cdot 10^{-5}$	$2.233 \cdot 10^{-5}$	$2.262 \cdot 10^{-5}$
Heat transfer coefficient ($W/m^2 \cdot K$)	224.16	226.28	239.04	223.61
Average Nusselt number	3.205	3.235	3.418	3.197
Colburn *j* factor	0.016	0.016	0.017	0.016
Schimdt number	0.316	0.316	0.315	0.315
Friction factor *f*	0.894	0.725	0.996	0.522

There is a little increase in pressure drop compared to the uniform arrangement of the fins (Nagarajan et al. [11]). The ripsaw and the inverted bolt fins do not have noticeable increase in pressure drop. All the obtained pressure drop values are good for safe operation. Due to the smaller heat transfer surface area the effectiveness obtained is also less. There is increase in the effectiveness of the heat exchanger and the ripsaw fin with thickness of 0.00005 m is found to have the highest effectiveness. Table 3 shows the pressure drop and temperature values for the staggered arrangement.

Table 3. Pressure drop and temperature difference between the inlet and the outlet for the flow channels

	ΔP in reacting flow channel (Pa)	ΔT in reacting flow channel (K)	ΔT in helium flow channel (K)	Temperature gradient in reacting flow channel (K/mm)	Mass diffusivity in the reacting channel D_{AB} ($m^2 \cdot s^{-1}$)	Effectiveness ε
Rectangular fins	28.41	135.13	55.58	20.90	$6.25 \cdot 10^{-6}$	0.544
Triangular fins	23.03	132.89	52.72	20.55	$6.26 \cdot 10^{-6}$	0.535
Inverted bolt fins	31.64	134.22	58.26	20.76	$6.27 \cdot 10^{-6}$	0.540
Ripsaw fin with thickness of 0.00005 m	16.59	137.35	59.85	21.24	$6.28 \cdot 10^{-6}$	0.553

V. CONCLUSION

The obtained average Nusselt number is higher for inverted bolt fins which is 3.418 followed by triangular fins which is 3.235. The obtained pressure drop for

the rectangular fins is higher compared to the triangular fins for similar heat transfer rate. For similar heat transfer rate the obtained pressure drop which is 16.59 Pa is less for the ripsaw fins compared to the other fins. Hence ripsaw fin with thickness of 0.00005 m is considered to be the best design with less pressure drop and reasonable heat transfer rate. The inverted bolt fins have the highest average Nusselt number followed by the triangular fins.

The values of the average Nusselt number for the triangular and the rectangular fins are very close. Even though the obtained average Nusselt number for the ripsaw fin with 0.00005 m thickness which is $\overline{(Nu)}$ = 3.2 is less compared to the other fins, the obtained pressure drop for the ripsaw fins is the least of all the four fins which is 16.59 Pa. Hence the ripsaw fin thickness of 0.00005 m is selected as the best design with good heat transfer rate of 0.494 W and minimum pressure drop of 18.73 Pa.

REFERENCES

[1] Hesselgreaves, J. E. (2001). Compact Heat Exchangers Selection, Design and Operation. Oxford, UK: Elsevier Science Ltd.

[2] Kayansayan, N. (1994). Heat Transfer Characterization in Plate-Fin Tube Heat Exchangers. International Journal of Refrigeration, 17, pp. 49-57.

[3] Ranganayakulu, C. & Seetharamu. K.N. (1999). The Combined Effects of Wall Longitudinal Heat Conduction, Inlet Fluid Flow Non-Uniformity and Temperature Non-Uniformity in Compact Tube-Fin Heat Exchangers: A Finite Element Method. International Journal of Heat and Mass Transfer, 42, pp. 263-73.

[4] Wen, J. & Liu. (2004). Study of Flow Distribution and Its Improvement on the Header of Plate-Fin Heat Exchanger. Cryogenics, 44(11), pp. 823-831.

[5] Manglik, R. M. &. Bergles, A. E. (1995). Heat Transfer and Pressure Drop Correlations for the Rectangular Offset Strip Fin Compact Heat Exchanger. Experimental Thermal and Fluid Science, 10, pp. 171-80.

[6] Bhowmik, H., &. Lee, K. (2008). Analysis of Heat Transfer and Pressure Drop Characteristics in an Offset Strip Fin Heat Exchanger. International Communications in Heat and Mass Transfer, 36(3), pp. 259-263.

[7] Ma, T., Wang, Q. W., Zeng, M., Chen, Y., Liu, Y., & Nagarajan, V. (2012). Study on Heat Transfer and Pressure Drop Performances of Ribbed Channel in the High Temperature Heat Exchanger. Applied energy, 99, pp. 393-401.

[8] Schulte-Fischedick, J., Dreibigacker, V., & Tamme, R. (2007). An Innovative Ceramic High Temperature Plate-Fin Heat Exchanger for EFCC Processes. Applied Thermal Engineering, 27(8-9), pp. 1285-94.

[9] Monteiro, D. &. B., & Batista De Mello, P.E. (2012). Thermal Performance and Pressure Drop in a Ceramic Heat Exchanger Evaluated Using CFD Simulations. Energy, 45, pp. 489-496.

[10] Ponyavin, V., Chen, Y., Mohamed, T., Trabia, M.B., Hechanova, A.E., & Wilson, M. (2012). Design of a Compact Ceramic High-Temperature Heat Exchanger and Chemical Decomposer for Hydrogen Production. Heat Transfer Engineering, 33(10), pp. 853-70.

[11] Nagarajan, V., Chen, Y., Wang, Q., & Ma, T. (2014). Hydraulic and Thermal Performances of a Novel Configuration of High Temperature Ceramic Plate-Fin Heat Exchanger. Applied Energy, 113, pp. 589-602.

[12] SOLIDWORKS 2013., SOLIDWORKS Corp.

[13] ANSYS Inc. (2011). ANSYS 14.5 user's guide.

[14] Patankar, S. (1980). Numerical Heat Transfer and Fluid Flow. New York.

[15] Manson, S. V. (1950). Correlations of Heat Transfer Data and Friction Data for Interrupted Plate Fins Staggered In Successive Rows. Washington DC: National Advisory Committee for Aeronautics.

[16] Wieting, A. R. (1975). Empirical Correlations for Heat Transfer and Flow Friction Characteristics of Rectangular Offset-Fin-Plate-Fin Heat Exchanger. ASME, Int J. Heat Transfer, 97, pp. 480-490.

Numerical Analysis of Fluid Flow and Heat Transfer for Different Fin Designs and Arrangements of Ceramic Plate-Fin High Temperature Heat Exchanger – Part II

Vijaisri Nagarajan[a], Yitung Chena*, Qiuwang Wang[b], Ting Ma[b]
[a] Department of Mechanical Engineering, University of Nevada, Las Vegas, NV 89154-4027, USA
[b] Key Laboratory of Thermo-Fluid Science and Engineering, MOE, Xi'an Jiaotong University, Xi'an, Shaanxi, 710049, China

Abstract - In this study numerical analysis is carried out for four different types of fins for top and bottom fin arrangement. The obtained results are compared with each other and the design with best heat transfer and minimum pressure drop is selected. The working fluids used in the model are sulfur trioxide, sulfur dioxide, oxygen and water vapor. The operating pressure is 1.5 MPa and the operating temperature ranges from 973 K to 1223 K. From the results it was found that the ripsaw fin design with thickness of 0.00005 m gives a good heat transfer rate with minimum pressure drop.

The inverted bolt fins also gives a good heat transfer rate but due to the fin arrangement and the flow disturbances caused by the arrangement the pressure drop is the highest compared to other fins. The pressure drop and the heat transfer obtained for the rectangular and triangular fins are similar to each other. Friction factor, Colburn j- factor and dimensionless numbers like Nusselt number, Schmidt number are calculated for all the models. The average Nusselt number obtained for the ripsaw fin design with thickness of 0.00005 m for the top and bottom arrangement is 3.023. The friction factor for the ripsaw fins for the top and bottom arrangement is 0.589.

Keywords - Heat transfer enhancement factor, Ceramic Plate-Fin (PFHE) Heat Exchanger, Nusselt number, Schmidt number, pressure drop.

I. INTRODUCTION

Compact heat exchangers (CHE) plays an important role in the field of aerospace, transportation, nuclear and other industries. The need for lightweight, space saving and economical heat exchangers have driven to the development of compact heat exchangers. Surface area density of greater than 700 m2/m3 is achieved by incorporating fins, ribs tec. The book by Hesselgreaves [1] describes different types of compact heat exchangers like plate-fin heat exchangers, spiral heat exchangers, printed circuit heat exchangers, tube fin heat exchangers etc. A plate-fin heat exchanger is a form of compact heat exchanger made of block of alternating layers of corrugated fins separated by parting sheets. Surface interruption prevents the continuous growth of the thermal boundary layer by periodically interrupting it. Thus the thicker thermal boundary layer which offers high thermal resistance to heat transfer are maintained thin and their resistance to heat transfer is reduced.

In a plate-fin heat exchanger, fins are easily rearranged resulting in cross-flow, counter-flow, cross-counter-flow or parallel flow arrangements. From the research done by Kayansayan [2] the effect of the performance of plate-fin and tube cross-flow heat exchangers due to the outer surface geometry was considered. In this study 10 geometrical configurations were tested and the Reynolds number was varied from 2,000 to 30,000.

The results showed that the heat transfer coefficient strongly depends on the finning factor ε and the value of ε increases with decrease in j-factor. Ranganayakaulu & Seetharamu [3] carried out an analysis of a cross-flow compact plate-fin heat exchanger for the combined effects of two-dimensional longitudinal heat conduction through the exchanger wall, flow non-uniformity and temperature distribution was carried out using the finite element method. The exchanger effectiveness and thermal deterioration due to these effects were studied for various design and operating conditions. Wen & Li [4] proposed a study in order to enhance the uniformity of flow distribution. In their study an improved header configuration of plate-fin heat exchanger was proposed. The results showed that the fluid flow maldistribution was very severe in the direction of header length for the conventional header used in the

industry due to poor header configuration. Manglik & Bergles [5] studied the heat transfer and pressure drop correlations for the rectangular offset strip-fin compact heat exchanger. The f and j parameters were also found for laminar, transition and turbulent flow regimes. Steady state three-dimensional numerical model was used to study the heat transfer and pressure drop characteristics of an offset strip-fin heat exchanger by Bhowmik & Lee [6] Three different performance criteria for heat exchangers were tested for different fluids and the appropriate performance criteria for Pr = 7 and Pr = 50 were found to be JF (thermal-hydraulic performance factor) and j/f1/3.

Research has been carried out by Ma et al. [7] to find heat transfer and pressure drop performances of ribbed channels in the high temperature heat exchanger. From the results it was found that the Nusselt number and the friction factor were unsuitable to compare heat transfer and pressure drop performances at different temperature conditions. Schulte-Fischedick et al. [8] proposed a ceramic high temperature plate-fin heat exchanger for externally fired combustion process. Thermal performance and pressure drop in ceramic heat exchanger was evaluated using CFD simulations by Monteiro et al. [9].

Correlations for the Colburn and the friction factors for the Reynolds number ranging from 500 to 1500 were evaluated. Simulations with conjugate heat transfer were conducted and the results show the influence of mass flow rate on pressure drop and effectiveness of the heat exchanger. Ponyavin et al. [10] carried out a numerical analysis on the three-dimensional computational model of the ceramic high-temperature heat exchanger to investigate fluid flow, heat transfer, and chemical reaction and stress analysis within the decomposer. A decomposition rate of 0.515% was achieved for SO3 using this design.

In this study numerical analysis of ceramic plate fin high temperature heat exchanger was carried out to investigate the fluid flow and heat transfer for different fin designs and fin arrangements. This study is an extension of the work done by Nagarajan et al. [11]. In order to save computational space and time a single channel model of the heat exchanger is modeled and studied. The main operating parameters for the heat exchanger design models for the current study are taken from the research done by Ponyavin et al. [10].

II. GEOMETRY OF THE MODEL AND MATERIAL PROPERTIES

In this study three-dimensional study of the fluid flow and heat transfer on four type of fins namely rectangular, triangular, inverted bolt fins and ripsaw fins for top and bottom arrangement is carried out. The computer aided geometry (CAD) geometry for all the models are modeled in Solid works [12] and simulations are carried out in ANSYS FLUENT 14.5. The geometry and dimensions for the current study is taken from the work done by Ponyavin et al. [10] and from his study it was found that mass flow rate in all channels can be made almost uniform with a proper design of manifold channels. Hence by applying that concept a single channel model is developed to reduce computational time and memory. Single-banking configuration is used where in the hot and the cold plates are stacked alternatively.

The current study has hot fluid channel, cold fluid channel and two silicon carbide (SiC) solid regions. Helium fluid flows through the hot channel placed above the solid region and mixture of sulfur trioxide, sulfur dioxide, oxygen and water vapor flows through the cold fluid channel which is placed between the two solid regions. The flow is counter flow where the hot and the cold fluids enter the model from –x and +x directions and exit in the +x and –x directions, respectively. Figure 1 shows the geometry and dimensions of the single channel of plate fin heat exchanger.

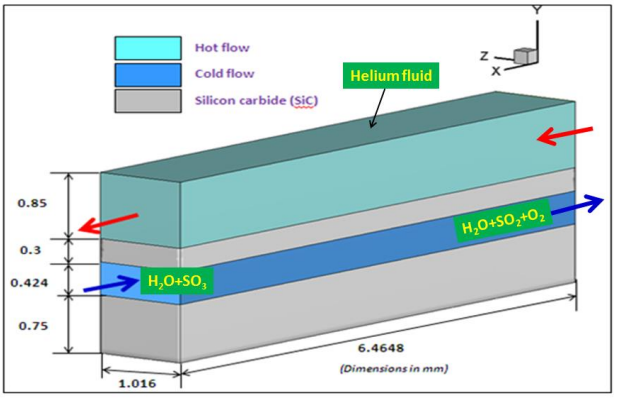

Fig .1. Geometry and dimensions of the channel

To enhance the thermal performance of the PFHE many fin designs are explored and studied. Table 1 shows the dimensions of all the fins

Table 1. Dimensions of various fins

Geometry	Definition
Rectangular fins	Height = 0.4 mm, length = 0.4 mm, width = 0.2 mm
Triangular fins	Height = 0.3 mm, breadth = 0.2 mm, length = 0.4 mm
Inverted bolt type fins	Diameter of top cylinder = 0.2 mm, diameter of bottom cylinder = 0.4 mm
Ripsaw fins	Larger height of the rectangle = 0.3 mm, smaller height of the rectangle = 0.15 mm, thickness = 0.05 m

In order to avoid backflow and provide entrance zone for each channel no fins are placed near the inlet and the outlet region on the cold channel. A study was carried out by increasing the length of the inlet and outlet to 5, 10 and 15 times the hydraulic diameter. At 10 times the hydraulic diameter the flow becomes fully developed and hence the length of the inlet and outlet are taken to be 10 times the hydraulic diameter. The material properties, boundary and operating conditions are taken from the work done by Nagarajan et al. [11].

III. NUMERICAL METHOD AND ALGORITHM

The finite volume method is one of the most versatile discretization techniques used in CFD. The governing equations are solved in the Cartesian coordinate system using a control volume finite difference method that is similar to the approach introduced by Patankar [14]. ANSYS FLUENT [13] a commercial CFD program based on the finite volume method is among the most powerful packages of existing software used for solving fluid flow and heat transfer problems. The pressure-based segregated solution algorithm is used for the given problem. It can be simply described as the process of solving the governing equations in a sequential order as opposed to simultaneously as with a coupled solver.

The geometry of the model is meshed in ANSYS WORKBENCH [13] mesh generator. Hexahedral elements are used for meshing. The mesh is refined near the walls particularly for the cold flow channel with fins. The mesh refinement near the wall helps in calculating the fluid flow and heat transfer properties accurately. In order to check the mesh dependence on fluid flow and heat transfer properties, the grid independent study was done for both staggered and top and bottom arrangement. From the study, optimum nodes with difference in pressure drop and heat transfer of less than 5% is selected for further study. Around 481,558 cells, 1,496,152 faces and 532,599 nodes are selected for further study for all the cases.The friction factor, the Colburn factor and the Prandtl number are calculated using the formula shown below:

$$f = \frac{\left(\frac{\Delta P}{L}\right) * D_h}{(0.5 \cdot \rho \cdot U^2)} \quad (1)$$

$$j = \frac{\overline{Nu}}{Re \cdot Pr^{\frac{1}{3}}} \quad (2)$$

$$Pr = \frac{\mu \cdot C_p}{K} \quad (3)$$

The Schmidt number which is the ratio of the viscous diffusion rate to the mass diffusion rate is calculated based on the average temperature of the reacting channel. The validation of the fluid flow and heat transfer for the rectangular and ripsaw fins was carried out in the previous study done by Nagarajan et al. [11]. The friction factor was compared with the published result by Manson [15] and the Colburn factor was compared with the correlation published by Wieting [16]. The obtained CFD result was in good agreement with the published result and the slight offset is due to the difference in the dimensions of the geometry. Since the numerical results agree closely with the published results and follow the same trend, further research is carried out for the selected design.

IV. RESULTS AND DISCUSSIONS

A. Fins Arranged on the Top and the Bottom Solid

In this study, the fins are arranged on both the top and the bottom solid regions to enhance the heat transfer. It is found that since the bottom solid region doesn't have any heat input and the heat transfer is only from top solid region there is a little increase in heat transfer rate compared to the uniform arrangement. The pressure drop obtained is higher compared to the other two arrangements because there is an increase in heat transfer surface area and more flow disturbances produced by the fins.

1. Case 1 (Single Channel Model with Rectangular Fins)

In this study the rectangular fins are arranged on both the top and bottom solid regions. The heat transfer surface area of the rectangular fin arrangement is 2.47·10-5 m2. The pressure drop obtained for this model is 56.49 Pa which is twice higher than the staggered arrangement. The friction and Colburn j-factor is 1.778 and 0.016, respectively. Due to the top and bottom arrangement there is strong flow disturbance which results in the increase of pressure drop.

Figure 2 shows the pressure and velocity contour for the single channel model with rectangular fins arranged on the top and the bottom solid regions.

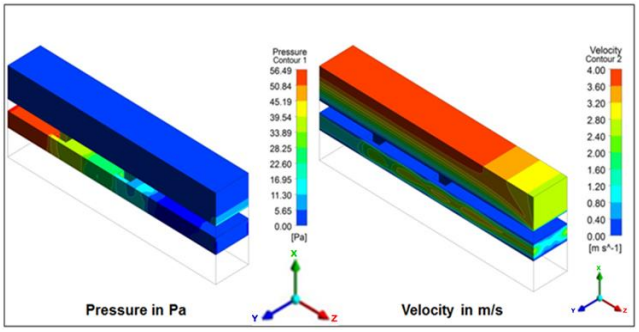

Fig .2. Pressure in Pa and velocity in m/s contour for single channel model with rectangular fins arranged on the top and bottom solid regions

The horseshoe vortex is formed at the beginning of the fins and it extends along the sides. Recirculation is formed behind the fins in the wake region. The shear layer separates and form twin vortices where one vortex rotates in the clockwise direction and the other in the opposite direction, In Figure 3, the recirculation can be seen clearly in the second and the fourth row of fins but not in the first and the third row. The y-plane is taken at a distance from three-fourth of the top fin and from one-fourth of the bottom fin. Hence more recirculation is found on the top fins.

From the streamline along the z-plane recirculation can be found alternately along the top and the bottom fins. Since the Reynolds number is only 244 there is no secondary vortex formed. The recirculation region is located at 0.00108 m and the reattachment region of the shear layer is located at 0.00201 m.

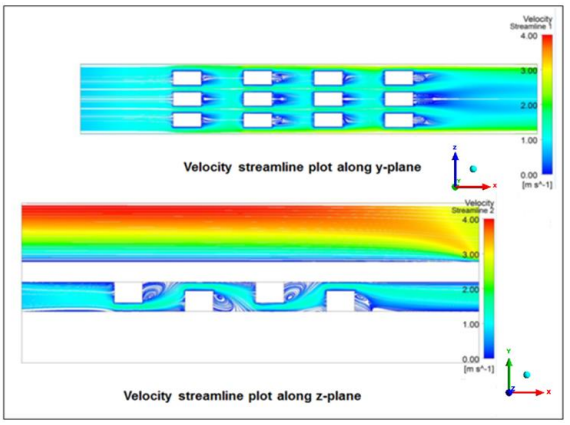

Fig .3. Velocity streamline for the single channel model with rectangular fins arranged on the top and bottom solid regions at y=0.0032 m and z=0.0053 m

Figure 4 shows the top and bottom arrangement of rectangular fins for pressure and velocity plots. The pressure decreases uniformly from inlet to P1 where the fins start. Pressure is high at P1 and it starts decreasing and reaches minimum at P2. Similarly the velocity increases as the fluid flow around the fins and becomes maximum at P2. Recirculation zone is formed behind the top fin and adverse pressure gradient is formed. Hence pressure increases at P3 and the velocity is minimum at P3.

The bottom fin starts and the pressure is low at P4 where there is no obstacle and the velocity increases. The pressure decreases as the fluid travels to the rear of the fins. The process continues till the end of the fourth fin and the pressure and velocity becomes stable till it reaches the outlet.

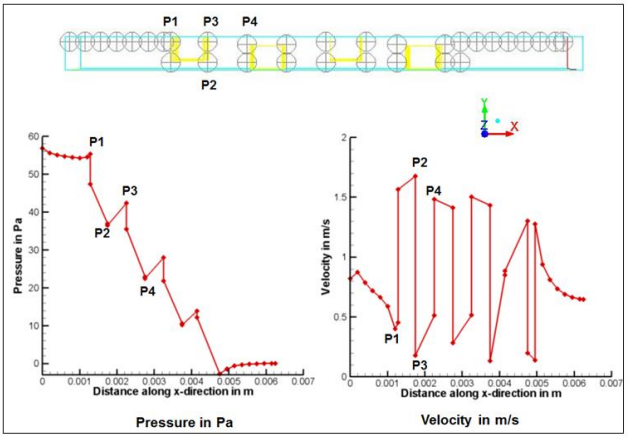

Fig .4. Pressure and velocity for single channel model with rectangular fins arranged on the top and bottom solid regions

Figure 5 shows the temperature and the local heat transfer coefficient for the rectangular fins. The temperature and the local heat transfer coefficient increases until it reaches P1. The local heat transfer coefficient decreases at P2, P3 which are placed away from the hot solid wall.

The temperature becomes high at P4. The fins placed on the bottom solid are away from the heat source and hence the temperature and the local heat transfer coefficient at P5 and P6 are small. The heat flux is high at the upper solid wall and it decreases away from the hot wall. The temperature increases at P7 where the top fin start and again decreases at P8. Away from the wall the temperature difference increases resulting in the decrease of the heat transfer coefficient.

The process repeats till the end of the fins and the temperature and the local heat transfer coefficient increases till the fluid reaches the outlet. Due to the increase in the heat transfer surface area, the obtained heat transfer rate is high compared to the uniform arrangement of rectangular fins.

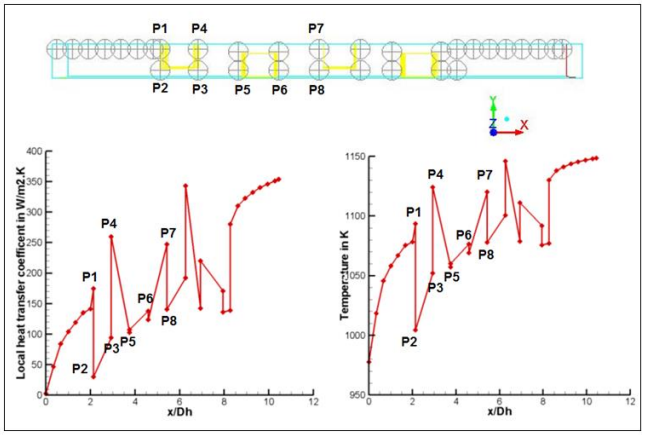

Fig .5. Temperature and local heat transfer coefficient of single channel model with rectangular fins arranged in the top and bottom solid regions

2. Case 2 (Single Channel Model with Triangular Fins)

Two rows with three triangular fins arranged in alternate manner along the top and bottom solid regions are studied. The heat transfer surface area of triangular fins is smaller than rectangular fins. The heat transfer surface area for the top and bottom fin arrangement is 2.342·10-5 m2. The pressure drop and the friction factor for this model are 34.04 Pa and 1.073, respectively. The average Nusselt number and the Colburn j-factor is 3.099 and 0.016, respectively. The obtained heat transfer rate and the pressure drop is less than the rectangular fins.

Figure 6 shows the velocity streamline for the triangular fins along y and z-planes. The obtained streamlines are similar to the rectangular fins. Recirculation zone is found in the wake region forming symmetrical twin vortices behind each fin. The recirculation region is located at 0.00123 m and the reattachment region is located at 0.00207 m.

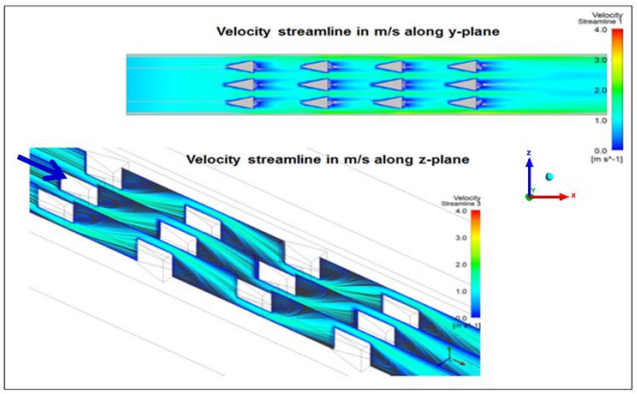

Fig .6. Velocity streamline for single channel model with triangular fins arranged on the top and bottom solid regions at y=0.0045 m and z=0.0059 m

It can be seen that recirculation zone is formed behind the top and bottom fins alternately. Since the Reynolds number is low there is no formation of secondary vortex. Though the bottom solid does not have any heat input the heat transfer rate of this model is more than the staggered triangular fin arrangement. The increase in heat transfer is due to the increase in heat transfer surface area. The pressure, velocity and local heat transfer coefficient plot for the triangular fins are similar to the rectangular fin model and hence not shown in this study.

3. Case 3 (Single Channel Model with Inverted Bolt Type Fins)

The obtained heat transfer rate is higher than the triangular and rectangular fins. The heat transfer surface area is 2.438·10-5 m2 which is higher than all the fins. The only disadvantage of this fin type is the high pressure drop and the friction factor. Due to the complex design and arrangement horseshoe vortices are formed which increases the pressure drop and the friction factor.

The obtained local heat transfer coefficient and the average Nusselt number are 221 W/m2·K and 3.16, respectively. The pressure and velocity for the inverted bolt fin are similar to the rectangular and triangular fins. The velocity streamline plot for the inverted fin mounted on the top and the bottom solids is shown in Figure 7. A strong horseshoe vortex is formed in front of the cylindrical fins and fluid flows around the cylinder to the rear side. The shear layers starts to separate and recirculation zone is formed in the rear side of the top fins for the top fins and in the rear side of the bottom fins for the bottom fins.

The recirculation zone covers almost three-fourth of the space between the fins and the shear layers reattach to the wall after the wake region. Again flow separation occurs and this results in periodic breaking of the boundary layer thus enhancing the heat transfer. The recirculation region is located at 0.00123 m and the reattachment region of the shear layer is located at 0.001978 m.

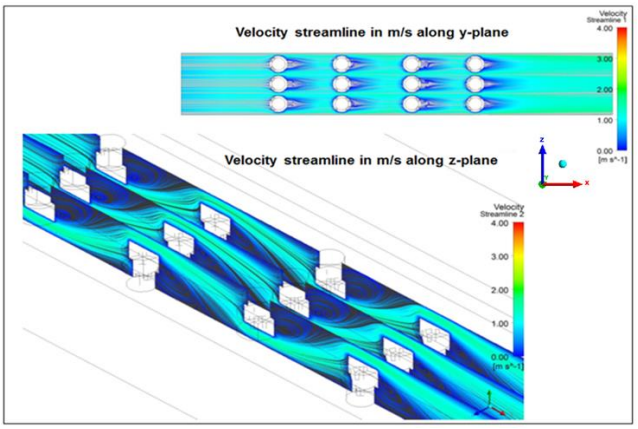

Fig .7. Velocity streamline for the single channel model with inverted bolt fins arranged on the top and bottom solid regions at y=0.0036 m and z=0.0045 m

Figure 8 shows the velocity and local heat transfer coefficient. The velocity along the flow is uniform till it reaches the fins. The velocity is low at P1 and the pressure is high. The velocity increases at P2 as the fluid flow around the fins and it reaches a maximum at P3. The pressure is least at this point. Recirculation takes place at the rear of the fins and the velocity is minimum at P4 and the pressure is maximum at P4. The fluid then flows through the bottom fins and the velocity is minimum at P5 and pressure is high at this point. The fluid velocity then reaches maximum at P6 and the pressure is minimum at P6.

The process continues until it reaches the fourth row of the fins and it becomes stable after the end of the fins. The local heat transfer coefficient is high for the top fins which are in contact with the solid wall. The temperature and local heat transfer coefficient is low at P2, P3, P5, etc. which are away from the hot solid surface. After the fourth tow of the fin the temperature increases without much fluctuation till reaches the outlet.

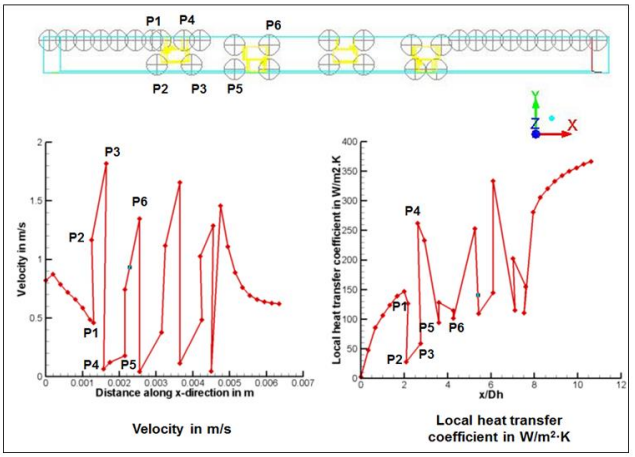

Fig .8. Velocity and local heat transfer coefficient for the single channel model with inverted bolt fins arranged on the top and bottom solid regions

4. Case 4 (Single Channel Model with Ripsaw Fin Thickness of 0.00005 m)

The last model studied in this research is the ripsaw fin thickness of 0.00005 m arranged on the top and bottom solid regions. The heat transfer surface area is 2.371·10-5 m2. This type of arrangement has no recirculation due to their shape. As a result of this the obtained pressure drop and the friction factor is also less. The obtained friction factor and the pressure drop is 0.589 and 18.73 Pa, respectively.

The obtained average heat transfer coefficient and the average Nusselt number is 211.43 W/m2·K and 3.023, respectively. The streamline velocity plot shows that there is no recirculation the streamlines are parallel to the flow direction. The obtained velocity and local heat transfer coefficient is similar to the other fins explained above. Figure 9 shows the velocity streamline along the y and z-planes.

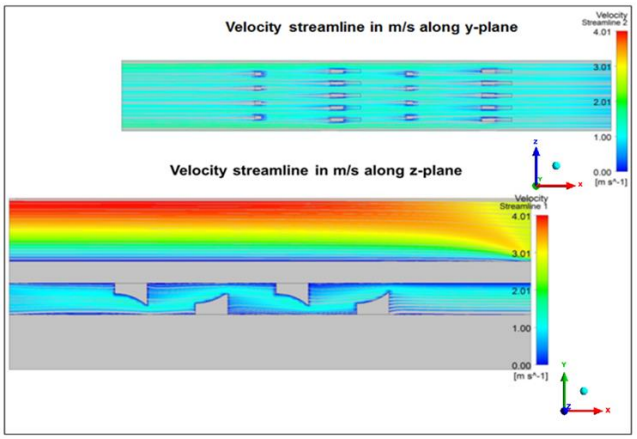

Fig .9. Velocity streamline for single channel model with ripsaw fin of thickness 0.00005 m arranged on the top and bottom solid regions at y=0.0032 m and y=0.0046 m

The pressure, temperature and local heat transfer coefficient plots are similar to the other fin types. The velocity is low and the pressure is high at the stagnation point and in the recirculation region. The temperature and the local heat transfer coefficient are high at places near the top solid wall and low at regions away from the hot solid wall.

From the results it is found that there is not significant increase in heat transfer for the top and bottom fin arrangement. The reason is because the bottom solid has no heat input and the heat is transferred only from the top solid. In the top and bottom arrangement there are only 6 fins placed in the hot solid wall and 6 placed in the cold solid wall. Hence the obtained heat transfer is less than the regular staggered arrangement of the fins.

In real case, the channel arrangement is periodic and the hot helium fluid flows below the cold solid wall and heat transfer will be increased by having fins on both the solid walls. However in the current study the hot flow channel is present only above the reacting channel and hence the heat transfer obtained is less. The obtained average Nusselt number and the Colburn j factor is similar to the uniform fin arrangement. The friction factor is increased and the ripsaw fin with thickness of 0.00005 m is found to have the lowest friction factor.

The effectiveness of the heat exchanger increases for the top and bottom arrangement. The pressure drop increases due to the presence of fins on both the top and bottom solids. In this arrangement recirculation and vortices are formed which increases the pressure drop and friction factor. The pressure drop is the highest for rectangular fins and least for the ripsaw fins. Hence ripsaw fin with thickness of 0.00005 m is considered to be the best design because it gives good heat transfer with minimum pressure drop. The obtained effectiveness is around 52 to 54% for all the fin designs. The heat transfer surface area is less and hence the effectiveness of the heat exchanger is less. The length of the heat exchanger channel with staggered rectangular, triangular and ripsaw fin with thickness of 0.00005 m is increased from 0.0064648 m to 0.064648 m.

The heat transfer area of the long staggered rectangular fins is 2.44·10-4 m2, triangular fins is 2.35·10-4 m2 and the ripsaws with thickness of 0.00005 m is 2.4354·10-4 m2. The obtained heat exchanger effectiveness for rectangular fin is 80.15%, triangular fin is 87.25% and ripsaw fins with thickness of 0.00005 m is 92.13%.

V. CONCLUSION

The obtained average Nusselt number is higher for inverted bolt fins which is 3.201 followed by triangular fins which is 3.099. The obtained pressure drop for the rectangular fins is higher compared to the triangular fins for similar heat transfer rate. For similar heat transfer rate the obtained pressure drop which is 18.73 Pa is less for the ripsaw fins compared to the other fins. Hence ripsaw fin with thickness of 0.00005 m is considered to be the best design with less pressure drop and reasonable heat transfer rate.

The inverted bolt fins have the highest average Nusselt number followed by the triangular fins. But the pressure drop for the rectangular fin which is 56.49 Pa is almost twice that of the triangular fin which is 34.08 Pa. Eventhough the obtained average Nusselt number for the ripsaw fin with 0.00005 m thickness which is $(Nu)^{-}$= 3.026 is less compared to the other fins, the obtained pressure drop for the ripsaw fins is the least of all the four fins which is 18.73 Pa.

Hence the ripsaw fin thickness of 0.00005 m is selected as the best design with good heat transfer rate of 0.475 W and minimum pressure drop of 18.73 Pa. The effectiveness increased from 52% for 0.0064648 m to 82% for 0.064648 m.

REFERENCES

[1] Hesselgreaves, J. E. (2001). Compact Heat Exchangers Selection, Design and Operation. Oxford, UK: Elsevier Science Ltd.

[2] Kayansayan, N. (1994). Heat Transfer Characterization in Plate-Fin Tube Heat Exchangers. International Journal of Refrigeration, 17, pp. 49-57.

[3] Ranganayakulu, C. & Seetharamu. K.N. (1999). The Combined Effects of Wall Longitudinal Heat Conduction, Inlet Fluid Flow Non-Uniformity and Temperature Non-Uniformity in Compact Tube-Fin Heat Exchangers: A Finite Element Method. International Journal of Heat and Mass Transfer, 42, pp. 263-73.

[4] Wen, J. & Liu. (2004). Study of Flow Distribution and Its Improvement on The Header of Plate-Fin Heat Exchanger. Cryogenics, 44(11), pp. 823-831.

[5] Manglik, R. M. &. Bergles, A. E. (1995). Heat Transfer and Pressure Drop Correlations for The Rectangular Offset Strip Fin Compact Heat Exchanger. Experimental Thermal and Fluid Science, 10, pp. 171-80.

[6] Bhowmik. H., &. Lee.K. (2008). Analysis of Heat Transfer and Pressure Drop Characteristics in an Offset Strip Fin Heat Exchanger. International Communications in Heat and Mass Transfer, 36(3), pp. 259-263.

[7] Ma, T., Wang, Q. W., Zeng, M., Chen, Y., Liu, Y., & Nagarajan, V. (2012). Study on Heat Transfer and Pressure Drop Performances of Ribbed Channel in the High Temperature Heat Exchanger. Applied energy, 99, pp. 393-401.

[8] Schulte-Fischedick, J., Dreibigacker, V., & Tamme, R. (2007). An Innovative Ceramic High Temperature Plate-Fin Heat Exchanger for EFCC Processes. Applied Thermal Engineering, 27(8-9), pp. 1285-94.

[9] Monteiro, D. &. B., & Batista, De Mello, P.E. (2012). Thermal Performance and Pressure Drop in a Ceramic Heat Exchanger Evaluated Using CFD Simulations. Energy, 45, pp. 489-496.

[10] Ponyavin, V., Chen, Y., Mohamed, T., Trabia, M.B., Hechanova, A.E., & Wilson, M. (2012). Design of a Compact Ceramic High-Temperature Heat Exchanger And Chemical Decomposer for Hydrogen Production. Heat Transfer Engineering, 33(10), pp. 853-70.

[11] Nagarajan, V., Chen, Y., Wang, Q., & Ma, T. (2014). Hydraulic and Thermal Performances of a Novel Configuration Of High Temperature Ceramic Plate-Fin Heat Exchanger. Applied Energy, 113, pp. 589-602.

[12] SOLIDWORKS 2013., SOLIDWORKS Corp.

[13] [ANSYS Inc. (2011). ANSYS 14.5 user's guide.

[14] Patankar, S. (1980). Numerical Heat Transfer and Fluid Flow. New York.

[15] Manson, S. V. (1950). Correlations of Heat Transfer Data and Friction Data for Interrupted Plate Fins Staggered in Successive Rows. Washington DC: National Advisory Committee for Aeronautics.

[16] Wieting, A. R. (1975). Empirical Correlations for Heat Transfer and Flow Friction Characteristics of Rectangular Offset-Fin-Plate-Fin Heat Exchanger. ASME, Int J. Heat Transfer, 97, pp. 480-490.

Aerodynamic Optimization of a Wind Turbine Blade Designed for Egypt's Saharan Environment Using a Genetic Algorithm

Khaled Yassin, Aya Diab, Zakaria Ghoneim
Mechanical Power Engineering Dept. Faculty of Engineering, Ain Shams University Cairo, Egypt
aya.diab@eng.asu.edu.eg

Abstract – This work aims to optimize the aerodynamic parameters (airfoil chord lengths and twist angles smoothed using Bezier curves) of the NREL 5MW wind turbine and a wind turbine designed for site-specific wind conditions to increase the wind turbine's annual energy production (AEP) under this site conditions. This optimization process is carried out using a Genetic Algorithm (GA) developed in MATLAB and coupled with NREL's FAST Modularization Framework. The results showed that after optimizing the NREL 5MW wind turbine design, the AEP was improved by 5.9% of the baseline design AEP, while a site-specific designed wind turbine using Schmitz equations showed 1.2% improvement in AEP. These results show that optimization of wind turbine blade aerodynamic parameters for site-specific wind conditions leads to improvement in AEP and hence decreasing cost of energy generated by wind turbines.

Keywords **-** Wind Turbine, aerodynamics, optimization, genetic algorithm, site-specific wind turbine.

I. INTRODUCTION

Wind energy is the fastest growing source of energy in the world today, with an average growth rate of nearly 30% per year over the past 10 years. With global warming, energy security, and rising fuel prices being main public concerns, it is reasonable to assume that the growth of the wind energy industry will continue at an unprecedented pace.

The global energy challenge is certainly not foreign to Egypt whose developmental needs mandate the addition of 2000-3000 MW of installed capacity each year. Luckily, Egypt is endowed with an excellent wind energy potential, especially in the Red Sea coast area where a capacity of 20,000 MW could be achieved, as the annual average wind speed is around 10 m/s. Egypt's national energy planning incorporates a target of 1,050 MW wind capacity to be installed by the end of the Sixth Five-Year Plan period (2007-2012). On the long term, the government envisages 20% of electricity to come from renewable energy by 2020. To meet this target, it is expected that 12% will be satisfied by wind power. With Egypt's wind energy potential and its ambitious plan to expand wind energy contribution in electric energy production, the need to develop its own technology in wind turbine becomes vital. In Egypt, while viable wind farm locations with high quality wind resources exist in the Gulf of Suez region (for example Zaafarana, and Jabal El-Zeit), improved blade design optimized for a particular location can significantly reduce the unit cost of electricity, amortized over the turbine lifetime. This is expected to expand the number of locations that are economically viable, such as the east and the west of the Nile.

In the last few years, the topic of developing and optimization of wind turbine rotors attracted a lot of attention. Maheri et al [1] applied a combined analytical/FEA coupled FSI to design and optimize bend-twist adaptive blades to increase average generated power over the operation wind speed. In their work, shell thickness, ply angles, and pre-twist distribution were optimized to increase the energy generated at this wind speed. Xiong et al.[2] presented an optimization model of HAWT blade using Weibull frequency distribution function (to simulate wind speeds around the year) and extended compact genetic algorithm (ECGA) to optimize airfoil shapes, chord lengths and twist angles of a 1.3 MW turbine blade to maximum annual energy production.

Xudong et al. [3] presented optimization procedure of wind turbine blade. This procedure includes both structural dynamics and Blade Element Momentum theory (BEM) to optimize annual energy production and cost of the rotor by variation of chord, twist and relative thickness. These procedures are applied on

three different wind turbines: 25 kW MEXICO experimental rotor, Tjaereborg 2MW rotor and NREL 5 MW rotor to compare between original and optimized performance of the mentioned three rotors. The main goal of this work is to design an optimized utility scale wind turbine as a step towards the ultimate long term goal of indigenously fabricating a utility scale wind turbine suitable for operation in the Egyptian harsh operating environment, particularly of high temperature, high humidity and the existence of sand and wind speeds that may reach 10-11 m/sec and a capacity factor of 60%.

Realization of this goal is a major task and has to be carried out progressively. Two of the main components of the turbine, the rotor blades, and the tower are obvious candidates. The present work concentrates on the use of genetic algorithm for the aerodynamic design optimization of the rotor blades of a utility scale wind turbines, which, according to Mohamed and Wetzel [4], is a major contributor to the wind turbine cost.

II. AERODYNAMIC BLADE DESIGN

The blade element momentum theory is well known and has been widely used. Blade Element Momentum (BEM) is an extension of the simple 1D momentum theory. The low computational cost of the relatively good accuracy has led to its widespread use in the wind turbine industry, both for design analysis and design optimization. The models based on BEM method are robust and simple to use but limited to simple boundary conditions, specifically limited to non-yaw and steady cases, where the upstream velocity is constant and perpendicular to the rotating plane. The rotor extracts kinetic energy from the wind and decelerates the airflow passing through the rotor plane. Consequently, the relative velocity between the blade element and the air is not equal to the geometric sum of the wind and peripheral velocities. Thus, the true velocity experienced by the elements from the air must be obtained after accounting for the slipstream. In this case, it is assumed that the axial and tangential induced velocities are distributed evenly and can be obtained by means of correction models.

The BEM theory is used to study the behavior and the properties of the wind turbine. The blade is divided to a number of elements, each having the same length. At each element, the generated forces are calculated for the middle of this element as its representative station. These forces combined with the radius at each station and the rotational speed of the rotor are summed to get the produced power and thrust. In the BEM theory, the blade is assumed to be divided into N sections which are called the blade elements. It is assumed that there is zero aerodynamic interaction between the blade elements and there is negligible spanwise velocity component on the blade. The forces on the blade element are solely determined by the lift and drag characteristics of 2D airfoils of the blade element; lift and drag components are defined perpendicular and parallel to the relative wind speed direction. The total tangential velocity experienced by the blade element is (1+a´)Ω r and the axial velocity is (1-a)U∞. The relative wind velocity at the blade is given by [5]:

$$W = \frac{U_\infty(1-a)}{sin\varphi} \quad (1)$$

Where a is the axial induction factor, a' is the rotational speed in the wake and U∞ is the wind speed. The angle between the relative wind velocity and the plane of rotation is given by:

$$tan\varphi = \frac{U_\infty(1-a)}{\Omega r(1-a')} = \frac{(1-a)}{(1-a')\lambda_r} \quad (2)$$

where λr is the local tip speed ratio at radius r from the rotation axis and Ω is the rotational speed of the rotor. The net force normal to the plane of rotation for each blade element and the resulting torque on each blade element can be written as:

$$dF = dLcos\varphi + dDsin\varphi \quad (3)$$

$$dQ = r(dLsin\varphi - dDcos\varphi) \quad (4)$$

where dL and dD are the lift and drag forces on the blade elements respectively. They are defined as follows:

$$dL = \frac{1}{2}C_L\rho W^2 cdr \quad (5)$$

$$dD = \frac{1}{2}C_D\rho W^2 cdr \quad (6)$$

where C_L is the lift coefficient of the airfoil at radius r, C_D is the drag coefficient at this radius and W is the relative velocity. For a multi-bladed wind turbine with B number of blades and φ is the angle between the plane of rotation and the relative velocity, the

equation becomes:

$$dF = B\frac{1}{2}\rho W^2(C_L cos\varphi + C_D sin\varphi)cdr \quad (7)$$

$$dQ = B\frac{1}{2}\rho W^2(C_L sin\varphi - C_D cos\varphi)cdr \quad (8)$$

Defining the local solidity as such:

$$\sigma' = \frac{Bc}{2\pi r} \quad (9)$$

Replacing W, the thrust and torque can be written as:

$$dF = \sigma'\pi\rho\frac{U_\infty^2(1-a)^2}{sin\varphi^2}(C_L cos\varphi + C_D sin\varphi)rdr \quad (10)$$

$$dQ = \sigma'\pi\rho\frac{U_\infty^2(1-a)^2}{sin\varphi^2}(C_L sin\varphi - C_D cos\varphi)r^2dr \quad (11)$$

Although the BEM theory does not include 3D characteristics of the flow and viscous losses due to separation and turbulence, some modification can be applied to the theory to take into account these losses. The first modification includes the tip-loss and Glauert corrections. The tip-loss model serves to correct the induced velocity resulting from the vortices shed from the blade tips into the wake on the induced velocity field, while the hub-loss model corrects the induced velocity resulting from a vortex being shed near the hub of the rotor. These losses are calculated as:

$$F_{tip} = \frac{2}{\pi}cos^{-1}\left(exp\left(-\frac{B}{2}\left(\frac{R-r}{rsin\varphi}\right)\right)\right) \quad (12)$$

$$F_{hub} = \frac{2}{\pi}cos^{-1}\left(exp\left(-\frac{B}{2}\left(\frac{r-r_{hub}}{r_{hub}sin\varphi}\right)\right)\right) \quad (13)$$

Hence, the total tip loss term can be calculated as follows:

$$F = F_{tip}F_{hub} \quad (14)$$

A Glauert correction factor as well as a Prandtl tip and hub loss correction factor need to be applied to the equations. The solution is obtained using a fixed point iteration scheme until both the axial and tangential induction factors converge to within a specified tolerance.

$$C_T = \frac{8}{9} + \left(4F - \frac{40}{9}\right)a + \left(\frac{50}{9} - 4F\right)a^2 \quad (15)$$

$$a = \frac{18F - 20 - 3\sqrt{C_T(50-36F)+12F(3F-4)}}{30F-50} \quad (16)$$

$$dF = 4F\rho U_\infty^2 a(1-a)\pi r dr$$

$$= \sigma'\pi\rho\frac{U_\infty^2(1-a)^2}{sin\varphi^2}(C_L cos\varphi + C_D sin\varphi) \quad (17)$$

$$Q = 4F\rho U_\infty a'(1-a)\Omega r^3\pi dr$$

$$= \sigma'\pi\rho\frac{U_\infty^2(1-a)^2}{sin\varphi^2}(C_L sin\varphi - C_D cos\varphi)r^2dr \quad (18)$$

where C_T is the coefficient of thrust. By equating the thrust force relation and torque relation, the axial induction factor and the angular induction factor a' can be calculated iteratively. When the iteration converges, the induction factors can be determined and are then used to calculate the angles of attacks and thrust for each blade element separately for the wind turbine performance analysis. Usually wind turbine rotors are designed at specific conditions; however with more and more wind penetration, the optimized design that minimizes the cost of energy becomes mandatory. Several studies have been motivated by this need, focusing on rotor optimization by considering blade chord and twist optimization. Particularly for countries in the MENA region, like Egypt, additional cost benefits can be achieved by considering site specific (wind conditions dictated by the histogram of the specific location under consideration) designs with low surface contamination sensitivity.

In this work, we considered Zaafarana site wind conditions for our optimization process and comparison of AEP with different designs. The AEP is calculated according to wind frequency distribution calculated by Weibull distribution [5]:

$$f_w(v) = \frac{k}{A}\left(\frac{v}{A}\right)^{k-1}.e^{\left(-\left(\frac{v}{A}\right)^k\right)} \quad (19)$$

where f_w is the frequency of wind velocity v. According to Mortensen et al. [6], Zaafarana site has a Weibull distribution shape factor k=3.19 and

$$A = \frac{U_{mean}}{\Gamma(1+1/k)} = 10.2\ m/s \quad (20)$$

This represents a very attractive site for wind farms.

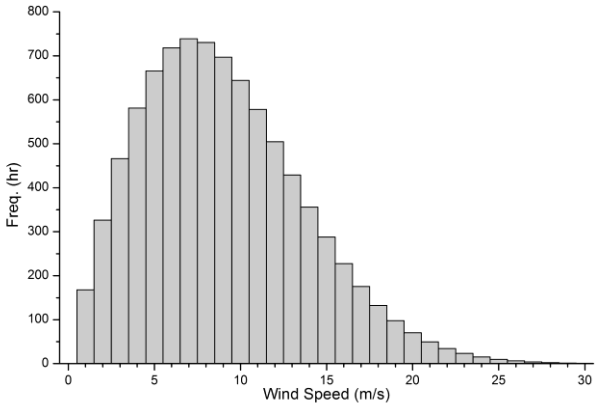

Fig .1. Weibull frequency distribution at k=3.19, A=10.2

The AEP of both NREL and site-specific wind turbine is calculating by using the equations:

$$\mathrm{AEP} = \sum_{i=1}^{n-1} (P_{v_i} - P_{v_{i-1}}).(f(v_i < v < v_{i+1}).8760 \quad (21)$$

$$\frac{U_{mean}@\text{Hub Height}}{U_{mean}@\text{Ref. Height}} = \left(\frac{90}{24.5}\right)^{\alpha} \quad (22)$$

where P_v is power generated by this wind turbine at wind velocity v, U_{mean} is the mean wind velocity at this site, α (wind shear exponent) = 0.2, Hub height = 90m and Ref. Height=24.5m (anemometer height above ground level).

III. GENETIC ALGORITHM (GA)

In general, optimization techniques fall into one of two main categories: gradient based methods and gradient free methods. Gradient free methods include genetic algorithms (GA), the Nedler-Mead simplex, and particle swarm optimization (PSO). Typical examples of gradient based methods include the conjugate gradient method the method of feasible decent and sequential quadratic programming.

One of the modern optimization techniques that are used widely in research, especially in wind turbine rotor optimization, is Genetic Algorithm. Unlike gradient based optimization methods, where objective function has to be continuous and differentiable to be solved, GA is a heuristic optimization method that the search for the optimum solution starts from a random set of solutions. These random solutions are then evaluated and the best solutions are then re-entered to the process several times until an optimum solution is found [7].

In this work, GA was used in the optimization process because it fits the wind turbine parameters optimization process more than other heuristic optimization methods. For example, Simulated Annealing (SA), despite its simplicity and flexibility, is not useful in problems where many local optimum values exist. Another example is the Ant System optimization method that mimics the behavior of ant colony in finding the shortest route to food. Despite the high reliability of this method, it is computationally more demanding than other methods since its generation complexity increases as the generation number increases. More information about heuristic optimization methods can be found in Maringer [7].

To avoid the high time consumption of the GA, the variables chord lengths and twist angles distribution along the blade were generated using Bezier curves with only five control points for each curve to decrease the complexity of the problem and at the same time to ensure smooth distribution of chord lengths and twist angles along the blade.

Genetic Algorithm was first invented by Holland [8] in the 1970s to mimic the evolution that happens in nature. This technique is achieved by generating a number of random individuals (called initial population); each consists of randomly chosen string of parameters to be optimized (called genes) and each individual is given a parameter that measures its proximity to the objective of the optimization process. This parameter is called fitness. After that, crossover (or mating) is achieved by splitting each two individuals (called parents) at a random point of the string and exchanging its half with the other to form a new string of genes called offspring or child. The choice of parents from the initial population is achieved by Tournament Selection technique that compares each two randomly chosen individuals.

The one which wins this comparison, i.e. has more fitness than the other, is promoted to the mating pool of parents. That is to say, the higher the fitness the higher the chance of the individuals genes to reach the next generations. More details about this technique can be found in Deb [9].

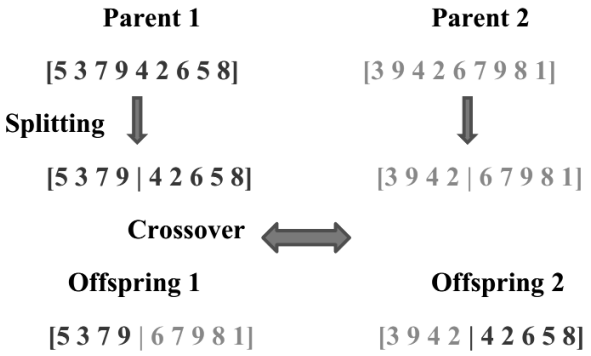

Fig .2. GA main procedure

The used technique in this work is called Multiple Elitism (ME) Genetic Algorithm presented by Soremekun et al. [10]. The difference between the ME technique and the technique described above is that after each crossover process, all parents and offspring are assembled in one pool and individuals with higher fitness are chosen to ensure fast conversion towards the optimum individual.

IV. DESIGN OF SITE SPECIFIC WIND TURBINE

In this design, the NREL S818, S830 and S831 were used to replace DU-91-W2-250, DU-93-W-210 and NACA-64-618 airfoils respectively in the baseline NREL 5MW wind turbine design. According to Diab et al. [11], the S-Airfoil family showed less deterioration in aerodynamic performance in dusty environments and hence this design will be suitable for MENA region, specially Egypt.

In this design, the NREL S818, S830 and S831 were used to replace DU-91-W2-250, DU-93-W-210 and NACA-64-618 airfoils respectively in the baseline NREL 5MW wind turbine design. According to Diab et al. [11], the S-Airfoil family showed less deterioration in aerodynamic performance in dusty environments and hence this design will be suitable for MENA region, specially Egypt. In the new design, the root airfoils (namely DU-99-W-405, DU-99-W-350 and DU-97-W-300) were not changed in the S-airfoil family design for the following reasons:

- There are no corresponding airfoils in the S-airfoil family to the root DU-family airfoils (having the same thickness to chord ratio. Root sections with high thickness to chord ratio are used in the wind turbine rotor to withstand bending moment. Hence, it cannot be replaced with other sections with low thickness to chord ratios.
- According to Rooij and Timmer [12], DU airfoils give the lowest roughness sensitivity for airfoils with thickness to chord ratios between 30% and 40%.
- The root section of the wind turbine blade has a little effect on the overall generated power of the rotor. Hence, performance deterioration due to dust accumulation on root airfoils will not have significant effect on generated power.

After selecting the airfoil shapes, the aerodynamic parameters (lift, drag and moment coefficients) are calculated using XFOIL software and hence the design angle of attack was selected to have the max C_L/C_D value. The twist angle and chord lengths were calculated using Schmitz equations [13]:

$$\beta(r)_{Schmitz} = \frac{2}{3}\tan^{-1}\frac{R}{r\lambda} - \alpha \quad (23)$$

$$c(r)_{Schmitz} = \frac{1}{B}\frac{16\pi r}{C_L} sin^2(\frac{1}{3}tan^{-1}(\frac{R}{\lambda r})) \quad (24)$$

where β(r) is the twist angle at radius r, R is the blade tip radius, λ is the tip speed ratio, α is the design angle of attack of the airfoil section, c(r) is the chord length of the airfoil section at radius r and C_L is the design lift coefficient of the airfoil sections.Since the root airfoils in the baseline NREL 5MW wind turbine are already designed for max C_L/C_D twist angles, these angles are not changed in the S-airfoil family design. The baseline design was simulated at wind velocities ranges from cut-in to cut-out speed, using FAST Modularization Framework [14] to calculate AEP at specified Weibull distribution.

V. RESULTS AND DISCUSSIONS

The Simulation and optimization process includes simulation of four wind turbine designs:

- Case 1: NREL 5MW baseline design (described in [15]).
- Case 2: Optimized NREL 5MW wind turbine.
- Case 3: Baseline site-specific wind turbine design using the S-Airfoil family.
- Case 4: Optimized site specific wind turbine design.

The baseline design (Case 1) power curve at each wind speed was verified against the power curve provided in the definition report of the NREL 5MW [15]. After that, the AEP was calculated for all cases.
After calculation of the AEP of the four cases and running optimization processes of cases 2 and 4 using a MATLAB optimization code coupled to FAST Modularization Framework to run the optimization process, the results were as follow.

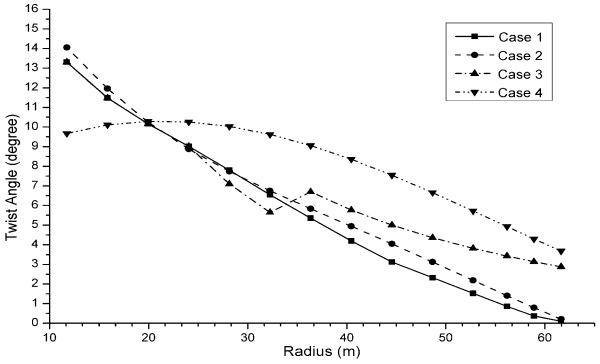

Fig .3. Twist angle distribution along the rotor blade for cases 1 to 4

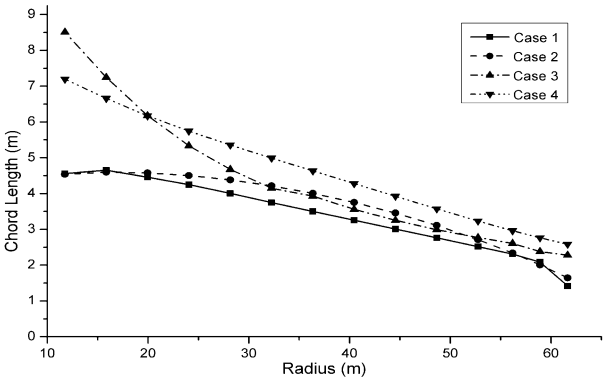

Fig .4. Chord length distribution along the rotor blade for cases 1 to 4

Table 1. AEP OF CASES 1 TO 4

Case No.	AEP (GWh)	Improvement from Baseline case (%)	Improvement from Case 1 (%)
1	32.88	-	-
2	34.83	5.9	5.9
3	32.18	-	-2.13
4	32.57	1.2	-0.94

The previous results show that a 5.9% improvement can be achieved on a baseline design after optimization for Zaafarana wind distribution. This highlights the importance of tailoring design and optimization of wind turbine aerodynamic parameters on specific wind distribution along the year and attracts attention towards the need of designing and manufacturing special wind turbines that serve in specific sites to increase the ability of energy extraction from wind.

On the other hand, for S-airfoil wind turbine rotor, the AEP is less than the optimized Baseline design. This is a result of replacing DU airfoils with NREL airfoils because DU airfoils have better aerodynamic characteristics than NREL airfoils. However, the NREL airfoil family is still recommended for Zaafarana wind farm since it is less surface contamination sensitive, according to Diab et al. [11].
According to roughness sensitivity data found in [11,12 and 16], the new aerodynamic performance of the rough airfoils of DU-91-W2-250, DU-97-W-300, S818, S830 and S831 were used to calculate the AEP of optimized wind turbine after dust accumulation, while the other airfoils were assumed to maintain the same aerodynamic performance as clean airfoils due. The optimized NREL 5MW wind turbine shows a drop in AEP form 34.83 to 29.75 GWh (-14.6% in AEP), while the S-airfoil family design shows a drop in AEP form 32.571 to 32.497 GWh due to dust accumulation on the blade surface. Hence, the loss in AEP along the year due to using NREL S-airfoil family airfoils will decrease the loss in AEP due to deterioration of aerodynamic characteristics of the DU and NACA airfoil sections in the baseline NREL 5MW rotor.

V. CONCLUSION

From the previously mentioned results, we can conclude that the new S-airfoil design and optimization resulted in a new design that is suitable for Saharan areas (like areas found in Egypt and many countries in the MENA region) with higher AEP than the baseline design. This work also concludes that design and optimization of site-specific wind turbine design play a very important role in increasing the wind turbine's AEP and hence decreasing the cost of energy generated from the wind turbine. Such techniques along with consideration of the conditions in which the turbine operates, such as dust, must be taken into consideration during the process of design or selection of wind turbines to be installed in a specific wind farm.

REFERENCES

[1] Maheri, A., Noroozi, S. and. Vinney, J. “Application of combined analytical/FEA coupled aero-structure simulation in design of wind turbine adaptive blades”. Renewable Energy. Volume 32. Issue 12, October 2007. Pages: 2011-2018.

[2] Xiong, L., Yan, C. and Zhiquan, Y. “Optimization model for rotor blades of horizontal axis wind turbines”. Frontiers of Mechanical Engineering in China. Pages: 483-488.

[3] Xudong, W., Jin, Ch., ZhongShen, W., Jun Zhu, and NørkærSørensen, J. “Shape optimization of wind turbine blades” . Wind Energy. Pages: 781-803.

[4] Mohamed, M. and Wetzel, K.. “3D Woven Carbon/Glass Hybrid Spar Cap for Wind Turbine Rotor Blade”. Tran. of ASME. Journal of Solar Energy Engineering. Issue 128 (2006). Pages:562-573.

[5] Hansen, M. Aerodynamics of Wind Turbines, 2nd ed. London: Earthscan. 2008.

[6] Mortensen, N., et al. “Wind atlas for Egypt: measurements, micro- and mesoscale modellin”. European Wind Energy Conference EWEC 2006. 2006.

[7] Maringer, D. “Portfolio Management with Heuristic Optimization”. Dordrecht: Springer, 2005.

[8] Holland, J. Adaptation in natural and articial systems. Ann Arbor, MI: The University of Michigan Press. 1975.Ann Arbor, MI: The University of Michigan Press. 1975.

[9] Deb, K. Multi-objective optimization using evolutionary algorithms. John Wiley and Sons Ltd. 2001.

[10] Soremekun, G., Gürdal, Z., Haftka, R.and Watson, L. “Composite laminate design optimization by genetic algorithm with generalized elitist selection”. Computers & Structures. Volume 79. Issue 2. January 2001. Pages: 131-143.

[11] Diab, A., Alaa, M., Hossam El-Din, A. , Salem, H.and Ghoniem, Z. “Performance Degradation of Wind Turbine Airfoils Dust Contamination: A Comparative Numerical Study”. ASME Turbo Expo. 2015 (2015).

[12] Rooij, R. and Timmer, W. "Roughness Sensitivity Considerations for Thick Rotor Blade Airfoils." Journal of Solar Energy Engineering 125.4 (2003). 468. Web.

[13] Gasch, R. and Twele J. “Wind Power Plants: Fundamentals, Design, Construction and Operation”. Berlin: Springer Berlin. 2011.

[14] Jonkman, J. and, Buhl, M. “FAST user’s guide”. Tech. Rep. Golden, Colorado: National Renewable Energy Laboratory. 2005.

[15] Jonkman, J. , Butterfield, S., Musial, W. and Scott, G. “Definition of a 5- MW Reference Wind Turbine for Offshore System Development” (2009)

[16] Buhl, M. "Wind Turbine Airfoil List.". Wind Turbine Airfoil List. NWTC. 6 July 2012. Web. 02 May 2015.

On the Long-term Behavior of Wind-Wave Climatology over the West Region of Scotland, UK

Tarek M. El-Geziry
Laboratory of Physical Oceanography, Division of Marine Environment, National Institute of Oceanography and Fisheries, Alexandria, Egypt
tarekelgeziry@yahoo.com

Abstract - Using 38 years (January 1973-December 2010) of hourly wind records, the present paper aims at drawing the possible long-term trends of winds and ten surface wave parameters over the west region of Scotland, using the quadratic regression approach.
Four dominant wind components were determined: the southern, the western, the south-western and the north-western. Two opposite groups of oscillations were proven: one for the southern groups and one for the western groups.

The examined wave parameters were: the wave frequency, the wave angular frequency, the peak angular frequency, the wave spectral density, the significant wave height, the peak period, both the peak and group velocities and lastly the wave energy and the wave power.

Results revealed that every examined parameter tended to have a cyclic behaviour except the wave spectral density, which appeared to be linearly decreasing. All wave frequencies were in an inverse correlation to the mean monthly wind speed. All other wave parameters appeared to be highly correlated to the mean monthly wind speed with correlation factors exceeding 0.95 except the wave power, which had a correlation factor of 0.89.

In conclusion, the general behaviours of the dominant wind components over the west region of Scotland, and of the different wave parameters tend to be cyclic. A longer time series, than that presently used, will be advantageous in order to strengthen this outcome with more robust investigation. This concluded cyclic behaviour may positively have impact on the engineering work within the wave energy resource off the western coasts of Scotland.

Keywords - Scotland, Anomaly, Wind, Wave, Quadratic regression, Cycles.

I. INTRODUCTION

It is well-known that air masses intrusion or replacement over any area or basin is the primary mechanism connecting atmospheric and oceanic characteristics through the transfer of heat, moisture and momentum at the sea surface (El- Geziry et al. 2013). Ocean waves are produced by the movement of these air masses (winds) over the sea surface. The faster the wind, the longer the wind blows, and the bigger the area over which the wind blows, the bigger the generated waves. Wave energy, i.e. energy of ocean surface waves, is created by the drag of winds over the sea (Mollison 1994).

The west region of Scotland (Fig. 1), extending along the Atlantic Ocean, tends to have one of the strongest and, meanwhile, steadiest wind system all over the world. The region is also believed to be one of the worldwide vital renewable energy resource with its surface wave characteristics. Geographically, the west region of Scotland covers the western half of both the Central Lowlands and Southern Uplands of Scotland. This comprises Kintyre, Strathclyde, Galloway and Dumfries. The region also includes the Isles of Tiree, Mull, Arran and Jura.

Factually, the examination of the long-term behaviour of wind at a given site is considered a clue to understand changes in both the wind system, as a key player in the generation of surface ocean waves, and the wave resource itself.

According to the UK Met Office climate wind data (http://www.metoffice.gov.uk/), the prevailing wind directions over the west region of Scotland lie between south and northwest for the majority of occasions, and the strongest winds nearly always blow from this range of directions. This is mainly attributed to the Atlantic depressions, which pass by the United Kingdom, and is considered the main cause of air mass movement over the region. Results of wind analysis by Corbel et al. (2007) revealed that

the occurrence of strong south westerly winds at sites around the Scottish coasts is closely linked to the behaviour of the North Atlantic Oscillation (NAO).

Most of the long-term wind analysis research and studies focused on the use of winds as a renewable energy resource, i.e. wind power, e.g. Youm et al. (2005); Sinden (2007); Lindsey (2011); Olaofe and Folly (2012); Anastasiades and McSharry (2013). The target has mainly been to specify conditions and characteristics of windy regions and to test the feasibility of wind farm construction according to density function, height variability, wind energy potential, turbine distribution…etc.

The behaviour of waves is determined by the spectrum of the sea state, S (f, θ), which specifies how the wave energy is distributed in terms of frequency and direction (Longuet-Higgins 1957; Mollison 1994). However, many models of the spectrum of wave measured at a certain point are widely-used regardless the wave direction. Generally speaking, there are two main types of these wave spectra: the mono-parameter spectrum (e.g. Pierson and Moskowitz 1964) and the multi-parameter spectrum (e.g. Bretschneider 1959; Hasselmann et al. 1973; Ochi-Hubble 1976). The spectrum type is determined based on the required number of the input parameters. Wind and wave properties in the shelf regions of the Atlantic Ocean, including the coasts of Scotland have been previously studied (e.g. Woolf and Challenor 2002; Wolf and Woolf 2005; Weisse and von Storch 2010).

Trends and cycles for climatological parameters, hydrography and fish catch have been investigated for long-term data in different regions worldwide, e.g. Maiyza 1984; Fedrouich 1985; Baumgartner et al. 1992; Kawasaki 1994; Levitus 1995; Hylen 2002; Klyashtorin and Lyubushin 2007; Sundby and Drinkwater 2007; Maiyza and Kamel 2009; 2010; Maiyza et al. 2011; Said et al. 2012; El-Geziry et al. 2013. Moreover, from a the behavioural point of view, long-term variations in winds have been previously investigated in the south-eastern Mediterranean Sea region (El-Geziry et al. 2013). All these studies proved the cyclic nature and strengthened the concept of oscillations of the examined parameters. The cycle of those oscillations have periods that may extend to centuries.

To the author's knowledge, the long-term trends of variations in the wind-wave climatology over the west region of Scotland have not been previously examined from a behavioural trend point of view. The present paper aims at drawing the possible long-term trends of winds and ten surface wave parameters over the west region of Scotland, using the quadratic regression approach. For those who work in the wave energy field, year-to -year and long term climatic variability are especially important for estimating the life time extremes that a structure will experience (Mollison 1994).

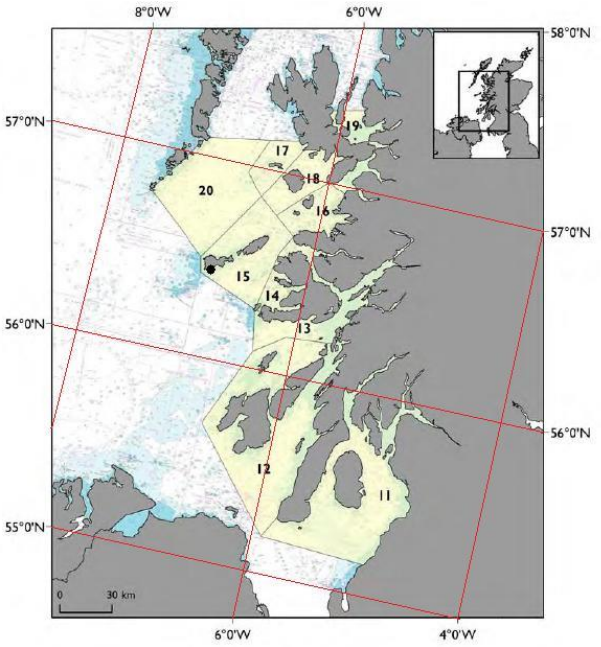

Fig .1. Map of the west region of Scotland showing the location of Tiree meteorological station (Adapted from Speedie et al., 2009)

II. DATA AND METHOD OF ANALYSIS

The selected data set of wind vectors (speed and direction) covers 38 years (January 1973 - December 2010) based on hourly records over the period of investigation.

This is obtained from Tiree meteorological station (56° 30.00' N; 6° 52.98' W; Fig. 1) placed at an elevation of 9 m above the Mean Sea Level (MSL) (http://gis.ncdc.noaa.gov/map/viewer/#app=cdo). This station, facing an open sea region, is used as a representative meteorological point for the whole western region of interest.

The dominant wind directions over the period of investigation have been specified through the calculation of the percentage of wind occurrence frequency.

The mean monthly wind speed (MMWS; mean for specific month every year) for the four most dominant wind components over the 38-year data set and the monthly mean speed (Wm; mean for specific month of all years) for every month in the whole data set are calculated. The deviation from the monthly mean (ΔW) is computed on monthly basis in order to express the monthly wind anomaly (MWA), using the following equation:

$$\Delta W \equiv MWA = MMWS - W_m \quad (1)$$

The general trend of the monthly variation in the MWA is examined, using the quadratic regression approach. The specific years of the lowest and highest calculated MWA are determined using the first derivative concept for the generated equations.
The available wind data and the location of Tiree meteorological station satisfy the assumptions of Pierson and Moskowitz (1964):

- North Atlantic data, specified on the sea state as a Fully Developed Sea (FDS)
- Deep water
- Unlimited fetch
- Unidirectional sea, and
- No swell

Therefore, the Pierson-Moskowitz spectrum model has been applied in the present research. The spectral function of the spectrum takes the form:

$$S(\omega) = \frac{\alpha}{\omega^5} g^2 e^{-\beta\left(\frac{\omega_o}{\omega}\right)^4} \quad (2)$$

Where, S (ω) is the wave spectral density function (m2s), α = 0.0081, ω is the wave angular frequency (rad/s), g is the acceleration of Earth's gravity (9.81 m/s2), β = 0.74 and ωo = g/U19.5 (rad/s). U19.5 is the wind speed (m/s) at a height of 19.5 m above the MSL; U19.5 = 1.075 U10. U10 is the measured wind speed (m/s) at a height of 10 m above the MSL. In the present work, U10 is the wind speed directly recorded by Tiree meteorological station.

The wave peak frequency (rad/s) and peak speed (m/s) of the Pierson-Moskowitz spectrum are, respectively, calculated by the Equations:

$$\omega_p = 0.877\ (g/U19.5) = 0.877\ \omega_o \quad (3)$$

$$cp = g/\omega p \quad (4)$$

The significant wave height (m) calculated from the Pierson-Moskowitz spectrum is

$$H_s = 0.21\left(\frac{U_{19.5}^2}{g}\right) \quad (5)$$

and the wave peak period (s) is

$$T_p = \frac{2\pi}{\omega_p} = 7.14\left(\frac{U_{19.5}}{g}\right) \quad (6)$$

In order to get the wave angular frequency to build-up the Pierson-Moskowitz spectrum for the present research, the satisfied FDS condition enabled to derive both the corrected wind speed (UA; m/s) and the wave period (T; s) using the following Equations (Holmes 2001):

$$U_A = 0.71\, U_{10}^{1.23} \quad (7)$$

$$T = 0.83\ UA \quad (8)$$

The wave energy (E; J) (Holthuijsen 2007) and the wave power (P; W/m2) (Phillips 1977) are calculated using the two following Equations, respectively:

$$E = \frac{1}{8}\rho g H_s^2 \quad (9)$$

Where E is the wave energy ρ is the ocean water density 1025 kg/m3

$$P = E\ C_g \quad (10)$$

Where,P is the wave power Cg is the wave group velocity (m/s), calculated as the half peak wave celerity for the present deep water wave status.The general trends of the long-term variations of the different wave parameters off the western coasts of Scotland have been produced using the quadratic regression approach. These parameters are the wave frequency, the wave angular frequency, the peak angular frequency, the wave spectral density, the significant wave height, the peak period, both the peak and group velocities and lastly the wave energy and the wave power.

III. RESULTS

1. Hourly Wind-Wave climatology

The raw data set downloaded directly from the meteorological site consists of 397340 hourly observations. This exceeds the supposed record of observation, 333096 hours, for the 38 years of study. This data excess is mainly attributed to data repetition and to the extra 10, 20 and 50 minutes of records in some months. Accordingly, the initial data set has been filtered and the final data set used for the present analysis has been set up to consist of 323866 hourly records of both wind speed and wind direction. This represents 97.23% of availability, with 9230 records (2.77%) missed. However, statistically speaking, these missed records do not affect the data quality to proceed for the proposed investigation. Over the period of investigation, the hourly wind speed varied between calm (0 m/s) and 38.89 m/s with an average of 7.34 m/s over the period of investigation. Moreover, 12 wind speed classes have been specified as shown in Table (1) and their percentage of occurrence has been figured out in Figure (2). While the dominant speed interval over the study period was >5:10 m/s, with an occurrence of 41.25%, the lowest speed interval was >35:40 m/s with 0.0006%.

Table 1. Hourly Wind Speed Classes

Wind Speed Classes (m/s)	No. of Observations
0 (Calm)	3628
>0:5	107312
>5:10	137408
>10:15	63083
>15:20	11273
>20:25	1071
>25:30	83
>30:35	6
>35:40	2
Missed data	9230

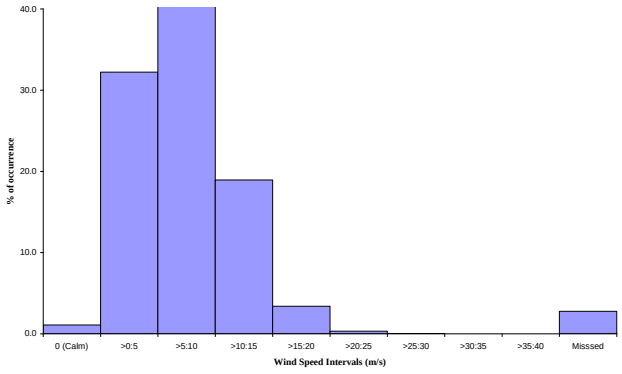

Fig .2. The percentage of occurrence of different wind speed intervals

The hourly statistics of the different wave parameters from January 1973 to December 2010 are shown in Table (2). The Pierson-Moskowitz wave spectrum for the present hourly wind speed is shown in Figure (3). Figure (4) shows the hourly significant wave height and hourly wave peak period calculated from the Pierson-Moskowitz spectrum.

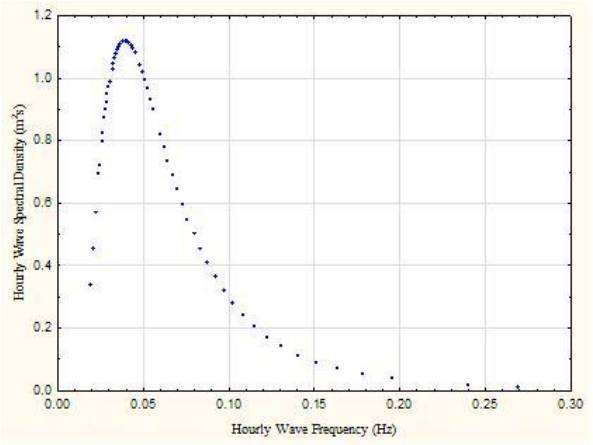

Fig .3. The FDS Pierson-Moskowitz spectrum off the western coasts of Scotland based on the hourly wind records

Table 2. Hourly statistics of the different wave parameters

	Minimum	Maximum	Mean
U_{10}, recorded wind speed, (m/s)	0	38.89	7.34
U_A, corrected wind speed, (m/s)	0	64.0	8.5
T, wave period, (s)	0	53.1	7.1
f , wave frequency, (Hz)	0.0187	0.280	0.250
ω, wave angular frequency, (rad/s)	0.1181	28.714	1.571
$U_{19.5}$, wind speed at 19.5 m above MSL, (m/s)	0	41.8	7.8
S (ω), wave spectral density, (m^2s)	0	1.122	0.189
ω_p, wave peak frequency, (rad/s)	0.2057	17.903	1.577
C_p, wave peak speed, (m/s)	0	47.6	8.9
H_s, significant wave height, (m)	0	37.4	1.7
T_p, wave peak period, (s)	0	30.4	5.7
E, wave energy, (J)	0	1759948	7467.19
C_g, wave group velcoity, (m/s)	0	23.7	4.4
P, wave power, (W/m^2)	0	41941970	64319.28

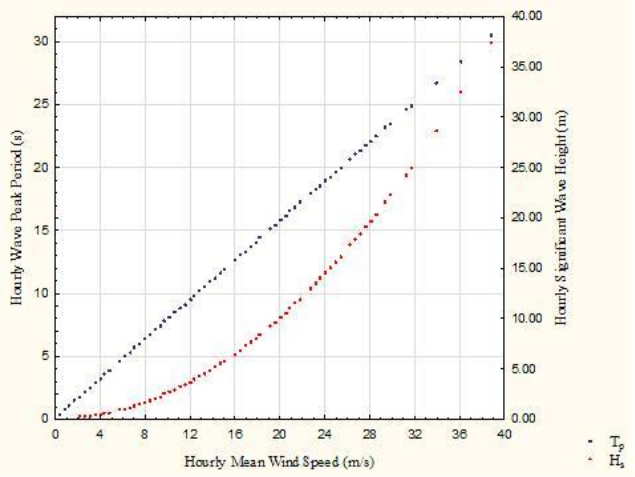

Fig .4. Significant wave height and period at the peak of the spectrum of FDS calculated from the Pierson-Moskowitz spectrum using Equations (5 and 6)

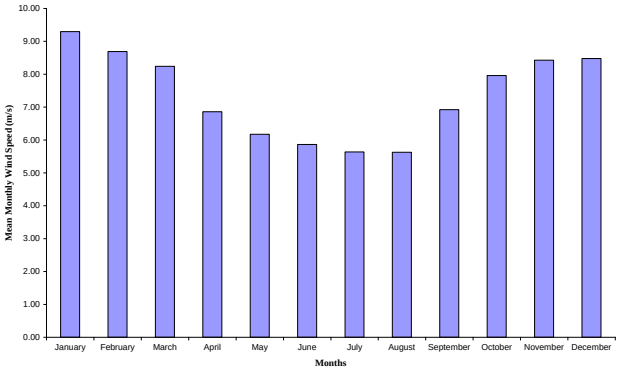

Fig .5. Histogram of the Mean Monthly Wind Speed (MMWS) over the study period

2. Dominant Wind Directions

The dominant wind directions in the present study have been determined using the percentage of wind occurrence frequency for the main 16 wind directions. Table (3) shows this percentage in a descending order. From this Table, the four major dominant winds during the period of investigation were the southern (S), the western (W), the south-western (SW) and the north-western (NW) winds.

This agrees with the general climatology of the wind direction prepared by the UK Met Office for the region of west of Scotland. The calm wind (0 m/s) represented 1.09% of the recorded wind data, i.e. 3628 hourly records.

A. Mean Monthly Wind speed (MMWS)

The mean monthly wind speed (MMWS) is one of the most important parameters in the wind profile of any given site.

Figure (5) shows the histogram of the MMWS variations. In Table (4), Vmin, Vmax and MMWS are the mean monthly minimum wind speed, mean monthly maximum wind speed and the mean monthly wind speed, respectively. It can be seen that the highest Vmax as well as the maximum MMWS occur during the three months of the winter season: January, February and December.

This reveals that these months might have the potential of recording the highest amount of exploited wave energy in the area of investigation.

Table 3. Percentage of occurrence frequency of wind directions

Wind Direction	No. of hourly records	% of occurrence frequency
S	34742	10.43
W	33310	10.00
SW	31777	9.54
NW	28646	8.60
SSW	25715	7.72
SE	24216	7.27
WSW	21784	6.54
SSE	21784	6.54
NWN	17421	5.23
WNW	16655	5.00
ESE	16055	4.82
E	10926	3.28
NE	10659	3.20
NNE	9560	2.87
N	9327	2.80
EEN	7661	2.30
Direction Records	320238	96.14
Calm wind (0 m/s)	3628	1.09
Missed Records	9230	2.77

Table 4. Minimum, maximum and mean monthly wind speeds over the study period

	V_{min} (m/s)	V_{max} (m/s)	MMWS ((m/s)
January	6.24	12.36	9.29
February	5.59	12.07	8.69
March	5.93	10.57	8.24
April	4.17	8.62	6.86
May	4.11	8.62	6.17
June	4.15	7.75	5.86
July	4.29	7.39	5.63
August	3.93	7.20	5.63
September	5.44	8.77	6.92
October	5.59	10.19	7.96
November	6.33	10.54	8.43
December	5.97	11.58	8.48

Over the period of investigation, the quadratic regression of the MMWS has a parabolic form (Fig. 6), which reflects an apparent cyclic trend in the changes of the MMWS over the investigated area. A longer time series of recorded wind data will be advantageous to confirm with more clarification this cyclic behaviour, i.e. cycle length and points of cycle-reverse. The quadratic regression model is represented by the Equation:

$$MMWS = 4.04E\text{-}06\ x^2 - 0.0035\ x + 7.8665 \qquad (11)$$

The month of the minimum MMWS occurrence is determined to be January 2009. The resultant parabola shows a general trend of decrease from January 1973 to January 2009 with a rate of 0.0017 ms-1/month (0.0204 ms-1/yr), followed by a very slow gradual increase up to the end of the investigated period with a rate of 0.00008 ms-1/month (0.00096 ms-1/yr).

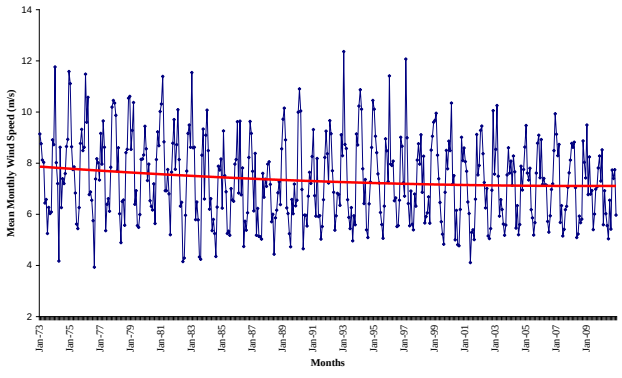

Fig .6. Quadratic regression model of the MMWS over the study period

B. The Four Major Dominant Wind Components

In the following discussion, the trend of variations of the four major main dominant components over the region of interest will be discussed. This will be presented according to the descending percentage of occurrence frequency (Table 3).

1. The Southern Wind Component (S)

Wind blowing from the south dominates the region of investigation. Over 38 years of hourly records, the southern wind represented 10.43% of occurrence. The quadratic trend of the southern variations is mathematically expressed by:

$$S\text{-}MWA = 1.6287E\text{-}06\ x2 - 0.0006\ x + 0.0132 \qquad (12)$$

This results in a parabolic cyclic variation (Fig. 7) with a minimum occurrence of the S-MWA in April 1988. A general decrease (0.0003 ms-1/month; 0.0036 ms-1/yr) occurred from January 1973 to April 1988 followed by a general increase (0.00044 ms-1/month; 0.00528 ms-1/yr) afterwards. The zero values of the S-MWA (points of intersection with the months' axis) occurred in November 1974 and September 2001.

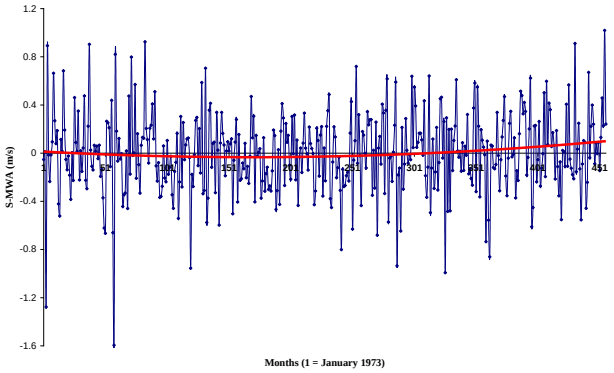

Fig .7. Quadratic trend of variation in the S-MWA over the period of investigation

2. The Western Wind Component (W)

Wind blowing from the west represented 10% of the recorded hourly data over the 38 years of investigation. In contrast to the south wind component, the quadratic regression model of the westerly MWA tends to produce a concave-down parabolic figure (Fig. 8), the maximum of which occurred in May 1995. There is an increasing rate from January 1973 to May 1995 (0.0003 ms-1/month; 0.0036 ms-1/yr) followed by a slight decreasing rate of

0.0002 ms-1/month (-0.0024 ms-1/yr) from May 1995 to December 2010.

The zero values of the W-MWA occurred in September 1982 and January 2008. The quadratic regression model of the W-MWA is mathematically represented by the following Equation:

W-MWA = -1.1136E-06 x2 + 0.0006 x – 0.0551 (13)

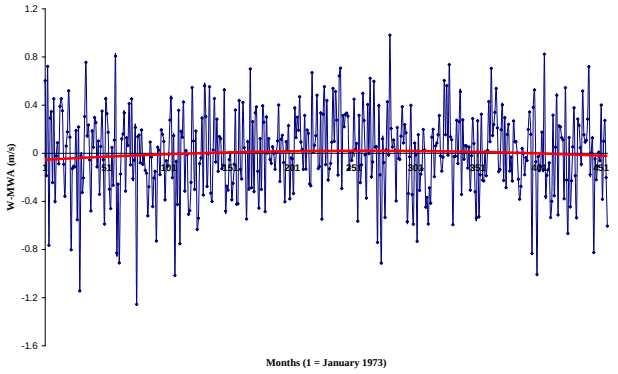

Fig .8. Quadratic trend of variation in the W-MWA over the period of investigation

3. The South-West Wind Component (SW)

The south-west wind component comes third in the frequent occurrence during the period of investigation, with 9.54%. The quadratic regression of the SW-MWA (Fig. 9) reflects a parabolic form the minimum of which is out of the present data in hand: May 1969. The apparent segment from the resultant parabola of the SW-MWA is an increasing segment with a rate of 0.00022 ms-1/month, i.e. 0.00264 ms-1/yr (Equation 14). The zero values of the SW-MWA occurred in September 1994 and January 1947.

SW-MWA = 4.9024E-07 x2 + 2.5313E-05 x – 0.0399 (14)

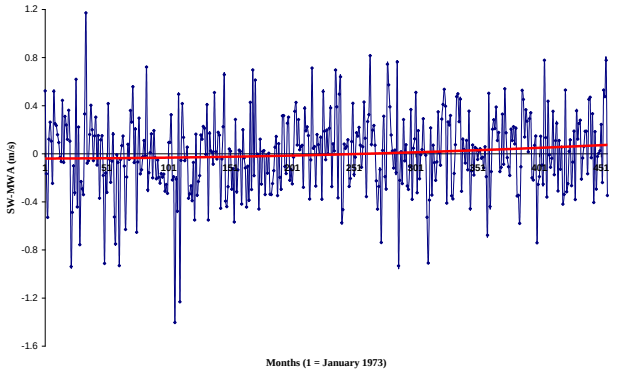

Fig .9. Quadratic trend of variation in the SW-MWA over the period of investigation

4. The North-West Wind Component (NW)

This wind component is the fourth dominant wind component over the study period with an 8.6% occurrence. The quadratic examination of changes of this monthly wind anomaly component (Fig. 10) reflects both an increasing rate and a decreasing rate over two successive time-interval segments. While the first is 0.011 ms-1/month (0.012 ms-1/yr) from January 1973 to July 1994, the second rate is -0.0017 ms-1/month (-0.0204 ms-1/yr) from July 1994 onwards. This apparent trend of the NW wind component followed that of the westerly component shown above. The zero values of the NW-MWA occurred in September 1975 and April 2000. The quadratic model equation which represents the NW-MAW is:

NW-MWA = -1.6602E-06 x2 + 0.0006 x – 0.018 (15)

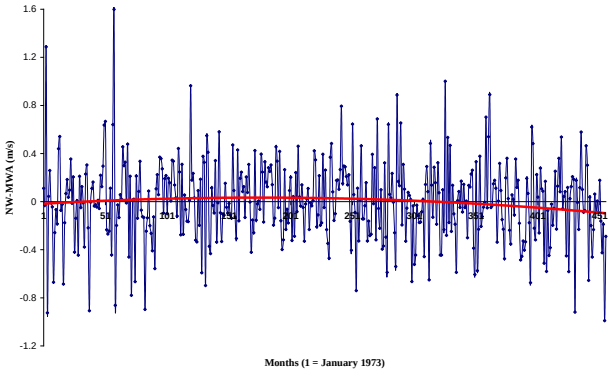

Fig .10. Quadratic trend of variation in the NW-MWA over the period of investigation

3. Quadratic Regression Models of the Different Wave Parameters

In order to describe the wave climate off the western coasts of Scotland, the long term changes in the ten mentioned wave parameters are considered.

The minimum mean monthly S (ω) was 0.01 m2s and the maximum was 0.53 m2s, with an average of 0.12 m2s over the study period. The mean monthly f ranged from 0.08 Hz to 0.32 Hz with an average of 0.16 Hz, and the mean monthly ω varied between 0.48 rad/s and 1.98 rad/s with an average of 0.98 rad/s over the study period. The mean monthly Hs and Tp calculated from the mean monthly Pierson-Moskowitz spectrum in the present study is shown in Figure (11). The mean monthly Hs ranged from 0.38 m to 3.78 m with an average of 1.40 m, and the Tp

varied between 3.07 s and 9.67 s with an average of 5.75 s, over the study period.

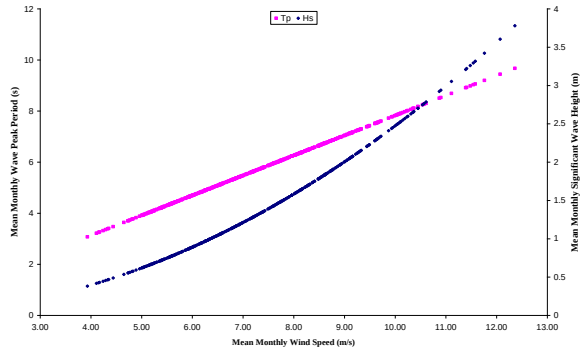

Fig .11. The mean monthly Hs and Tp of the mean monthly Pierson-Moskowitz spectrum over the study period

The examination of the long term trends of variations of the different wave parameters reveals that the mean monthly f is in an inverse relationship to the mean monthly winds speed (MMWS), with a correlation factor of -0.96. This is the same situation for both ω and ωp. The latter varied between 0.65 rad/s and 2.00 rad/s, with an average of 1.14 rad/s over the study period. The general trends of the three frequencies are shown in Figures (12-14).

The mean monthly f (MMf) is quadratically expressed by the Equation:

$$MMf = -1E\text{-}07\ x2 + 1E\text{-}04\ x + 0.1442 \quad (16)$$

This mathematically expresses a concave-down parabola, the increase rate of which is 0.018 Hzyr-1, with a maximum occurrence in August 2014.

The mean monthly ω (MMω) tends to have the same parabolic form but with a maximum occurrence in August 2000, i.e. preceding that of the MMf by 14 years. This is expressed by the following Equation:

$$MM\omega = -9E\text{-}07\ x2 + 0.0006\ x + 0.9062 \quad (17)$$

This implies an initial increasing rate in the MMω of 0.003 rads-1yr-1 from January 1973 to August 2000 followed by a decreasing rate of 0.001 rads-1yr-1 afterwards.

The quadratic expression of variations in the mean monthly ωp (MM ωp) is:

$$MM\omega p = -8E\text{-}07\ x2 + 0.0006\ x + 1.0707 \quad (18)$$

The MMωp increased from January 1973 to March 2003 followed by a gradual decrease afterwards, with rates of 0.004 rads-1yr-1and -0.02 rads-1yr-1, respectively.

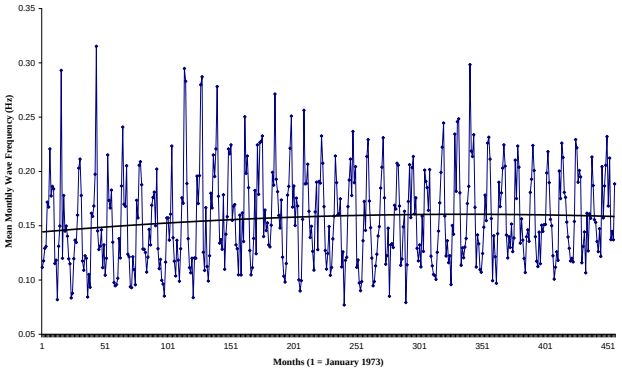

Fig .12. The mean monthly Hs and Tp of the mean monthly Pierson-Moskowitz spectrum over the study period

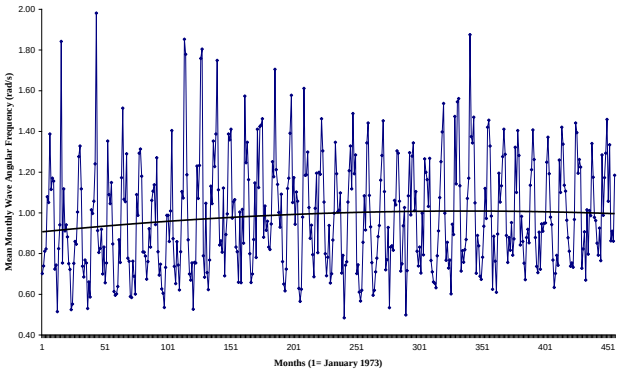

Fig .13. Quadratic trend of variation of the MMω over the period of investigation

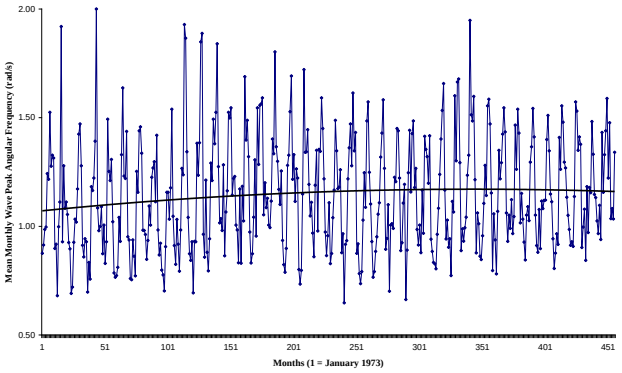

Fig .14. Quadratic trend of variation of the MMωp over the period of investigation

Over the period of investigation, the mean monthly wave spectral density, MMS(ω), did not show any parabolic form or a cyclic behaviour. In contrast, a general decrease trend is more obvious for the MMS(ω), with both the quadratic (Blue solid line) and

linear (Red dashed-line) regressions almost super-imposable (Fig. 15). While the first has a rate of -0.0018 m2syr-1 the second has a rate of -0.0012 m2syr-1. The correlation factor between the MMS(ω) and the MMWS is 0.98. The quadratic regression model of the MMS(ω) is given by the following Equation:

$$MMS(\omega) = 1E\text{-}07x2 - 0.0002\,x + 0.1515 \quad (19)$$

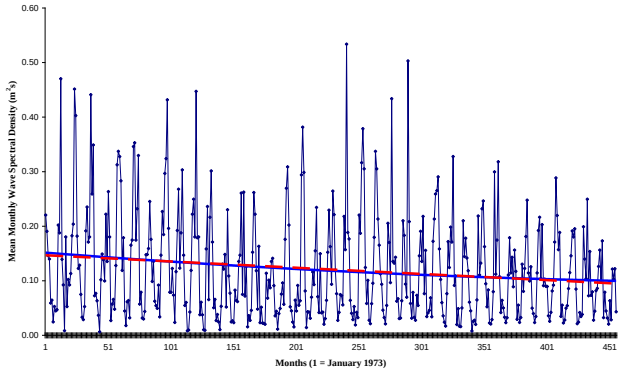

Fig .15. The mean monthly trends of variation of the MMS(ω) over the study period

During the study period, the mean monthly Hs (MMHs) was highly correlated to the MMWS, with a correlation factor of 0.98. The long-term variations in the MMHs have a parabolic form (Fig. 16), which reflects a cyclic behaviour for this wave parameter. The MMHs decreased from January 1973 to May 2008, followed by a gradual increase afterwards. This is mathematically expressed by the following Equation:

$$MMHs = 2E\text{-}06\,x2 - 0.0017\,x + 1.9563 \quad (20)$$

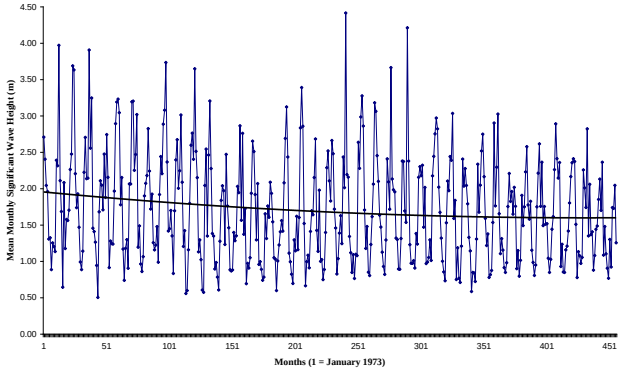

Fig .16. Quadratic trend of variation of the MMHs over the study period

The general trend of the mean monthly Tp (MMTp) tends to be cyclic (Fig. 17) with a quadratic expression as:

$$MMTp = 3E\text{-}06\,x2 - 0.00298\,x + 6.1694 \quad (21)$$

This reflects a large cycle with a minimum occurrence in May 2014, which is obviously out of the present data set and comes 6 years after the minimum occurrence of the MMHs. The MMTp is highly correlated to the MMWS, with a factor of 0.998.

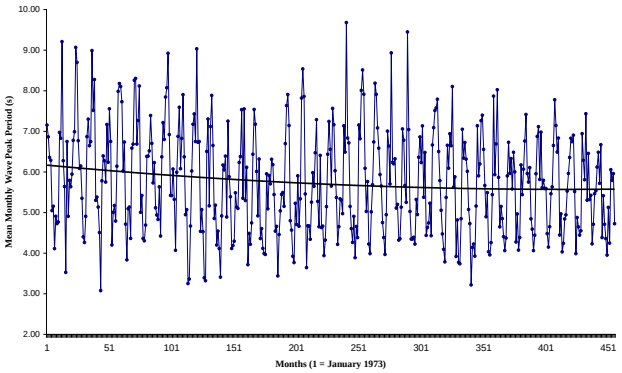

Fig .17. Quadratic trend of variation of the MMTp over the study period

Both the mean monthly Cp (MMCp) and Cg (MMCg) are positively correlated to the MMWS, with a factor of 0.998, and both tend to have a cyclic behaviour of variations. While the minimum occurrence of the MMCp occurred in January 2010 (Fig. 18), one year after that of the MMWS, the minimum MMCg occurred in January 2003 (Fig. 19), six years before that of the MMWS. The Equation, which represents the variations of the MMCp is:

$$MMCp = 5E\text{-}06\,x2 - 0.00445x + 9.663 \quad (22)$$

The yearly rate of the MMCp decrease is 0.0265 ms-1yr-1from January 1973 to January 2010, followed by a very slow rate of increase of 0.00066 ms-1yr-1 afterwards. The MMCp varied from 4.91 m/s to 15.15 m/s with an average of 9 m/s over the period of investigation.

The quadratic Equation, which represents the variations of the MMC_g is:

$$MMCg = 3E\text{-}06\,x2 - 0.00217x + 4.8287 \quad (23)$$

This results in two segments of variations (Fig. 19), the first of which has a rate of -0.012 ms-1yr-1 from January 1973 to January 2003, followed by an

increasing segment with a rate of 0.0042 ms-1yr-1. The MMCg ranged between 2.45 m/s and 7.58 m/s, with an average of 4.5 m/s over the study period.

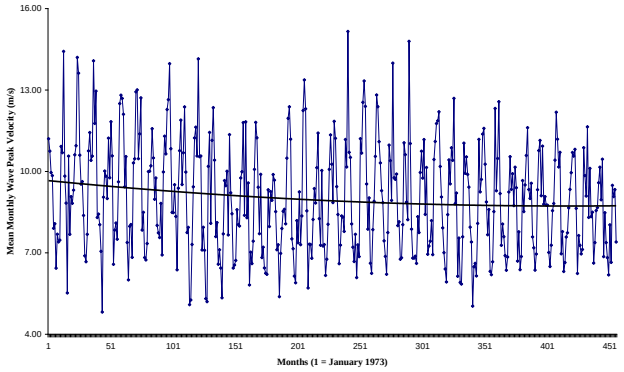

Fig .18. Quadratic trend of variation of the MMCp over the study period

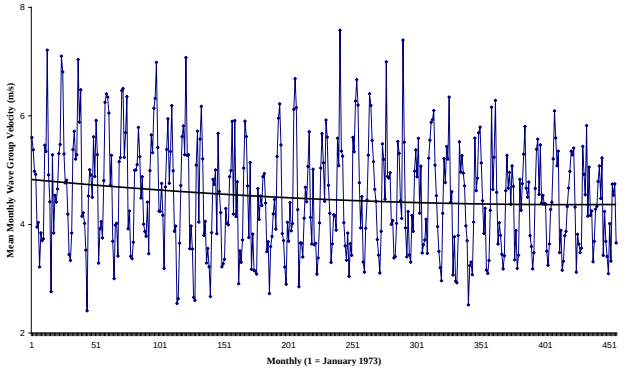

Fig .19. Quadratic trend of variation of the MMCg over the study period

Over the period of investigation, the quadratic regression of the mean monthly E (MME) has a well-observed parabolic form (Fig. 20), which reflects an apparent cyclic behaviour for the changes of the wave energy in the investigated area. The quadratic regression model is represented by the Equation:

$$MME = 0.0172\ x2 - 14.11602\ x + 9536.2 \quad (24)$$

The MME varied from 183.49 J to 17951.93 J with an average of 2953.63 J over the study period. The minimum MME occurred in February 2007. The resultant parabola shows a general trend of decrease from January 1973 to February 2007 with a yearly rate of -160.5 Jyr-1. This is followed by an increase up to the end of the investigated period with a rate of 688.2 Jyr-1. The MME is highly correlated to the MMWS, with a correlation factor of 0.93.

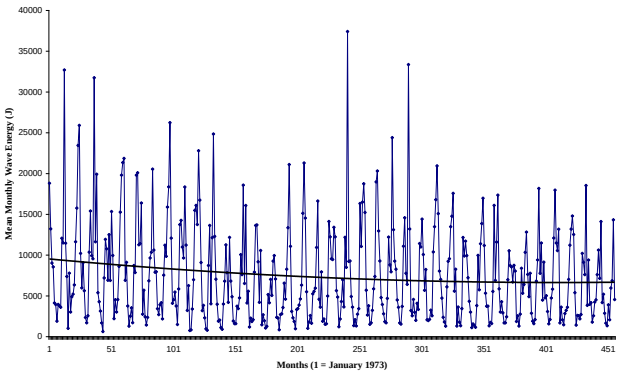

Fig .20. Quadratic trend of variation in the MME over the study period

The mean monthly P (MMP) is positively correlated to the MMWS. However, it appears to be the weakest wave parameter, among the investigated parameters, to be correlated to the MMWS having a correlation factor of 0.89.

From January 1973 to December 2010, the MMP appeared to have a cyclic trend of variations (Fig. 21) with a minimum occurrence in May 2005. The two yearly rates of variations are -952.86 Wm-2yr-1 from January 1973 to May 2005, and 163.44 Wm-2yr-1 from May 2005 to the end of the study period. The MMP varied from 450 W/m2 to 135990.49 W/m2 with an average of 15809.21 W/m2 over the period of investigation. The representative Equation of these variations is:

$$MMP = 0.2049\ x2 - 159.5203\ x + 86890 \quad (25)$$

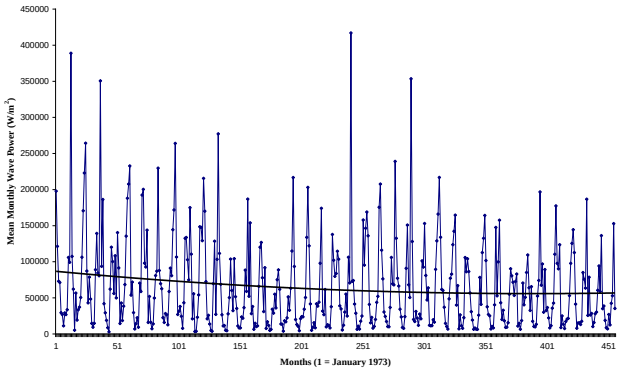

Fig .21. Quadratic trend of variation in the MMP over the study period

IV. DISCUSSION AND CONCLUSION

To the author's knowledge, no work has dealt before with the changes in the long-term behaviour of wind-wave climatology over the west region of Scotland.

The present study can be considered as an initial fair trial to get closer to the general behaviour of the major wind components and ten main wave parameters over this region.
The long-term variations of the wind-wave climatology have been examined using the quadratic regression model approach.

According to the percentage of occurrence frequency during the period January 1973-December 2010, the dominant wind components came from the south (S), the west (W), the southwest (SW) and the northwest (NW). All have the Atlantic Ocean origin and result mainly from the Atlantic depressions passing over the UK. This percentage computation agrees with the given information by the UK Met Office.

All over the period of investigation, the hourly wind speed varied between calm wind (0 m/s) to a maximum of 38.89 m/s, with an hourly average speed of 7.34 m/s. Twelve hourly wind-classes have been specified for the area of investigation with the dominant speed interval >5:10 m/s (occurrence of 41.259%), and the lowest speed interval was >35:40 m/s with 0.0006%.

The quadratic regression model of the mean monthly wind speed (MMWS) has a parabolic form, which reflects a cyclic behaviour of occurrence. From a quadratic point of view, the approach applied in this research to examine periodicity and cyclic behaviour, it can be deduced that the two major southern components have a common parabolic trend and the two major western components have another opposite common parabolic trend. Both the S and the SW monthly winds anomalies have concave-up parabola with minimum MWA speed occurrence in April 1988 and May 1969, respectively. The later, minimum of the SW-MWA, is obviously out of the present in-hand set but meanwhile, reflects the possibility of existence of large cycles of occurrence for this wind component.

Both the W and the NW monthly wind anomaly speeds have concave-down parabola with maximum occurrence in May 1995 and July 1994, respectively.
From the calculations of the zero values of the different WMA parabolas, September has appeared a common month when the MWA half-cycle reverses its path, whether upward or downward, i.e. positively with an increasing rate or negatively with a decreasing rate.
The Pierson-Moskowitz spectrum conditions have been satisfied to apply the model in order to represent the wave climatology of the area of investigation. The spectrum has been previously discussed and applied in many regions, which satisfy the conditions of Pierson and Moskowitz (1964), e.g. Holmes (2001); Alves and Banner (2003); Sorensen (2006). Both significant wave height and wave peak period have been calculated form the Pierson-Moskowitz spectrum and the resultant relationships with the MMWS and between the two parameters are in good agreement with the results of Harrison and Wallace (2005).

All wave frequencies are in an inverse correlation to the MMWS. All other wave parameters appear to be highly correlated to the mean monthly wind speed with correlation factors exceeding 0.95 except the wave power, which has a correlation factor of 0.89.

In conclusion, the general behaviour of the dominant winds over the western region of Scotland tended to be cyclic. Two opposite cycles appeared to dominate: one for the southern components (S & SW) and one for the western components (W & NW). September was a month of cycle reverse for the MWA over the region. The general behaviour of the ten examined wave parameters over the western region of Scotland also tended to be cyclic.

A longer time series, than that presently used, will be advantageous in order to strengthen this outcome of this natural cyclic behaviour with more robust investigation. Longer time series will also enable to determine the cycle period for each of the investigated parameters. This concluded cyclic behaviour may positively impact on the engineering work within the wave energy resource off the western coasts of Scotland.

REFERENCES

[1] [Alves, J.H, Banner, M.L (2003) A Symptotic Limits for Fully Developed Wind Waves. Journal of Physical Oceanography 33: 1301-1323.

[2] Anastasiades, G. and McSharry, P.E. (2013) Extreme Value Analysis for Estimating 50 Year Return Wind Speeds from Reanalysis Data. Wind Energy 17(8): pp.1231-1245.

[3] Baumgartner, T.R., Soutar, A., and Ferreira-Bartrina V (1992) Reconstruction of the History of Pacific Sardine and Northern Pacific Anchovy

Populations over the Past Two Millennia from Sediments of the Santa Barbara Basin. CalCOFI Reports 33: pp 24-40.

[4] Bretschneider, C.L. (1959) Wave Variability and Wave Spectra for Wind-Generated Gravity Waves U.S. Army Corps of Engineers, Beach Erosion Board, Technical Memorandum pp. 118: 192.

[5] Corbel G, Allen JT, Woolf DK, Gibb S (2007) Wind Trends in the Highlands and Islands of Scotland 1960–2004 and their Relation to the North Atlantic Oscillation. 19th Conference on Climate Variability and Change, San Antonio, Texas, January 2007.

[6] El-Geziry, T.M., Maiyza, I.A., Abdel-Hafez, S., Maiyza, ShI. and Kamel, M.S. (2013) Interannual Variability of the South-Eastern Mediterranean Catch and Its Relation to Hydrographical and Air-Temperature Anomalies". Journal of King Abdul-Aziz University: Marine Science 24 (1):43-54.

[7] El-Geziry, T.M., Maiyza, I.A., Maiyza, H.I. (2013) General Trend of Wind Anomalies in the South-Eastern Mediterranean Sea. Journal of King Abdul-Aziz University (JKAU), Marine Sciences 24 (2): pp 85-97.

[8] Fedrouich, L.A (1985) Regular Formation of Large Scale Temperature Anomalies of the Surface Layer in the Northern Pacific Ocean. Ph.D. Thesis, Moscow University.

[9] Harrison GP, Wallace AR (2005) "Sensitivity of Wave Energy to Climate Change. Energy Conversion" 20 (4):pp 870-877.

[10] Hasselmann, K., Barnett, T.P., Bouws, E. ET AL (1973) Measurements of Wind-Wave Growth and Swell Decay During the Joint North Sea Wave Project (JONSWAP). Report No.12, Deutches Hydrographisches Institute: p95.

[11] Holmes, P. (2001) Coastal Processes: Waves. In: "A Course in Coastal Defence Systems". Professional Development Programme: Coastal Infrastructure Design, Construction and Maintenance. St. Lucia, West Indies, 22p.

[12] Holthuijsen, L.H (2007) Linear Wave Theory (Oceanic Waters). In: "Waves in Oceanic and Coastal Waters". Cambridge University Press, pp 106-143.

[13] Hylen, A. (2002) Fluctuations in Abundance of Northeast Arctic Cod During the 20th Century. ICES Marine Science Symposia: 534-550.

[14] Kawasaki, T. (1994) A Decade of the Regime Shift of Small Pelagics. Bulletin of the Japanese Society of Fisheries Oceanography 58: pp 321-333.

[15] Klyashtorin, L.B, and Lyubushin, A.A (2007) Cyclic Climate Changes and Fish Reproductivity. Editors: Gary D. Sharp. VNIRO Publishing, Moscow.

[16] Levitus, S. (1995) Interannual to Decadal Scale Variability of the World Ocean. IAPSO XXI General Assembly, Honolulu, Hawaii, USA, August 5-12, 1995.

[17] Lindsey DT (2011) "A High Wind Statistical Prediction Model for the Northern Front Range of Colorado". National Weather Association, Electronic Journal of Operational Meteorology, 2011-EJ03.

[18] Longuet-Higgins, M.S (1957) The Statistical Analysis of a Random Moving Surface. Philosophical Transactions of the Royal Society of London, Series A: Mathematical and Physical Sciences 249 (966): pp321-387.

[19] Maiyza, I.A. and Kamel, M.S. (2009) Climatological Trend of Sea Surface Temperature Anomalies in the South Eastern Mediterranean Sea. Journal of King Abdul-Aziz University: Marine Science 20: 59-66.

[20] Maiyza, I.A and Kamel, M.S. (2010) Climatological Trend of Sea Surface Salinity anomalies in the South Eastern Mediterranean Sea. Journal of King Abdul-Aziz University: Marine Science 21(2): 63-72.

[21] Maiyza, I.A. (1984) Long -Term Variation of Water Temperature in the Eastern Part of the Mediterranean Sea, Ph. D. Thesis, Moscow University.

[22] Maiyza, I.A, El-Geziry, T.M, Maiyza, H.I. and

Kamel, M.S (2011) Climatological Trend of Air Temperature Anomalies in the South-Eastern Mediterranean Sea. Journal of King Abdul-Aziz University: Marine Science 22 (2): 55-65.

[23] Mollison, D. (1994) Assessing the Wave Energy Resource. In: Statistics for Environment 2. Barnett and Turkman Eds. Wiley press, pp 205-220.

[24] Ochi, M.K. and Hubble, E.N. (1976) Six-Parameter Wave Spectra. In: Coastal Engineering, pp 301-328.

[25] Olaofe, Z.O. and Folly, K.A. (2012) Statistical Analysis of the Wind Resources at Darling for Energy Production. International Journal of Renewable Energy Research 2 (2): pp 250-261.

[26] Phillips, O.M. (1977) The Dynamics of the Upper Ocean (2nd ed.). Cambridge University Press.

[27] Pierson ,W.J. and Moskowitz, L. (1964) A Proposed Spectral form for Fully Developed Wind Seas Based on the Similarity Theory of A. A. Kitaigorodskii. Journal of Geophysical Research 69: pp 5181–5190.

[28] Said, M.A, El-Geziry, T.M, Radwan, A.A (2012) Long-Term Trends of Extreme Climate Events over Alexandria Region, Egypt. International Conference on "Land-Sea Interactions in the Coastal Zone" Jounieh - Lebanon, 06-08 November 2012: pp 286-293.

[29] Sinden, G. (2007) Characteristics of the UK Wind Resource: Long-Term Patterns and Relationship to Electricity Demand. Energy Policy 35 (1): 112-127.

[30] Sorensen, R.M. (2006) Wind-Generated Waves. In: "Basic Coastal Engineering. Springer", pp: 157-194.

[31] Speedie, C.D, Johnson, L.A. and Witt, M.J (2009) Basking Shark Hotspots on the West Coast of Scotland: Key sites, "Threats and Implications for Conservation of the Species". Commissioned Report 339: 58p.

[32] Sundby, S. And Drinkwater, K. (2007) On the Mechanisms Behind Salinity Anomaly Signal of the Northern North Atlanti. Progress in Oceanography 73: pp190–202.

[33] Youm, I., Sarr, J., Sall, M., Ndiaye, A. and Kane, M.M (2005) "Analysis of Wind Data and Wind Energy Potential along the Northern Coast of Senegal". La Revue des Energies Renouvelables 8: pp 95 – 108.

[34] Woolf ,D.K, and Challenor, P.G (2002) Variability and Predictability of the North Atlantic Wave Climate. Journal of Geophysical research 107 (C10): doi: 10.1029/2001JC001124, p 14.

[35] Wolf, J. and Woolf, D.K. (2005) Waves and Climate Change in the Sea of the Hebrides. Proceedings of the 15th International Offshore and Polar Engineering Conference, Seoul, Korea, June 19-24, 2005: pp 100-107.

[36] Weisse, R. and Storch, V. H. (2010) Marine Climate and Climate Change. Springer Praxis, p 219.

A Brief Introduction to Building Information Modeling (BIM) and its interoperability with TRNSYS

A. Boukara[a] & A. Naamane[b]
[a] École Nationale Supérieure d'Architecture de Marseille, L'unité de recherche PROJECT[s]
email: abdelaziz.boukara@marseille.archi.fr
[b] Aix Marseille Université, CNRS, ENSAM, Université de Toulon, LSIS UMR 7296, 13397, Marseille France, email: aziz.naamane@lsis.org

Abstract - Hand-drafted print, sketching and hand modeling were the standard for building designs before the advent of computer aided design (CAD) systems. Nowadays CAD systems are better understood, their adoption increased until the 2D, 3D CAD system and the virtual reality system have become the norm. Their natural evolution has given rise to a new and more complex generation of building design tools known as building information modeling, or BIM.

There is insufficient clarity about what BIM is, although this is improving, and there is much shared understanding. There is agreement that BIM is not just software. BIM is not just CAD, or geometric data. BIM is a collaboratively generated and maintained data rich information source for the life of the design process and beyond. In this paper, we present briefly the greatest value derived from BIM in the use and maintenance of buildings and the use of TRNSYS with BIM.

Nomenclature –

BIM	Building Information Modeling
CAD	Computer Assisted Design
MEP	Mechanical, Electrical & Plumbing
TRNSYS	Transient Simulation Program

I. INTRODUCTION

Wikipedia defines Building Information Modeling (BIM) as the process of generating and managing building data during its life cycle using three-dimensional, real-time, dynamic building modeling software to decrease wasted time and resources in building design and construction. This process produces the building information model (also abbreviated BIM), which encompasses building geometry, spatial relationships, geographic information, and quantities and properties of building components, including the life-cycle processes of construction and facility operation. Building Information Modeling (BIM, the process) began as a common name for a variety of activities in object-oriented computer-aided design (CAD) that support the representation of building elements in terms of their 3D geometric and non-geometric (functional) attributes and relationships[2].

II. WHAT IS BIM?

BIM is an intelligent model-based process that provides insight to help you plan, design, construct, and manage buildings and infrastructure. So BIM goes further than traditional CAD drawings by providing intelligence to individual building components (e.g. windows, walls or chillers) as well as providing system- and building-wide information and awareness (system flows or building loads) in addition to simple spatial relationships.

The BIM process involves participants from the entire project life cycle (architect, engineer, contractor, owner, facilities management, etc.) who all contribute and communicate with BIM designers, who are asked to provide more accurate energy modelling data. It is important to not consider and think that BIM is a software; BIM should be considered as the process of creating and using digital models for design, construction and/or operations of building projects. These models combine intelligent 2D and 3D objects used to define a building design, along with external factors, such as geographic location and local conditions, into a virtual building database that provides a single, integrated source for all information associated with that building's design.

The "intelligence" attributed to the objects includes parametrically-defined graphical and non-graphical information, giving the architects, MEP engineers, and contractors the ability to represent geometric and functional relationships between building elements. This information feeds an integrated database, which in turn feeds all design documents and schedules for

the building project. When a change is made to the building model, all graphical views (plan, elevation, detail, and other construction drawings), as well as non-graphical views, such as the design documents and schedules, automatically reflect the change. Therefore, the main advantages of BIM are:

A. Improved information flow

Because a digital model represents a unified description of a building, it can significantly improve the flow of information in every stage of the design, construction, and life cycle of a building The digital model can be accessed by the architects, MEP engineers, contractors, facilities managers, and owners at different phases in the building life cycle to add, extract, or modify information in support of their role. A clear vision of the project is maintained to promote informed decisions, reduce errors, and improve productivity[5].

B. Better design visualization

The ability to predict how occupants, visitors, and neighbors will react to and interact with a building is a crucial part of the design process for architects and engineers. However, the virtual building model created during the BIM process also provides an important benefit in helping MEP engineers optimize the layout of the HVAC system within the space constraints of the building design [2]. Whether placing an air handler in a mechanical room, or routing piping or ductwork, the ability to virtually build the HVAC system and visually examine it in 3D can provide added assurance that all components will fit when construction begins [3].

C. Improved cost estimating

BIM can simplify and help provide better cost estimates because of the depth and precision of the information it provides. The relative ease with which material and assembly quantities can be extracted from the model can increase the speed and accuracy of estimates, providing a better gauge of the impact of design changes so that budget concerns can be dealt with proactively.

D. Improved energy analysis

Here again, BIM can simplify and improve the accuracy of energy analysis because the data required to perform such analysis is resident in the digital building model [4].

E. Reduced construction costs

Clash detection can be used long before construction begins to show where parts of the design occupy the same space. This can reduce or eliminate the need for changes in the field during construction. BIM models can also be used to help prefabricate building components, such as duct or pipe runs, with confidence. This can save in costs associated with assembly and installation.

F. Building history

As a building passes through design, construction, and into occupancy, the digital model can serve as an important information library for owners and service contractors. For example, if a building component fails, the building information model can be used to identify its location, manufacturer, model number, performance specifications, and other pertinent data to most efficiently repair or replace that component. If a portion of the building is being remodeled, the building information model can be used to identify concealed components, such as piping, ductwork, and electrical equipment to promote informed decisions on the remodel design[6].

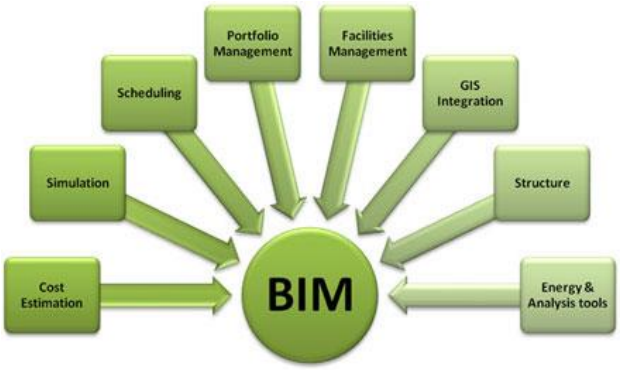

Fig .1 Bim environment

III. TRYNSYS AND BIM

TRNSYS is a complete, modular, and expansible simulation environment for the transient simulation of thermal systems including multi-zone buildings [1], [8]. It is used by engineers and researchers around the world to validate new energy concepts, from simple solar domestic hot water systems to the design and simulation of buildings and their equipment, including control strategies, occupant behavior, alternative energy systems (wind, solar, photovoltaic, hydrogen systems), etc.

One of the key factors in TRNSYS' success over the last 25 years is its open, modularstructure. The source code of the kernel as well as the component models is delivered to theusers. This simplifies extending existing models to make them fit the user's specific needs. No single computer application can support all of the tasks associated with building design and production. Interoperability depicts the need to pass data and knowledge between applications, allowing multiple types of experts and applications to contribute to the work at hand. Interoperability has traditionally relied on file -based exchange formats, such as DXF (Drawing eXchange Format, or another type of date as dwg and more) and IGES that exchange only geometry. In this part, we present how TRNSYS is used in BIM Framework.

IV. STUDY CASE: DYNAMIC THERMAL SIMULATION OF A BUILDING

The project consists of 8 buildings as shown on the below ground plane.

The study will focus on building E. The objective is to analyze the thermal behaviour of the building and evaluate the impact of technical or architectural choices in order to justify the proposed solution. In this case, the standard building, initially defined without insulation on the external envelop was modified by taking into account the glazing surface in the building.

The simple glazing was changed to a double glazing layer incorporated with Argon. A dynamic thermal simulation with TRNSYS software was conducted. The simulation results are presented as output data, hour by hour: temperature, moisture, powers of air conditioning, energy consumption, and so forth, related to the building behaviour and its occupants.

The different steps carried out in the simulation are the following:

A. Step 1

The building is obtained on a graphical format compatible with sketch up environment

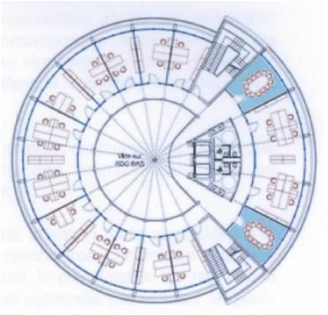

Fig .2 CAD Format

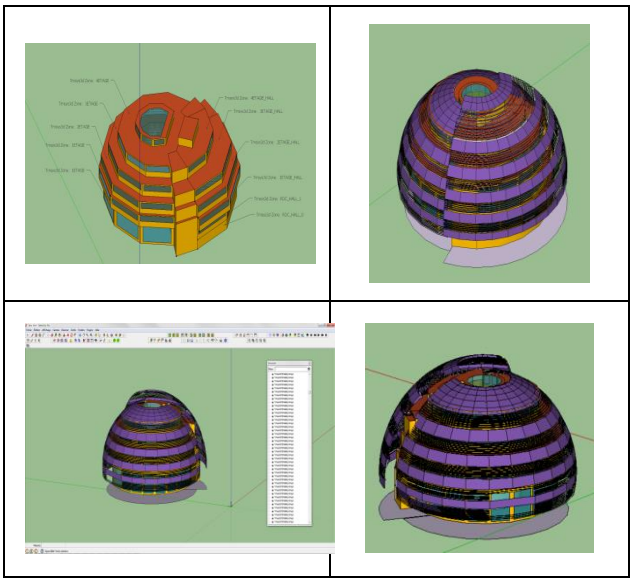

Fig .3 Sketchup view using TRNS3D (Open Studio) plugin

B. Step 2

Thermophysical properties are affected to the external envelop

Type de paroi	Composition	Coefficient U En W/m².K	Facteur solaire
Plancher bas	Dalle béton	0.58	-
Plancher sous combles	Dalle béton	0.95	
Vitrages	Vitrage simple clair	Ug = 5.8	82%
Murs extérieurs	Béton	3.94	-
Cloisons intérieures	Plâtre /Laine de verre 5cm	0.67	-
Terrasse	Dalle béton	0.952	

Once the operation has been completed the file is saved in an appropriate format idf. This enables to make the connection between Sketchup and TRNSYS.

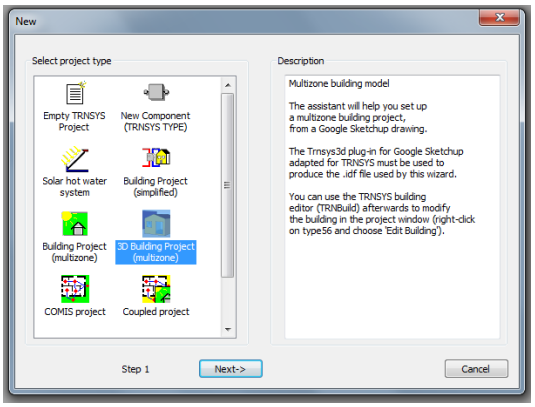

Fig .4 Opening the idf format on simulation Studio

TRNsys is loaded with features that allow making the link between the geometric modeling and thermal modeling, so it minimizes the time and the loss of the data; this interface returns fully under the BIM approach.The tool that is used to set all the thermophysical, properties and in this case the different consumption and internal inputs as a function of the scenarri is TRNbuild. The latter allows thermophysical modifications at the level of the envelope and its properties.

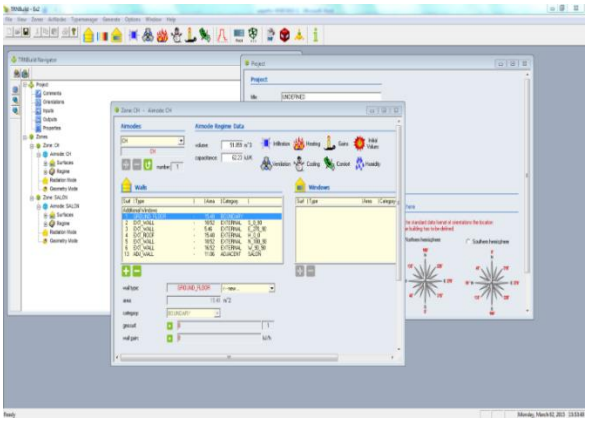

Fig .5 TRNbuild environment

Heat transfer calculations are made in TRNbuild and forwarded to the studio simulation environment in which the building is being updated (data).

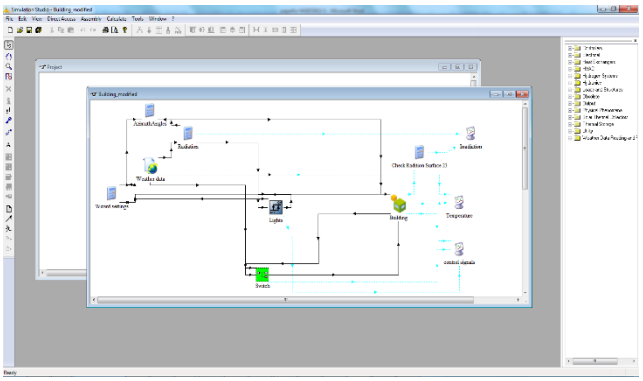

Fig .6 Managing the project on Open studio environment

V. SIMULATION RESULTS

After making several parametric simulations, we obtained the following results concerning the comfort temperature and energy consumption (summer comfort) parameters.

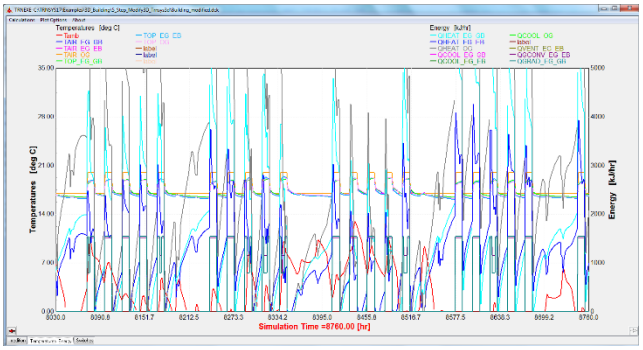

Fig .7 Simulation results (type 65, online plotter)

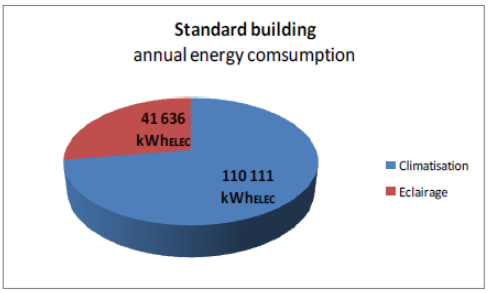

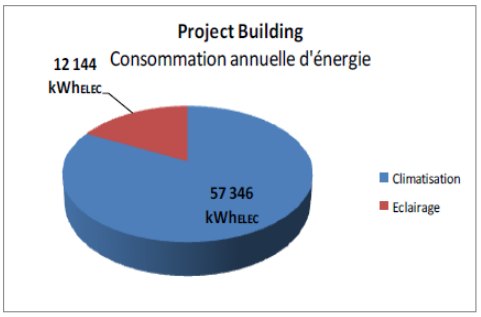

Saving energy-54%

Over a period of 20 years, the building designed by the project management team will allow an economy of exploitation of €326 529, or an average of €16 326 / year. Such building designed by the project management team will enable a saving of 82 257 kWh of electricity / year.

V. CONCLUSION

Those who have adopted BIM continue to tell us about the real benefits it delivers. For the design team, there are clear benefits of collaboration, visualisation, coordination and information retrieval. This readily translates into increased cost efficiencies and profitability. The use and sophistication of BIM will continue to grow as more of the benefits of the technology have become evident. The number of buildings designed using the technology and the number of BIM users has grown dramatically over the past few years, and this trend is expected to continue. The benefits of BIM adoption depend on all parties being able to engage and collaborate in a well-informed way. In the BIM world all participants depend on each other to succeed. There may be a lot of focus on technology, but BIM is also about people and processes. People need to understand the opportunities offered by technology and make choices about how to use it.

REFERENCES

[1] Klein, S. A., Beckman, W., Mitchell, J. W., Duffie, A. J., Duffie, N. A., Freeman, T. L., Mitchell, J. C., Braun, J. E., Evans, B. L., Kummer, J. P., Urban, R. E., Fiksel, A., Thornton, J., Blair, N. J.,Williams, P. M., Bradley, D. E., McDoweel, T. P. & Kummert, M. 2004. TRNSYS 160- A TRaNsient SYstem Simulation program, User Manual, adison, Solar Energy Laboratory, University of isconsin-Madison.

[2] Laine, T., et al., 2010. Energy and Thermal Performance Management Through Utilisation of Building Information Models NBDM, Neutral Building Data Model, http://nbdm.org/

[3] Nytsch-Geusen, C. et al., 2003. Integration of CAAD, Thermal Building Simulation and CFD by using IFC Data Exchange Format, Eigth International IBPSA Conference, Eindhoven, Netherland.

[4] Bazjanac, V. 2008. IFC BIM-based methodology for semi-automated building energy performance simulation. In L. Rischmoller (ed.), CIB W78, Proc. 25th conf.

[5] Ford, S., Aouad, G., Kirkham, J., Brandon, P., Brown, F., Child, T., Cooper, G., Oxman, R., Young, B., 1995. An information engineering approach to modelling building design, Automation in Construction 4(1), pp. 5-15.

[6] Sacks, R., Eastman, C.M., Lee, G., 2004. Parametric 3D modeling in building construction with examples from precast concrete, Automation in Construction 13(3), pp. 291-312.

[7] Migilinskas, D., Ustinovichius, L., 2006. Computer-aided modelling, evaluation and management of construction project according PLM concept,Lecture Notes in Computer Science 4101, pp. 242-250.

[8] Eastman, C., Teicholz, P., Sacks, R., Listo, K., 2008. BIM handbook: A guide to building information modeling for owners, managers, designers,engineers, and contractors. Hoboken (New Jersey): Wiley, p. 490.

A Mechanism for Using Renewable Energy Applications in Remote Areas

Safwat Abdel Fattah Seleem
High Institute of Engineering, 15 th May City,
Former General Manager,
Safwat.seleem@yahoo.com

Abstract - Currently our world is facing the challenge of natural resources depletion, specifically the depletion of fossil fuel resources. Accordingly, the implementation of sustainable energy sources is no longer a luxury, but a key issue for survival. Egypt is one of the most fortunate locations when it comes to renewable energies, such as wind and the sun but implementation remains lacking. This paper addresses this matter by offering simple applicable solutions for remote areas, such as Al-Wadi Al-Jadid and Sinai. The idea is based on creating a self-sustaining simple closed system that can be replicated in different settlements, which offers prosperity for the local communities.

The proposed system will be designed to address the technical, financial and social barriers that prevent renewable energies from becoming widespread in Egypt. Such a system would consist of financial institutions, suppliers, local technical capacity building and local awareness raising and education. In addition, they use fly ash material in construction of different projects that contains concrete, plaster, and bricks. The use of fly ash material aims at saving energy and reduces the use of cement, as the fly ash replaces about 25 % of cement quantity in concrete and plaster works and about 60 % of brick ingredients.

Accordingly, the use of fly ash material leads to reducing the emission of CO2 resulting from the factories of cement. Simply, in order to spread the use of renewable energy on a large scale, the community as a whole must benefit and private individuals must also benefit by being able to make life easier and reduce pollution levels.

Keywords - Renewable energy, Sustainable, Friendly environmental concrete, Fly ash, Remote areas.

I. INTRODUCTION

One of the main concerns in Egypt is to guarantee modern electricity resources for all citizens. This target matches with the concept of sustainable development, which is defined as “development that meets the needs of the present without compromising the ability of future generations to meet their own needs” [1]. The main factor in attaining sustainability is how to implement it effectively. The key points are the design of a realistic work system that meets the needs of the society and that can be easily implemented. The awareness of the community plays an important role as well. This is where the idea of sustainable communities starts emerging.

Sustainable communities can be defined through different ways; one common definition is “communities that meet the diverse needs of existing and future residents, their children and other users, contribute to a high quality of life and provide opportunity and choice. They achieve this in ways that make effective use of natural resources, enhance the environment, promote social cohesion and inclusion and strengthen economic prosperity” [2]. Figure 1 represents the main components of sustainable communities.

In this regard, the idea of the paper has been highlighted. It aims to create a sustained community based on available local resources and components. Providing vulnerable underprivileged rural households with a sustainable and environmentally friendly source of energy will improve the quality of living. It will allow for covering their basic needs of food, safety and security by making the operation of small fridges possible and providing a storage facility.

This will also allow for reducing transportation expenditures and the use of and dependency on fossil fuels. Having access to electricity, saving energy via using fly ash material as a friendly environment material, the youth in the village will also be able to study in the evenings, since they typically have to help their parents in farming after school.

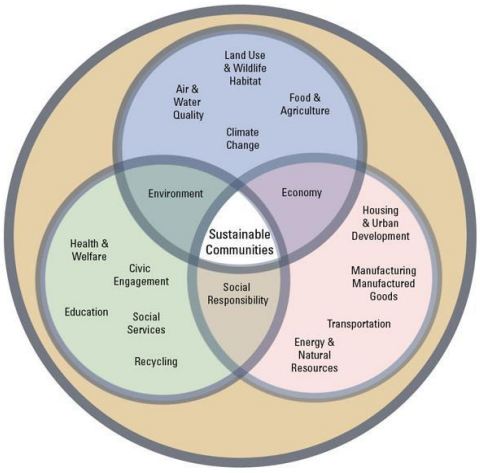

Fig .1. Components of Sustainable Communities [3]

II. PROJECT DESCRIPTION

The proposed mechanism is based on three main pillars which fulfill the needs of the local community by finding suitable applications for renewable energy, using the friendly environmental concrete, plaster works, and bricks which use the fly ash material by replacing about 25 % instead of cement in concrete structures and plaster works, and about 60 % of brick ingredients. The third pillar is creating a system (a loop of work) that ensures the attainment of sustainability. By establishing these pillars in a model community, the idea will roll-out to spread through different local communities (governorates) in Egypt.

Locations such as Al-Wadi Al-Jadid and Sinai could be potential areas to apply the proposed approach. That is because both governorates represent more than 50% of the country's borders. Therefore, their development and growth in population is crucial. Moreover, the low population density and large deserted areas give a way to various possible innovations for the two places and their communities. And also, this facilitates the involvement of the local communities in the planning process for the development projects to be carried out. Some basic information about the two locations, Al-Wadi Al- Jadid and Sinai, work methodology and an outline for the system are as follows:

A. Background

The first step of this approach is to identify the candidate locations for the study. The selection criteria resulted in two locations that represent important marginalized governorates in Egypt, which are Al-Wadi Al-Jadid and Sinai.

Al-Wadi Al-Jadid governorate is located in the southern west of Egypt. It represents the western border of Egypt with Libya and the southern one with Sudan. The size of the governorate is 440,098 km2 representing 44% of Egypt's total area, a considerably large one. The governorate lies at the border of Giza, Marsa Matruh, and El-Menya governorates from the north, Assuit, Sohag, Qena and Aswan from the east. Unfortunately, although it is the largest governorate with regard to area, it is the smallest one with regard to population (209,597).

Figure 2 shows the location of the governorate in Egypt and its surrounding borders and it can be observed that Al-Wadi Al-Jadid represents around 50% of Egypt's political land borders. [4, 5]

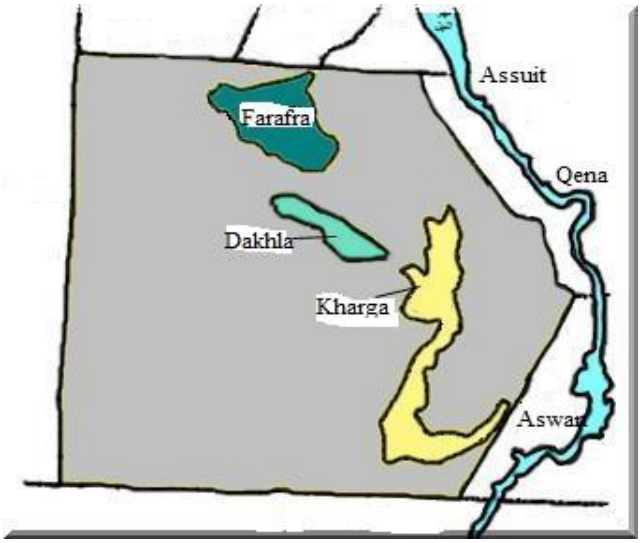

Fig .2. Map showing the location of Al-Wadi Al-Jadid governorate and its surrounding borders

People activities in Al-Wadi Al-Jadid are focused on tourism, agriculture and traditional fabrications. Olives, dates, orange, beans, mango, and apple are the most agriculture productions. Regarding the tourism industry, various touristic sites from different areas are found in the governorate as well as eco-touristic sites, such as Gilf El- Kebir area.In addition, herding sheep and cattle are also one of the main income sources for farmers. On the other hand, fabricating traditional and decorated Pottery, Arabesque, and Kilim rugs are attractive to tourists. In this regard, there are two airports: El-Dakhla airport and El-Kharga airport.

Concerning available resources, water wells are the main source for water supply. As for electricity, the National Electricity Grid mainly feeds Abu-Tartur mining project to produce phosphate and partially El-Kharga, El-Dakhla, El-Farafra, and Paris cities. Meanwhile, other districts distributed in the governorate use diesel to generate electricity for a certain period during the day, maximum 6 hours. This means that people could not use modern energy applications.On the other hand, districts are distributed in different places and are very far from the national grid, ranging between 50 to 210 km, which makes expanding electricity network to these places unviable. So the most applicable solution is to use decentralized systems to feed these districts with its needs of electricity. Tables (1) and (2) list some detailed information on electrical supplies in the governorate.

Table 1. Substations Details at Al-Wadi Al-Jadid Governorate

Substation	Transmitted Electricity (W)	Beneficiary Districts
El-Kharga	163,862,888	El-Kharga City and its villages
Paris	10,800,000	-
Balat	159,086,542	Balat City and its villages
El-Dakhla		Moot City and its villages
El-Farafra	14,544,970	El-Farafra City and its villages

Table 2. Villages and Districts Electricity supplies

City / Date	Darb El-Arbaeen				Balat City	El-Farafra City
Village	Bir Alshab				El-Zayat Village	Ain El-Teneen
	#1	#2	#3	#4		
No. of Houses	80	80	80	80	46	60
Current source of electricity	-	-	-	-		
Distance from the National Grid of Electricity (km)	210	200	190	180	0.2	70

Lack of electrification has proved to be a blocking element against economic and social development. The proof lies in the synergies brought by the electrification of the Nile valley and Delta. Nevertheless, electrification of scattered communities in the Egyptian deserts as well as the construction of friendly environmental concrete structures is a challenge brought in by the financial burden for electrifying and housing the population dispersed over a large geographical area.

However, economic and social development to this population is mandatory to integrate them within the larger society.

The second location, Sinai, is in the eastern side of Egypt falling on the borders with Israel and Palestine and surrounded with the Mediterranean Sea on the north side and the Red Sea from south. It has an area of 60,000 km2. The land is divided into two governorates, North Sinai and South Sinai. Sinai is renowned as a famous touristic site. Figure 3 shows maps for Sinai Peninsula.

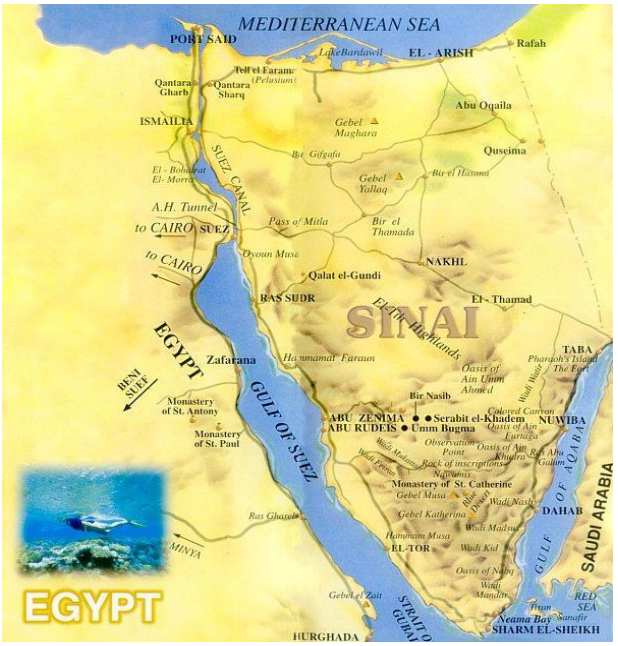

Fig .3. Maps showing location of Sinai Peninsula [6, 7]

North Sinai, where Arish represents its capital city, has a population of 357,900. It has an illiteracy rate of 24.2% while the unemployment rate is only 3.8% yet of which 45.9% have received higher education degrees. The percentage of people living underneath the poverty line is the same in both North and South Sinai, 11.1% (earning less than 185 EGP/month).

As for South Sinai governorate, it has a population of 152,500, which is the lowest population in Egypt, yet it has the highest annual growth rate. The illiteracy rate is 11.6% in the governorate while the unemployment rate is 7.8%, of which 5.3% have received higher education degrees. [ ] Al-Tur city is the capital city of South Sinai.

B. Problem Definition

The current paper identifies the community needs, land opportunities, using environmentally friendly concrete and bricks in housing projects and models of possible renewable energy applications. In order to reach such a goal, the usage of natural resources needs to be optimized; availablility of both renewable sources of energy and capabilities should be studied, as well as analyzing the society's social and economical needs. Merging both sides in a harmonized scheme socially, economically and environmentally, will lead to a pioneer study able to be replicated in similar communities.

Fundraising need to be partially self-generated. Consequently, the study will attempt to answer how these communities could perform their own economic development based on their resources, capabilities and objectives.

From this context, the available opportunities that lie in Al-Wadi Al-Jadid and Sinai locations are their low population density – 2, 12.8, and 4.8 per km2 for Al-Wadi Al- Jadid, North Sinai and South Sinai respectively – with their vast land area that can be used in various projects – agricultural, touristic, etc. – that can be replicated in other governorates.It is important to note three main advantages that lie in the choice of these two governorates.

The first advantage is addressing a major problem: a part of Egypt's society has been marginalized for a long time; therefore, such a development project would strengthen their sense of belonging to their country and give them the urge to prove it through their contribution to their larger community. The second one is the location of each governorate, which lies at the borders of the country, making its development and prosperity an important issue for Egypt's security. The last one is developing these communities will be reflected directly into the national GDP, as a result of attracting more tourists.

Figure 4 shows the contributing factors that should be well studied in order to achieve sustainability.

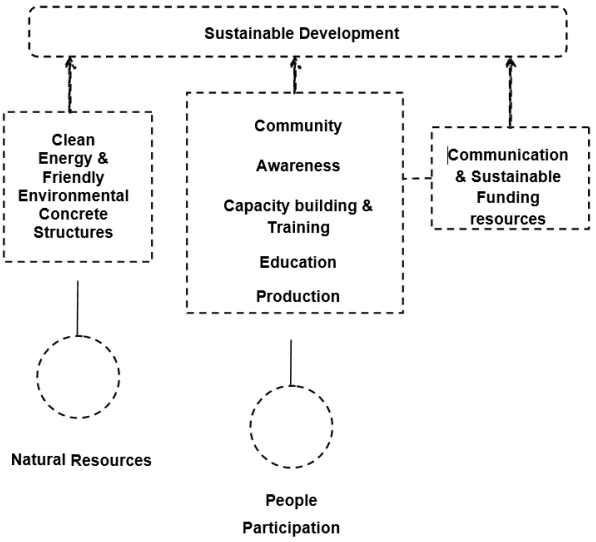

Fig .4. Factors affecting sustainability

C. Methodology

The main outline of work is based on building a self-sustained cycle ensuring continuous development while preserving the concept of sustainable development where it is based on three main pillars:

1. Renewable Energy (RE) System

One of the principal activities to be taking place is the analysis and design of renewable energy system, whether stand-alone such as solar energy system or a hybrid system consisting of a combination of solar, wind and/or biogas energies. The importance of renewable energy systems lies in the opportunities they offer starting from the ability to expand community facilities and create new jobs to enhancing the quality of life for the society. This cannot be done by national grid expansions due to its high cost, difficulty of planning and needed maintenance which render off-grid renewable energy system a favored substitute. Moreover, it is an already known fact that the national grid is suffering from overload and meeting current demands. Implementation in such deserted community would help promoting awareness on using new and renewable sources of energy in other governorates.

2. Renewable Energy (RE) System

Cement industry is the third largest source of environmental pollution, specially the emission of CO2.The fly ash material is a byproduct powder

resulting from electrical power stations in general and those using coal fuel in particular, as well as the industrial furnaces of steel and iron factories. The fly ash is a powder similar to cement but its particles are very fine and finer than those of cement powder. It is bagged also in bags similar to those of cement and has the same weight (50 kg for each bag). The fly ash is available in Egypt on a large scale. A vast array of possible applications using renewable energy can be carried out. It is an important issue to use the fly ash material in concrete structures and in manufacturing bricks as well as in plaster works. This will reduce about 60 % in the industry of cement production. In addition, this will lead to reducing pollution by preventing emission of about 50 % of CO2. The key issue is finding what is most suitable for the society and its needs concerning jobs creation, filling electrical power needs, looked for expansions and so forth. Of course, this should be done without losing the identity of the community or enforcing a complicated system.

The targeted applications should be carefully chosen through several social surveys and study of land potentials and expected outcomes on the long run. In Egypt, we are using now the fly ash material in the construction of (Metro Tunnels) such as concrete, lining of their interior walls as well as plaster works in order to achieve two targets. The first target is as friendly environmental material and the second target to be used as a fire resistant material. U.S.A, India, Japan, and European countries are the main users of fly ash material in different fields of constructions.

Figures (5-a) and (5-b) illustrate the percentage of fly ash material used in the field of concrete and bricks. The fly ash materials are replaced in concrete and plaster works and bricks instead of cement.

3. Sustainable Funding Entity

The continuous improvement is highly dependent on the presence of an entity that can be dedicated to financially support the development and upgrading of the community projects. Such entity could be an existing one (for example a national foundation such as the Social Fund for Development (SFD) or an international organization working on aiding development projects, such as the (World Bank). Creation of a channel between the local community and such proposed entity is to facilitate communication as well as empower local citizens.

In order to reach an effective communication stream, capacity building program will be needed for local citizens where the local government and city councils can play a role in such aspect. A main objective of the study is to design a system that allows the communities to earn income from the renewable energy systems and friendly environmental housing projects in a way that enable them to sustainably finance their future energy systems. The proposal team members have already had positive initial contact with international agencies and local private sector firms who can provide the initial financing and on-going financial support.

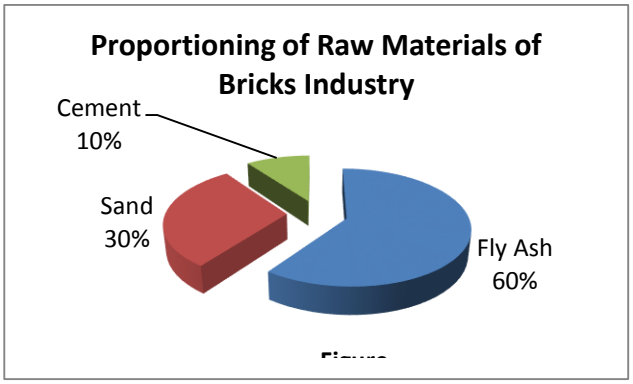

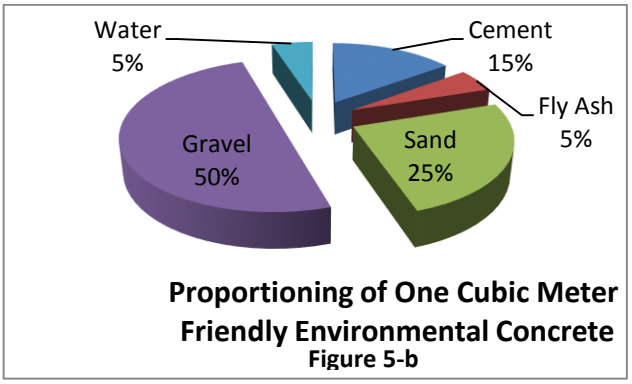

Figure 5-b

In order to achieve this work cycle, several steps should be taking place:

- Several site visits are expected to take place in order to collect needed data, understand and study the nature of the land, and carry out measurements such as for the nearest cement factories, solar and wind data as well as assess possible locations for implementations

- Social Surveys will be carried out through different forms – meetings, oral and written questionnaires, focus group and so forth. – to analyze the current status of the society concerning educational levels, employment rates,

main jobs sector as well as knowing the needs of the society including electrical power needed.

- Renewable Resources identification whether solar, wind, biomass, etc: This requires desk research to establish a quantitative data base of the selected site data and to analyze different combinations of hybrid systems and stand-alone ones.

- Energy Requirements identification of both the energy requirement of the settlement together with the load profile: This requires an understanding of the social and economic pattern at the settlement.

- Energy Mix Optimization provided the availability of renewable energy resources data, the availability of using the fly ash material in the industry of cement, the load profile and generation requirements. A techno- economic study shall be performed to provide the most economic generation mix together with the least Loss of Load Probability. Homer software is one candidate for this study.

- Technology Selection and Project Financial Feasibility Study where translating the proposed generation mix into technology is governed by the simplicity of the adopted technology together with its economics. The primary selection of the technology is dependent on its simplicity and suitability to the population. The second selection that follows is the prefeasibility of the project. Rest screen shall be used to perform the pre- feasibility study of the optimum generation mix.

- Project Generalization is based upon the obtained results which shall be generalized so that they can be used with other settlements. This requires carrying out sensitivity analyses. The results shall be summarized in user friendly tables and charts.

- Project Engineering Equipment Specifications and cost estimates as well as cost benefit analysis of the project shall be prepared by the project team. The provided document shall be the basis for the future tender for the actual implementation of the project.

III. CONCLUSION

The main outcomes that this project is looking for can be summarized in the following points:

- Using environmentally friendly concrete structures and bricks via replacing the material of fly ash instead of about 25 % of cement in concrete structures and about 60 % of bricks ingredients, which should lead to reducing the emission of about 50 % of CO2. This will lead to keeping on the heat of indoor houses and consequently saving energy.

- Satisfying community needs through the implementation of renewable energy systems that meet the required growth and prosperity of land and society.

- Empowering local citizens by offering needed guidelines, training and capacity building to be able to take decisions needed to help their community and reserve the environment which they live in.

- Introduce a talent fundraising approach.

- Promoting sustainability awareness by giving Al-Wadi Al-Jadid and Sinai as model governorates for a sustainable community.

- Promoting the use of renewable energy and fly ash systems where Egypt has great potentials in that field. This could help in solving electricity shortage problems and reduce the load on the national grid by using off-grid energy systems for remote areas and reducing the emission of CO2 via preventing the production of about 50 % of cement.

- Helping in improving the quality of Egypt's tourism sector as well as increasing its revenue.

- Developing a replicable sustainable model.

- Develop an evaluation scheme based on monitoring socio-economic parameters during different implementation phases.

REFERENCES

[1] International Institute for Sustainable Development (iisd); http://www.iisd.org/sd/

[2] The Egan Review: Skills for Sustainable Communities http://dera.ioe.ac.uk/11854/1/Egan_Review.pdf

[3] Sustainable Communities Components; http://goo.gl/1OSCQ

[4] Al-Wadi Al-Jadid Governorate official site; http://www.newvalley.gov.eg/html/nabza1.htm

[5] Luventicus Academy of Sciences; http://www.luventicus.org/maps/egypt/newvalley governorate.html

[6] Map of Sinai Peninsula; http://goo.gl/DDBK9

[7] Map of Egypt; http://goo.gl/UXGdg

[8] Egypt Human Development Report 2010 – UNDP

[9] CLAYTON, N., and LENNON, T. High-grade concrete columns in fires. Concrete. Vol. 34, No.3. March 2000, p.51.

[10] THOMAN, T., When Hull freezes over. Tunnels and Tunneling International, Vol. 32, No.10. October 2000, pp. 16-17

[11] THE CONCRETE SOCIETY. Design guidance for high strength concrete. Technical Report 49, 1998, 176 pp.

Energy Retrofitting of the Mediterranean Terrace Dwellings

D.K.SERGHIDES M.MARKIDES & M.C.KATAFYGIOTOU
Department of Environmental Science and Technology Cyprus University of Technology (CUT) Limassol, Cyprus
despina.serghides@cut.ac.cy, markidesmarina@gmail.com, martha.katafygiotou@cut.ac.cy

Abstract **-** The building sector in Europe is responsible for an estimated 40% of the total energy consumption. This paper focuses on the existing terrace housing in Mediterranean island of Cyprus. The collection of statistical data and the building typologies were developed based on a harmonised structure for European building typologies according to the IEE EPISCOPE project.

A representative terrace-housing complex was used as a showcase for demonstrating the energy performance and the potential of energy savings, by applying energy conservation measures. This research aims at filling in the current knowledge gap. It also portrays that building typologies can be a useful instrument to facilitate the energy performance assessment of the building stock.

Keywords **-** Energy performance, Building typology, Terrace housing, Existing building stock.

I. INTRODUCTION

The increasing energy consumption already threatens the future of the planet, as studies show that 10% of the world population exploits 90% of energy resources [1]. Under this threat, the European Union aims to achieve a more sustainable future and therefore focuses on the existing building stock by identifying the potential energy conservation of the building sector. However this venture presents many obstacles and it seems very difficult to find data on the European or on the national levels [2].

In 2000, it was estimated that 45% of the energy produced in Europe was used in the building sector and 50% of air pollution was caused by this sector [3]. The existing residential building stock exceeds the number of newly built dwellings in most developed countries. Moreover residential buildings are responsible for approximately 2/3 of the energy consumption of the building sector [4]. While new buildings add at most 1% per year to the existing stock, the other 99% of the buildings are already built and produce about 26% of the energy-use induced carbon emissions [5]. Thus, there is greater potential of energy savings and reduction of carbon emissions, in the existing residential buildings than the newly built ones.The improvement of the energy performance of the existing residential stock in every country is essential since the operational cost; the energy consumption and the carbon dioxide emissions are major issues worldwide. This paper is based on information laid out by the European, IEE Episcope Project [6]. The study focuses on the Terrace Family House (TFH) typology, which is one of the main residential typologies identified in Cyprus; three representative buildings from this typology were selected to conduct the research. This paper is a multiple case study and aims at reducing the energy consumption and CO_2 emissions of the dwelling through energy efficient refurbishment measures.

II. METHODOLOGY

According to previous studies by the EU, IEE Project EPISCOPE [6], twelve residential building stock typologies were established as typical and representative of the national residential building stock in Cyprus. These are classified according to their chronological period of construction and their architectural and constructional characteristics. The three building typologies consist of; the Multi-storey Family Houses (MFH), the Terrace Family Houses (TFH) and the Single Family Houses (SFH). These are divided into four different chronological periods, supported by the data collected from the Cyprus Statistical Service [7]. Each chronological division was defined based on the different constructional regulations and techniques that were applicable throughout the years, formulating the four distinctive chronological categories, before 1980, between 1981-2006, between 2007-2013 and after 2014. These divisions were also guided by the rapid growth of the construction industry in Cyprus, which occurred after 1980, by the adoption of the European Directive in 2007 [9] and the amendment of the Directive, which was enforced in beginning of 2014.

For the purpose of this paper only, one residential building typology is examined; the Terrace Family House of the second chronological period between

1981-2006. Three exemplary building units were selected from a Terrace Family House complex; the middle one and the two end dwellings. These building units have the same constructional characteristics, the same electromechanical systems and they are typical and representative samples for their construction period. The scope of the study is to compare the energy performance concerning the varied location of the buildings (one fully attached house in the middle of the complex and two semi-detached on either end, which have different orientations). The effect of the orientation and the dissimilar exposed facades of the three houses are examined and conclusions towards the energy consumption of the building are derived.

The buildings' design, specifically their construction characteristics, are selected through field inspections and are examined through parametric simulations using the software iSBEMcy. This is the official governmental software used for the categorization of energy efficiency in buildings and also for the calculation of CO_2 emissions according to the European Directive 2002/91/EC [8]. The software calculates the energy consumption of the building and concludes to its energy performance certificate, which states the energy categorization of the building. All the European member countries have similar software in order to examine the energy classification of their buildings. Energy rating of a building can provide useful information on its energy consumption. The rating is performed through standard measurements under a specific experimental protocol.

The total area of each building, the heated living volume and the other elements that form the building envelope were documented. Specifically, the characteristics of the roof, the wall, the floor slab, the frame structure and the openings were recorded. Their U-Value as well as their thermal capacity was calculated. The installed electromechanical systems were documented, their energy efficiency investigated and documented in the simulation as well. Due to the lack of the available data, mainly concerning the existing electromechanical systems installed in the representative buildings, certain assumptions were made concerning length, type of pipes and condition of the systems.

The energy auditing of the buildings under study investigates the aspects that affect their energy efficiency. Initially, the simulations conclude to the energy consumption of the existing building. As energy consumption of a building is affected by its construction elements, alternative strategies and techniques for energy efficiency must be used to create a comfortable indoor environment, which at the same time will achieve energy conservation and reduce the operational cost. Therefore, based on the energy categorization of the buildings, one retrofitting scenario was studied in the simulations.

This scenario concerns the energy conservation measures (ECMs), which were based on the new requirements of the EPBD Directive [9] and were enforced in the beginning of 2014. The retrofitting interventions are restricted on the building envelope, while the electromechanical systems for heating and cooling together with the hot water system remained the same. Finally, the pay-back period of retrofitting interventions was also calculated using the official tool published by the Ministry of Energy, Commerce, Industry and Tourism of Cyprus for the cost optimal [10] EMCs.

III. CASE STUDIES AND RESULTS

The representative dwellings that were identified and studied concern the Terrace Family House (TFH) typology of the second chronological period (1981-2006). As shown on Fig. 1, this complex consists of seven Terrace Family Houses (TFH). The chosen buildings for the study are the two end dwellings and the middle one, as illustrated on the Figure. Each building was extensively studied. Information regarding the size, the heated living volume and the thermal characteristics of the building envelope were documented. Furthermore, the characteristics of the heating and cooling systems were recorded.

Fig .1. The TFH complex under study

A. Existing condition of buildings

The Terrace Family Housing Complex (TFH) is located in the capital City of Nicosia, situated in the inland area of the island. It belongs to the second chronological period between 1981-2006 and was built in the early 2000's. The dwellings have a non-insulated tiled pitched roof with horizontal ceiling, rendered brick walls, the floor slabs in contact with the ground and aluminum-framed single glazed windows. Nowadays, owners of the dwellings replaced their windows with double glazed windows for better indoor comfort and more energy efficiency. The houses have a living room, a dining room, one kitchen, a small WC on the ground floor, three bedrooms and a family bathroom on the first floor. They have an un-insulated constant temperature oil boiler, with a water storage tank, which is connected to the solar thermal panels on the roof and backed up by an electric element for domestic hot water. The cooling system installed is a standard air-conditioning with split units installed in the living room, kitchen and bedrooms of the houses. The thermal characteristics of the building envelope for the TFH and specifically their U-Values are calculated as shown on Table 1.

Table 1. THERMAL CHARACTERISTICS OF THE BUILDING ENVELOPE FOR TFH

Construction Element	U-Value W/(m^{2}k)
Pitched roof with horizontal ceiling	3.42
External Walls	1.42
Floor in contact with the ground	0.91
Double glazed windows	3.80

The first selected Family House (TFH01) is at the end of the Terrace complex and it has North East to South West orientation, with three windows covering 11m2 facing south, as shown on Fig. 2. The total heated living area is 112m2, the heated living volume is 705.6m3 and it is the second large unit, of the three selected houses of the study.

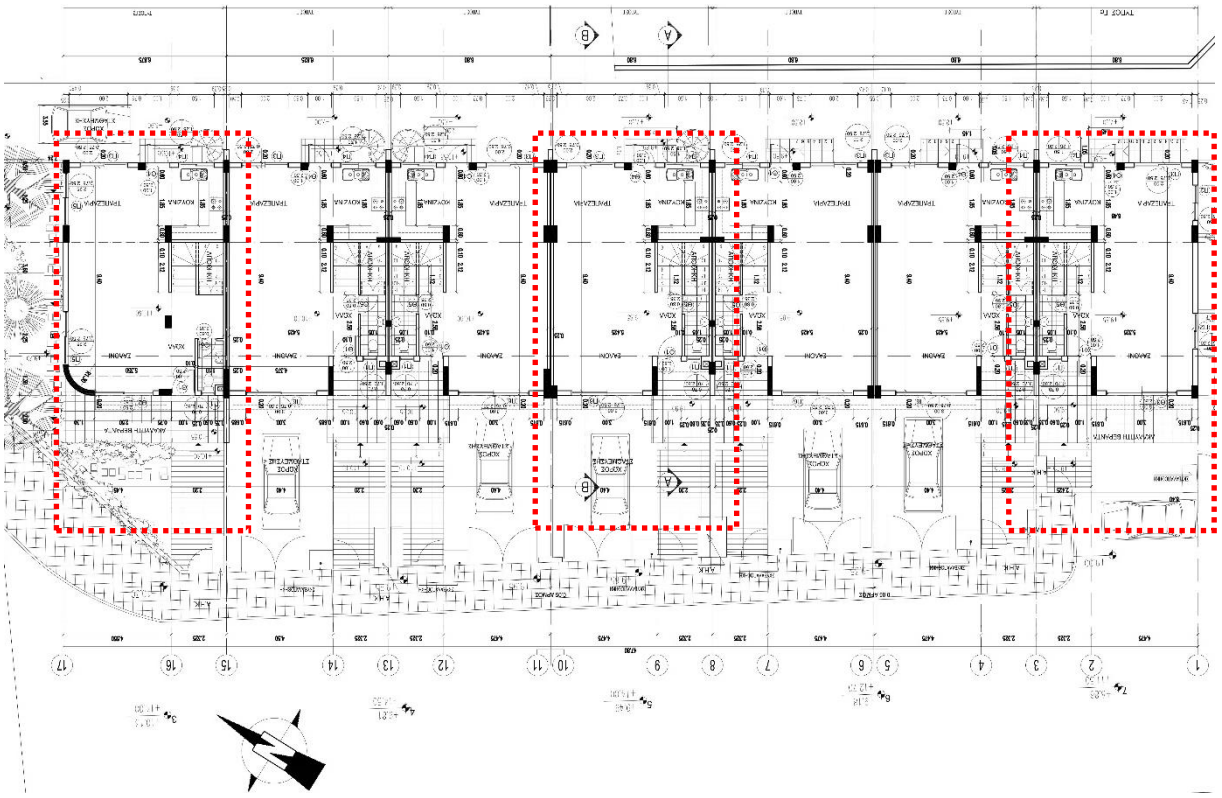

Fig .2. The Architectural plans TFH complex under study

The calculated Total Primary Energy Consumption for the TFH01 is 525.52kWh/(m^{2}a), 7kWh/(m^{2}a) of which are produced from Renewable Energy Sources (RES), the solar thermal panels on the roof for domestic hot water consumption. The total energy consumption for the TFH01 reaches the 248kWh/(m^{2}a), the energy consumption for heating is 90.22kWh/(m^{2}a), for cooling is 136.14kWh/(m^{2}a), for domestic hot water is 6.36kWh/(m^{2}a) and for lighting is 15.40kWh/(m2a), as shown in Fig. 3. The Carbon Dioxide emissions are calculated at 159.60kgCO_2/(m^{2}a). The Energy Performance Certificate (EPC) Categorization falls in class F.

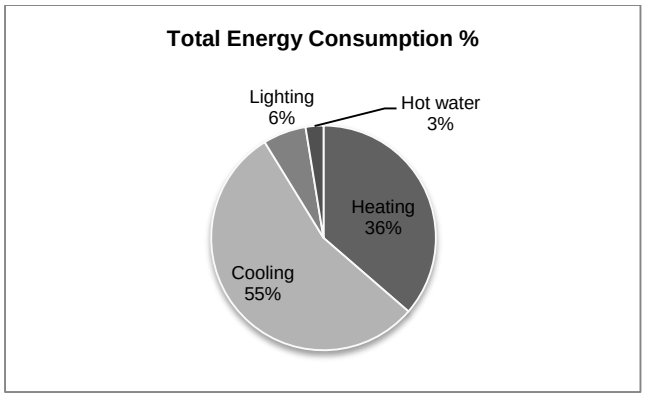

Fig .3. TFH01 Percentage of Total Energy Consumption

The second Family House (TFH02) is in the middle of the Terrace complex and has a North-East and South-West orientation, as shown on Fig. 2. The total heated living area is 110m2, whereas the heated living volume is 699.3m3. It is the smallest of the three Terrace houses under study.

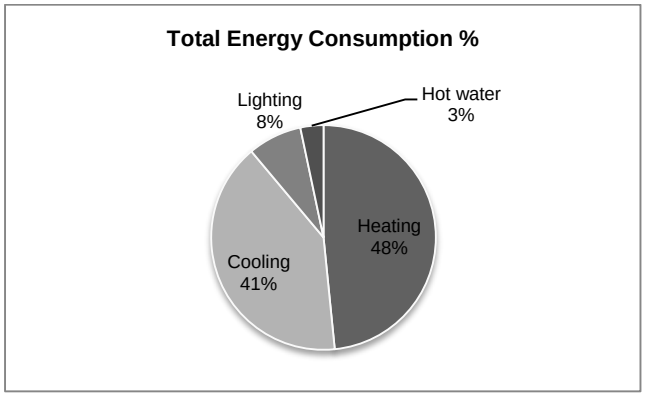

Fig .4. TFH02 Percentage of Total Energy Consumption

The calculated Total Primary Energy Consumption for the TFH02 is 404.42kWh/(m^{2}a), 7kWh/(m^{2}a) of which are produced from Renewable Energy Sources (RES), the solar thermal panels on the roof for domestic hot water consumption. The total energy consumption reaches the 210.31kWh/(m^{2}a), the energy consumption for heating is 102.14kWh/(m2a), for cooling is 85.45kWh/(m^{2}a), for domestic hot water is 7kWh/(m2a) and for lighting is 16.42kWh/(m^{2}a), as shown in Fig. 4. The Carbon Dioxide emissions are calculated at 113.06kgCO_2/(m^{2}a). Its Energy Performance Certificate (EPC) Categorization falls in class E. The third Family House (TFH03) is at the end of the Terrace complex and it has a northeast and northwest orientation. It has two large windows and a smaller one covering 14 m2 facing north, as shown on Fig. 2. The total heated living area is 118.5m2, the heated living volume is 746.55m3 and it is the largest of the three Terrace houses that are being studied in the research.

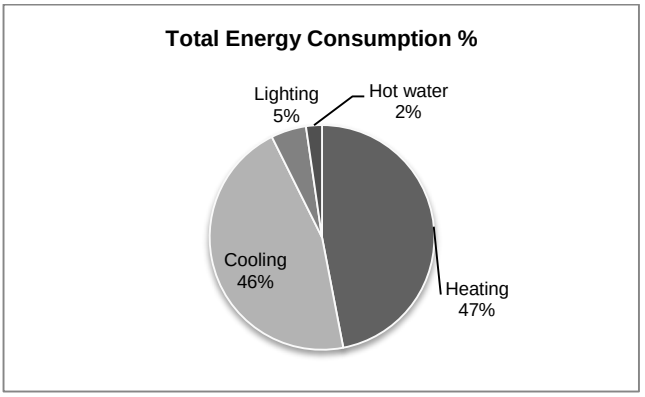

Fig .5. TFH03 Percentage of Total Energy Consumption

The calculated Total Primary Energy Consumption for the TFH03 is 601.16kWh/ (m^{2}a), 7kWh/ (m^{2}a) of which are produced from Renewable Energy Sources (RES), the solar thermal panels on the roof for domestic hot water consumption. The total final energy consumption for the TFH03 reaches 307.63kWh/(m^{2}a), from which the energy consumption for heating is 143.40kWh/(m^{2}a), for cooling is 139.43kWh/(m^{2}a), for domestic hot water is 9.31kWh/(m^{2}a) and for lighting is 15.49kWh/(m^{2}a) as shown in Fig. 5. The Carbon Dioxide emissions are calculated at 168.54kg CO_2/ (m^{2}a). The Energy Performance Certificate (EPC) Categorization falls in class F.

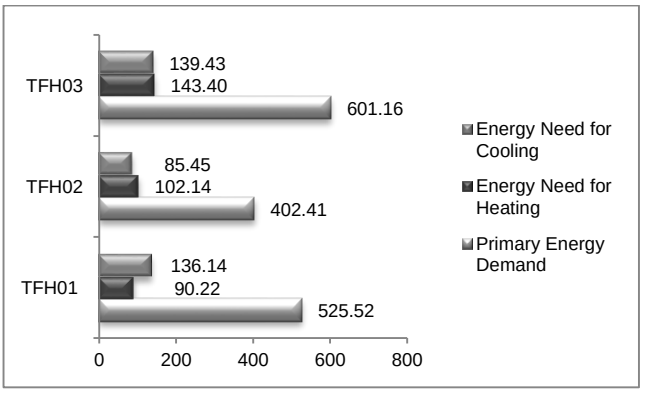

Fig .6. Comparing the Primary Energy Consumption, Energy need for heating and cooling for the existing TFH01, TFH02, TFH03

Through comparative studies of the above results and as indicated in Fig. 6, the energy needs of the third Terrace Family House (TFH03) are the highest followed by the first Terrace Family House (TFH01) and the second Terrace Family House (TFH02) with the lowest. All the three houses have the same

thermal characteristics and the same HVAC systems. Their only differentiating variables are their orientation, their different exposed surface areas, their heated living areas and their heated living volumes.

Comparing the results of the two end houses of the complex, TFH01 and TFH03, it is concluded that they fall under the same EPC category F; the TFH03 has a larger heating living area by 6.5m2 and therefore a higher primary energy consumption of 68.16kWh/(m2a), than TFH01. The difference of the primary energy consumption is also attributed to the different orientation of the two houses. More specifically, the TFH01 has windows and exposed surface area facing south, whereas the TFH03 has the same exposed surface area and larger windows facing north and, therefore it has a higher energy consumption for heating due to the lack of solar gains. The differences are accentuated when their heating consumption is compared. The TFH01 has a heating consumption of 90.22kWh/(m2a); whereas the heating consumption for the THF03 is 143.40kWh/(m2a).

Comparing their cooling consumption, the difference is not significant; the TFH01 has a cooling consumption of 136.14kWh/(m2a), which is lower than the 139.43kWh/(m2a) of the TFH03. The westward orientation causes slightly bigger overheating than the eastward orientation. The results indicate the significant role of the orientation in the buildings' design. In this case study, the TFH01 benefits from the southern sun during the winter and from the cooler breezes of the southwest during the summer, consequently it has an improved energy performance with less energy consumption all over the year. The second Terrace Family House TFH02, situated in the middle of the complex, has the lowest primary energy consumption and energy demand for cooling and heating. It is classified as (E), one class higher than the other two (F). Since it is located in the middle of the terrace complex, it benefits from the adjacent buildings, which act as a buffer on the left and right, and more specifically on the Southeast and the Northwest orientations. It also has less exposed surface area, and therefore fewer amounts of heat are lost from the building envelope.

B. Refurbishment Scenarios

As the energy consumption of a building is affected by its construction elements, alternative techniques must be used to create a comfortable indoor environment, which at the same time will achieve energy conservation [11,12,13,14]. Therefore, the retrofitting interventions are restricted on the building envelope, while the electromechanical systems for heating and cooling remained the same. Thus, a retrofitting scenario was developed using energy conservation measures (ECMs) that were based on the new requirements of the EPBD Directive [9] enforced on the beginning of 2014.

In order to meet the minimum requirements for the building envelope for EPBD Directive [9]; 30mm of thermal insulation (expanded polystyrene) is added externally on the walls, 50mm of thermal insulation (expanded polystyrene) is also installed internally on the horizontal ceiling and finally, the windows are replaced with new double glazed windows. After the retrofitting interventions, the new U-Values of the building envelopes of all the three Terrace Family Houses stay the same and are calculated as shown on Table 2.

Table 2 THERMAL CHARACTERISTICS OF THE BUILDING ENVELOPE FOR TFH

Construction Element	U-Value W/(m^{2}k)
Pitched roof with horizontal ceiling	0.60
External Walls	0.69
Floor in contact with the ground	0.91
Double glazed windows	3.23

Using these EMCs, the TFH01 has moved up two EPC categories from (F) to (D). The calculated total Primary Energy Consumption for the refurbishment scenario of TFH01 is now 319.36kWh/(m2a) which means a saving percentage of 39.23%. The total Delivered Energy Consumption is reduced to 149.08kWh/(m2a), from which the energy consumption of heating is 51.98kWh/(m2a), with savings up to 42.40% and of cooling is 75.36kWh/(m2a) with savings up to 44.60%. Lighting and domestic hot water consumption remained the same. The Carbon Dioxide emissions are calculated at 90.93kgCO_2/(m2a), presenting a reduction of 43%. After this refurbishment scenario, the dwelling has an average energy saving percentage up to 42.30% (as shown in figure 7).

The installation and construction cost for the refurbishment scenario for the first Terrace Family House (TFH01) was approximately €7,090 based on the current market values. The refurbishment

scenario for the TFH01 has a payback period of 2 years only. The operational cost savings reach €3,591 per year. The pay-back period was calculated using the official tool published by the Ministry of Energy, Commerce, Industry and Tourism of Cyprus for the cost optimal [10] EMCs.

Using the same EMCs, the TFH02 has also moved up two EPC categories from (E) to (C). The calculated total Primary Energy Consumption for the refurbishment scenario of TFH02 is now 212.17kWh/(m^2a) and this means a saving percentage of 47.50%. The total Delivered Energy consumption is reduced to 112.44kWh/(m^2a), from which the energy consumption for heating is 51.13kWh/(m2a), with savings up to 44% and as for cooling is 32.58kWh/(m2a) with savings up to 61.87%. Lighting and domestic hot water consumption remained the same.

The Carbon Dioxide emissions are calculated at 59.11kgCO_2/(m^2a), presenting a reduction of 47.72%. After the refurbishment scenario, the TFH02 has an average energy saving percentage of 50.27% (as shown in figure 7). The installation and construction cost for the refurbishment measures for the second Terrace Family House (TFH02) was approximately €6,665 based on the current market values. The refurbishment scenario for the TFH02 has a pay-back period of 2.5 years only. The operational cost savings reach €2,840 per year.

Finally, using the same EMCs the TFH03 has moved up two EPC categories from (F) to (D). The calculated total Primary Energy Consumption for the refurbishment scenario of TFH03 is now 212.17kWh/ (m^2a) and this means a saving percentage of 36.64%. The total Delivered Energy Consumption is reduced to 190.47kWh/ (m^2a), from which the energy consumption for heating is 83.38kWh/ (m^2a), and for cooling is 82.30kWh/ (m^2a) with savings of 41.85% and of 40.97% respectively. Lighting and domestic hot water consumption remained the same. The Carbon Dioxide emissions are calculated at 107.21kgCO_2/ (m^2a), presenting a reduction of 36.39%. After the refurbishment scenario, the TFH03 has an average energy savings percentage of 38.96% (as shown in figure 7).

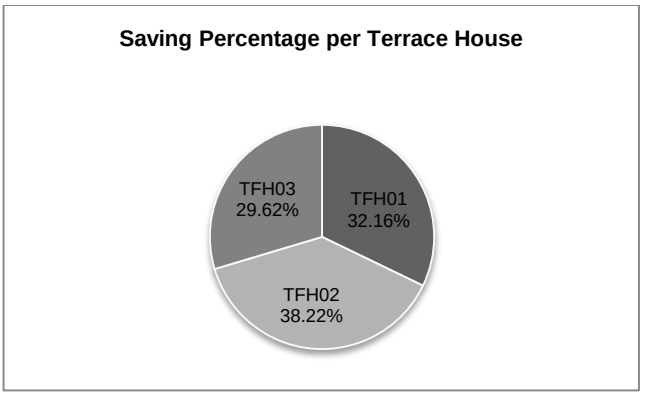

Fig .7. Average Saving Percentages for each Terrace House (TFH01, TFH02 and TFH03)

The installation and construction cost for the refurbishment measures for the third Terrace Family House was approximately €7,545 based on the current market values. The refurbishment scenario for the TFH03 has a payback period of 2 years only and the operational cost savings reach € 4,514 per year. As shown on Figure 8 the first Terrace Family House (TFH01) has a Primary Energy Consumption reduction of 39.23%, the second Terrace Family House (TFH02) has the highest percentage of Primary Energy Consumption reduction of 47.53% ; whereas the third Terrace Family House (TFH03) has the lowest reduction percentage of 36.60%. The operational cost as calculated by the national method of cost optimum is divided in fuel (oil/diesel) consumption and electricity consumption. Even though the payback period for all three dwellings was between 2-2,5 years, the TFH03 has the largest operational cost saving of €4,514.

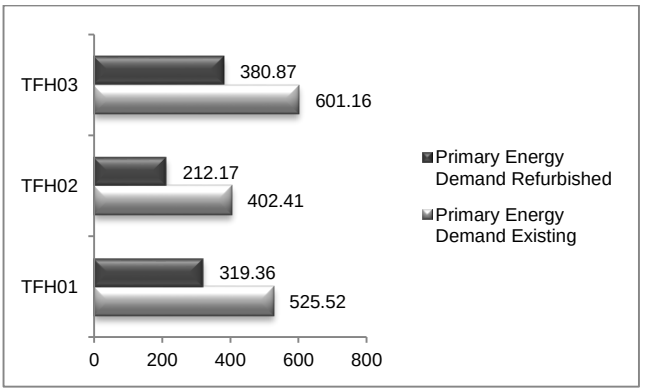

Fig .8. Calculated Primary Energy Consumption for the existing and the refurbishment for TFH01, TFH02 and TFH03

Although the TFH03 has the highest installation and construction cost amongst the buildings under study, it has the largest savings due to the reduction in litres

of oil consumed during the heating season. The TFH01 and TFH02 have larger savings on electricity consumption; yet electricity has a lower price per kWh. The TFH02 has the smallest operational cost savings of €2,839 due to the fact that it has a fewer calculated savings in both electricity and oil consumption. Furthermore, TFH02 was classified one category higher than the TFH01 and TFH03.There were fewer savings due to the fact that the same EMCs were applied on all three dwellings and the TFH02 initially had less energy consumption, so there was less to save [15].

IV. CONCLUSION

The study was performed in order to model the energy performance of a terrace family house typology complex. The scope was to compare the variance in energy consumption of similar units within the complex, which differ in terms of their orientation and their exposed facades areas. In this framework, an energy-retrofitting scenario was developed based on interventions on the building envelope of the dwellings to meet the minimum standards for the thermal envelope of the latest EPDB requirements. Indeed, the comparative studies of the energy consumption of the three terrace houses under study, prior the refurbishment interventions, show that the orientation of the surface areas of the units and their fenestration are determining factors for their energy consumption.

The results of the simulations, adopting retrofitting technics, indicate that the application of thermal insulation on the building envelope could have a significant impact on the buildings' performance. By introducing simple retrofitting interventions, such as 30mm of external thermal insulation on the walls, 50mm of thermal insulation on the roof and better double glazing of the end house of the Terrace complex, facing North East to South West, achieved a reduction of 39.23% in Primary Energy Consumption, 43% on CO_2 emissions, 42.4% for heating and 44.64% for cooling. With the same interventions, the middle unit of the building had a calculated decrease of 47.53% in Primary Energy Consumption, 47.72% on CO_2 emissions, 44% for heating and 61.87% for cooling. The application of the same energy conservation measures on the end unit of the Terrace complex facing northeast and northwest, had a calculated decrease of 36.60% in Primary Energy Consumption, 36.39% on CO_2 emissions, 41.85% for heating and 40.97% for cooling. The Energy Performance Certificate (EPC) category for the three Terrace Family Houses was raised by two classes; the First and the Third were upgraded from (F) to (D) category; whereas the second was upgraded to category (E) from (C). The payback period varies between 2 and 2,5 years; whereas the TFH03 has the largest operational cost savings, followed by the TFH02 and the TFH01 which have the lowest operational cost saving.

The calculated savings vary from one dwelling to another. This is directly related to the existing energy consumption, which is a result of the thermal capacity of the building envelope, the heating area, the electromechanical systems as well as the location and orientation of each dwelling. Since the dwellings have the same thermal characteristics and thermal capacity of the building envelope, heating area and electromechanical systems, it is concluded that the location within the terrace complex and the orientation of each dwelling exert high impact on the savings of their energy consumption. It is therefore imperative to take these aspects into consideration at the design and setting stages of the buildings. Furthermore, the poor energy performance of the existing national residential building stock, especially those dwellings that were built before the enforcement of the European Directives, is evident. The urgency for immediate actions and simple retrofitting guidelines to improve the performance of the buildings' envelope and their energy consumption is confirmed.

REFERENCES

[1] NATO Science Series (2005) Thermal Energy Storage for Sustainable Energy Fundamentals, Case Studies and Design. Volume 234 pp. Preface ix.

[2] Meijer, F. Itard, L. Sunikka-Blank, M. (2009) Comparing European Residential Building Stocks: Performance Renovation. Building Research & Information pp. 533-551.

[3] Ilaria Ballarini, Vincenzo Corrado (2009) Application of Energy Rating Methods to the Existing Building Stock: Analysis of Some Residential Buildings in Turin. pp. 790 – 800.

[4] Konstantinou, T., Knaack, U. (2013) An Approach to Integrate Energy Efficiency Upgrade into Refurbishment Design Process,

Applied in Two Case Study Buildings in Northern European Climate. Energy and Buildings 59, pp.301-309.

[5] Konstantinou, T., Knaack, U. (2011) Refurbishment of Residential Buildings: A Design Approach to Energy-Efficiency Upgrades. Procedia Engineering 21, pp. 666 – 675.

[6] IEE EPISCOPE Project: http://episcope.eu/index.php?id=97

[7] Typology of the Building Stock in Cyprus published (May 2012). Statistical Service of Cyprus.

[8] http://www.mcit.gov.cy/mcit/mcit.nsf/dmlperformance_gr/dmlperformance_gr? (Accessed 20 November 2014) OpenDocument

[9] Directive2002/91/EC:http://eur-lex.europa.eu/legacontent/EN/TXT/?uri=CELEX:32002L0091

[10] Costoptimaltool:http://www.mcit.gov.cy/mcit/mcit.nsf/All/E074577C58AD9EFCC22575B60047BEA8? OpenDocument.

[11] DK Serghides, MC Katafygiotou (2013). The Role of Materials in the Energy Efficient Retrofitting of Traditional Buildings. Materials and Processes for Energy: Communicating Current Research and Technological Developments pp. 978-84.

[12] Katafygiotou, M. C., & Serghides, D. K. (2014). Analysis of Structural Elements and Energy Consumption of School Building Stock in Cyprus: Energy Simulations and Upgrade Scenarios of a Typical School. Energy and Buildings, 72, 8-16.

[13] Serghides D.K., Georgakis C., (2012). The Building Envelope of Mediterranean Houses – Optimisation of Mass and Insulation. Journal of Building Physics, Volume 36 No1, ISSN: 1744-2591. Pp.83-98.

[14] Serghides, D. et al (2014). Energy Efficient Refurbishment of Existing Buildings: A Multiple Case Study of Terraced Family Housing. World Renewable Energy Congress 12- WREC XIII Aug. 2014 p.23.

[15] Serghides D.K., (2009). Optimisation of Insulation on Mediterranean Houses. ICPSR Journal: ISESCO Science and Technology Vision, Volume 5, Issue n° 8- Novembre 2009. Pp.79-83.

SUSTAINABLE MANAGEMENT OF CLIMATE CHANGE: THE CASE OF THE MIDDLE EAST AND NORTH AFRICA REGION

ADEL M. AL TAWEEL[1*], V. ISMET UGURSAL[1] AND DONNIE BOODLAL[2]
[1] Dalhousie University, Halifax NS, CANADA
[2] The University of Trinidad and Tobago, Point Lisas Campus, Trinidad and Tobago WI,
[*] Corresponding author: al.taweel@dal.ca

Abstract - Climate change is one of the major environmental challenges facing the world. Particularly vulnerable are arid and low-laying coastal areas, conditions that prevail through most of the Middle East and North Africa [MENA]. This region is an economically diverse one, including both the oil-rich economies in the Gulf and countries that are resource-scarce in relation to their population. However, with about 23 percent of MENA's population living on less than $2 a day, it is imperative that the climate change management strategies adopted be cost-effective and emphasize economic, social and human development while addressing the concerns arising from anthropogenic climate change.

Over the past decades several national and international mechanisms were developed in an attempt to reduce the emissions considered to be mainly responsible for climate change, and to assist in coping with the adverse effects that are beginning to occur as a result of climate change. Unfortunately, many of these approaches are presently associated with economic penalties that often adversely affect the socio-economic welfare of the populace, particularly in low-, and medium-income countries. In this regard, it is informative to note the experience recently gained by Trinidad and Tobago [T&T] in its attempt to reduce GHG emissions without affecting the competitiveness of the industrial and agricultural sectors. Using appropriate decision making tools and a policy environment based on a combination of regulations and incentives, the environmental challenges can be turned into a vehicle for sustainable development.

This paper discusses the factors that need to be considered while developing a sustainable climate change management approach for the MENA region and develops some recommendations that may be essential for achieving the desired climate change mitigation/adaptation actions while minimizing social disruption.Greenhouse gas emissions

Keywords - Climate change, MENA region, Global and regional energy production/consumption trends, Energy and wealth, Need for adaptation, Managing GHG emissions, Sustainable development, Building local capacity.

Nomenclature –

CEBC	Clean Energy Business Council of the Middle East and North Africa
CER	Certified Emission Reductions
CNG	Compressed natural gas
EU	European Union
GCC	Gulf cooperation council
GDP	Gross national product
GNI	Gross National Income
HDI	Human development index
LED	Low emission strategies
LNG	Liquefied natural gas
MAPS	Mitigation Action Plans and Scenarios
PCGDPI	Per Capita Gross GDP
PPP	Purchasing power parity
tpa	Tonne per annum
T&T	Trinidad and Tobago
UN	United Nations

I. INTRODUCTION

Energy is one of the key commodities required to sustain human existence and advancement and is one of the largest components of the world economy. Consequently, global energy consumption has been rapidly increasing over the past two centuries but the pace of change has recently accelerated due to the increase in the total world's population and the rapid improvement in the standard of living in a large segment of the world's populace. However, the negative environmental aspects associated with the increasing consumption of energy necessitate that such trends be properly managed for the overall benefits of humanity (Brundtland et al. 2010). Climate change is a multi-faceted problem that requires the numerous stakeholders to contribute knowledge, skills and energy to plan for the impacts of a warmer planet and to take action to mitigate rising GHG

emissions. Such actions must however be based on meeting the socio-economic challenges faced in any particular country/region yet help in achieving the overall objectives of protecting the global environment.

Nowhere are the climate change and sustainability issues more acute than in the MENA countries which are likely to be severely affected by climate change. The predicted rise in temperature and sea level may affect coastal areas, while the current severe water stress is likely to be exacerbated (Cherfane 2010, Ghaddar 2010). Water supply sources in MENA – two-thirds of which originate outside the region— are being stretched to their limits threatening to lead to national confrontations over this vital resource. Adapting to climate change is not a new phenomenon for the NEMA region. For thousands of years, the people in this region have coped with the challenges of climate variability by adapting their survival strategies to changes in rainfall and temperature. But over the next century global climatic variability is predicted to increase, and NEMA countries may experience unprecedented extremes in climate (World Bank MENA Region, 2007).

This paper discusses the factors that need to be considered while developing a sustainable climate change management approach for the MENA region. Some of the recommendations developed in this paper may be essential for achieving the desired climate change mitigation/adaptation actions while minimizing social disruption particularly in low-income countries.

II. THE IMPACT OF ENERGY PRODUCTION AND UTILIZATION ON THE SOCIO-ECONOMIC CONDITIONS IN MENA COUNTRIES

The evolution of population, prosperity, and energy consumption has been substantially different in different parts of the world, resulting in large disparities amongst nations and regions in terms of wealth and the state of human development. This is particularly evident in the Middle East and North Africa, a region which includes both the energy-rich economies in the Gulf as well as countries that are amongst the poorest in the world. Figure 1 clearly illustrates this phenomenon where the 22 MENA countries considered in this investigation (Algeria, Bahrain, Egypt, Eritrea, Iraq, Israel, Jordan, Kuwait, Lebanon, Libya, Mauritania, Morocco, Oman, Palestine, Qatar, Saudi Arabia, Somalia, Sudan, Syria, Tunisia, UAE, Yemen) were organized in ascending order in accordance with their economic wealth using the World Bank data for the annual per capita gross domestic product (PCGDP). Although the cost of living variation between the different countries is already taken into consideration through the purchasing power parity [PPP] factor, the value of the per capita GDP was found to vary between these countries by a factor of up to about 150, thus creating a very difficult situation in which it is virtually impossible to develop a singular strategy that meets the needs of the whole region. Conversely, the presence of countries depicting a wide spectrum of developmental stages can create an opportunity for complementary/synergistic action that can benefit the population of both the wealthy and poor countries. Appropriate strategies and frameworks are however needed in order to achieve such goals.

The discrepancy between the various countries in the MENA region becomes less sever when one utilizes more comprehensive indicators of the socio-economic development stage for any particular country. The Human Development Index [HDI] used in Figure 2 is a composite indicator introduced by the UN in 1990 and provides a better measure of the socio-economic state of development of the populace by combining three basic dimensions: life expectancy, educational attainment (through literacy index and registration combined index) and economic performance (through per capita PPP GNI in international dollars) (UNDP, 2010). The use of this more appropriate indicator reduced the inter-country discrepancy within the MENA region to about 3-fold.

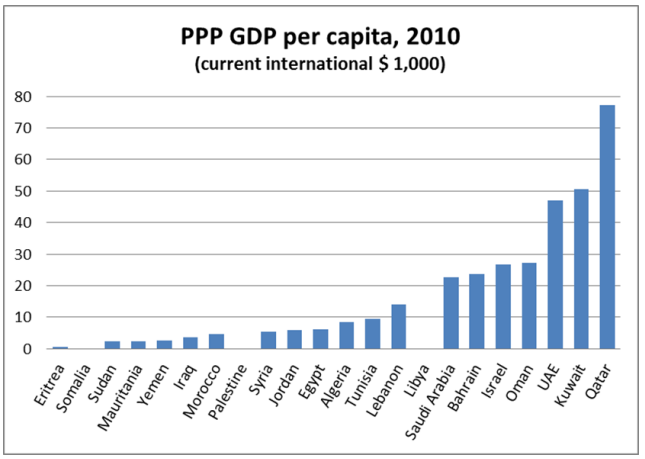

Fig .1. – Intra-region variation of the Per capita GDP

(Source of data: World Bank Databank, PPP 2011)

However, it is worthwhile to note that whereas only three countries in the region have achieved a high stage of human development (HDI ≥ 0.8), five countries can be considered as still being in a low stage of human development (HDI < 0.5), with the remaining 14 countries being in the moderate stage of human development (0.5 ≤ HDI < 0.8).

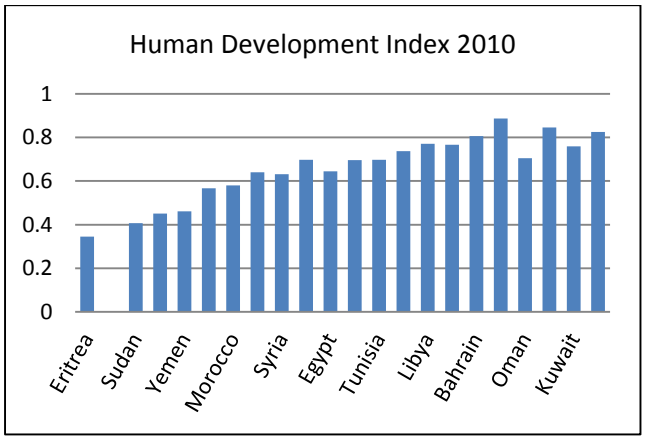

Fig .2. – Regional Variation in the Human Development Index (2011) The scale used for labeling the countries in Fig. 2 resulted in half of the countries being omitted in the formatted version

A significant part of the GDP generated by prosperous MENA countries can be attributed to the production and utilization of non-renewable energy resources (energy-related revenues can be as high as 55% of the GDP for countries that are primarily oil exporters). Two-thirds of the Organization of Petroleum Exporting Countries (OPEC) are thus located in the MENA region, which has 57% of the world's proven conventional oil reserves and 41% of proven conventional natural gas resources. These reserves generated an estimated US$ 785 billion in revenues in 2011 (Fattouh and El-Katiri, 2012) and sovereign investment funds are being increasingly considered as means for ensuring the prosperity of future generations in countries presently endowed with large non-renewable natural resources.

The importance to the energy sector in determining the state of prosperity in MENA countries becomes very clear when one considers the per capita level of GHG emissions and its variation amongst the different countries of the region (Figure 3). With the exception of Israel, the most prosperous MENA countries are those with abundant energy resources and energy-based industries (e.g. the processing of petroleum and natural gas as well as petrochemicals).However, the activities associated with the extraction, processing and export of the oil and gas resources, and the rapidly-expanding energy-based industrial sector, are large GHG emitters. Continued development of these energy resources along historic lines is therefore expected to result in exasperating the level of GHG emissions unless certain measures are taken to reduce the overall environmental impact of such development. On the other hand, any viable GHG emission reduction strategy will have to consider the fact that the near-term demand for fossil fuels is predicted to increase as a result of the increase in the world's population, and the increased per capita demand particularly in the rapidly expanding economies such as China, India, and Indonesia. Policies and procedures aimed at implementing cleaner energy extraction/production/utilization are therefore urgently needed, particularly in the wealthy energy-rich countries. Such measures can strongly reduce the environmental impacts of present and future development of energy resources in the region.

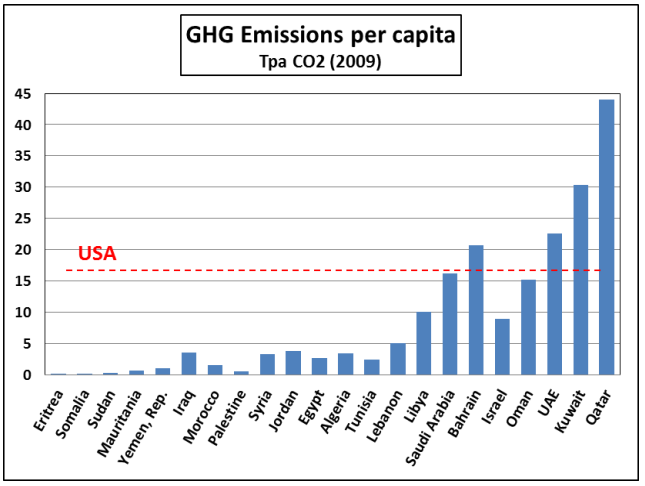

Fig .3. – Regional variation in GHG emissions (Source of data: World Bank Databank)

Previous studies confirmed the existence of strong correlation between the wealth of the citizens of a country and their energy consumption pattern (Sütterlin 2012, Floyd 2012, Estiri et al. 2013), a situation that applies to all countries regardless of their state of human development. Prosperous and developed countries thus have a high level of energy consumption that is used for the production of goods and services, to support the transport and telecommunications sectors, and to achieve a high level of comfort for the citizens. A large part of their

energy demand is presently supplied (directly and indirectly) by fossil fuels whereas a significant part of the energy demand in low-income countries is supplied by traditional biomass (wood and charcoal). Unfortunately, The increasing use of biomass for energy purposes in middle and low-income MENA countries is one of the major forces driving the desertification process and is driven by the local availability of relatively inexpensive biomass in a world where the price of fossil fuels is relatively high.

As shown in Figure 3, the same qualitative relationship exists in the MENA region. The average fossil fuel energy consumption in the major oil and gas producers (Bahrain, Iraq, Libya, Qatar, Saudi Arabia, and UAE) are more than 300-fold higher than that in the low-income countries in the region. Unfortunately, these emission levels are also many-fold higher than the present day world-average emission levels (4.6 tpa CO_2 Equivalent) as well as the emission levels in developed countries that are strongly dependent on the exploitation of natural resources (Canada = 15.2 tpa CO_2 equivalent; Australia = 18.2 tpa CO_2 equivalent). Amongst the factors contributing to this state of affairs are: the heavy dependence of affluent MENA countries on energy-intensive industries, the export of raw materials with limited local value-added (e.g. crude oil and LNG), and the limited contribution of the agricultural and service sectors to the overall prosperity of the citizens. Concerted efforts have been ongoing to change this situation, but is recommended that special attention be given to the use of low-emission-development routes (e.g. energy efficiency and waste minimization) in order to ensure that the increase in the level of local value added does not result in further exasperating the environmental problems.

The heavy dependence of a country's prosperity and the level of energy resource utilization is reflected in the essentially linear relationship between the per capita GDP and the level of GHG emissions in MENA countries (Figure 4). This is mainly caused by the heavy dependence of affluent MENA countries on energy-intensive industries, the export of raw materials with limited value-added processing, and the limited contribution of the agricultural and service sectors to the welfare of the citizens.

III. ENERGY CONSUMPTION, POWER GENERATION AND THE STANDARD OF LIVING

Accepting that most countries do not want to suffer a reduction in their prosperity level while attempting to address the climate change challenge, the question becomes how the level of

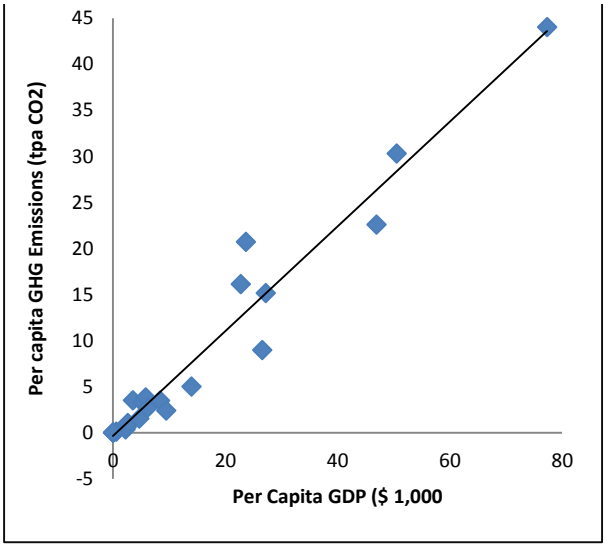

Fig .4. The relationship between PCGDP and the GHG emissions level (Source of data: World Bank Databank, MENA region)

GHG emissions can be reduced while maintaining the prosperity at its present level or even higher. An indication the efficiency by which energy is utilized to generate wealth can be obtained by calculating the amount of GHG emissions associated with every $ 1,000 PPP GDP produced. This indicator which is frequently used for benchmarking purposes is based on the fact that most of the world's large consumers of energy still rely heavily on fossil fuel for power generation. The large intra-regional variation in the energy use per unit GDP is clearly evident from the results depicted in Figure 5.

An in-depth investigation of the factors contributing to this phenomenon (e.g. internal strife, the contribution of the service sector, the emphasis on high-value added production, the role of the agricultural sector, the role of hydro power) is needed to develop better understanding of the factors hindering the accelerated development of this region as a whole, and to identify novel means by which the prosperity of the region can be enhanced. It is however noteworthy that the prosperous MENA countries are about 3-7 fold less efficient in converting their energy resources into national wealth than it is the case in the USA and EU (Figure 6). Thus, whereas the generation of a $1,000

of GDP in the former group is associated with the emission of 700-1000 kg of CO2 equ., the same is achieved while emitting 100-180 kg of CO2 equ. in more developed societies. This suggests that there is a substantial potential for improving the efficiency by which energy resources are converted into revenue-generating economic activities in the prosperous, hydrocarbon-rich MENA countries. On the other hand, the high energy utilization efficiencies exhibited by the poorest three MENA countries are not indicative of high energy utilization efficiencies but are typical of their developmental stage (HDI < 0.5) where energy (fossil fuels in particular) plays a less significant role in determining the GDP. The very low energy utilization efficiency observed in the case of Iraq in 2009 could most probably be attributed to the internal strife in the country and its negative impact on the GDP. In that regard, it is important to note that although China has been rapidly increasing its power generation capacity to cope with the escalating demand, it has been able to achieve a remarkable increase in the energy use efficiency of energy utilization over the past 30 years. This is largely due to the use of better manufacturing technologies and the gradual shift towards the production of high-value added products and services.

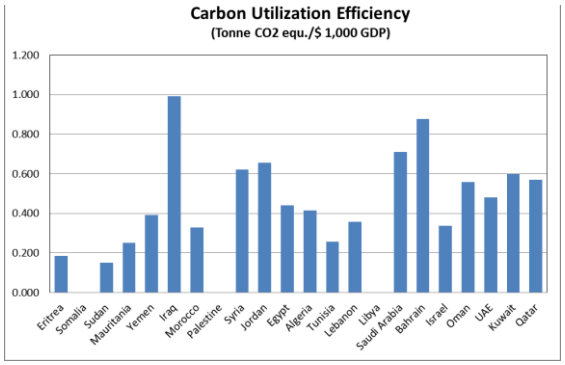

Fig .5. Regional variation in energy utilization efficiency

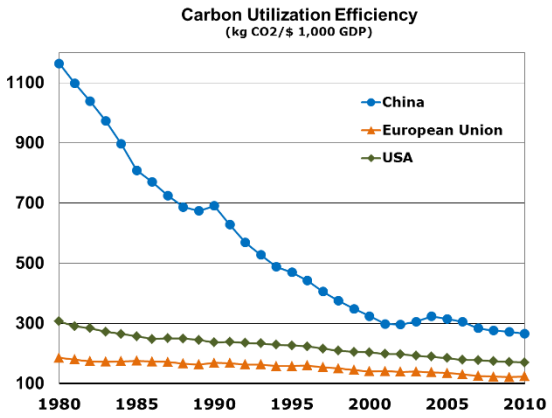

Fig .6. Evolution of energy use per unit of GDP (Source of data: World Bank Databank)

IV. ENERGY CONSUMPTION, POWER GENERATION AND THE STANDARD OF LIVING

In order to develop sustainable MENA-focused strategies for coping with the problem of climate change it is important that, in a fashion similar to other rapidly-developing regions of the world, the MENA region assumes its responsibility with respect to reducing its GHG emissions while undertaking unquestionably necessary adaptation projects (Verner, 2012). In the meantime, it should also attempt to achieve two important socioeconomic objectives:

- Avoid socially disruptive situations by reducing the large discrepancy in prosperity levels of the citizens within the MENA region.

- Address the need for securing long-term prosperity for the citizens of the countries whose present prosperity levels depend on exhaustible non-renewable energy resources.

The question is how these apparently contradictory demands can concurrently be met particularly by governments that have limited funds and need to spend them in a fashion that addresses urgently needed socio-economic challenges while trying to reduce emissions?. Considering the fact that about 23% of the population in MENA lives below the poverty level of less than $2 a day, a concerted effort aimed at improving the standard of living in the region as a whole is desperately needed if social turmoil is to be minimized. It is however imperative that the strategies adopted emphasize economic, social and human development objectives while addressing the concerns arising from climate change. However, the financial and human resources needed for such an effort can be limiting factors considering the multi-faceted needs in the region in a period of budgetary constraints throughout much of the world.

In a recent study based on data from 112 countries (Ugursal, 2013), it was noted that the relationship between the HDI and energy consumption depends very much on the country's developmental stage (Figure 7). Thus, for example, a substantial increase in the per capita energy consumption is needed before any significant improvement can be noted in the human development level can be noted for countries with HDI < 0.5. On the other hand,

significant reductions in the energy consumption levels can be achieved without substantial reduction in the standard of living in countries with HDI ≥ 0.8; while, small increases in energy consumption result in substantial increases in the HDI of countries within the moderate HDI range (0.5-0.8).

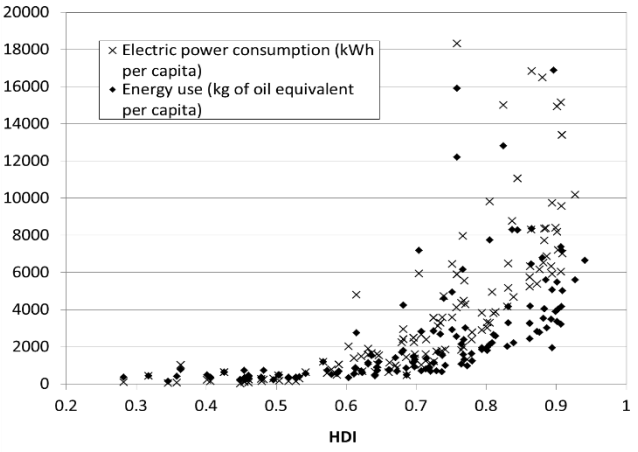

Fig .7. Relationship between a country's HDI and its per capita energy consumption rate (Ugursal, 2013).

It is therefore projected that substantial investment in power generation and utilization will be needed in most of the 19 countries having HDI less than 0.8. Such a massive undertaking will adversely affect climate change with the impact being mitigated if low emission development [LED] strategies are adopted in the new projects and measures for improving the efficiency of existing operations are adopted (Clapp et al., 2010). Considering the fact that the population of the region is in excess of 330 million with an average per-capita GHG emission of 5.85 tpa CO2 equivalent per year, the full impact of unplanned development is equivalent to adding a GHG emitter that is equivalent to 2/3 that of the USA (until recently, the world's largest emitter).

Innovative means for the planning, financing, execution, and managing of such a major undertaking are therefore needed in order to avoid the adverse impact of combined social, economic, and environmental upheavals. The concept of "Sustainable Development" with its emphasis on balancing the needs of the society with those of the environment in an economically viable fashion represents one of the most promising avenues for achieving the aforementioned balanced objectives. However, the challenge of managing this global problem in a sustainable fashion is quite daunting particularly considering the conflicting interests of the various regions and countries, particularly those at radically different stages of development.

The increase in GHG emissions associated with the accelerated development of low-, and medium-income MENA countries can be partially compensated by improving the environmental efficiency of the enormous oil and gas sector operating in various MENA countries. Many such countries (e.g. Algeria, Egypt, Iraq, Kuwait, Libya, Oman, Qatar, Saudi Arabia, and UAE) have very large oil and gas operations, a situation that offers the opportunity for achieving significant reductions in GHG emissions at little, or even negative, costs. A review of the GHG mitigation efforts in most of the MENA countries was recently given by Abdel Gelil (2009). Once identified, the private sector may be interested in profitable emission reduction schemes but some additional incentives may be needed for high-risk border line cases. Typical examples are:

- Reducing the wasteful release of undesired energy by-products (e.g. flares).
- Replacing high-carbon fuels with low-cost low-emission alternatives.
- Enhancing the efficiency of power generation plants and power transmission systems,
- Enhancing the efficiency of energy utilization in large industrial operations, and
- Identifying opportunities for reusing some of the CO2 captured in the many petrochemical plants present in the region for enhancing oil recovery in nearby fields.

It is hard to overemphasize the importance of energy efficiency as an economically-viable tool for mitigating GHG emissions. The experience in many European countries, combined with the recent financial crunch, resulted in the recent adoption by the EU of "Directive 2012/27/EU" on energy efficiency. This Directive establishes a common framework of the promotion of energy efficiency within the EU in order to ensure the achievement of its 2020 target on energy efficiency, and to pave the way for further energy efficiency improvements beyond that date. It also lays down rules designed to remove barriers in the energy market and overcome market failures that impede

efficiency in the supply and use of energy, and provides for the establishment of indicative national energy efficiency targets for 2020 Marginal MENA cases may be eligible for financial support through various international programs, such as the Clean Development Mechanism [CDM] program and the Global Environment Facility fund. It is however imperative that such border-line project meet the sustainability criteria and urgently addresses the socio-economic needs of the population.

The potential for significantly reducing GHG emissions at little or no cost is not a situation that is unique to MENA and was identified to exist in several countries. For example, it is estimated that a significant reduction in Australian GHG emissions can be achieved (30% below 1999 levels by 2020) can be achieved without major technological breakthroughs or lifestyle changes. These reductions can be achieved by using existing approaches and by deploying mature or rapidly developing technologies to improve the carbon efficiency of the Australian economy (Gomer and Lewis, 2008) It is, however, essential to redress the imbalance presently existing in the various methodologies used to estimate GHG emissions. For example, equitable mechanisms may have to be developed by which the GHG emissions associated with the production, export, and transport of natural gas (10-12% of the carbon content in the case of LNG) can be split between the exporting counties and those which use it to replace coal in power generating plants.

V. AN EXAMPLE OF A SUSTAINABLE CLIMATE CHANGE MITIGATION EFFORT

Over the past few years, several national and international mechanisms were developed in an attempt to reduce GHG emissions and to assist in coping with the adverse effects that are beginning to occur as a result of climate change. Unfortunately, many of these approaches are presently associated with economic penalties that often adversely affect the socio-economic welfare of the populace particularly in low-, and medium-income countries. In this regard, it is informative to note the experience recently gained by Trinidad and Tobago [T&T] in its attempt to reduce GHG emissions without affecting the competitiveness of its industrial and agricultural sectors.

Although the GHG emissions of Trinidad and Tobago are not very large when compared to larger countries (estimated at 53 M tonne CO2 Equivalent per year in), it is one of the world's largest GHG emitters per capita (40 tpa CO2 Equivalent in 2009). Initial attempts were made to meet its international obligations, focused on policies/measures similar to those used in developed economies (energy efficient cars, replacing incandescent bulbs etc.). However, a recent inventory of the sources of GHG emissions clearly showed the inability of such simple measures to achieve substantial reductions in GHG emissions (Figure 8), since more than 80% of the GHG emissions are generated by industrial activities.

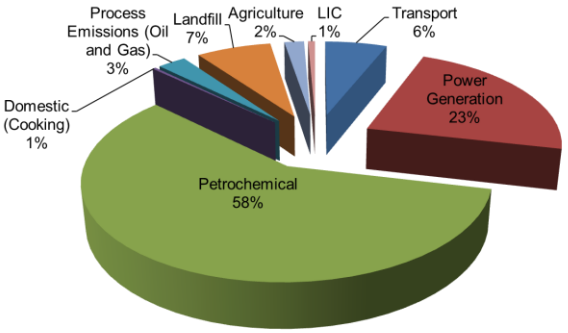

Fig .8. Sources of GHG emissions in T&T, 2010 (adapted from Boodlal and Al Taweel, 2013)

Conventional environmental management concepts were applied to identify means by which GHG emissions can be reduced without significantly affecting the value of the welfare of the country (Figure 9). Based on the results of an inventory of GHG emissions in T&T, and the costs associated with each GHG reduction option, an indigenous action plan was proposed (Boodlal and Al Taweel, 2013) which includes identification of the optimal carbon reduction opportunities in the country (Figure 10).

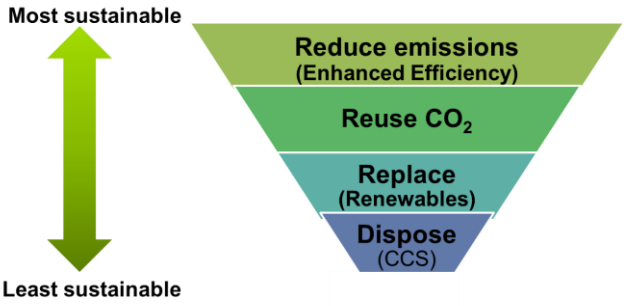

Fig . 9. Identifying the most sustainable GHG reduction strategies

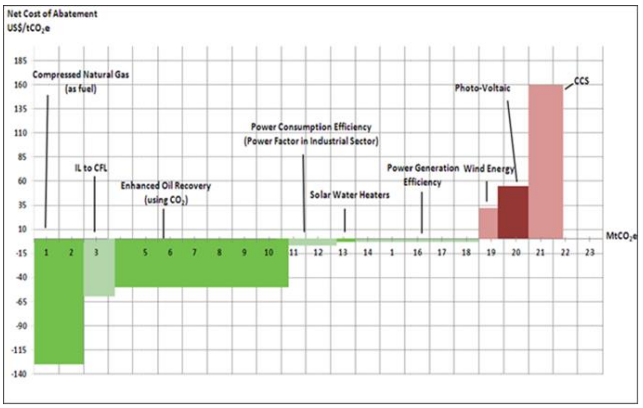

Fig . 10. Cost associated with the various options for reducing GHG emissions in T&T (adapted from Boodlal and Al Taweel, 2013)

Very conservative cost estimates were used in this study since its primary purpose is to serve as a policy development tool rather than for profitability analysis; yet several negative-cost opportunities were identified (Figure 10). This suggests that the implementation of such measures will be beneficial for the country's economy while, simultaneously, reducing its GHG emissions. A policy environment based on a combination of regulations and incentives was also recommended to attract investment to cost-effective emission reduction measures. In this way, environmental challenges can be turned into economic opportunities and a vehicle for sustainable development. To achieve this goal it is, however, necessary to use appropriate decision-making tools and adopt innovative site-specific solutions that take into consideration the socio-economic welfare of the disadvantaged segment of the population.

The most financially attractive option for reducing GHG emission in T&T is the replacement of liquid fuels (diesel and gasoline) by compressed or liquefied natural gas. For the past several decades, diesel and gasoline have been heavily subsidized in T&T in order to facilitate the transport of individuals and goods, particularly for the low-income citizens. The price of liquid fuels has been fixed for many years at the fixed prices of: TT$ 1.50/liter of diesel, TT$ 2.60/liter of regular gasoline, and TT$ 4.20/liter of premium gasoline (6.5 TT$ = 1 US$). In addition to encouraging energy-wasteful behaviour, the annual subsidy for these fuels was about US$ 500 per person with large quantities of the subsidized diesel fuel being illegally exported. Significant savings can therefore be achieved by converting cars and trucks so that they can use natural gas instead of the afore-mentioned liquid fuels. In addition to the financial benefits accrued by such conversions, the air quality is expected to improve as a result of using the clean-burning fuel and the GHG emissions are lower than those achieved when using the conventional heavier fuels.

The need for promoting such a conversion has been recognized many years before and both CNG and LNG are easily available as a by-product of the existing LNG production facility (used to export 58% of all the natural gas produced in T&T). However, the progress achieved on that front has been slow because of the lack of a concerted effort to promote such conversion and the limited number of re-fueling stations equipped to handle CNG.
Following the drop in the price of natural gas and its impact on the country's royalties, this issue is being more seriously addressed. The price of premium gasoline was recently raised to TT$ 5.75 and a plan for increasing the number of stations equipped to handle CNG is being implemented. A growing number of public transport buses are being converted to CNG while the Environmental Management Authority has launched a programme to convert its vehicle fleet to CNG.

This approach is not a novel one since natural gas is a commonly used alternative fuel used by trucks and transit bus fleet operators interested in reducing the cost and environmental impact of their operations. Many factory-built natural gas vehicles are available, which incorporate engine technologies that have been designed specifically for natural gas with power, torque, and fuel efficiency similar to diesel engines. Warranty coverage is also comparable to what is available on diesel engines.

Natural gas presently powers more than 15 million vehicles around the world and the number of natural gas fueled vehicles has been increasing by more than 15% a year over the past decade (NGV Global, 2012). There are more than 20,000 refueling stations in use globally, with the majority of these stations dispensing CNG, although LNG projects have been announced in several countries for both on-road truck and marine use. The trend of using CNG/LNG to power vehicles is expected to grow as the price differential between natural gas and liquid fuels increases as a result of the abundant availability of natural gas in the market place (Figure 11).
The development of a cost-effective natural-gas

based alternate to LPG (Liquefied Petroleum Gases that are extensively used in the region for cooking and heating purposes) could similarly benefit NEMA countries that are heavily dependent on the use of this type of fuel for domestic purposes.

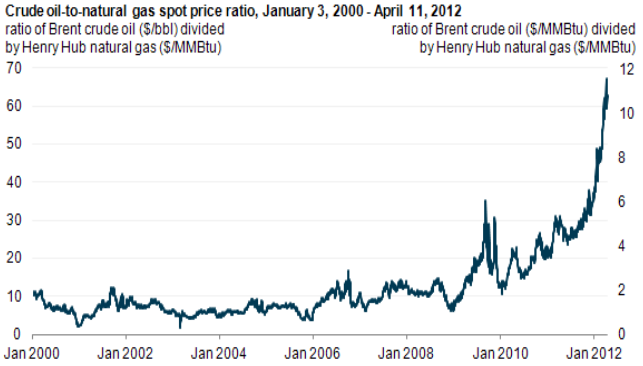

Fig . 11. Price ratio of crude oil to natural gas (U.S. Energy Information Administration)

VI. BALANCING CLIMATE CHANGE ABATEMENT MEASURES AGAINST DEVELOPMENTAL NEEDS

Global climate change is projected to result in a set of diverse and regionally-specific impacts on natural ecosystems and human societies. A growing literature suggests that while mitigation strategies are necessary, those alone are unlikely to be sufficient to cope with these changes. Therefore, pursuing a complementary strategy of enabling countries to adapt to global change and negate many of the expected adverse impacts is equally, if not more, urgent (Burton et al., 2002; Verner, 2012). However, with about 23% of MENA's population living on less than $2 a day, it is imperative that the climate change management strategies adopted be cost-effective and emphasize economic, social and human development, while addressing the environmental concerns arising from anthropogenic climate change.

Poverty alleviation is often linked to economic development resulting in job creation, increased energy production and consumption, GDP growth, energy security, and reducing all of inequality, which usually translates into increased emissions levels. Policy makers in low-income countries are therefore faced with the dilemma of having to allocate limited resources in an attempt to alleviate poverty while, at the same time, try to slow down GHG emissions. The need for integrating the environment in development planning has been strongly promoted for many years (Tolba M. K., 2008) and it may be now necessary to emphasize the need for integrating development into environmental planning particularly for low- and middle-income countries Over the past few years, several tools have been developed to facilitate rational decision making and achieving a balance between development needs and protecting the environment. (e.g. Low-Emission Development Strategies [LEDS], and Mitigation Action Plans and Scenarios [MAPS]). A detailed discussion of these tools is beyond the scope of this investigation but a quick introduction to their recent application to developing countries was given by Clapp et al. (2010) and Boyd (2013).

Though no formally agreed definition exists, LEDS are generally used to describe forward-looking national economic development plans and strategies that encompass low-emission and/or climate-resilient economic growth. LEDS can serve multiple purposes but are primarily intended to help advance national climate change and development policy in a more co-ordinated, coherent and strategic manner. By providing integrated economic development and climate change planning, an LEDS can provide value-added to the myriad of existing climate change and development related strategies and reports that already exist. Because of its benefits, the Copenhagen Accord recognised that a LEDS is indispensable to sustainable development.

VII. FINANCING SUSTAINABLE INTEGRATED DEVELOPMENT PROJECTS WITH CLIMATE CHANGE MITIGATION/ ADAPTATION COMPONENTS

Achieving sustainable development goals that integrate climate change adaptation/mitigation measures within a holistic framework requires that announced commitments be translated into strategies, policies and actions. The scale of such anticipated efforts in the MENA region requires massive multi-billion dollar financing that needs to be secured from internal and external sources. The financial aspects of climate change issues in the MENA region has recently received much attention from a large number of investigators (Abaza, 2008; Babiker and M. Fehaid, 2011; Fattouh and El-Katiri, 2012; Nakhooda et al., 2012; Saidi, 2012) whose findings provide valuable insight into the real state of affairs. A high level of investment in climate change related projects by resource-rich MENA countries is

already underway, largely supported with domestic and private sector financing. Many large-scale wind and solar energy projects are also investing in for both domestic use and export, while significant investments are being planned in energy efficiency and carbon reduction projects. However, the financing of similar projects in resource-limited MENA countries faces many challenges.

Climate change funding by international agencies has been rather limited in the MENA region. Although about US$ 1 Billion in finance has been dedicated since 2004, less than US$ 200 million was approved as grants in support of a large number of relatively small-scale projects, which are concentrated in 12 MENA countries (Nakhooda et al., 2012). Similarly, the region's share of the CDM funding is less than 2% of the global CER market in spite of the multitude of oil, gas, and petrochemical operations that are spread throughout the region and usually offer good opportunities for CDM support.

To further complicate matters, prices for CERs collapsed from about US$20 a tonne in 2008 to less than US$ 1 by the end of 2012. This is mainly driven by the Eurozone debt crisis reducing the industrial activity and the over-allocation of emission allowances under the European Union Emissions Trading Scheme" . Furthermore, some of the projects contemplated for support can hardly be considered as being "sustainable" when, for example, the citizens of a developing country end up supporting the development of a promising technology by substantially subsidizing the cost of the power generated over the project's life span (typically 20-30 years in this case).

On the other hand, there exists excellent opportunity for drawing upon the substantial financial resources that are generated within the MENA region itself. These can be utilized to accelerate the development of equitable, holistic, and sustainable climate change projects in the region, provided that a proper framework is developed that secures the equity, long-term viability, and security of such financing efforts. A similar example is presently being considered for the case of the five major emerging national economies of: Brazil, Russia, India, China and South Africa [BRICS], where the need for financial cooperation in the five-nation bloc has led to a recent agreement to establish a BRICS development bank, which could properly utilize the huge savings pool of the bloc countries.

In this regard, it is worthwhile to note that the high oil and gas prices have generated an extraordinary level of international assets and liquidity in the hydrocarbon exporting countries of the MENA region, with gross foreign assets forecast to reach some USD 2.3 trillion by end-2012 (Saidi, 2012). Consequently, governments and corporations in such countries have traditionally been cash rich and not reliant on market financing. However, the global financial crisis, the contagion effects of the Eurozone's continuing crisis and retrenchment of EU banks, along with growing financial sophistication of both the public sector and private businesses in the GCC countries, changed their financial strategy, particularly since the GCC countries are keen to lead in innovative finance as they develop financial centers and diversify their economies (Saidi, 2012).

In this context, Sukuk (Tradable financial instruments that comply with the Islamic law and its investment principles, which prohibit the charging of and/or paying interest) may be a suitable investment instrument for the MENA region, as it would meet the investment requirements of investors from the GCC, Asia and other Shariah-compliant global institutional investors. Several organizations, such as the Green Sukuk Working Group, the Clean Energy Business Council of the MENA Region and the Gulf Bond and Sukuk Association, were formed to address this need (Climatebonds, 2015).

In light of the above, the Clean Energy Business Council of the Middle East and North Africa (CEBC), the Climate Bonds Initiative and the Gulf Bond and Sukuk Association have launched a Green Sukuk Working Group. The group aims to channel market expertise to develop best practices and promote the issuance of sukuk for climate change solutions investments, such as renewable energy and clean tech projects (Saidi, 2012). Green Sukuk are Shariah securities and investments that use criteria for climate solutions developed by the International Climate Bond Standards scheme. The CEBC plans to help investors more easily identify Shariah-compliant opportunities while assisting in providing the investment capital for clean energy and other climate-friendly projects in the region.

Another financing option to be considered is based on the development of a framework by which MENA

countries with high per capita GHG emissions can gain credit in exchange for financing climate change mitigation/adaptation projects within low- and intermediate-income countries in the region.

VIII. BUILDING THE CAPACITY TO MANAGE CLIMATE CHANGE AND DEVELOPMENT CHALLENGES IN MENA

The development of sustainable solutions to the multitude of climate change issues facing the MENA region requires in-depth knowledge of site-specific conditions prevalent in the various countries and the ability to identify/develop appropriate solutions that can meet the socio-economic needs of the local population. Much of the expertise needed is already available in the region but is scattered amongst many countries, ministries, universities and NGOs. It is therefore necessary to develop a regional network of institutions that have the knowledge and ability to accomplish such goals, and equip it with a project management team that can coordinate the efforts of the various individuals. This network should encourage flexibility in problem-solving, the development of cost-effective innovative approaches, and emphasize the importance of addressing the needs of the various stakeholders and the balance of power among the various interest groups.

Such a network can also draw upon the world-wide pool of expertise, but the translation of the experience of others into a MENA-specific plan of action could best be handled on the local level where the active participation by the various stakeholders (particularly the most vulnerable sectors of the population) is a necessary condition for the success of any sustainable development program.

IX. CONCLUSION

Based on the analysis presented in this investigation it can be concluded that:

- Socioeconomic analysis of the MENA countries and their GHG emissions shows that they can be split into three categories: the affluent resource-rich countries, the middle-income countries, and a few low-income countries. The former group of countries has the world's highest level of per capita GHG emissions while the latter has almost negligible emissions. Although the variation in per capita GDP amongst these countries is very high, this does not reflect in a similar disparity of human development level.
    - Massive investments are needed to accelerate the pace of economic development in lower-and middle income countries in order to improve the standard of living and minimize social disruption. Such efforts will be accompanied by an increase in the emission levels that can be minimized by adopting low emission development strategies and by implementing cost effective means for reducing the emissions associated with the development of the oil/natural gas/petrochemical sectors.
- With about 23% of MENA's population living on less than $2 a day, it is imperative that the climate change management strategies adopted be cost-effective and emphasize economic, social and human development while addressing the concerns arising from anthropogenic climate change. This will avoid duplicating efforts, minimize the capital requirements, and facilitate the acceptance of such measures by the population at large.
- The carbon reduction experience of T&T clearly identified several negative-cost opportunities for reducing carbon emissions. The savings accrued by implementing such measures can be used for adaptation or economic development purposes. In this fashion, environmental challenges can be turned into economic opportunities and a vehicle for sustainable development.
- Converting cars and trucks so that they can use natural gas instead of gasoline or diesel reduces the GHG emissions and improves the air quality in urban centres. Significant financial benefits can also be accrued by such conversions due to the large difference in the cost per unit energy of the two fuels and the elimination of the subsidies needed to make transportation more affordable. It is, however, essential that such conversion plans be carefully implemented in a fashion that renders it the natural choice of the consumer rather than the socially disruptive price hikes.
- The extent of financial support received from international agencies by MENA countries for

mitigation/adaptation measures is relatively low. This is most probably driven by the financial difficulties through which some of the world's leading economies are presently going through, a situation, which is not predicted to change in the near future. The region should therefore rely primarily on internally-generated financing driven by intelligent self-motivated interests.

- There apparently is a growing interest in developing Shariah-compliant financing istruments that can be used for climate change solutions investments. This is driven by the high liquidity levels prevalent in the public and private sectors in many resources-rich MENA countries and the desire of the GCC countries to diversify their economies and develop financial centers that lead in innovative finance. This approach is similar to that recently adopted the recent agreement by the BRICS countries to establish their own development bank, which could utilize their huge savings pool to enhance their collective interests.

- An alternate financing scheme may be achieved by having large GHG emitters gain credit for financing climate change mitigation/adaptation projects within low- and intermediate-income countries in the region.

Although no single formula can apply to a collection of countries as diverse as those in the NEMA region, it is recommended that the various MENA countries undertake the initial four steps needed to create a Low-Emission Development strategy [LEDS] which entail:

- Development of vision/goal: An over-arching vision or goal is needed to help guide in the development of long-term policy decisions related to economic development and climate change priorities.

- Assessment of current situation: A clear understanding of major GHG emitting sectors and the socio-economic indicators is fundamental to determining the path forward.

- Emission projections, mitigation potential and costs: Planned pathways for business-as- usual emissions can help provide a sense of the national emission trajectory, while mitigation potential and costs associated with the various emission reduction options are needed as a first step towards identifying promising mitigation actions.

- Vulnerability assessment: Indications of how a country or region may be impacted by climate change can help engage stakeholders, including the general public, and can help identify adaptation needs and the range of possible cost-effective adaptation outcomes.

Much of this information is already available in the many MENA-related studies conducted by several local and international agencies. What is needed is to collect and update the information and ensure its correctness, fill in any gaps, and analyse the findings in a fashion that allows for the identification of cost-effective projects that emphasize economic, social and human development while addressing the environmental concerns arising from anthropogenic climate change.

ACKNOWLEDGEMENT

The financial support of the Natural Sciences and Engineering Research Council of Canada is gratefully acknowledged. The stimulating intellectual input and contribution of all the members of the Trinidad and Tobago Carbon Reduction Strategy Task Force is greatly appreciated.

REFERENCES

[1] Abaza H., 2008, Financing of Environment Programmes: Private-Public Partnership, in Arab Environment: Future Challenges, M. K. and N. W. Saab Edit., Report of The Arab Forum For Environment And Development, 2008.

[2] Abdel Gelil I., 2009. GHG Emissions: Mitigation Efforts in the Arab Countries, in Arab Environment: Climate Change, M. K. Tolba and N. W. Saab Edit., Report of The Arab Forum For Environment And Development, 2008.

[3] Babiker M. and M. Fehaid, 2011, Climate Change Policy in the MENA Region: Prospects, Challenges, and the implication of Market Instruments, Economic Research Forum paper # 588.

[4] Boodlal, D. and A. M. Al Taweel. 2015. Sustainable Reduction of GHG Emissions: The Case of Trinidad and Tobago, Submitted for publication in "Process Safety and Environmental Protection". Institution of Chemical Engineers (UK).

[5] Boyd A., 2013. http://www.mapsprogramme.org/normalising-apples-and-oranges-comparing-trade-offs-for-pro-poor- itigation-options/ (last accessed March 16th, 2013).

[6] Brundtland G.H. et al., 2012, Environment and Development Challenges: The Imperative to Act, Final summary report of the "The Blue Planet Prize laureates" promoted by the Asahi Glass Foundation.

[7] Burton I., S. Huq, B. Lim, O. Pilifosova, and E.L. Schipper. 2002, From impacts assessment to adaptation to adaptation priorities: the shaping of adaptation policy, Climate Policy 2: 145-159.

[8] Cherfane C.C., 2010, Regional Initiatives to Assess the impact of Climate Change on Water Resources, Paper presented at the Arab Water Forum.

[9] Clapp, C., G. Briner, and K. Karousakis, 2010, Low-emission development Strategies (LEDS): Technical, Institutional and policy lessons, Report # JT03292873, OECD/IEA.

[10] Climatebonds, 2015, http://www.climatebonds.net/tags/green-sukuk-working-group (last accessed on May 20, 2015)

[11] Estiri H., R. Gabriel, E. Howard, L. Wang, 2013, Different Regions, Differences in Energy Consumption- Working Paper no. 134, Center for Statistics and the Social Sciences, University of Washington.

[12] Floyd J. 2012, Beyond this Brief Anomaly- A systemic inquiry into energy and society, (http://beyondthisbriefanomaly.org/; last accessed on May 25th, 2015)

[13] Fattouh, B. and L. El-Katiri, 2012. Energy Subsidies in the Arab World. Arab Human Development Report, Research Paper Series. United Nations Development Programme, Regional Bureau for Arab States.

[14] Ghaddar N., 2010, Climate Change Research on Energy Efficiency in the Arab Region, Report submitted to the UNDP, Regional Bureau for Arab States (RBAS),

[15] Gomer S. and Lewis A., 2008. An Australian Cost Curve for Greenhouse Gas Reduction. Mckinsey and Company.

[16] Klawitter J., 2011, Implications of Climate Change on Energy and Security in the MENA Region http://www.mei.edu/ , (last accessed March 15th, 2013)

[17] ngv. 2012, http://www.ngv2012.com/ (last accessed March 24th, 2013).

[18] Nakhooda S., A. Caravani, P. Seth and L. Schalatek, 2012. Climate Finance for the Middle East and North Africa: Confronting the challenges of climate change, Heinrich Böll Stiftung North America.

[19] Saidi N. H., 2012, http://hawkamah.org/wp-content/uploads/2014/10/Harnessing-Green-Sukuk-for-Sustainable-Development.pdf (last accessed, May 20th, 2015).

[20] Sütterlin B.S., 2012, Segmentation and Characterization of Energy Consumers: Consumer Differences in Energy-Related Behaviours and Commonalities in Perceptions of "Others" Behaviours, Ph.D. Thesis, ETH Zurich Switzerland.

[21] Tolba M. K., 2008, Integrating Environment in Development Planning, in Arab Environment: Future Challenges, M. K. and N. W. Saab Edit., Report of the Arab Forum for Environment And Development, 2008.

[22] Tolba M.K. and N.W. Saab, 2010, Impact of Climate Change on Arab Countries, REPORT OF THE Arab Forum for Environment and Development.

[23] UNDP, 2010, http://hdr.undp.org/en (last accessed May 20th, 2015)

[24] Ugursal V. I., 2013, Energy Use and Energy Conservation. Chapter 21 in The World Scientific

[25] Handbook of Energy, edited by Gerard M Crawley, World Scientific Publishing Co., 2013.

[26] Verner D. ed. 2012. Adaptation to a Changing Climate in the Arab Countries. Washington, DC: World Bank. DOI: 10.1596/978-0-8213-9458-8.

[27] Wingqvist G. Ö. and O. Drakenberg, 2010, Environmental and Climate Change Policy Brief - MENA1

[28] World Bank Databank, 2013. http://databank.worldbank.org/ (Last accessed March 18, 2013).

[29] World Bank MENA Region, 2007, Sustainable Development Sector Department (MNSSD) Regional Business Strategy to Address Climate Change Preliminary draft for consultation and feedback.

Durability Probabilistic Evaluation of RC Structures Subjected to Chloride Ion

Han-Seung Lee[1], Mohamed A. Ismail[1,*], Mohd Warid Hussin[2]
[1]School of Architecture & Architectural Engineering, Hanyang University, Ansan, S. Korea
[2]Construction Research Centre (UTM CRC), Institute for Smart Infrastructure and Innovative Construction, Universiti Teknologi Malaysia, 81310 UTM Johor Bahru, Johor, Malaysia
[*]Corresponding Author Email: mismail@hanyang.ac.kr, phone: +82-31- 4005181, fax: +82-31- 4368169

Abstract - Chloride attack on concrete structures is becoming a primary factor that deteriorates the durability of concrete structures. For this reason, research has been conducted on chloride ion penetration and diffusion. This research produced an accurate durability life prediction through reliability assessments and proposes a prediction method for the chloride ion diffusion coefficient of a concrete applied assessment program for reliability. As a result, test materials were fabricated using different admixtures, and chloride ion diffusion coefficient was calculated by applying an RCPT test at each equivalent age. Based on the results, reliability prediction formulas were indicated through the reliability analysis for a durability life design using a Monte Carlo method. In addition, results were verified through comparisons and analysis using the proposed formula with the investigated data for chloride ion diffusion.

Keywords - Evaluation of durability life, Chloride ion diffusion coefficient, Monte Carlo method.

I. INTRODUCTION

It is widely known that the ingress of chloride ions constitutes a major source of durability problems affecting reinforced concrete structures that are exposed to saline environments. Once a sufficient quantity of chloride ions has accumulated around the embedded steel, pitting corrosion of the metal is liable to occur unless the environmental conditions are strongly anaerobic. In the design of concrete structures, the influence of chloride ingress on service life must be considered [Metha 2006; Papadakis 2000; Nielsen et al. 2003; Han 2007; Song et al. 2007].

The common service life model for the chloride induced corrosion of reinforcing steel in concrete involves two time periods. The first is the time for chloride diffusion until a sufficient concentration of chlorides is available at the reinforcing bar depth to initiate corrosion. The second is the time for corrosion damage (from initiation to cracking and spalling of the cover concrete) to the end of functional service life.
An apparent diffusion process, based on Fick's second law, can be used to model the time for chloride to reach and initiate corrosion, where first repair and rehabilitation at reinforcing steel depths will take place. When solved for the condition of constant surface chloride and a one-dimensional infinite depth, Fick's second law takes the following form [Kim et al. 2007]:

$$C(x,t) = C_0(1 - erf(x/\sqrt{4 * D_C * t})) \quad (1)$$

Where $C(x,t)$ is chloride concentration at depth and time; C_0 is surface chloride concentration; D_C is apparent chloride ion diffusion coefficient; t is time for diffusion; x is concrete cover depth and erf is statistical error function. When $C(x,t)$ is set equal to the chloride corrosion initiation concentration and Eq. (1) is solved for t, the time for the diffusing chloride ions reaches rebar and initiates corrosion. However, for a given real condition, the values of $C(x,t)$, C_0 D_C and x are random variables, each with their own statistical distributions, means, and variances. A solution to Eq. (1) for the time of diffusion should include the probabilistic nature of the input variables [Kirkpatrick *et al.* 2002; Enright and Frangopo 1998]. The time for corrosion damage to the end of functional service life is also a random variable and depends on the corrosion rate, concrete cover depth, reinforcing steel bar spacing, and size [Liu and Weyers 1998]. To predict the whole service life, the probabilistic nature of these variables should also be considered.

One common modern statistical technique is called Monte Carlo simulation. Monte Carlo is a general class of repeated sampling methods, where a desired response is determined by repeatedly solving a mathematical model using values randomly sampled from probability distributions of the input variables [Kalos and Whitlock 1986].

II. SUMMARY OF CHLORIDE PENETRATION TEST

A. Experimental Program

Mineral components for improvement of chloride blocking property were tested in the same environment. To examine diffusion blocking properties, Rapid Chloride Penetration Test (RCPT) was done. Configurations of test are presented in Table 1. Water-binding material ratio has two levels: 40% and 50%. Fly Ash (FA), Blast furnace Slag (BS), Silica Fume (SF) and Meta Kaolin (MK) were used in 3 different levels.

Table 1. Dimensions of various fins

Water- binding material ratio (%)	Admixture type		Admixture replacement ratio (%)	Measurement item	Measurement aging (day)
40, 50	Non-blending	Designation	-	Compressive strength Chlorine ion diffusion coefficient	7, 28, 56, 91
	Fly ash	FA	10, 20, 30		
	Blast-furnace slag	BS	30, 50, 70		
	Silica fume	SF	5, 10, 15		
	MetaKaolin	MK	5, 10, 15		

Table 2 shows composition of the plain concrete, without adding mineral components, to accomplish slump 18 ± 2.5cm and air entrained quantity, high efficiency AE water reducing agent. For the test of chloride penetration, RCPT, which was proposed by Tang & Nilsson, was referred to as illustrated in Fig. 1. Accordingly, each side of the cell is filled with 0.3M of sodium hydroxide (NaOH) as anode and 3% of sodium chloride (NaCl) as cathode. After that 30V was applied to the cell. The test was maintained for 8 hours; then 0.1 N water solution of silver nitrate (AgNO3) was sprayed after the split test body. As a result, the color of affected area changed. The colored depth was measured by Vernier calipers. The chloride ion diffusion coefficient was calculated using Eq. (2) based on the measured results.

$$D = \frac{RTL}{zFU} \cdot \frac{x_d - a\sqrt{x_d}}{t}$$

$$\left(a = 2\sqrt{\frac{RTL}{zFU}} \cdot erf^{-1}\left(1 - \frac{2c_d}{c_0}\right) \right) \qquad (2)$$

Where:

D	diffusion coefficient (m^2/s)
z	atomic value of ion (z=1 for chloride ion)
F	Faraday constant (96,481.04 J/Vmol)
U	Voltage differences between positive and negative pulse (V)
R	gas constant (8.314 J/Kmol)
T	solution temperature (K)
L	specimen thickness (m)
x_d	penetration depth of chloride ion (m)
t	test sustaining time
erf	error function
c_d	chloride ion density at the section changed in color by $AgNO_3$
c_0	chloride ion density of cell located in a negative pole

Table 2. Composition of the plain concrete

Water-cement ratio (%)	Fine aggregate ratio (%)	Unit weight (kg/m^3)			
		water	cement	fine aggregate	coarse aggregate
40	45.6	158	395	793	954
50	47.7	158	316	861	951

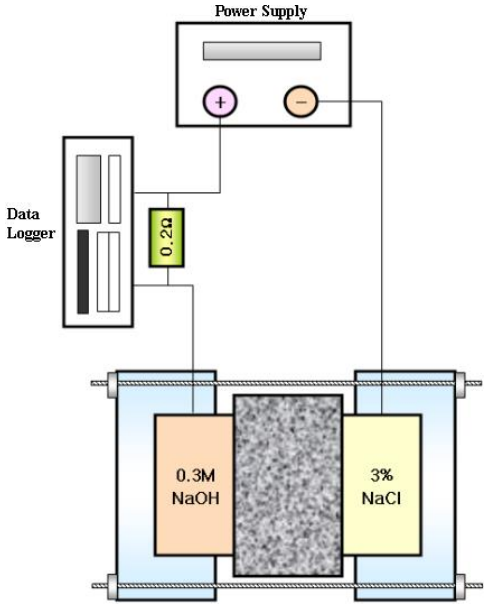

Fig .1. Diagram of chloride ion diffusion test equipment

Fig. 2 demonstrates the procedure of rapid chloride penetration test to examine chloride ion diffusion coefficient of chloride ion.

Fig .2. Procedure of rapid chloride penetration test

III. EVALUATION OF PROBABILISTIC DURABILITY LIFE

A. In the latent period

Corrosion in RC structure assumed to have occurred by the attack of salt. In this case, chloride concentration depth is determined by Eq. (3); it is also assumed that if chloride concentration is over the limits of (1.2 kg/m3) at steel bar position then it is the end of service for the structure. In this study, durability of the structure in sea environment was statistically analyzed by Monte Carlo method. Table 3 shows the factors of statistical analysis. D0 is determined by RCPT, Dm is calculated by Eqs. (4a) and (4b) is used with chloride ion diffusion coefficient of chloride on the 28th day.

$$x(t) = 2erf^{-1}(1-\frac{C_{cr}}{C_s})\cdot\sqrt{D_m t} \quad (3)$$

$$D_m = \frac{D_0}{1-n}(\frac{t_0}{t})\ (t<t_c) \quad (4a)$$

$$D_m = D_0[1+\frac{t_0}{t}\cdot\frac{n}{1-n}](\frac{t_0}{t})^n\ (t\geq t_c) \quad (4b)$$

Where:

C_{cr}	critical chloride content ion density at the beginning of corrosion (kg/m3)
Cs	chloride ion density at the surface of concrete (kg/m3)
Dm	average chloride ion diffusion coefficient until time t (m2/s)
Do	chloride ion diffusion coefficient at t0 (m2/s)
tC	perpetual time of chloride ion diffusion coefficient (assumed as 30 years)
t	time lapse (years)
n	time dependent coefficient

Table 3. Factors of statistical analysis

Factor	Average	Standard deviation
D_0	Test result	1.2
N	Test result	0.08
d(mm)	40	7
$C_{cr}(kg/m^3)$	1.2	0.24
$C_s(kg/m^3)$	9	1.8

B. In the progress period

Progress period means the period that starts after the beginning of corrosion and until the crack begins. In this period, if the corrosion quantity is larger than corrosion quantity when structure cracked, service year will be end. The amount of corrosion in steel bars can be calculated using Eq. (5).

$$W(spe) = I/(2F) * [Fe(OH)_3^{\ 1}] * t_{corr} \quad (5)$$

$$(I = 0.025 * C(d,t)^{1.5} \quad (6)$$

$$C(d,t) = C_s(1 - erf(\frac{d}{2\sqrt{D_m \cdot t}})) + C_i)) \quad (7)$$

Where:

I	corrosion current density (μA/cm2)
C(d,t)	chloride ion density at the shield d(cm) and time t(year) (kg/m3)
W(spe)	amount of steel bar corrosion(g/cm2)
F	Faraday constant (96500C/mol)
Fe(OH)3	molecular weight of Fe(OH)3 (Ⅲ) (106.9g/mol)
t_{corr}	time lapse (years) from the beginning of the time that exceeds the corrosion occurred critical chloride content ion density
Ci	chloride ion density in the early stage (kg/m3)(=0)
Dm	Average chloride ion diffusion coefficient at t (year) (m2/s) (Eqs. 3a, 3b)

If the shield thickness is considered with factor k, Eq. (5) will be expressed as Eq. (8). Eq. (9a) and Eq. (9b) considers diameter and shield thickness to get factor k. C(d, t) is calculated by Eq. (7); Dm is calculated by (4a) and (4b) as a latent period. Ci assumed as 0 and steel bar diameter is assumed as 13 mm. If corrosion calculated by Eq. (8) is larger than Wcr, which is calculated by Eq. (10), it is assumed that its service year has ended. As a process of the latent period, possibility of crack is calculated in the progress period.

$$W = k * W(spe) \quad (8)$$

$$k = 1.0\ (3*D \geq d) \quad (9a)$$

$$k = 3 * D/d\ (3*D < d) \quad (9b)$$

$$Wcr = \frac{0.02d}{3D} \quad (10)$$

Where:

W	corrosion speed of steel bars
k	shield parameter that affects corrosion speed
D	steel bar diameter (cm)
d	shield thickness (cm)
Wcr	corrosion quantity when cracking begins(g/cm2)

IV. TEST ANALYSIS

The 28th day compressive strength of this study is found to be between 30~40 MPa, as shown in Fig 3, whereas Fig. 4 the chloride ion diffusion coefficient of plain concrete for W/C is between 0.4 and 0.5. The estimation of the chloride ion diffusion coefficient DPC, can be produced using Eq. (11).

$$D_{PC} = 0.547e^{3.95W/C} \quad (11)$$

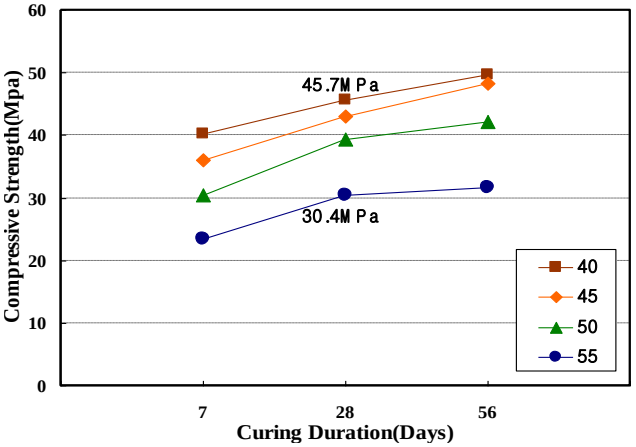

Fig .3. Compressive strength development with time

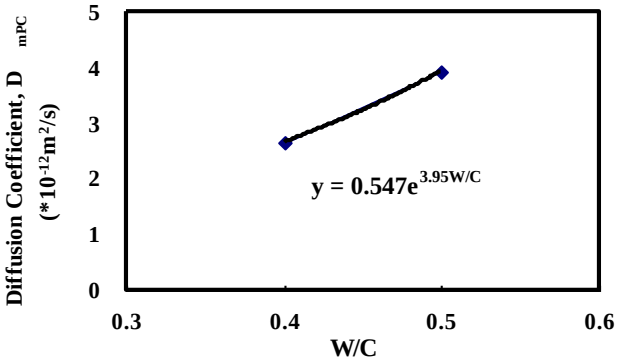

Fig .4. Diffusion coefficient of plain concrete W/C 0.4 and 0.5

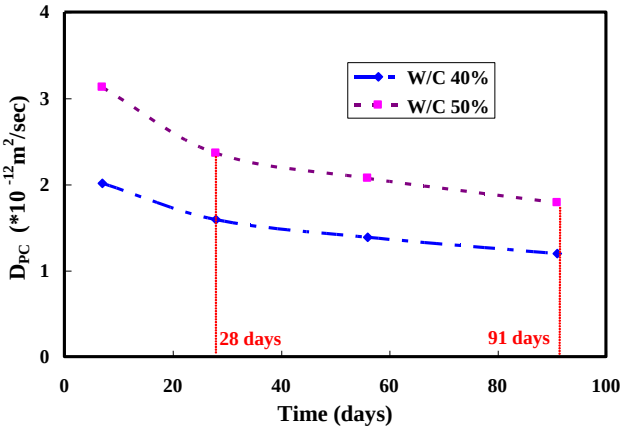

Fig .5. Diffusion coefficient according to time passage (W/C 0.4 and 0.5)

In this study, chloride ion diffusion coefficient according to time passage (Fig. 5) was determined by RCPT and Eqs. (4a) and (4b). With this result, variation of diffusion coefficient was calculated. Fig. 6 shows diffusion coefficient ratio when the plain concrete was replaced by admixture. According to Fig. 6, equation for determining the diffusion coefficient of each admixture was suggested in Table 4.

To estimate possibility of failure according to the time dependent coefficient variation, durability failure possibilities according to the service year was calculated when SF15%, time dependent coefficient n=0, 0.4 and 0.8 (Fig. 7). Chloride ion diffusion coefficient can calculated by Eq. (12) when the concrete property according to the time dependent is considered. According to Eq. (13), induced by Eq. (12) and test result, the variation of time dependent parameter [n] is shown in Fig. 8.

$$D(t) = Do(\frac{t_0}{t})^n \quad (12)$$

$$n = \log Do(\frac{t_0}{t})^{D(t)} \quad (13)$$

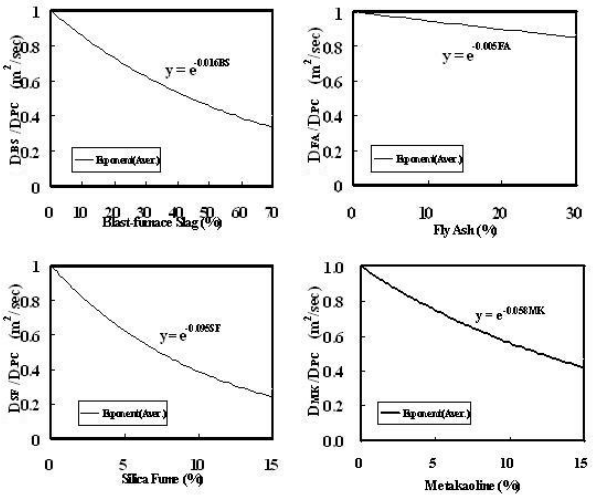

Fig .6. Type of admixture and substitution ratio

Table 4. Diffusion coefficient of each admixture

Component	Equation(m^2/sec)
BS	$D_{PC}\cdot e^{-0.016\cdot SF}$
FA	$D_{PC}\cdot e^{-0.005\cdot SF}$
SF	$D_{PC}\cdot e^{-0.016\cdot SF}$
MK	$D_{PC}\cdot e^{-0.016\cdot SF}$

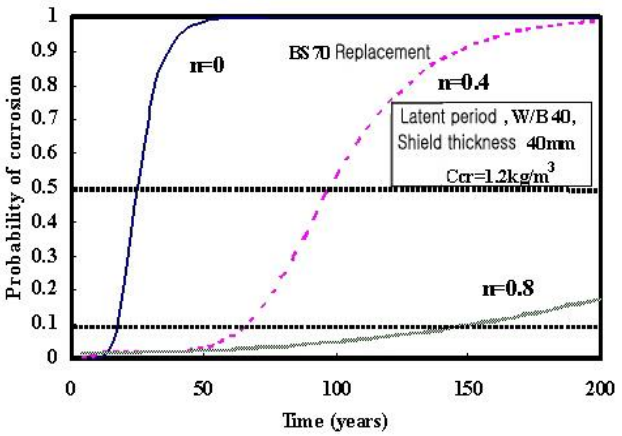

Fig .7. Durability failure possibilities according to the time dependent coefficient

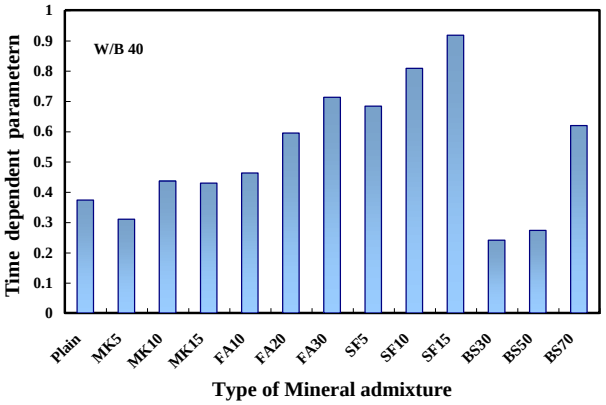

Fig .8. Time dependent parameter by type and quantity of mineral admixture

Probabilistic durability analysis for the latent period and the progress period were shown in Fig. 9. Meanwhile fly ash does not have any efficiency to improve durability, wherea blast furnace slag, silica fume and MetaKaolin do improve durability.

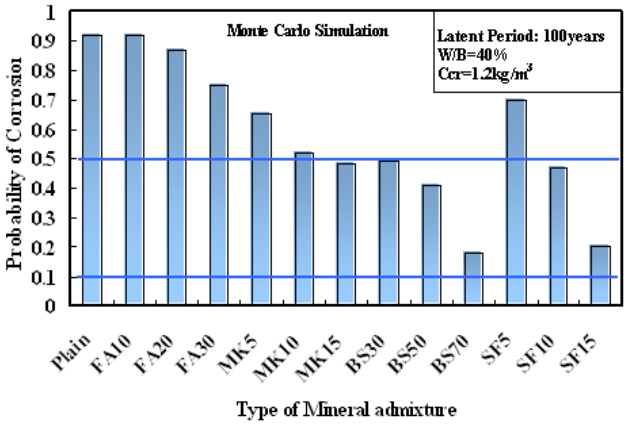

Fig .9. Possibility of durability failure by type and quantity of mineral admixture

Fig. 10 shows the durability failure possibility according to shield thickness. If the shield thickness of steel bar is increased, distance from concrete surface to the steel is also increased. Consequently, resistance of chloride ion is increased and durability failure possibility is decreased. Fig. 11 shows durability failure possibility in latent period according to time. It is also replaced by SF 15% and BS 70% is most efficient to improve durability. The point of the possibility of durability failure will be 10% in the 80th year.

Fig. 12 shows durability failure possibility when admixture type and replacement ratio are different. According to this graph, the deviation of admixture type is smaller than the deviation of replacement ratio. Durability failure possibility is also approximately 30% smaller.

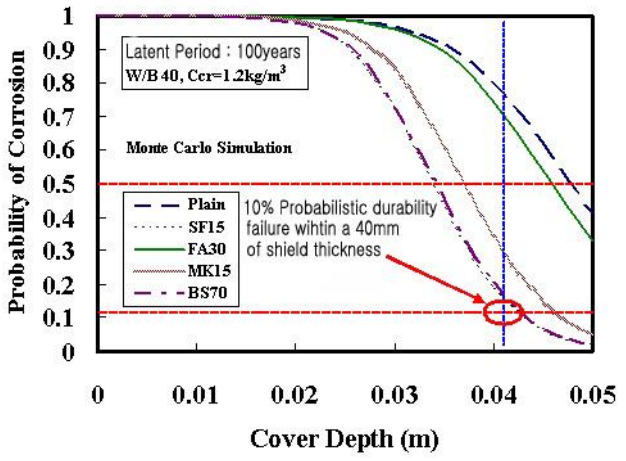

Fig .10. Durability failure possibility according to shield thickness

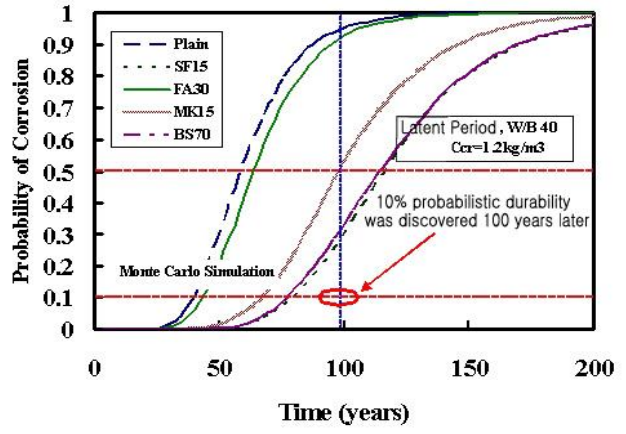

Fig .11. Durability failure possibility according to time

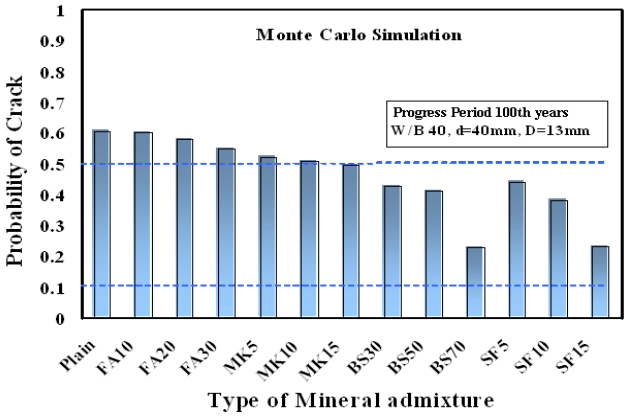

Fig .12. Durability failure possibility of admixture type and replacement variation

Fig. 13 presents the result of durability failure possibility according to the shield thickness, while Fig. 14 shows durability failure possibility in progress period according to time. In the latent period, nothing satisfied the durability failure possibility under 10% when shield thickness was 40mm and over 100 years. However, when replaced by silica fume 15% and blast furnace slag 70%, the durability failure possibility was reduced to 9 % in the progress period, which satisfied possibility under 10%. Other parameters have durability failure possibility over 30%.

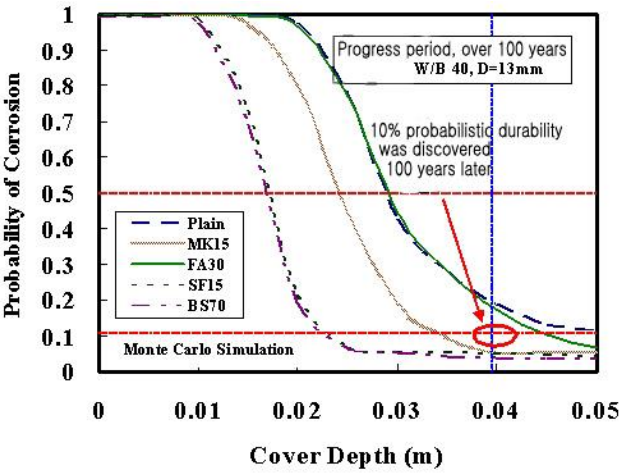

Fig .13. Durability failure possibility according to shield thickness

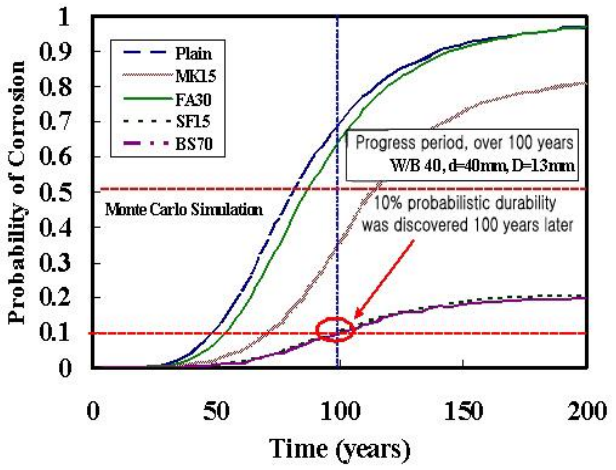

Fig .14. Durability failure possibility according to time

V. CONCLUSION

In this paper, based on experimental results of chloride diffusion coefficients and Monte Carlo method, the service of concrete structure incorporating different mineral components, such as fly ash (FA), blast furnace slag (BS), silica fume (SF) and metakaolin (MK) was predicted. The proposed model incorporates the statistical nature of chloride induced corrosion of reinforced concrete and can be used to evaluate the time of first repair and rehabilitation of concrete structures.

This study obtained a DPC equation with a W/C using the chloride ion diffusion coefficient and time dependent coefficient (n) calculated by the experiment. It proposes an estimation equation for the chloride ion diffusion coefficient according to the blending ratio of admixtures, using the chloride ion diffusion coefficient of the plain concrete and admixture blended concrete. Large differences of 20, 40, and 160 years at a 10 % probabilistic durability failure rate were evident by varying the time dependent index to 0.0, 0.4, and 0.8 under the same conditions of the probabilistic durability life test. It was clear that the time dependent index significantly affected the evaluation of the durability life. Thus, it is necessary to precisely calculate the time dependent index.

ACKNOWLEDGEMENT

This work was supported by Sustainable Building Research Center Hanyang University, which was funded by the SRC/ERC program of MOST (#R11-2005-056-04003-0). This paper is an extended abstract that was published in Korea by AIK.

REFERENCES

[1] P. Kumar Metha (2006). Concrete-Microstructure, Properties and Materials. MaGraw-Hill, New York.

[2] Vagelis G. Papadakis (2000). Effect of supplementary cementing materials on concrete resistance against carbonation and chloride ingress. Cem Concr Res 30: 291-299.

[3] Erik P. Nielsen, Mette R. Geiker (2003) Chloride diffusion in partially saturated cementitious material. Cem Concr Res 33: 133-138.

[4] Sang-Hun Han (2007) Influence of diffusion coefficient on chloride ion penetration of concrete structure. Constr Buil 21:370-378.

[5] Ha-won Song, Jong-Chul Jang, Velu Saraswathy, Keun-Joo Byun (2007) An estimation of the diffusivity of silica fume concrete. Bldg Envir 42:1358-1367.

[6] Dongseok Kim, Hanseung Lee, Seongmin Lee, Xiaoyong Wang.(2007) A study on the evaluation of probabilistic durability life for RC Structures deteriorated by chloride ion, Advances in fracture and damage mechanics VI, FDM 2007, Portugal, edited by J.Alfaiate, M.H.Aliabadi, M.Guagliano, L.Susmei, pp.417-421.

[7] Trevor J. Kirkpatrick, Richard E. Weyers , Christine M. Anderson-Cook, Michael M. Sprinkel (2002) Probabilistic model for the chloride-induced corrosion service life of bridge decks, Cem Concr Res 32 :1943–1960.

[8] Mchael P. Enright and Dam M. Frangopol (1998) Probabilistic analysis of resistance degradation of reinforced concrete bridge beams under corrosion, Eng Struct 20: 960-971.

[9] Y. Liu, R.E. Weyers (1998) Modeling the time-to-corrosion cracking in chloride contaminated reinforced concrete structures, ACI Mater. J.95: 675– 681.

[10] M.H. Kalos, P.A. Whitlock (1986) Monte Carlo Methods: Volume I. Basics, Wiley, New York.

A Sustainability Assessment Framework for Waterfront Communities Increasing the Resilience of the Abu Qir Waterfront Community in Alexandria

Sally El.Deeb[1], Rania AbelGalil[1], Alaa Sarhan[1]
[1]Architectural Engineering and Environmental Design Department,
Arab Academy for Science, Technology & Maritime Transport,
AbuQir campus, Alexandria, Egypt.

Abstract - It is predicted that the global phenomena of Climate change will have far reaching effects and implications on different local urban systems. For incidence, global average sea levels are expected to rise between 7 and 36 cm by the 2050s, and between 9 and 69 cm by the 2080s. Waterfront communities are the first to be affected by such impacts, putting them at high risk. Planning strategies are needed to assist these communities and increase their adaptive and learning capacities in the face of diverse challenges to their urban sub-systems.

The research investigates a number of sustainability frameworks and assessment rating systems for neighbourhoods and communities. It investigates the sustainable evaluation criteria carried out by three assessment rating systems. First is the LEED (Leadership in Energy & Environmental Design, USA), the second is the BREEAM (Building Research Establishment Environmental Assessment Method, UK), and the third is the Estidama PEARL rating system (UAE).Examples of waterfront communities which applied the previous rating systems are analysed in order to determine the applicability and relevance of these systems to waterfront communities in particular.

The research concludes with a proposed framework of indicators for waterfront communities. The similarities and differences between the three rating systems and featured indicators specific to waterfront planning applied in the analysed examples; yet absent in the three rating systems, have informed the selection of indicators in the proposed assessment framework. The proposed framework could be an effective tool for the planning and development of à waterfront community in the MENA (the port region). In order to validate the framework, the set of environmental and physical indicators were applied on the case study of Abu Qir waterfront, Alexandria, Egypt. Conclusions and recommendations are made that would enhance the resilience of this waterfront community and provide a comprehensive tool for its sustainable planning.

Keywords - waterfront communities, sustainability, rating systems, assessment framework.

I. INTRODUCTION

Waterfront regeneration is becoming one of the most celebrated practices of urban renewal in contemporary cities of the North. At the same time, developing regions have suffered prolonged inattention which lead to a gap between both (Giovinazzi & Moretti, 2010). Urban waterfronts throughout the world suffered a series of deteriorating conditions related to environmental, social and economic issues.

Some of these issues include changing land uses, large areas of derelict land, lack of services and affordable housing for communities, contaminated air, water and soil, lack of connectivity and inefficient transport. With increased awareness of impacts of climate change, cities are facing big challenges with environmental conditions accomanied by pressures that threaten urban systems to accommodate rapid growth and development. Planning for long term growth and increasing the resilience of urban areas in such a manner that addresses the number of crucial economic, environmental and social conditions is an important quest, more particularly for developing countries with surging population.

This paper addresses this quest through providing a framework of indicators to assess the environmental and physical aspects of water front communities. The paper is divided into six sections, following the introduction. The second section explores principles agreed upon for the sustainability of waterfronts. The third section analyses the three rating systems

designed for urban communities. Moreover, it organises the indicators of those systems according to common categories critically assessing the importance granted to each one. The fourth section explores some international examples and their use of the rating systems plus any appendages made. The fifth section applies a framework to the case study done the area designated at Abu Quir to uncover priority themes based on the inputs collected from the field survey together with the interviews conducted, in order to facilitate the sustainable planning of this waterfront community. Lessons learnt are drawn in the sixth section with concluding remarks that can be made use of by other MENA (the port region), any coastal areas.

II. PRINCIPLES OF SUSTAINABLE WATERFRONTS

In the context of the initiatives for the Global Conference on The Urban Future (Urban 21) held in Berlin in July 2000 (Hall and Pfeiffer, 2000) and in the course of the EXPO 2000 World Exhibition (Giovinazzi,2008), 10 Principles for a Sustainable Development of Urban Waterfront Areas were approved. These principles are shown in Table 1:

Table 1. Principles of Sustainable Waterfronts

Principles of sustainable waterfronts:
1 - Secure the quality of water and the environment
2 - Waterfronts are part of the existing urban fabric
3 - The historic identity gives character
4 - Mixed use is a priority
5 - Public access is a prerequisite
6 - Public participation is an element of sustainability
7 - Planning in public private partnerships speeds the process
8 - Waterfronts are long term projects
9 - Waterfronts profit from international networking
10 - Re-vitalization is an ongoing process

It is concluded from the set of principles of Urban 21 shown above that it offers general international concepts of sustainability that can be applied on waterfronts, specifically by methods which respect nature and human needs to make a vital waterfront. But an assessment tool is needed as an evaluative mechanism to measure the rate of sustainability. The following section will show such attempts. However, it must be noted that the rating systems could apply to any urban area ; and not particularly waterfront communities. It should be critically assessed whether the rating systems will fully consider the above-mentioned principles or not. If so, their applicability to waterfronts could be possible. Further to this step, their application on some examples of waterfront communities are studied in section 4.

III. SUSTAINABILITY ASSESSMENT RATING SYSTEMS

Sustainability has become an accepted meta narrative, almost certain to be integrated into any future scenario of development (Campbell, 1996). A lot of institutions in different cities began to call for applying the principles of sustainable development (WCED, 1987; IUCN, 1991;Bell & Morse,2008). Different approaches have been developed; these include assessment techniques, indicators, audits, footprint studies and ecological accounts (Munda, 2001; Rydin et al, 2003, Tanguay et al. 2009), all viewed as approaches translating a concept that is presumed to be agreed in principle into something workable on the ground (Owens and Cowell, 2002).

Assessment rating systems are considered an important approach which has become popular worldwide and even obligatory in some places to classify who would barely fulfill the requirements of sustainability and who would exceed it. Examples of these rating systems are the LEED (American system), BREEAM (European system), CASBEE (Japanese system), Green Star (Australian system), and Pearl (UAE system). Three rating systems will be analysed. LEED and BREEAM were selected in this study as they are the most commonly known rating systems, and the Pearl system as it is a rating system used in the Middle East (United Arab Emirates) which is similar to the Egyptian context.

A. LEED Indicators

LEED stands for Leadership in Energy and Environmental Design which is a green building rating system, originally developed in 1998 by the U.S. Green Building Council (USGBC) to provide a recognized standard for the construction industry for assessing the environmental sustainability of building designs. LEED for neighborhood development was later developed in 2007 and updated in 2009(USGBC,

2009).

B. *BREEAM Indicators*

BREEAM (Building Research Establishment's Environmental Assessment Method) is an environmental assessment method which was first addressed in 1990 for buildings to set the standard for best practice in sustainable design. Eventually, In 2002 BREEAM released and published a comprehensive framework for the early stage of development called, « A Sustainability Checklist for Developments », a common framework for developers and local authorities BREEAM Communities. (BRE, 2009).

C. *PEARL Indicators*

The Pearl Rating System for Estidama (which means sustainability in Arabic) is the first government initiative released in the Middle East region, by Estidama program of the Abu Dhabi Urban Planning Council in 2010. The Program includes a standard rating system for buildings, villas, and other neighborhoods. Its aim is to create more sustainable communities, cities and global enterprises, balancing between the four pillars of Estidama: environmental, economic, cultural and social. Estidama itself is also a part of Abu Dhabi's 20-year plan, known as « A Plan for Abu Dhabi 2030 » which attempts to redefine how a contemporary Arab city should look like to encourage sustainable growth and progress. (AbuDhabi Urban Planning Council, 2010)

D. Comparison between the Categories of the 3 Rating Systems

After analyzing the 3 previous rating systems, it is observed that there is a considerable overlap between the three systems and that they all include the same main categories shown in Table 2. These are community layout, buildings, transportation, water, energy, materials, waste, environment, and innovation (though the categories have different names within each rating system). On the other hand, each system still has its own particularities and definitions under each category. The similarities between the 3 rating systems are examined and the criteria for sustainability to be followed are collated in a framework. Five categories were reached.

The framework ,including the five categories, is set to assess the sustainability and resilience of waterfronts, and thus they can be applied in the case study of Abu Qir area .

Table2.demonstrates the common indicators between Pearl, BREEAM, and LEED rating systems (after grouping categories under headings devised by the researcher)

Table 2. demonstrates the common indicators between Pearl, BREEAM, and LEED rating systems (after grouping categories under headings devised by the researcher)

Category	LEED Indicator		BREEAM Indicator		PEARL Indicator	
Community layout	**Smart Location & Linkage**	-Smart Location - Proximity to water & waste water infrastructure - Floodplain Avoidance - Brownfields Redevelopment - High Priority Brownfields Redevelopment - Site Design of Habitat /Wetland Conservation -Housing and Jobs Proximity -School Proximity - Conservation Management of Habitat or Wetlands --Open community - Compact Development - Diversity of Uses - Reduced Parking Footprint - Access to Surrounding Vicinity - Access to Public Spaces - Access to Active Spaces - Universal Accessibility - Community Outreach and Involvement	**Community / Place Shaping**	- Inclusive Communities - Community Consultation - Information / Ownership - Land Use - Form of Development - Open Space - Inclusive Design - Mix of Use	**Livable communities & Integrated Development**	-Integrated Development Strategy - Sustainable Building Guidelines - Community-Dedicated-Infrastructure-Basic Commissioning - Life Cycle Costing - Plan 2030 - Urban Systems Assessment - Provision of Amenities and Facilities - Outdoor Thermal Comfort Strategy - Neighborhood Connectivity - Open Space Network - Accessible Community Facilities - Community Walkability - Active Urban Environments - Travel Plan - Safe and Secure Community -Regionally Responsive Planning

Buildings		**Green Construction & Technology**	- Diversity of Housing Types - Affordable Rental Housing - Affordable For-Sale Housing -Construction Activity Pollution Prevention -LEED Certified Green Buildings - Energy Efficiency in Buildings - Reduced Water Use - Building Reuse and Adaptive Reuse -Reuse of Historic Buildings	**Buildings**	-Residential Buildings (CSH or EcoHomes) -Non-Domestic Buildings (BREEAM)	**Livable communities**	- Minimum Pearl Rated Buildings Within Communities -Housing Diversity
Transportation		**Neighborhood pattern & Design**	-Reduced Automobile Dependence -Walkable streets -Street Network -Transit facilities -Transportation demand management	**Transport**	- Public Transport - Cycling Requirements - Car Parking -Traffic Management	**Livablecommunities**	- Transit Supportive Practices
Environmental Issues	**Ecology**	**Green Construction & Technology**	- Imperiled Species and Ecological Communities - Wetland and Water Body Conservation - Agricultural Land Conservation - Minimize Site Disturbance Through Site Design. - Minimize Site Disturbance During Construction. - Contaminant Reduction in Brownfields Remediation - Heat Island Reduction - Solar Orientation	**Ecology & Resources**	- Ecological Survey - Biodiversity Action Plan - Native Flora - Wildlife Corridor - Pollution Issues - Land Remediation	**Natural Systems**	-Natural Systems Assessment -Natural Systems Protection -Natural Systems Design &Management Strategy -Reuse of Land -Remediation of Contaminated Land -Ecological Enhancement -Habitat Creation and Restoration -Food Systems -Improved Outdoor Thermal Comfort -Construction Environmental Management
	Water	**Green Construction & Technology**	-Stormwater Management	**Resources**	- Water Resources Management -Flood Risk Issues -Water Consumption Management	**Precious Water**	-Community Water Strategy -Building Water Guidelines -Water Monitoring and Leak Detection -Community Water Use Reduction: Landscaping -Community Water Use Reduction: Heat Rejection -Community Water Use Reduction: Water Features -Storm water Management -Water Efficient Buildings
	Energy	**Green Construction & Technology**	- On-Site Energy Generation - On-Site Renewable Energy Sources - District Heating & Cooling -Infrastructure Energy Efficiency	**Climate & Energy**	-Passive Design Principles -Energy Consumption Management -Infrastructure	**Resourceful Energy**	-Community Energy Strategy -Building Energy Guidelines -Energy Monitoring and Reporting -Community Strategies for Passive Cooling -Urban Heat Reduction -Efficient Infrastructure: Lighting -Efficient Infrastructure: District Cooling -Efficient Infrastructure: -Smart Grid Technology -Renewable Energy: Onsite -Renewable Energy:Offsite -Energy EfficientBuildings
	Waste	**Green Construction & Technology**	-Construction Waste Management -Comprehensive Waste Management	**Resources**	-Waste Management (Operation and Construction)	**StewardingMaterials**	- Basic Construction Waste Management - Basic Operational Waste Management - Improved Construction Waste Management - Improved Operational Waste Management - Organic Waste Management 2 - Hazardous Waste Management
	Materials	**Green Construction & Technology**	- Recycled Content in Infrastructure	**Resources**	-Impact of Materials	**Stewarding Materials**	-CCA Treated Timber Elimination -Modular Pavement & Hardscape Cover -Regional Materials -Recycled Materials -Reused or Certified Timber
Innovation		**Innovation**	-Innovation and Exemplary Performance -LEED Accredited Professional	**Business**	-Business Investment -Employment -Business Facilities -Connectivity	**Innovating Practice**	-Showcase of Regional & Cultural Practices -Innovating Practice -Sustainability Awareness

E. Comparison between the Weightings of Each Category in the 3 Rating Systems LEED, BREEAM and PEARL.

Table 3 shows the relative weights in each rating system according to five categories arrived at from the previous analysis. The weighting of each category is measured as a percentage of each system's total credit points.

Table 3. shows the relative weights in each rating system to the following main categories

Categories		LEED	BREEAM	Pearl
Community layout		43.5%	31%	13%
Buildings		16%	4%	10%
Transportation		11.5%	22%	1%
Environmental Issues	Water	8.5%	6.5%	24%
	Energy	5.5%	10.5%	25%
	Materials	1%	3%	7%
	Waste	2%	3%	4.5%
	Ecology	6.5%	15%	14%
Innovation		5.5%	5%	2%

It is shown in the table above that each system gives a different weighting to each category, as each region focuses mainly on one category more than the other in terms of the issues-at- stake and according to the policies or strategies of the region towards sustainability. LEED's main focus is on community layout reflecting the United States most common planning problems. BREEAM's main focus is on community layout and transportation.

PEARL's main focus is on environmental issues, specifically water and energy issues as the very hot weather and the scarce water resources are considered problems of main concern in the United Arab Emirates. Similarly, a new rating system for neighbourhoods has to be made for the Egyptian context as it is a different region with its own characteristics and own needs. Moreover, waterfront neighbourhoods have specific issues reflected in the principles outlined in section 3. The following section will examine some examples of waterfront communities which applied the three above - mentioned rating systems to deduce any aspects that had been added and how useful the indicators are.

IV. ANALYTICAL EXAMPLES OF WATERFRONT COMMUNITIES APPLYING SUSTAINABILITY RATING SYSTEMS

Three types of waterfront cities which apply the categories of the sustainability rating systems are studied and analyzed. The first example is the city of Toronto, Canada, which applied the guidelines of LEED rating system on West Don Lands waterfront community. The second is Media city, UK, which applied the guidelines of the BREEAM rating system on the waterfront area. The third is Abu Dhabi, UAE, which applied the guidelines of the PEARL rating system on Mina Zayed waterfront community. The framework previously discussed will be used to compare between these examples and their implementation to methods of sustainability.

The case studies were selected by a simple methodology which is demonstrating the principles of sustainability. This concept is seen in the 3 examples but with different applicability due to their location, and this is the reason for analyzing examples in three different regions to learn how each region dealt with its surrounding environment to be sustainable.

A. West Don Lands, Toronto, Canada (TWDI, 2002)

The Toronto waterfront development has received the LEED for neighborhood development gold certificate with a total of 61 points achieved. Shown in Table 4 is a summary of the application of Toronto waterfront to the LEED points of sustainable development.

Table 4. Summary of Toronto's application of LEED

Common Categories		Application (Toronto LEED achievement)
Community layout		• smart mixed use neighborhood design • HIGH % Parks & opens spaces connected to the waterfront • 90% within ¼ mile to transit stops, 50% within ½ mile to services, 99% within ½ mile to schools
Buildings		• 60 % LEED certified buildings - 20% Affordable renting
Transportation		• Increased % multi modal transport, cycling, reduced car use
Environment	Water	• 15% reduction in water consumption due to Enwave project • New storm water collection system
	Energy	• 27% reduction in energy use • 30% energy supplied renewable sources Enwave deep water technology
	Materials	• Using recycled materials in infrastructure
	Waste	• Recycling 50% of construction waste - Waste diversion
	Ecology	• Preservation of the habitat near the water body by natural parks • Enwave technology reduces tones of CO2 emissions

Table 5. Summary of Media city application of BREEAM

Common Categories		Application (BREEAM achievement)
Community layout		• Mixed use compact development • Decreased % of industrial sites & increased % of commercial & residential to 96% • Radial planning centered towards waterfront • One Huge open space on the waterfront
Buildings		• 80% BREEAM certified buildings
Transportation		• Using canal in water transportation • Increased % of multi modal transport • Encouraging cycling through providing special lanes
Environment	Water	• Water resources management • Use of water from the canal to create a combined heat & power plant energy system (Tri Gen plant)
	Energy	• Tri Gen plant as a renewable source of energy
	Materials	• 80% of construction timber environmentally friendly
	Waste	• New waste management plan for waste collection and recycling • Production of fuel from waste & using it in a power plant on site
	Ecology	• Reduce air pollution by the tri gen plant & the increased use of public transport • Major Brownfield urban regeneration

B. Media City, UK (BRE Global, 2006), (BREEAM Communities, 2009)

MEDIACITY UK is the first scheme in the world to become a BREEAM approved sustainable community. The project achieved a Score of 76%: Potential Final Certificate Excellent.

Table 5 below is a summary of the application of Media city waterfront to the BREEAM points of sustainable development.

C. Mina Zayed Community, Abu Dhabi, UAE (Abu Dhabi Urban Planning Council,2010)

Mina Zayed is a new community mixed use project development on the waterfront of Abu Dhabi developed by ALDAR corporation. Mina Zayed's ambition is to create an integrated and sustainable new waterfront community that affords a vibrant example for the future development of Abu Dhabi. Table 6 below incorporates many practices for achieving Estidama.

Table 6. Summary of Abu Dhabi application of Pearl

Common Categories		Application (pearl achievement)
Community layout		• Mixed use compact development • 20% open spaces & parks on the waterfront • continuous shaded pedestrian routes that link the center to it's waterfront.
Buildings		• 99% PEARL certified buildings • Housing variety
Transportation		• Multiple transportation options and transit supportive practicesto reduce car use • Street management between car lanes, rails & walking lanes
Environment	Water	• Low water use landscape • Utilize biological water treatment systems with least energy consumption
	Energy	• District cooling strategy • Green roofs & compact development for shading & cooling
	Materials	• Use of local materials, reuse and recycle materials
	Waste	• waste management plan • recycle a large % of the demolition of industrial site
	Ecology	• Conserving the shoreline • Re-introducing nature on a formerindustrial site • High % of parks reinforce the natural systems and help in habitat creation

The analysis of the three previous examples and their implementation of the different rating systems prove that all the previous rating systems are concerned with the environmental factor of sustainability more than the social and economic factors (Given that Environmental, Social and Economic are the 3 pillars of sustainability(WCED, 1987).

Another conclusion is that all the rating systems when dealing with a waterfront community include rating categories like waterfront (water body or wetland) conservation either from pollution or from habitat extinction which are environmental aspects, but there are no rating categories for integration with the waterfront ; the social and economic aspects (other 2 pillars of sustainability) for example, specifying the percentage of open spaces which must be on the waterfron or the type of land use on the waterfront, or the percentage of recreational facilities which must be on the waterfront as all these principles increase the social and physical interaction between people and the waterfront as well as the economic values pointed by the principles in section 2.

Although these indicators were not required in the rating systems, the examples succeeded in applying some of them to integrate with the waterfront, which means that integration with the waterfront is an important feature for sustainable planning and must be considered under any rating system when dealing with a waterfront. So, a set of new indicators concerning waterfront development, including environmental, social and economic aspects of sustainability along with the categories discussed before will be taken to form a rating system to be implemented on the case study of Abu Qir area.

Integration with the waterfront, a comparison		Principles of sustainable waterfronts:
Toronto	•Reduce water consumption from the river •Benefit from water by Enwave water technology	1 - Secure the quality of water and the environment
Media city	•planning order is almost radial (centered towards the waterfront) •Huge open space on the waterfront	2 - Waterfronts are part of the existing urban fabric
		3 - The historic identity gives character
		4 - Mixed use is a priority
		5 - Public access is a prerequisite
Mina Zayed	•Preventing pollution of the water by removing former industrial land •20% of the project's total area is dedicated for open spaces, parks and green areas, most of these spaces are on the waterfront interconnected to each other by the green lanes	6 - Public participation is an element of sustainability
		7 - Planning in public private partnerships speeds the process
		8 - Waterfronts are long term projects
		9 - Waterfronts profit from international networking
		10 - Re-vitalization is an ongoing process

A set of Indicators « Integration With The Waterfront »

Degree of Integration with the water body
Degree of benefiting from the water source
Sea Level Rise management using network of streets and parks
% Open spaces on the waterfront
Land use adjacent to or on the waterfront
% Recreational facilities on the waterfront
Linked facilities and open spaces on the waterfront

Common Categories	
Community layout	
Buildings	
Transportation	
Environment	Water
	Energy
	Materials
	Waste
	Ecology
Innovation	
Integration with the waterfront	

Fig .1. Conclusion, addition of a new category « Integration With The Waterfront » & the indicators under it

V. ANALYTICAL REVIEW OF ALEXANDRIA'S WATERFRONT (ABU QIR AS A CASE STUDY)

Abu Qir area analysis includes a study of it's physical, environmental and historical features. In the following subsections, the problems of the area are concluded and organized in terms of priority, under the five categories of the framework.This helps in determining what the biggest problem of the area is like, which must be considered first. Afterwards, the other potential problems should be considered prior to the urban development of the area as well. The study is based on a document review of the future comprehensive planning for the development strategy of Abu Qir area, including site visits, observtions, interviews, together with consulting experts of urban planning, coastal planning and environmental design.

A. Abu Qir Review

Alexandria city is the second largest city in Egypt, either in terms of population or economical growth. Located on the Mediterranean sea with a length of 93.5 km on the waterfront from Abu Qir bay on the east up to Matrouh city on the west. Abu Qir (shown in Fig.2) is one of the communities of Montazah District in Alexandria city with an area of 60 km2 from the total area of the Montazah district which is 81 km2 (Alexandria Governorate, 1984). Abu Qir with a population range of 200,000 residents consists of 3 neighborhoods which are Abu Qir, Toson, and Mamoura Elbalad. It represents one of the most important historical places in Egypt (Alexandria

comprehensive plan 2017).

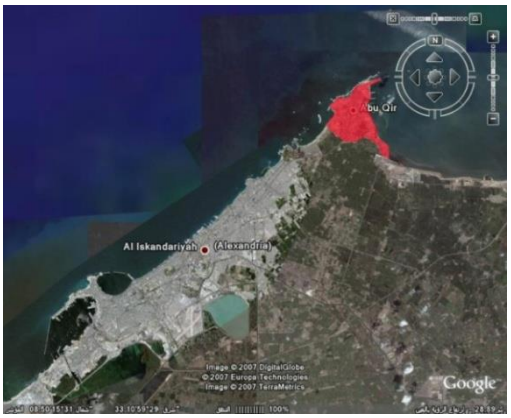

Fig .2. Location of Abu Qir
Source: Google maps, accessed June 2011

B. Motives for Replanning

- It is a strategic location as it is considered an eastern gate to Alexandria.
- There are a lot of motives for development: a waterfront with many brownfields, unplanned open spaces, historical sites and sunken treasures (Goddio, 2007; Encyclopaedia of the orient, May 2011)
- It has three important historical fortresses: El-Sabaa, Tawfeekeya and El-Raml fortresses, which could form an important historical tour in Alexandria as they represent an important era in the history of Egypt. Unfortunately, they strongly need a great work of rehabilitation and renovation.
- Abu Qir bay (lying on a Dead Sea area) is considered a fertile marine habitat when compared with other Egyptian Mediterranean coastal waters (ASRT, 1984; Hamouda & Abdelsalam, 2010).
- Abu Qir bay can be used for a variety of purposes: commercial and recreational fishing, shipping, recreational boating, yachting, swimming and diving to explore sunken monuments.
- Abu Qir is famous for its warm temperature and warm seawater which facilitate the development of a lot of recreational beaches and touristic facilities on the waterfront which can enhance and promote the economic development of the area.

C. Site Analysis:

In the map below having a master plan for the city, we can observe from the land use, accessibility and building conditions analysis that martial sites occupy a large area of the waterfront which act as a barrier between central Abu Qir and the waterfront. As a result, scattered parts of groups of buildings are left in the center. Another barrier is the train line which seperates west Abu Qir from east Abu Qir.

Fig .3. Map showing the Master plan, street layout in Abu Qir
Source: the researcher

D. Problems of the Site

After analyzing the context of Abu Qir area as a whole, its natural, historical, economic and touristic features along with its land use, accessibility and building conditions, the following problems are concluded as follows.

- Problems Related to Community Layout and Integration with the Waterfront

Abu Qir area is not well connected to it's waterfront due to the following :

1- The absence of pedestrian accessible streets leading to the waterfront (either very narrow streets between slums which are the residential areas on the waterfront, or inaccessible streets inside military sites on the waterfront).

2- Inefficient street layouts which lead to the presence of only one main street as an entrance to Abu Qir and Touson areas after Mamoura neighborhood (Gabr, 2009)

3- The absence of connected open spaces on the waterfront.stable till it reaches the outlet.

Fig .4. Presence of a lot of high illegal buildings on the waterfront

4- The absence of well developed attractive beaches or recreational facilities on the waterfront

5- The absence of usable (opened) marines which can connect the area altogether if water transport is present.

6- The presence of military sites in separated zones on the waterfront which cut the way between Abu Qir downtown and the waterfront.

Fig .5. presence of martial sites in separated zones

7- The land use in Abu Qir area is either residential or industrial, plus the martial sites which occupy large areas in Abu Qir region (no mixed land use).

8- The presence of unplanned areas and scattered slums.

9- The presence of a lot of agricultural or space lands which separate Abu Qir urban zone from the rest of Alexandria.

10- The calculations of population density in Abu Qir community, made by Alexandria governorate have proven that there is a continuous growth in population density in Abu Qir area without a balance in job opportunities, facilities, housing and infrastructure (Alexandria comprehensive plan for 2017, 1997)

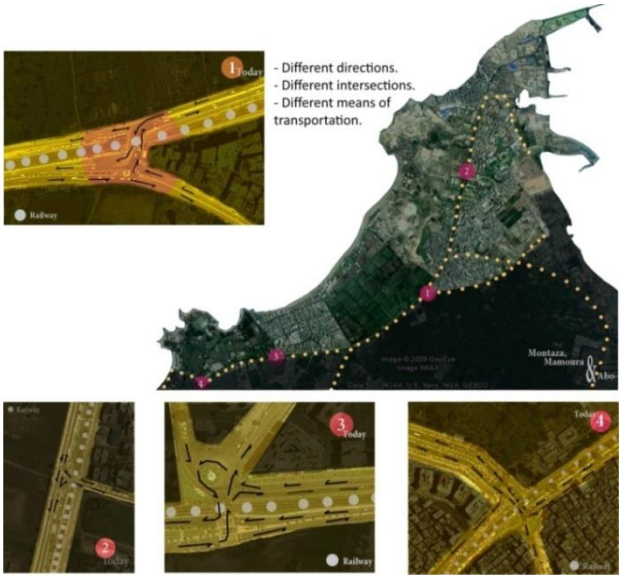

Fig .6. Trafic Problems in Abu Qir
Source : Researcher

- Problems Related to Transportation

1- Growth in population with insufficient public transportation leads to increasing reliance on private cars and buses

2- Occurence of continuous traffic jam due to increasing number of cars.

3- Occurence of traffic problems and accidents due to unplanned intersections and the absence of stop signs.

4- Number of trains reaching Abu Qir train station is not big enough to meet the need targeted as it is the only means of transportation for most workers in Abu Qir area. Moreover, trains and train lines are too old, dirty and don't work with full power (Gabr, 2009)

5- Train lines occupy large space of the street width increasing traffic conjestion. They also form a barrier between west and east of Abu Qir as they are closed with a high wall barrier.

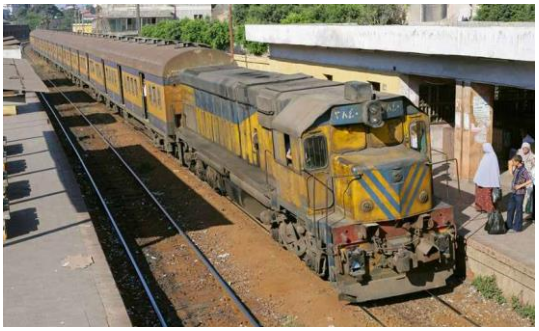

Fig .7. The problems of transport in Abu Qir source : researcher

- Problems Related to Transportation

1- Illegal high buildings on the waterfront of Abu Qir (Alexandria governorate, 1997)

2- The Presence of slums and narrow streets, with deteriorated buildings scattered here and there makes it impossible to supply such places with efficient infrastructure needed (waste, water supply, electricity, gas, sewage grid, telephone lines …. etc)

3- The presence of illegal fast construction projects everywhere, streching out to the sea shore leads to the sloping down of buildings and in some cases collapsing. They also lead to the emergence of unplanned streets and narrow corridors. These illegal buildings never comply with the architectural character of theplace.

Fig .8. The problems of buildings in Abu Qir Source: http://www.flickr.com/photos/david_vilder

- Problems Related to Waste

1- The presence of a lot of areas with no supply of drainage pipes leading to draining in wells. These wells cannot be reached by maintainace cars because the streets are very narrow, consequently a blockage of these wells occurs leading to sanitary problems.

2- Water pollution of Abu Qir bay due to untreated sewage and industrial waste discharged from different sources like El-Tabia pumping station. This station discharges polluted industrial waste from factories of food processing, canning, paper, fertilizers and textiles. The outlet of Idku Lake which contains drainage water from agriculture, usually containing pesticides, is another source of pollution. Added to this is the Rosetta mouth of the Nile River which discharges fresh water carring agricultural waste from cultivated lands. (Nasr, et al., 2003)

3- No waste collection which leads to accumulation of waste in front of buildings and houses.

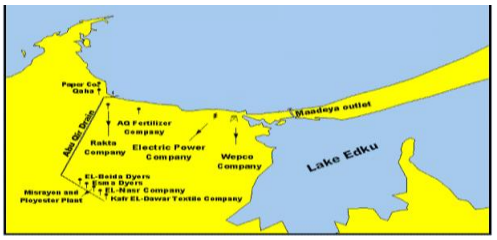

Fig .9. The study area where the arrows indicate the sources of pollution along Abu-Qir Bay Source: the researcher

Fig .10. The problems of waste in Abu Qir Source: http://www.flickr.com/photos/david_vilder

- Problems Related to Water

  1- Infrastructure problem related to sewage grid, leading to insufficient number of sewers that cause water blockage in the streets during rainy days of the year. (Alexandria governorate comprehensive plan for 2017)

  2- No water supply in many areas (particularly slums) which drives many citizens to practice unlawful activities to have water supply connections.

- Problems Related to Environment

  1- Air pollution from different industrial factories in Abu Qir (Kamel, 2002)

  2- Water pollution in the eastern area of Abu Qir bay (Dead sea) from ships and marine waste (Gabr, 2009)

  3- The problem of climate change is being taken seriously by the Egyptian authorities. The low lying land in the Nile Delta region is considered to be at risk due to the potential effects of any sea level rise resulting from global warming. In particular, the cities of Alexandria, Rosetta and Port Said, which are major industrial and economic centres, are expected to experience serious environmental impacts, if no action is taken (El-Raey, 2009).Therefore, as long as Abu Qir region represents a large area of the coast of Alexandria, it is considered to be at a high risk of submerging.

- Problems Related to Energy

  1- The absence of any means of energy saving in buildings or in the community as a whole due to all the previous problems.

  2- Although Abu Qir area in particular (and Alexandria in general) is one of the most sunny places in the world, still there is no benefit from the sun as a renewable source of energy.

E. Conclusion

Referring to the previous problems, the document review of the future comprehensive planning for development strategy of Abu Qir area, the site visits, the interviews, plus the consulting experts in urban and coastal planning as well as environmental design, it is concluded that most of the problems which are present in Abu Qir area are problems related to community planning and integration with the waterfront. Moreover, the other problems of transportation, buildings and environment are all due to the unplanned community of Abu Qir, and can be solved if community planning and integration with the waterfront are maintained. As a result, community layout and integration with the waterfront should have the highest priority (as shown in Fig.10) when considering a developmentproject. The problem of transportation, which is the second significant issue comes next. It should be solved instantly as Abu Qir area is full of workplaces and important facilities that have to be easily reached and made use of. Next to transportaion is the problem of existing buildings. Though it is not as important as transportation; still the field study and survey show that building conditions, heights and utilities constitute a major problem of concern. Then comes the environmental category that forms higher levels of sustainability. This is explained by colouring priority table from red as the highest priority to violet as the lowest one.

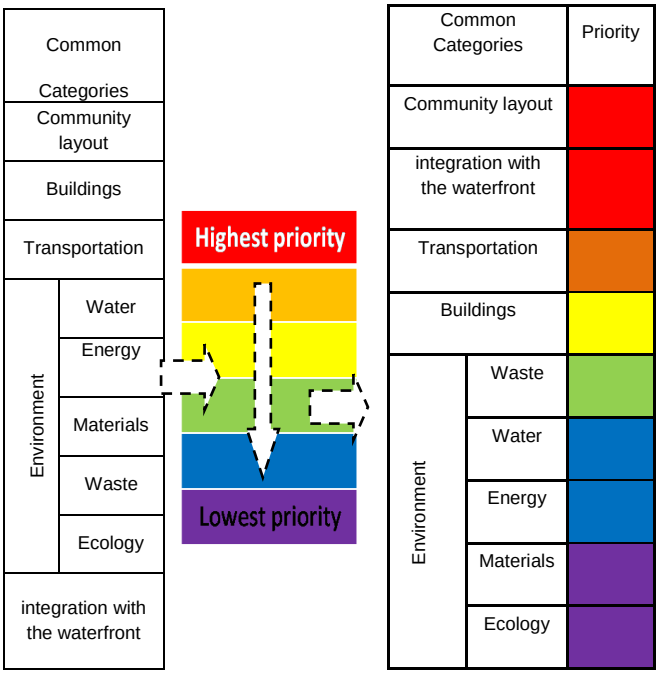

Fig .11. Defining priorities from problems of the case

F. Implementations of Sustainability Guidelines in Development of Abu Qir

Abu Qir community sustainable urban planning needs to consider all of the previous categories resulting from the problems discussed above, bearing in mind to follow the same priority order. Rrenovation and rehabilitaion works should be environmentally, socially and economically sustainable. Each indicator under those categories is chosen from one of the rating systems analyzed, The indicators chosen are only the indicators that concern the problems in Abu Qir area. In addition to the indicators specific for the waterfront (concluded in section 4), a checklist of recommended criteria should be set for the replanning of Abu Qir area.

Table 7. shows The Checklist of criteria produced for sustainable replanning of Abu Qir

Category	Indicator
Community layout	Open community
	Compact development
	Diversity of uses
	Street network
	Access to public spaces
	Universal accessibility
	Community outreach & involvement
Integration with the waterfront	Degree of Integration with the water body
	Degree of benefiting from the water source
	Open spaces on the waterfront
	Land use adjacent to or on the waterfront
	Recreational facilities on the waterfront
	Linked facilities and open spaces on the waterfront
Transport	Public transport
	Reduced automobile dependence
	Bicycle network
	Transportation demand management
	Transit facilities
	Street network
	Walkable streets
	Reduced parking footprint
	Traffic management
Buildings	Energy efficient buildings
	Construction pollution prevention
	Reuse of historic buildings
	Building reuse & adaptive reuse
	Housing & jobs proximity
	Diversity of housing types
	Affordable housing
Environment – Waste	Waste management
	Proximity to waste water infrastructure
	Construction waste management
Environment – Water	Water resources management
	Water consumption management
	Community water strategy
	Wet land & water body conservation
	Building water guidelines
	Water monitoring & leak detection
	Community water use reduction: Landscaping
	Community water use reduction: Heat rejection
	Community water use reduction: Water features
	Storm water management
	Water efficient buildings
	Proximity to water infrastructure
Environment – Energy	Energy consumption management
	Community energy strategy
	Building energy guidelines
	Energy monitoring & reporting
	Community strategies for passive cooling
	Urban heat reduction
	Renewable energy: Onsite
	Renewable energy: Offsite
	Energy efficient buildings
	Infrastructure energy efficiency
Environment – erial	Local materials
	Recycled materials
Environment – Ecology	Biodiversity
	Conservation management of habitat & wetland
	Natural systems protection
	Reuse of land
	Remediation of contaminated land
	Habitat creation & restoration
	Local food production
	Minimize site disturbance through site design
	Minimize site disturbance during construction
	Heat island reduction
	Solar orientation
	Reduce air pollution

VI. CONCLUSION

There is a need to develop a rating system specifically for the evaluation and upgrading of Abu Qir as a waterfront community. The rating system should consider the following:

- Priorities first (biggest problems are the first

to be solved).

- Creation of connections between waterfront and inner City districts.
- Benefit from the water source either physically or environmentally.
- Water as a means of transportation to reduce city traffic and improve the quality of the urban environment.
- Public accessibility to the waterfront by linking open spaces and recreational facilities to increase social and economic income.
- Utilization of unused land on the waterfront to serve the previous point.
- Revival of the waterfront with attractive uses, high-quality public spaces, and publicly oriented water-dependent uses, integrated with adjacent communities.
- Maintenance and improvement of the environmental quality of water bodies, land and air.

VII. Concluding Remarks

Waterfront sustainable development is now an obligation for all waterfront cities. However, Waterfront planning differs from one place to another according to the needs and problems of the region.That is why all rating system must have it's own weighting sustainable strategies are the same worldwide, they all call for the same principles. On the other hand, different obligations, rules and regulations are applied to them according to the needs and problems of each region. The Egyptian region (Waterfront in particular) needs its own sustainability rating system. Pursuing strategies to improve the sustainability of the city's waterfront, the government should focus on increasing resilience to climate change and projected sea-level rise. Economic interests must be balanced with environmental and social concerns. However, waterfront work is not just about economic development; yet it is not simply a design question or only about environmental issues. Rather, it is a fusion of these elements and related disciplines like Balance-People-Recreation-Public access-Open space-Safety-Suitable and Diverse Living-Mix of Uses- Environment- Transport which are all principles of sustainability.

REFERENCES

[1] Abdel-Shafy, H., & El-Saharty, A. (2007). RAINWATER ISSUE in EGYPT: QUANTITY, QUALITY AND ENDEAVOR of HARVESTING. Alexandria: Water Research & Pollution Control Department, National Research Centre, National Institute of Oceanography and Fisheries.

[2] Abu Dhabi Urban Planning Council. (2010, August). Estidama A to Z. Retrieved October 12, 2010, from Abu Dhabi Urban Planning Council,: www.upc.gov.ae

[3] Abu Dhabi Urban Planning Council. (2010). Estidama Excellence Projects. Abu Dhabi: Estidama.

[4] Abu Dhabi Urban Planning Council. (2010). The Pearl Rating System for Estidama: Community Rating System. Abu Dhabi.

[5] [Academy Center of Engineering Consultancy & Development. (2009). Project Proposal For Strategic Planning of Abu Qir. Alexandria.

[6] Alexandria Governorate. (1984). Alexandria Comprehensive Plan for 2005. Alexandria University.

[7] Alexandria Governorate, (1984). Comprehensive Plan Alexandria 2005. Comprehensive Master Plan Project, Final Report 1984.

[8] Bell, S., & Morse, S. (2008). Sustainability Indicators: Measuring the Immeasurable? UK: Earthscan.

[9] BRE. (2009). Certification Scheme for BREEAM COMMUNITIES. UK: BRE Global Ltd.

[10] BRE Global. (2006). Creating Sustainable Communities. UK.

[11] BREEAM communities. (2009). Improve, Measure & Independently Certify the Sustainability Of Planning Proposals. UK: BRE Global LTD.

[12] (2002). BREEAM Communities:Sustainable Assessment Framework. UK: BRE-Global.

[13] Breen, A., & Rigby, D. (1996). The New Waterfront. New York: McGraw Hill.

[14] Brundtland, & al., G. (1987). Our Common Future. Oxford: Oxford University Press.

[15] Campbell, S. (1996) Green Cities, Growing Cities, Just Cities? Urban Planning and the Contradictions of Sustainable Development, Journal of the American Planning Association (summer 1996) [online]. Available at: http://www-personal.umich.edu/~sdcamp/Ecoeco?Greencities.html [accessed 7/6/2005]

[16] Consultant Body for the Follow up of Alexandria Comprehensive Planning. (2003). Abu Qir Economic Resources. Alexandria: Alexandria University.

[17] Consultant Body for the Follow up of Alexandria Comprehensive Planning. (2003). Futuristic Planning of Abu Qir. Alexandria University.

[18] Egyptian Green Building Council (EGBC). (2009). The GREEN PYRAMID Rating System,. Egypt.

[19] El-Raey, M. (1999). “Impact of Climate Change on Egypt”. Retrieved July 14, 2009, from Environmental Software and Services: http://www.ess.co.at/GAIA/CASES/EGY/impact.html

[20] Gabr, M. (2009). Futuristic Vision for Urban Planning of Abu Qir District- Alexandria. Alexandria: Urban Planning Center, College of Engineering, Arab Academy for Science & Technology.

[21] Giovinazzi, O., & Giovinazzi, S. (2008). Waterfront Planning: A Window of Opportunities for Post Disaster Reconstruction. Italy: i-Rec.

[22] Giovinazzi, O., & Moretti, M. (March 2010). Port Cities and Urban Waterfront: Transformations and Opportunities. TeMaLab journal of Mobility, Land Use and Environment, Selected Papers 2009 , Vol 3 - SP - (P.57 - 64).

[23] Goddio, F. (2007). EGYPTIAN MONUMENTS. Retrieved September 25, 2007, from EGYPT SITES: www.egyptsites.co.uk/lower/delta/western/abuqir.html

[24] GOPP. (1997). General Plan for Alexandria City For 2017, Cairo, Egypt

[25] Hamouda, A., & Abdel Salam, K. (January, 2010). Acoustic Seabed Classification of Marine Habitats:Studies in the Abu-Qir Bay, Egypt. Journal of Oceanography and Marine Science , Vol. 1(1). pp. 011-022.

[26] Hall Peter, Pfeiffer Ulrich (2000), Urban Future 21. A Global Agenda for Twenty First Century Cities, London, E& FN Spon, 363pp., ISBN 0-415-24075-1

[27] Hansen, L. (2008). "Rising Sea Levels Threaten Egypt's Ancient Cities". Retrieved July 28, 2009, from http://www.npr.org/templates/story/story.php?storyId=89660898

[28] International Centre Cities on Water. (2005). Waterfront Redevelopment As Strategic Factor of Urban Regeneration. Venice (Italy): International Centre Cities on Water.

[29] JULIEN, A. (2006). BREEAM VS LEED. SUSTAIN' , vo.9, i06, p.30-33.

[30] Kamel, W. (2002). Integrated Environmental Study Of Abu Qir. Alexandria.

[31] M.Dill, P., & J.Bedford, P. (2001). MAKING WAVES: PRINCIPLES fOR BUILDING TORONTO’S WATERFRONT, CENTRAL WATERFRONT PART II PLAN. Toronto.

[32] Marshall, R. (2001). Waterfronts in Post-Industrial Cities. Spon Press.

[33] Merz, S. K. (2009). BREEAM Communities-Media city. Retrieved June 12, 2010, from BREEAM Communities: www.breeam.org/communities

[34] Ministry of State for Environmental Affairs. (2007). Environment 2006- Number of Garbage Recycling Factories. Alexandria: Alexandria Governorate- Comprehensive plan 2015.

[35] Munda, G (2001) Indicators and Evaluation Tools for the Assessment of Urban Sustainability [online]. Available at: www.h-economicauab.es/cat/papers/10-2001.pdf [accessed 23/5/2003]

[36] Nasr, S., El-Raey, M., El-Shenawy, M., Okbah, M., Abulsoeud, A., El-Hattab, M., et al. (2003). Assessment of Water Quality of Abu-Qir Bay Along The Mediterranean Coast Of Egypt. Alexandria: Institute of Graduate Studies & Research, Alexandria University.

[37] Owens, S. and Cowell, R. (2002) Land and Limits – Interpreting Sustainability in the Planning Process. London: Routledge.

[38] Palmer, A. (2008). "Rising Sea Levels, The World Bank Report". Retrieved July 12, 2009, from http://www.theworldincrisis.com/artman2/publish/climate/Rising_Sea_Levels.shtml

[39] Rydin Y, Holman N and Wolff E (2003) Local Sustainability Indicators,Local Environment, 8 (6), pp. 581–589.

[40] Said, R. (2001). Sunken treasures, sunken myths,. Al-Ahram Weekly Online , Issue No.553, 27 Sep. - 3 Oct.

[41] Tanguay, G., J., Rajaonson, Lefebvre, J-F & Lanoie, P. (2009) Measuring the Sustainability of Cities: A Survey-Based Analysis of the Use of Local Indicators. CIRANO: Scientific series, 2009s-02.

[42] Toronto Waterfront Design Initiative. (2002). Urban Design Report 1 . Toronto: Toronto Waterfront Revitalization Corporation.

[43] TORONTO WATERFRONT REVITALIZATION CORPORATION. (2005). EAST BAYFRONT PRECINCT PLAN. TORONTO: TORONTO WATERFRONT REVITALIZATION CORPORATION.

[44] TORONTO WATERFRONT REVITALIZATION CORPORATION. (2005). EAST BAYFRONT PRECINCT PLAN., (pp. 11-20). Toronto.

[45] Toronto, W. (2008). LEED for Neighbourhood Development. Toronto: Credit Valley Conservation Authority – Strategic Sustainability Workshop.

[46] USGBC, C. f. (2009). LEED for Neighborhood Development. United States: U.S Green Building Council.

[47] Vallega, A. (2001). Urban Waterfront Facing Integrated Coastal Management. Ocean & Coastal Management, ElSevier , Volume 44, P.379–410.

[48] Waterfront Toronto. (2009). Mandatory Green Building Requirements. Toronto.

[49] Waterfront Toronto. (March 2010). Waterfront Toronto Environmental Management Plan for Project-Related Activities. Toronto.

TRIPLE –E VESSELS: TONNAGE MEASUREMENT AND SUEZ CANAL DUES ASSESSMENT

ELSAYED HUSSIEN GALAL
Vice director of Suez Canal transit department
Email: galallelsayed@gmail.com

Abstract **-** Container industry is growing faster than GDP; Shipping lines always attempt to augment efficiency by reducing cost and by attracting larger volumes of containers. As a result, rising container freight rates leads to an increase of the economic scale of the lines that have been driven, by building mega ships and making more efficient port calls. In 2011 Maersk line ordered up to 20 new "Triple- E "Class of container vessels to be delivered between 2013- 2015. This class of mega container vessels has its way through Suez Canal. Other companies like CMAand CGM also ordered this type of mega container vessels in order to reach higher profits due to the achieved economic scale. It is believed that 20000 TEU could be the next target size. Present mega container fleet of vessels and any future potential vessel capacity demand an expansion for Suez Canal route to handle vessels larger than 18000 TEU. This will put Suez Canal route in strong competitive position. Meanwhile Panama Canal will not be able to handle vessels larger than 12600 TEU even after its expansion in 2015.

Keywords **-** Triple – E Vessels – Tonnage measurement – Suez Canal rules.

I. INTRODUCTION

Various types of vessels transit Suez Canal. On top of these ships, come container vessels which represent 56% of total Suez Canal net tonnages and 60% of Suez Canal total revenues. Specifications and characteristics of Triple –E vessels have been studied. It is worth mentioning that Triple-E vessel pay about one million US dollars as transport dues when transiting Suez Canal. At the same time the cost of TEU transiting Suez Canal for this type of vessel is less than small types such as New – Panamax (12500 TEU) or New –Post Panamax (15000 TEU), thereby achieving high economic scale. This paper mainly highlights various methods of tonnage measurements in general and various methods of tonnage measurements for Suez Canal in particular.

II. CONTAINER VESSELS EVOLUTION

Container ships carry more than 95% of the world's manufactured goods.In the last decades container vessels became larger carriers trying to achieve high economic scales by increasing the container vessels capacity and consequently the emergence of so-called mega container vessels or ultra-large container vessels has taken place. This new generation of ships is called "Triple-E". "Triple-E" vessels have emerged taking into account the following specifications:

- Energy efficiency.
- Economics of scale.
- Environmental improvements, reducing Co2 emission by 50% per container carried.

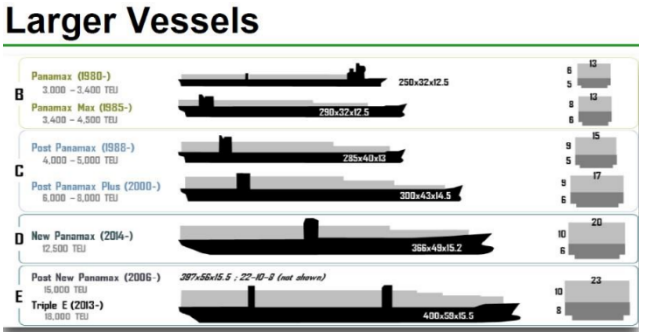

Fig .1. Evolution of Container ships

Fig .2. TRIPLE-Class

Such ships need new ports and container terminals with high specifications and sustainable maritime system. Nowadays, this type of vessels uses ASIA-Europe lane through Suez- Canal

III. TRIPLE- E CLASS IN FIGURES

Its length is approximately 400m, its width is approximately 59m, its draught is about 14.5m and its capacity is 18200 TEU (on deck approx. 10600 TEU in holds 7600 TEU). Its displacement is 55000 tons. A reefer container's capacity is 600 TEU. Its height is 73m. Its maximum speed is 23 knots, average speed is approximately 17-18 knots. Rows in hold/ on hatches are about 21/23, Tiers in hold/ on Hatches are about 11/10.

Fig .3. TRIPLE-Class

The HHI 18,000 TEU Class container ship is the largest container vessel ever developed by HHI. The vessel is based on HHI's advanced ship-building technology and experience. A single-skeg hull form has been adopted and optimised for various operating draughts and speeds, reflecting various clients' needs.

TEXT: JEIWOO JANG, HYUNDAI HEAVY INDUSTRIES CO., LTD.

Fig .4. Longitudinal Section of 18000 TEU Ship

The economics of ship size are the driving force for increasing numbers of containers transported. The aforementioned dimensions of "triple- E" vessels are outside the ability of Panama Canal dimensions even after its recent expansion project. Also it has 30% less power per ton displacement than the other vessels (EMMA MAERSK, MARCO POLO). This is mainly because the "triple- E" vessels will be sailing at the utmost power speed because it has a full U-shaped body and is more spacious than traditional containerships; accordingly one extra row of containers has to be accommodated. The engine room has been put at the rear of the ship instead of the middle, so it is able to fit in more containers behind the navigation bridge and in the hull.

IV. ENERGY EFFICIENCY OF TRIPLE-E VESSELS

A waste heat recovery system helps propel the ship by capturing energy from the engine's exhaust gas. This cuts fuel by up to 10%. The, energy is also used to produce electricity for the onboard accommodations. The waste heat recovery system on "Tripe – E" vessels has allowed to use a smaller and less energy, consuming main engine speeds in the range of 20- 25 knots. Now, these speeds had dropped to 15-17 knots lesser than it was commonplace 5 years ago,

V. ENVIRONMENTAL IMPROVEMENT

Triple-E" vessels are a combination of carefully thought-of technological and ecological solutions, as well as the result of many years of engineering work. They will enhance the ecological solutions and performance.

Better fuel efficiency may be the easiest way to cut down on both air pollution and greenhouse gases. Thus, "Triple-E" vessel innovative design and technological features will help reduce its CO2 emissions by more than 50% for every container it moves. Also it has a waste heat recovery system that reduces fuel consumption. Emissions of air pollutants from the shipping sector have increased substantially in the last two decades, contributing to both climate change and air pollution problems. In 2007 shipping sector was responsible for 3.3% of global carbon dioxide emissions. This sector has contributed to the growing of emissions by 4% per year over the next decade .If ships reduced their speed by 10% , which is known as " slow steaming ", they could cut and reduce carbon footprint.

VI. PROBLEMS FACING TRIPLE- E VESSELS

The greater outreach required to service the ship's extra row of containers will mean longer booms. The booms also must be located at a greater height than the height of the ship's container stacks which also creates a number of new stresses. The wind forces on the crane will be higher which has an impact on wheel loads [1].

The capital cost per TEU moved has increased even, considering the increase in slot size of the vessels.

Furthermore, due to the increase in transportation duration, the capital cost and insurance of goods transported have gone up. Furthermore the cost increase could be influenced by the time-length taken by goods that need longer to get from the world's production centers to the markets. Goods that move faster cost less. Shipping lines are demanding ever shorter port stay in order to make the economies of scale work. Longer vessels of 400 yards (such as Maersk Line's "Triple-E" class) will lead to more berth wastage to handle efficiently. High port productivity and reliability are essential to enable carriers to operate within schedules. The bigger the ship, the greater the cost of hours lost in port, and an increased port stay is a diseconomy of scale [2].

VII. IMPORTANCE OF CONTAINER SHIPS IN SUEZ CANAL

The Suez Canal plays a pivotal role in today's global container shipping network, particularly in accommodating vessels that sail on the important. ASIA- EUROPE trade lane. Container ships accounted for about 56% of Suez Canal total net tonnages and 60% of total revenues. The charge of containerized cargo also is still rising. The number of TEUs transiting the Suez Canal is still growing , it has reached (42.1 million TEUs) in 2014 , (38.2 million TEUs) in 2013 and (37.7 million TEUs) in 2012 .The following data illustrates the importance of container vessels traffic through Suez Canal (as stated on tables 1 & 2).

Table 1. Number of container ships and its net tonnages (2010- 2014) : Source: Suez Canal Authority

Year	No. of Container vessels	Container ships net tonnages (million tons)	Total net tonnages of ships in Suez Canal (Million Tons)	Ratio of net tonnage of container ships%
2010	6852	465.7	846.4	55
2011	7178	519.3	928.5	55.9
2012	6332	507.1	928.5	54.6
2013	6014	508.2	915.5	55.5
2014	6129	536.3	962.7	55.7

Table 2. Containerized Cargo in Suez Canal : Source: Suez Canal Authority

Year	Containerized cargo (million tons)	Total Cargo (Million Tons)	Ratio of containerized Cargo %
2010	367.0	646.1	56.8
2011	397.2	691.8	57.4
2012	398.0	739.9	53.8
2013	406.1	754.5	53.8
2014	435.0	822.3	52.9

Comparing containerized cargo with the total cargo in Suez Canal, we find it ranging between 54% to 57% as stated in table 2.

VIII. IMPORTANCE OF TONNAGE IN MARITIME WORLD

Maritime institutes and departments of ship engineering in Egyptian Universities does not give sufficient importance to the study of ship tonnage measurement rules in spite of its importance in maritime world. The tonnage of a ship has become important as one of its defining characteristics.

This paper is intended to define and point out briefly some of the ways that tonnage factors influence ship design. It also sheds light on how tonnage factors affect the financial responsibility of ship-owners who pay dues in accordance with the amount of net tonnage, gross tonnage or net registered tonnage.

Practically all seagoing merchant vessels operating on the open seas, bays, rivers, lakes and waterways are measured for the assignment of national gross and net registered tonnages. Also vessels intending to transit Suez Canal and Panama are measured according to the rules of the respective canal authorities. IMO rules refer always to tonnage base to its laws. Harbors and waterways dues are depending on net tonnage base or gross tonnage. Light house dues, pilotage dues, dry dock dues, wharves dues and similar facilities throughout the life of the vessel depend on its tonnage. Also, there is a correlation between tonnage and the balance and the safety rules of a ship.

The tonnage figures are used for statistics in maritime trade and for charging taxes. They are also used for comparison of national fleets, framing of policies on trade of shipping, granting of subsidies, comparison of shipbuilding, scrapping, regulatory application basis for manning, registration and survey charges, insurance premium and limitation liability in cases of pollution. For vessel registration, tonnage indicators must be offered. Shipping tonnage was a useful indicator of a country's commercial strength. It also indicates the physical carrying capacity of a ship as well as the comparison of trade and movement of goods. Tonnage has been used to indicate the relative magnitude of ships for centuries.

IX. EVOLUTION OF TONNAGE MEASUREMENT SYSTEM

A. Moorsom's system 185

Traditionally, tonnage was related to the carrying capacity of the ship. Moorsom's [3] concept related tonnage to the total volume of enclosed spaces. Being the colonial power, the British maritime legislation spread throughout the world. During the second half of the 19th century, Moorsom's system was the basis for tonnage measurement around the world, though the rules varied from one jurisdiction to another [4].

B. Suez Canal Rules 1873[5]

Initially the net register tonnage was used as a basis for Suez Canal Company tolls. Since the revenue of Suez Canal was inadequate to meet the expenses and owing to the questionable propelling power deduction for steamers, gross register tonnage was adapted as the basis from July 1872, leading to higher charges. Shipping companies and owners opposed this change. Thus, an international tonnage commission, formed to resolve the issue, adopted separate rules for Suez Canal tonnage in 1873 at Constantinople. It was expected that the 1873 rules would be adopted by the countries represented at Constantinople leading to a universal system. Separate rules for Suez Canal tonnage came into existence.

It is important here to cite the text of Annex 2 regulation for the measurement of tonnage recommended by the international tonnage commission assembled at Constantinople 1873: "General principles: The gross tonnage or total capacity of ships comprises the exact measurement of all spaces (without any exception) below the upper deck, as well as of all permanent covered and closed-in erections on that deck".N. B. by permanent covered and closed- in erections on the upper deck are to be understood all those which are separated off by decks or coverings, or fixed partitions and therefore represent an increase of capacity which might be used for the stowage of merchandises, or for the berthing and accommodation of the passengers or of officers and crew[6].This text in the Constantinople convention is the philosophical basis for estimating the Suez Canal tonnage so far.

C. Panama Canal Ad measurement system

The tonnage measurement system used in the Panama Canal is known as: Panama Canal Universal measurement system (PC/UMS), following the rules of ITC- 1969, using its parameters to determine the total volume of a vessel with the additional variations established by the authority. The ACP ad measurement system for a full container vessel reflects the international standard for a container TEU. This measurement considers the full container carrying capacity of vessels (above and below deck). In October 2002, the Panama Canal Authority decided to charge container vessels in a new method based on TEU, since the PC/UMS net tonnage was not representing the earning or economic capacity of

container vessels[7].

D. International convention on Tonnage Measurement of ships, 1969 (ITC- 69)

The efforts for a uniform method materialized when the convention on tonnage measurement of ships (ITC- 69) was adopted at an international conference held in London from 27th May to 23 June 1969. It was the second successful attempt to introduce a universal tonnage measurement system. The first attempt in 1873, when the Maritime powers assembled at Constantinople and adopted the rules of Suez Canal measurement system.

ITC- 69 applies to ships above 24 meters long and came into force on 18th July 1982. A phase in period was given for the ships built before that date to retain the existing tonnage figures up to 18th July 1994, for a smooth transition to the new system. The Suez Canal and Panama Canal Company continued with their separate methods for tonnage measurement even after adopting (ITC- 69).150 states amounting to 98.9% of world tonnage have ratified the convention, as of 31th July 2010 [8]. Under ITC-69 the overall size and useful capacity of a ship are indicated by dimensionless figures, GT and NT respectively (instead of GRT and NRT under Moorson's system). Calculated based on the total molded volume of enclosed spaces and volume of cargo spaces[9].

Therefore, GT= K,1 V, whereby V= Total Volume of all enclosed spaces in cubic meters, and K1= a coefficient as tabulated in appendix 2 (of the convention). This coefficient ranges from 0.22 to 0.32 for the smallest to the largest volumes and cares for results being similar to the former tonnage figures based on 100 cubic feet. For the calculation of NT, same coefficient is used together with the volume of cargo spaces, the depth and the draught. NT shall not be taken as less than 0.30 GT. Thus GT and NT are calculated independently[10].

X. SUEZ CANAL TRANSIT FEES OF TRIPLE-E VESSELS

The tonnage on which all dues and charges to be paid by vessels are assessed, is the net tonnage resulting from the system of measurement laid down by the international commission held in Constantinople in 1873, and duly entered, on the special tonnage certificate issued by the competent authorities in each country[11]. The containers on upper deck are considered as closed in spaces increasing the carriage capacity of the ship when situated over the main deck[12]. Tolls are calculated on the basis of Suez Canal net tonnage plus a Ratio specified for the number of tiers on the upper deck according to circular No. 3/2014 of Suez Canal are as follows:

1. Northbound Container Vessels

- 4% for vessels carrying one tier.
- 6% for vessels carrying two tiers.
- 8% for vessels carrying three tiers.
- 11% for vessels carrying four tiers.
- 15% for vessels carrying five tiers.
- 21% for vessels carrying six tiers.

An increase of 2% shall be applied for each tier in excess of six tiers, which means that a surcharge of 23% shall be applied on vessels carrying seven tiers and 25% surcharge if vessels carrying 8 tiers…etc.: South bound vessels, circular No. 2/2007 shall remain in force, for example container vessel carrying 8 tiers on deck shall pay 20% surcharge [13].

2. Southbound container vessel

- 2% for vessels carrying one tier.
- 4% for vessels carrying two tiers.
- 6% for vessels carrying three tiers.
- 8% for vessels carrying four tiers.
- 12% for vessels carrying five tiers.
- 16% for vessels carrying six tiers.
- 18% for vessels carrying seven tiers.

An increase of 2% shall be applied for each tier in excess of seven tiers, which means that a surcharge of 20% shall be applied on vessels carrying 8 tiers on deck….etc.

3. Example

- Northbound transit

Triple– E" class transited Suez Canal from its gross tonnage= 200532 tons. Net tonnage= 180528 tons. Carrying 8 layers of containers on upper deck. So additional dues 25% are taxed, plus extra dues for escorting tugs and pilots. The total Canal dues were 932741 U.S $. That means the transfer cost of TEU in Suez Canal is 64.4 U.S. $. So the more TEU the ship carry the less cost are realized. Another triple- E class vessel's cost of TEU through the Suez Canal is 58.8 U.S $.

- Southbound Transit

Cost of TEU transiting Suez Canal ranges between 56 and 59 U.S $, according to the number containers the ship were transporting.

- EMMA- MAERSK class vessel

This type of container vessel capacity 15000 TEU, the cost of TEU for transiting Suez Canal was 71.8 U.S. $ in case of 68% utilization.

Table 3. TEU fees in Suez Canal

TEU Cost U.S. $.	Utilization
a- Triple- E Direction (Northbound):	
67.5	76.0%
64.5	80.4%
58.8	88.9%
b- Triple- E Direction (Southbound):	
56.1	88.4%
59.1	86.0%
59.5	85.0%
c- EMMA MAERSK Class (Southbound):	68.0%

TEU transport Cost through Suez Canal decrease, the higher the numbers of TEU can the ship carry.

XI. ADVANTAGES GRANTED TO CONTAINER VESSELS

- Allow to the vessel carrying 10 TEUs on the higher tier without calculating it as tier.
- If protuberance part of open TEUs on the last tier exceeds half height of container, then consider one tier.
- If the ship carries empty containers only, then Suez Canal dues shall be calculated as ballast, provided that containers carried be belonged to the owner or charters

V. CONCLUSION

- Container vessels represent the bulk of the Suez Canal revenues.
- There is correlation between mega projects and economics of scale.
- Varying utilization of mega container ship affect the cost of TEU transiting Suez Canal.
- The slot cost increase for diminishing utilization.
- The importance of tonnage measurement of a container ship in particular for its operating economics.
- The need to pay attention to the rules of tonnage measurement of ships in the maritime institutes and colleges of engineering (Departments of Ship Engineering).
- New Suez Canal will cut time of transiting, consequently affecting "Triple-E" economics by saving time.

REFERENCES

[1] The Journal of Commerce, March 4, vol. 14, No.5, 2013.

[2] Cullian, K & Khanna, 'Economies of Scale in Large Container Ships. Journal of Transport Economics and Policies, March 2000, vol. 33. pp. 185- 207 e-journal: www.bath.ac.uk.

[3] George Moorsom, Secretary Board of Trade in Britain, the 1854 British Tonnage Rules, British Merchant Shipping Act of 1854.

[4] Corkhill, Michael, Andrew Moysa, 'The Tonnage Measurement of Ships', Fairplay Publication. London, 1980.

[5] Lane, Frederic, Tonnage Medieval and Modern. The Economic History Review. Second series, pp.17 (2) (213- 233) electronic version.

[6] Elsayed Hussein Galal,'The International Conflict over the Exploitation of Suez Canal (1869- 1882) Arabic Edition', 1979, pp. 197- 292, General Egyptian Book organization.

[7] Suez Canal Authority: Rules of Navigation (2007), part. 4, p. 169.

[8] Aji Vasudevan, 'Tonnage Measurement of Ships: Historical Evolution, Current Issues and Proposals for the Way Forward', 2010, p. 21. World Maritime University, Malmo. Sweden.

[9] Architecture of Instruction and Delight, Ibid, pp. 43- 44.

[10] International Maritime Origination issues, IMO, 1982.

[11] International Maritime Origination issues, IMO, 1982. Op. Cit.

[12] Suez Canal Authority, Rules of Navigation (1995) p. 190.

[13] Architecture of Instruction and Delight, Ibid, Art. 98, pp. 194.

THE ECO-EFFICIENCY AND SUSTAIBLE NATIONAL PROJECTS IN EGYPT

KHALED EL-SAKTY
Head of Transport Logistics Department & Vice Dean of College of International Transport and Logistics,
Arab Academy for Science and Technology and Maritime Transport, Cairo, Egypt.,
Tel: +2 0100 833 4341, E-mails: khaled.sakty@aast.edu

Abstract - As a national mega project, the Suez Canal Area Development Project has logistically imposed two main questions. First: how can the project spot an ideal solution for balancing the business and environmental concerns? Second: how can the project enhance the trade-off between these two dimensions? In order to answer these two questions, the efficient frontier between the profitability and the environmental impact needs to be investigated. In this paper, the Strategic Thinking Approach will be discussed for improving the Eco-efficiency. The main purpose of this paper is to discuss the eco-efficiency solution and to identify the appropriate way for measuring the environmental performance in such a project.

Keywords - Eco-efficiency, Suez Canal Area Development Project , Eco-efficiency Analysis.

I. INTRODUCTION

In a supply chain context, suppliers, customers and governments have recently increased their attention towards the balance between the profitability of establishing mega national projects on one hand and the environmental and societal impacts on the other. Hence, governments have changed the 'end-of-pipe' laws to more comprehensive one, worldwide. Here, one question arises: which trade-offs would be counted for between the environmental impacts of an activity project such as the Suez Canal Area Development Project, known as "New Suez Canal Project" and the associated costs of the project?. In other words, what are the best solutions balancing between the ecological and economic concerns of such a project?

These questions lead to a concept of eco-efficiency as displayed in Figure 1. The axes represent the economic value and the environmental quality of economic activity expected from establishing a mega project. The eco-efficiency curve provides either decreasing the environmental pressure without decreasing the economic value added, or increasing economic value without restricting environmental quality. In both cases, the right direction is to move to the efficient frontier. As each point on the efficient frontier is Pareto optimal, it is up to the decision makers to decide which improvement path is preferred. In most cases, increasing environmental quality without losing economic value means moving to the right direction when establishing new projects. In other words, increasing economic value without losing environmental quality means moving up (Neto et. al., 2007).

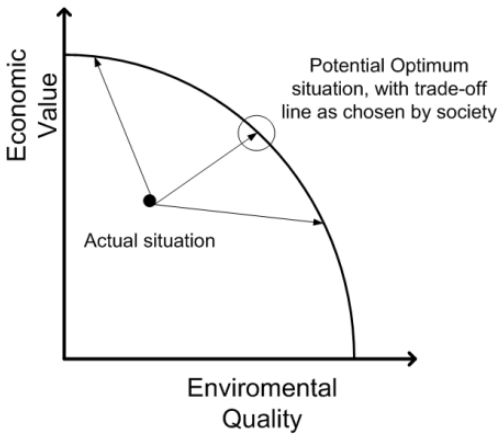

Fig .1. Eco-efficiency of Mega Project
Source: Huppes and Ishikawa, 2005

According to a management philosophy, the eco-efficiency aims to combine business excellence with business excellence that can support sustainable development. Concerning the strategic framework of economic and social Development Plan in Egypt 2022, the economic value can be realized when the investment policies (including financial, monetary and commercial policies) are directed towards enhancing demand on work in national mega projects. In addition, institutional and legislative reforms should be added to the policies, focusing on developing unorganized labor market. Environmentally, the environment should support small and micro projects as well as young

businessmen to improve the chances of having land, loans, and instructional services. In many projects, the quality of environment is affected due to unsustainable use of natural resources, shortage in water resources, and many environmental problems related to different activities in agriculture, industry drinking water, sanitary sewage sectors and other problems.

According to a United Nation Program definition of environment as “green economy”, we understand that environment could be seen as a tool to help modify unsustainable consumption and production attitude resulting in pollution. It can also help modify the overuse of natural resources, especially energy sources and its emissions. Accordingly, the national mega projects in Egypt such as the Suez Canal Area Development Project should consider this new attitude that leads to more efficient and diverse economy in terms of usage and production of the resources which preserve environment and create proper job opportunities. Such a project must encourage sustainable trade operations in order to limit the rate of poverty and achieve social justice.

Moreover, the objectives of the Suez Canal Area Development Project should include the following: creating extended job opportunities, generating investment projects, increasing exportation scale, promoting world trade activities, ensuring long-term economic growth by integrating the existing activities and attracting new foreign investment, using the available resources to find out best practices in the field of sustainable development, and upgrading the efficiency of Egyptian laborers to meet the international advanced labor standards. Consequently, the potential optimum can be attained by reviewing the economic value together with the quality of the environment as displayed in Figure 1. In the next section, the importance of eco-efficiency in improving the performance of any logistic system will be discussed.

II. RESEARCH PROBLEM

In national mega projects, a management philosophy often aims at encouraging business to develop and commercialize products with environmental improvements that would yield economic benefits. There are two challenges facing managers in this case. First, they need to know what the potential drivers that affect the environmental performance are. Second, they need to have tools that can be applied by them to achieve comprehensive environmental and economic benefits for such projects. This paper is trying to seek out a solution for these two problems. The paper is limited to identify the appropriate methodology for managing an environmental performance in national projects.

III. METHODOLOGY

Exploratory approach was conducted in this paper to help understand the research problem and provide significant insights into a given situation. It relies on secondary research such as reviewing available literature, qualitative approach and projective methods. This approach helps build strength around the linkage between process elements, metrics, best practices and opportunities for eco-efficiency in logistics cluster. In this research, the exploratory approach helps to understand the scientific thinking process for improving the Eco-efficiency in such a project.

IV. ECO-EFFICIENCY AND BUSINESS CASE

Eco-efficiency includes creating economic value and reducing environmental impact and resource use at the same time. This leads to a more significant value to be added to any project. Five aspects of eco-efficiency have been identified that make it an indispensable strategic element in business project. These aspects are:

- Eco-innovation
- Optimized processes
- Networks/virtual organizations
- New services
- Waste recycling

Any project includes a set of activities, where eco-efficiency can be implemented along the entire value chain of a product or service. Implementing the eco-efficiency can be achieved through seven key approaches:

- Reduce material intensity
- Energy intensity minimized

- Dispersion of toxic substances is reduced
- Undertake recycling
- Capitalize on use of renewables
- Extend product durability
- Service intensity is increased.

V. ECO-EFFICIENCY AND LOGISTICS NETWORK

Increasing importance of sustainable development has lead eco-efficiency to find a specific position in literature. Eco-efficiency means producing goods and delivering services by using lower energy and raw material which together result in lower amount of waste, pollution and cost. Hence, eco-efficiency considers two aspects: economic and environmental.
As a methodology, using the eco-efficiency concept in assessing the trade-off in logistics networks has recently received attention (Neto et al., 2008). Determining the eco-efficient frontier regarding business and the environment for the design of sustainable logistics networks in Suez region requires using such measures. Three measures can be used to describe the eco-efficiency of any project (Krikke et al., 2003). These measures are cost, energy/resource usage and waste. On the other hand, consumers and legislators have pushed companies to re-design their logistics networks in order to mitigate negative environmental impacts. The objective in the design of logistics networks has changed, therefore, from cost minimization only, to cost and environmental impact minimization.

In general, a logistics network has a number of players that influence business costs and environment impact. Suppliers, manufactures, consumers, operators, third parties operating in testing, refurbishing, recycling and energy producers for the end-of-life products are the main players (Neto et al., 2008). These players affect both businesses and the environment. These activities are related to manufacturing, transportation, usage and end-of-life products' and destination as shown in Figure 2. The decisions regarding these activities will, therefore, determine the network costs and environmental impact. These decisions are strategic (e.g. location of proposed projects in the New Suez Canal Area Development Project), tactical (e.g. the destination of end-of-life products), and operational (e.g. the choice of suppliers, third parties, investors, etc.).

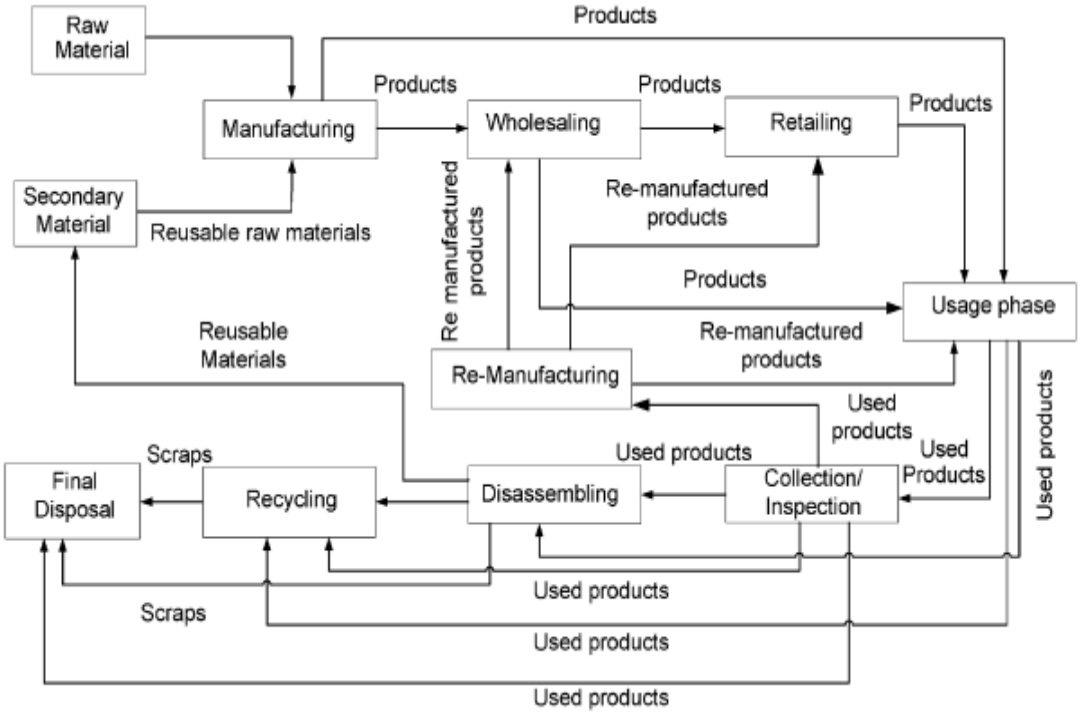

Fig .2. Framework for a sustainable Logistics Network Source: Neto et al., 2008.

Hence, it is obvious that choosing the right activities in demonstrating definite logistics nets is fundamental. In the available Literature, logistics network design is commonly divided in two approaches: minimizing costs (or maximizing profits) and minimizing environmental impact. However, there is little done integrating these two formulations (Bloemhof-Ruwaard et al., 2004). In other words, there is a lack of integration or capturing the trade-offs between the logistics network costs and its respective environmental footprint. Thus, the eco-efficiency is applied in this research for this purpose.

VI. ECO-EFFICIENCY AND NEW SUEZ CANAL PROJECT

The maritime sector is composed of highly competitive businesses. This is because the industry has often faced governmental mandates for achieving regulatory compliance, including safety, security or environmental requirements. Meeting these requirements has been typically perceived as added costs that impede to compete in the sea trade marketplace. With applying the eco-efficiency concept on the New Suez Canal Project and the Suez logistics corridor project in order to make a trade-off between business and environment, a set of attributes can be applied for this purpose (Adams et al., 2009).

VII. BUSINESS APPROACHES

The Suez logistics corridor and the New Canal projects must comply with their applicable environmental laws and regulations in order to avoid enforcement actions by the responsible government agencies. Targeted investors are looking forward to motivating 'greening' initiatives. Recently, 'green' and 'sustainability' issues have become essential requirements for improving maritime transport (IMO, 2014). On the other hand, there are three potential reasons that a business may invest in improving its environmental performance: 1) social license to operate, 2) corporate conscience, and/or 3) competitive advantage. The most important issue for any business established in the corridor is to avoid water or air pollution problems or congestion problems as this will affect the environment as well as the business itself.

VIII. DRIVERS FOR ENVIRONMENTAL INITIATIVES

The drivers for Suez Logistics Corridor investments in environmental performance are many and varied. On top of the list are regulatory compliance and court-ordered activities where businesses, ports and logistics adding-value activities are forced to make investment to avoid further legal action. There are other drivers, motivations, and considerations as listed in Table 1.

Table 1. Potential Essential Motives and Drivers Source: Adams et al., 2009

MOTIVES	DRIVERS	
Regulatory compliance (1)	International Marine and/or environmental legislation	Regional environmental legislation
	Local (e.g. provincial) environmental legislation	Self-regulation
Response to societal pressures (and enjoy resulting direct economics benefits) (2)	Corporate and Social Responsibility	Local communities concerns and public relations
	Environment's protection and/or quality improvement	Assess environmental impact of port's activities
	Economic Incentives (Tax exemption, subsidies, capitalization, revenues)	Insurance premium & liabilities reductions
	Environmental management (e.g. Pollution Prevention)	Profit: Emissions trading market
Development & Planning (3)	Coastal zones planning	Port policy and planning
	Component of port's sustainable development program	
Operational issues (4)	Operational performance	Costs reduction and control
	Health and safety issues	Labor relations
	Processes standardization	Environmental problem-solving and remediation plan
Gain competitive advantage (5)	Competition between regional ports	Corporate strategy
	Short sea shipping promotion	New Markets
	Create/Enhance/Promote "green logistics"	Collaborative logistics
	External business pressure (e.g. Shipping lines, terminal operators)	Strategic alliances
	Commercial and marketing interest	

IX. INCREASING PRESSURE AND MOTIVATIONS

Port, Maritime and shipping industries have become targets for public environmental policy regulations (IMO, 2014). Proper management of water bodies and sediments, air emissions, waste reception facilities, and modal split of port related hinterland traffic are 'hot button' issues in today's port policy agendas. To a certain extent, ports are being pressured to respond to problems related to environmental harm resulting from shipping activities, whether moved by ships or trucks. Also, the rapid growth of cargo volumes over the years and expanding port infrastructure led to an increase in both environmental problems and societal pressures.

Figure 3. shows the overview of total sea pollution due to an increase in cargo volumes handled at seaports, worldwide.

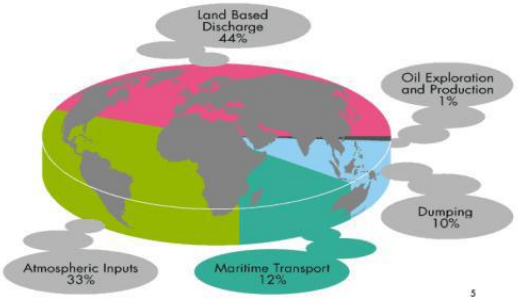

Fig .3. Overview of Total Sea Pollution
Source: IMO, 2012

X. SPILLOVER EFFECTS AND TIMELINES

As an eco-efficiency dynamic, the 'green' practices create spillover effects. Once a business in the Suez region begins to address environmental matters, the interdependent nature of ecological and physical elements inevitably will lead towards ever-broader responses. Hence, green suppliers and transporters became a mandatory requirement to any business enterprise and supply chains become greener.

XI. RESULTS

As discussed in Table 1, there are many drivers affecting the environmental performance in national mega projects. It is recommended in this paper to apply an Eco-Efficiency Analysis (EEA) that provides businesses and organizations with more fully-measured footprint of their projects or processes. This tool aims at evaluating the economic and environmental impacts of a product or process. It differs from other tools such as the Life Cycle Assessment (LCA) tool that eco-efficiency analyses evaluate both environmental burdens and economic costs, whereas LCA evaluate only environmental burdens. EEA works as follows:

- It provides managers with both environmental and economic data around a project.
- An EEA can accurately analyze those potential drivers in a project relying on the credible baseline data.
- From that baseline, an environmental footprint can be prioritized or cost reduction efforts.
- It helps to identify broader the optimization targets in a project.
- The level of detail and data provided is far beyond that available in a life cycle analysis and can be the basis for attaining higher sustainability goals.

As the methodology in this paper is Exploratory (inductive in nature) rather than Explanatory approach, this paper aims at understanding and finding the appropriate methodology that can be used by managers in such mega projects to measure the environmental performance. As further research in future, it is recommended to apply EEA tool in the Suez Canal Area Development Project when data will be available and accessible.

XII. CONCLUSION

This research is trying to seek out an answer as to how any project can spot the preferred solution for balancing the business and environmental concerns, and how any project can enhance the trade-off between those two dimensions. Answering these two questions, the efficient frontier between the profitability and the environmental impact has been discussed.

Establishing such new national mega projects such as the New Suez Canal and the Suez Canal Area Development Project will certainly affect carrier and shipper market practices. Ports, transporters,

investors, businesses and other players in these projects should be prepared to proactively address the environmental issues that are emerging, which may also have a potential impact on costs and carrier market practices.

Making a balance/trade-off between business and the environment has received little attention in the available literature so far. Hence, this research has discussed some attributes that can attain this goal using the eco-efficiency concept. These issues may have even greater impacts on both projects for doing global maritime business, particularly if dealt with reactively. On the other hand, if dealt with from an anticipatory perspective, there may be a possibility of improving a port's competitive position while reducing costs to shippers and carriers. Environmental issues can no longer be considered only as added costs but actively treated as business opportunities. As the purpose of this paper is limited to find the appropriate methodology for managing the environmental performance in national projects, Eco-Efficiency Analysis (EEA) is recommended to be applied in the future using Explanatory approach when the required data are available.

REFERENCES

[1] Adams, M., QUINONEZ, P., Pallis, A., and Wakeman, T. (2009) Environmental Issues in Port Competitiveness. Dalhousie University: Halifax.

[2] Bloemhof-Ruwaard, J.M., Krikk, H. and Van Wassenhove, L.N. (2004) OR Models for Eco–Eco Closed-Loop Supply Chain Optimization. Vol. 1, Springer, Berlin: Heiderberg.

[3] Huppes, G.and Ishikawa, M. A. (2005) Framework for Quantified Eco-efficiency Analysis. Journal of Industrial Ecology, Vol. 9(4), pp. 25–41.

[4] Krikke, H., Bloemhof-Ruwaard, J.M. and Van Wassenhove, L. N. (2003) Current Product and Closed Loop Supply Chain Design with an Application to Refrigerators. International Journal of Production Research, Vol. 41(16), pp.3689–3719.

[5] Quariguasi Frota Neto, J., Bloemhof-Ruwaard, J, Van Nunen, J.A.E.E. and Van Heck, E. (2008) Designing and evaluating sustainable logistics networks. International Journal of Production Economics, pp. 195-208.

[6] Quariguasi Frota Neto, J., Walther, G.,.Bloemhof, J., J.A.E.E Van Nunen and Spengler, T. (2007) Methodology for Assessing Eco-Efficiency in Logistics Networks ERIM, , pp. 1-37.

[7] Ministery of Planning and International Cooperation (June 2012) Strategic Framework for Economic and Social Development plan 2022

[8] IMO, (2014) A Concept of A Sustainable Maritime Transportation System. International Shipping Facts and Figures.

[9] IMO, (2012) Information Resources on Trade, Safety, Security, Environment.

Culture - independent Pathogenic Bacterial Communities in Bottled Mineral Water

Hamdy A. Hassan
Environmental Biotechnology Department, Genetic Engineering and Biotechnology Research Institute,
Sadat city University - Sadat city – Egypt

Abstract **-** Bottled mineral water (BMW) is an alternative to mains water and consider it to be better and safer. Access to safe BMW from the bacteria involving potential health hazard is essential to health. Cultivation-independent technique PCR-based single-strand conformation polymorphism (SSCP) for genetic profiling of PCR-amplified 16S rRNA genes was performed using Com primer set targeting the 16S rRNA genes for detection of pathogenic bacteria in bottled mineral water from the final product of six factories for BMW in Wadi El-natron region- Egypt.

These factories use often ozone technology to treat large quantities of water because of its effectiveness in purifying and conditioning water. A total of 27 single products were isolated from the profiles by PCR re-amplification and cloning. Sequence analysis of 27 SSCP bands revealed that the 16S rRNA sequences were clustered into seven operational taxonomic units (OTUs) and the compositions of the communities of the six samples were all common.

The results showed that most communities from phyla Alphaproteobacteria and certainly in the Sphingomonas sp. Culture-independent approaches produced complementary information, thus generating a more accurate view for the bacterial community in the BMW, particularly in the disinfection step, as it constitutes the final barrier before BMW distribution to the consumer

Keywords **-** Bottled mineral water, Pathogenic bacteria, Culture- independent, PCR-SSCP, 16S rRNA genes.

I. INTRODUCTION

Bottled mineral water (BMW) is often recommended for patients with immune-system deficiencies as well as marketed as ideal for infant nutrition and reconstitution of foods (Warburton, 1993). Mineral water is an oligotrophic environment; their content of viable bacterial cell is as low as 10cfu ml-1 (Ferreira et al., 1994). These lows, count of native organisms are of little concern to the healthy consumer. Outbreaks of infectious bacteria via the use of contaminated tap drinking water still pose a serious health threat worldwide, despite that drinking water is one of the most closely monitored and strictly regulated resources. Both bottled water and tap water may contain the same microorganisms, which originated from the same sources (Papapetropoulou et al., 1997; Ahmed et al., 2013).

The European Union Council Directive on the quality of water intended for human consumption restricts the presence of E. coli, Clostridium perfringens, Pseudomonas aeruginosa, enterococci and coliforms and recommends a total heterotrophic colony count only in the case of water offered for sale in bottles or containers (The Council of the European Union 1998; Ahmed et al., 2013). By using conventional cultivation techniques, less than 1% of the bacterial population can be cultivated from oligotrophic systems such as the drinking water distribution system and the related microbial population (Kalmbach et al., 1997; Falcone-Dias et al., 2015). The real significance of of pathogenic bacteria in the drinking water is poorly understood (Guzman et al., 2010).

Sphingomonas spp. are widely distributed in nature and are resistant to many disinfecting and toxic chemicals (Laskin and White, 1999), and has been isolated from drinking water and drinking water distribution systems. Some Sphingomonas strains are well known for metabolizing complex organic pollutants, but some are opportunistic human pathogens as Sphingomonas paucimobilis and S.

parapaucimobilis (Anon, 2000, Guzman et al., 2010, Gesumaria et al., 2011). A developed protocol was used, which allows the application of single-strand-conformation polymorphism (SSCP) (Orita et al., 1989; Hayashi, 1991; Gasser et al., 2007) for the culture-independent assessment of microbial-community diversity (Schwieger and Tebbe, 1998; Gasser et al., 2007; Jean and Georges , 2008;

Keskes et al., 2012). The SSCP method has the potential to be more easily applied (Lee et al., 1996) and the SSCP produced a number of sharp bands and differentiated the bacterial community structures (Tomoyuki et al., 2006). SSCP was optimized to analyze only one of the complementary single strands (Schwieger and Tebbe, 1998; Meng-zhi et al., 2008), by preferentially degrading with lambda exonuclease the one strand generated with a phosphorylated primer.

This development aims to avoid heteroduplex formations, or overlapping of forward-reverse strands from different amplicons during separation, allowing the separation of mixtures of fragments of identical size but different in sequence. The application of this modified technique was focused on studies of taxonomic shifts in microbial communities by targeting 16S rRNA genes (Peters et al., 2000; Schmalenberger et al., 2001; Schwieger and Tebbe, 2000, 2003). However, a potential application to assess diversity of functional genes was foreseen (Stach and Burns, 2002).

The aim of this study was to identify the common uncultured bacterial community via SSCP in the BMW from the end product of six factories for mineral water located in Wadi El-natroon region, which is one of the largest industrial regions for mineral water in Egypt.

II. GEOMETRY OF THE MODEL AND MATERIAL PROPERTIES

A. DNA Extraction from the six water samples

Six water samples equal volumes each 2 liters were collected from the final product of BMW from six factories in Wadi El-natroon region, The filtration was implemented under sterile conditions with a filtering device actuated by a motor driven pump, the filter sandwich with the bacteria was cut into small pieces with a sterile scalpel and transferred to The MULTIMIX 2 Tissue Matrix Tub, add 978 µl Sodium Phosphate Buffer and 122 µl MT Buffer from fast DNA SPIN Kit for Soil Bio 101 and follow the DNA extraction according to the protocol for DNA extraction with the Fastprep DNA kit for soil (Bio 101). DNA was visualized on 1% agarose gels. Yield of genomic DNA was determined spectrophotometrically by measuring the absorbance at 260 nm.

Purity was determined by calculating the ratio of absorbance at 260 nm to absorbance at 280 nm (a pure DNA has an A260/A280 The DNA extracts from water samples containing approximately 200 ng ml-1 DNA were 50- or 100-fold diluted in Tris-HCl buffer (10 mM, pH 8.0) and used as template DNA in PCR.

B. SSCP for six BMW samples collected from the final product of six factories in Wadi El-natroon region

The primers Com1 (5`CAGCAGCCGCGGTAATAC3`) targeting the position (519-536) and Com2-Ph (5`CCGTCAATTCCTTTGAGTTT3`) targeting the position (907-926) were chosen for the amplification of bacterial 16S rRNA genes (Schwieger and Tebbe 1998). Single-stranded DNA (ssDNA) from PCR products was obtained as previously described (Schwieger and Tebbe, 1998). Briefly, PCR as performed with one of the primers being 5` phosphorylated, Each amplification was carried out using 2 ng DNA template in a final volume of 50 µl, starting with an initial denaturation for 15 min at 95°C.

A total of 30 cycles (30s at 95°C, 30s at 55°C, and 1 min at 72°C was followed by a final elongation for 10 min at 72°C. Amplification was achieved using Hot Star Taq DNA polymerase (Fermentas). PCR products were eluted from agarose gels (see Figure. 1), and the phosphorylated strands were digested by lambda exonuclease (NEB). The remaining single-strands were purified with GeneJET PCR Purification Kit (Fermentas), dried by vacuum centrifugation, resuspended in 6 µl of loading buffer (95% formamide, 0.25% bromophenol blue and 0.25% xylene cyanol), and denatured for 5 minutes at 94 °C, followed by instant cooling on water ice bath for 3 minutes.

The separation conditions were standardized in a DCode System for PCR-SSCP, optimized running parameters were 120V (10 mA) for 18 h at a constant temperature of 26°C on 20 cm x 20 cm x 0,75 mm 0.6X MDE gels in 0.7X TBE (Sambrook et al., 1989) as a running buffer. Optimal results were obtained when ssDNA obtained from 100 - 400 ng dsDNA was loaded onto the gels and a slightly enhanced resolution was achieved when the amplified single-strands of the reverse primer were subjected to PCR-SSCP analysis. For nucleic acid detection, gels were silver stained as reported previously (Bassam et al., 1991).

Single-strand electrophoretic mobilities corresponding to different conformations were excised from dried gels, and DNA extracted by the “Crush and Soak” method (Sambrook et al., 1989) PCR reamplification of the excised and eluted single-strands was made with the same primers used to generate the original dsDNA fragment.

C. Data Deposition

The sequences reported in this paper have been deposited in the GenBank database (27 sequences for the independent culture bacteria accession numbers (JF793682- JF793708).

D. RESULTS

Com Primer set were used to amplify the eubacterial 16S rRNA gene sequences (see Figure 1) including the variable regions yielded complex SSCP patterns, SSCP community profiling showed highly diverse and distinct microbial communities for the BMW water samples, BMW sample 5 displayed the largest numbers of bands, while BMW sample 6 displayed less numbers of bands (see Figure 2 A, B). By PCR, the opposite strands were regenerated and the products were reamplified. SSCP gel electrophoresis was used to evaluate the purities and identities of the reamplified 27 products, as shown for products obtained from PCR targeting the hypervariable samples 16S rRNA genes only 27 were appeared (see Figure 3). In most cases, reamplification products corresponded to the expected positions in the community patterns and no additional products were observed. These products were then directly used for cloning and DNA sequencing.

To identify the predominant products by DNA sequencing, a total of 27 different DNA single strands ("bands") were excised, 27 sequences were in good appearance. By comparing the 27 sequences accession numbers from JF793682- JF793708 with the related taxa, revealed 7different operational taxonomic units OTUs of bacteria, and that the most compositions of the communities of the six BMW samples were all common. The phylogenetic tree (see Figure 4) constructed from the partial sequences of the 16S rRNA amplicons from the 6 BMW samples showed a predominance of Alphaproteobacteria, especially family Sphingomonas sp. (Table 1).

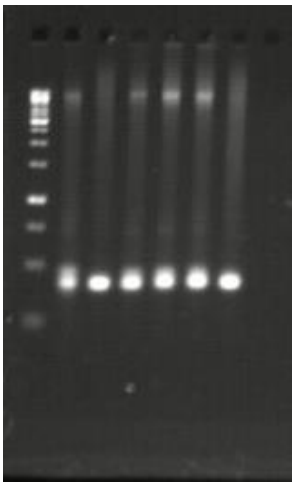

Fig .1. PCR with com primers targeting the 16SrRNA genes for the four DNA extracted samples from the six water samples collected from the final product of BMW from six factories in Wadi El-natroon region (lanes 1, 2, 3, 4,5,6) , C is the controle without DNA and M is 1Kb DNA Ladder GeneRuler™, Fermentas.

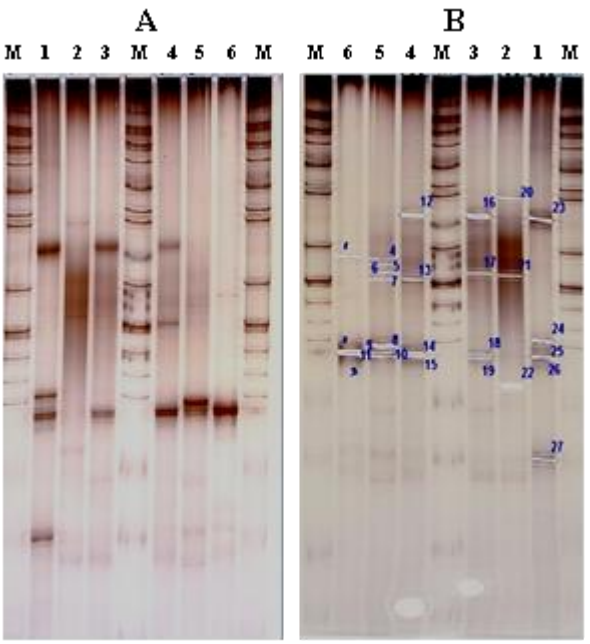

Fig .2. (A) SSCP on a polyacrylamide gel for the Six BMW samples before cutting the bands, (B) after cutting the bands.

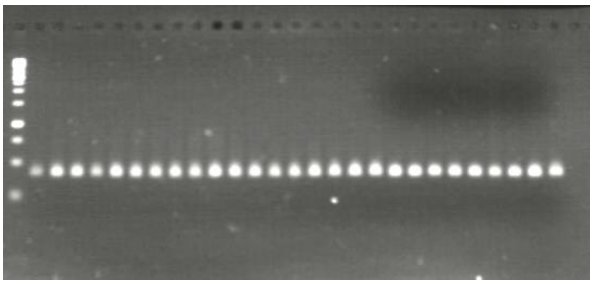

Fig .3. PCR reamplification of the excised and eluted single-strands with the same com primers to generate the original dsDNA fragment lans 1-27 are the product of the reamplification, C is the control without any template, M is 1Kb DNA Ladder GeneRuler™, Fermentas.

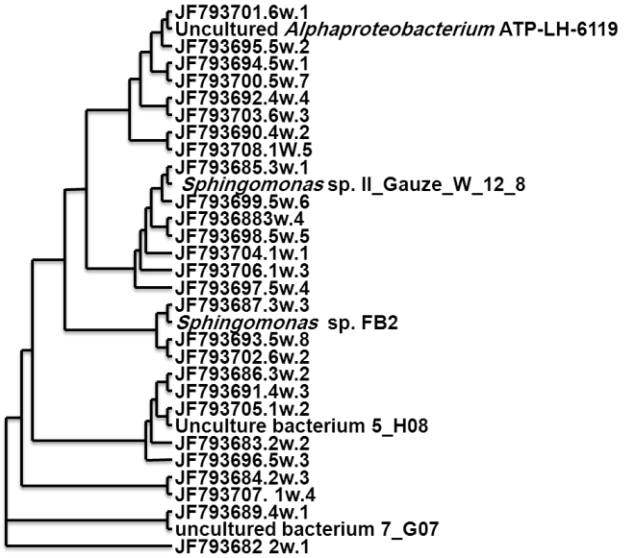

Fig .4. Phylogenetic tree of partial 16S rRNA gene sequences for the SSCP bands from the six BMW samples and its high similarity.

Table 1. Phylogenetic assignment of sequences of prominent bands in SSCP gel profiles of the six BMW samples communities., showed the sample number and the band number i.e 6W1 means BMW sample number 6 and 1 is the band number in this sample.

Band Number	OUT#	Accession Number	bp	Most closest related sequence	Similarity (%)	Accession Number
6w.1	1	JF793701	348	uncultured alpha proteobacterium ATB-LH-6119	98.7	FJ535117
6w.2	3	JF793702	353	uncultured bacterium; BF0001B016	89.6	AM696990
6w.3	1	JF793703	345	uncultured alpha proteobacterium ATB-LH-6119	97.9	FJ535117
5w.1	1	JF793694	344	uncultured bacterium; BF0001B016	94.7	AM696990
5w.2	1	JF793695	351	uncultured bacterium; 13_D04	96.2	FN421620
5w.3	4	JF793696	350	uncultured bacterium; BF0002B019	100	AM697069
5w.4	2	JF793697	346	*Sphingomonas* sp. II_Gauze_W_12_8	97.2	FJ267571
5w.5	2	JF793698	358	uncultured bacterium; BF0002B019	97.2	AM697069
5w.6	2	JF793699	353	uncultured alpha proteobacterium; ATB-LH-6119	95.6	FJ535117
5w.7	1	JF793700	344	uncultured alpha proteobacterium ATB-LH-6119	98.7	FJ535117
4w.1	6	JF793689	355	uncultured bacterium BF0002B019	97.4	AM697069
4w.2	1	JF793690	391	uncultured bacterium; BF0001B024	96.4	AM696998
4w.3	4	JF793691	343	uncultured bacterium; 5_H08	92.8	FN421996
4w.4	1	JF793692	345	uncultured alpha ATB-LH-6119	98.7	FJ535117
4w.5	3	JF793693	344	uncultured bacterium; 4_H07	94.6	FN421778
3w.1	2	JF793685	347	uncultured bacterium; 2_E05	91.1	FN421872
3w.2	4	JF793686	352	uncultured bacterium; 13_F05	94.6	FN421638
3w.3	3	JF793687	359	*Sphingomonas* sp. FB2	95.1	AM933496
3w.4	2	JF793688	355	uncultured bacterium BF0002B019	96.2	AM697069
2w.1	7	JF793682	359	*Sphingomonas* sp Ens34	96.2	DQ339629
2w.2	4	JF793683	362	uncultured bacterium BF0002B019	96.4	AM697069
2w.3	5	JF793684	387	uncultured bacterium7_G07	95.1	FN421898
1w.1	2	JF793704	353	uncultured bacterium; 4_H03	95.7	FN421776
1w.2	4	JF793705	345	uncultured alpha proteobacterium ATB-LH-6119	94.6	FJ535117
1w.3	2	JF793706	392	uncultured bacterium1_C11	94.4	FN421586
1w.4	5	JF793707	396	unculturedbacterium1_D12	96.7	FN421594
1w.5	1	JF793708	389	uncultured bacterium; BF0002B019	92.6	AM697069

III. DISCUSSION

The cultivation independent methods, based on amplification of environmental DNA followed by acrylamide gel electrophoresis, separate sequence specific DNA fragments of the same length, have the potential for accurate comparison of environmental samples in a short period of time. In this study, we have shown that SSCP analysis of 16S rRNA genes amplified from directly extracted DNA from the six BMW samples from the different end product manufactories can be used to visualize all the community structures included the pathogenic species in the BMW, and also this indicate the high potential of this technique to monitor microbial communities and their variation qualitatively and quantitatively (Peters et al., 2000).

Culture-independent techniques were used for the detection of pathogenic bacteria in BMW at potentially critical control points in the end products of BMW six factories in Wadi El-natroon region – Egypt. PCR-SSCP in the BMW from the end product samples. BMW sample number 5 displayed the largest bands than the other bands maybe possibly due to different reasons, because the factory was near from urban but the other factories were a little bit far, and may be also due to the handling of the workers.

As more gene sequences become available, PCR-SSCP-mediated monitoring of different subgroups or microorganisms, due to optimized primer design, will become even more attractive, almost all of these OTUs from the indirect culture (Table 2) in this study are belonging to the phyla Alphaproteobacteria (Falcone-Dias et al. 2015) and certainly related to Sphingomonas species, which are widely distributed in nature. Sphingomonas have been recovered from sea water (Cavicchioli et al. 1999; Gesumaria et al., 2011), sea ice (Bowman et al. 1997), river water (Tabata et al. 1999), waste water (Neef et al. 1999), polluted ground water (Männistö et al. 1999), mineral water (Ferreira et al. 1996; Vachee et al. 1997), sterile water' used in hospitals (Oie et al. 1998), drinking water (Gauthier et al. 1999).

The widespread distribution of sphingomonas can be explained by their ability to survive and grow at low temperature, low nutrient concentration and in toxic chemical environments (Laskin and White, 1999). Because sphingomonas are relatively slow growing (The Council of the European Union 1998). Therefore, the presence of sphingomonas in BMW and also in the drinking water environment may be much more common than has been reported so far and deserves further study not only by culture bacteria but also by culture- independent bacterial molecular techniques. Two species of Sphingomonas, S. paucimobilis and S. parapaucimobilis, have been classifed to Hazard Group 2 in the European Community regulations (Anon, 2000), all species of Sphingomonas contain glycosphingolipids in their cell envelope. Glycosphingolipids (Kawahara et al., 1999).

Glycosphingolipids of sphingomonas have been shown to induce tumour necrosis factor and other monokine production in human mononuclear cells (Krziwon et al. 1995), stimulate phagosytosis and phagosome lysosome fusion (Miyazaki et al. 1995), activate the human complement system (Wiese et al. 1996) and inhibit protein kinase C and possibly function as endogenous modulators of cell function and as second messengers (Hannun and Bell, 1989). These factors may partly explain the pathogenic features of hospital sphingomonas infections.

V. CONCLUSION

This study provides a better method for understanding the uncultured bacterial community in the BMW and providing new information that might be used for improving BMW quality and safety. The above findings underline the fact that BMW sold in Egypt and tested as free from culture pathogenic still have uncultured potential bacterial pathogens. Therefore, in a country such as Egypt , where the quality of tap water is uncertain, it is recommended that there should be stringent regulation of bottled water quality whilst boiled tap water could be a safe alternative.

It is important that consumers are aware that the perception that bottled water is always safer than tap water can be misleading as the former can also contain the same microorganisms commonly found in tap water. This study gives an attention that BMW is not completely safe either for BMW producer to try to solve BMW problems or for the user to be careful during use BMW for infant nutrition and reconstitution of foods.

REFERENCES

[1] Ahmed, W., Yusuf, R., Hasan, I., Ashraf, W., Goonetilleke, A., Toze, S., & Gardner, T. (2013). Fecal indicators and bacterial pathogens in

bottled water from Dhaka, Bangladesh. Brazilian Journal of Microbiology, 44(1), pp.97–103.

[2] Amann, R.I., Ludwig, W. and Schleifer, K.H. (1995) Phylogenetic identification and in situ detection of individual microbial cells without cultivation. Microbiol. Rev. 59: pp. 143-169.

[3] Anon. (2000) Bacterial nomenclature up-to-date. www.dsmz.de/bactnom/bactname.htm.

[4] Bassam, B. J., Caetano-Anolles, G. and Gresshoff, P. M. (1991) Fast and sensitive silver staining of DNA in polyacrylamide gels. Anal Biochem 196: pp. 80–83.

[5] Blumenroth, P., and Wagner-Dobler, I. (1998) Survival of inoculants in polluted sediments: effect of strain origin and carbon source competition. Microb. Ecol. 35:pp. 279–288

[6] Cavicchioli, R., F. Fegatella, M. Ostrowski, M. E. and Gottschal, J. (1999) Sphingomonas from marine environments. Journal of Industrial Microbiology and Biotechnology 23: pp. 268-272.

[7] Falcone-Dias, M. F., Centrón, D., Pavan, F., Moura, A. C. da S., Naveca, F. G., de Souza, V. C., Leite, C. Q. F. (2015) Opportunistic Pathogens and Elements of the Resistome that Are Common in Bottled Mineral Water Support the Need for Continuous Surveillance. PLoS ONE, 10 (3).

[8] Ferreira,A.C., Morais, P.V. and Da Costa, M. (1994). Alterations in total bacteria, iodonitrophenyltetrazolium (1NT)-positive bacteria, and heterotrophic plate counts of bottled mineral water. Canadian Journal of Microbiology 40: pp. 72-77.

[9] Ferreira, A.C., Morais,P.V., Gomes, C. and da Costa. M.S. (1996) Computer-aided comparison of protein electrophoretic patterns for grouping and identi®cation of heterotrophic bacteria from mineral water. Journal of Applied Bacteriology 80: pp. 479-486.

[10] Gasser, R.B, Chilton, H. M, NB, Campbell, B.E, Jex, A.J, Otranto, D, et al. (2007) Single-strand conformation polymorphism (SSCP) for the analysis of genetic variation. Nature Protocols 1, (6):pp. 3121 - 3128.

[11] Gesumaria, R., Microbiology of Bottled Water: A Molecular View (2011). Undergraduate Honors Theses. Paper 671.

[12] Gusman V., Jelesic, Z. Mihajlovic-Ukropina, M., Medic, D. , Pavlovic, G. and Radosavljevic, B. (2010) Isolation of Sphingomonas paucimobilis from drinking water using novel automated system. HealthMED. 4:pp. 1068-1071.

[13] Gauthier, V., Redercher, S. and Block. J. C. (1999) Chlorine inactivation of Sphingomonas cells attached to goethite particles in drinking water. . Appl Environ Microbiol 65: pp. 355-357.

[14] Hannun, Y. and Block, R.M. Bell. (1989) Function of sphingolipids and sphingolipid breakdown products in cellular regulation. Science 243: pp. 500-507.

[15] Hayashi, K. (1991) PCR-SSCP: A Simple and Sensitive Method for Detection of Mutations in The Genomic DNA. PCR Methods Appl. 1:pp. 34-38.

[16] Jean-Luc J. and Georges, B. (2008) Culture-Independent Methods for Identifying Microbial Communities in Cheese. Food Microbiology 25: pp. 839-848

[17] Keskes S, Hmaied, F., Gannoun,H., Bouallagui, H ., Godon, J. J. and Hamdi, M. (2012) Performance of a submerged membrane bioreactor for the aerobic treatment of abattoir wastewater. Bioresour Technol. 103: pp. 28-34.

[18] Kalmbach, S., Manz, W. and Szewzyk, U. (1997) Isolation of New Bacterial Species from Drinking Water Biofilms and Proof of Their in Situ Dominance with Highly Specific 16S Rrna Probes. . Appl Environ Microbiol 63: pp. 4164-4170.

[19] Kawahara, K., Kuraishi, H. and ZaÈhringer, U. (1999) Chemical structure and function of glycosphingolipids of Sphingomonas spp. and their distribution among members of the alfa-4 subclass of Proteobacteria. Journal of Industrial Microbiology and Biotechnology 23: pp. 408-413.

[20] Krziwon, C., ZaÈhringer, U., Kawahara, K., Weidemann, B., Kusumoto, S., Rietschel, E., Flad, H. D. and Ulmer, A. J. (1995) Glycosphingolipids from Sphingomonas paucimobilis induce monokine production in human mononuclear cells. Infection and Immunity 63: pp. 2899-2905.

[21] Laskin, A.I. and White, D.C. (1999) Special issue on the genus Sphingomonas. Journal of Industrial Microbiology and Biotechnology 23: pp. 231±408

[22] Lee, D.H., Zu, Y.G. and Kim, S.J. (1996) Nonradioactive method to study genetic profiles of natural bacterial communities by PCR-single strand conformation polymorphism. Appl. Environ. Microbiol. 62: pp. 3112-3120.

[23] Männistö, M., Tiirola, M., Salkinoja-Salonen, M., Kulomaa, M. and Puhakka, J. (1999) Diversity of chlorophenol-degrading bacteria isolated from contaminated boreal groundwater. Archives of Microbiology 171, pp. 189±197.

[24] Meng-zhi, W., Hong-rong W., Heng-chun C.A.O, Guo-xiang L.I and Jie Z. (2008). Effects of Limiting Amino Acids on Rumen Fermentation and Microbial Community. In vitro. Agricultural Sciences in China 7: pp. 1524-1531.

[25] Miyazaki, Y., Oka, S., Yamaguchi, S., Mizuno, S. and Yano, I. (1995) Stimulation of phagosytosis and phagosome-lysosome fusion by sphingolipids from Sphingomonas paucimobilis. Journal of Biochemistry 118: pp. 271-277.

[26] Neef, A., Witzenberg, R. and KaÈmpfer. P. (1999) Detection of sphingomonads and in situ identification in activated sludge using 16S rRNA-targeted oligonucleotide probes. Journal of Industrial Microbiology and Biotechnology 23: pp. 261-267.

[27] Oie, S., Oomaki, M., Yorioka, K., Tatsumi, T., Amasaki, M., Fukuda, T., Hakuno, H., Nagano, K., Matsuda, M., Hirata, N., Miyano, N., and Kamiya, A. (1998) Microbial contamination of `sterile water' used in Japanese hospitals. Journal of Hospital Infection 38: pp. 61-65.

[28] Orita, M., Iwahana, H., Kanazawa, Hayashi, H. K. and Sekyia, T. (1989) Detection of polymorphisms of human DNA by gel electrophoresis as single-strand conformation polymorphisms. Proc. Nat. Acad. Sci. USA 86: pp. 2766-2770.

[29] Papapetropoulou M., Tsintzou, A. and Vantarakis, A. (1997) Environmental mycolacteria in botled table waters in Greece. Can. J. Microbiology 43: pp. 499 - 502.

[30] Peters, S., Koschinsky, S., Schwieger, F. and Tebbe, C. C. (2000) Succession of microbial communities during hot composting asdetected by PCR-single-strand-conformation polymorphism-based genetic profiles of small-subunit rRNA genes. Appl Environ Microbiol. pp. 66:930-936.

[31] Sambrook, J., Fritsch, E. F. and Maniatis, T. (1989) Molecular cloning: a laboratory manual. Second edition. Cold Spring Harbor Laboratory Press, Cold Spring Harbor, New York, USA.

[32] Schmalenberger, A., Schwieger, F. and Tebbe, C.C. (2000) Effect of primers hybridizing to different evolutionarily conserved regions of the small-subunit rRNA gene in PCR-based microbial community analyses and genetic profiling. Appl Environ Microbiol. 67: pp. 3557-3563.

[33] Schmalenberger, A. and Tebbe, C.C. (2003) Bacterial diversity in maize rhizospheres: conclusions on the use of genetic profiles based on PCR-amplified partial small subunit rRNA genes in ecological studies. Mol Ecol. 12: pp. 251-262.

[34] Schwieger, F., and Tebbe, C. C. (1998) A new approach to utilize PCR-single-strand-conformation polymorphism for 16S rRNA gene-based microbial community analysis. Appl. Environ. Microbiol. 64: pp. 4870-4876.

[35] Schwieger, F. and Tebbe, C.C. (2000) Effect of field of inoculation with Sinorhizobium meliloti L33 on the composition of bacterial communities in rhizospheres of a target plant (Medicago sativa) and a non-target plant (Chenopodium album)-linking of 16S rRNA gene-based single-strand conformation polymorphism community profiles to the diversity of cultivated bacteria.

Appl Environ Microbiol. 66: pp. 3556-3565.

[36] Stach, J. E. M. and Burns, R.G. (2002) Enrichment versus biofilm culture: a functional and phylogenetic comparison of polycyclic aromatic hydrocarbon- degrading microbial communities. Environ Microbiol. 4: pp. 169-182.

[37] The Council of the European Union. 1998. Council directive on the quality of water intended for human consumption. Council Directive 98/83/EC 3 November, 1998. The Official Journal of the European Communities L 330, pp. 32-34.

[38] Tomoyuki H., Shin, H., Yoshiyuki, U., Masaharu, I. and Yasuo, I. (2006) Direct comparison of single-strand conformation polymorphism (SSCP) and denaturing gradient gel electrophoresis (DGGE) to characterize a microbial community on the basis of 16S rRNA gene fragments. Journal of Microbiological Methods 66: pp.165-169.

[39] Warburton, D. W. (1993) A review of the microbiological quality of bottled water sold in Canada. Part 2. The need for more stringent standards and regulations. Can. J. Microbiology 39: pp. 158–168.

[40] Wiese, A., Reiners, J., Brandenburg, K., Kawahara, K., ZaÈhringer, U. and Seydel, U. (1996) Planar asymmetric lipid bilayers of glycosphingolipid or lipopolysaccharide on one side and phospholipids on the other: Membrane potential, porin function, and complement activation. Biophysical Journal 70: pp. 321-329.

Rule-Based Control of Off-Grid Desalination Powered by Renewable Energies

A. Serna[1], F. Tadeo[1], D. Torrijos[2]
[1] University of Valladolid, 47005 Valladolid, Spain
E-mail: fernando@autom.uva.es,
[2]SETA S.L., Rivas-Vaciamadrid, Madrid, Spain

Abstract **-** A rule-based control is presented for desalination plants operating under variable, renewable power availability. This control algorithm is based on two sets of rules: first, a list that prioritizes the reverse osmosis (RO) units of the plant, based on the current state and the expected water demand; secondly, the available energy is then dispatched to these units following this prioritized list. The selected strategy is tested on a specific case study: a reverse osmosis plant designed for the production of desalinated water powered by wind and wave energy. Simulation results illustrate the correct performance of the plant under this control strategy.

Keywords **-** Renewable energies, off-grid, desalination, rule-based control, reverse osmosis.

I. INTRODUCTION

Desalination is becoming increasingly used in many areas of the world to satisfy the demand of water. This process produces water (for human or industrial use) by removing most of the salts, generally from sea or brackish waters. Desalination systems are ubiquitous. The capacity estimation for 2015 goes beyond 120 Mm3/day and the cost of drinkable water obtained from desalination is steadily decreasing. Although currently most large-scale desalination plants are connected to the grid, renewable energies are being introduced especially in small desalination plants located in areas without a reliable electricity grid. Australia is an important exception, where the biggest seawater desalination plants are powered by renewable energies: see [1] and [2] for a detailed description of desalination plants powered by renewable energy sources.

This paper concentrates on Reverse Osmosis (RO) plants, as this is the most frequently used process for small and medium sized plants. RO uses high pressures to force water molecules through a semi permeable membrane, retaining salt particles on the high pressure side (see, for example [3], and [4] for some general references of RO desalination). The pressure required goes from 40 to 80 bars, depending on the salt concentrations (see for example [5]). This pressure is supplied by high-pressure pumps (positive-displacement, centrifugal, etc) that consume a significant amount of electric power. When renewable energy sources are the main source of energy, a central problem is balancing the power consumption with the power production; this is solved here using the active load concept used in micro grids (see [6], [7] and references therein).

More precisely, small desalination plants are considered here, as they are frequently installed in remote areas powered by renewable energies (see [8] and [9]), and a proposal for its control, that has been developed in the context of the H2 Ocean Project*, is presented and evaluated here. In fact, many different ideas have been proposed in the literature for the control of these systems, as control significantly improves the performance (see for example [10], [11], [12] and [13] for some previous control proposals). In this case, following the proposal studied by some of the authors in [14], the desalination plant is considered to be partitioned in several stages, consisting of parallel lines connected through buffer tanks.

Each of them operates at a constant working point and can be connected or disconnected depending on the available energy and the amount of water stored in each tank. Thus, the control proposal discussed here is based on deciding which sections would be switched on or shut down. So, only the energy available at each time is used; while unused energy would be temporarily stored in batteries for later use. In order to minimize the use of batteries, most of the power should be immediately consumed by the desalination system; yet at the same time the water in all the sections of the process should be secured (by ensuring that the water is properly stored in the buffer tanks), and thus no production is lost.
The rest of the paper is organized as follows. In

Section II the problem statement is presented. Section III discusses the control system. Section IV presents the case study. Section V evaluates the results and a discussion is given. Finally the paper ends with a conclusion section.

II. PROBLEM STATEMENT

Figure 1 presents the main components of the desalination plants studied here. If the power supply changes by time, the production of water is also going to change by time in order to adapt to the available power. Changing the working point of the plant by selecting a different flow/pressure set point is not adequate for most Reverse Osmosis systems, as they are designed to correctly operate at a given set point, although connection and disconnection of the devices of the desalination plant may have constraint in practice. Thus, in a previous paper by the authors [14], it was proposed to partition the high pressure part of the RO plant in

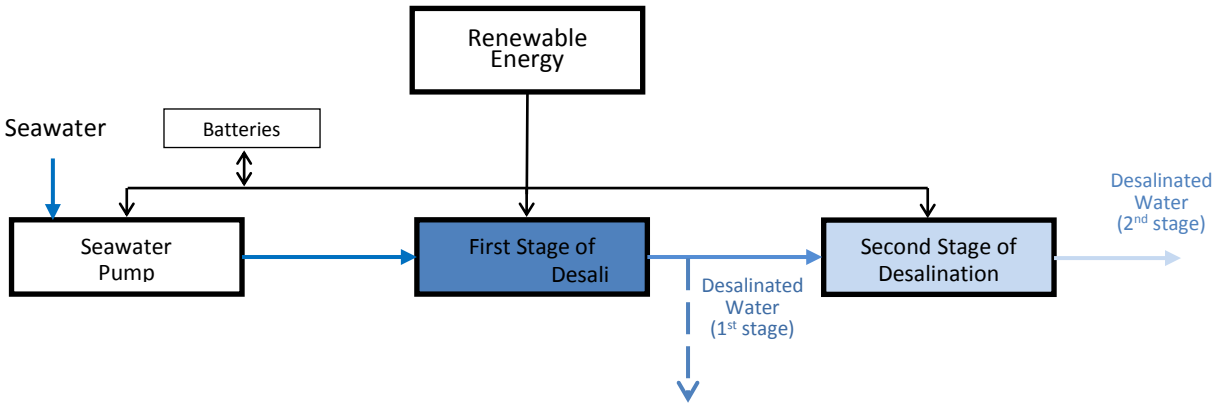

Fig .1. Renewable-Energy Powered Desalination system under study

the devices of the desalination plant may have constraint in practice. Thus, in a previous paper by the authors [14], it was proposed to partition the high pressure part of the RO plant in different parallel sections. Each section is operating as a standard RO plant (producing water at a fixed working point), regardless of being connected or disconnected when needed, as it follows a pre-programmed sequential functional chart. This proposal was selected as it is simple to implement in the existing control systems of Desalination Plants, making it possible to operate the whole plant as an active load by temporally disconnecting components until the predicted electrical consumption is fully used.

Unfortunately, the approach previously presented is not suitable enough in case there is a significant number of units of consumption being used, as it would conflict with the control objectives. Particularly speaking, it is not quite adequate for multi-stage desalination plants operated by lines, as the number of components with high electrical consumption (high pressure pumps) is too big to make a functional block diagram that accurately represents the control objectives. Thus, an alternative procedure is presented in the next section, which combines the possibility of implementation of existing control hardware (PLCs) with the fulfillment of conflicting control objectives.

III. CONTROL SYSTEM

This section studies the control system to be developed for that class of desalination plants. There are some previous works that use rule-based control strategies in the case of energy management [15, 16]. In [15] a rule-based control for a case of a series of a hybrid vehicle is designed; whereas in [16] a type of control strategy in case of ice storage systems is developed. In our proposal, we have selected a ruled-based control strategy for a reverse osmosis plant powered by renewable energy as it is simple enough to be implemented and give good results out of its operation.

A. Control Structure

For simplicity, the controller is presented for a single

seawater pump plant with two high pressure pumps for the first stage and two high pressure pumps for the second stage of the reverse osmosis. Parallel approaches can be developed for other configurations, maybe by adding more components and supplying different rated powers. The main aim is to ensure a smooth operation of the facility by means of the control system. We need to balance power consumption with the available power, by deciding which components of the plant are connected or disconnected. These components are:

- The seawater pump (SWP).
- Each of the lines and stages of the desalination system: in the simplified structure presented in Figure 2, they would be denoted RO1A, RO1B, RO2A and RO2B.

The control variables are then the connection of the SWP and the different sections of the Reverse Osmosis (see Figure 2).

B. Control Objectives

The main objectives can be written in a prioritized way as follows:

- Keep all the buffer tanks over a minimum level, so the next section can operate properly.
- Once a unit of consumption is connected, it should be kept operating at its nominal value as long as there is enough energy.

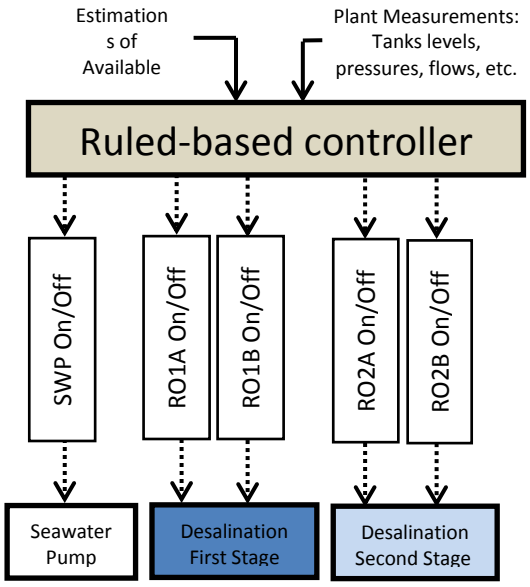

Fig .2. Proposed structure of the control system

C. Control Algorithm

The control strategy is based on two consecutive steps that are defined by different rules:

1. At each sampling time

create a prioritized list of units of the water plant based on the current state of the plant (i.e., the tank levels and the units that are currently operating) and the expected water demand. This list of prioritized units is denoted $\{U_i\}_{i=1}^{N}$. Another list of predicted energy demands should be associated, denoted $\{E_i\}_{i=1}^{N}$. These lists are generated based on the knowledge of the process, in order to fulfill the requirements given in section III.B. For example, the following algorithm is used for the structure in Figure Figure 3 to generate

- Initialize:
  $\{U_i\}\{SWP, RO1A, RO1B, RO2A, RO2B\}$
- At each sample time:

IF the level of SWT is LOW THEN
increase the priority of SWP
decrease the priority of RO1A and RO1B

IF the level of BT1 is LOW THEN
increase the priority of RO1A and RO1B
decrease the priority of RO2A and RO2B

IF the level of BT2 is LOW THEN
increase the priority of RO2A and RO2B

IF the level of SWT is HIGH THEN
decrease the priority of SWP
increase the priority of RO1A and RO1B

IF the level of BT1 is HIGH THEN
decrease the priority of RO1A and RO1B
increase the priority of RO2A and RO2B

IF the level of BT2 is HIGH THEN
decrease the priority of RO2A and RO2B

2. Distribute the available energy

from among the units, following the prioritized list $\{U_i\}_{i=1}^{N}$;; when possible, energy is assigned to those units with a higher priority. That is, a list of units that would be operating during the next sample, denoted $\{O_j\}_{j=1}^{m}$, is generated together with the corresponding list of predicted energy demands$\{EO_j\}_{j=1}^{m}$. The disconnected elements would be $\{D_j\}_{j=1}^{N-m}$,, with the corresponding unsatisfied energy demands$\{ED_j\}_{j=1}^{N-m}$.The energy consumed by the connected units fulfill $\sum_{j=1}^{m} EO_j \leq E$, while all the units in the set of disconnected units fulfill $E - \sum_{j=1}^{m} EO_j \leq ED_k \quad \forall k$

These lists can be generated by examining the list of predicted energy demands, $\{E_i\}_{i=1}^{N}$,, generated in parallel with $\{U_i\}_{i=1}^{N}$,, as given by the following Algorithm:

1. At each sampling time

- Initialize $\{EO\} = \{\}$; $\{ED\} = \{\}$; $m=0$;
- FOR $i = 1:N$

IF $E_i \leq E - \sum_{j=1}^{m} EO_j$ THEN

$m=m+1$

$O_m = U_i$

$EO_m = E_i$

OTHERWISE

$D_{i-m} = U_i$

$ED_{i-m} = E_i$

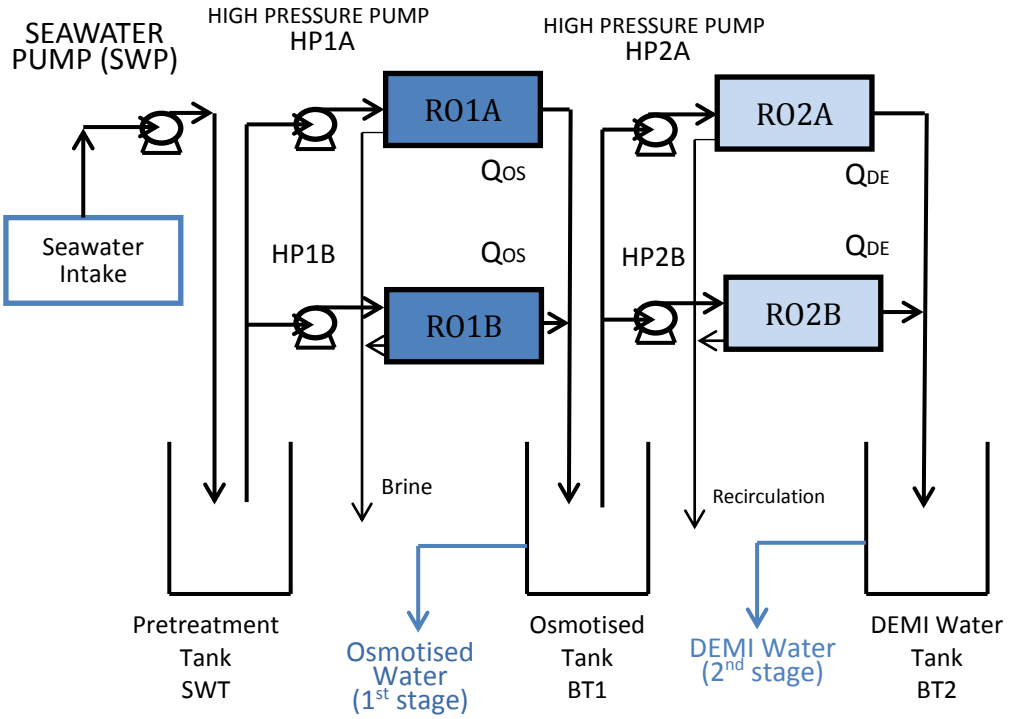

Figure 3: Structure of the desalination plants under study

IV. CASE STUDY

As a practical case study, the proposed control strategy was applied to a desalination plant for an industrial process designed to produce up to 68 m3/h of demineralized (DEMI) water and up to 20 m3/h of drinkable and service water. It consumes renewable electricity with variable production. A schematic diagram is presented in Figure 4.

The characteristics of each of its units of consumption are as follows:

- A 51 kW (PSWP) seawater pump that provides a nominal flow rate of 256 m³/h (QSW).

- The first stage of the Reverse Osmosis plant RO1 consists of two similar lines, each designed to produce 57 m^3/h (QOS) of water when connected (with a recovery ratio of around 45%), consuming 155 kW (PHP1) per line (corresponding to approximately 2.7 kWh/m^3) when they are operating.

- The second stage, RO2, also consists of two similar lines, which, when connected, produces 34 m3/h (QDE) of demineralized water (recovery ratio of 75%), in each line, consuming around 38 kW (PHP2) per line (approximately 1 kWh/m^3 of demineralized water produced).

To validate the proposed control system, meteorological data at the target location was used, and previously derived production models for power and water were used [7, 13, 14].

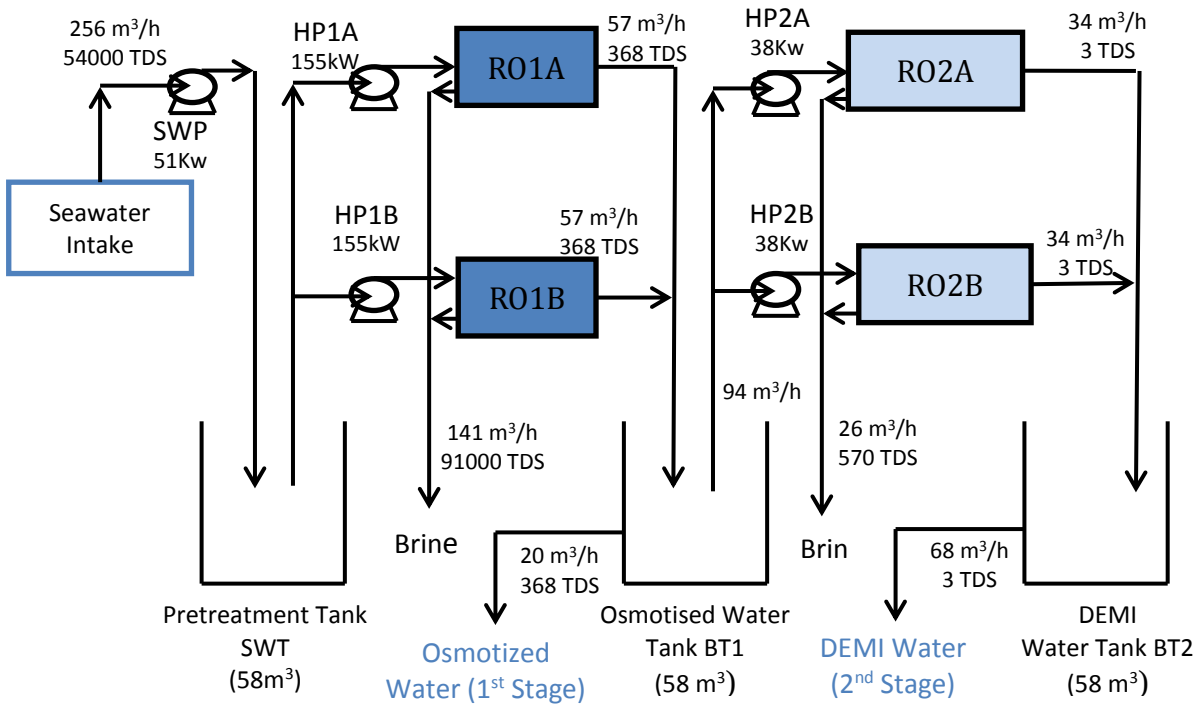

Figure 4: Case Study

V. RESULTS AND DISCUSSION

Some preliminary results for 20 days of operation are shown in Figures 5 to 13. The evaluation over 20 days confirms the correct operation of the control system for the parameters considered in the previous sections. As can be seen in Figure 5, the value of the power consumed by the system is lower than the available power. Figure 6 depicts the amount of DEMI water that is consumed in the electrolysis process. Figure 7 shows the pretreatment level tank.

Figure 8 shows the osmotized level tank. Figure 9 shows the DEMI water tank. In all cases, the levels are between the minimum and maximum defined to maintain them within a safety range. Figure 10 depicts the operation of the SWP. SWP is not switched on/off very frequently (the exact value can be seen in Table 1). Figures 11 and 12 show the operation of the first and second Reverse Osmosis stages, respectively. As in the previous figure, the performance of both stages of the Reverse Osmosis process can be considered correct. Figure 13 gives a zoom of the simulation results during 3 days of operation of all the figures explained above.

Finally, Table 1 summarizes the total parameters and consumption for the summer results. This corresponds to a mean production of 32.39 m3/h of water for the electrolysis, consuming a mean power of 219.79 kW.

Table 1. Parameters and consumptions

Mean Power Available (kW)	Mean Power Consumed (kW)	DEMI Water (m^3/h)	Osmotised Water (m^3/h)
271.66	219.79	32.39	55.71

Sea Water Pump ON/OFF (times/day)	1st Reverse Osmosis Stage ON/OFF (times/day)	2nd Reverse Osmosis Stage ON/OFF (times/day)
5.8	6.2	14.6

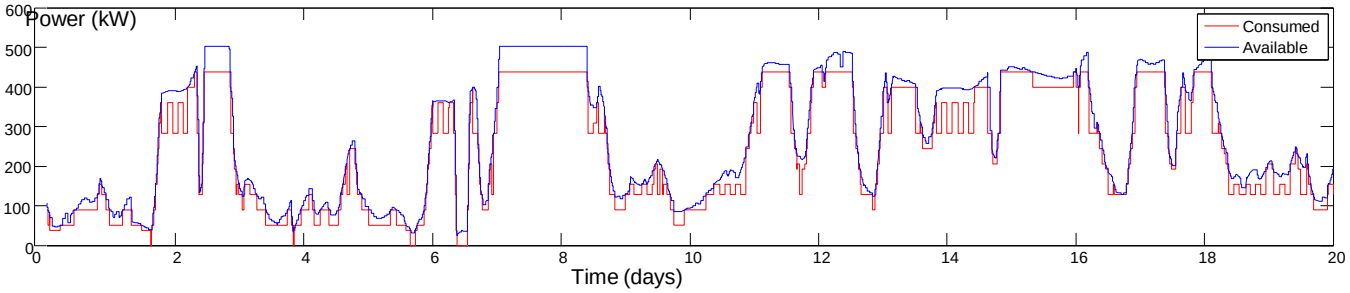

Figure 5 Power available and consumed by the desalination unit

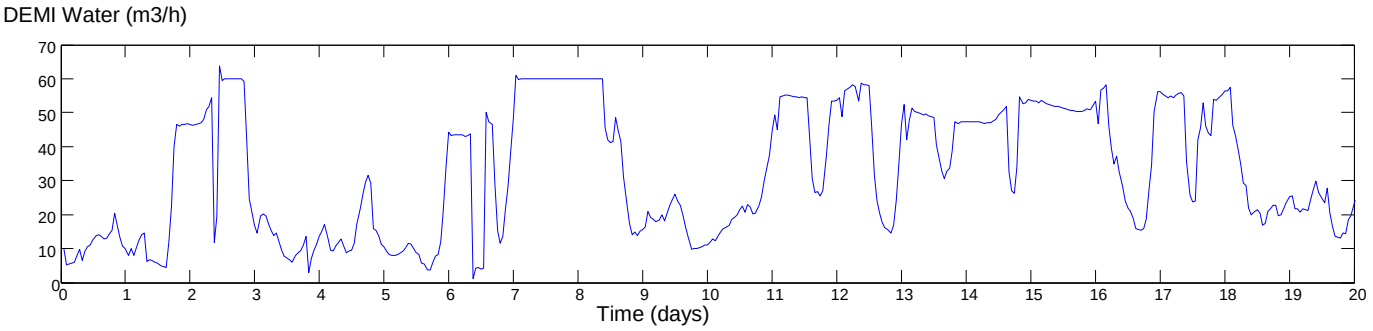

Figure 6 Demineralized (DEMI) water

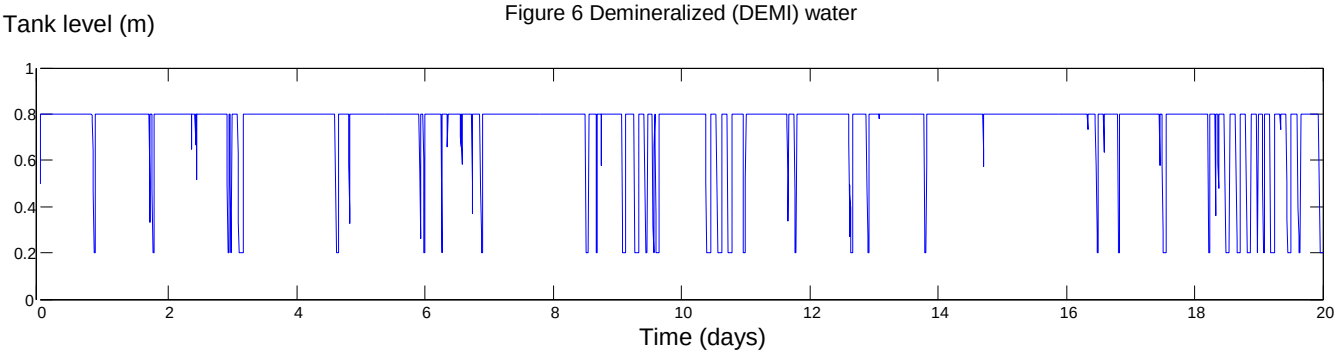

Figure 7 Pretreatment Tank level (winter)

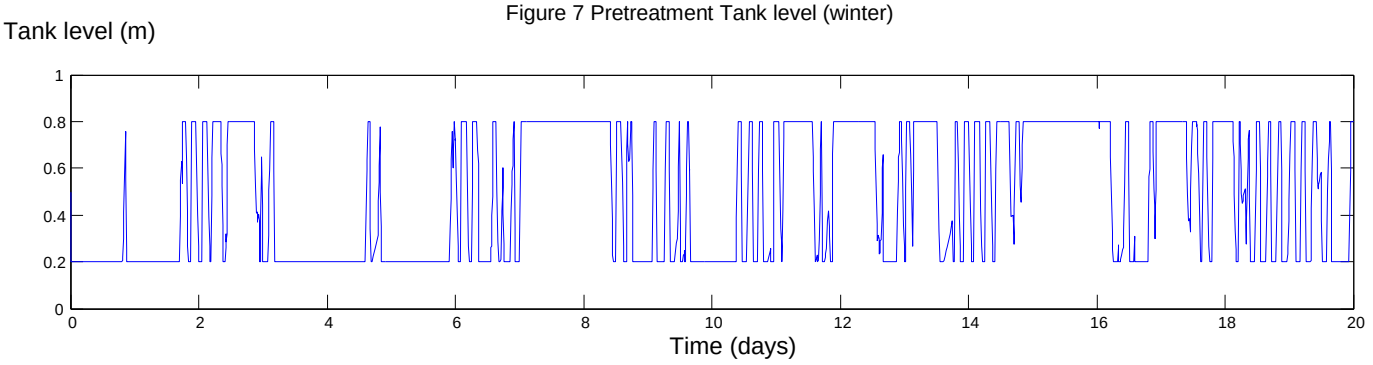

Figure 8 Osmotized Tank level (winter)

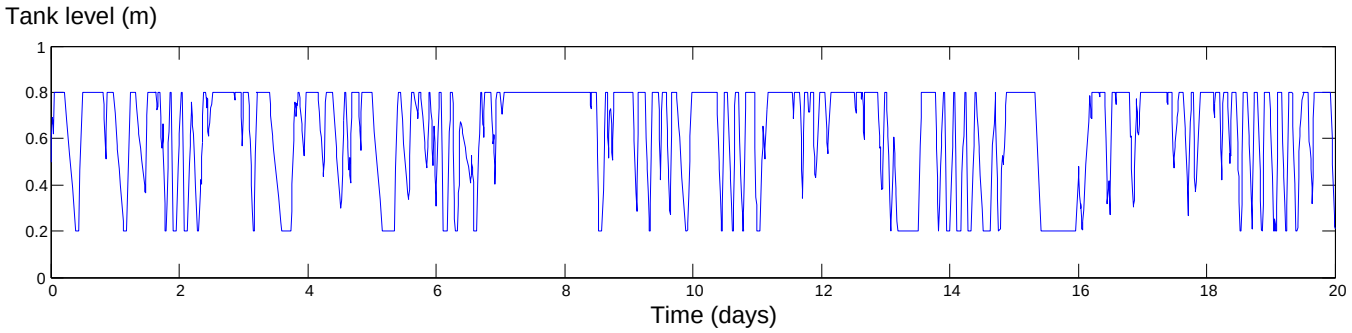

500

Figure 9 DEMI Tank level (winter)

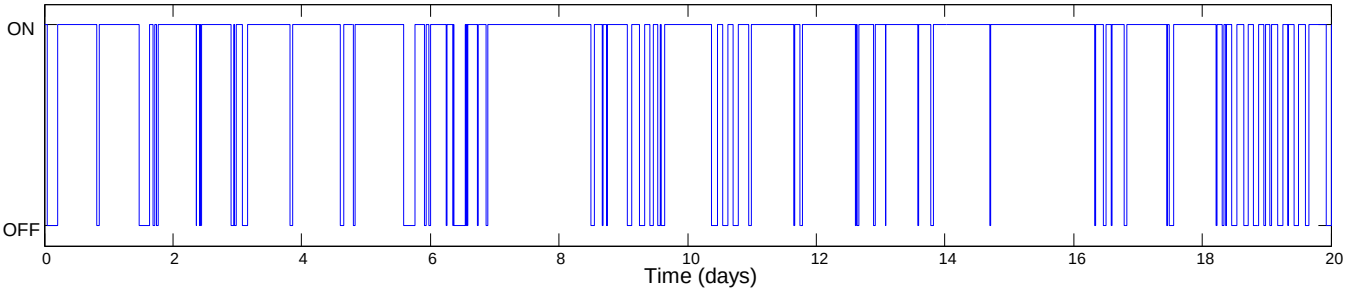

Figure 10 Operation of the seawater pump (SWP)

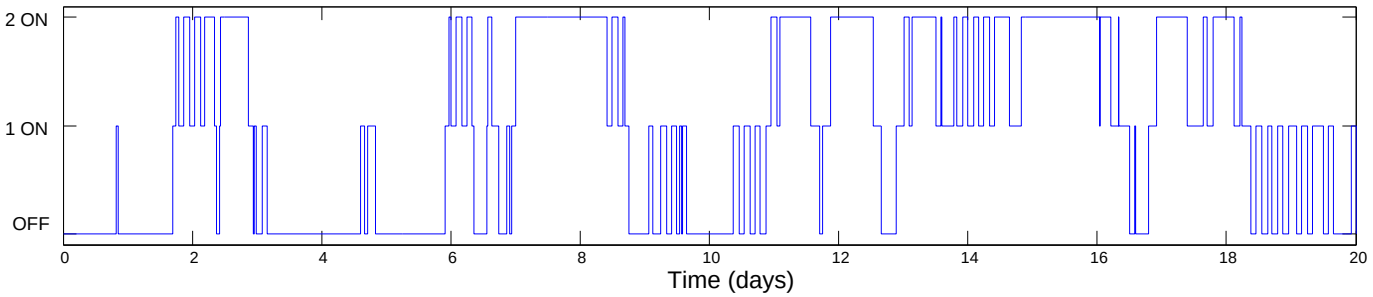

Figure 11 Operation of the first stage of the desalination unit (RO1A + RO1B)

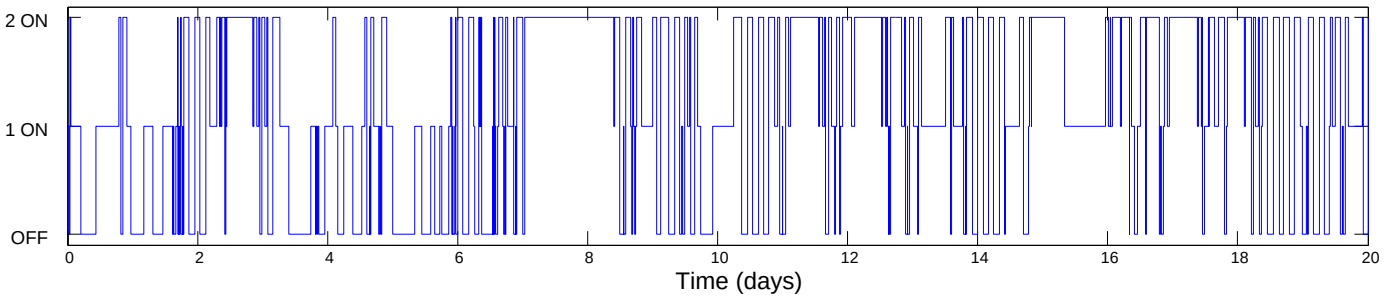

Figure 12 Operation of the second stage of the desalination unit (RO2A + RO2B)

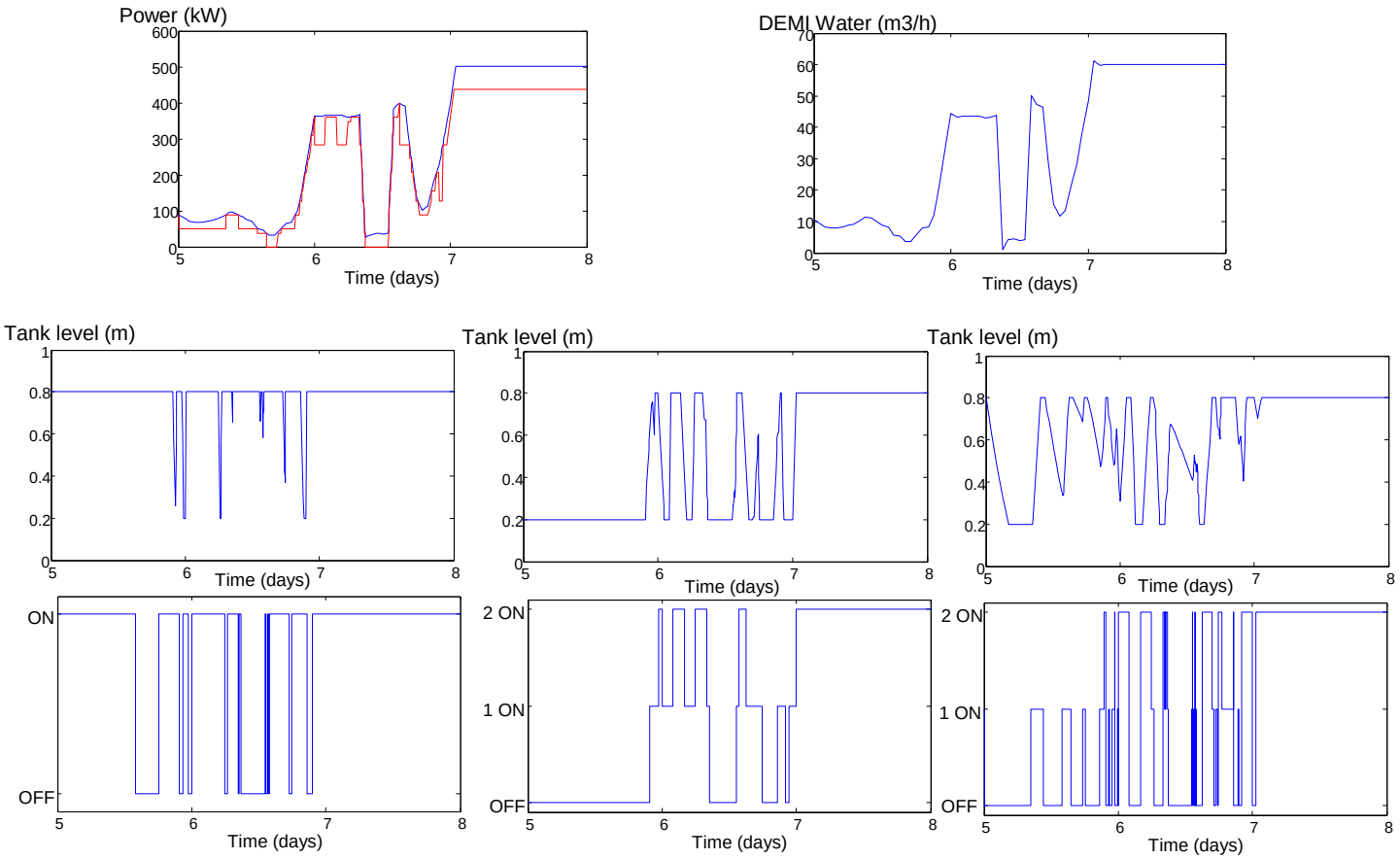

Figure 13 Zoom. From up to down and left to right: Power available and consumed by the desalination unit, water flow to electrolyzers, pretreatment, osmotized and DEMI tank level, operation of the SWP, first and second stage of the desalination unit.

VI. CONCLUSION

This work has discussed the problem of operating reverse osmosis (RO) plants under variable power availability conditions, which is a problem encountered when local green energy sources are used in off-grid locations. A rule-based control strategy has been designed based on giving preference, at each sample time, to the operation of the high pressure (HP) pumps of the RO plant that require action to avoid the occurrence of not fulfilling the water demand. The tanks make it possible to dampen variations in production as long as they have enough water stored; so a central aspect of the control system is the use of the information from the measured tank levels.

The proposed controller was evaluated for a specific RO plant, powered by wind and wave energies that produce demineralized water. Simulation results are provided to depict the correct operation of the plant with the designed controller. It must be pointed out that the proposed estimation is based on lines that operate at a fixed working point. However, current technical advances in the integration of frequency variators in HP pumps would enable some more adequate applications to operate the lines at variable set points: the adaptation of the proposed rule-based control strategy to these alternative installations would be the aim of future work. Finally, it is planned to include information on predicted energy availability and water demand.

REFERENCES

[1] Rodriguez, L.G. (2002) Seawater Desalination Driven by Renewable Energies: A Review Desalination, 143:pp.103–113.

[2] Mathioulakis, E., Belessiotis, V. and Delyannis, E. (2007) Desalination by Using Alternative Energy: Review and State-of-the-Art, Desalination. 203:pp.346–365.

[3] Fritzmann, C. Lowenberg, J. Wintgens, T. and Melin, T. (2007) State-of-the-Art of Reverse Osmosis Desalination, Desalination, 216:pp.1–76.

[4] Penate, B. and Rodriguez, L. G, (2012) Current Trends and Future Prospects in the Design of Seawater Reverse Osmosis Desalination Technology, Desalination, 284:pp.1–8.

[5] Wong, M. C., Martinez, K. G., Ramon, Z. and Hoek, E. M. V. (2012) Impacts of Operating Conditions and Solution Chemistry on Osmotic Membrane Structure and Performance. Desalination, 287:pp. 340–349.

[6] Lopes, J.A., Moreira C. L. and Madureira, A. G. (2006) Defining Control Strategies for Microgrids Islanded Operation. IEEE Transactions on Power Systems, 21(2), pp.916-924.

[7] Vandoorn, T. L., Renders B., Degroote, L., Meersman, B. and Vandevelde, L. (2011) Active Load Control in Islanded Microgrids Based on the Grid Voltage. IEEE Transactions on Smart Grid, 2(1), pp.139-151.

[8] Seibert, U., Vogt, G., Brenning, C., Gebhard, R. and Holz, F. (2004) Autonomous, Desalination System Concepts for Seawater and Brackish Water in Rural Areas with Renewable Energies. Desalination, vol. 168, pp. 29-37.

[9] Tadeo, F., Palacin, L. G., Salazar J. and de Prada C., (2011) Desalination in Remote Areas: A Prediction-Based Approach, in Proc. IDA World Congress, Perth, Australia.

[10] Robertson, M. W., Watters, J. C., Desphande P. B., Assef, J. Z , Alatiqi, I. M. (1996) Model Based Control for Reverse Osmosis Desalination Processes. Desalination, 104:pp.59–68.

[11] Gambier, A. and Badreddin, E. (2003) Application of Hybrid Modeling and Control Techniques to Desalination Plants. Desalination, 152:pp.175–184.

[12] McFall, C., Bartman, A., Christofides, P. and Cohen, Y. (2008) Control and Monitoring of a High-Recovery Reverse-Osmosis Desalination Process. Industrial & Engineering Chemistry Research, 47:pp.6698–6710.

[13] Palacin, L., Tadeo, F., de Prada, C., Elfil, H. and Salazar, J. (2011) Operation of Desalination Plants Using Hybrid Control, Desalination and Water Treatment. Vol. 25, pp. 119-126.

[14] Serna, A. and Tadeo, F. (2013) Offshore Desalination Using Wave Energy, Advances in Mechanical Engineering vol., Article ID 539857, 8 pages.

[15] Jalil, N., Kheir, N.A. and Salman, M. (1997) A Rule-Based Energy Management Strategy for a Series Hybrid Vehicle, American Control Conference, 1997. Proceedings of the 1997 (Vol. 1, pp. 689-693). IEEE.

[16] Drees, K.H, and Braun. J.E. (1996) Development and Evaluation of a Rule-Based Control Strategy for Ice Storage Systems. HVAC&R Research, 2(4), pp.312-334.

SELF SHIELDING TREATMENT TO PERFORM CELL CALCULATION FOR SEED FUEL IN THORIUM/URANIUM PWR USING DRAGON CODE

Ahmed Amin ABD El-HAMEED[1], Mohammed NAGY[2], Hanaa ABOU-GABAL[3]
[1] BSc in Nuclear Engineering and MSc degree researcher, Nuclear Engineering Department, Alexandria University, Egypt
[2] Professor Emirates, Nuclear Engineering Department, Alexandria University, Egypt,
[3] Professor and Head, Nuclear Engineering Department, Alexandria University, Egypt

Abstract - Time and precision of the results are the most important factors in any code used for nuclear calculations. Despite the high accuracy of Monte Carlo codes, MCNP and Serpent, in many cases their relatively long computational time causes difficulties in using any of them as the main calculation code. Monte Carlo codes are used mainly to benchmark the results. Ideally, the flux distribution in the lattice would be determined by solving the transport equation in the exact geometry of the lattice using continuous energy cross sections, the way a Monte Carlo code might. But because of time constraints, the calculation scheme within a lattice physics code is intended to reduce the overall computation time without sacrificing too much accuracy. The nuclear deterministic codes have limited precision due to the approximations made to solve the multi-group transport equation. Self –shielding treatment is responsible for the biggest error in any deterministic code; it is an algorithm that produces an average cross-section defined over the complete energy domain of the neutrons in a nuclear reactor.

The inaccuracy in deterministic codes is increased dramatically in the resonance period, where a small change in the neutron's energy may lead to a great change in the corresponding microscopic cross section. There are mainly two resonance self-shielding models commonly applied: models based on equivalence and dilution and models based on subgroup approach. The fundamental problem with any self-shielding method is that it treats any isotope as there are no other isotopes with resonance present in the reactor. The most practical way to solve this problem is to use multi-energy groups (50-200) that are chosen in a way that allows us to use all major resonances without self-shielding. This paper offers the best use of a known International Program (DRAGON Code) for nuclear reactor fresh cell calculations by using different methodologies, hypothesis and different Nuclear Data Library, with comparison of other well-known international codes, particularly MCNP5 code and WIMS-D5 Nuclear Data. Similar self-shielding methodologies were tested in other studies. However, all of these studies are concentrated on the low enriched nuclear fuel (3%) which is the standard fuel enrichment of most of nowadays nuclear power reactors. However, there are new designs which propose the use of higher enriched fuel for economical and safety purposes. In higher enriched fuel the effect of resonance interference of uranium isotopes is expected to change. Hence, it is important to test the validity of these self-shielding methodologies and hypothesis in such case. One of these new designs introduces the idea of developing thorium/uranium fueled PWRs. This design has been characterized by its good economics, wide safety margins, minimal waste burden and high proliferation resistance. In such design whole assembly seed and blanket are used, where individual seed and blanket regions each occupy one full size PWR assembly.

The seed fuel pin in this design has enrichment close to those used in research reactors (about 20%). In this paper, we selected the fresh seed fuel pin, which is used in thorium/uranium reactors, to be our physical model. Then, we performed cell calculations by solving 172 energy group transport equation using the deterministic DRAGON code. Two types of self-shielding models (equivalence and dilution models and subgroup models) are used. The data libraries used are WIMS-D5 and DRAGON libraries. To obtain the accuracy of the self –shielding treatments, the results are compared with the result obtained from the stochastic MCNP5 code. We also tested the sensitivity of the results to a specific change in self-shielding method implemented, for example the effect of applying Livolant-Jeanpierre Normalization scheme and Rimman Integration improvement on the

equivalence and dilution method, and the effect of using Ribbon extended approach on sub-group method.

Keywords **-** Nuclear Cell Calculation; Self-Shielding Treatment; Precision of Nuclear Deterministic Codes, DRAGON, MCNP5.

I. INTRODUCTION

Nuclear fuel cell calculation is one of the most complicated steps of neutron transport problems in the reactor core [1]. Broadly speaking, neutron physics problems need to be solved at three levels of precision with respect to the energy variable:

- In the epithermal domain, the many resonances of heavy nuclei such as uranium 238 typically require a few tens of thousands of energy groups in order to properly describe each of the resonances. It is not essential to handle the heterogeneities very precisely at this level; in fact, by using equivalence we can relate the real geometry to a homogeneous geometry.

- Handling the spectrum requires about a hundred energy groups; this can be done at the assembly constituting the elementary “mesh” of the core of a nuclear reactor, but it requires “microscopic” heterogeneity to be taken into account; this means on the scale of the fuel element or assembly.

- In practice, the multiplication factor of a core and the power distribution in it can be calculated to a few energy groups only, e.g. two groups for the usual calculations for pressurized water reactor cores. This calculation takes “macroscopic” heterogeneity into account, i.e. the differences between assemblies and axial variations. These three types of calculation must be performed one after the other: when calculations have been carried out at a given level, the mean values in space (homogenization) and energy (condensation) must be taken in order to prepare for the calculation at the next level. [8]

The first step in building lattice physics code is to create an energy group-dependent cross section library. This is the first approximation – which we assume we can accurately represent cross sections over a range of energies using constant values as opposed to point-wise data.

The number of energy groups needed and the location of the group boundaries are determined by the lattice physics code’s range of application. For example, analysis on mixed-oxide fuel requires different energy detail than does analysis on Uranium-oxide fuel; analysis on fast reactors requires different energy detail than does analysis on thermal reactors; analysis on light water reactors requires different energy detail than does analysis on heavy water reactors, and so on. From the early WIMS days through the1980s, the cross section libraries associated with production-level lattice physics codes were limited to 100 energy groups or fewer.

The original WIMS library contained 69 energy groups and many early lattice physics codes replicated that structure. In the early 1990s, HELIOS was released with a master library containing 190 energy groups, although this group structure was rarely used for analysis. Instead, a smaller library with 35 groups was routinely utilized. Today, it is common for libraries to contain hundreds of energy groups. [10] There are two generations of physical codes used to solve neutron transport problems. A few first generation lattice codes based of the four-factor formula are still in production use today.

The second generation lattice codes features a consistent multi-group (between 50 and 400 groups) representation of the neutron energies.
The main components of a typical second generation lattice code are the following:

- Library access and temperature interpolation.

- Resonance self-shielding calculation.

- Main flux calculation.

- Homogenization and condensation of the reaction rates

- SPH factor calculation.

- Isotopic depletion calculation; figure (1) illustrates the main components of a second generation lattice code [9]

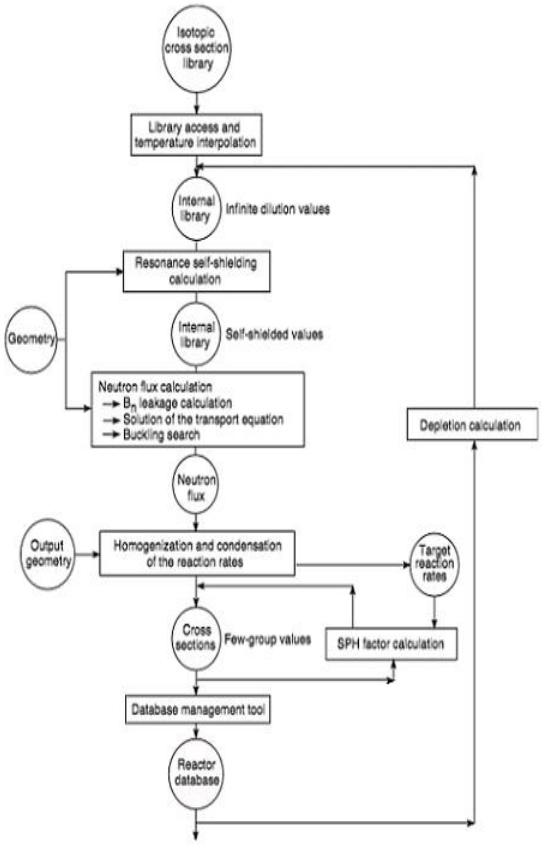

Fig .1. The main components of a second generation lattice code

For realistic systems with complex geometry and detailed energy dependency, transport equation can only be solved by using numerical methods implemented in the lattice codes. Those calculations go through several levels before the final solution is obtained. Each level of the calculation has its own characteristics, and any simplification at any step can lead to a poor final result. [2] In this paper, we focus on the self-shielding step as it is responsible of the biggest inaccuracy in any lattice code used to solve the multi-energy transport equation.

A self-shielding model is required in any lattice code in order to take into account the resonant behavior of the cross sections. [3] Self- Shielding is an algorithm that produces an average cross-section defined over the complete energy domain of the neutrons in a nuclear reactor. The microscopic self-shielded cross section for any reaction ρ in group g (σ_(ρ,g)^(˜)) which is defined in equation (1) as:

$$\tilde{\sigma}_{\rho,g}=\mu_g \frac{\int_{U_{g-1}}^{U_g} du\ \sigma_\rho\ \Phi(u)}{\int_{U_{g-1}}^{U_g} du\ \Phi(u)} \quad (1)$$

where u is the lethargy (= ln(E0/E)), ug is the upper lethargy limit of group g, μg is the SPH factor obtained from the multi-group equivalence procedure, φ(u) is the neutron flux inside the resonances and σρ(u) is the microscopic cross section for nuclear reaction ρ. [3],[5] The development of methodologies used to treat resonance self-shielding with respect to energy was improved from assuming that the resonant material was purely absorbent to the improvement made by applying the approach used by Michel Livolant and his doctoral student Françoise Jeanpierre in the late 1960s.

This improvement allowed for scattering and slowing down by the resonant material, which affected self-shielding factors, heterogeneous-homogeneous equivalence, Dancoff effect and Doppler Effect. This theory was introduced at that time in the first version of APOLLO. With the new developments introduced in Version 2 of this code, there was renewed interest in the theory of resonant absorption of neutrons, because the inadequacies of Livolant and Jeanpierre's original theory had been clearly identified. [8]

Two resonance self-shielding shielding models are commonly applied [2]:

- Model based on equivalence and dilution:

This approach is based on the rational expansion of fuel to fuel collision probabilities, either in closed or open cell (or assembly). For infinite and homogeneous problems, each self-shielded cross section of each resonant isotope is tabulated against the dilution parameter.

For heterogeneous problems, a heterogeneous resonant situation is replaced with a linear combination of homogeneous resonant problems. In its simplest form, this technique reduced to the use of Bell and Dancoff factors. This kind of model is implemented in the deterministic code WIMS-D5. The extension of this model has been proposed by Stamm'ler and Abbate (PHOENIX code) and later by Hébert and Marleu (DRAGON code, SHI module) [11].

It is known as a generalized Stamm'ler model (GSM). To achieve better accuracy with the GSM model, two additional improvements are implemented in the Dragon code:

- Use of the Nordheim distributed self -shielding effects in a fuel rod (Level=1 in DRAGON code)

- The Nordheim distributed self-shielding model and use of the Riemann integration method (Level=2).

II. MATERIALS AND METHOD

A. *Physical Model (Case study)*

To perform cell calculations, we selected our physical to be the initial composition of the seed fuel pin used Thorium/Uranium fuel. This design uses Whole assembly Seed and Blanket, where individual seed and blanket regions each occupy one full size PWR assembly. Figure 2 illustrates SBU and WASB Assembly Configuration & Pin Cell Models of Seed and Blanket. The initial composition and the design parameters are illustrated in tables 1, 2 respectively.[4]

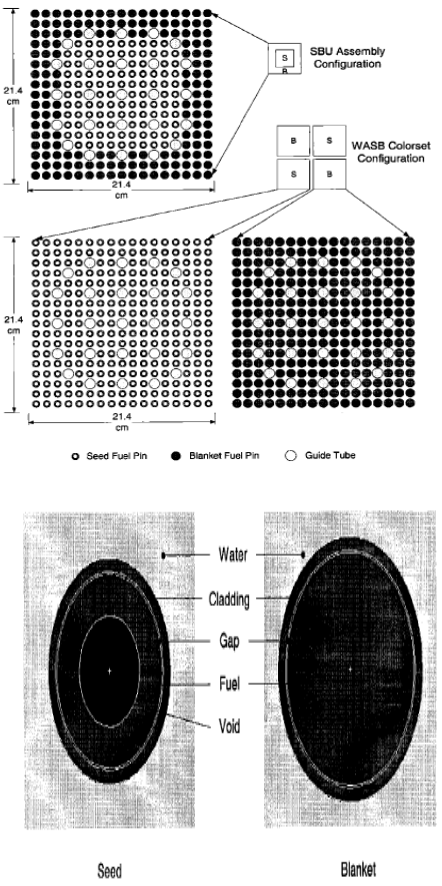

Fig .2. SBU and WASB Assembly Configuration & Pin Cell Models of Seed and Blanket

Table 1. Initial Isotopic Composition

		Nuclide	Weight Percent w/o	Number Density 1/ cm^3
Fuel	Seed	U-234	0.1410	3.73911E+19
		U-235	17.6300	4.65393E+21
		U-238	70.3790	1.83438E+22
		O-16	11.8500	4.59793E+22
	Blanket	Th-232	79.0955	1.92206E+22
		U-234	0.0071	1.71054E+18
		U-235	0.8814	2.11441E+20
		U-238	7.9326	1.87893E+21
		O-16	12.0834	4.26071E+22
Coolant, H_2O		H-1	11.19	6.66295E+22
		O-16	88.81	3.33339E+22
Cladding Zircaloy-4		O	0.125	3.08281E+20
		Cr	0.100	7.58663E+19
		Fe	0.210	1.48338E+20
		Zr	98.115	4.24275E+22
		Sn	1.450	4.81835E+20

Table 2. Pin Cells design Parameters

Parameter	Value	
	Seed	Blanket
Fuel Pellet Radius, cm	0.22-0.385	0.4646
Cladding Inner Radius, cm	0.3932	0.4728
Pin Pitch, cm	1.26	1.26
Fuel Density, g/cm^3	10.3024	9.3624
Coolant Density, g/cm^3	0.977	
Cladding Density, g/cm^3	6.55	
Power Density, kW/liter	129.58	79.42

B. *Self-shielding calculations*

The neutronic calculations were carried out using DRAGON code with DRAGON library (or WIMS-5D library) and two self-shielding modules (SHI for equivalence and dilution method, USS for sub-group method) to calculate Kinf. The results are then benchmarked using the well-known Monte Carlo MCNP5 code. Hence, various self-shielding modules and data libraries are tested. Also, the sensitivity to various self-shielding deterministic approximations are tested.

C. *Nuclear Codes Used for Analysis*

Two different classes of codes are available in respect to solving transport equation: stochastic and deterministic models. In our study we used stochastic models in MCNP, which are the most accurate but

also the most time consuming, as well as the deterministic code DRAGON Version 4. The nuclear codes used for cell calculations are:

- MCNP5 [6]

It is a general-purpose Monte Carlo N–Particle code that can be used for neutron, photon, electron, or coupled neutron/photon/electron transport, including the capability to calculate Eigen values for critical systems. The code treats an arbitrary three-dimensional configuration of materials in geometric cells bounded by first- and second-degree surfaces and fourth-degree elliptical tori. It was tested on several criticality benchmarks, so it is verified to be a reliable and accurate code.

Therefore, in this paper obtained value kinf of fresh seed fuel is set to be the reference value of all deterministic calculations, because it has point wise consentaneous energy data that eliminates self-shielding issue of multi-groups.

- DRAGON [7], [2]

The computer code DRAGON contains a collection of models, which can simulate the neutronic behavior of a unit cell or a fuel assembly in a nuclear reactor. It includes all of the functions that characterize a lattice cell code, namely: the interpolation of microscopic cross sections which are supplied by means of standard libraries; resonance self-shielding calculations in multidimensional geometries; multi-group and multidimensional neutron flux calculations which can take into account neutron leakage; transport or transport-diffusion equivalence calculations as well as editing of condensed and homogenized nuclear properties for reactor calculations, and finally isotopic depletion calculations.

The code DRAGON contains a multi-group iterator conceived to control a number of different algorithms for the solution of the neutron transport equation. Each of these algorithms is presented in the form of a one group solution procedure where the contributions from other energy groups are included in a source term. The current version of DRAGON contains many such algorithms.

The SYBIL option which solves the integral transport equation using the collision probability method for simple one dimensional (1–D) geometries (either plane, cylindrical or spherical) and the interface current method for 2–D Cartesian or hexagonal assemblies. The EXCELL option solves the integral transport equation using the collision probability method for general 2–D geometries and for three-dimensional (3–D) assemblies. The MCCG option solves the integro-differential transport equation using the long characteristics method for general 2–D and 3–D geometries. The execution of DRAGON is controlled by the generalized GAN driver. [2] Version 4 is a new distribution of the reactor physics computer code sat GAN .Its components are:

DRAGR module in NJOY, GAN lib tools, and Modules (calculation operators) of the following codes:

- Dragon: lattice code
- Trivac: reactor (full core) code Donjon: simulation of reactor operation
- Optex: reactor design optimization.[9]

D. Nuclear Data Libraries used

In order to obtain the final solution, isotopic cross section libraries are required. We used the following libraries:

- 172 energy group WIMS-D5 library format based on ENDF/B-VII.0 evaluated nuclear data library (WIMS-D5)
- 172group DRAGON-lib library format based on ENDF/B-VII.0 evaluated nuclear data library (DRAGON 4)
- A compact ENDF ACE format in MCNP5 based on ENDF/B-VII.0

E. Deterministic Methods used

In this paper, we study sixteen deterministic methods; each method is given an identification number from 1 to 16. All these methods are implemented using the same lattice code-DRAGON Version4- and calculated for the same number of energy groups (172), but they have different tracking modules and data libraries(DRAGON-lib/ WIMS-D5-lib).

These sixteen deterministic methods are:

- One dimensional self-shielding calculations are made using the equivalence and dilution method to obtain the microscopic cross-sections of isotopes with resonance present in the material without using neither Norhdeim distribution nor Rimman integration improvements on the equivalence and dilution method (SHI level=0 in DRAGON code). Also, Livolant and Jeanpierre normalization scheme (which modifies the self-shielded averaged neutron fluxes in heterogeneous geometries) is not used (NOLJ module in DRAGON code). The data library used is 172 energy groups WIMS-D5 library.

- One dimensional self-shielding calculations are made using the equivalence and dilution method with Norhdeim distribution improvement (SHI Level=1 module). But without Livolant and Jeanpierre normalization scheme (NOLJ). The data library used is 172 energy groupsWIMS-D5 library.

- One dimensional self-shielding calculations are made using the equivalence and dilution method using both Norhdeim distribution and Riemann Integration improvements (SHI Level=2 module). But Livolant and Jeanpierre normalization scheme (NOLJ module) is not used. The data library used is 172 energy groups WIMS-D5 library.

- One dimensional self-shielding calculations are made using the equivalence and dilution method with resonance present in the material without using any improvements on the equivalence and dilution method (SHI Level=0 module). Livolant and Jeanpierre normalization scheme (LJ module) is used. The data library used is 172 energy groups WIMS-D5 library.

- One dimensional self-shielding calculations are made using the equivalence and dilution method with using Norhdeim distribution improvement (SHI Level =1 module). Livolant and Jeanpierre normalization scheme (LJ module) is used. The data library used is 172 energy groups WIMS-D5 data library.

- One dimensional self-shielding calculations are made using the equivalence and dilution method using Norhdeim distribution and Rimman integration improvements (SHI Level=2 module). Livolant and Jeanpierre normalization scheme (LJ module) is used. The data library used is 172 energy groups-DRAGON library.

- One dimensional self-shielding calculations are made using the equivalence and dilution method without any improvements on the equivalence and dilution method (SHI Level=0 module). Livolant and Jeanpierre normalization scheme is not used (NOLJ module). The data library used is 172 energy groups- DRAGON library.

- One dimensional self-shielding calculations are made using the equivalence and dilution method Norhdeim distribution improvement (SHI Level=1 module). Livolant and Jeanpierre normalization scheme is not used (NOLJ module). The data library used is 172 energy group DRAGON library.

- One dimensional self-shielding calculations are made using the equivalence and dilution method with using Norhdeim distribution and Rimman integration improvements (SHI Level=2 module). Livolant and Jeanpierre normalization scheme is not used (NOLJ module). The data library used is 172 energy groups DRAGON library.

- One dimensional self-shielding calculations are made using the equivalence and dilution method without using any improvements on the equivalence and dilution method (SHI Level=0 module) with the Livolant and Jeanpierre normalization scheme (LJ module). The data library used is 172 energy groups DRAGON library.

- One dimensional self-shielding calculations are made using the equivalence and dilution method using Norhdeim distribution improvement (SHI Level=1 module). Livolant and Jeanpierre normalization scheme (LJ) is used. The data library used is 172 energy groups DRAGON library.

- One dimensional self-shielding calculations are made using the equivalence and dilution method using Norhdeim distribution and Rimman integration improvements Livolant and Jeanpierre normalization scheme (LJ) is used. The data

library used 172 energy groups- DRAGON library.

- Two dimensional Self-shielding calculations are made using the subgroup with 172 energy groups WIMS-D LIB calculations with SUBG method where the physical Probability Tables are computed using the RMS approach (root-mean-square).

- Two dimensional Self-shielding calculations are made using the subgroup with 172 energy groups WIMS-D LIB calculations with PTSL method where mathematical probability tables and slowing down correlated weight matrices can be computed in selected energy groups using the Ribbon extended approach.

- Two dimensional Self-shielding calculations are made using the subgroup with 172 energy groups DRAGON calculations with SUBG method where the physical probability tables are computed using the RMS approach (root-mean-square).

- Two dimensional self-shielding calculations are made using the subgroup with 172 energy groups DRAGON library calculations with PTSL method where mathematical probability tables and slowing down correlated weight matrices can be computed in selected energy groups using the Ribbon extended approach.

These sixteen deterministic methods are summarized in table 3 as follows:

Table 3. Sixteen self-shielding methodologies which are applied and tested

Method Number	Code Used	Tracking Module	Data Library
1	DRAGON	SYBIL+SHI (L=0) NOLJ	172gWIMS-D
2	DRAGON	SYBIL+SHI (L=1) NOLJ	172g WIMS-D
3	DRAGON	SYBIL+SHI (L=2) NOLJ	172gWIMS-D
4	DRAGON	SYBIL+SHI (L=0) LJ	172gWIMS-D
5	DRAGON	SYBIL+SHI (L=1) LJ	172g WIMS-D
6	DRAGON	SYBIL+SHI (L=2) LJ	172g WIMS-D
7	DRAGON	SYBIL+SHI (L=0)NOLJ	172g DRAGON
8	DRAGON	SYBIL+SHI (L=1) NOLJ	172g DRAGON
9	DRAGON	SYBIL+SHI (L=2) NOLJ	172g DRA GON
10	DRAGON	SYBIL+SHI (L=0) LJ	172g DRAGON
11	DRAGON	SYBIL+SHI (L=1) LJ	172g DRAGON
12	DRAGON	SYBIL+SHI (L=2) LJ	172g DRA GON
13	DRAGON	USS-SUBG	172gWIMS-D
14	DRAGON	USS-PTSL	172gWIMS-D
15	DRAGON	USS-SUBG	172g DRAGON
16	DRAGON	USS-PTSL	172g DRAGON

III. RESULTS AND DISCUSSION

A. MCNP5 Result of K_{inf}

For our physical Model (fresh seed cell used in thorium/uranium PWR) using MNCP 5 the resultant value of Kinf is 1.66440 with an estimated standard deviation of 0.00061. Figure (2) illustrates the MCNP5 simulation of fresh seed fuel cell drawn by Vised program, the design parameters are as indicated in tables 1 and 2.

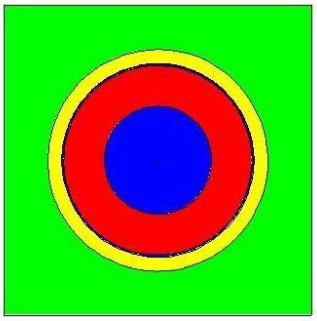

Fig .3. MCNP5 seed cell simulation

In this paper, sixteen deterministic self-shielding methods are tested by comparing the resultant Kinf with the reference value obtained by MCNP5 code. The resultant values of Kinf for different modules in DRAGON code compared with the reference MCNP value of Kinf illustrated in figure 3, show that of the sixteen tested deterministic methods the best are methods of numbers 11, 12, 15, and 16. In these methods, high accuracy was that found using the equivalence and dilution method with Norhdeim distribution and Rimman integration improvements and Livolant and Jeanpierre normalization scheme with 172 energy groups DRAGONLIB. (Method number 12)The absolute error in this case is 0.000662 which is approximately the standard deviation of the Monte Carlo result of Kinf. Also, using subgroup method with SUBG with 172 energy groups DRAGON-library is also a very sufficient self-shielding treatment as its absolute error is only 0.001039.

B. Sensitivity of Kinf to various deterministic modules and data libraries

Using DRAGON code the sensitivity of the obtained value of Kinf to the various modules and data libraries is studied to identify the impact of each of these modules on the efficiency of the self-shielding treatment used.

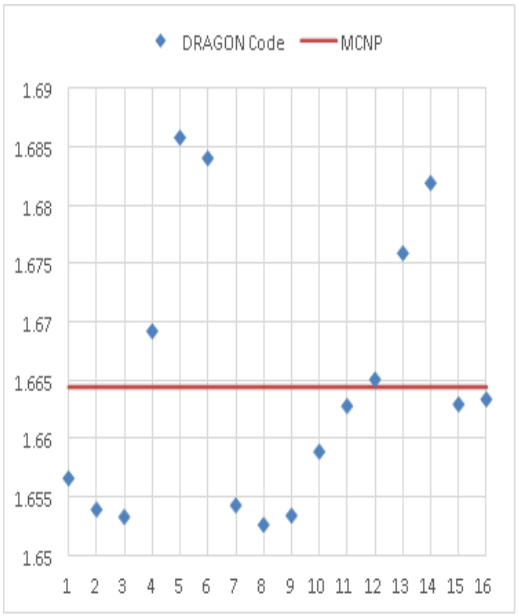

Fig .4. K_{inf} as obtained by the different 16 self-shielding methodologies implemented in DRAGON code Vs. the reference value obtained by MCNP5 code.

C. Effect of changing data libs. on SHI module

The resultant values of Kinf in case of using equivalence and dilution method for various deterministic options are LJ/NOLJ, L=0 / L=1 / L=2. These calculations are performed using DRAGON-LIB/ WIMS-LIB is illustrated in Fig 4. It shows that there is advantage of using DRAGON-LIB with the equivalence and dilution method of self-shielding treatment.

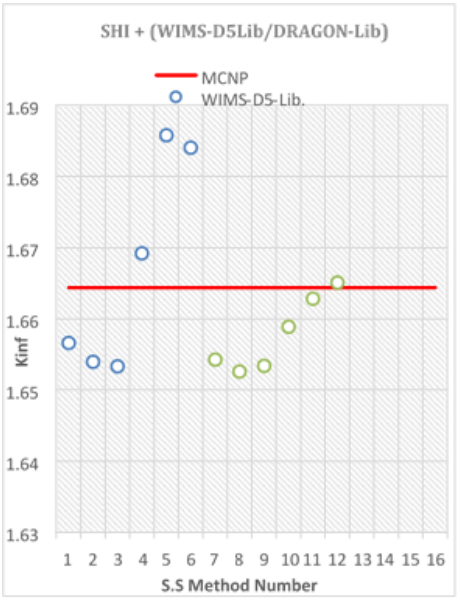

Fig .5. K_{inf} using SHI module for WIMS-D5 Lib implemented in DRAGON code Vs. The reference value obtained by MCNP5 code

The results show that a high accuracy is obtained using DRAGONLIB especially with the LJ module.

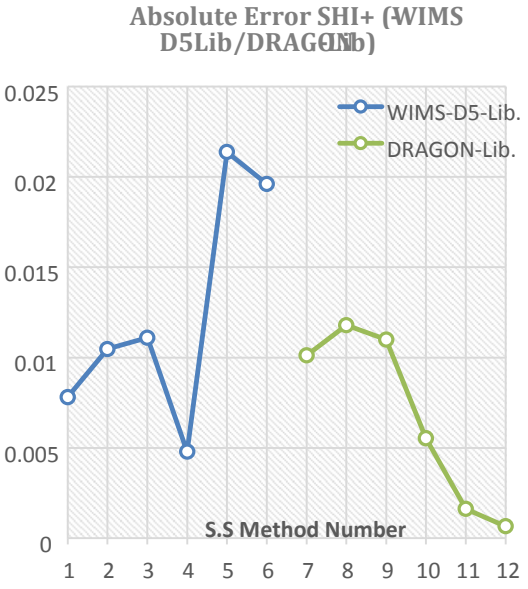

Fig .6. Absolute error in Kinf using SHI module for different Libraries

The absolute error in Kinf for SHI with DRAGON library and WIMS-D5 library (figure 5) may be divided into two periods:

- Period contains points (1, 2, 3, 4) for WIMS-D5 library and points (7, 8, 9, 10) for DRAGON library.

- Period contains points (5, 6) for WIMS-5D-library and points (7,8) in DRAGON library.

It is observed in Fig.5 that the effect of changing Data-lib in the first period is trivial, but the effect of changing Data-lib in the second period has a significant effect. Hence, it can be concluded that for equivalence and dilution and without Livolant and Jeanpierre normalization scheme (SHI + NOLJ), changing between WIMS-D5 and DRAGON libraries has a trivial effect. However, the results also show that DRAGON library is more suitable with Livolant and Jeanpierre normalization scheme (SHI +LJ) than WIMS-D5 library as higher accuracy is obtained.

D. Effect of changing data libraries on USS module

The use of DRAGON-LIB and WIMS-LIB for self-shielding using sub-group method and SUBG / PTSL modules (Fig. 6) illustrates that the result of Kinf using DRAGON library results in higher accuracy than WIMS-SD library.

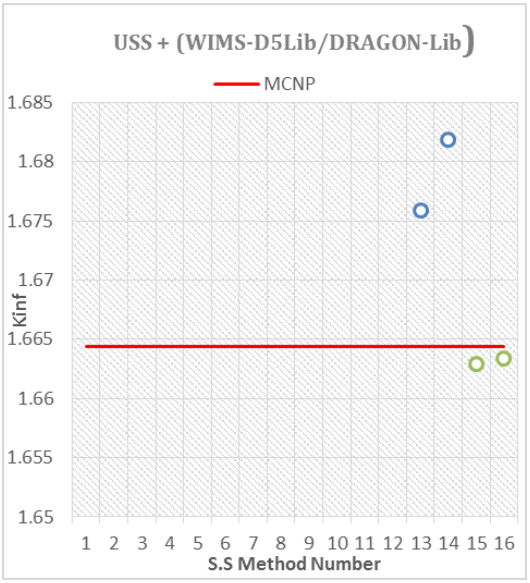

Fig .7. Kinf results of using USS module for WIMS-D5/DRAGON data libraries compared with reference value obtained by MCNP5

E. Effect of Norhdeim Distribution and Rimman Integration Improvements

In figure 7, the effect of Norhdeim distribution alone (level=1), normalization distribution and Riemann Integration improvements (level=2) on improving the results of a deterministic module uses equivalence and dilution method with LJ normalization scheme. The effect was tested by comparing the resultant value of Kinf in each case with the reference value obtained using the Monte Carlo MCNP5 code.

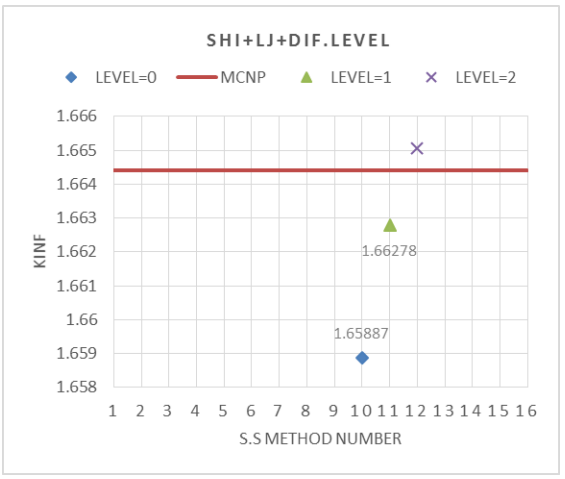

Fig .8. Ki_{nf} using SHI module for different improvement levels compared with the reference value obtained by MCNP5

The results show that the improvements are sufficient to obtain higher accuracy. Where level=0 stands for the case in which neither Norhdeim distribution nor Riemann integrations are used.

IV. CONCLUSION

For our standard fresh seed fuel, the following items are concluded:

- For equivalence and dilution self –shielding method without applying Livolant and Jeanpierre normalization scheme (SHI + NOLJ), changing between WIMS-D5 and DRAGON data libraries has a trivial effect. However, the results also show that DRAGON library is more suitable if Livolant and Jeanpierre normalization scheme is used (SHI +LJ) than WIMS-D5 library, as higher accuracy is obtained.

- Using equivalence and dilution method with Norhdeim distribution and Rimman integration improvements and Livolant and Jeanpierre

normalization scheme is a very sufficient deterministic method to deal with resonant self-shielding problem for fresh fuel – even with a relatively high U-235 concentration, as the absolute error is only 0.000662 .

- Using sub-group method with PTSL or SUBG with 172 energy groups DRAGON library method shows high accuracy for fresh fuel.

- Norhdeim distribution and Rimman integration improvements are sufficient to improve the results id DRAGON library is used.

REFERENCES

[1] M. Shafii, Z. S. (2012). “Nuclear Fuel Cell Calculation Using Collision Probability with Linear Non Flat Flux Approach”. World Journal of Nuclear Science and Technology, 2, 49-53.

[2] DušanĆalić, MarjanKromar, Andrej Trkov. (2011). “Use of Monte Carlo and Deterministic Codes for Calculation of Plutonium Radial Distribution in a Fuel Cell. International conference of Nuclear Energy for Europe.

[3] H´ebert, A. (April 6 – 11, 2003). Development of a new resonance self-shielding methodology based on probability tables. Proc. Int. Mtg. on Nuclear Mathematical and Computational Sciences . Gatlinburg, Tennessee.

[4] Wang, M. S., & DriscollD, M. J. (June 2003). PHD Thesis : “Optimization of a Seed and Blanket Thorium-Uranium Fuel Cycle for Pressurized Water Reactors” . MIT. Retrieved from http://dspace.mit.edu/handle/1721.1/29956

[5] H´EBERT, A. (April 25-29, 2004). “A Mutual Resonance Shielding Model Consistent with Ribon Subgroup Equations. PHYSOR - the Physics of Fuel Cycles and Advanced Nuclear Systems: Global Developments”, (pp. on CD-ROM, American Nuclear Society, Lagrange Park, IL. (2004)). Chicago, Illinois.

[6] Team, X.-5. M. (April, 2003). MCNP5 “User Manual” (Vol. Volume I: Overview and Theory). LANL

[7] G.Marleau, A. H. (April 25, 2012). “User Guide for DRAGON Version4. Institut de g´enie nucl´eaire D´epartement de g´enie m´ecanique ´ Ecole Polytechnique de Montr´eal”. Retrieved from www.polymtl.ca/merlin/downloads/IGE294.pdf

[8] Reuss, P. (2008). Neutron Physics. France: EDP Sciences.

[9] AlainH´ebert. (2008). "Neutronslowing-down and resonance self-shielding". In Course ENE6101. Institut de g´enie nucl´eaire Ecole Polytechnique de Montr´eal.

[10] Cullen, D. E. (n.d.). "Nuclear Data Preperation" In D. G. Cacui, Handbook of Nuclear Engineering, Volume 1 (p. 279).

[11] Marleau, A. H. (1991). "Generalization of the Stamm’ler Method for the Self-Shielding of Resonant Isotopes in Arbitrary Geometries". Nuclear Science and Engineering , 108, 230-239. Retrieved from http://www.ans.org/pubs/journals/nse/a_23821

Economical Feedback of Increasing Fuel Enrichment on Electricity Cost for VVER-1000

Dwiddar,M. S[1]., Badawi, A[1]. A., Abou-Gabal, H. H[1]. El-Osery, I. A.[2], Badawy, M. R[2],
[1] Faculty of Engineering, Alexandria University
Alexandria, Egypt.,
[2]Nuclear Power Plants Authority, Nasr City, Cairo, Egypt.

Abstract **-** A methodology of evaluating the economics of the front-end nuclear fuel cycle with a price change sensitivity analysis for a VVER-1000 reactor core as a case study is presented. The effect of increasing the fuel enrichment and its corresponding reactor cycle length on the energy cost is investigated. The enrichment component was found to represent the highly expenses dynamic component affecting the economics of the front-end fuel cycle. Nevertheless, the increase of the fuel enrichment will increase the reactor cycle length, which will have a positive feedback on the electricity generation cost (cent/KWh). A long reactor operation time with a cheaper energy cost set the nuclear energy as a competitive alternative when compared with other energy sources.

Keywords **-** Front end fuel cycle economics; electricity cost; VVER-1000.

NOMENCLATURE –

a: Conversion factor for uranium yellow cake (U3O8)
AF: Availability Factor
CL: Cycle length (days)
Cfab: Cost of fabrication (M$)
Cen: Cost of enrichment (M$)
Cconv: Cost of conversion (M$)
CYC: Cost of yellow cake (M$)
CTotal: Front-end fuel cycle total cost(M$)
Celec: Direct electricity generated cost (cent/kWh)
ef: Fraction of U-235 in the uranium feed
ep: Fraction of U-235 charged in the reactor
et: Fraction of U-235 in the tails
lC: Material losses of uranium conversion process
lF: Material Losses in fabrication process
Mcycle: Mass of uranium charged in the reactor
Mf: Mass of uranium feed to the enrichment process
Mp: Mass of uranium in the enriched stream
Mt: Mass of uranium in the tails
Mconv: Mass of uranium for conversion process
MYC: Mass of yellow cake
M$: Million Dollar
P1: Monetary units per lb U3O8 for uranium purchase ($/lbU3O8)
P2: Monetary units per Kg U for fuel conversion ($/kgU)
P3: Monetary units per SWU for fuel enrichment ($/SWU)
P4: Monetary units per Kg U for fuel fabrication ($/kgU)
Qe: Electrical Power (MW)
Qth: Thermal Power (MW)
R: average rate of nuclear fuel burn-up (MWd/MTU)
S: Separative work unit requirements (SWU)
Vx: Value function - x subscript for f, p or t

I. INTRODUCTION

The economics of nuclear fuel cycle for nuclear power plants depends generally on two main issues, the nuclear fuel cycle components and the reactor core cycle length. The nuclear fuel cycle can be divided into three stages: front-end, at-reactor and back-end. These, in turn, can be sub-divided into more specific components [1].To identify the generating electricity costs from a typical nuclear power plant, the economics of fuel cycle must be clear. Actually, most countries study the economics and properties for the first two stages of nuclear fuel cycle; front-end and reactor operation time as there is no clear long term strategy made for the back-end part till now. Moreover the large dependency on storage of spent fuels in reactor site increases this foggy vision of the nuclear fuel cycle back-end strategy.

Over the past decade the discharge irradiation level (burn-up) of both Pressurized Water Reactor (PWR) and Boiling Water Reactor (BWR) fuels has increased steadily. This development is mainly attributable to the increased economic benefit that is associated with higher fuel burn-up.

This benefit comes from the reduced throughput of fuel that results from higher burn-up [2]. In this paper, we calculate the generating electricity costs for PWR being the most prevalent reactor type in the world as it represents 274 of the world's 436 reactors now operating [3]. The calculations are performed considering a typical VVER-1000 reactor [4] as a case study.

II. VVER-1000 GENERATING ELECTRICITY COST

A. Front-end Fuel Cycle Cost

The front-end component is composed of uranium purchase, conversion of yellow cake into uranium hexafluoride (UF6), enrichment (isotope separation process to rise the content of fissile materials, U235, in the fuel) and uranium oxide fuel fabrication into assemblies. Based on a direct cost analysis for the front-end fuel cycle components, the amount and price of each component can be defined [1]. Table 1 gives the magnitude of each front-end component unit price [5]. Most fuel contracts are made based on long term contracts not on spot prices so the front-end components unit prices are taken as average values for the past three years.

Table 1. FRONT-END COMPONENTS UNIT PRICES (5)

Component	Price*
Uranium purchase (P1)	\$45/lbU3O8
Conversion (P2)	\$8/KgU
Enrichment (P3)	\$120/SWU**
Fabrication (P4)	\$260/KgU

* average prices over the past 3 years.
** SWU: Separative Work Unit

Based on the VVER-1000 reactor core configuration and the plant design parameters [4], the amount of required fuel charged to the reactor each cycle can be calculated using (1) [6].

$$M_{cycle} = \frac{Q_{th} \cdot CL}{R} \quad (1)$$

Within the context of Dwiddar, M.S., et al.'s previous work on the VVER-1000 reactor core and its improvements to achieve the new design of VVER-1200reactor core, MCNP-X code was used to calculate the core cycle length and the burn up [7].The VVER-1000 validated model showed that for a 3000 MWth, the average value of fuel burn-up is 11800MWd/MTU and the core cycle length is 300 days [7].

Using (1) the amount of required fuel is 76.2 tons of uranium. The value of burn-up is assumed to be an average value for the whole core for one cycle length time. The reactor core consists of three batches and only one batch will be replaced each cycle. Therefore, the output of (1) will be divided by 3 as it will be 76.2/3 = 25.4 tons of uranium, which represents the amount of required fuel for each cycle length. Going backwards through the front-end components, this amount of uranium represents the output of fabrication stage.

The mass of uranium, Mp, required for the fabrication is slightly more than the mass of UO2in the core, Mcycle, due to fabrication losses. To calculate the amount needed for the fabrication stage, the occurring losses must be considered. The loss factor of fabrication stage is 1.0% [1]. Thus applying (2) [1], a value of 25.65 tons is obtained for Mp.

$$M_p = M_{cycle} \cdot (1 + l_F) \quad (2)$$

Using (3) [1] the cost of this amount is calculated based on the price value in table 1, and is found to be equal to 6.669 M\$.

$$C_{Fab} = M_p \cdot P_4 \quad (3)$$

Moving to the enrichment stage, to calculate the amount of uranium required for the enrichment process, both the enriched and depleted assays (ep & et) must be well known. The fuel enrichment batch charged for the VVER-1000 case study is 3.3% – which will be refueled to the reactor core each cycle – so the enriched assay output for the enrichment process is 3.3%. The depleted assay is assumed to be 0.25% which is the prevalent value for the enrichment process in Russia. According to (4) [1] the feed material for the enrichment process is calculated and a value of 169701.73 Kg U is obtained. Equation (5) [1] gives the amount of depleted uranium from this specific enrichment process and it is equal to 144051.73 Kg U.

$$M_f = \left[\frac{e_p - e_t}{e_f - e_t}\right] \cdot M_p \quad (4)$$

$$M_t = M_f - M_p \quad (5)$$

Since the price of enrichment services is expressed per separative work unit (SWU), the quantity of SWUs necessary to obtain the enriched uranium quantity (Mp) at the required enrichment level (3.3%) must be calculated. This quantity can be estimated depending on the 'value' of a mixture (V) which is

estimated on equation (6) as a function of the U235 content. Equation (7) [1] gives the SWU required for this specific enrichment process. According to (7), the separative work need for this process is equal to 113289 SWU.

$$V_x = (2 \cdot e_x - 1) \cdot \ln\left[\frac{e_x}{1-e_x}\right] \quad (6)$$

$$S = M_p \cdot V_p + M_t \cdot V_t - M_f \cdot V_f \quad (7)$$

Thus, the cost of enrichment is calculated using (8) [1] and is found to be equal to 13.7M$.

$$C_{en} = S \cdot P_3 \cdot (1 + l_F) \quad (8)$$

Moving to the conversion stage, the amount of uranium required is calculated using (9) [1]. This amount is equal to 170550.24Kg U considering the loss factor of conversion stage to be 0.5% [1]. According to the calculated uranium amount and using (10) [1] the cost of conversion process is calculated to be 1.364 M$.

$$M_{conv} = M_f \cdot (1 + l_C) \quad (9)$$

$$C_{conv} = M_{conv} \cdot P_2 \quad (10)$$

Finally, the amount and cost of yellow cake to be purchased for starting the nuclear fuel cycle processes have to be calculated. Equations (11) and (12) [1] give the amount and the cost respectively. The amount of yellow cake is equal to 443430.63 lb and the cost is 19.95 M$.

$$M_{YC} = M_{conv} \cdot a \quad (11)$$

$$C_{YC} = M_{YC} \cdot P_1 \quad (12)$$

Fig. 1 summarizes the actual annual front-end fuel cycle requirements for the VVER-1000 case study. The total front-end fuel cost is the sum of all its components cost. Equation (13) [1] gives the total cost which is equal to 41.69 M$.

$$C_{Total} = C_{YC} + C_{conv} + C_{en} + C_{Fab} \quad (13)$$

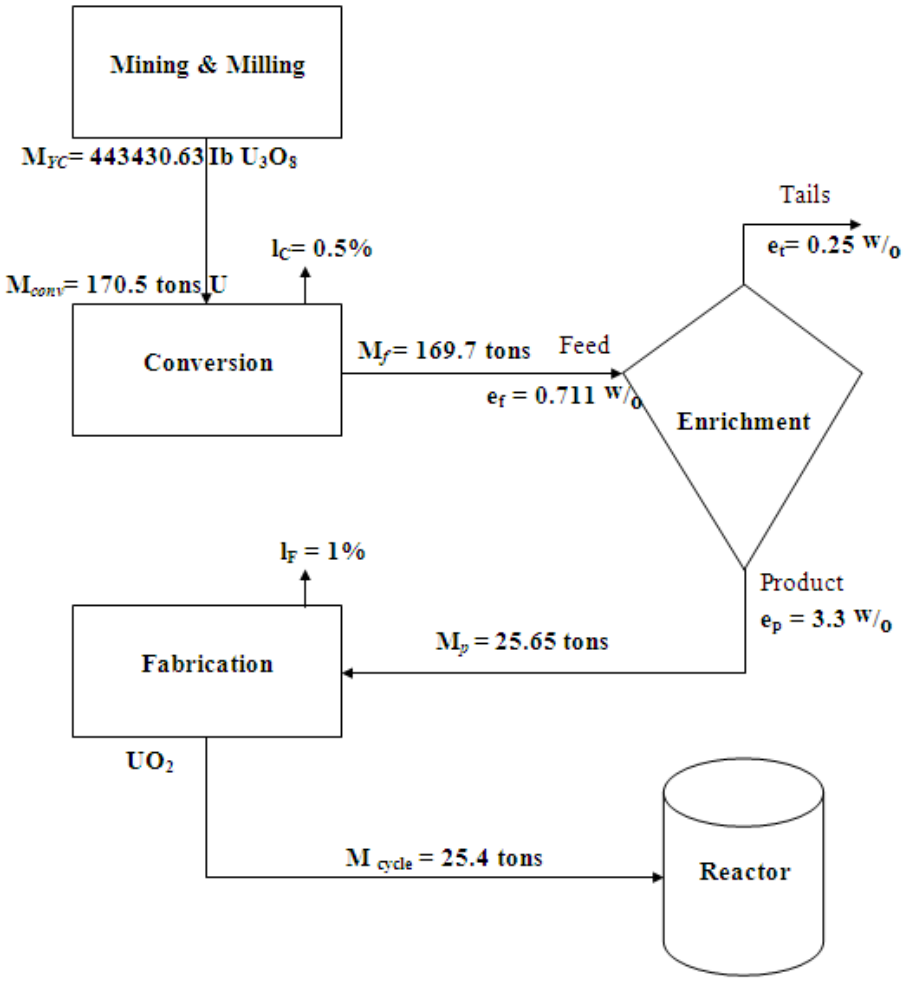

Fig .1. Annual VVER-1000 front-end fuel cycle requirements

From the calculated front-end fuel cycle total cost and considering a plant's availability factor of 82%, (14) estimates the direct fuel cost for the unit electricity generation to be 0.7047 cent/kWh. This value represents the direct electricity generation cost according to the front-end fuel cycle economics.

$$C_{elec} = \frac{C_{Total}}{Q_e \cdot CL \cdot AF \cdot 24} \times \frac{100\ (Cent/\$)}{1000\ (kWh/MWh)} \quad (14)$$

B. Price Sensitivity Analysis

A sensitivity analysis has been carried out with respect to the unit prices for the front-end fuel cycle components. The sensitivity range for front-end service prices generally reflects the upper and lower bound values seen from the extrapolation of component spot prices in international market [1]. The values used for the sensitivity analysis are shown in table 2.

Table 2. SENSITIVITY RANGE FOR THE FRONT-END COMPONENT UNIT PRICES

Component	Price sensitivity range*
Uranium purchase	22.5-90 $/lb U
Conversion	3.75-15 $/Kg U
Enrichment	$60-240 $/SWU
Fabrication	130-520 $/Kg U

Fig. 2 gives the results of the front end fuel cycle components prices sensitivity analysis applied on the direct electricity cost. It is clear that although the uranium purchase is the highly significant component, enrichment cost is the most effective because it is the dynamic process that affects all other components. So it may be deduced that the enrichment cost forms a significant component of the front-end fuel cycle costs.

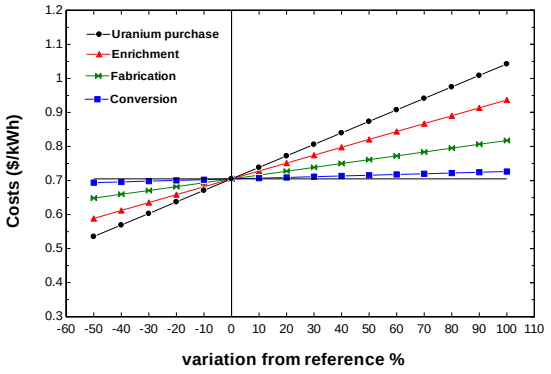

Fig .2. Effect of front end fuel cycle components price change on electricity direct costs

C. Effects of Increasing Enrichment and Core Cycle Length

For increasing the reactor core cycle length, it is required to increase the fissile material content in the reactor core. This will affect the economics of fuel cycle components. From international practice, the maximum allowable enrichment for PWRs is 5%. For saving the design basis parameters for the VVER-1000 case study, the minimum enrichment batch of VVER-1000 model is increased by a step of 0.1. The enrichments of the other batches are also increased keeping the same ratio of enrichment between the three batches as in the reference case. According to this assumption, the maximum enrichment calculated is 4.95 %. [7] Table 3 gives all probable improvements of fuel batches enrichment within the maximum allowable value with the corresponding reactor cycle length and core average burn up. The reactor cycle length and the core average burn up are out data from the MCNP-X code [7].

Table 3. CHANGES CONSIDERED IN THE ENRICHMENT OF THE FUEL BATCHES [7]

Cases	Enrichment of Fuel Batches			Cycle length (days)	Average burnup (MWd/ MTU)
	Batch 1	Batch 2	Batch3		
A (Ref. Case)	2	3	3.3	300	11800
B	2.1	3.15	3.465	336	13213
C	2.2	3.3	3.63	372	14626
D	2.3	3.45	3.795	408	16039
E	2.4	3.6	3.96	444	17452
F	2.5	3.75	4.125	480	18865
G	2.6	3.9	4.29	516	20278
H	2.7	4.05	4.455	552	21691
I	2.8	4.2	4.62	588	23104
J	2.9	4.35	4.785	624	24517
K (Max. Enrich.)	3.0	4.5	4.95	660	25930

According to the output data given in table 3, Fig. 3 shows that the fuel burn-up is directly proportional to the core cycle length.

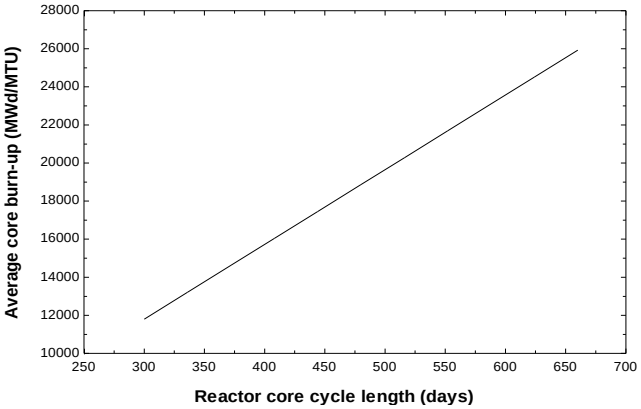

Fig .3. Relation between core cycle length and fuel burn-up

Similarly to case A already considered in section A, (1) to (14) were used to calculate the front end fuel cycle economics and its effect on the electricity generation cost for the other cases.

Calculating the fuel mass required each cycle for the different cases results in a constant value as shown in Fig. 4. This can be explained by the proportionality relation obtained between the core cycle length and the fuel burn-up. As (2) and (3) do not depend on the enrichment percentage, this constant value of fuel mass required each cycle will be reflected in a constant value for both the required mass for the fabrication stage and its cost, namely 25.65 tons and 6.669 M$ respectively.

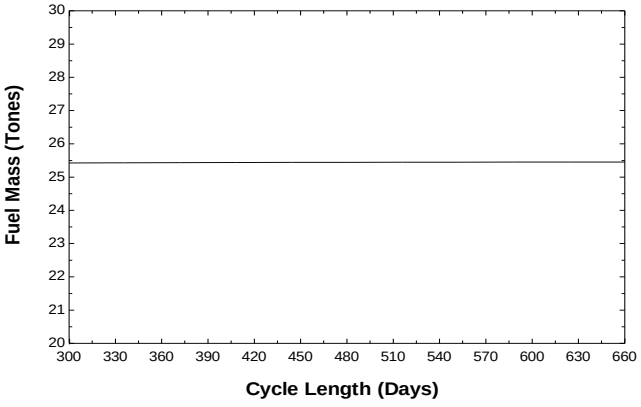

Fig .4 Fuel mass required each cycle for the different cases in table 3

However as fuel enrichment increases, the feed material will increase. Consequently the enrichment cost will increase due to the need for more separative work units as seen in Fig. 5. Fig. 6 shows that the cost of enrichment process is directly proportional to the mass of uranium feed.

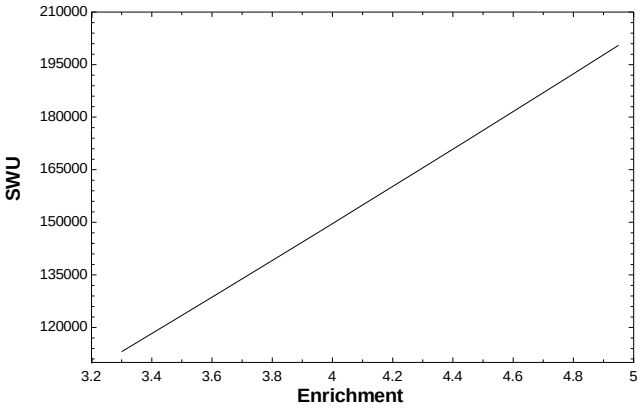

Fig .5 Amount of required SWU for different fuel enrichments

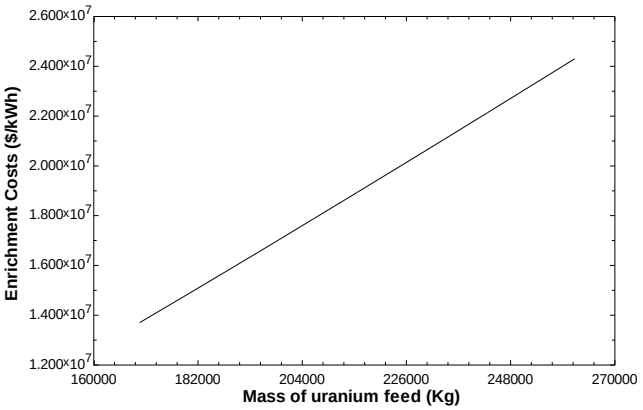

Fig .6 Enrichment process cost versus the mass of uranium feed

The increase in the uranium feed to the enrichment process leads to the need for more uranium for both the conversion and the uranium purchase components resulting in an increase in their costs as illustrated in Figs. 7 and 8.

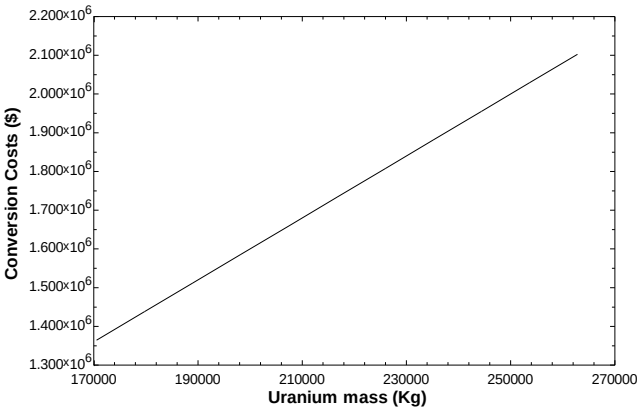

Fig .7 Conversion costs versus the mass of uranium

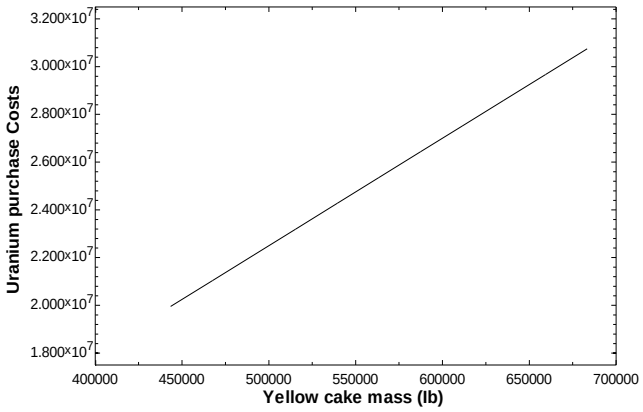

Fig .8 Uranium purchase costs versus the mass of uranium

As a consequence of the increase in the costs of the uranium enrichment, the conversion and the uranium purchase components, the total cost of the front end fuel cycle will increase. But since the increase in the uranium enrichment will lead to longer reactor core cycle length due to the higher fuel burn-up, the resulting electricity cost decreases as shown in Fig. 9.

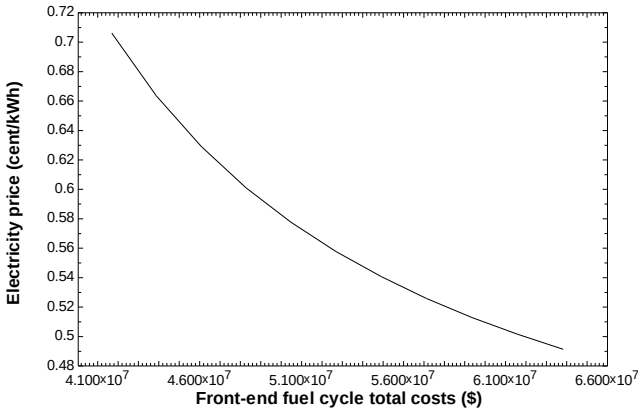

Fig .9 Direct electricity cost versus total front-end cost

III. CONCLUSION

The effect of increasing the nuclear fuel enrichment on the electricity cost has been considered. A typical VVER-1000 reactor has been selected as the case study. The fuel enrichment has been increased up to 5% which is the maximum allowable value for PWRs. Excluding the fabrication component, increasing fuel enrichment was found to increase the uranium masses needed for all the front-end components and consequently their costs.

A sensitivity analysis was performed with respect to the unit prices for the front-end fuel cycle components and their effects on the electricity direct cost. It was noticed that although the uranium purchase is the most effective component, the uranium enrichment still has the highly priority effect due to its dynamic properties and its consequences on the other front-end fuel cycle components. Although increasing the fuel enrichment resulted in a higher total cost of the front end fuel cycle, it was found to extend the reactor core cycle allowing the reactor to operate for more than 12 months. This fact results in a decrease in the electricity generation cost.

Therefore, increasing the nuclear fuel enrichment within the limit allowable internationally for the PWRs will have a positive economic feedback leading to a cheaper electricity cost. This makes the nuclear energy a strong competitor to the other energy sources

REFERENCES

[1] Nuclear Energy Agency, The economical on nuclear fuel cycle (1994) , Organization for economic co-operation and development, Paris, France.

[2] Christopher S. (June 1998) Economic and Fuel Performance Analysis of Extended Operating Cycles in Existing Light Water Reactors (LWRs), Handwork, Massachusetts Institute of Technology,

[3] PRIS, IAEA,(August 2014) Power Reactor Information System. www.iaea.org/PRIS/WorldStatistics/OperationalReactorByTupe.aspx

[4] IAEA, (November 1995) In-core fuel management code package validation for WWERs. IAEA-TECDOC-847.

[5] The Ux Consulting Company (August 2014). www.uxc.com/review/UxCProces.aspx

[6] Cacuci, D. G. (2010) Handbook of Nuclear Engineering, Institute for Nuclear Technology and Reactor Safety. KarlsruherInstitut fur Technologie, Germany.

[7] Dwiddar, M. S. (May 2014) From VVER-1000 to VVER-1200: investigation of the effect of the changes in core. The third international conference on physics and technology of reactors and applications, Tetuan, Morocco.

Scan the QR Code

Journal of

Renewable Energy and Sustainable Development

RESD

Volume 1, June 2015 ISSN 2356-8569

ISSN 2356-8569

http://apc.aast.edu